

IMPULSIVE LOADING ON REINFORCED CONCRETE SLABS

Thesis submitted to
The University of Sheffield
for the degree of

Doctor of Philosophy

in the

Faculty of Engineering
Department of Civil and Structural Engineering

by

N. Duranovic

February 1994

**PAGE
NUMBERING
AS
ORIGINAL**

SUMMARY

A number of reinforced concrete slabs have been exposed to blast and impact loading in order to access modes of slab behaviour under these extreme dynamic loadings.

Two sizes of specimens were used; small scale slabs modelled the large slabs at 1: 2.5 scale.

Impact loads were produced by a free falling hammer impacting coaxially onto a cylindrical bar of steel placed at rest in the centre of the slab. The steel bar was instrumented with electrical strain gauges which recorded the stress pulses produced by the impact.

Blast loads were produced using explosive charges made of Plastic Explosive PE4. In most cases the charge used was hemispherical in shape and was placed centrally above the slab at close range standoffs, i.e. up to 10 times the radius of the charge.

Additional blast tests were conducted in order to monitor the transient and spatial pressure distribution across the slab by using the pressure gauges placed in replica steel slab.

Transient deflections of the slabs under both types of load were obtained using long stroke displacement transducers, whilst transient strains in the steel reinforcement of the slabs were obtained using electrical resistance strain gauges bonded to the steel bars at mid span point.

A rotating prism high speed camera was used to film the damage on some of the small scale specimens at rates of up to 10,000 pictures per second.

The Hopkinson pressure bar tests were used to obtain the dynamic characteristics of the concretes used at high rates of loading. Different concrete mixes were used for the 1:1 and 1:2.5 scale slabs.

An analytical function of the spatial and transient blast pressure distribution based on the detonation pressure of PE4 was established. This is in close agreement to experimentally measured results.

The nature of the local and overall failure are discussed, and the time sequence of the slab failure is established for the case of explosive loading.

The crack pattern that occurs soon after the explosion in area of local failure has been established from the high speed films whilst the overall deflected shape was obtained from the displacement vs time records.

After test scab sizes and slab perforations were used to establish a relation between the slab thickness, amount of explosive and the slab damage in respect to scabbing and perforation.

The displacement records and the shape of after test damage provided the basis for comments on "gravity neglected - the ultimate strength" modelling law that was employed in this research.

ACKNOWLEDGEMENTS

I want first and foremost to express my gratitude to Dr. Alan J. Watson for his guidance, encouragement and supervision throughout the research program.

I also want to thank the Defence Research Agency, Farnborough, for financing the work and, in particular, Dr. Jim Sheridan for his valuable suggestions and comments.

The technical assistance of Mr. A. Hindle and Mr. R. Mellor from the Harpur Hill - CEDUS laboratories of The University of Sheffield made the testing more enjoyable and successful, whilst the patient typing of the reports and most of the thesis by Mrs. B. Mason gave me valuable time to concentrate on the testing and analysis of the results.

Lastly, but probably most importantly, I want to thank my wife Zorica for providing me and our children with a warm, worry - free family environment in which my comittment to completing the thesis was never considered as something personal, but as a worthy effort for all four of us.

CONTENTS

	Page
List of Figures	VII
List of Tables	X
List of Plates	XI
1. INTRODUCTION	
1.0 General Introduction	1
1.1 Dynamic loading	2
1.2 Impact and impulse loading in the field of Civil Engineering	4
1.3 R.C. slabs under transient loading	6
1.4 Present investigation	7
2. LITERATURE SURVEY	
2.1 Impact and blast loading of R.C. slabs	9
2.2 Material properties under high rates of strain	17
2.2.1 Concrete properties	21
2.2.1.1 Stress-strain diagram	21
2.2.1.2 Compressive strength	23
2.2.1.3 Tensile strength	26
2.2.1.4 Poisson ratio	31
2.2.1.5 Energy absorption and modulus of rupture	31
2.2.2 Reinforcement properties	32
2.3 Local response of R.C. slabs to impact and close range blast loading	34
2.3.1 Stress-wave propagation	34
2.3.2 Cracking	36
2.3.3 Penetration	38
2.3.4 Shear plug formation	38
2.4 Overall response of R.C. slabs to impact and close range blast loading	40
2.4.1 Inertial loading	40

2.4.2	Resistance function	41
2.5	Blast pressure characteristics	45
2.5.1	Introduction	45
2.5.2	Blast wave scaling and parameters	48
2.5.3	Interaction of shock waves with plane surfaces	49
2.5.4	Loading due to a short range explosion	51
2.6	Modelling considerations	54
2.6.1	Dimensional analysis	54
2.6.2	Theory of modelling for structures exposed to impact and blast	55
2.7	Some theoretical approaches to the problem	57
2.7.1	Timoshenko (1951)	57
2.7.2	Goldsmith (1960)	57
2.7.3	Norris (1964)	58
2.7.4	Ezra (Johnson, 1972)	59
2.7.5	Popov (1976)	60
2.7.6	Symonds (Watson, 1991)	61
2.8	Standard recommendations	62
3.	EXPERIMENTAL TECHNIQUES	
3.0	Introduction	65
3.1	Test specimen	66
3.1.1	Slab dimensions	66
3.1.2	Materials	68
3.1.2.1	Concrete	68
3.1.2.1.1	Microconcrete mix	69
3.1.2.1.2	Macroconcrete mix	73
3.1.2.2	Steel reinforcement	76
3.1.2.2.1	H.Y. grade 460 deformed reinforcement bars	77
3.1.2.2.2	H.Y. BS4483 square reinforcement mesh	77
3.1.2.2.3	Heavy Twilweld reinforcement mesh	78
3.1.3	Fabrication of the specimen	79

3.1.3.1	Reinforcement mesh	79
3.1.3.2	Preparation of moulds	80
3.1.3.3	Concrete mixing, casting and curing	81
3.1.3.4	Control specimen	81
3.1.3.5	Preparations prior to testing	82
3.2	Test instrumentation	82
3.2.1	Displacement transducers	82
3.2.2	Digital storage oscilloscopes	83
3.2.3	Strain gauges	84
3.2.4	D.C.-Bridge amplifier - 359 - TA	86
3.2.5	Microswitches	86
3.2.6	Slotted opto-switches	87
3.2.7	Universal counter timer	87
3.2.8	D.C. Power supply	88
3.2.9	Photec IV - 16mm High Speed Camera	88
3.2.10	FS-10 Firing system	89
3.2.11	Pressure transducers	90
3.2.12	Hycam - K 2001 R - 16mm High Speed Camera	91
3.3	Test arrangements	92
3.3.1	Support conditions	92
3.3.1.1	Free supports	92
3.3.1.2	Inner supports	93
3.3.1.3	Fixed support	94
3.3.2	Loading conditions	95
3.3.2.1	Impact test	96
3.3.2.2	Impulse test	98
3.3.2.2.1	Test arena	98
3.3.2.2.2	Explosive charge	99
3.3.2.3	Static test	100
3.3.3	Specimen response record	101

3.3.3.1	Impact load measurements	102
3.3.3.2	Hammer velocity measurements	105
3.3.3.3	Blast pressure measurements	106
3.3.3.4	Reinforcement strain measurements	107
3.3.3.5	Deflection measurements	108
3.3.3.6	High-speed filming	111
3.3.3.7	After test damage assessment	113
3.3.4	Test set up, procedure and event synchronisation	113
3.3.4.1	Impact test	113
3.3.4.2	Impulse test	116
3.3.5	Experimental programme and variables	117
4.	EXPERIMENTAL RESULTS	
4.0	Introduction	120
4.1	Impact tests	121
4.1.1	1:2.5 Scale slabs	121
4.1.1.1	Pressure bar record and velocity measurement	122
4.1.1.2	Displacement record	124
4.1.1.3	Reinforcement strain record	125
4.1.1.4	High speed films	128
4.1.1.5	Crack patterns and slab cross-sections	130
4.1.2	1:1 Scale slabs	132
4.1.2.1	Pressure bar record and velocity measurement	133
4.1.2.2	Displacement record	135
4.1.2.3	Strain record	137
4.1.2.4	Crack pattern	138
4.1.3	Conclusions	139
4.2	Impulse tests	140
4.2.1	1:2.5 Scale slabs	140
4.2.1.1	Blast pressure records	142
4.2.1.2	Displacement record	145

4.2.1.3	Reinforcement strain record	147
4.2.1.4	High speed films	149
4.2.1.5	Crack patterns and slab cross-sections	152
4.2.2	1:1 Scale slabs	154
4.2.2.1	Displacement record	154
4.2.2.2	Reinforcement strain record	156
4.2.2.3	Crack patterns	157
4.2.3	Conclusions	158
5.	DISCUSSION	
5.1	Introduction	160
5.1.1	Loading function	161
5.1.1.1	Calculation of blast loading function	161
5.1.1.2	Attenuation of the loading function and inertia	168
5.1.2	Dynamic character of material behaviour	169
5.1.3	Dual nature of the slab response	170
5.2	Local response	171
5.2.1	Formation of an area of local response	172
5.2.1.1	High speed films	173
5.2.1.2	Stress wave theory approach	175
5.2.2	Development of cracking within the area of local response	181
5.2.3	Ultimate state conditions in the area of local response and failure	183
5.2.3.1	Spalling, scabbing and perforation of the slab	183
5.2.3.2	Prediction of the damage	193
5.2.4	Load transfer from the area of local response to the rest of the slab	197
5.3	Overall response of the slab	199
5.3.1	Crack type analysis	200
5.3.1.1	Top surface cracks	200
5.3.1.2	Bottom surface cracks	202
5.3.1.3	Cross sectional cracks	205
5.3.2	Deflection analysis	205

5.3.3	Energy considerations due to close range explosion	217
5.4	Connection between local and flexural response	217
5.5	Time sequence of events in the blast loading of R.C. slabs and	219
5.6	Modelling	222
5.6.1	Local damage	222
5.6.2	Overall flexural damage	222
5.6.3	Displacement record	223
6.	CONCLUSIONS	
6.1	Modelling	224
6.2	Instrumentation	225
6.3	Dynamic properties of materials and the blast loading function	226
6.4	Local response	227
6.5	Overall flexural response	230
7.	FUTURE WORK	232
	REFERENCES	
	APPENDICES	
Appendix A1	1:1 Scale impact test results	
Appendix A2	1:2.5 Scale impact test results	
Appendix A3	Impact tests - High speed films	
Appendix B1	1:1 Scale impulse test results	
Appendix B2	1:2.5 Scale impulse test results	
Appendix B3	Impulse tests - High speed films	
Appendix C1	Static test results	

LIST OF FIGURES

- Fig. 1.1 Accelerogram of the Montenegro earthquake, 1979 (Petrovic, 1985)
- Fig. 1.2 The car impact loading function (Bangash, 1993)
- Fig. 1.3 Typical dynamic loading function in case of blast loading (Fertis, 1975)
- Fig. 1.4 Typical pressure-time relation
- Fig. 1.5 Typical load time history produced by a soft impact
- Fig. 1.6 Typical load time history produced by a hard impact
- @
- Fig. 2.1 Load-deflection curve for slabs with edges restrained against lateral movement (Park, 1964)
- Fig. 2.2 Front side crack pattern (Nilsson and Sahlin, 1980)
- Fig. 2.3 Explosive tests on concrete slabs (Watson and Sanderson, 1984)
- Fig. 2.4 Slab failure modes (Watson and Al-Azawi, 1984)
- Fig. 2.5 Empirical Model for Shear Stress-Shear Slip Relationship (Krauthammer et al, 1986)
- Fig. 2.6 Cracking patterns (experiment) (Yamaguchi and Fujimoto, 1991)
- Fig. 2.7 Stress-strain diagrams for two concretes at different rates of straining (Mainstone, 1975)
- Fig. 2.8 Influence of a high stress rate upon the stress-strain relationship for concrete in uniaxial tension (Zielinski et al, 1981)
- Fig. 2.9 Variation of modulus of elasticity with stress and strain rate (Mainstone, 1975)
- Fig. 2.10 Influence of stress and strain rate on compressive properties of concrete (CEB Bulletin No. 187, 1988)
- Fig. 2.11 Variation of ultimate strength of concrete in direct compression with average rate of loading or straining (Mainstone, 1975)
- Fig. 2.12 Strength ratio vs strain rate (Atchley and Howard, 1967)
- Fig. 2.13 Influence of stress and strain rate on tensile properties of concrete (CEB Bulletin No. 187, 1988)
- Fig. 2.14 Relative impact tensile strength as a function of load and strain rate (Veen and Blaauwendraad, 1983)
- Fig. 2.15 Relation between tensile strength and loading rate (Reinhardt, 1982)
- Fig. 2.16 Influence of different strain rates on the ratio between compressive and tensile concrete strength (Reinhardt, 1982)
- Fig. 2.17 Influence of W/C ratio on dynamic tensile strength of concrete, (Hughes and Gregory, 1972)
- Fig. 2.18 Effect of changes in loading/casting direction upon the impact fatigue tensile strength (Reinhardt, 1982)
- Fig. 2.19 Effect of loading history on concrete behaviour (CEB Bulletin No. 187, 1988)
- Fig. 2.20 Relative MOR versus Strain-Rate for Mortar and Concrete (Suaris and Shah, 1983)
- Fig. 2.21 Stress-strain diagrams for three steels at different rates of straining (Mainstone et al, 1975)
- Fig. 2.22 Variation of upper yield strength of steel in direct tension or compression with rate of straining or loading (Mainstone, 1975)
- Fig. 2.23 τ - δ relation at four loading rates for concrete with a cube strength of 22.7N/mm² (Reinhardt, 1982)
- Fig. 2.24 Experimental crack velocity (V) versus strain rate $\dot{\epsilon}$ relationship (John and Shah, 1986)
- Fig. 2.25 Critical angle ϕ_c versus stress rate $\dot{\sigma}$ (Zielinsky et al, 1981)
- Fig. 2.26 Idealised behaviour of punching cone (Eibl, 1988)
- Fig. 2.27 Variation of shear cone angle with the striker velocity (CEB Bulletin 187, 1988)
- Fig. 2.28 Distribution of inertia forces P, moments and shear forces for extreme values α (Eibl and Feyerabend, 1985)
- Fig. 2.29 Bilinear resistance function (Biggs, 1964)
- Fig. 2.30 Effective linear resistance function (Biggs, 1964)
- Fig. 2.31 Two degree of freedom model (Eibl, 1988)
- Fig. 2.32 Idealised elastoplastic material (Eibl, 1988)
- Fig. 2.33 Resistance-Deflection (Tankreto, 1991)
- Fig. 2.34 Resistance Function (Smith and Mlakar, 1991)
- Fig. 2.35 Resistance function (Kyger and Hyde, 1987)
- Fig. 2.36 Typical overpressure-time relation produced by the blast wave
- Fig. 2.37 Typical pressure-time curves for successive distances after an explosion (Kinney and Graham, 1985)
- Fig. 2.38 Reflection of a low overpressure spherical shock (Watson, 1991)
- Fig. 2.39 Formation of Mach stem (Kinney and Graham, 1985)
- Fig. 2.40 Oblique shock reflection (Kinney and Graham, 1985)

- Fig. 2.41 Outburst pattern for the nearby explosion (Henrych, 1979)
- Fig. 2.42 Nearby explosion above a circular plate (Henrych, 1979)
- Fig. 2.43 Central impact on a simply supported beam (Goldsmith, 1960)
- Fig. 2.44 Notation for flexural vibration (Norris, 1964)
- Fig. 2.45 Characteristic shapes of first three normal modes of vibration (Norris, 1964)
- Fig. 2.46 Travelling plastic hinge (Johnson, 1972)
- Fig. 2.47 Behaviour of an elastic system under an impact force (Popov, 1976)
- Fig. 2.48 Symond's analysis - load function (Watson, 1991)
- Fig. 2.49 Symond's analysis - overall load, shear force and moment

- @
- Fig. 3.1 Slab reinforcement details
 - Fig. 3.2 Sand sieve analysis
 - Fig. 3.3 Gravel sieve analysis
 - Fig. 3.4 Microconcrete stress-strain diagram
 - Fig. 3.5 Hopkinson Pressure Bar Test Rig
 - Fig. 3.6 Hopkinson pressure bar test results for microconcrete
 - Fig. 3.7 Hopkinson pressure bar test results for macroconcrete
 - Fig. 3.8 Confined concrete test arrangement
 - Fig. 3.9 Confined concrete test results
 - Fig. 3.10 H.Y. steel reinforcement bar stress-strain curve
 - Fig. 3.11 Stress-strain curve for the BS4483 A393 reinforcement mesh
 - Fig. 3.12 Stress-strain curve for the Heavy Twilweld reinforcement mesh
 - Fig. 3.13 Slab mould
 - Fig. 3.14 Displacement transducer
 - Fig. 3.15 Displacement transducer test results
 - Fig. 3.16 Effect of using too long strain gauge
 - Fig. 3.17 Pressure gauge calibration and test results
 - Fig. 3.18 Free supports
 - Fig. 3.19 Inner supports
 - Fig. 3.20 Fixed supports
 - Fig. 3.21 Drop hammer test rig
 - Fig. 3.22 Static test loading arrangement
 - Fig. 3.23 Pressure bar set-up and strain gauge station arrangement
 - Fig. 3.24 1:1 Scale pressure bar - static calibration results
 - Fig. 3.25 Arrangement for measuring drop-hammer velocity by microswitches
 - Fig. 3.26 Arrangement for measuring drop-hammer velocity by opto-switches
 - Fig. 3.27 Instrumentation for pressure measurement
 - Fig. 3.28 Pressure test set-up
 - Fig. 3.29 Wheatstone bridge circuitry for measuring the strain in the reinforcement
 - Fig. 3.30 RPDT positions
 - Fig. 3.31 Instrumentation for deflection measurements
 - Fig. 3.32 The area that was filmed by the High Speed Camera
 - Fig. 3.33 High speed camera arrangements
 - Fig. 3.34 Testing programme

- @
- Fig. 4.1 Small scale slab, hard impact test, typical force vs time record
 - Fig. 4.2 Small scale slab, soft impact test, typical pressure bar record
 - Fig. 4.3 Small scale slab, hard impact test - typical deflection vs time record
 - Fig. 4.4 Small scale impact test - full reinforcement strain record
 - Fig. 4.5 Small scale impact test - partial reinforcement strain record
 - Fig. 4.6 Typical 16mm Frame details - Impact test
 - Fig. 4.7 Failure propagation for hard and soft impact tests
 - Fig. 4.8 Small scale slabs - hard impact tests - crack patterns
 - Fig. 4.9 Small scale slabs - soft impact tests - crack patterns
 - Fig. 4.10 Small scale slabs - hard impact test - cross-sections
 - Fig. 4.11 Small scale slabs - soft impact test - cross-sections
 - Fig. 4.12 Full scale slab - hard impact test - typical load-time record
 - Fig. 4.13 Full scale slab - soft impact test - typical load time record
 - Fig. 4.14 Full scale slabs - hard impact test - typical displacement vs time record
 - Fig. 4.15 Full scale slabs - soft impact test - typical displacement vs time record
 - Fig. 4.16 Full scale slabs - hard impact test - typical strain record

- Fig. 4.17 Full scale slabs - soft impact test - typical strain record
- Fig. 4.18 Large scale slabs - impact tests - crack patterns
- Fig. 4.19 Typical pressure-time record for the 78g PE4 hemispherical charge - flat side facing the gauges
- Fig. 4.20 Typical pressure-time record for the 78g PE4 hemispherical charge curved side facing the gauges
- Fig. 4.21 Typical pressure-time record for the 78g PE4 cylindrical charge
- Fig. 4.22 Spatial pressure distribution from the 78g PE4 hemispherical charge -curved side facing the gauges
- Fig. 4.23 Blast pressures taken at 420mm off centre of the plate from the curved side of the 78g PE4 hemispherical charge
- Fig. 4.24 Small slabs - Impulse test - Typical deflection time record
- Fig. 4.25 Small slabs - Impulse test - Example of deflection record with electrical disturbance
- Fig. 4.26 Small slab - Impulse test -Typical reinforcement strain record
- Fig. 4.27 Small slabs - Impulse test - Partial strain gauge record
- Fig. 4.28 16mm Film frame details- Blast impulse tests
- Fig. 4.29 Small slab SE17 - Blast Impulse Test - Typical frames taken from the high speed film
- Fig. 4.30 Small slabs - Impulse test - crack patterns
- Fig. 4.31 Small slabs - Impulse test - cross-sections
- Fig. 4.32 Full scale slab - Impulse test - typical displacement record
- Fig. 4.33 Full scale slab - Impulse test - typical reinforcement strain record
- Fig. 4.34 Large scale slabs - Impulse tests - crack patterns

@

- Fig. 5.1 Loading function
- Fig. 5.2 Pressure vs time profile for 78g PE4 charge according to Henrych (1979) - 50mm standoff
- Fig. 5.3 Pressure vs time profile for 78g PE4 charge according to Henrych (1979) - 100mm standoff
- Fig. 5.4 Pressure vs time profile for 78g PE4 charge according to Henrych (1979) - 200mm standoff
- Fig. 5.5 Pressure vs time profile for 78g PE4 charge according to Henrych (1979) - 300mm standoff
- Fig. 5.6 Pressure vs time profile for 78g PE4 charge according to Henrych (1979) - 400mm standoff
- Fig. 5.7 Pressure vs time profile for 78g PE4 charge according to Henrych (1979) - 500mm standoff
- Fig. 5.8 Static type concrete failure
- Fig. 5.9 Dynamic type concrete failure
- Fig. 5.10 Shape of the incident pulse
- Fig. 5.11 Stress wave reflection
- Fig. 5.12 Divergence of the stress wave
- Fig. 5.13 Scab thickness
- Fig. 5.14 Development of area of local response
- Fig.5.15 Symmetrical segmentation of the outer ring (ring B) and random segmentation of the inner ring (ring A)
- Fig. 5.16 Typical impact punched hole
- Fig. 5.17 Punched hole Type A
- Fig. 5.18 Punched hole Type B
- Fig. 5.19 Estimate of the slab damage
- Fig. 5.20 Damage Classification (Kropatscheck, 1983)
- Fig. 5.21 Load transfer from the area of local response
- Fig. 5.22 Deflection profiles of small slab SS1 - static test
- Fig. 5.23 Deflection profiles of small slab SS2 - static test
- Fig. 5.24 Deflection profile of small slab S10 - soft impact
- Fig. 5.25 Deflection profiles of small slab S11 - soft impact
- Fig. 5.26 Deflection profiles of small slab S12 - soft impact
- Fig. 5.27 Deflection profiles of small slabs S15 and S16 - hard impact
- Fig. 5.28 Deflection profiles of large slab LS5 - soft impact and LS2 - hard impact
- Fig. 5.29 Deflection profiles of small slabs under blast loading
- Fig. 5.30 Deflection profiles of large slab LSE3 - blast loading test
- Fig. 5.31 Deflection profiles of large slab LSE5 - blast loading test
- Fig. 5.32 Radial expansion of the stress wave
- Fig. 5.32 Flexural mechanism forces

@

- Fig. 7.1 Fixed supports

LIST OF TABLES

Table 1.1	Type of loading - strain rate relation
@	
Table 2.1	Summary of scale factors for dynamic loading
@	
Table 3.1	Specimen dimensions
Table 3.2	Mix proportions
Table 3.3	Hopkinson pressure bar test results for small scale concrete
Table 3.4	Control specimen test results
Table 3.5	Hopkinson pressure bar test results for the macroconcrete
@	
Table 4.1	Small scale impact tests - test variables
Table 4.2	Small scale slabs - force time records
Table 4.3	Small scale impact tests - reinforcement strain record
Table 4.4	Small scale impact test - high speed film details
Table 4.5	Full scale slabs - impact test - test details
Table 4.6	Full scale slab - impact test - load function results
Table 4.7	Full scale slab - impact test - displacement record details
Table 4.8	Full scale slabs - impact test - strain record
Table 4.9	Small slabs - impulse tests - test details
Table 4.10	Blast pressure test results for the cylindrical and hemispherical 78g PE4 charge
Table 4.11	Small slabs - impulse tests - strain record
Table 4.12	Small slabs - impulse tests - high speed film details
Table 4.13	Full scale slabs - impulse tests - test details
Table 4.14	Full scale slabs - impulse test - displacement vs time record details
Table 4.15	Full scale slabs - impulse test - reinforcement strain record details
@	
Table 5.1	Comparison between the measured and calculated pressures
Table 5.2	Details of slab bottom face damage - 1:2.5 scale impact tests Slabs S1 to S15
Table 5.3	Details of slab bottom face damage - 1:2.5 scale impact tests Slabs S16 to S19 and 1:1 scale Slabs LS1 to LS5
Table 5.4	Details of slabs top and bottom face damage - 1:2.5 Scale Impulse tests - Slabs SE1 to SE10
Table 5.5	Details of slabs top and bottom face damage - 1:2.5 Scale Impulse tests - Slabs SE11 to SE19
Table 5.6	Details of slab's top and bottom face damage 1:1 Scale Impulse tests - Slabs LSE1 to LSE5
Table 5.7	Values for Fig. 5.2.3.2.2
Table 5.8	Blast Impulse Tests, displacement scaling

LIST OF PLATES

Plate 1.1 Demolition by implosion (New Civil Engineer, 22.2.1990)

@

- Plate 3.1 Slab mould
- Plate 3.2 Digital storage oscilloscope OS 4020
- Plate 3.3 FILDE DC - Bridge Amplifier
- Plate 3.4 Microswitch
- Plate 3.5 Slotted opto switch
- Plate 3.6 Universal counter timer 9903
- Plate 3.7 D.C. Bench Power Supply
- Plate 3.8 Photec IV - 16mm High Speed Camera
- Plate 3.9 F.S.10 - Firing System
- Plate 3.10 HKM-375-1000 Kulite pressure transducer
- Plate 3.11 16mm HYCAM camera
- Plate 3.12 1:2.5 Scale impulse test site
- Plate 3.13 RPDT slab fixing
- Plate 3.14 Small scale slab, impact test set up
- Plate 3.15 Large scale slab, impulse test set up
- Plate 3.16 Small scale slab, impulse test set up

@

- Plate 5.1 Top face of Slab S12 - soft impact test, 3.0m drop
- Plate 5.2 Top face of SE5 - hemispherical charge 100mm standoff
- Plate 5.3 Bottom face of Slab S12 - soft impact test - 3.0m drop
- Plate 5.4 Bottom face of Slab SE16 - hemispherical charge - 60mm standoff
- Plate 5.5 Slab SE17, larger size cracks
- Plate 5.6 Slab SE17, smaller size cracks

CHAPTER 1

INTRODUCTION

1.0 General introduction

This thesis presents the findings of an experimental study into the behaviour of reinforced concrete slabs under impact and blast loading. The work, initially funded for 18 months but later extended for another 24 months, was commissioned by the Defence Research Agency, Farnborough. It provided the Special Services Division of the Mott MacDonald Group, Consulting Engineers, Croydon, with the necessary test results and explanations of R.C. slab behaviour in order to contribute in developing computer software that deals with the blast and impact loading of R.C. slabs. The study presented here was conducted from February 1990 to December 1993.

The experimental work was carried out at the laboratories for Civil Engineering Dynamics, University of Sheffield (CEDUS), Sheffield University Research Laboratories, Harpur Hill, Buxton.

The impact loading was produced by a free falling hammer whilst plastic explosive PE4 charges of up to 1.3 kg were used to explosively load the specimens.

The tests were performed on specimens of two sizes; the small scale slabs modelled the large scale slabs at 1: 2.5 scale.

1.1 Dynamic loading

In addition to long term static loads civil engineering structures might also be exposed to dynamic loads. They can be of different nature and origin but most of them could fall in one of these three categories.

1. Earthquake loading
2. Impact loading
3. Impulse loading

While in the case of static loading time relation of the structural response is usually not of major importance, in the case of dynamic loads it becomes the factor that most influences the structural behaviour. The three above mentioned types of loading are usually best identifiable by the shapes of their loading functions, Fig. 1.1, Fig. 1.2 and Fig. 1.3.

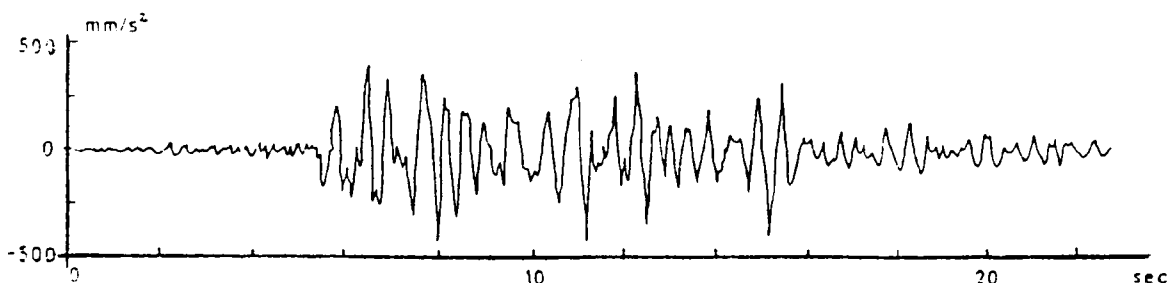


Fig. 1.1 Accelerogram of the Montenegro earthquake, 1979, (Petrovic, 1985)

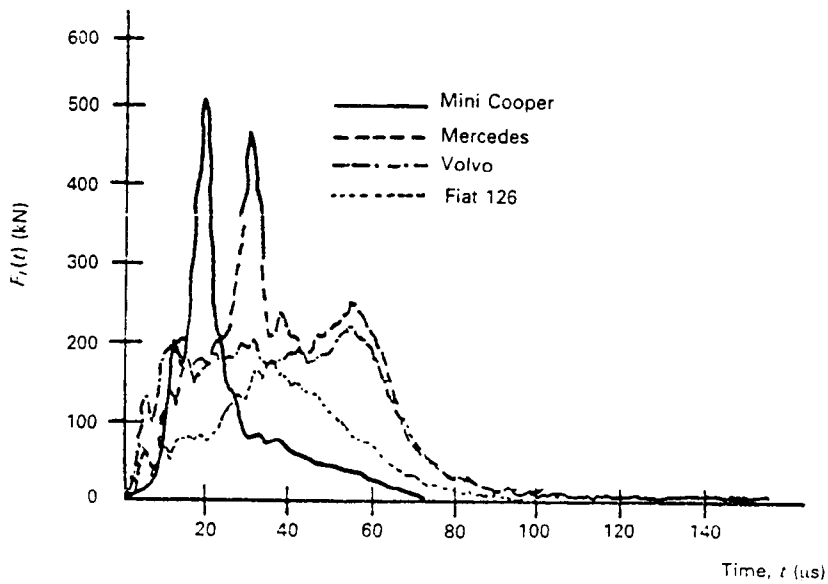


Fig. 1.2 The car impact loading function (Bangash, 1993)

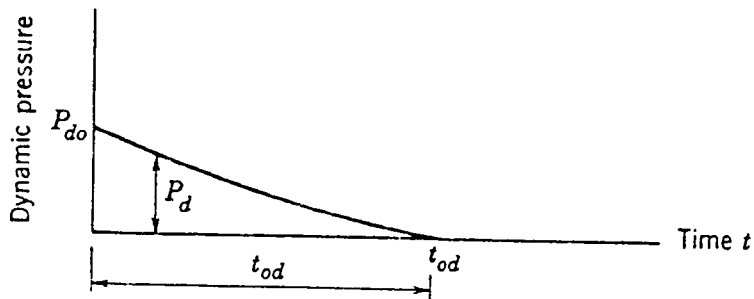


Fig. 1.3 Typical dynamic loading function in case of blast loading (Fertis, 1975)

Earthquake loading usually lasts from a few seconds to a few minutes and structural response can not be studied through the response of a single structural element but as a response of the structure as a whole.

Impact loading result from the collision of two solid bodies when at least one of them has an initial velocity. The loading functions presented in Fig. 1.2 are the result of the impact against the steel and aluminium barriers at speeds of up to 90km/hour.

Impulse loading are distinguished from impact loads when the stationary object is not struck by a solid but by an overpressure. An overpressure acts on a structure in the form of dynamic pressure as given in Fig. 1.3.

Both impact and impulse loading may cause fast initial deformation of the impacted body which may then transfer displacement by overall response of the structure. Studies of these two

phenomena are not only into the behaviour of the structure as a whole but very often concentrate on the response of a particular element of the structure that is directly exposed to the loading.

Rapidly applied loads produce high strain rates in the structural member. Some typical strain rates for various types of dynamic loading are shown in Table 1.1.

TYPE OF LOADING	STRAIN RATE (sec ⁻¹)
Traffic caused loads	10 ⁻⁶ to 10 ⁻⁴
Gas explosions	5 x 10 ⁻⁵ to 5 x 10 ⁻⁴
Earthquake	5 x 10 ⁻³ to 5 x 10 ⁻¹
Pile driving	10 ⁻² to 10 ⁰
Aeroplane crash	5 x 10 ⁻² to 2 x 10 ⁰
Hard impact	10 ⁰ to 5 x 10 ¹
Hypervelocity impact	10 ² to 10 ⁶

Table 1.1 Type of loading - strain rate relation

1.2 Impact and impulse loading in the field of Civil Engineering

Short duration intensive loads that cause a dynamic response of structures are very rapidly increasing in their importance. The most frequent and best known examples of these loads in the civil engineering field can be divided into the following categories:

- (a) Loads caused by falling objects.
- (b) Loads caused by impact of moving vehicles.
- (c) Loads caused by waves in water.
- (d) Concrete pile driving.
- (e) Crashing aircraft.
- (f) Explosions from chemical or military explosives.
- (g) Gas explosions.
- (h) Extreme wind loading.
- (i) Demolition (Plate 1.1).



Plate 1.1 Demolition by implosion (New Civil Engineer, 22.2. 1990)

The design of structures against all of these loads are predominantly determined by:

- (a) The probability of the dynamic load occurrence and the costs of resistant design.
- (b) The characteristics of the dynamic load.
- (c) The level of damage that the whole structure or individual elements can suffer.
- (d) The response of the structure and its constitutive materials under high rates of loading.

Loading functions for both impact and impulse loading are characterised by a very short duration which may be less than the natural period of the structure in which case the structure responds to the impulse. When the load is long relative to the natural period then the structure responds to the peak force that usually occurs at the beginning of the loading pulse.

Typical pressure-time history produced by an explosion is shown in Fig. 1.4.

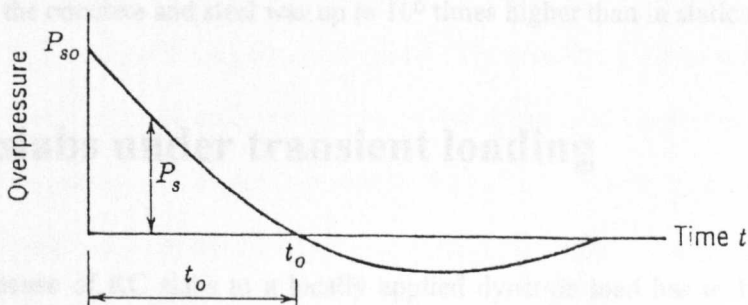


Fig. 1.4 Typical pressure-time relation

Under impulse loads the structure is usually loaded by air type pressure, but impact load is produced by a solid body whose mass, hardness and velocity greatly influences the response of the impacted element. The term "soft impact" is widely used when the impactor's stiffness is significantly lower than that of the structure and consequently a great amount of energy gets absorbed in deforming the impactor, Fig. 1.5.

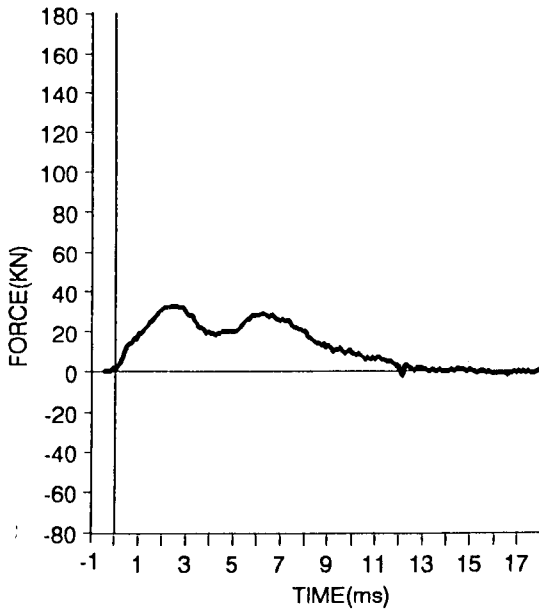


Fig. 1.5 Typical load time history produced by a soft impact

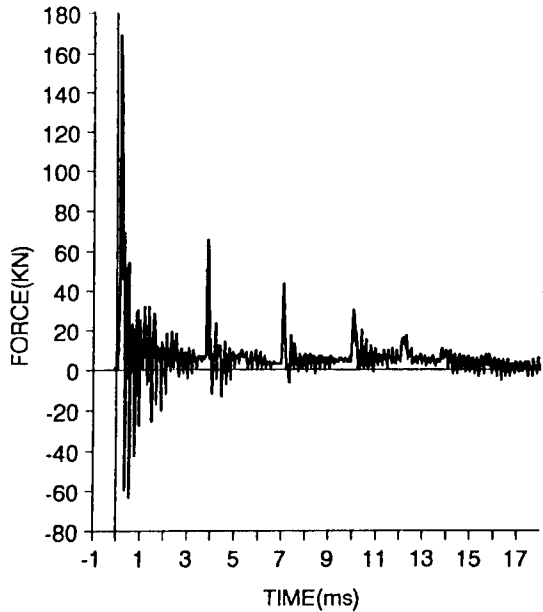


Fig. 1.6 Typical load time history produced by a hard impact

Hard impact, Fig. 1.6, is produced when the stiffness of the impactor is relatively so great that it does not deform during the impact and consequently most of the impact energy has to be absorbed by the structure.

A very important aspect in the case of loading that produce high rate straining, is the change of characteristics of structural materials under these strain rates. In this research the straining rate of the concrete and steel was up to 10^6 times higher than in static case loading.

1.3 R.C. slabs under transient loading

The response of RC slabs to a locally applied dynamic load has to be divided into the local response in the region just under and very close to the area of load application, and to the overall response of the whole slab.

The difference in the overall response of the structure and the local response, is that the overall deformation is associated with the time dependence of flexural response to the natural period of oscillation but the local, shear-punching response is independent of this parameter.

Inertial loading of the slab, becomes very important in cases of very fast loading and greatly influences the overall response of the slab. The contribution of inertia to the local response is in the control of crack velocity and there is hardly any flexural deformation in this period.

Parameters and phenomena that are most often used to describe R.C. slab response mechanisms to these fast, centrally applied loads are punching, cratering, spalling, shear response, flexural response, shear plug formation, crack patterns and deflection profile of the slab. Consequently due care has to be taken to choose parameters that would describe and explain not only its local but also overall response.

1.4 Present investigation

The specific purpose of the experiments described in this report was to determine the shear and flexural modes of behaviour in the response of reinforced concrete 2-way spanning slabs to impact from a free falling drop hammer or, more importantly, from an explosive blast from the detonation of a charge at close range. Materials tests at maximum rates of strain of 10^3 strain/sec, were carried out using a split Hopkinson or Kolsky bar, to obtain stress-strain curves for the concrete used in the slabs.

Scale effects were obtained by carrying out the experiments on two sizes of slabs. The larger slabs were 110mm deep x 2000mm square. Using a scale factor of 1:2.5 produced the model dimensions of 44mm deep x 800mm square slabs. The reinforcement and the concrete were scaled as much as possible, by the same factor. Three concrete cubes and three cylinders to give compressive and tensile splitting strength, were cast at the same time as each specimen, using 100mm cubes and cylinders of 100mm diameter for the full size specimens and 50mm size for the model scale specimens. These were usually tested at the same age as the slab specimen.

In each impact test the force-time relationship to which the specimen was subjected, was obtained by making the hammer impact coaxially onto a cylindrical bar of steel placed at rest in

the centre of the specimen. The steel bar was instrumented with electrical resistance strain gauges which recorded the stress pulses produced by the impact and is referred to as a pressure bar. Blast pressure gauges were used to measure the pressure-time curves at different distances. These results can be used in an analysis to estimate how pressure contours varied over the surface of the specimen. The details of the drop hammers, the explosive charges, the support conditions and the instrumentation used at each scale, are given in Chapter 3.

Transient deflections of the beam and slab specimens under the dynamic loads, were obtained using long stroke, rectilinear potentiometric displacement transducers (RPDT).

Transient strains in the steel reinforcement of the beam and slab specimens, were obtained using electrical resistance strain gauges bonded to the tensile bars at mid span. These gauges had a sensitivity limited by a gauge factor given by the manufacturer, and the bonding technique and instrumentation to record their voltage-time output are also described in Chapter 3.

Attempts have also been made to photograph the transient deformation and crack development of the reinforced concrete slabs. A rotating prism, high speed cine camera was used at rates up to 10,000 p.p.s.

In both the impulse and impact tests, nineteen slabs were tested at 1:2.5 scale and five slabs at full 1:1 scale. Five 1:2.5 scale slabs were tested statically.

CHAPTER 2

LITERATURE SURVEY

2.1 Impact and blast loading of R.C. slabs

It was observed a long time ago that material characteristics and the overall response of structures are not the same under different loading rates. With advances in technology and special measuring equipment, research in the fields of rapidly applied load was intensified. Now there is a lot of available literature, publications and papers that deal with these problems. To obtain high rates of loading different rigs for applying load were used. Generally, they were: static-dynamic rig (*Watstein,1953*), drop-hammer (*Hughes and Gregory,1972, Hughes and Watson,1978, Suaris and Shah,1981 and 1983, Khawandi,1991*), Charpy rig (*Gopalaratnam et al, 1984, John and Shah,1986*), air gun (*Cernica and Chagnon,1963, Kaminskiy,1993*), Hopkinson pressure bar (*Zech and Witman,1980, Zielinski and Reinhardt,1982 and 1984, Tyas,1993*), and finally

direct explosive tests (*Colton and Herman,1975, Watson and Sanderson,1984, Wright,1991*). Depending on testing arrangement used, different rates of loading were produced and consequently different material characteristics and slab behaviour parameters were obtained. In the following pages an attempt is made to summarise some of the available data which can be directly related to the work carried out in this research.

Park, (1964), developed a theory for determination of the static ultimate strength of uniformly loaded rectangular R.C. slabs which have either all or three edges restrained against lateral movement, by using rigid-plastic strip approximation. Compressive membrane action in the slab, which increases ultimate moments at the yield lines was introduced and the load deflection curve was as shown in Fig. 2.1.

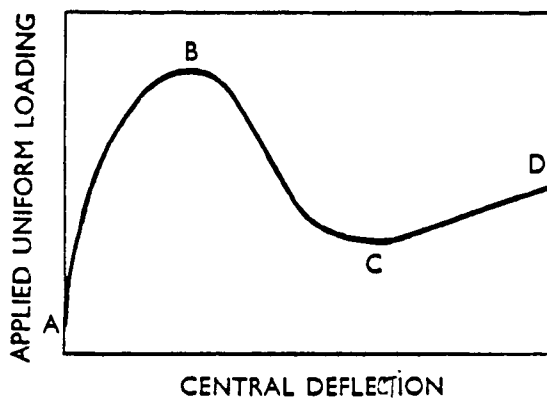


Fig. 2.1 Load-deflection curve for slabs with edges restrained against lateral movement (Park, 1964)

Where: Point B - maximum load capacity

Region B - C- for increasing deflection, the load-capacity decreases because of the decrease in bending resistance and compressive membrane stresses

Point C - point where membrane forces change from compressive to tensile

Region C - D - load is carried mostly by reinforcement in tension because the cracks have already extended throughout the depth of the slab.

For slabs with all edges fully fixed, compressive membrane action was taken into account for both directions.

Nilsson and Sahlin, (1982), impact tested two reinforced concrete slabs of 3000mm diameter, and 150mm thick. The impact velocity of the 250mm diameter and 650mm long

hammer was about 4.8m/sec. Maximum reinforcement strain recorded was 0.15%. Typical front side crack pattern is shown in Fig. 2.2.

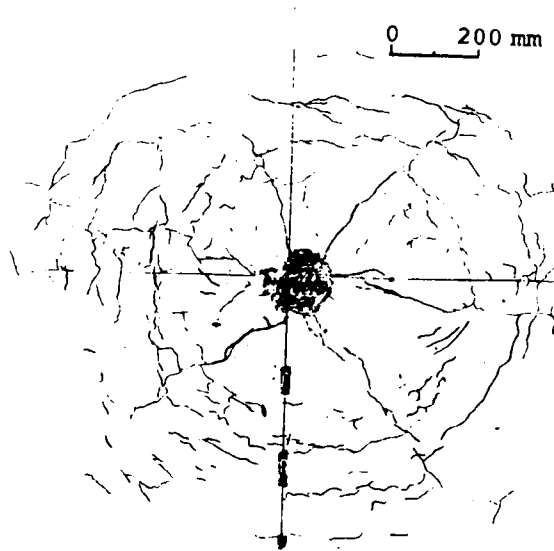


Fig. 2.2 Front side crack pattern (Nilsson and Sahlin, 1980)

Watson and Sanderson, (1984), tested ninety concrete slabs (300mm x 300mm x 50mm) using up to 10g of explosive. A method of locating subcrater fractures by ultrasonic pulse transmission has been employed. Fluorescent oil was used to mark the cracks. Most of the cracks observed were bond cracks around the aggregate particles. The way in which slabs were tested is shown in Fig.2.3.

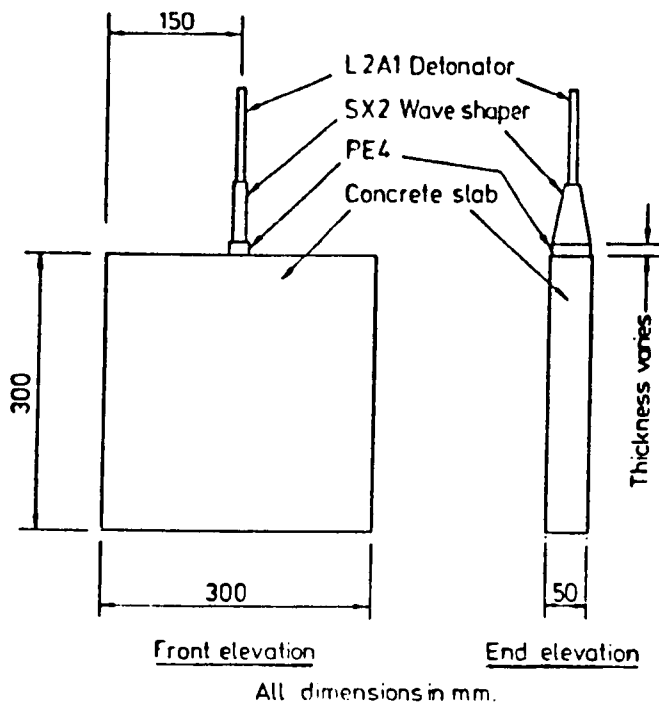


Fig. 2.3 Explosive tests on concrete slabs (Watson and Sanderson, 1984)

Maximum measured concentration of the crack lengths inside the specimen was 3.5cm/cm^2 . This suggested that there was limiting crack density of about 4cm/cm^2 above which the concrete no longer could remain intact.

Watson and Al-Azawi, (1984), used a 33.7Kg drop-hammer to test two-way simply supported R.C. slabs (525mm x 465mm x 42mm or 54mm). Typical failure modes are shown in Fig. 2.4.

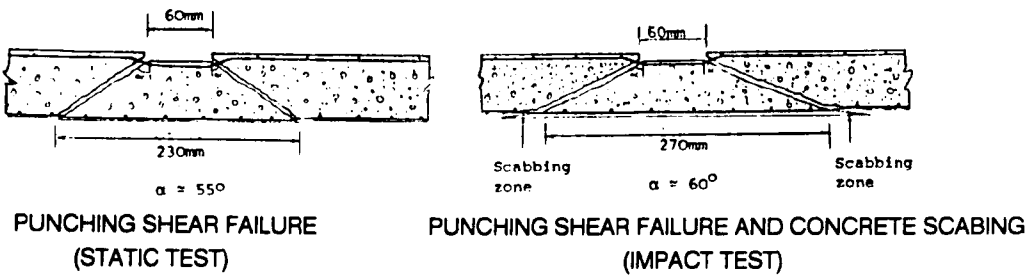


Fig. 2.4 Slab failure modes (Watson and Al-Azawi, 1984)

All tested slabs suffered punching shear failure and showed the same crack pattern. The slabs static load capacity was not reduced even after they had been impacted by a blow of energy equal to the static energy absorption capacity of the slab. They failed only after being impacted by 88% greater energy than in static case.

Abdel-Rohman and Sawan, (1985), proposed three different analytical approaches to estimate the impact effects on R.C. slabs.

(a) **The Impact Factor Method** employed the principle of conservation of energy with the assumptions that the slab had one degree of freedom, that the striker was rigid, that two bodies were not separated after the impact, that the slab remained elastic and that type of deformation and behaviour of slab were the same as for the static loading. Then:

$$K_d = 1 + \sqrt{1 + \frac{V_o^2}{g \cdot \delta_{st}} \left[\frac{1}{1 + K_m \cdot \frac{Q_o}{Q}} \right]}$$

where: K_d - impact factor

δ_{st} - maximum deflection due to static load Q (m)

K_m - mass reduction factor

Q_o - slab weight (kg)

V_o - velocity of the striking body (m/sec)

g - acceleration of gravity (m/sec²)

Dynamic values for maximum deflection, stress and force were then calculated by multiplying the static values obtained by applying the same weight statically, by the impact factor K_d .

(b) **The Method of Equivalent Mass** assumed that the slab was a one degree of freedom system, that impact would happen in the centre of the slab and that damping was negligible.

The equation of motion for the slab:

$$M_e \cdot \ddot{y} + K_e \cdot y = P(t)$$

where: y - slab mid span deflection (m)

M_e - equivalent mass (kg)

K_e - equivalent stiffness $\left(\frac{N}{m}\right)$

$P(t)$ - dynamic force is the only unknown which can be obtained by combining Petry formula for penetration depth:

$$X = K \cdot A \cdot V' \cdot R \quad \text{and Newton's law :} \quad P(t) = m \cdot \ddot{X}$$

where: X - depth of penetration into the slab (m)

K - material property constant (for concrete $2.97 \times 10^{-2} \text{ m}^3/\text{kN}$)

A - ratio of weight of impact and area of contact surface (kg/m²)

V' - striker velocity factor, $V' = \log(1 + (\text{initial velocity at impact})^2/19,973 \text{ m}^2/\text{sec}^2)$

R - penetration ratio, $R = \frac{Q_o}{2\pi \cdot r \cdot X}$, r - radius of a ball of equivalent weight Q_o

m - impactor mass (kg)

(c) **The Continuous Mass Method** used Timoshenko's equation of motion for an elastic slab under a concentrated load:

$$\rho \cdot H \cdot \frac{\partial^2 y}{\partial t^2} + N \cdot \frac{\partial^4 y}{\partial x^2 \partial z^2} = P(x, z, t) \cdot \delta\left(x - \frac{a}{2}\right) \cdot \delta\left(z - \frac{b}{2}\right)$$

where: ρ - mass density of slab (kg/m³)

H - slab thickness (m)

N - flexural rigidity (Nm²)

P - impact load (N)

a, b - dimensions of the slab (m)

δ - Dirac delta function

Impact load P was determined as in method (b) and the dynamic response of the simply supported slab was given by implementing boundary conditions for the slab and initial loading conditions .

Henter, Limberger and Brandes, (1985), observed three typical failure modes on R.C. slabs exposed to impact loads:

1. "Primary punching failure" - real punching failure with only small bending deformations.
2. "Secondary punching failure" - greater plastic bending deformations and local bending cracks which induce the shear failure.
3. "Overall flexural failure" - failure occurs because the ultimate rotational capacity of the yield lines is exceeded.

Ross and Krawinkler, (1985), investigated direct shear failure in fixed supports slabs caused by dynamic loading. Assumptions included in the analysis were:

1. Bending or shear failure will take place at the support of the slab.
2. Shear failure will occur if shear failure level is reached before the bending moment reaches the bending strength.
3. Rate effects are included by increasing the static strength values for shear and bending.
4. Wave propagation through the slab thickness is neglected.
5. A one-way slab can be treated as a beam.
6. Elastic behaviour describes structural response.
7. Dynamic direct shear failure behaves as static one.

The Timoshenko beam model was used as a base for the analytical theory. Equations for bending moment $M(o, t)$ and shear force at the support $V(o, t)$ when shear failure takes place were given as:

$$M(o,t) = -E \cdot I \cdot \sum_n \frac{\phi_n'(o)}{w_n} \int_0^t G_n(\tau) \cdot \sin w_n(t-\tau) dt$$

$$V(o,t) = K' \cdot A \cdot G \cdot \sum_n \frac{Y_n'(o) - \phi_n(o)}{w_n} \int_0^t G_n(\tau) \cdot \sin w_n(t-\tau) dt$$

where: E - modulus of elasticity (N/mm²)

G - shear modulus (N/mm²)

I - moment of inertia (mm⁴)

A - cross-sectional area (mm²)

K' - shear deformation coefficient of the beam

w_n - natural frequency corresponding to the n-th mode of vibration (sec⁻¹)

ϕ_n - beam n-th normal mode due to bending rotation (mm)

τ - integration variable

Krauthammer, Bazeos and Holmquist, (1986), used SDOF analysis to determine the behaviour of reinforced concrete box-type structures. A proposed model for the dynamic shear resistance function of slabs vs shear slip is presented in Fig. 2.5.

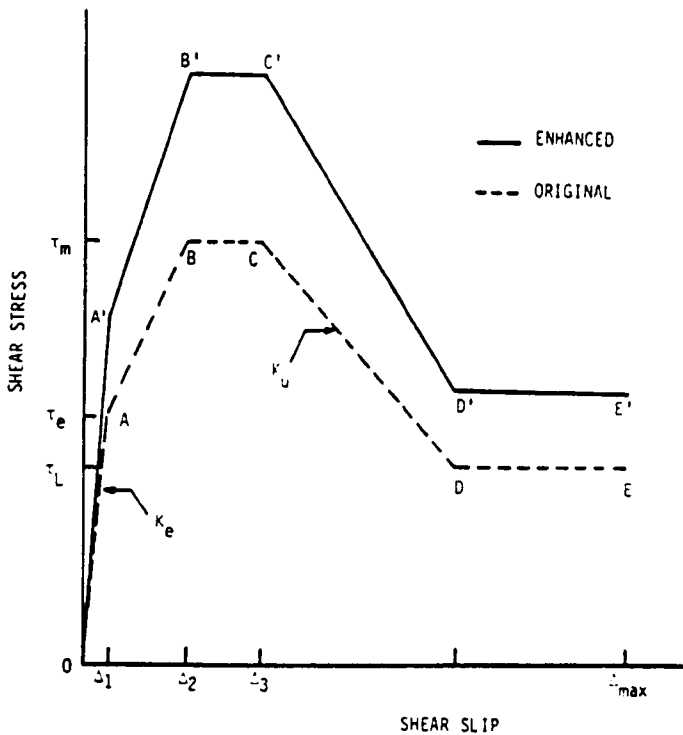


Fig. 2.5 Empirical Model for Shear Stress-Shear Slip Relationship (Krauthammer et al, 1986)

where: $\tau_e = 165 + 0.157 f_c'$

$$\tau_m = 8\sqrt{f_c'} + 0.8 \rho_{vt} \cdot f_y \leq 0.35 f_c'$$

$$\tau_L = \frac{0.85 \cdot A_{sb} f_s'}{A_c}$$

τ_e - elastic shear strength (N/mm²)

τ_m - maximum shear strength (N/mm²)

τ_L - limiting shear capacity (N/mm²)

$$\rho_{vt} = \frac{\text{total reinforcement area}}{\text{area of plane that crosses total reinforcement area}}$$

f_c' - concrete uniaxial strength (N/mm²)

f_y - the yield strength of reinforcement (N/mm²)

A_{sb} - area of bottom reinforcement (mm²)

f_s' - tensile strength of bottom reinforcement (N/mm²)

A_c - cross-sectional area (mm²)

Sawan and Abdel-Rohman, (1986). tested reinforced concrete slabs (dimensions 750 x 750 x 50mm, with six different steel percentages; 0.45% to 1.47%) using 6.9kg heavy steel ball released to fall freely from heights of up to 120mm. The midspan deflection measurements were taken. Total dynamic deflection decreased with the increase of the steel ratio but proportionately less for steel ratios of more than 1.07%.

Eibl and Schluter, (1987), presented an empirical method which included a parametric study of the slab characteristics like thickness, span, percentage of bending and shear reinforcement, shape and distribution of the dynamic load and support condition. Assumptions that cracks are allowed to open and close and that the shear modulus is reduced depending on the crack width were incorporated in the analysis that was based on a finite element approach. It was concluded that all parameters mentioned above highly influence punching behaviour of the slab.

Tancreto, (1991), applied close-in blast load on 12 reinforced concrete slabs (2286mm x 2286mm x 114mm to 254mm) with reinforcement percentages from 0.15% to 2.54%. He used a 27.2kg spherical charge. The spalling was reduced by reducing the spacing of reinforcement.

Because of the many different variables as percentage of reinforcement, spacing of the reinforcement, span to depth ratio and standoff, no further conclusions seem reliable.

Yamaguchi and Fujimoto, (1991), impact tested reinforced concrete slabs (300mm diameter and 40mm thick) with the 30Kg hammer released from 200mm and 400mm heights. Displacements were obtained from the acceleration data measured during the test. The authors observed a dynamic increase in the modulus of elasticity of concrete at failure. On the other hand the elastic modulus of reinforcement did not show any increase. The dynamic failure crack pattern observed in the tests is shown in Fig. 2.6.

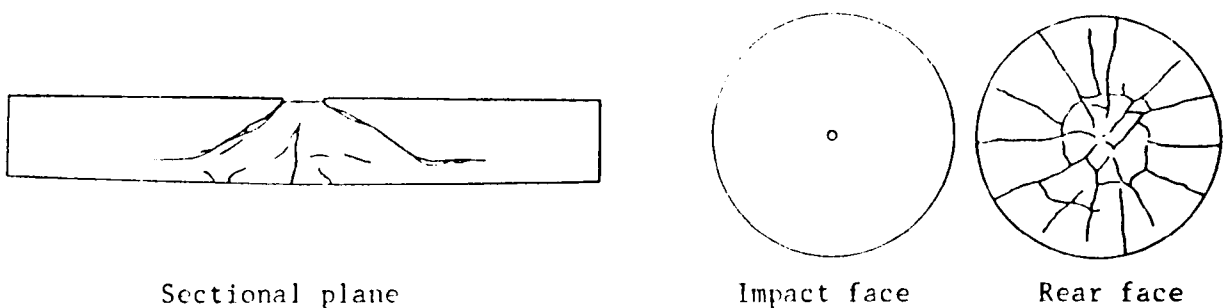


Fig. 2.6 Cracking patterns (experiment) (Yamaguchi and Fujimoto, 1991)

2.2 Material properties under high rates of strain

Watstein, (1953), tested concrete cylinders in a drop-hammer machine. Maximum strain rate was 10 strain/sec while the duration of impact was 0.3msec. Average ratio of dynamic to static compressive strength was 1.85, modulus of elasticity increased about 33% and resistance to impact, measured by the specimen's ability to absorb energy, 2.2 times. The ultimate strain was also significantly higher for higher load rates.

Green, (1964), impactly tested concrete cubes (102mm) to see if the mix proportions, type of coarse aggregate, sand grading, type of cement, method of curing and age of the specimen influenced impact strength. The absorbed energy was smaller for water-stored than for air-stored specimens. The impact strength of the specimen increased compared to the static compressive strength with the same rate of increase for each type of aggregate and condition of storage. For

the same static compressive strength the impact strength was greater for the concretes made with aggregate of greater angularity and surface roughness.

Atchley and Howard, (1967), impact tested 152mm diameter x 305mm long concrete cylinders of three different compressive strengths with free hammer drops of up to 305mm to define the energy absorption and strength capacity of the concrete. Some of the slow dynamic tests were performed by deforming the specimens at a speed of 165mm/min or 0.009 strain/sec. The authors found that the rate of loading influences the amount of energy absorbed at failure and the failure strength of material. The ratio of energy absorbed in dynamic and static tests was proved to be dependent on the strain rate but not on the static strength of concrete and it was found to be in the range of 1.26 - 1.72. The strain rates were up to 4.48 strain/sec. By increasing the stress and strain rate the dynamic strength approached a constant value.

Hughes and Gregory, (1972), carried out drop-hammer tests on concrete cubes and prisms to obtain load-time and strain-time curves. The failure patterns seemed similar to those in static tests. The ratio of impact to static strength varied around 1.90. Impact compressive strength was not affected by the aggregate size but it was increased by the larger proportion of fine aggregate in the concrete mix.

Hughes and Watson, (1978), impact tested different kinds of concrete cubes to obtain compressive strength, ultimate strain, energy absorption and deformation modulus. The maximum measured drop velocity of the 106Kg hammer was 5.8m/sec. The authors observed that changes in cement/water relation affect impact strength in the same way they affect the static strength. The amount of cement content did not cause any changes but limestone concrete showed better impact resistance than gravel concrete. The largest increase in the compressive strength of concrete was 35% of that obtained in the static test. The impact ultimate strain had decreased with higher rates of strain. By increasing the age of concrete, the impact compressive strength increased but the ultimate strain decreased. A stress wave analysis was used to interpret the measurements made during the tests.

Zech and Wittman, (1980), carried out experimental investigations into the behaviour of mortar bars exposed to impact load. The crack velocity in mortar has been estimated as 400m/sec. The highest rate of stressing used in these tests was 5×10^4 N/mm²/sec. The coefficient of

variability of strength of mortar remained unchanged as the rate of loading increased while the absolute scatter of strength increased with the increase of rate of loading.

Zielinski, Reinhardt and Kormeling, (1981), used the Split Hopkinson Bar technique to test concrete specimens by releasing a freely falling weight. Impact strengths were 1.33 to 2.34 times greater than the static ones but they differed for different mixes. By decreasing the maximum size of the aggregate, impact strength increased which may be partly explained by the lower bond strength of larger aggregate particles. The higher cement content gave higher strength but cement type and quality and way of curing did not influence impact strength. Concrete loaded in the direction of the casting showed lower impact resistance than one tested normally to that direction.

The authors consider crack propagation as the main reason for different characteristics of material under different rates of loading. When the load slowly increases the fracture process starts from existing micro and macrocracks which have time to propagate and develop along the paths of least energy requirements but under dynamic tensile loading cracks are forced to develop along a shorter path of higher resistance which results in higher energy capacity and hence strength of material.

Tensile impact strength of concrete was considerably reduced in the case of repeated impacts.

Suaris and Shah, (1981), performed impact flexural tests on concrete beams of different sizes to validate their analytical approach for calculation of inertial effects in dynamic testing. Impact velocities were 1 to 3m/sec. The modulus of rupture had up to four times higher value in dynamic than in static tests. For soft impacts applied through a rubber pad, the dynamic compressive strength was 1.7 times greater than the static one. The authors considered that a soft pad between the specimen and the striker eliminated inertial effects in dynamic tests and their measurements show that in such cases applied load was equal to the static bending load carried by the specimen.

Suaris and Shah, (1983), impact tested concrete and fibre-reinforced concrete prisms to study concrete properties under a wide range of strain rates. The strain in the concrete, the impact load and the deflection of the specimen were measured. The impact velocity was 1m/sec. It was observed that the higher the value of the static flexural strength the lower is the relative increase in

the flexural strength of the specimen under high strain rates. The tensile response was more strain rate sensitive than the compressive one. Drier specimens showed lower strain rate sensitivity. The load-deflection curves become more linear with the increase of the strain rate. Since the nonlinearity in concrete behaviour is the produce of microcracking, the conclusion was that the amount of microcracking decreases with the increase in strain rate.

The energy absorption measured as the area under the load deflection curve, substantially increased with the strain rate.

Zielinski, (1984), presented a theoretical model to highlight the problem of tensile fracture of concrete at high rates of loading. The microcracks, which exists because of the heterogeneous nature of concrete, are pointed out as a potential initiator of fracture. Since microcracks mostly exist at the interfaces of aggregate particles and mortar matrix, they will, under slow increased loading, grow along these interfaces without going through the aggregate. But for dynamic loading, the time in which that propagation should happen is extremely short, and cracks will be forced to propagate along the shortest possible paths even of much higher resistance. The criterion which determines where the fracture will occur is the position of the aggregate particles with respect to crack planes and the rate of loading which influences the crack velocity.

Fracture energy is obtained as a sum of energies absorbed by fracture in the matrix and aggregate phases and in the interfacial bond phase of concrete. For dynamic loading the energy absorbed by fracture of the aggregates gains in importance, because of shorter "energy paths" and consequently a greater amount of broken aggregate particles.

Comparison of the theoretical with the experimental results proved a high degree of applicability of the theory.

Gopalaratnam et al, (1984), tested concrete specimens (229mm x 25mm x 76mm) in a modified Charpy test. Impact velocities varied in the range of 0.7 - 2.4m/sec. In some of the tests a damping rubber pad was placed between the striker and the specimen in order to reduce inertial effects. Maximum strain rates were 0.3 strain/sec and the dynamic flexural strength was up to 150% of the static one. Failures were mostly the result of pure bending and very similar to those obtained under static loading. Microcracking was identified as the reason for the nonlinear behaviour of concrete at higher impact velocities.

Authors made an attempt to estimate the period of inertial oscillation, i.e. the oscillations caused by the inertia loading only, and its amplitude, the frequency of oscillation and maximum difference between the applied and support load by using a two degrees of freedom model.

John and Shah, (1986), tested concrete prisms of 203mm x 25mm x 76mm with a single-edge notch 17mm deep and 2.5mm wide, to study crack propagation in concrete subjected to dynamic loading. The load was applied through a rubber pad in a Charpy testing machine. Strain rates were up to 0.4 strain/sec. For those strain rates crack velocities were linearly related to strain rates and the maximum observed velocity was about 2.4% of the longitudinal wave velocity in the material. From crack velocity-time curves it can be seen that at the beginning velocity increases, then stays constant and after it decreases. Authors observed that the amount of cracks was smaller for higher strain rates and that the decrease in nonlinearity at higher rates of strain was due to the reduced amount of slow crack growth.

An attempt has been made to establish the stress intensity factor as a function of the applied load, the geometrical characteristic of the specimen, the length of crack and ratio of crack length and depth of specimen.

Oh, (1987), proposed a theoretical model for analysing behaviour of concrete under dynamic tensile loads by producing rate-independent nonlinear stress-strain relations for concrete. Strain rate sensibility was introduced by fitting experimental results and assuming similarities in shapes of stress-strain curves for different strain rates.

2.2.1 Concrete properties

2.2.1.1 Stress-strain diagram

The overall stress-strain diagram for concrete is to a large extent affected by changes in loading rate. Both the ultimate stress and strain have higher values for higher rates of strain which is sometimes related to the changes in the Young's modulus of elasticity with an increase in the stress and strain rate.

Typical stress-strain diagrams for different loading rates are shown in Fig. 2.7 (compression) and Fig. 2.8 (tension).

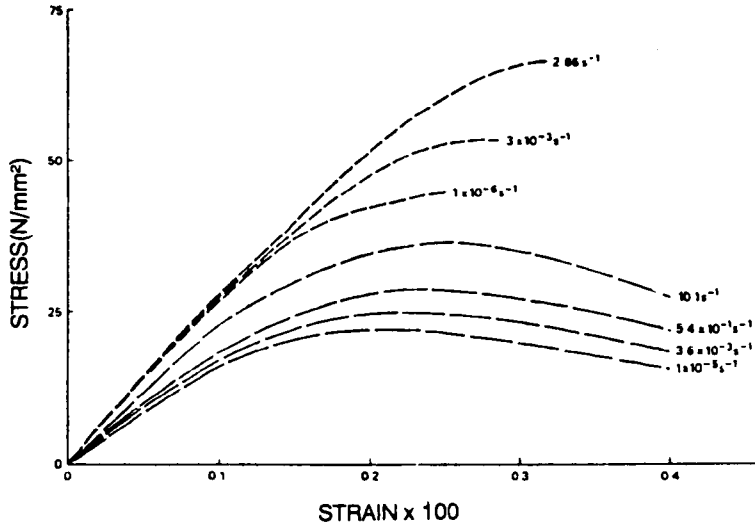


Fig. 2.7 Stress-strain diagrams for two concretes at different rates of straining (Mainstone, 1975)

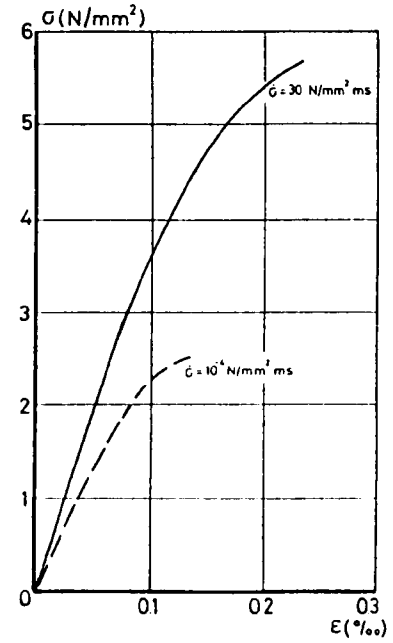


Fig. 2.8 Influence of a stress rate upon the stress-strain relationship for concrete in uniaxial tension (Zielinski et al, 1981)

The ratio of impact and static value of elastic modulus was given in *CEB Bulletin No.187, (1988)*, as:

$$\frac{E_{imp}}{E_{st}} = \left(\frac{\dot{\sigma}}{\sigma_o} \right)^A = \left(\frac{\dot{\epsilon}}{\epsilon_o} \right)^B$$

where: $\dot{\sigma}_o = 1 \text{ N/mm}^2 \text{ sec}$ for compression and $0.1 \text{ N/mm}^2 \text{ sec}$ for tension and $\dot{\epsilon}_o = 30 \cdot 10^{-6} \text{ sec}^{-1}$

$A = 0.25$ for compression and 0.016 for tension

$B = 0.26$ for compression and 0.017 for tension

σ_o and ϵ_o are described as static stress and strain rates respectively.

The formula for calculating the strain rate dependent modulus of elasticity is also given

by:

$$E_{dyn} = 0.1 E_{stat} \left(\log \frac{\dot{\sigma}}{\sigma_o} + 10 \right)$$

but here: $\dot{\sigma}_o = 0.5 \text{ N/mm}^2 \text{ sec}$.

The increase of Young's modulus is not always proportional to the increase in the strength of concrete.

From previous experimental investigations a relation between modulus of elasticity and stress or strain rate can be given as shown in Fig. 2.9.

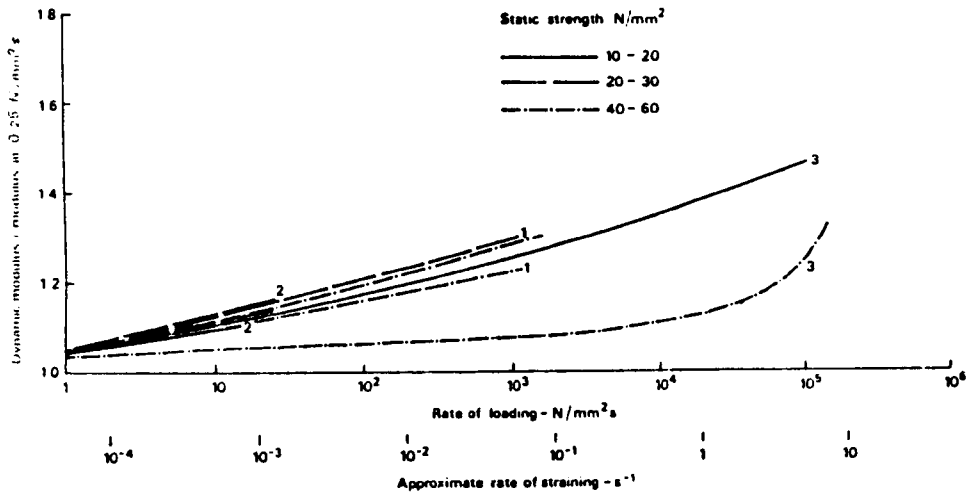


Fig. 2.9 Variation of modulus of elasticity with stress and strain rate (Mainstone, 1975)

The ultimate stress is usually much higher under dynamic than under static loading conditions. The relation between ultimate strain, stress and strain rates may be calculated as:

$$\epsilon_{ult,imp} = \left(\frac{\dot{\sigma}}{\dot{\sigma}_o} \right)^{0.020} = \left(\frac{\dot{\epsilon}}{\dot{\epsilon}_o} \right)^{0.020}$$

where $\dot{\sigma}_o$ and $\dot{\epsilon}_o$ are the same as above. They concluded that higher ultimate strains in dynamic tests were caused by inertial effects and enhanced cracking.

2.2.1.2 Compressive strength

Dynamic compressive strength is highly dependent on stress and strain rate. The enhancement ratio between dynamic and static values can be given as in *CEB Bulletin No. 187, (1988)*:

$$\frac{f_{imp}}{f_{stat}} = \left(\frac{\dot{\sigma}}{\dot{\sigma}_o} \right)^\alpha$$

for $\dot{\sigma} < 10^6 \text{N/mm}^2\text{sec}$ and:

$$\frac{f_{imp}}{f_{stat}} = \beta \cdot \dot{\sigma}^{.1/3}$$

for $\dot{\sigma} > 10^6 \text{N/mm}^2\text{sec}$, where:

$$f - \text{compressive strength}, \quad \alpha = \frac{1}{5 + 0.75f_{cm}}, \quad \beta = 6\alpha - 2 \quad \text{and} \quad f_{cm} - \text{cube static strength.}$$

If the predicted influence of strain rate on the Young's modulus is taken into account then:

$$\frac{f_{imp}}{f_{stat}} = \left(\frac{\dot{\epsilon}}{\dot{\epsilon}_o} \right)^{1.026\alpha}$$

for $\dot{\epsilon} < 30 \text{ sec}^{-1}$ and :

$$\frac{f_{imp}}{f_{stat}} = \gamma \cdot \dot{\epsilon}^{.1/3}$$

for $\dot{\epsilon} > 30 \text{ sec}^{-1}$, where: $\log \gamma = 6.156\alpha - 0.492$. From these expressions it can be seen that the stress-strain relation is divided into the two regions (Fig. 2.10), i.e. stress rates lower and higher than $10^6 \text{N/mm}^2\text{sec}$ or strain rates above and below 50 strain/sec.

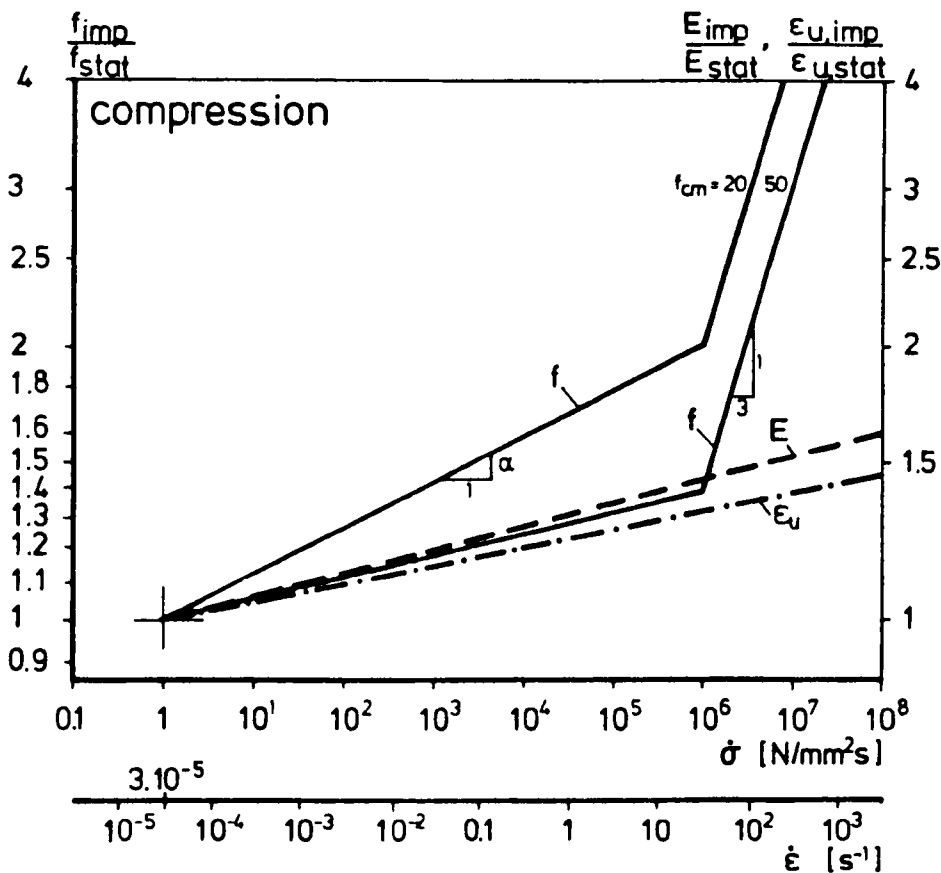


Fig. 2.10 Influence of stress and strain rate on compressive properties of concrete (CEB Bulletin No. 187,1988)

This critical value has been observed by several authors. A similar relation has also been presented by *Mainstone, (1975)*, (Fig. 2.11).

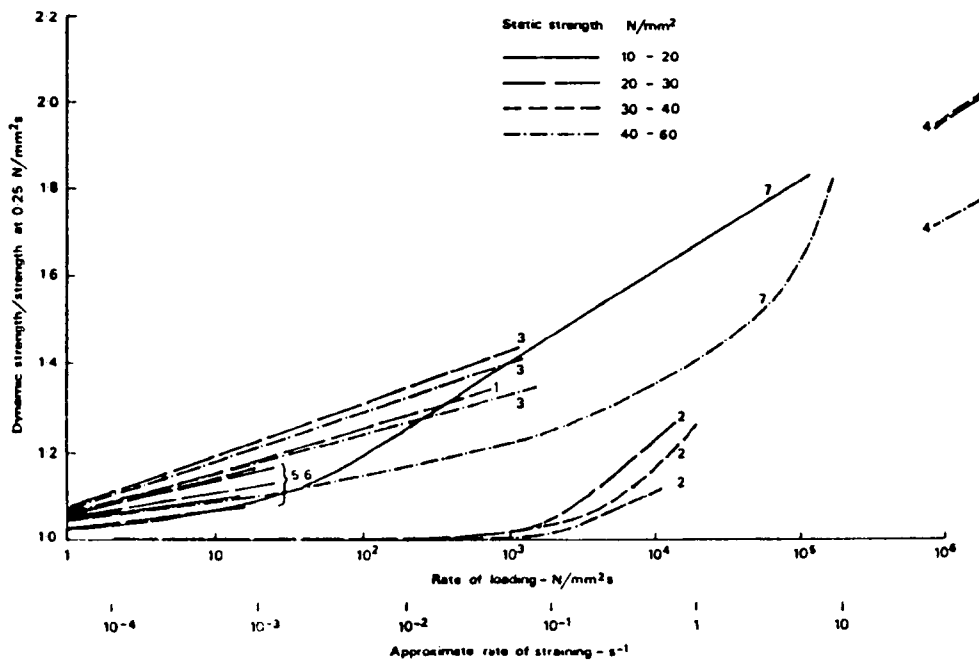


Fig. 2.11 Variation of ultimate strength of concrete in direct compression with average rate of loading or straining (Mainstone, 1975)

On the other hand, *Hughes and Watson, (1978)*, do not report any changes in compressive strength for stress rates of up to $1.6 \cdot 10^5 N/mm^2sec$ and strain rates of up to $8sec^{-1}$, while for strain rate of $14sec^{-1}$ they report an increase in compressive strength of only 25%. Fig. 2.12 gives more experimental data for the strain rates of up to $10 sec^{-1}$.

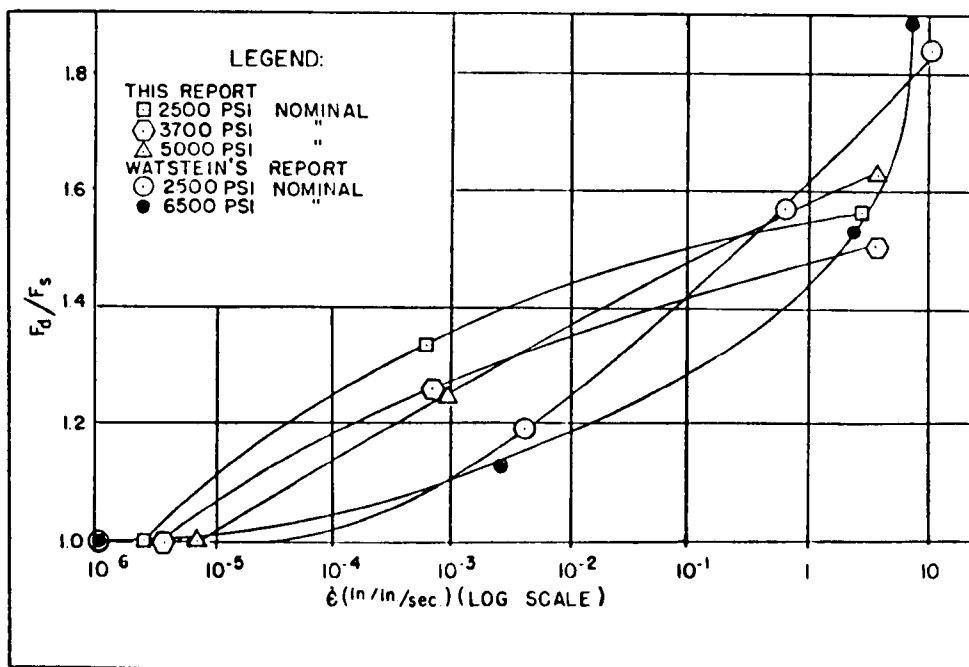


Fig. 2.12 Strength ratio vs strain rate (Atchley and Howard, 1967)

Finally, it can be concluded that the compressive strength of concrete increases with the rate of stress and strain but there is still some amount of uncertainty which follows any predictions of compressive strength under high rates of loading.

2.2.1.3 Tensile strength

A function that describes the tensile strength of concrete under dynamic loads is the same as that for compressive strength, explained in section 2.2.1.2, but here:

$$\alpha = \frac{1}{10 + 0.5f}, \quad \dot{\sigma} = 0.1 \text{ N/mm}^2 \text{sec} \quad \text{and} \quad \beta = 7\alpha - 2.$$

The stress rate of $10^6 \text{ N/mm}^2 \text{sec}$ and strain rate of 50 strain/sec have again been considered as the dividing point in the behaviour of concrete under high rates of loading (Fig. 2.13).

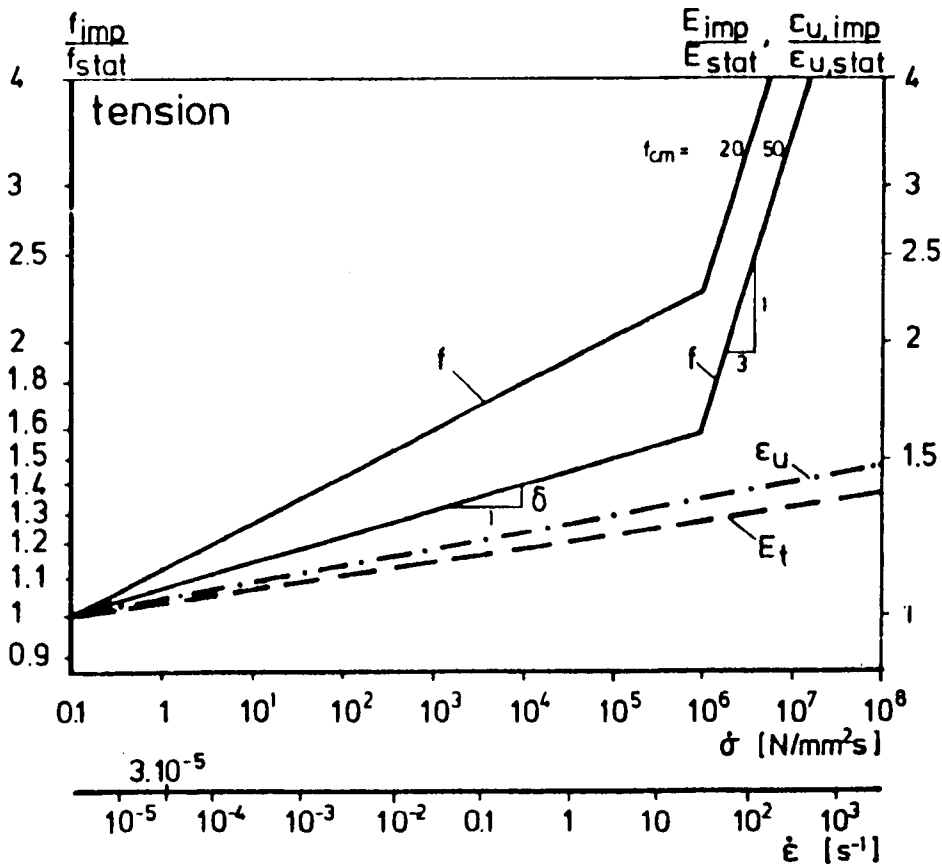


Fig 2.13 Influence of stress and strain rate on tensile properties of concrete (CEB Bulletin No. 187, 1988)

The relationship between tensile strength and stress or strain rates can also be given as function of strain rate where:

$$\frac{f_{imp}}{f_{stat}} = \left(\frac{\dot{\epsilon}}{\dot{\epsilon}_0} \right)^\alpha$$

for $\dot{\epsilon} \leq 30 \text{sec}^{-1}$ and:

$$\frac{f_{imp}}{f_{stat}} = \eta \dot{\epsilon}^{.1/3}$$

for $\dot{\epsilon} > 30 \text{sec}^{-1}$, where: $\log \eta = 6.933\alpha - 0.492$.

These equations all include the predicted influence of changes in Young's modulus under high rates of loading.

Veen and Blaauwendraad, (1983), recommend relation based on previous experimental investigations (Fig. 2.14):

$$\ln f_{cdt} = 151 + 0.043 \ln \dot{\sigma}$$

where: f_{cdt} - average tensile strength (N/mm^2)

$\dot{\sigma}$ - stressing rate ($\text{N/mm}^2\text{msec}$)

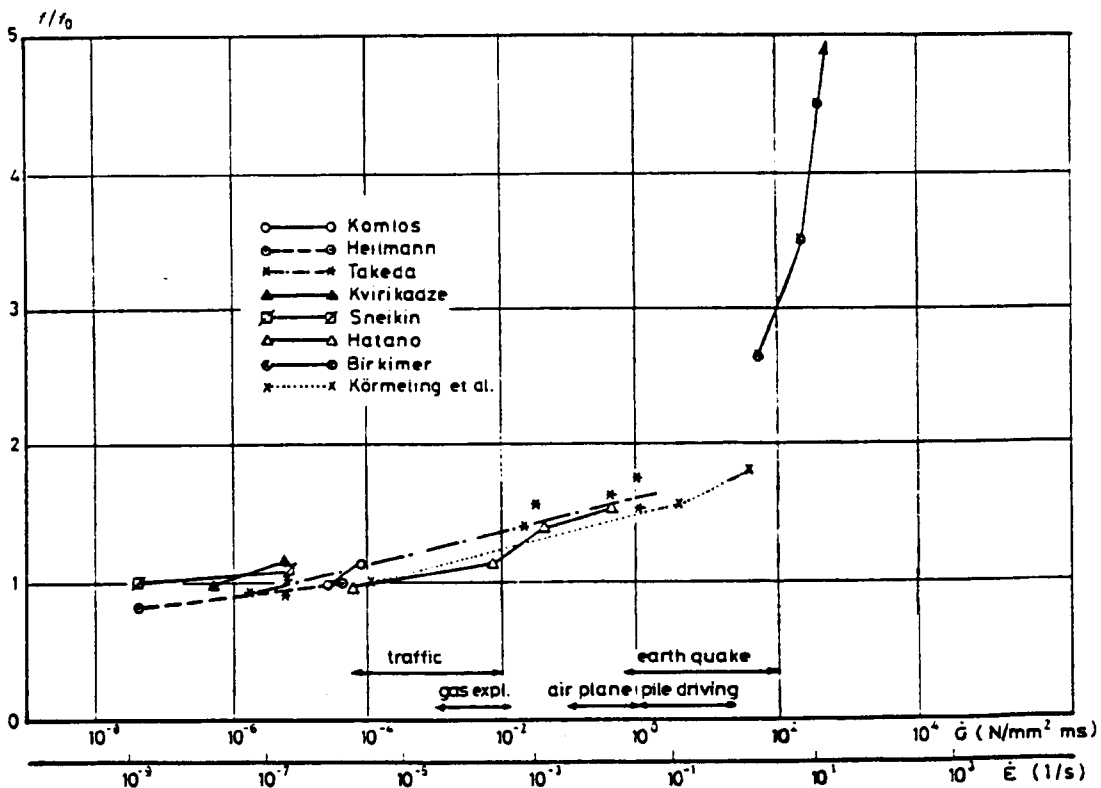


Fig. 2.14 Relative impact tensile strength as a function of load and strain rate (Veen and Blaauwendraad, 1983)

It must be noted, that in all of these tests stress rates were in the order of up to 10^2sec^{-1} . For these relatively low stress rates tensile strength in 90% of cases increases inside dotted lines as shown in Fig. 2.15.

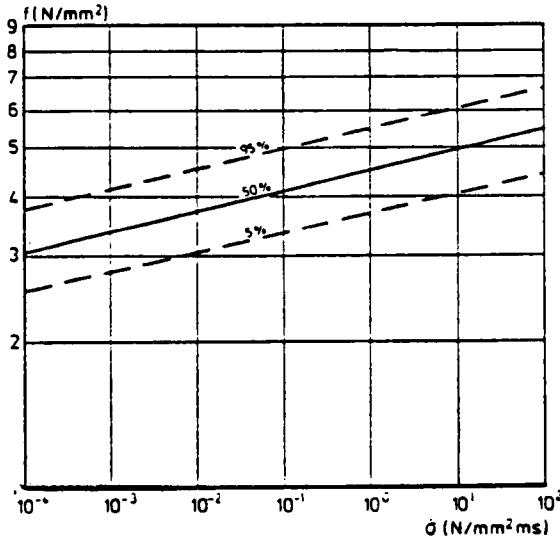


Fig. 2.15 Relation between tensile strength and loading rate (Reinhardt,1982)

Reinhardt, (1982), also tries to establish relationships between f_{cm} - cube compressive static strength and f_{tm} - static tensile strength and its behaviour under different stress rates (Fig. 2.16). Here $\dot{\sigma}$ and $\dot{\sigma}_0$ are dynamic and static strain rates respectively.

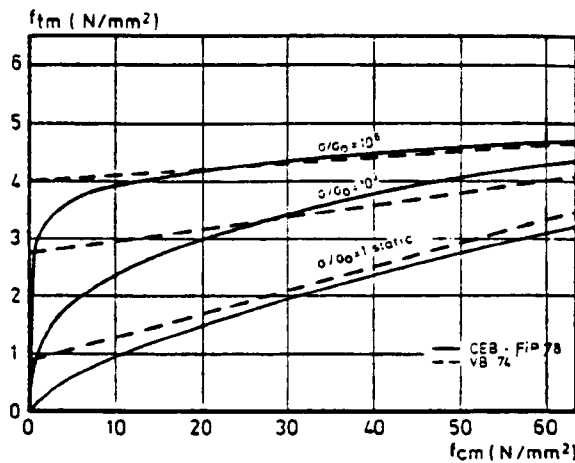


Fig. 2.16 Influence of different strain rates on the ratio between compressive and tensile concrete strength (Reinhardt, 1982)

A decrease in the water/cement ratio tends to increase static strength of concrete. It also increases the dynamic tensile strength (Reinhardt,1982). That change can easily be seen even when concretes made of different types of aggregate were used, Fig. 2.17.

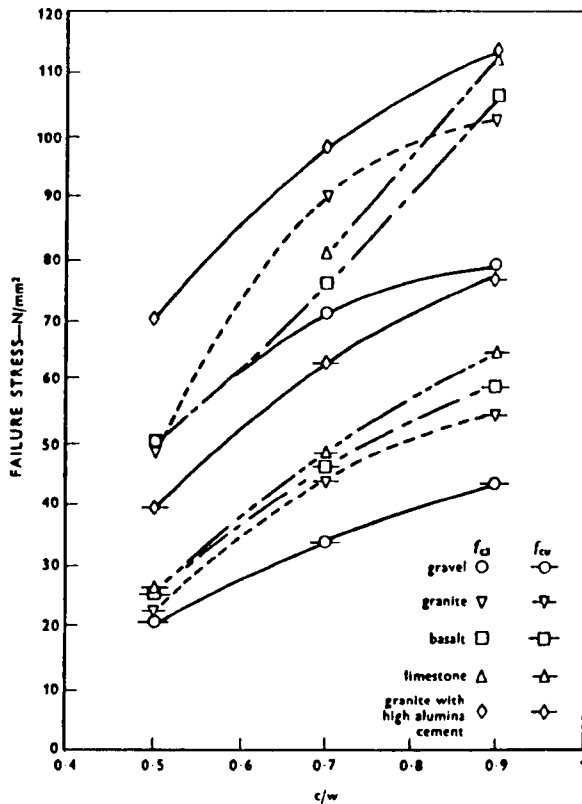


Fig. 2.17 Influence of W/C ratio on dynamic tensile strength of concrete (Hughes and Gregory, 1972)

In contrast there are some reports, *Zielinsky et al* ,(1981), which lead to the conclusion that a change in the W/C ratio does not produce consistent changes in concrete dynamic strength.

By increasing the maximum aggregate size the concrete dynamic tensile strength has been found to decrease (*Zielinsky et al* ,(1981), *Reinhardt* ,(1982)) which could be explained by a lower bond strength for concretes with the larger aggregates particles and by the relative increase in aggregate surface area for the concretes of smaller aggregate particles. Concrete with a limestone aggregate showed greater dynamic strength than gravel aggregate, *Hughes and Watson*, (1978). The aggregates that are angular in shape and have a rough surface show a tendency to produce a higher dynamic resistance, *Green*, (1964). All available information seems to suggest that any improvement in bond between the aggregate and the mortar matrix, which is the concrete's weakest area when tested dynamically, leads to an increase in strength.

For most of the concretes studied, any quantity of cement within the British Standard recommendations showed no effect on the behaviour of concrete. Some investigators however did observe a higher dynamic strength if the cement content was 375kg/m³ instead of 325kg/m³ and they explain this by the poor workability that leaves excessive air voids compared with that when a smaller amount of cement was used.

The effect of moisture content on the strength of concrete has been studied by very few authors. Some of them concluded that the moisture content of the specimen did not affect the mechanical properties of concrete (*Zielinski et al,(1981) and Reinhardt,(1982)*) while others found that the relatively wet specimens exhibited a slightly higher strain rate sensitivity than the drier specimens (*Suaris and Shah, (1983)*).

Direction of casting and loading highly influences the dynamic behaviour of concrete., Fig. 2.18. The tests performed in the direction parallel to the direction of casting showed 20% to 30% lower tensile strength than those performed in a perpendicular direction.

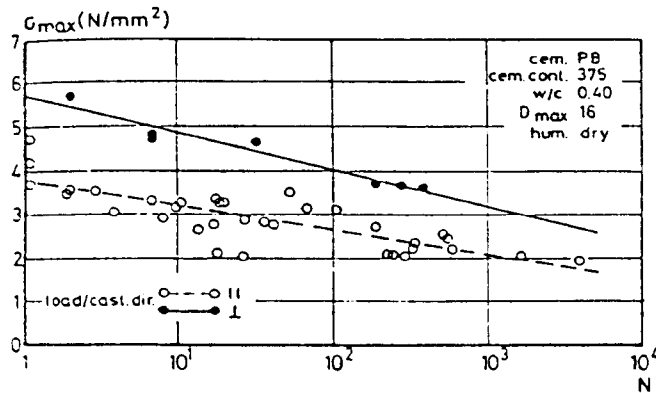


Fig. 2.18 Effect of changes in loading/casting direction upon the impact fatigue tensile strength (Reinhardt, 1982)

The load history of any rapidly applied load, that is larger than 80% of the static strength of the specimen, is a very important factor that can determine the behaviour of concrete. The specimen may suffer failure even during unloading if it takes place slowly after the rapid loading. Some of typical cases can be seen in Fig. 2.19.

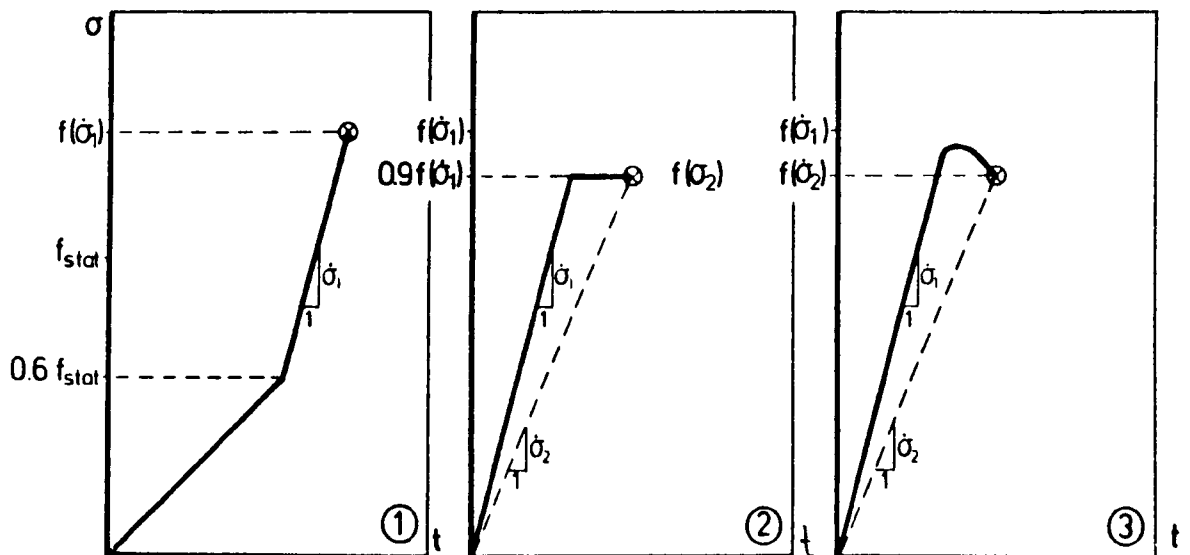


Fig. 2.19 Effect of loading history on concrete behaviour (CEB Bulletin No. 187, 1988)

2.2.1.4 Poisson's ratio

There is some evidence that Poisson's ratio, for both compression and tension, does not depend on the stress or strain rate.

2.2.1.5 Energy absorption and modulus of rupture

The energy absorption per unit volume is usually defined as the area under the stress-strain curve. Since much higher stresses occur in dynamic than in static tests, the energy absorption must be higher for the specimens exposed to rapidly applied load. For a load applied more than 10^6 times faster than in the static test, the energy absorbed was reported as 70% higher than in the static test and this value increased with the strength of concrete, *Atchley and Howard, (1967)*.

The modulus of rupture as a measure of the flexural strength of concrete changes with strain rate. It can be seen that the change of strain rate from 10^{-6} sec^{-1} to 1 sec^{-1} cause a 1.6 to 2.0 times increase in flexural strength of concrete and mortar (Fig. 2.20).

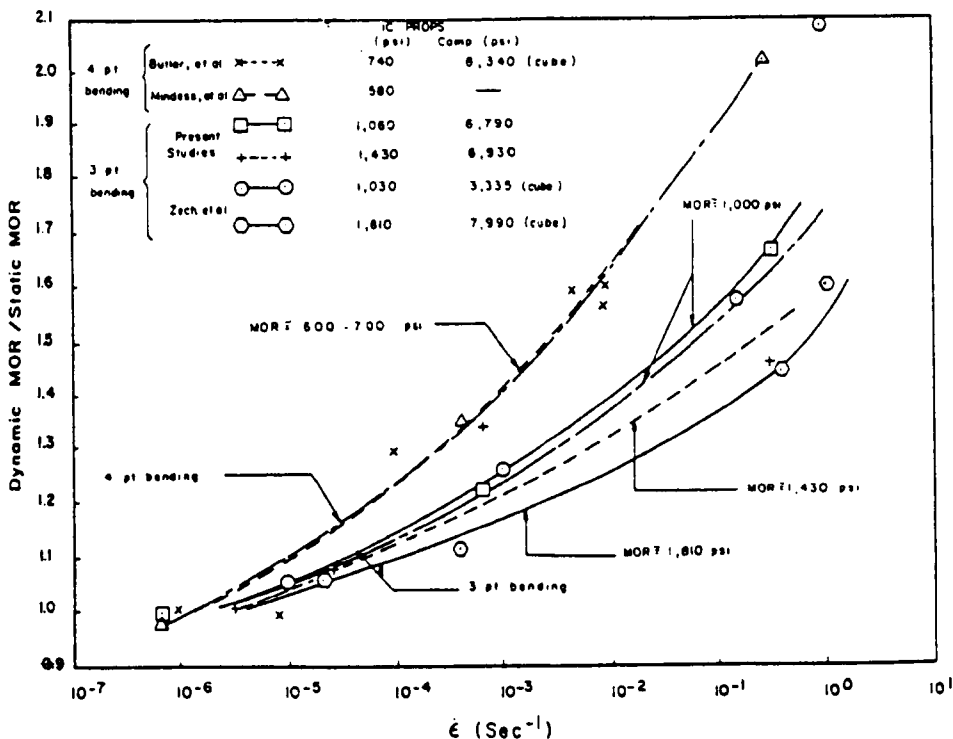


Fig. 2.20 Relative MOR vs. Strain-Rate for Mortar and Concrete, (Suaris and Shah, 1983)

The increase in MOR is greater for hard than for soft impact, obtained by placing a rubber pad between the striker and the specimen, *Suaris and Shah, (1981)*. All of these investigations

cover strain rates of up to 1sec^{-1} and no data are available for higher strain rates. The values presented were calculated assuming linear behaviour of the material.

2.2.2 Reinforcement properties

Reinforcement properties also exhibit considerable change under dynamic loading. These changes are best seen from stress-strain diagrams for different kinds of steel under the different rates of loading, Fig. 2.21.

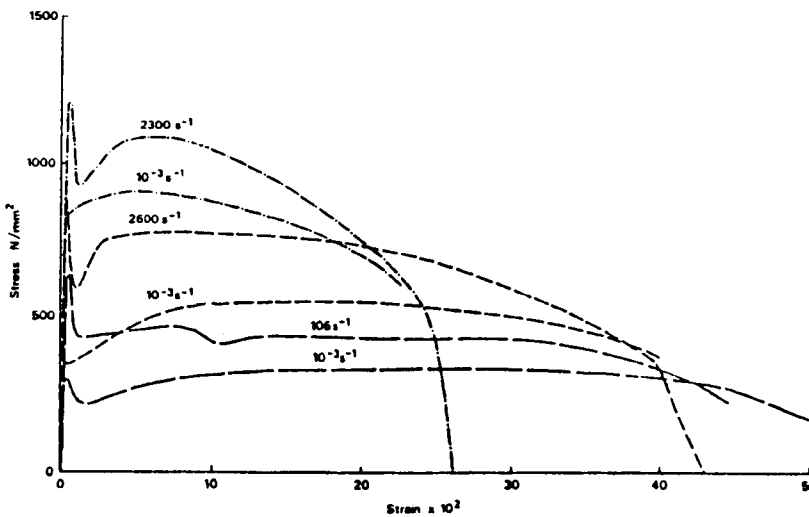


Fig. 2.21 Stress-strain diagrams for three steels at different rates of straining. (Mainstone et al, 1975)

A significant difference between upper and lower yield points can be seen for all kinds of steel and is described as a major characteristic of the behaviour of steel subjected to high loading rates. The increase of yield stress is much more pronounced than any changes in ultimate tensile strength. The relationship between lower yield point and the strain rate for dynamic and static loading itself may be given as in *Veen and Blaauwendraad, (1983)*, and *CEB Bulletin No. 187, (1988)*:

$$\frac{\sigma_{y\text{dyn}}}{\sigma_{y\text{stat}}} = 1 + \left(\frac{\dot{\epsilon}_s}{40} \right)^{1/5}$$

where: σ_y - yield stress and $\dot{\epsilon}_s$ - straining rate.

The various experimental results (Fig. 2.22) graphically show the increase of the upper yield point in dynamic test.

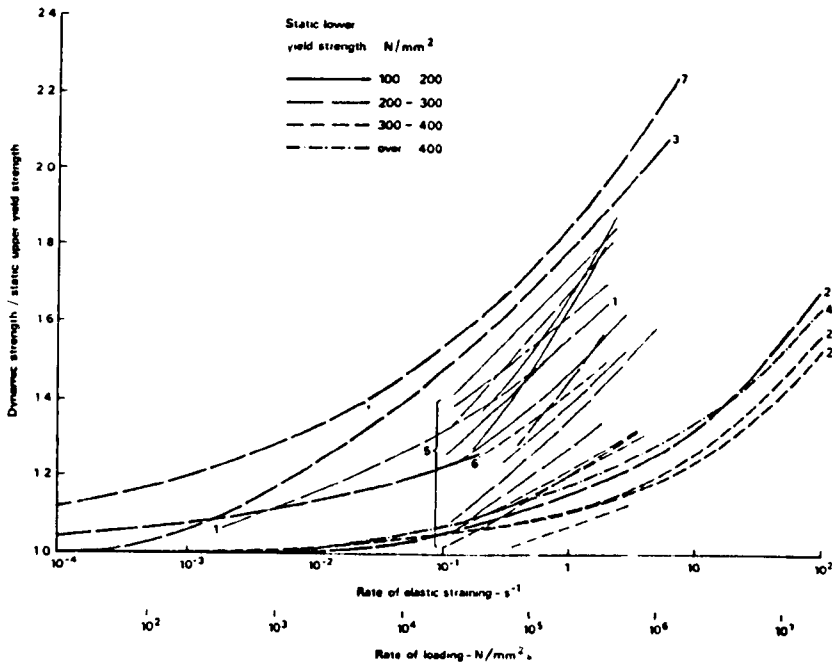


Fig. 2.22 Variation of upper yield strength of steel in direct tension or compression with rate of straining or loading. (Mainstone 1975)

The ultimate strain in steel seems not to be influenced by the strain rate (*Veen and Blaauwendraad, 1983, CEB Bulletin No 187, 1988, Mainstone, 1975*). Young's modulus of elasticity also remains almost unchanged ($E_{dyn} = 2.06 \times 10^5 N/mm^2$) under high rates of loading.

The bond between the steel and concrete, materials of completely different characteristics, has been considered as one of the weak regions in the overall structural response under dynamic loading, but despite this there is not a lot of available data about this issue. Generally it can be said that the influence of stress rate on the bond of smooth bars is negligible (*Reinhardt, 1982*) while the ribbed steel characteristics are considerably different. This influence is mostly seen as an increase in pull-out resistance of deformed bars under different rates of pull-out force, Fig. 2.23.

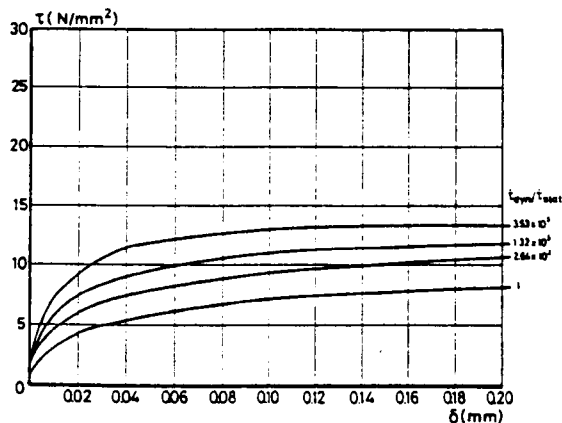


Fig. 2.23 τ - δ relation at four loading rates for concrete with a cube strength of $22.7 N/mm^2$ (Reinhardt, 1982)

With the increase of concrete strength this becomes even more pronounced and the relationship between bond stresses under dynamic $\dot{\tau}$ and static τ_o stress rates can be given as :

$$\frac{\tau}{\tau_o} = \left(\frac{\dot{\tau}}{\dot{\tau}_o} \right)^\eta$$

where: $\eta = \frac{0.7(1-2.5\delta)}{f_c^{0.8}}$

δ - relative displacement of reinforcement bar (mm) and

f_c - static cube strength (N/mm²)

2.3 Local response of RC slab to impact and close range blast loading

2.3.1 Stress-wave propagation

The dynamic nature of impact and impulsive loading produces changes in the stress state of the part of the structure exposed to the load. A rapid rise of external load requires that the material under pressure quickly develops the internal stresses necessary to balance the external load. The nature of solid bodies requires that the stresses in two points close together, have to be in equilibrium and the consequent result is the initiation of stress waves which are propagated at a definite speed across the structure.

As long as the structural element remains in the elastic region, the stress changes are caused by elastic stress waves. They are usually divided into longitudinal elastic stress waves, associated with the dilatation of the particles and torsional stress waves that are also called the waves of distortion.

Longitudinal waves that propagate through the body can be initiated by the compression (disturbed particles move in the direction of the stress waves) or tensile stresses (particles move in direction opposite to the stress wave propagation) and its speed is given as:

$$C_L = \sqrt{\frac{E}{\rho}}$$

and they are the fastest propagating waves. The speed of torsional waves is given as:

$$C_T = \sqrt{\frac{G}{\rho}}$$

E and G are modulus of elasticity and shear modulus, respectively and ρ is the density. The main characteristic of torsional waves is that they cause the particles to oscillate inside the plane orthogonal to the direction of wave propagation.

If the lateral dimensions of the body are large then the change of lateral dimension (Poisson's ratio) is included in the analysis, and the speed of these two fundamental types of wave is given as:

$$C_L = \sqrt{\frac{E \cdot (1 - \nu)}{\rho \cdot (1 + \nu) \cdot (1 - 2\nu)}}$$

$$C_T = \frac{E}{2\rho} \cdot (1 + \nu)$$

A third type of elastic stress waves that propagates on the surface or just inside the material body are surface or Rayleigh waves. Since their intensity decreases exponentially with the depth of the element their importance is much greater for the thin structures than for the thicker elements like RC beams. The elastic stress wave intensity σ is directly proportional to the density of the element ρ , velocity of the stress wave C and the velocity of the impacting particle V so their relationship is given as:

$$\sigma = \rho \cdot C \cdot V$$

As soon as the behaviour of the structural element becomes a part of the plastic response the nature of the stress waves becomes dual and there are now new types of waves, called plastic waves. They are associated with the permanent type of damage inflicted onto the RC elements and are, in nature, more complicated than the elastic ones. Its complexity is usually associated with the nonlinear behaviour of the concrete in the plastic region and, because of this, wave speed is a function of ρ and also of the change of stress under different strains. Since the modulus of plasticity is always lower than the Young's modulus in the elastic region, plastic stress waves are slower than the elastic ones.

Kolsky,(1963), Goldsmith,(1960), and Johnson,(1972), also discuss the nature of flexural stress waves, body waves, visco-elastic waves and Love waves.

2.3.2 Cracking

Dynamic load and the heterogeneous nature of concrete make the understanding of cracking even more complicated. The microcracks, air voids, interfacial bond failures between different concrete phases are the main source of fracture initiation and cracking, *Zielinski, (1984)*. The cracks always start to propagate in the mortar matrix or in the mortar/aggregate interfaces and they can be stopped only if the stresses are reduced or if the local strength becomes higher, for example at an aggregate particle. In the case of dynamic load the cracks initiated at lower stress levels do not have enough time to propagate through the regions of lower resistance before the stress increases and they can then propagate through aggregate particles which obviously have much greater strength than the mortar matrix. This eventually causes higher concrete strength under rapidly applied loads. The cracks also propagate through the aggregate particles particularly in dynamic failures. The maximum crack velocity is about 25% of the elastic longitudinal wave velocity and its strain rate dependence is shown in Fig. 2.24.

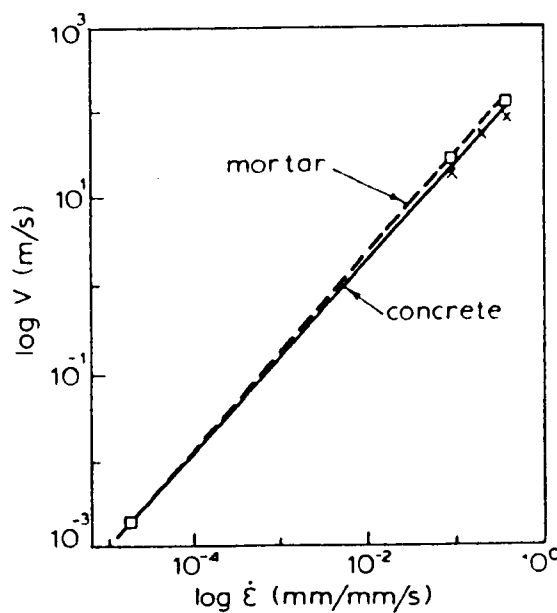


Fig. 2.24 Experimental crack velocity (V) versus strain rate $\dot{\epsilon}$ relationship (John and Shah, 1986)

An attempt was made (*Zielinski, 1984*) to establish a fracture criterion which determines whether a crack would propagate through an aggregate particle or around the aggregates as occurs in most static tests. It was concluded that the angle between the crack front and the aggregate

surface, is a major influence on the fracture criterion. The critical value of that angle was a function of the loading rate and its values are given in Fig. 2.25.

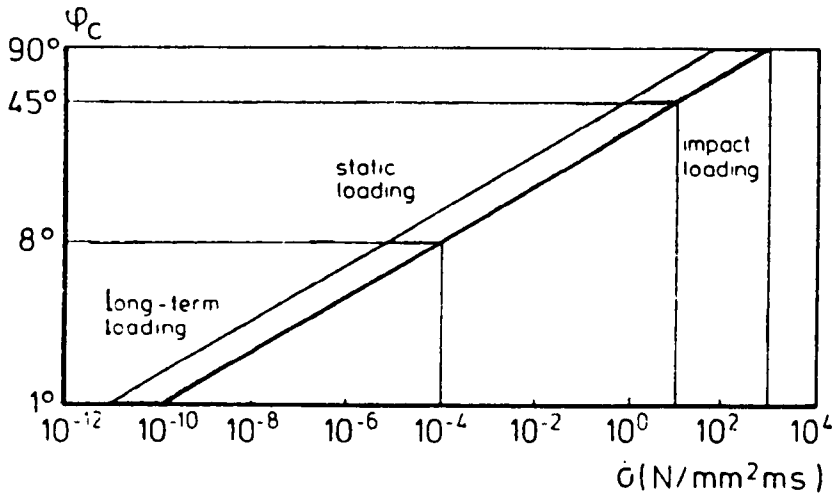


Fig. 2.25 Critical angle φ_c versus stress rate $\dot{\sigma}$ (Zielinsky et al, 1981)

The total crack density could also be used as a failure criterion. The value of 3.5cm/cm^2 has been considered as the ultimate one by *Watson and Sanderson, (1984)*.

Spalling is the phenomenon which happens on the top surface of the specimen when a solid striker or blast front impacts the concrete. It can be defined as ejection of pieces of concrete from the front face region surrounding the area of impact or the epicentre of the blast. The ejected pieces in the great majority of cases will be formed from the concrete cover to the top side reinforcement. The product of spalling is known as a front crater. Spalling is thought to be caused primarily by the compressive stress wave crushing the concrete and producing radial cracks.

Scabbing occurs when the tensile strength of the concrete close to the back side of the specimen is exceeded and is characterised by the fast ejection of concrete pieces from that side of the slab. It is caused by the reflection of the compressive wave as tension. For cylindrical dropped objects, if the scabbing number N_{scab} , given as:

$$N_{scab} = \frac{m^{0.5} \cdot V_i \cdot d_e^{0.5}}{d_o \cdot e \cdot (1 + \frac{e}{d_o})} \cdot \frac{E_c^{0.5}}{f_t}$$

is less than 50 then scabbing will not happen, *CEB Bulletin 187, (1988)*. For $N_{scab} > 60$, the scabbing is almost certain to occur. In this formula: d_e is the diameter of the impact area (m), m

is the mass of the dropped cylinder (kg) and d_o is its diameter (m), V_i is the impact velocity (m/s), e is the thickness of the concrete (m), f_t is the tensile strength of concrete (Pa) and E_c is the Young's modulus of elasticity (GPa). This formula shows that scabbing does not depend on the spacing of the back face reinforcement but the cover concrete is usually part of the scab.

In the case of explosive blast loading the size of the scab can best be related to the peak blast pressures that occur on the top surface of the slab and to the pulse duration, since the reflected tensile stress wave that causes scabbing is initiated by the blast wave. The thickness of the slab is determined by the shape of the stress pulse and the attenuation of the peak of the stress wave.

2.3.3 Penetration

Penetration is the depth to which a projectile or the load transmitter, enters an RC slab without passing through it. In an ideal case the concrete is not assumed to scab on the back face. There are a lot of formulae dealing with this problem but we will consider the situation in which the heavy solid cylinder was dropped on to the specimen. The penetration distance X (m) may be given as:

$$X = 10N_{pen} \cdot d_e$$

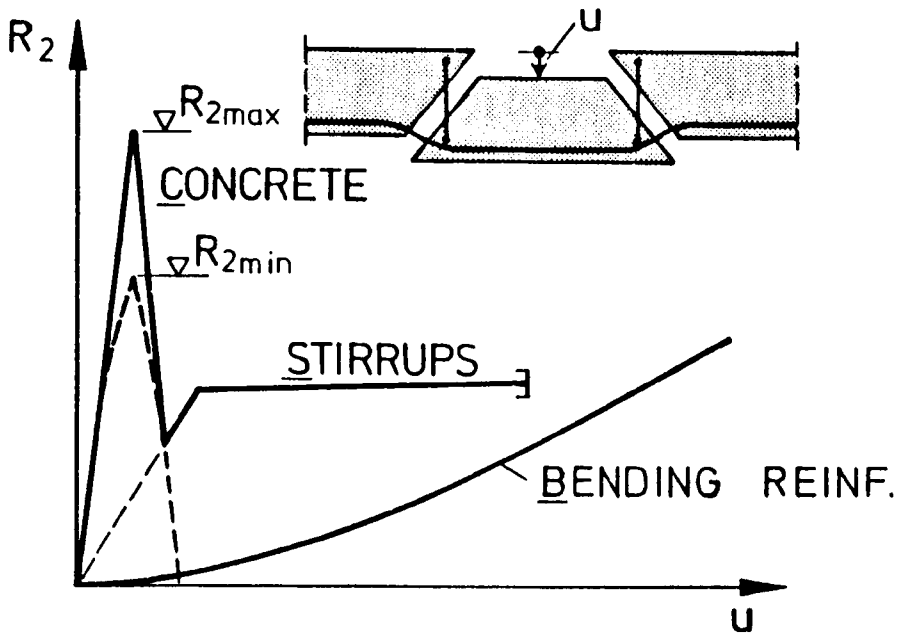
where: $N_{pen} = \frac{m^{0.5} \cdot V_i}{E_c^{0.5} \cdot d_e^{1.5}}$ and all the other notation is the same as previously given.

Perforation represents the full penetration of the target in the case of impact loading. In the case of the blast loading it is closely related to the formation of the top and back side craters.

2.3.4 Shear plug formation

This phenomena is closely related to scabbing, which can be part of the shear plug. Different forces and mechanisms take part in this process as can be seen from the Fig. 2.26.

This shows the mutual behaviour of concrete, stirrups and bending reinforcement which all share the load. When concrete is intact it takes almost all the load but once it has failed, then the reinforcement holds the load and even the concrete plug in place.



R - Resistance function and u - displacement

Fig. 2.26 Idealised behaviour of punching cone (Eibl, 1987)

Dragosavic and Beuwel, (1974), claim that punching resistance and consequently the shear plug are not influenced by the reinforcement at all. They explain punching resistance in the case of impact load, as a function of the effective depth of the section, the splitting tensile strength of the concrete and the diameter through which the load was applied. In the case of impulse loading it is related to the area of distribution and intensity of the blast pressure, and the R.C. section characteristics.

All investigators appear to agree that the size of the shear cone under impact loading is mainly dependent on the striker velocity (Fig. 2.27).

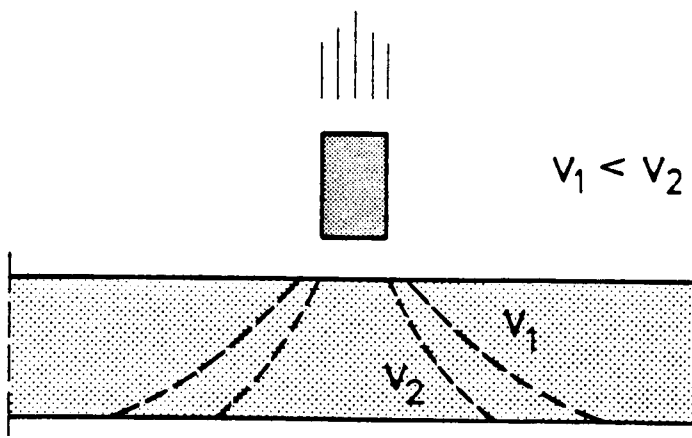


Fig. 2.27 Variation of shear cone angle with the striker velocity (CEB Bulletin 187,1988)

2.4 Overall response of R.C. slab to impact and close range blast loading

2.4.1 Inertial loading

In the cases of fast loading when the deflection rates of the specimen amount to tens of metres per second and strain rates of up to 10sec^{-1} it is not possible to neglect the existence of inertial forces that act on the structure. These forces by their nature act in the direction opposite to that of the specimen motion and their intensity F is given by Newton's equation:

$$F = m \cdot \ddot{x}$$

where m is the mass of the body and x is the displacement.

It can be said that all dynamics problems that are not stress wave propagation problems only, could partly be considered as inertial problems. This is particularly evident in the case of large deformation of elasto plastic structures under fast sudden loading.

If the inertial forces are linearly distributed, its intensity could be given as (*Eibl and Feyerabend, (1985)*):

$$R = \int_0^L p dx = \alpha \cdot F$$

where: α - percentage of the applied load

R - overall intensity of inertial force p

F - external load

Obviously for a static load $\alpha = 0$, while for the case of $\alpha = 1$ all of the external applied load F is carried by the inertia and the support reactions are zero. Shear forces Q and moments M for both of these two extreme cases are given in Fig. 2.28.

The main problem in this approach is obviously the assumption of the shape of the displacement curve and consequently accelerations and inertia forces. It can be overcome by experimentally obtaining the real acceleration distribution across the structure.

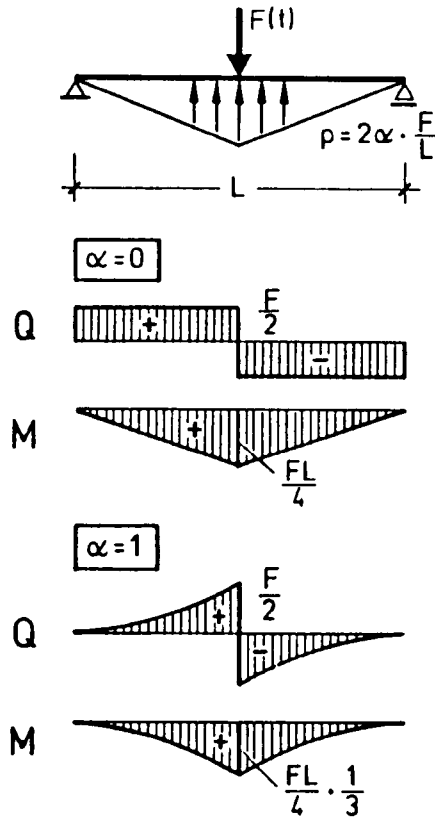


Fig. 2.28 Distribution of inertia forces P , moments and shear forces for extreme values α (Eibl, 1987)

Bentur et al, (1986), established that the time required for this inertial load to be absorbed was about three times the period of the apparent specimen oscillation. The relation of the resulting bending load $P_b(t)$ measured applied load $P_a(t)$ and inertial load $P_i(t)$ was given as :

$$P_b(t) = P_a(t) - P_i(t)$$

2.4.2 Resistance function

The problems in defining the resistance function of an R.C. slab exposed to locally applied fast transient loading are due to the dual nature of the specimen response, mainly shear response locally and flexure dominated response overall. All available information indicates that the exact resistance function is not likely to be just simple superimposition of the responses mentioned above but a time-load-deflection related expression that would reflect interference and a combination of these responses, with some of them being predominant in particular phases of response for example shear in the initial phase of the load application, leaving the remaining to dominate in the following phase or phases.

Biggs, (1964), considered an ideal, one degree of freedom system represented by the bilinear resistance function (Fig. 2.29).

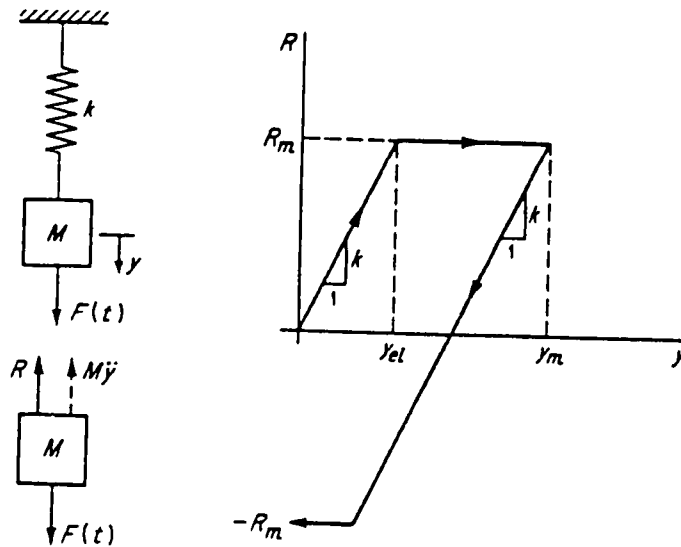


Fig. 2.29 Bilinear resistance function (Biggs, 1964)

The reversal part of the resistance trace means that the system assumes that the ultimate displacement has not been reached. This idealisation of the actual behaviour can be expressed in terms of the equations of motion as follows:

$$\begin{aligned}
 M\ddot{y} + ky - F(t) &= 0 & \text{for: } 0 < y < y_{el} \\
 M\ddot{y} + R_m - F(t) &= 0 & \text{for: } Y_{el} < Y < Y_m \text{ and} \\
 M\ddot{y} + R_m - k(Y_m - Y) - F(t) &= 0 & \text{for: } (Y_m - 2Y_{el}) < Y < Y_m
 \end{aligned}$$

For the real structure Biggs employed a trilinear resistance function Fig. 2.30.

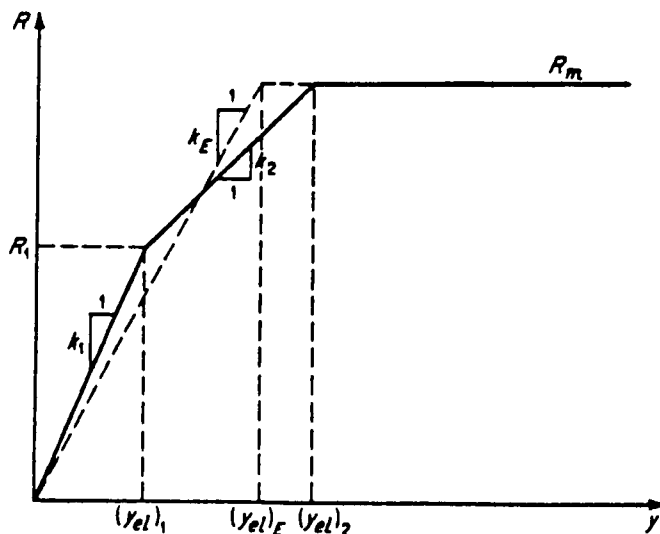


Fig. 2.30 Effective linear resistance function (Biggs, 1964)

The solid line represents a real structural response, where R_1 is considered to be the resistance before the first (support) hinge forms while R_m is the resistance after the span hinge formation. The dotted line represents an idealisation obtained by choosing stiffness K_E in a way that it gives the same area under the curve as the real structural response line.

For the case of two-way spanning RC slabs under uniformly distributed dynamic triangular shape pulse loading the response was based on the behaviour inside the elastic region and on the idealised yield lines that occur during plastic distortion.

Eibl, (1988), proposes a SDOF model but only when flexural failure occurs along yield lines. When punching failure is also present the response has to be approximated with a two degree of freedom model Fig. 2.31.

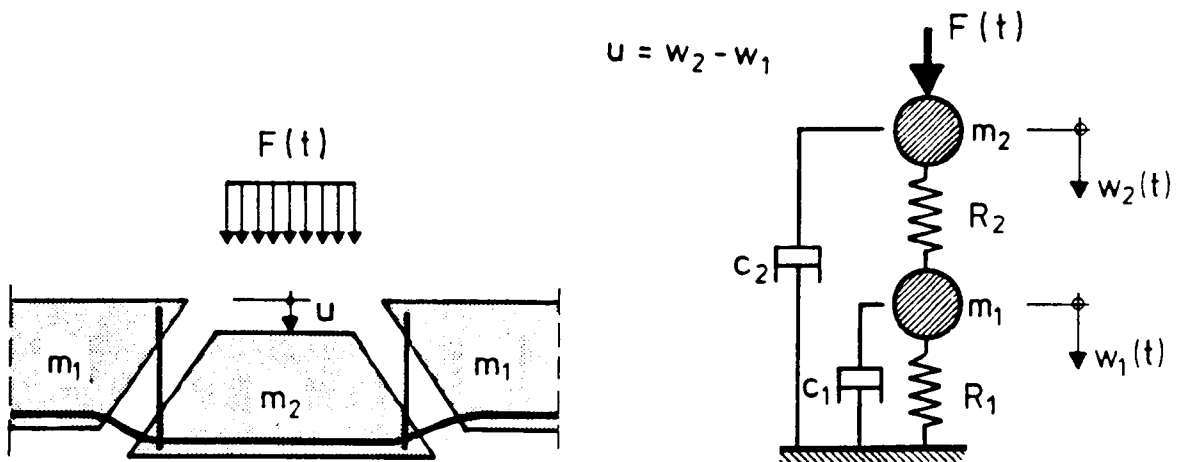


Fig. 2.31 Two degree of freedom model (Eibl, 1988)

Resistance R_1 is related to the bending of the slab according to elastic plastic type of behaviour, Fig. 2.32, while resistance R_2 represents contributions from the tensile strength of the concrete along the cone boundaries (very minor), stirrups elongation across the crack opening and from the bending reinforcement in case of large deformations, usually called dowel action, Fig. 2.31.

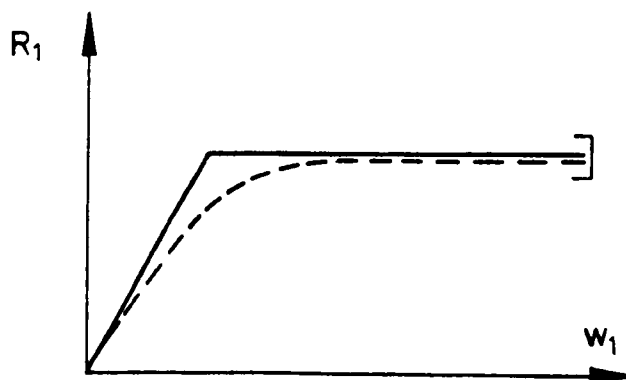


Fig. 2.32 Idealised elastoplastic material (Eibl, 1988)

Krauthammer, (1986), introduces a dynamic shear resistance function that is the same as the static one described by *Muntha and Holland, (1981)*, with a 40% linear increase in all resistance contributions due to the rate sensitive increase in material strengths, Fig. 2.5.

Point A' represents the end of the elastic response when the dowel action influence on the response is still negligible and when the max crack opening is about 0.1mm. Point B' represents a crack opening of about 0.3mm while the region B' to C' does not exhibit any resistance increase and lasts till cracks become about 0.6mm wide. The slope of the curve in area C' to D' does not seem to be influenced by the amount of reinforcement crossing the shear plane. Point E' represents a point of shear failure which happens in the support region along the vertical plane.

Tankreto, (1991), presented the resistance function for a slab explosively loaded as given in Fig. 2.33, while *Smith and Mlakar, (1991)*, used the bilinear function as in Fig. 2.34.

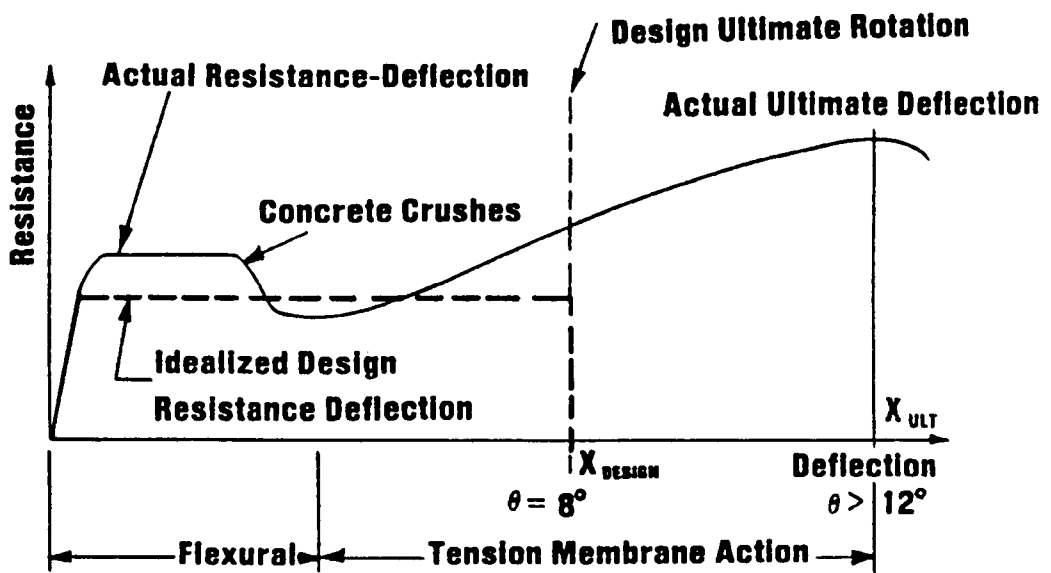


Fig. 2.33 Resistance-Deflection (Tankreto, 1991)

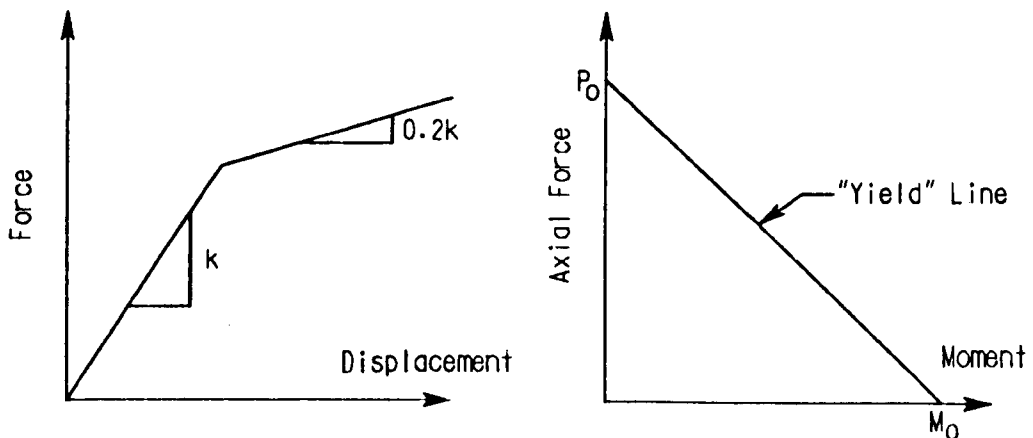


Fig. 2.34 Resistance Function (Smith and Mlakar, 1991)

Kyger and Hyde, (1987), presented the resistance function Fig. 2.35 for a two way slab that includes the effects of membrane action enhancing the flexural capacity of the slab.

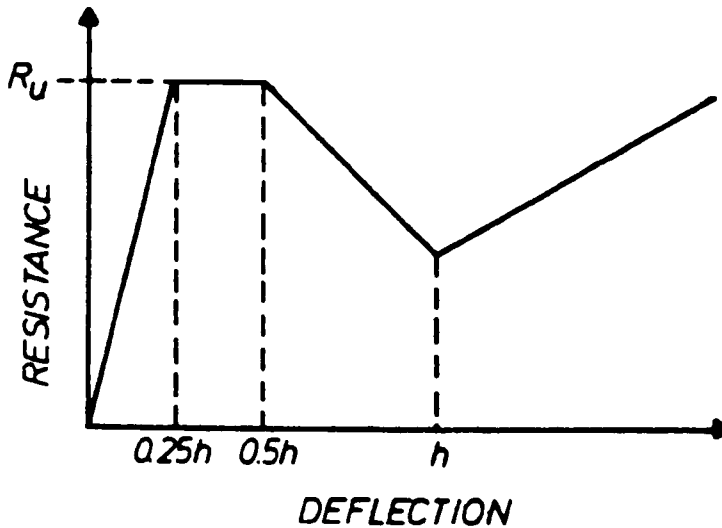


Fig. 2.35 Resistance function (Kyger and Hyde, 1987)

The reduction in peak resistance at $0.5h$ is caused by the crushing of the concrete, loss of compressive membrane action and large deformations in the slab. When the peak displacement increases to about the slab height (h) it is then mostly controlled by the tensile strength of the bending reinforcement.

2.5 Blast pressure characteristics

2.5.1 Introduction

An explosion is a phenomenon resulting from a sudden release of energy. The energy required for activation of the explosion of high explosives, such as the Plastic Explosive PE4 employed in this research, is mechanical in its nature and always produced by shock pressure forces. This process is called detonation and it proceeds at speeds of $V = 5,000 - 10,000\text{m/sec}$. Explosion is always followed by the blast wave - a pulse of air in which the pressure increases sharply at the front and is accompanied by blast winds. Typical above atmospheric pressure, overpressure vs time relation produced by a blast wave from an explosion source at a fixed distance is shown in Fig. 2.36.

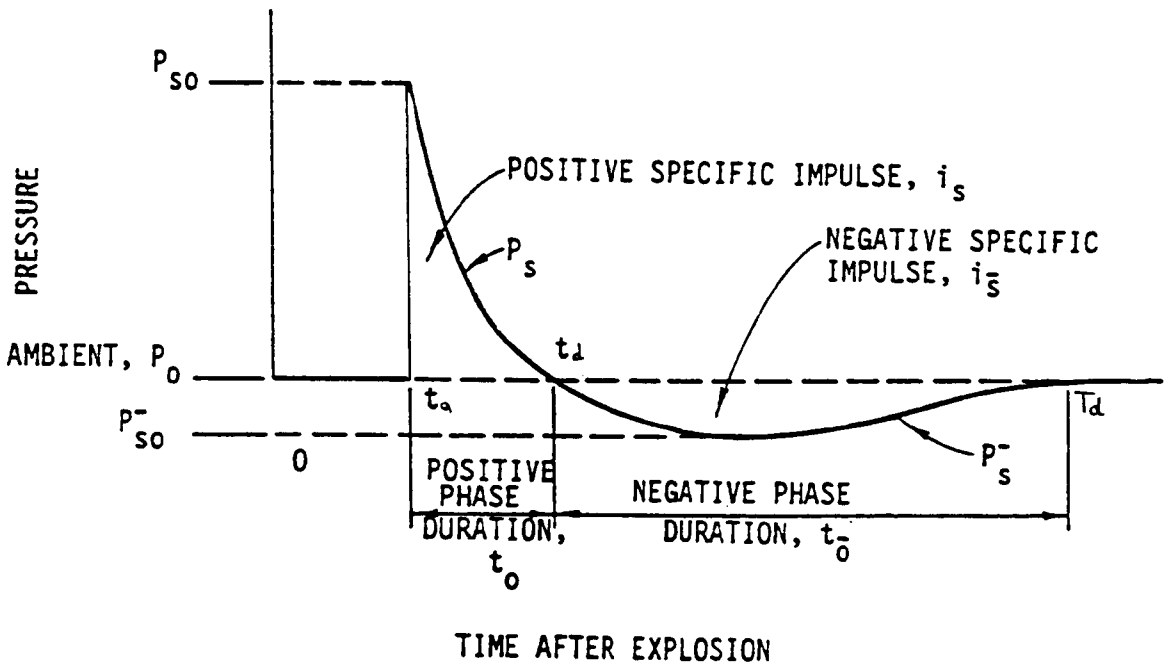


Fig. 2.36 Typical overpressure-time relation produced by the blast wave

The finite time interval required for the blast wave to travel from the centre of an explosion to any particular location is known as the arrival time. It can be calculated from:

$$t_a = \frac{1}{U_x} \int_{r_c}^r \sqrt{\frac{1}{1 + \frac{6P_{so}}{7P_a}}} dr$$

where: U_x - the speed of sound in the air (m/sec)

P_{so} - peak overpressure (bar)

r_c - radial distance (m)

P_a - atmospheric pressure (bar)

The interval between the time of arrival of the blast wave t_a and the time for the magnitude of the blast produced pressure to return to ambient atmospheric pressure is known as the duration of the pulse T_d and it increases with the distance from the charge.

A length of time between the arrival of the pulse t_a and the end of the positive part of the pulse t_d is known as the positive duration of the pulse and is closely related to the positive impulse of the pulse which represents the area under the positive part of the pressure time record and is given as:

$$I^+ = \int_{t_a}^{t_d} P_s(t) dt$$

Consequently a period of time from t_d to T_d is known as a negative phase of the pulse and is related to the negative impulse:

$$I^- = \int_{t_d}^{T_d} P_s(t) dt$$

Overpressure $P_s(t)$ decays with time at a fixed location, while the peak overpressure P_m decreases with distance from the source till it finally becomes a sound wave.

Typical pressure-time curves for successive distances are shown in Fig. 2.37.

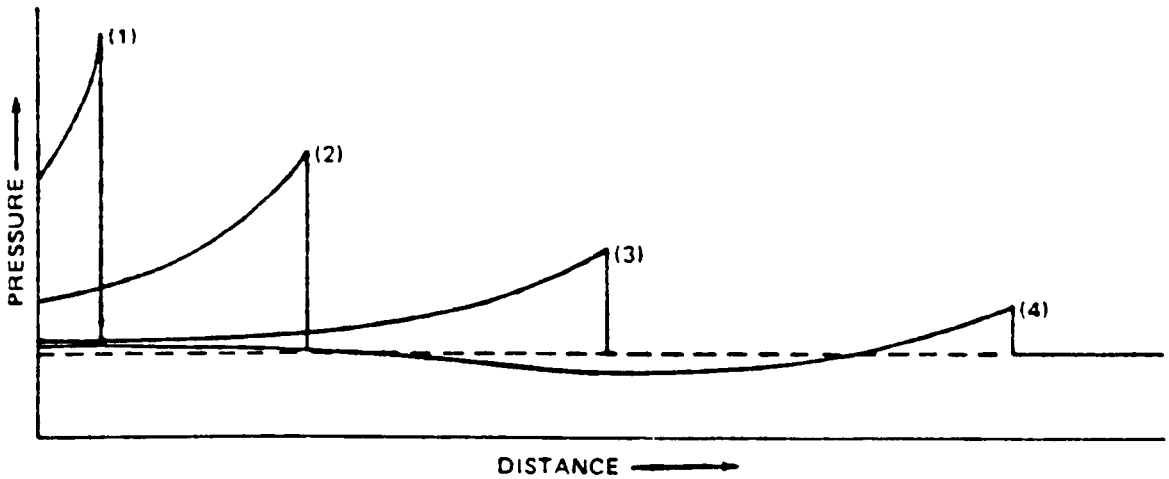


Fig. 2.37 Typical pressure-time curves for successive distances after an explosion (Kinney and Graham, 1985)

The total amount of energy transferred from an explosive to its blast wave gives the energy of the explosion:

$$E = \int_1^2 P dv$$

where: P - pressure produced in explosion and v - volume. The energy of the shock front over a unit of surface area of shock decreases with the distance squared from the explosion. A relative measure for the energy of the explosion is the explosion yield W and is related to the energy released in the explosion of TNT (symmetrical 2,4,6 - trinitrotoluene). The standard gram TNT is defined as the blast energy of 4610J (1100cal).

The velocity of a shock front of blast wave is given by:

$$U_{sf} = U_s + \frac{5P_s}{7P_a} \sqrt{1 + \frac{6P_s}{7P_a}}$$

Mach number M is another important parameter of a blast wave. It represents a dimensionless index of speed given as the ratio of the magnitude of a velocity to the speed of sound in the surrounding medium.

2.5.2 Blast wave scaling and parameters

Since the TNT equivalent has been widely accepted as a measure of the characteristics of different explosives, a spherical charge of conventional chemical explosive with energy release equivalent to one kilogram TNT will be taken into consideration in the following text.

The scaling law for explosions is based on conservation of momentum and geometrical similarity. Geometrical similarity of three dimensional bodies such as an explosive charge leads to a third power of ratio relations which are often represented in all blast wave scaling applications.

Two explosions can be expected to produce identical blast waves at distances which are proportional to the cube root of the respective energy release which is taken as the controlling parameter. Conservation of momentum can be introduced through the density of the atmosphere as a measure of the mass of the air which leads to the expression for the scaled distances Z as:

$$Z = \frac{f_a \cdot (\text{actual distance})}{\sqrt[3]{W}}$$

where: f_a - dimensionless ratio of the density of the atmosphere through which an explosive shock travels and that of the atmosphere for the reference explosion.

W - explosion yield (kg of TNT)

If f_a is taken as one, it can be shown that two charges of the same shape and explosive type but different masses M_1 and M_2 have peak overpressures that occur at distances that are related as:

$$R_1 = k \cdot R_2 \quad \text{where : } k = \sqrt[3]{\frac{M_1}{M_2}}$$

Although the peak overpressures will be the same at R_1 and R_2 , the scaling of times will mean that the other important parameters as duration of the pulse T_d and its impulse I are not the same and they can also be given as:

$$I_1 = k \cdot I_2 \quad \text{and} \quad Td_1 = k \cdot Td_2$$

If non uniform atmospheres are considered f_a cannot be taken as one and the above mentioned relations have to be adjusted for temperature and atmospheric density factors.

2.5.3 Interaction of shock waves with plane surfaces

A blast shock wave of spherical shape and low overpressure reflects from a plane surface as if the reflected wave comes from an imaginary identical source on the opposite side of the barrier and travels at the same velocity, Fig. 2.38.

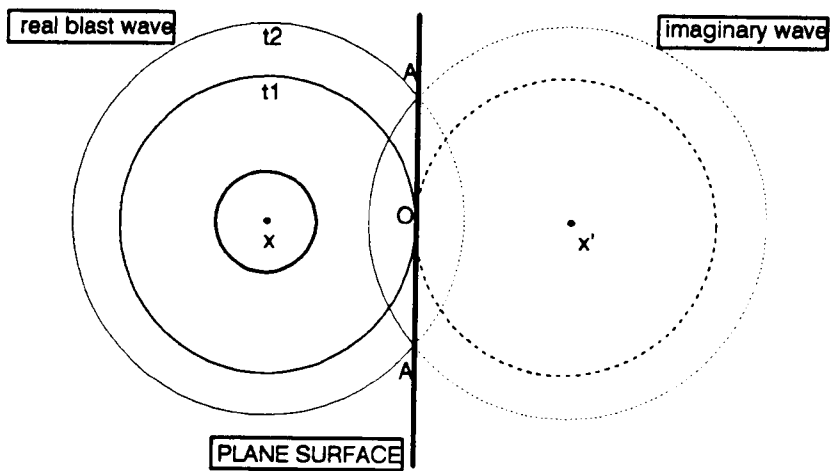


Fig. 2.38 Reflection of a low overpressure spherical shock (Watson, 1991)

Reflected overpressure P_r can be given in terms of overpressure P_s as:

$$P_r = 2P_s \cdot \frac{7P_a - 4P_s}{7P_a + P_s}$$

where P_a is atmospheric pressure.

Reflection coefficient λ_n represents the ratio of reflected overpressure to the overpressure in the incident shock. In the case of normal reflection from the rigid barrier reflection coefficient for an ideal gas can be given as:

$$\lambda_n = \frac{8M_x^2 + 4}{M_x^2 + 5}$$

where: M_x - Mach number for an incident shock.

In the case where the Mach number becomes close to one (low overpressure waves that are starting to transform to a sound wave) λ_n becomes 2 and consequently the reflected overpressure has twice the value of an incident pulse overpressure.

In all cases where the angle of incidence is up to 35° it can be said that reflected overpressure almost doubles the incident one. In the cases of not rigid, yielding barriers this factor is much lower.

Strong overpressure shocks happen under much greater Mach numbers and because of that the reflection coefficient can take any value up to 8. The reflection process for these waves is more complicated and apart from the incident and reflection waves it comprises of a new shock wave - the so called Mach stem that connects the ring of intersection points of these two waves, Fig. 2.39.

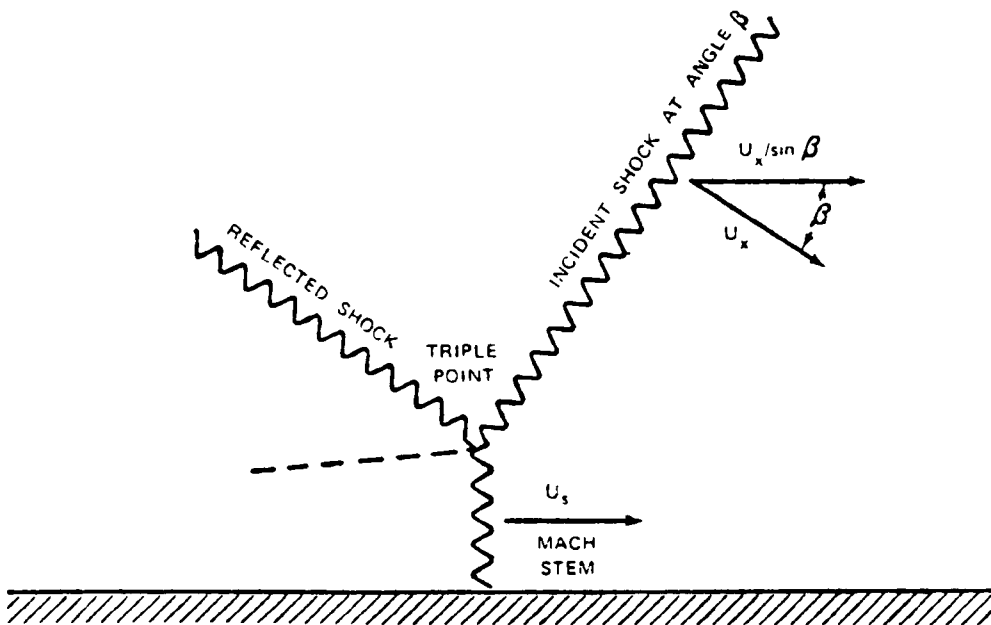


Fig. 2.39 Formation of Mach stem (Kinney and Graham, 1985)

If the duration of the incident shock wave is significantly greater than the natural period of the surface then the structural response is similar to that of a spring loaded with a constant static load.

If the duration of the shock wave is significantly smaller than the natural period then the overpressure reduces to zero before there is any significant deflection of the structure which, because of that, does not show any resistance.

The deflection rate of the structure \dot{y} can be given as:

$$\dot{y} = \int \ddot{y} t_a = \int \frac{P}{M} t_a$$

and since impulse $I = \int P t_a$ where: P - overpressure and t_a - time duration of its application and M - effective mass of the structure i.e. the mass of the structure that is actually moving, we can calculate the kinetic energy K that sets the structure in motion as:

$$K = \frac{1}{2} M \cdot V^2 = \frac{I^2}{2M}$$

Oblique reflections occur when the shock impinges at an angle onto an unyielding surface, Fig. 2.40.

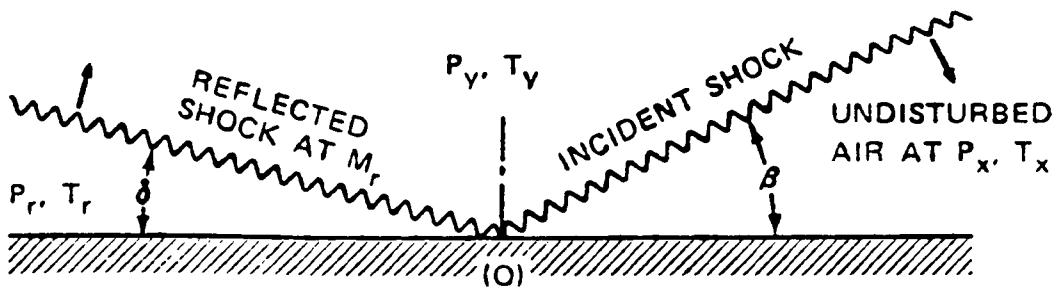


Fig. 2.40 Oblique shock reflection (Kinney and Graham, 1985)

The angle of reflection δ for an ideal gas can be given as:

$$\frac{\tan(\beta - \delta)}{\tan \beta} = \frac{5 + M_x^2}{6M_x^2}$$

The reflection coefficient for oblique reflections λ_o is given by:

$$\lambda_o = \frac{(7M_r^2 - 1) \cdot (7M_x^2 - 1) - 36}{42(M_x^2 - 1)}$$

where r means the reflected wave.

2.5.4 Loading due to a short range explosion

The case when $R_w < a \leq 10R_w$ where R_w is the radius of the charge and a is the distance of the structure from the charge centre is considered as a short range or nearby explosion. All of the blast tests in this research belong to this category. The outburst pattern produced by this type of explosion for the case of spherical charge is shown in Fig. 2.41.

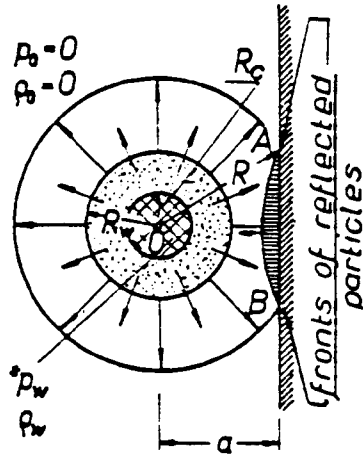


Fig. 2.41 Outburst pattern for the nearby explosion (Henrych, 1979)

If the central region of the slab is still at rest and the velocity of the outflowing particles of the explosion products $U = \text{const}$ then $\frac{\partial U}{\partial t} = 0$ and $\frac{\partial U}{\partial R} = 0$ then:

$$\frac{\partial U}{\partial t} + u \cdot \frac{\partial U}{\partial R} + \frac{1}{\rho} \cdot \frac{\partial P}{\partial R} = 0 \quad (\text{Henrych, 1979})$$

reduces to:

$$\frac{1}{\rho} \cdot \frac{\partial P}{\partial R} = 0 \quad \text{and since} \quad \frac{1}{\rho} \neq 0 \quad \text{then} \quad \frac{\partial P}{\partial R} = 0$$

which means that in the whole region, except for the hatched area in which the reflection of the waves started to take place, the pressure at a given time is constant.

At a particular time instant t , R_c can be calculated as:

$$R_c = R_w \left(1 - \frac{t}{\tau} \right)$$

where τ is the period for which the pressure acts on the obstacle. It usually lasts up to 10^{-4} sec and can be given as:

$$\tau = R_w \cdot \left(\frac{1}{U_x} + \frac{1}{N_{xw}} \right)$$

where N_{xw} - displacement velocity of the outburst surface.

These equations provide a relation between the co-ordinate of a point on the surface of the obstacle and the time t measured from the moment of incidence of the first particle. The relation between explosion product density ρ , distance and time can be given as:

$$\rho = \frac{N_{xw}}{U_x + N_{xw}} \cdot \rho_w \cdot \left(\frac{R_w}{R} \right)^{(\nu-1)} \cdot \left(1 - \frac{t}{\tau} \right)^{(\nu-1)}$$

where $(\nu - 1) = 2$ for the spherical charge.

It can also be found that the pressure at any point on the obstacle can be given as:

$$P = \rho \cdot (1 + \kappa \cdot r)$$

where ρ can be calculated as above and κ - coefficient of restitution:

$$\kappa = \frac{N_{xw}}{U_x} < 1$$

For the very short period of time for which this pressure acts the structural loading does not depend only on the magnitude of the pressure P but on the specific impulse i . At point A it can be given as:

$$i = \frac{A_o \cdot W}{a^2} \cos^4 \alpha$$

where: $W = \frac{4}{3} \pi \cdot \rho_w \cdot R_w^3$ - mass of the spherical charge and $A_o = \frac{N_{xw} + U_x}{4\pi}$.

If we consider an explosion occurring above the centre of the circular plate the total impulse of explosive loading is given as $\int_0^r i dr$ which leads to:

$$I = \pi \cdot A_o \cdot W \sin^2 \alpha_o$$

where: α_o is given in Fig. 2.42.

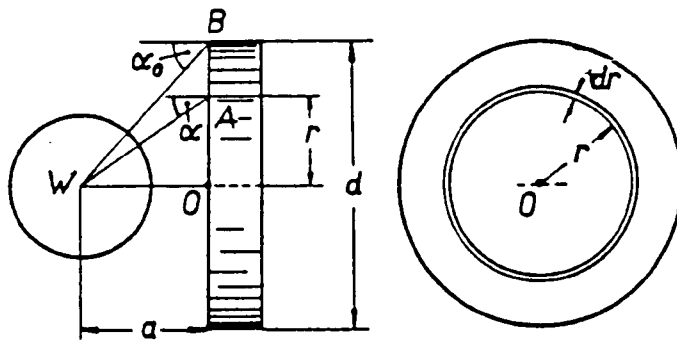


Fig. 2.42 Nearby explosion above a circular plate (Henrych, 1979)

In the case when the charge dimensions are greatly smaller than the plate size (plate of infinite dimensions) and since $\alpha_o \rightarrow \frac{\pi}{2} = 90^\circ$ total impulse is given as:

$$I = \pi \cdot A_o \cdot W$$

Further explanations of phenomena and relations connected to the blast loading and its characteristics are given in much more detail in *Watson (lecture notes 1991), Kinney and Graham (1985), Henrych (1979), Baker (1973) and Cook (1958)*.

2.6 Modelling considerations

Structural modelling has been widely and successfully used for assessing the characteristics and behaviour of materials and structures produced at different scales. There is great economic and practical advantage in using smaller structures exposed to scaled loads that represent the real structure and loads. Additionally when tests require the use of explosives as in this research, structural modelling provides the powerful tool for avoiding use of greater amounts of explosive so eliminating unnecessary risks.

A structural model is usually described as structural element or assembly of structural elements built to a reduced scale (in comparison with full size structures) which is to be tested, and for which laws of similitude must be employed to interpret test results.

2.6.1 Dimensional analysis

The similitude requirements that relate the model to the real structure are based upon the theory of modelling which is derived from a dimensional analysis of the physical phenomena involved in the behaviour of the structure.

The dimensional characteristics widely used for describing the physical phenomena are:

- (a) Length
- (b) Force (or mass)
- (c) Time
- (d) Temperature
- (e) Electric charge

Since most of the structural problems are of a mechanical nature the first three above mentioned dimensions are the most important for structural engineering.

The main requirement of dimensional analysis is that any mathematical relationship that describes the behaviour of a structure must be dimensionally valid regardless of the parameters that quantify the effects.

This implies that any relation of the form $F(X_1, X_2, \dots, X_n) = 0$ can be expressed in term of $G(\pi_1, \pi_2, \dots, \pi_m) = 0$ where the π 's are dimensionless measures of physical effects previously given in the form of X_1 to X_n .

This allows a reduction of the unknown quantities that fully represent physical behaviour of the structure because $m = n - r$ where the r is the number of fundamental dimensions that are involved in the physical phenomena. This means that a dynamic problem that combines the effects of say 6 different parameters can be effectively reduced in our case to three dimensionless parameters because $r = 3$ (length, time and mass).

Dimensional analysis and structural modelling can use replica models of complete similarity with the prototype when all of the dimensionless products are exactly the same in both model and prototype or adequate models that provide a close similarity but eliminate those variables that are not considered of relevant importance. Since it is usually very difficult to obtain exact similitude replica modelling adequate models are most frequently used.

2.6.2 Theory of modelling for structures exposed to impact and blast loading

Modelling considerations for transient dynamic loading include the loading function (force, pressure, time, gravitational acceleration and velocity) the geometry of the specimen (linear dimensions, displacement and strain) and the material characteristics (modulus of elasticity, stress, Poisson's ratio, mass and mass density).

The approach that would provide a so called true replica model would require selection of three physical quantities for independent scaling since there are three independent basic quantities (M,L,T) that describe the phenomena. Since in all possible combinations the gravity acceleration must be the same for the model and the prototype, two additional quantities can be chosen as say Poisson's ratio and velocity V . To fulfil the dimensional analysis requirements, time, linear dimensions and displacement would need to be scaled with a linear scaling factor. Strain, gravity

acceleration, Poisson's ratio and velocity would be the same for the model and the prototype, but scaling of mass density, mass, modulus of elasticity, force and pressure would require an additional change of modulus of elasticity of the material. This inevitably leads to the use of different material than concrete which is obviously not acceptable and consequently this true replica model can not be of great use in dynamic modelling of structures.

The model that one would naturally be expected to use would require the same material characteristics in the model and prototype and a linear scaling of geometry. An adequate model which would provide these requirements is called a Gravity Forces Neglected model and has been widely used for dynamic modelling and is also used in this research. The main difference with a true replica model is that gravitational acceleration g is neglected and this is acceptable since gravitation forces do not represent a significant part of the loading function in the cases of impact and blast loading. The relationship of the physical quantities for model specimens and those of the real structure, the full scale specimens, used in this research are given in Table 2.1.

M, L and T represent units for mass, length and time respectively, S1 is the linear scaling factor between the model and the prototype and 1 means that values are the same in both scales.

PHYSICAL QUANTITIES	DIMENSION	GRAVITY FORCES NEGLECTED ADEQUATE MODEL
Force	M	S1 ²
Pressure	ML ⁻²	1
Time	T	S1
Gravitational acceleration	LT ⁻²	Neglected
Velocity	LT ⁻¹	1
Linear dimensions	L	S1
Displacement	L	S1
Strain	-	1
Modulus of elasticity	ML ⁻²	1
Stress	ML ⁻²	1
Poisson's ratio	-	1
Mass density	MT ² L ⁻⁴	1

Table 2.1 Summary of scale factors for dynamic loading

The rules that govern the modelling of blast pressure function quantifiers are given in section 2.5.2 of this chapter.

Works by *Sabnis et al (1983) and Noor and Boswell,(1992)*, provide further details about structural modelling of structures exposed to dynamic loading.

2.7 Some theoretical approaches to the problem

2.7.1 Timoshenko, (1951)

He studied the problem of an impacted beam by introducing assumptions that:

- (1) The beam mass can be neglected if it is small in comparison with mass of falling body.
- (2) The stresses are in the elastic region so there is no energy loss due to plastic deformation.
- (3) The deflection curve during impact has the same shape as that during a static test.

Since there is no energy loss, the energy stored in the beam is the same as the work done by a static force. Then for impact at the mid span of a beam with a rectangular cross-section :

$$\delta = \delta_{st} + \sqrt{\delta_{st}^2 + \frac{1}{g} \cdot \delta_{st} \cdot V^2}$$

$$\text{where: } \delta_{st} = \frac{W \cdot l^3}{48E \cdot I}, \quad V = \sqrt{2g \cdot h} \quad \text{and} \quad \sigma_{max} = \sqrt{\frac{W \cdot V^2}{2g} \cdot \frac{18E}{l \cdot A}}$$

By introducing a reduced mass for the beam of $m = \frac{17}{35} \cdot \frac{q \cdot l}{g}$ then the maximum deflection

becomes:

$$\delta = \delta_{st} + \sqrt{\delta_{st}^2 + \frac{\delta_{st} \cdot V^2}{g} \cdot \frac{1}{1 + \frac{17}{35} \cdot \frac{q \cdot l}{W}}}$$

2.7.2 Goldsmith, (1960)

Impact by a rigid striker on a uniform straight beam has been studied using the equations of energy balance of the system, i.e. initial kinetic energy of the striker and maximum strain energy stored by the spring, which represents the beam, at the instant of maximum dynamic deflection.

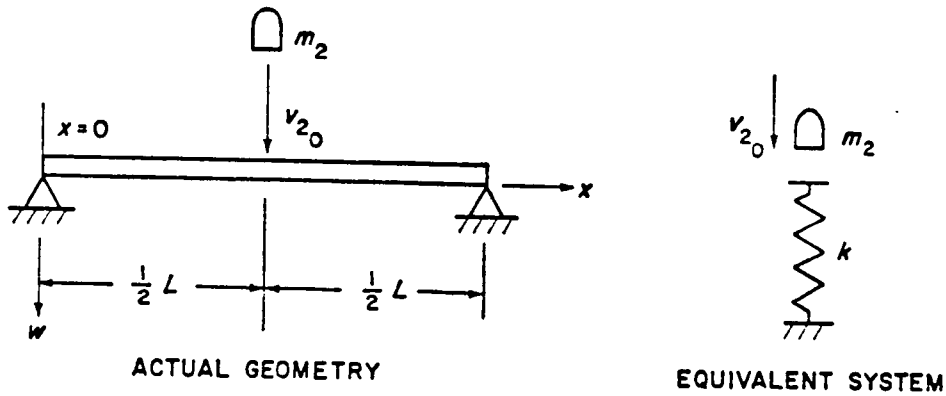


Fig. 2.43 Central impact on a simply supported beam (Goldsmith, 1960)

If the effects of change of potential energy of the striking mass are to be included, then the maximum dynamic deflection is:

$$W_m = \frac{m \cdot g}{k} \left(1 + \sqrt{1 + \frac{K \cdot v}{m \cdot g^2}} \right)$$

where: K - stiffness of the beam

v - striker velocity (m/sec)

m - mass of the striker (kg)

g - gravity (ms^{-2})

2.7.3 Norris, (1964)

He used the differential equation of motion for beams where the beam is considered to be loaded and to move in one plane only. Shear deformations, rotations and axial movement of the beam were neglected, Fig. 2.44.

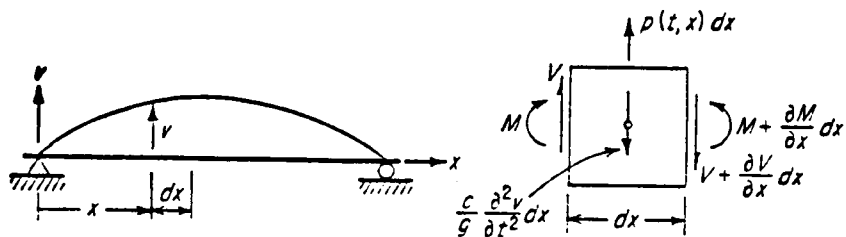


Fig. 2.44 Notation for flexural vibration (Norris, 1964)

$$w = p(f_{1x}) - \frac{c}{g} \cdot \frac{d^2 v}{dt^2} \quad \text{then:}$$

$$\frac{d^2}{dx^2} (E \cdot I \cdot \frac{d^2 v}{dx^2}) + \frac{c}{g} \cdot \frac{d^2 v}{dt^2} = p(f_{1x})$$

- where: w - intensity of load (per unit of length)
 $p(f_{1x})$ - dynamic load intensity (per unit of length)
 $\frac{c}{g} \cdot \frac{d^2 v}{dt^2}$ - inertial load (per unit of length)
 v - transverse deflection
 c - weight (per unit of length)
 $E \cdot I$ - flexural rigidity of beam

Solution of these equations was obtained by applying boundary conditions for different support conditions. In the case of the simply supported beam the solution gives the characteristic shapes of the first three normal modes of vibrations as presented in Fig. 2.45.

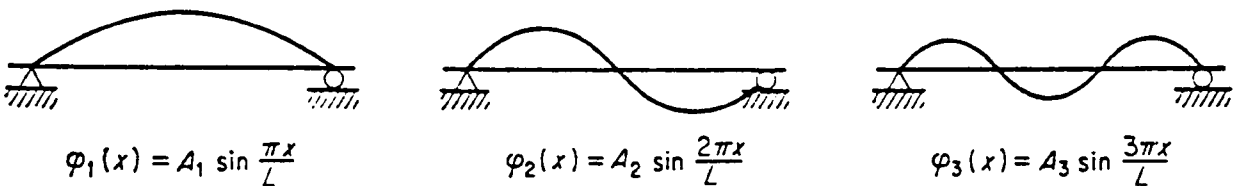


Fig. 2.45 Characteristics shapes of first three normal modes of vibration (Norris, 1964)

2.7.4 Ezra, (Johnson, 1972)

He describes an analysis by Ezra for a uniform simply supported beam dynamically loaded at its midspan by a rigid striker. It is considered that the kinetic energy delivered by the striker is dissipated in the moving plastic hinges and is of greater magnitude than the ultimate elastic strain energy for the beam.

At the moment of impact a plastic hinge is formed at the impact point and two more hinges travel outwards from it. These travelling plastic hinges become stationary and always lie between $0.67L$ and $0.59L$, Fig. 2.46.

According to this analysis, the deflection at midspan is:

$$Z = \frac{M^2 \cdot V_0^2}{12 M_p \cdot m} \cdot \left[l_n \left(1 + \frac{m}{M} \cdot x \right) - \frac{m \cdot x \cdot (2M + m \cdot x)}{2(M + m \cdot x)^2} \right]$$

where: M - mass (Kg)

V_o - velocity at time of impact (m/sec)

M_p - moment of plasticity (Nm)

m - unit mass (kg/m)

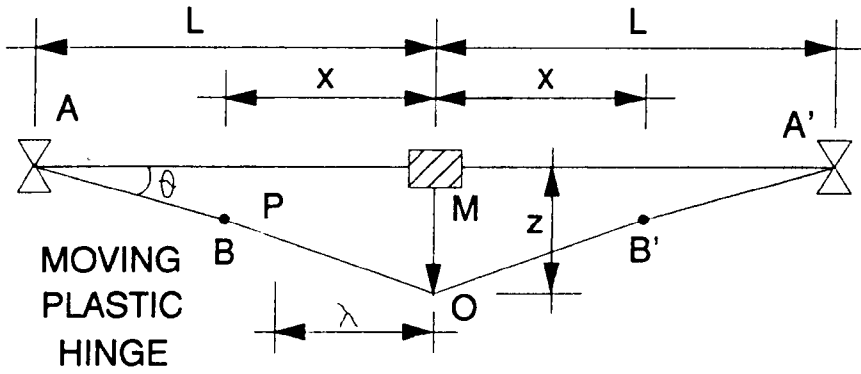


Fig. 2.46 Travelling plastic hinge (Johnson, 1972)

2.7.5 Popov, (1976)

He considered a free falling body which strikes a structure to deliver an impact load, Fig. 2.47.

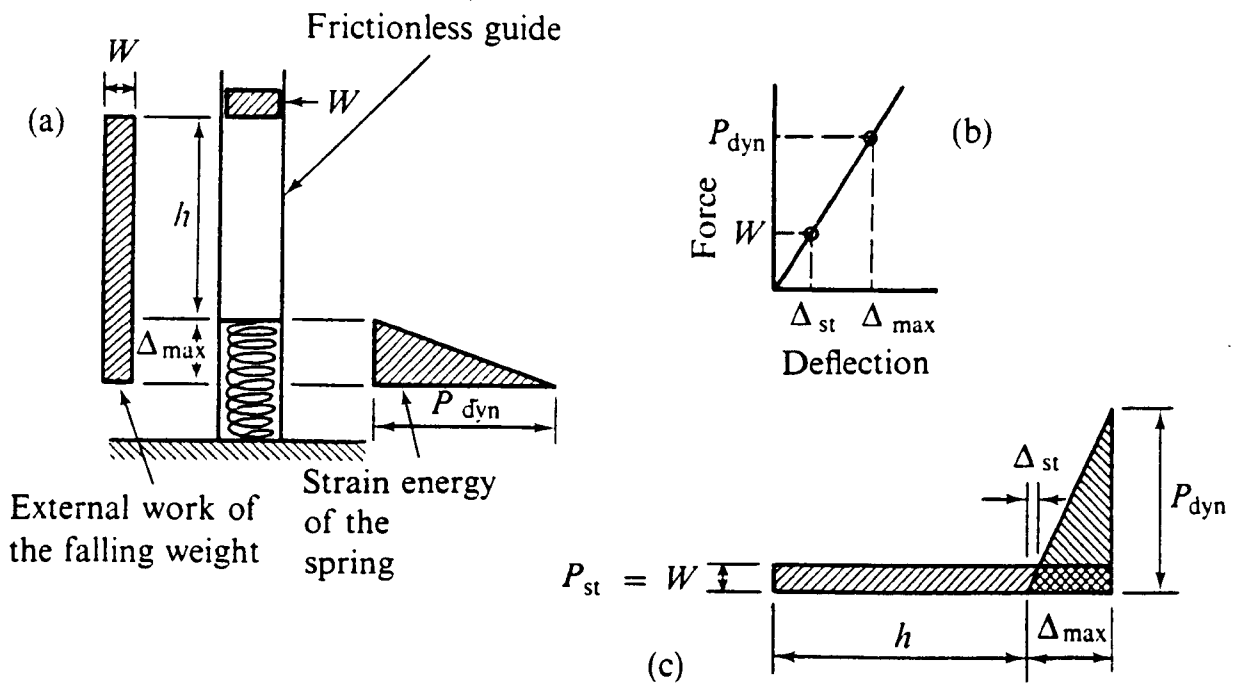


Fig. 2.47 Behaviour of an elastic system under an impact force (Popov, 1976)

His assumptions for analysing the problem are that there is no dissipation of energy at the point of impact or at the supports, that materials behave elastically, that inertia forces of a system are negligible and that deflection of the system is always directly proportional to the force applied, From the equality of external work to internal strain energy:

$$W \cdot (h + \Delta_{\max}) = \frac{1}{2} P_{\text{dyn}} \cdot \Delta_{\max} \quad \text{and} \quad P_{\text{dyn}} = \frac{\Delta_{\max}}{\Delta_{st}} \cdot W$$

Then:
$$P_{\text{dyn}} = W \cdot \left(1 + \sqrt{1 + \frac{2h}{\Delta_{st}}} \right) \quad \text{and} \quad \Delta_{\max} = \Delta_{st} \cdot \left(1 + \sqrt{\frac{2h}{\Delta_{st}}} \right)$$

2.7.6 Symond, (Watson, 1991)

Symond's analysis of a simply supported beam of unit mass m and plastic moment of resistance M_p under the uniformly distributed blast type loading $P(t)$ neglects elastic deformation of the beam (Fig. 2.48).

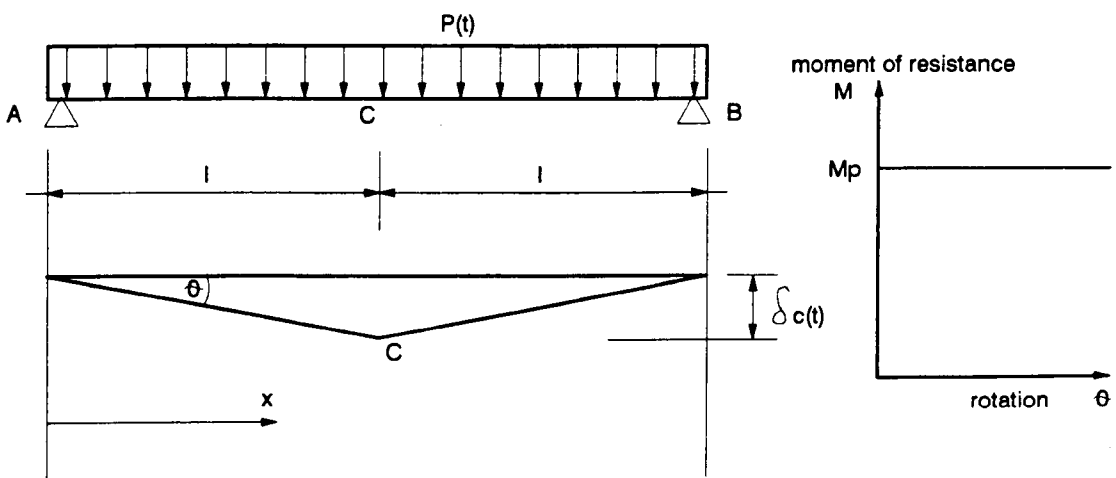


Fig. 2.48 Symond's analysis - load function (Watson, 1991)

It can be seen that Symond assumes rigid-plastic behaviour of the structure, and a hinge must form at a midspan point C before any rotation can take place.

Since $M_c = \frac{P \cdot L}{4}$ then if $M_c < M_p$ there is no rotation θ at the ends and no deformation

but if $M_c \geq M_p$ a hinge is formed at the centre and the only forces that oppose the deformation are inertial forces - $m \cdot a$ where a is acceleration of the beam. If the uniformly distributed load $P(t)$ is greater than inertial forces then (Fig 2.49):

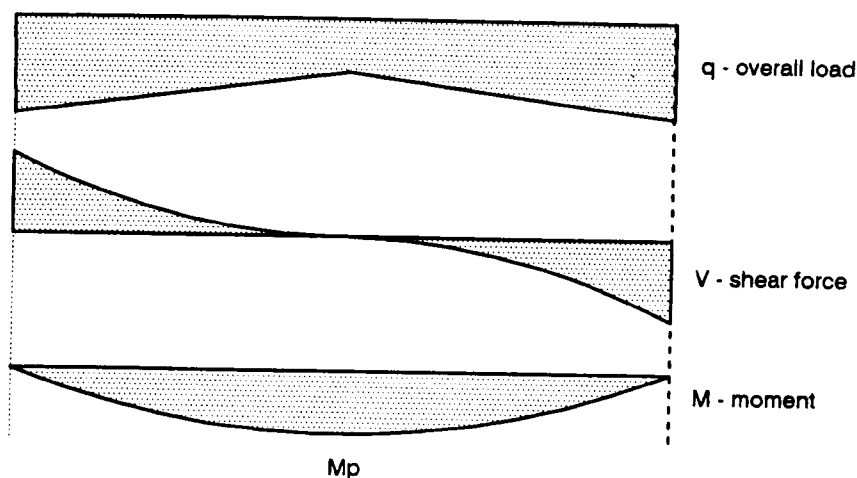


Fig. 2.49 Symond's analysis - overall load, shear force and moment

The intensity of uniformly distributed load $P(t)$ that can produce a plastic hinge at midspan C can be obtained from the equation of angular motion about the plastic hinge point:

$$M_c + I \cdot \ddot{\omega} = 0$$

where: I - moment of inertia and

$\ddot{\omega}$ - angular acceleration

It can be shown that if:

$$\frac{4M_p}{l} \leq P(t) \leq \frac{12M_p}{l}$$

then residual deflections can occur, but not necessarily collapse if the hinge rotation, calculated from equation of angular motion, can absorb all the energy. If $P(t)$ reaches $\frac{12M_p}{l}$ then the plastic hinge forms at C and the maximum deflection occurs at time $t = \frac{l}{4M_p} \cdot \int P dt$ which can be derived from the maximum deflection requirement that $\dot{\omega} = 0$.

If $P(t)$ is greater than $\frac{12M_p}{l}$ then instead of having a single point hinge at C, we have a "hinge region" where plasticity occurs, while the rest of the beam is still rigid.

2.8 Standard recommendations

The standards that deal with the dynamic problems of fast transient loads can be divided into two basic categories:

- (a) Standard recommendations for ordinary reinforced concrete structures, and

- (b) Standard recommendations for structures of particular interest (domestic shelters, nuclear reactors, key military installations, structures of strategic importance etc.)

The most common approach is to give a safety factor allowance (usually 1.20 to 1.50) on all designed loads when there is an indication of a possible case for this type of load. *HMSO guide on domestic shelters, 1975, (Bangash, 1993)* introduces ultimate unit resistance r_u as:

$$r_u = F_I \cdot \frac{1}{1 - 0.5\mu}$$

where: F_I - resistance force and

μ - damage factor.

For the case of moderate damage factor $\mu = 3$, ultimate unit resistance becomes:

$$r_u = 1.2F_I$$

The ultimate shear capacity is given as $0.4f_{cu}$ and for fixed ends boundary conditions it shall not exceed 17.2N/mm^2 .

The minimum area of high tensile flexural reinforcement in the tensile zone of the specimen should not be less than 0.2% of the effective cross-section.

The value of the ultimate unit resistance for a two-way slab can be written as:

$$r_u = \frac{8(M_{HN} + M_{HP}) \cdot (3L - x)}{H^2 \cdot (3L - 4x)} \quad \text{for the shorter span}$$

$$\text{and } r_u = \frac{5(M_{HN} - M_{HP})}{x^2} \quad \text{for the longer span}$$

where: M_{HN} and M_{HP} - ultimate unit negative moment capacity at support and midspan point respectively

L - span and

H - height of the section.

M_{HN} and M_{HP} can be calculated using either of:

$$M = f_{y(dyn)} \cdot A_s \cdot Z \quad \text{or:}$$

$$M = 0.225f_{cu(dyn)} \cdot b \cdot d^2 \quad \text{where:}$$

$$Z = \frac{d \cdot (1 - 0.84 f_{y(\text{dyn})} \cdot A_s)}{f_{cu(\text{dyn})} \cdot b \cdot d} < 0.95d$$

BS8110 states that when accidental loads are anticipated, a safety factor of 1.05 should be applied to the defined loads.

Most of the available and applicable standard recommendations refer to American Concrete Institute codes and other American codes. *ASCE Manual 42* and *TM5-1300* (both from *Bangash, 1993*) for the explosive and impact loading on structural element with both tensile A_s and compression zone reinforcement A'_s give ultimate unit resistance moment, for the width b , as:

$$M_u = \frac{A_s - A'_s}{b} \cdot f_y \cdot \left(d - \frac{a}{2}\right) + \frac{A'_s \cdot f_y}{b} \cdot (d - d')$$

where: d' - distance from the extreme compression fibre to the centre of compression zone reinforcement

a - depth of equivalent rectangular stress block

The difference between the reinforcement percentages of tensile and compressive zone reinforcement must not exceed 0.75 of the ratio that produces a balanced reinforced concrete section. The minimum amount of tensile flexural reinforcement for the high pressure range loading on two-way R.C. slabs can not be less than 0.25% of $b \cdot d_c$ while in the compression zone it can not be less than 0.18% $b \cdot d_c$.

The ultimate shear capacity is calculated by replacing the static value for the concrete strength with the corresponding dynamic value which means that the strain rate must be known.

ACI Standard 318-77, (1977) gives a safety factor as 1.7 (applied to all live and impact loads) while *ACI - 349-76, Appendix C, (1977)* increases the static characteristics of materials ranging from 10% for the concrete exposed to shear to 20% for the high yield steel.

European codes for concrete *CEB - FIP, (1978)*, for ordinary reinforced concrete structures classify impact and blast into the category of incidental loads. To reduce the effects of these loads, in the cases when they are not considered as very likely in the life time of structure, codes suggest design of the structure in such a way that, when an element is directly exposed to dynamic overload and destroyed, this will not cause disproportionate structural collapse.

CHAPTER 3

EXPERIMENTAL TECHNIQUES

3.0 Introduction

The reinforced concrete slab specimens used in this research are based on typical structural elements which can exist in various types of structure (for example bridges and industrial buildings). The models have been designed to represent approximately 1:4 scale and 1:10 scale models of typical prototypes. In the remainder of this report the 1:10 scale will be called small or model specimens and the 1:4 scale the large or full scale specimens. Thus the small specimens model the large specimens at 1:2.5 scale. This chapter will explain the methods of manufacturing these two sizes of structural specimen, specify the concrete and steel used in their production and fabrication and describe the manufacture of specimens used to obtain the properties of the materials.

The test equipment consists of a drop hammer impact rig and explosive blast cells appropriate for the model and full size tests. The test equipment and the instrumentation used on the specimens and on the rig are described in section 3.2. The explosive charges and their calibration are described in section 3.3.2.

3.1 TEST SPECIMEN

3.1.1 Slab dimensions

All outside dimensions for the model slab are 2.5 times smaller than for the prototype specimens. The slabs were all square shaped, had rectangular cross-sections and the overall dimensions are given in Table 3.1.

		SMALL SLABS	LARGE SLABS
CROSS SECTION		44 x 800mm	110 x 2000mm
LENGTH		800mm	2000mm
SPAN	FIXED SUPPORTS	640mm	1600mm
	FREE SUPPORTS	720mm	-

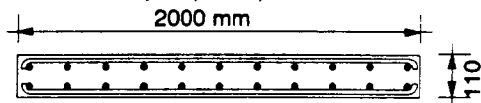
Table 3.1 Specimen dimensions

According to BS8110 the balanced section for design purposes is defined as one in which the steel stress reaches the design strength of $0.87 f_y$ simultaneously as the concrete reaches the strain of 0.0035. For the concrete used in this investigation with the target static compressive strength $f_{cu} = 40\text{N/mm}^2$ and high yield steel of $f_y = 460\text{N/mm}^2$, a balanced section is obtained when the reinforcement ratio is $\rho = 2.52\%$. After taking into account design requirements for the spacing and the size of the bars it was decided to use tensile reinforcement in all possible conditions i.e. over reinforced, balanced and under reinforced section, with 85% of the specimens being of the under reinforced section out of which the great majority were just lightly reinforced (0.26% for the small specimen and 0.41% for the large scale slabs).

The specimen details are shown in Fig. 3.1.

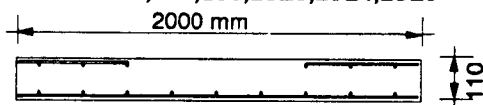
1:1 SCALE SLABS

SLABS:LS1,LS2,LSE1,LSE2



top reinforcement:
11 No 16 mm H.Y. steel bars, each way
bottom reinforcement:
11 No 16 mm H.Y. steel bars, each way
cover: 10 mm

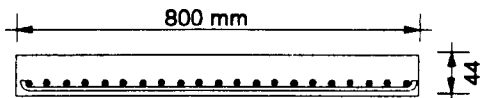
SLABS:LS3,LS4,LS5,LSE3,LSE4,LSE5



top layer reinforcement:
R.MESH : B.S.4483 A393 10/200/200 mm
(without central region 1.0 X 1.0 m)
bottom layer reinforcement:
R.MESH : B.S.4483 A393 10/200/200 mm
cover: 10 mm

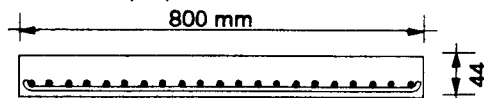
1:2.5 SCALE SLABS

SLABS:S1,S2,SE1,SE2



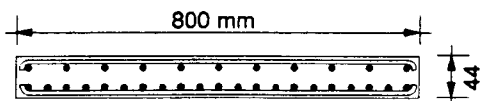
top reinforcement: -
bottom reinforcement:
11 No 8 mm H.Y. + 10 No 6 mm H.Y., each way
cover: 4 mm

SLABS:S3,S4,SE3



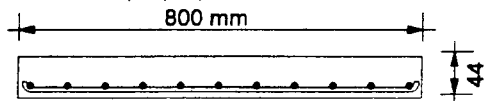
top reinforcement: -
bottom reinforcement:
21 No 6 mm H.Y., each way
cover: 4 mm

SLAB:SE4



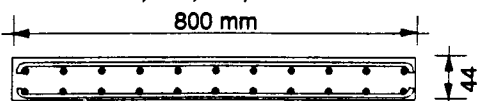
top reinforcement:
11 No 6 mm H.Y., each way
bottom reinforcement:
21 No 6 mm H.Y., each way
cover: 4 mm

SLABS:S5,S6,S7,S8



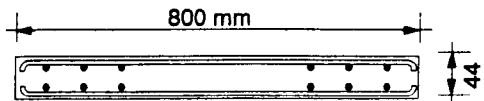
top reinforcement: -
bottom reinforcement:
11 No 6 mm H.Y., each way
cover: 4 mm

SLABS:SE5,SE6,SE7,SE8



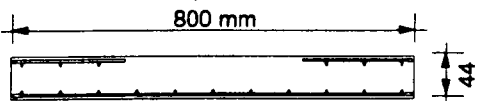
top reinforcement:
11 No 6 mm H.Y., each way
bottom reinforcement:
11 No 6 mm H.Y., each way
cover: 4 mm

SLAB:SE9



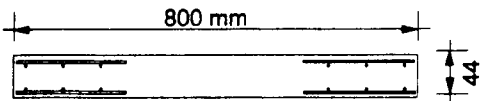
top reinforcement:
6 No 6 mm H.Y., each way
bottom reinforcement:
6 No 6 mm H.Y., each way
cover: 4 mm

SLABS:S9 to S18,SE10 to SE19 and SS1 to SS5



top layer reinforcement:
R.MESH : 3.15 mm DIAM. / 76.2 mm CENTRES
(without central region 400 X 400 mm)
bottom layer reinforcement:
R.MESH : 3.15 mm DIAM. / 76.2 mm CENTRES
cover: 4 mm

SLAB:S19



top layer reinforcement:
R.MESH : 3.15 mm DIAM. / 76.2 mm CENTRES
(without central region 400 X 400 mm)
bottom layer reinforcement:
R.MESH : 3.15 mm DIAM. / 76.2 mm CENTRES
(without central region 400 X 400 mm)
cover: 4 mm

Fig. 3.1 Slab reinforcement details

50mm cubes and 50mm diameter cylinders were used to obtain the static compressive and tensile strength for the concrete used for the model specimens. Corresponding strengths for the full scale concrete were obtained from 100mm cubes and cylinders. The compressive stress-strain curves for both concretes at high rates of strain, were obtained from 50mm diameter cores.

3.1.2 Materials

3.1.2.1 Concrete

An attempt was made to produce concrete of similar mechanical characteristics for slabs of both scales. In order to do this the maximum size of aggregate used in full scale specimens was scaled 1:2.5. The same kind of cement, but different mix proportions were used.

Both kinds of concrete, microconcrete (used for the small specimens) and macroconcrete (used for the large specimens), were designed to achieve an early compressive strength of 40N/mm² so that testing of the specimens could be done at 7 days after casting.

Natural washed river sand was used with a nominal maximum particle size of 4mm and grading to zone 3, BS882. The sieve analysis was carried out according to BS410 and is given in Fig. 3.2. The sand was supplied by ARC-Concrete Ltd, .

The coarse aggregate used in this research was uncrushed river gravel with a maximum particle size of 10mm. The percentage of absorbed water in aggregates of both sizes was determined by using the Speedy Moisture equipment and it was found to vary between 1% and 2%. A sieve analysis for the gravel was also carried out and the results are given in Fig. 3.3. The gravel was supplied by ARC-Concrete Ltd.

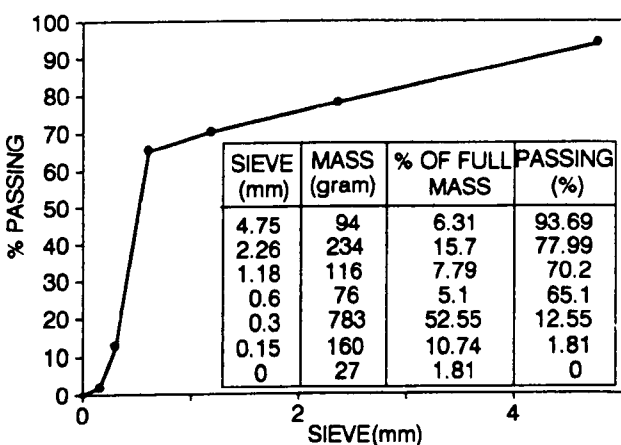


Fig. 3.2 Sand sieve analysis

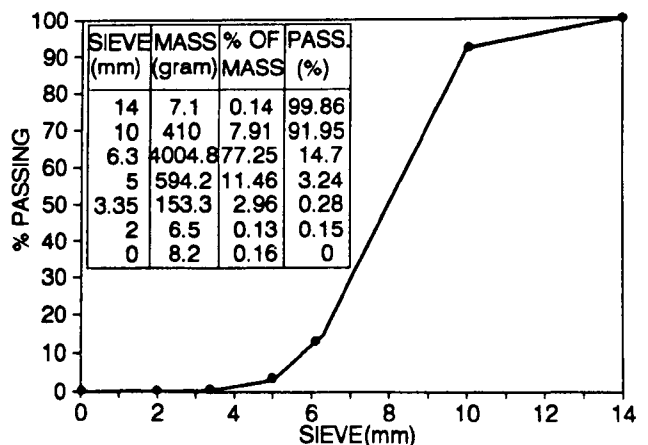


Fig. 3.3 Gravel sieve analysis

Ordinary grade rapid hardening Portland cement (RHPC) (made by the Blue Circle Group) was used in these concretes to give the early strength and shorter time of curing.

3.1.2.1.1 Microconcrete mix

This mix was used for the production of the small scale slabs and it contained the river sand as aggregate and none of the river gravel. The proportions by weight are given in Table 3.2.

	CEMENT	SAND	GRAVEL	WATER
MICROCONCRETE MIX	1	3	-	0.6
MACROCONCRETE MIX	1	2.28	3	0.6

Table 3.2 Mix proportions

The workability of the microconcrete mix was medium giving an average slump of 56mm and good compaction in the mould was easily reached. The average 7 days cube compressive strength (50mm x 50mm x 50mm) and cylinder tension strength (50mm dia x 100mm long) for microconcrete prepared with these mix proportions were 38.97 N/mm² and 4.20 N/mm² respectively. The control specimens were made and later tested in accordance with *BS1881* at the test age of the specimen cast from the same batch. The results are given in Table 3.4

Loading rates for static cube compressive and split cylinder tensile strength for this kind of specimen were 15N/mm²/min and 1.5N/mm²/min respectively.

Static compressive stress-strain relationships for the microconcrete have been obtained by testing 102mm diameter x 306mm long concrete cylinders in the ELE static loading rate cube crusher. Altogether three tests were conducted by using the concrete from the same mix. All three cylinders had the same kind of electrical resistance KYOWA 50mm long strain gauges which were bonded to the concrete using KYOWA CC-33A strain gauge cement. Typical results and test arrangements together with the ultimate stresses and strains for all three tests are shown in Fig. 3.4.

Static modulus of elasticity E, for the microconcrete was about 27kN/mm². The cylinder strength was found to be 75% of the cube compressive strength (taken from the 100mm cube) which is in the range of 70% to 90% given by ASTM.

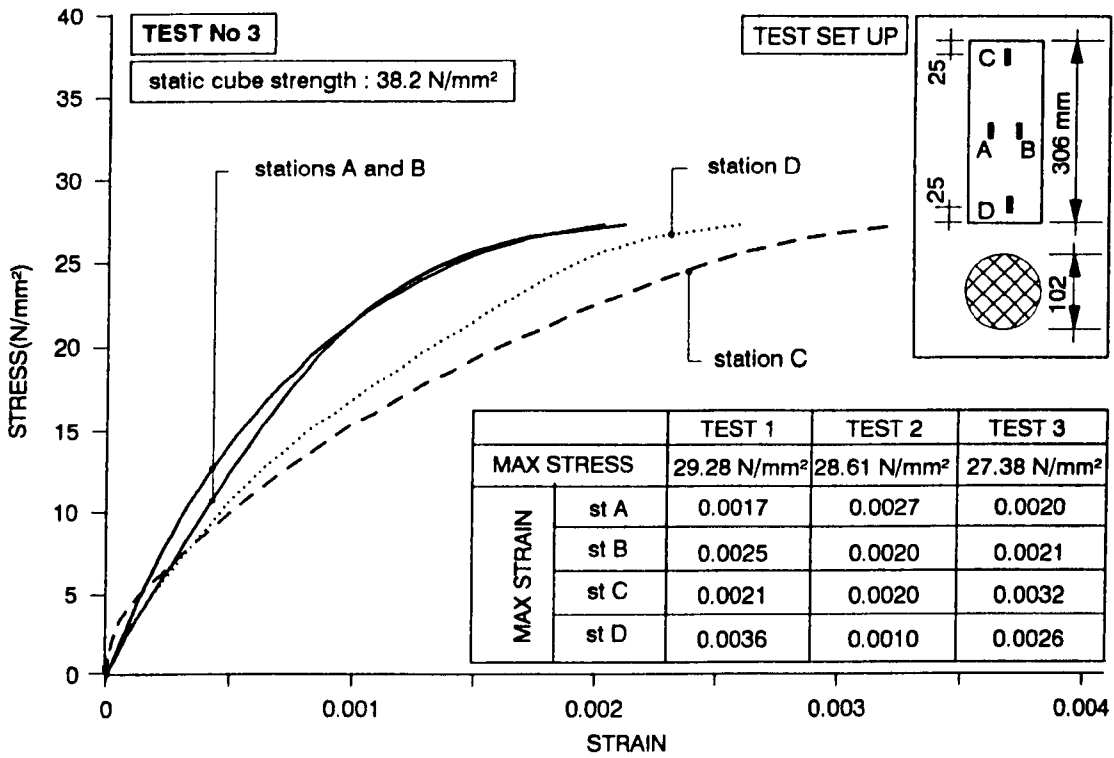


Fig. 3.4 Microconcrete stress-strain diagram

The stress-strain curves produced from these cylinder tests at so called static rates of strain, 10⁻⁶ strain/sec, can be compared with the stress-strain curves obtained from the split Hopkinson bar by testing the same kind of concrete but in this case under high strain rates of up to 2 x 10³ strain/sec which represents the behaviour of concrete in the main slab tests more accurately.

The apparatus used for the Hopkinson pressure bar tests has already been used in previous investigations and it consists of two 51.2mm diameter EN26 pressure bars suspended in a cradle of steel wires, Fig. 3.5. The strain gauge stations are located at two points, to measure the incident ϵ_I , reflected ϵ_R and transmitted ϵ_T strain pulses from which the stress strain relation was obtained for the 50mm dia concrete specimens. The relations between these pulses and concrete characteristics are:

$$\sigma_s = \frac{E \cdot A}{A_s} \cdot \epsilon_T, \quad \epsilon_s = -\frac{2C_o}{l_o} \int_0^{ld} \epsilon_R dt, \quad \text{and} \quad \dot{\epsilon}_s = -\frac{2C_o}{l_o} \cdot \epsilon_R$$

- where : σ_s - average stress in the specimen
 ϵ_s - average strain in the specimen
 E - Young's modulus for the steel
 A - cross-section area of the specimen
 C_o - longitudinal wave velocity in the steel
 l_o - length of the specimen

Specimens 50mm diameter x 16mm long (for the 1:1 scale concrete) and 50mm diameter x 10mm long (for the 2.5 scale concrete) were obtained from 450mm diameter x 125mm thick concrete discs by coring, slicing and surface grinding. This technique avoided the wall effect which would have been a significant feature of 50mm diameter cast cores. After initial trials an explosive charge of 45mm diameter and 3mm thick SX2 explosive, was chosen to produce the high rate of strain sufficient to produce failure of the concrete.

The specimen itself was obtained from concrete which was cured in the same manner as slabs. Eighteen specimens were tested from both microconcrete and macroconcrete mixes.

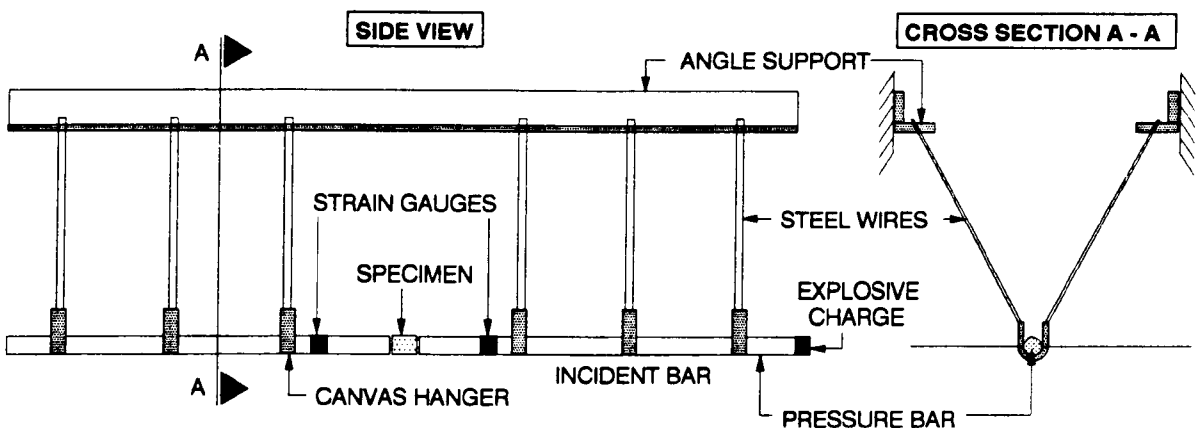


Fig. 3.5 Hopkinson Pressure Bar Test Rig

Dynamic modulus of elasticity E_d calculated from these results was about 22kN/mm^2 and the dynamic compressive strengths, strains at max stress and peak strain rates of the microconcrete at different ages are given in Table 3.3.

Typical results for these tests are shown in Fig. 3.6

1:2.5 SCALE CONCRETE				
AGE days	TEST	MAX STRESS N/mm ²	STRAIN AT MAX STRESS	MAX STRAIN RATE X 10 ³ Sec ⁻¹
11	1	103.21	0.0207	2.02
	2	114.56	0.0089	1.88
	3	110.81	0.0070	1.88
13	1	112.64	0.0056	2.23
	2	110.36	0.0291	2.17
	3	108.80	0.0098	2.13
15	1	142.73	0.0204	2.06
	2	127.86	0.0183	2.29
	3	129.43	0.0049	2.04

Table 3.3 Hopkinson pressure bar test results for small scale concrete

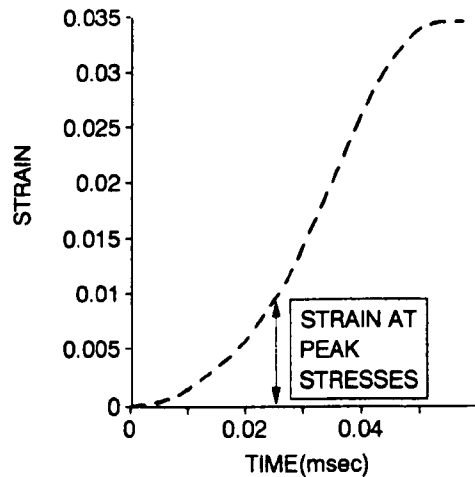
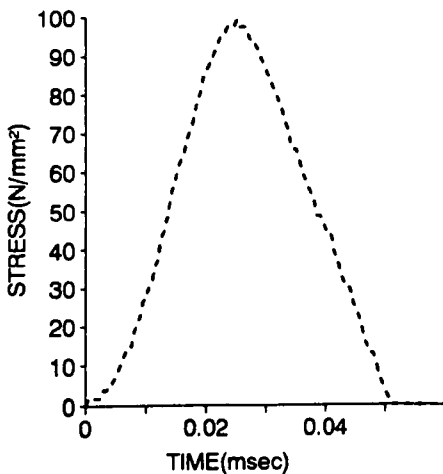
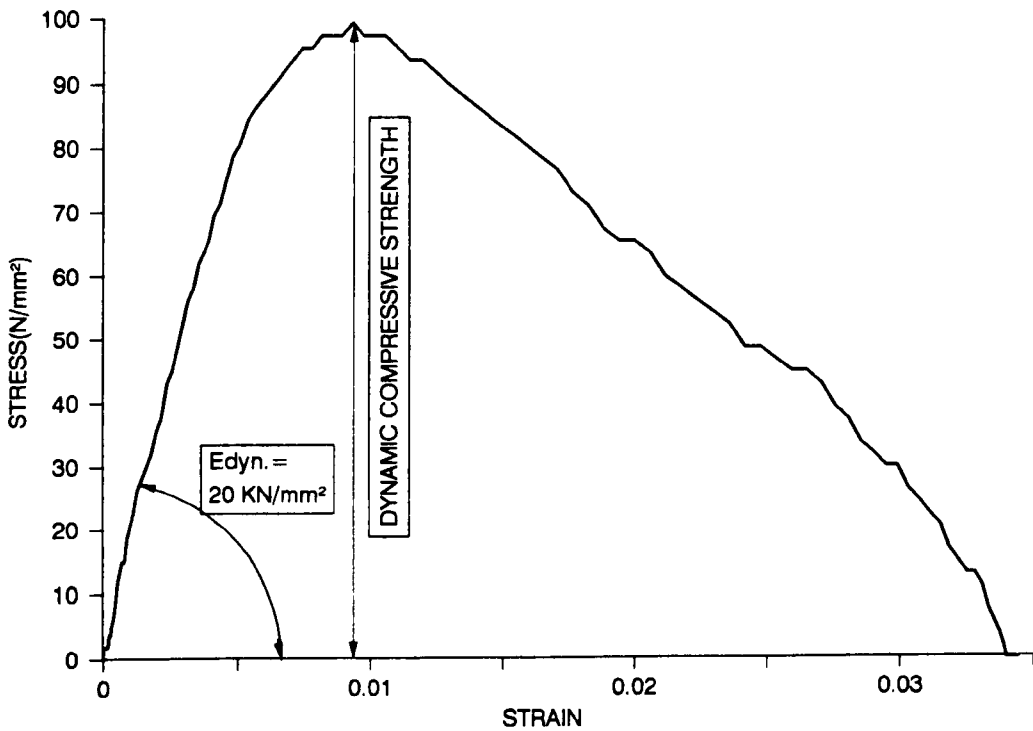


Fig. 3.6 Hopkinson pressure bar test results for microconcrete

3.1.2.1.2 Macroconcrete mix

This mix was used for the production of the large scale slabs and it contained both river sand and river gravel in the proportions by weight given in Table 3.2. The W/C ratio was again 0.6 and the aggregate/cement ratio was 5.28. These mix proportions reduce the creep and shrinkage effects in the concrete prior to testing. The workability was good and gave an average slump of 54mm. The average 7 days cube compressive strength (100mm x 100mm x 100mm) and split cylinder tensile strength (100mm dia x 200mm long) for these mix proportions were: 45.6N/mm² and 3.42 N/mm² respectively.

The compression machine used for the static testing of the cube and cylinder specimens was an ELE (Engineering Laboratory Equipment Ltd) cube crusher. The loading rates were inside the static range of 0.2 to 0.4 N/mm²sec and 0.02 to 0.04 N/mm²sec respectively, *BS1881, parts 116 and 117*.

The results for all of the tests are given in Table 3.4 and related to the small scale slabs, S1 - S19 (impact tests), SS1 to SS5 (static tests) and SE1 to SE19 (impulse tests), and to the large scale slabs, LS1 to LS5 (impact tests) and LSE1 to LSE5 (impulse tests).

TEST	S1/2	S3/4	S5/6	S7/8	S9/10	S11-13	S14-16	S17-19	SS1-2	SS3-5
COMP.STRENGTH (N/mm ²)	35.7	37.7	37.6	36.6	40.0	43.3	45.3	48.4	49.5	51.6
TENS.STRENGTH (N/mm ²)	3.90	4.12	4.33	4.02	4.03	4.58	4.88	4.62	4.08	4.33
TEST	SE1/2	SE3/4	SE5/6	SE7/8	SE9	SE10-12	SE13-15	SE16-18	SE19	-
COMP.STRENGTH (N/mm ²)	47.7	43.3	38.4	36.8	30.3	37.3	40.7	39.3	40.0	-
TENS.STRENGTH (N/mm ²)	4.55	3.69	4.12	4.41	3.0	3.52	4.65	5.05	4.03	-
TEST	LS1	LS2	LS3	LS4	LS5	LSE1	LSE2	LSE3	LSE4	LSE5
COMP.STRENGTH (N/mm ²)	47.8	46.8	56.0	43.9	41.9	45.0	45.3	39.1	38.7	36.4
TENS.STRENGTH (N/mm ²)	3.78	3.86	3.59	3.44	3.32	3.37	3.28	3.61	3.54	3.24

Table 3.4 Control specimen test results

Macroconcrete has also been tested in the Hopkinson Pressure bar arrangements (Fig. 3.5) and typical stress-strain trace together with the corresponding stress-time, strain-time, and strain rate-time results are presented in Fig. 3.7.

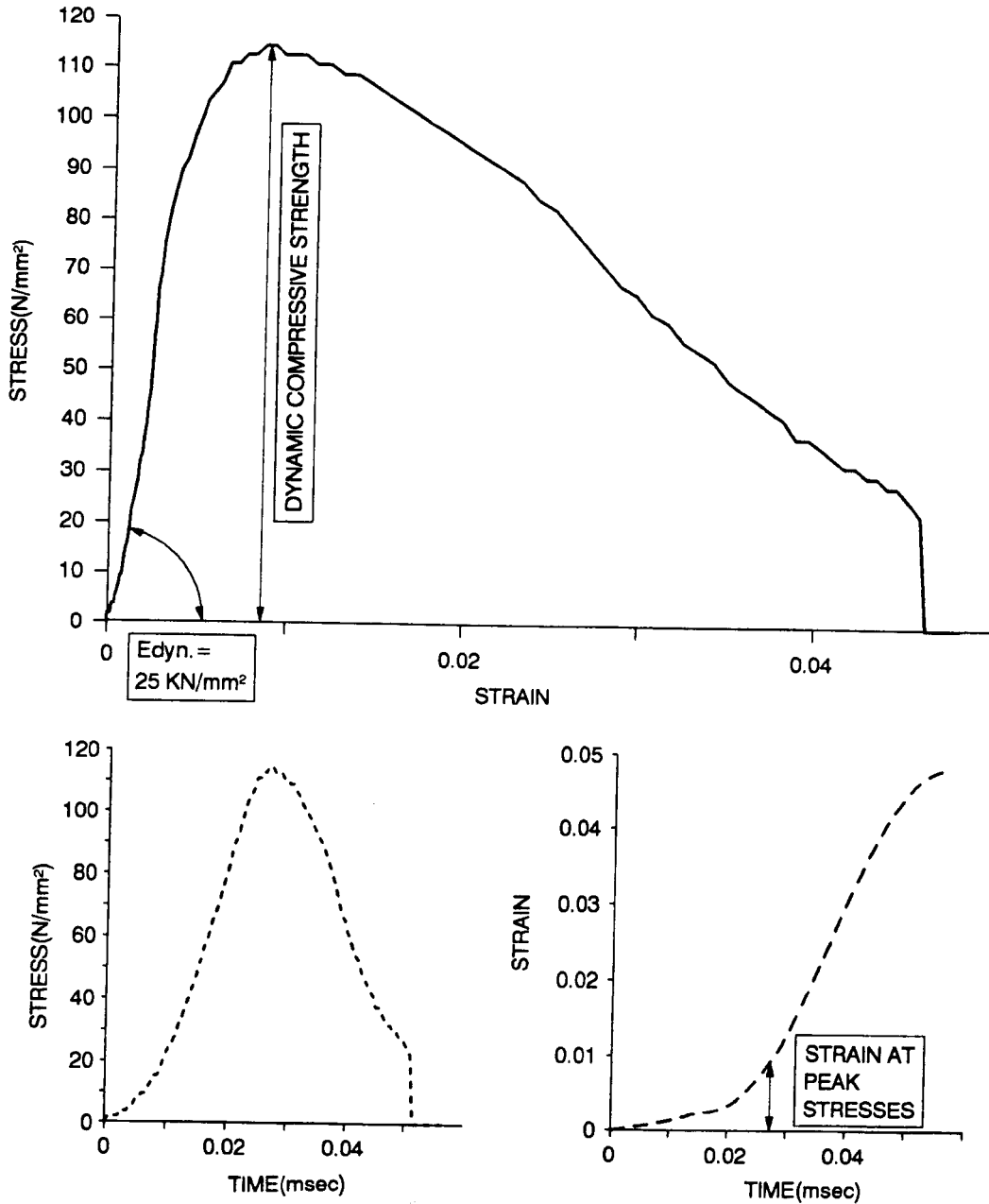


Fig. 3.7 Hopkinson pressure bar test results for macroconcrete

Maximum dynamic compressive stresses, corresponding strains and ultimate strain rates for the macroconcrete of different ages are given in Table 3.5.

1:1 SCALE CONCRETE				
AGE days	TEST	MAX STRESS N/mm ²	STRAIN AT MAX STRESS	MAX STRAIN RATE X 10 ³ Sec ⁻¹
8	1	99.30	0.0093	1.20
	2	97.74	0.0081	1.21
	3	90.36	0.0072	1.13
10	1	91.87	0.0121	1.46
	2	103.13	0.0106	1.33
	3	114.29	0.0143	1.31
14	1	95.7	0.0132	1.33
	2	95.55	0.0075	1.40

Table 3.5 Hopkinson pressure bar test results for the macroconcrete

In the case where the loads are rapidly applied to a limited area of the reinforced concrete slabs, there is an increase in compressive strength of concrete due to the speed of loading, and a further increase in compressive strength which can be associated with the confinement effect of the neighbouring areas of concrete. Additional tests on macroconcrete in confined conditions were performed in which six confined concrete cylinders were statically tested. The arrangement is shown in Fig. 3.8.

STEEL TUBE LENGTH:

150mm (TEST 1-3)
300mm (TEST 4-6)

OUTSIDE DIAMETER: 101.6mm

WALL THICKNESS: 12.7mm

INSIDE DIAMETER: 76.2mm

STRAIN GAUGE FACTOR: 2.15

STRAIN GAUGE RESISTANCE: 119.8ohms

STRAIN GAUGE LENGTH: 30mm

SINGLE ARM WHEATSTONE BRIDGE

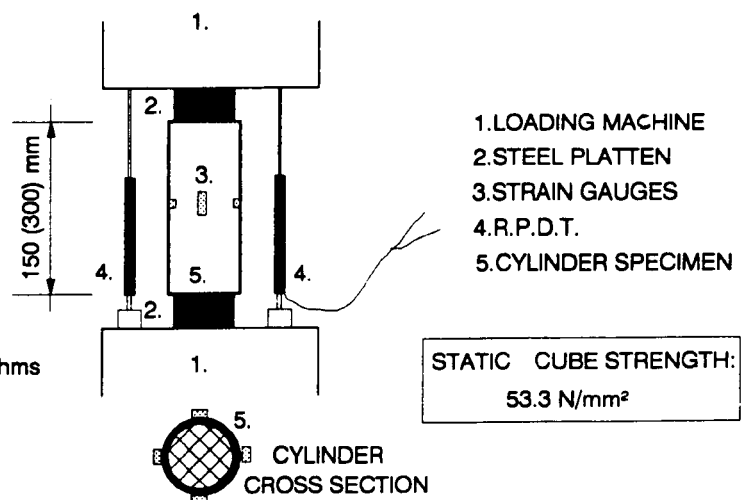


Fig. 3.8 Confined concrete test arrangement

Confinement was provided by a high yield steel tube with wall thickness 12.75mm and inner diameter, 101.6mm. Three cylinders were 150mm long and three were 300mm long. The load was applied by an Amsler loading machine of maximum capacity 2000kN and loads of up to 1950kN were produced.

The strain in the steel tube was recorded both axially and circumferentially by ERSG's. The movement of concrete inside the steel tube was measured by LVDTs attached to the upper and lower machine faces. Since the length of the steel tube was equal to the length of the concrete specimen the load had to be applied through specially made platens placed on both ends of the specimen, with diameter 1mm smaller than the inner diameter of the tube, Fig. 3.8. Strain in the platens was deducted from the overall strain obtained from the displacement record to give real strain in the concrete cylinder. Typical stress-strain curves obtained in the test are shown in Fig. 3.9.

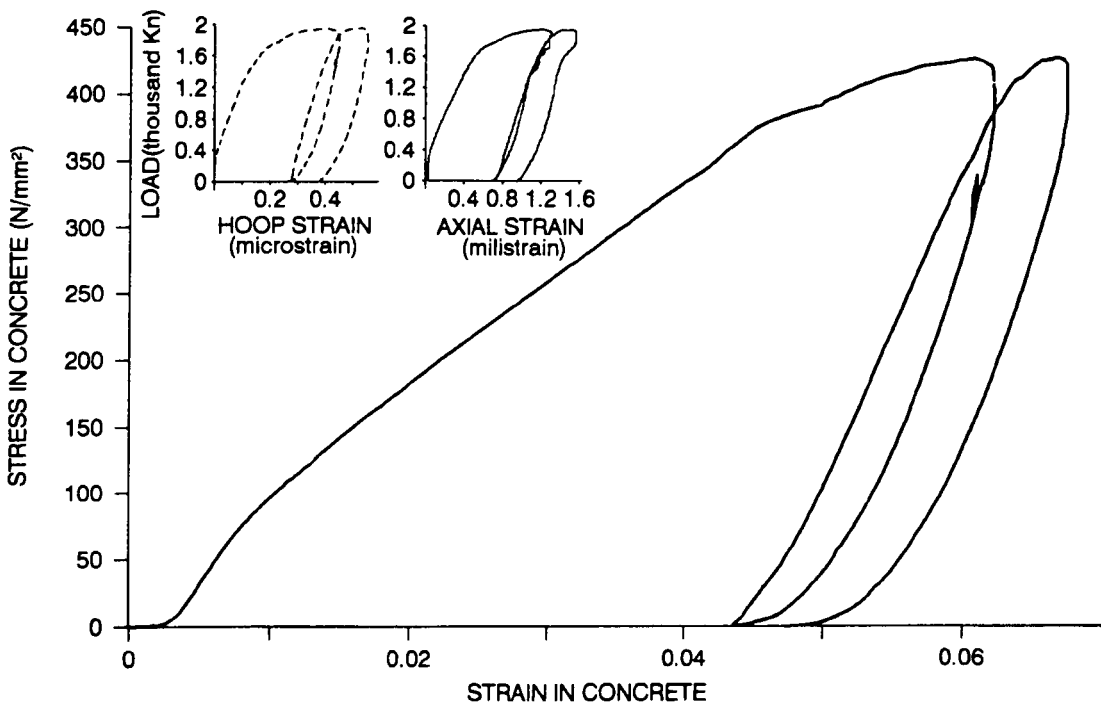


Fig. 3.9 Confined concrete test results

3.1.2.2 Steel Reinforcement

Two main types of reinforcement were used: H.Y. steel reinforcement bars, later used to produce reinforcement meshes, and ready made welded reinforcement meshes. A constant percentage of reinforcement in the small and large specimens, which is one of the main modelling requirements, could have been achieved if the bar spacing and diameter were both scaled down by the 2.5 scale factor. That requirement was almost fulfilled in the slabs using reinforcement bars (16mm bars large scale and 6mm bars small scale tests, H.Y. steel grade 460 in both cases, and scaled spacing) but in the case of the welded reinforcement meshes it was not possible because the

necessary bar size and spacing of the mesh that would be used for the small scale specimens was not available in widely used H.Y. grade 460N/mm² steel. So for the large slabs *BS4483*, A393 H.Y characteristic strength 460N/mm² reinforcement mesh (bar size 10mm and spacing 200mm x 200mm) was used, but for the small size slabs the reinforcement mesh with bar spacing and steel characteristics closest to that required, H.Y. 460N/mm², bar size 2.5mm and spacing of 80mm x 80mm reinforcement mesh, was Heavy Twilweld self coloured 600N/mm² mesh with the bar diameter of 3.15mm and bar spacing of 76.2mm x 76.2mm. This mesh had a tensile capacity of about 113% of that required for the model slab whilst very importantly, the bar spacing was kept at about 95% of that required.

3.1.2.2.1 High Yield grade 460 deformed reinforcement bars

These bars were used in the production of reinforcement meshes for some of the small and large scale slabs (S1-8, SE1-9, LS1-2 and LSE1-2). The nominal stress at yield for this type of reinforcement is $f_y = 460\text{N/mm}^2$ and the same was obtained in the test. The typical stress-strain curves were obtained by testing the samples in the existing Amsler loading machine and they are presented in Fig. 3.10

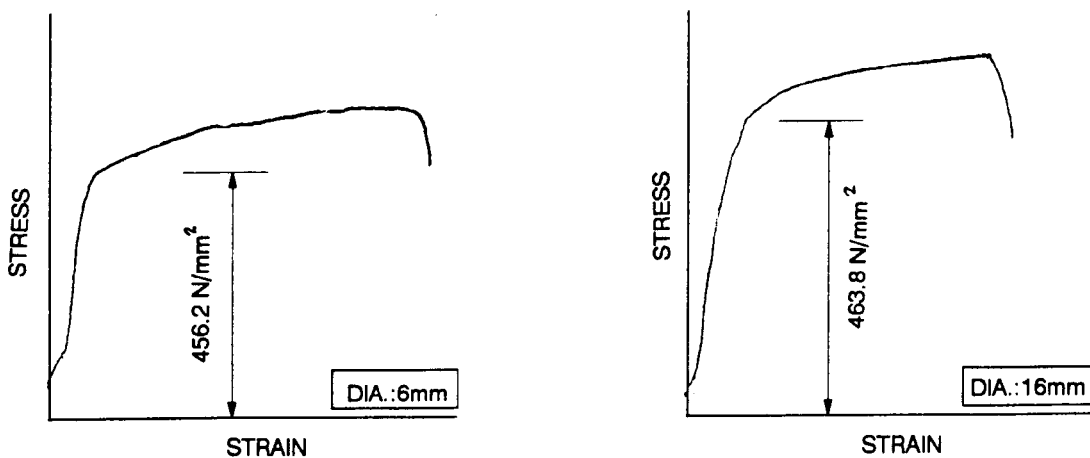


Fig. 3.10 H.Y. steel reinforcement bar stress - strain curve

3.1.2.2.2 H.Y. BS4483 square reinforcement mesh

Ready made meshes were found to be much easier to use than built up meshes using reinforcing bars. So for some of the large scale slabs (LSE3-5 and LS3-5) BS4483 A393 square

meshes of 10mm diameter plain bars with 200mm x 200mm bar spacing were used. They were produced by Allied Reinforcement - Sheffield from cold drawn wire complying with BS4482 with a characteristic strength not less than 460N/mm². We found that the yield tensile strength was $f_y = 550\text{N/mm}^2$ and modulus of elasticity was $E_s = 220\text{N/mm}^2$. A typical stress-strain curve obtained by testing a 300mm long piece of the mesh is given in Fig. 3.11.

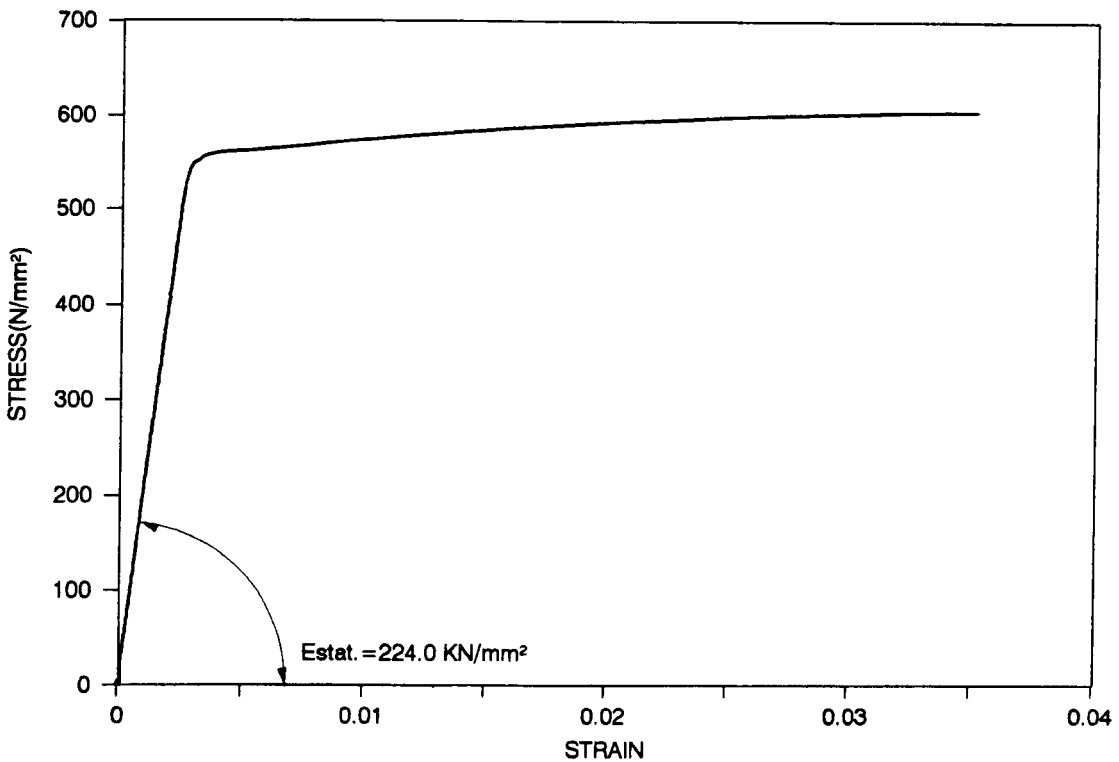


Fig. 3.11 Stress-strain curve for the BS4483 A393 reinforcement mesh

3.1.2.2.3 Heavy Twilweld reinforcement mesh

These meshes were produced by Rigby Wireworks and Co - Sheffield and were used in the production of small slabs S9 -19 and SE10 - 19. The bar diameter was given by the manufacturer as 10 gauge (3.15mm) while the spacing was 76.2mm x 76.2mm. The stress-strain curves were again obtained by testing about a 300mm long piece of mesh in the static Amsler loading machine. As in previous cases the bar was equipped with the KYOWA type 5mm long, foil type, strain gauges connected into a quarter bridge Wheatstone circuit in the same way as in the main slab tests.

A typical stress-strain trace is given in Fig. 3.12.

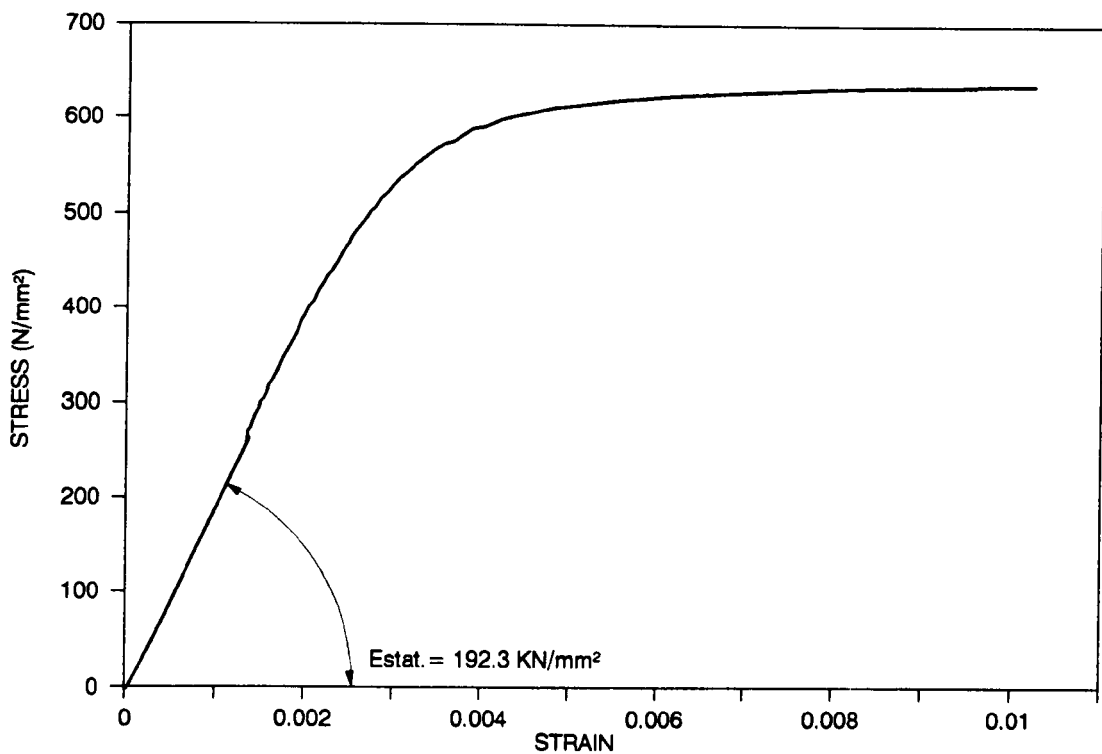


Fig. 3.12 Stress-strain curve for the Heavy Twilweld reinforcement mesh

3.1.3 Fabrication of the specimen

In all phases of the fabrication of the specimen due care was taken to provide specimens of consistent mechanical and physical characteristics. To achieve that uniformity certain steps and procedures were followed and they are described on the following pages.

3.1.3.1 Reinforcement mesh

For the specimens of both sizes, two different methods were used, to fabricate the reinforcement meshes. These were, individual high yield steel reinforcement bars, and already made welded reinforcement meshes. In the case when the individual H.Y. steel bars were used the following procedures were followed:

Steel bars were bought in 6m lengths and prior to being used were first brushed and visually inspected and then cut into 1m lengths using an available steel cutter. Both ends of the bar were then bent to 90° using an existing bar bender and the excessive lengths of the bar ends were cut before the bars were used to produce reinforcement meshes. The required number of lower layer bars was supported by the wooden holders and the positions for the bars of the

opposite directions were marked. The reinforcement meshes were then formed by tying orthogonal bars with wire of 0.75 dia and 1.5mm dia for the small and large scale specimens, respectively.

In all cases when two layers of mesh were used (tensile zone and compressive zone reinforcement) the necessary vertical spacing between them was provided by wire spacers that kept both meshes at the required distance from each other.

In the final phase of the work when only lightly reinforced sections were used, it was decided to use ready-made welded reinforcement meshes. They were provided in sheets of 2.44 x 1.22m for the small scale slabs and 4.8 x 2.4m for the large scale slabs. Both types were then cut into the right size in such a way that the central bars of the mesh ran through the centre of the slab. These meshes did not have the ends of the bars bent but the vertical spacing between them was again provided using wire spacers.

It is worth pointing out that with both types of mesh, their overall size was determined by allowing side concrete cover identical to that for the faces of the slab, i.e. 4mm and 10mm for small and large specimens respectively.

3.1.3.2 Preparation of moulds

Test specimens were cast in specially designed steel moulds. They were cast in sets of two or three for the small scale specimens and one for the large specimens. Before pouring the concrete, the mould was properly cleaned from the previous casting, carefully assembled and then a thin film of mould oil was applied on the internal surface of the mould, so that the specimen could be moved out of the mould more easily. One of the small size moulds used in the research is shown in Fig. 3.13 and Plate 3.1. The same procedure was followed for preparation of the moulds for the control specimens.

Reinforcement mesh was then placed into the mould and fixed to the mould by using thin wire which would not later prevent easy demoulding.

The minimum concrete cover, 4mm for the small specimens and 10mm for the large specimens, was provided by attaching steel spacers to the bottom bars. The top cover was again checked once the cage was fixed into the mould.

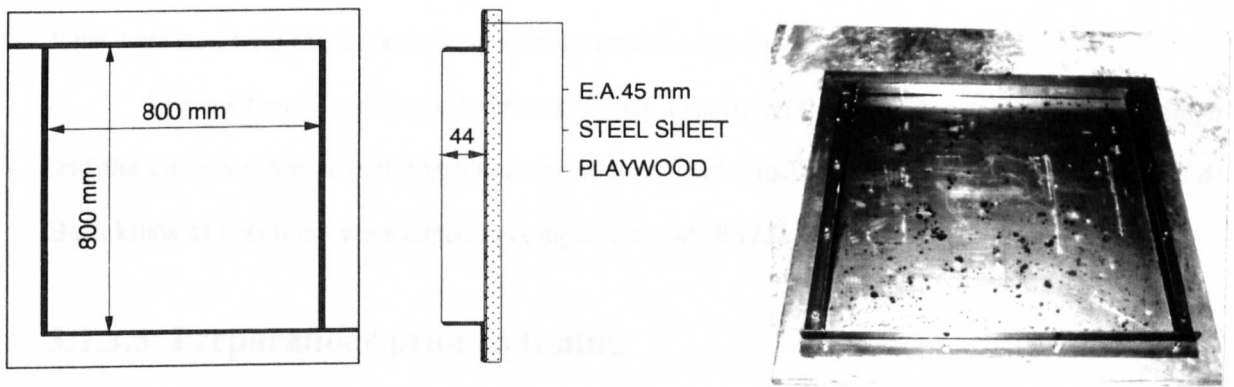


Fig. 3.13 and Plate 3.1 Slab mould

3.1.3.3 Concrete mixing, casting and curing

Both coarse and fine aggregates were poured into the mixer and mixed dry for 2 minutes. Then the cement was added and mixed dry with the aggregates for another 2 minutes. About half the required amount of water was then poured in and whilst mixing, the rest of the water was gradually added. During the mixing a small amount of hand mixing was used to ensure no pockets of dry materials remained. The contents were then mixed for a few minutes until a good mix was visible.

A non-tilting electrical mixer, capacity 0.25m^3 was used for both types of concrete.

The concrete was cast in the moulds in two layers, and each layer was vibrated with the vibrating poker until no air bubbles appeared on the concrete surface.

An hour after casting, the specimens were finally smooth finished by hand trowelling, covered with polythene sheets and left for 24 hours. For the next six days they were left under damp sacking and polythene sheets in an effort to secure almost 100% R.H. The average temperature in the room was $12 \pm 5^\circ\text{C}$.

3.1.3.4 Control specimen

In order to monitor the consistency and characteristics of the concrete that was used for the manufacturing of the slabs, it was necessary to cast additional cube and cylinder control specimens together with the main specimens. For the small scale slabs (microconcrete) there were

three concrete cubes of 50mm sides and three concrete cylinders of 50mm diameter x 100mm long. Three cubes of 100mm sides together with three cylinders of 100mm diameter x 200mm long were cast with the large scale specimens (macroconcrete).

These strength specimens were tested later, usually on the same day as the main specimen and the cube compressive strength and cylinder indirect tensile strengths are given in Table 3.4. Both kinds of specimen were tested in compliance with *BS1881*.

3.1.3.5 Preparations prior to testing

Prior to testing every slab specimen was painted white and then grid lines were drawn so that cracks could be more easily observed and mapped later. In the case of the small slabs the grid size was 36mm x 36mm whilst for the large slabs it was 90mm x 90mm and for both of them lines were marked starting from the central line of the slab.

3.2 Test instrumentation

3.2.1 Displacement transducers

The main type of displacement transducers used for the dynamic testing were Penny and Giles' Hybrid Track Rectilinear Potentiometers. These consist of two basic part, a moving stroke on which a two-part conductive plastic wiper is attached whose linear movement across the second main part, a resistive track of infinite resolution, is directly proportional to the voltage difference in the output of the two. In the case of our tests the rectilinear potentiometer displacement transducers, RPDT's, were powered by 10 volt DC and produced good results. Special mountings were provided on both ends of the transducer so enabling good connection between the stiff steel RPDT holder and the specimen itself.

A 3D-cross section of the transducer is given in Fig. 3.14 and typical static calibration traces together with some results are shown in Fig. 3.15. All transducers used in the tests were statically calibrated with the same electrical connections as in the dynamic tests. The RPDT static calibration rig consisted of a micrometer screw gauge and a dial gauge that together with the

Digital Voltage Meter gave the relation between the voltage output and the displacement of the RPDT's stroke.

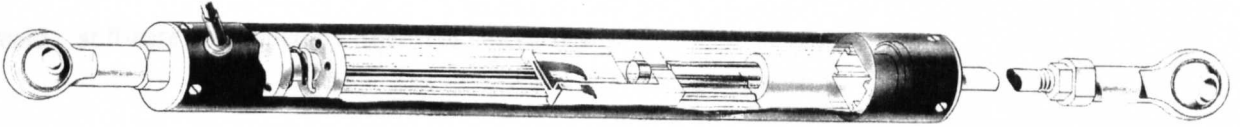


Fig. 3.14 Displacement transducer

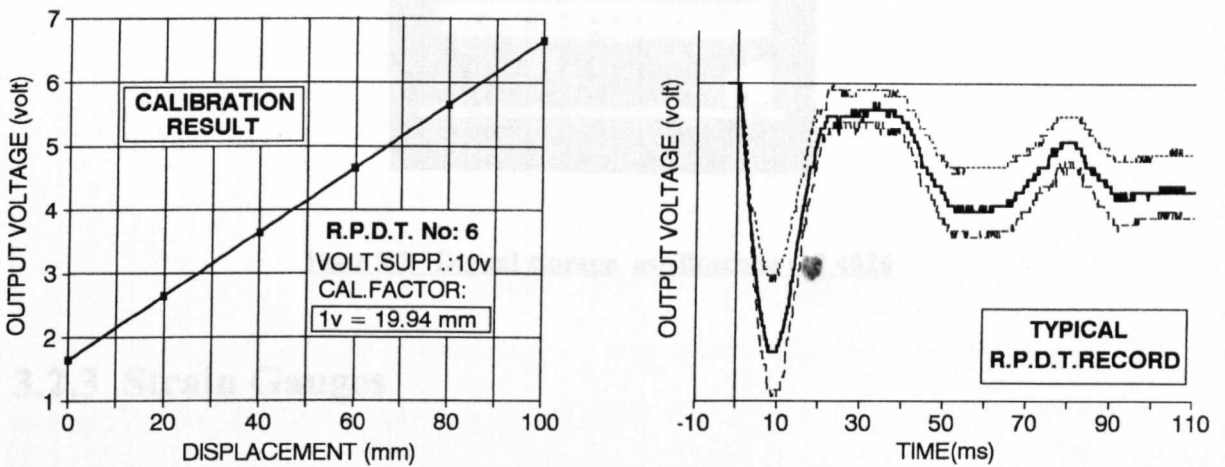


Fig. 3.15 Displacement transducer test results

3.2.2 Digital Storage Oscilloscopes

These were used in all dynamic tests to record and temporarily store the outputs from the transducer measuring devices, i.e. electrical resistance strain gauges, RPDTs, opto switches and pressure gauges before transfer to the personal computer. Five different kinds of oscilloscopes were used, and the "GOULD" digital storage oscilloscope OS 4020 (Plate 3.2) will be taken as a typical example. The OS 4020 is a high speed dual channel storage system in which each channel stores 2047 data points. It can be set for sensitivities from 5mv/cm to 20v/cm vertical resolution and capture rate of 200 μ s/cm to 0.50s/cm of screen so covering any event lasting from 2ms to 5 sec at a frequency of up to 1MHz. Both channels are synchronised on the same time base.

Triggering to start recording can be done externally or by the pulse from the event itself with pretrigger varying from 25% to 100% of the record in 25% steps. The system offers post storage expansion of up to 50 times.

After capturing the event on the oscilloscope it was later transferred to the computer by using software developed by Sheffield University.

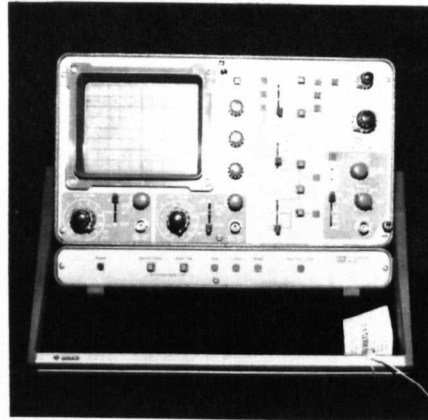


Plate 3.2 Digital storage oscilloscope OS 4020

3.2.3 Strain Gauges

Electrical resistance strain gauges were used to measure the tensile strain in the reinforcement and pressure bars (load cells) in the static and dynamic tests and to obtain static stress-strain relations for the materials used in the slabs. The principle of the operation is that the change in electrical resistance caused by elongation of the specimen due to stresses, is measured.

Since:

$$R = \frac{S \cdot L}{A}$$

where: R - electrical resistance

L - length of wire

S - specific resistance

A - cross-sectional area

then:
$$\frac{\Delta R}{R} = K \cdot \frac{\Delta L}{L}$$

where : K - the gauge factor (2 to 2.2)

The strain gauge length is very important because the strain recorded is the average strain over its length (Fig.3.16). Generally, the shorter the strain gauge the better.

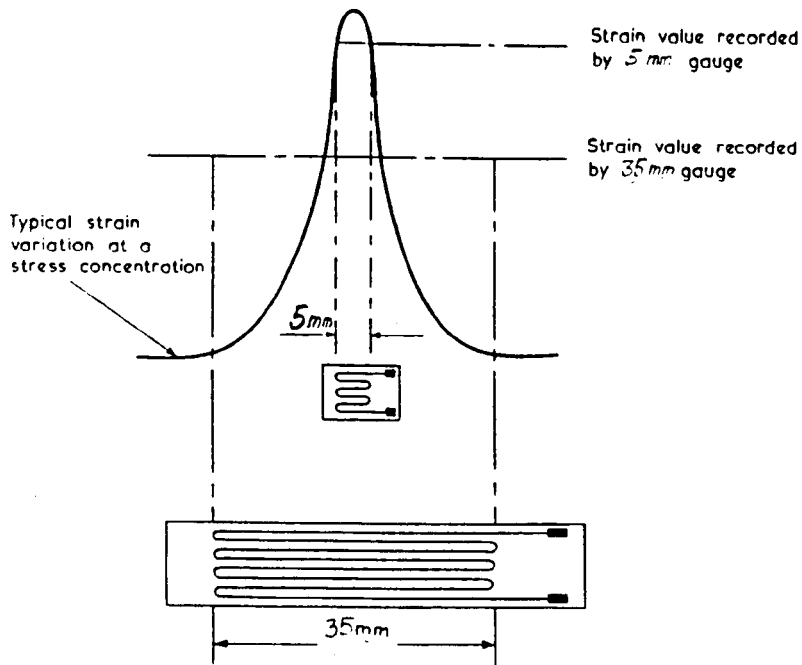


Fig. 3.16 Effect of using too long strain gauge

The efficient attaching of strain gauges is vital because all further measurements are very dependent on the quality of installation and protection from the moisture. For all our tests it was done as follows:

- (a) The reinforcement was cleaned to remove any rust, scale and grease and the surface was given a smooth finish.
- (b) The position for the gauge was marked.
- (c) The KYOWA CC-33A strain gauge cement was applied to the back of the gauge and then positioned carefully.
- (d) Pressure was then applied to the gauge through a thin polythene sheet.
- (e) The wires from the gauges were connected via terminals to the main twin pair insulated and shielded signal cables.
- (f) After checking their resistance the gauges were moisture sealed using polyurethane varnish and then covered with adhesive lined heat shrink sleeving.

For our tests we used "KYOWA" foil type strain gauges and terminals with the typical gauge characteristics being 120 Ω resistance, 5mm and 30mm long and gauge factors $K = 2.15$ or 2.08 .

3.2.4 DC - Bridge Amplifier - FE359 - TA

Fylde type DC - Bridge amplifiers (Plate 3.3) were used to power and amplify the outputs from the electrical resistance strain gauge Wheatstone bridge circuits employed on load cells, pressure gauges and reinforcement bars and so eliminate or reduce disruptions in the output signal caused by the noise produced by damp and radio interference. Analogue voltage signals can be amplified up to 10000 times to give up to 10v full scale output. The control facilities consist of amplification voltage controls (up to 10mv, 100mv, and 1V), bridge balancing controls (coarse and fine balancing), calibration controls and input voltage controls. Each amplifier is connected to one channel of a storage oscilloscope. In our case the amplification of the signal varied from 250 for circuits on reinforcing bars to 2500 times for some of the pressure gauge measurements. Circuits were powered from 4 to 10 volts DC.

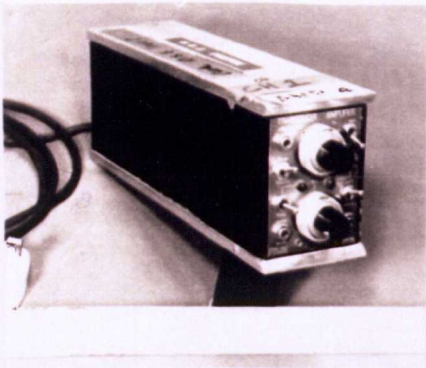


Plate 3.3 FILDE DC - Bridge Amplifier

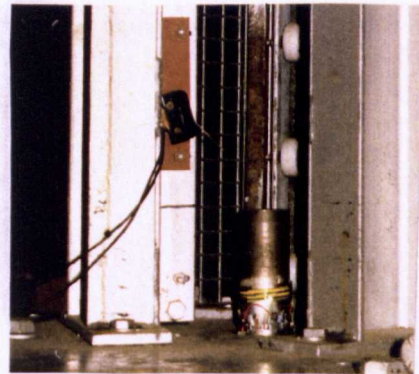


Plate 3.4 Microswitch

3.2.5 Microswitches

Long lever microswitches (Plate 3.4) were initially used on the small scale impact rig to trigger the timer for velocity measurements and the flash gun to mark the beginning of impact on the high speed film. It had a maximum travel of 2.79mm and maximum distance between triggering points of 1.27mm which made the maximum velocity error 0.13m/s or 2.3% of the average velocity obtained in the tests.

3.2.6 Slotted Opto-Switches

The infra red light opto switches (Plate 3.5) were used to measure more precisely the velocity of the drop hammer in both small and large scale impact tests. Both major parts, the infra-red source and the sensor, were housed in a slotted plastic mounting. When the trigger blade passes through the slot it produces a sharp edged signal from which velocities were later taken. This system proved to be much more precise than the microswitches, because the point where it triggers is constant. The circuits were usually powered with 5 volts DC and each system contained two sets of emitters and sensors so giving, for certain sizes of passing blade, four independent results.

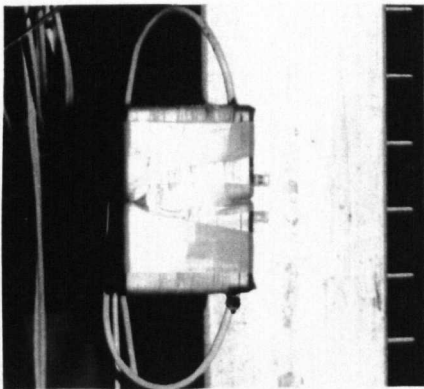


Plate 3.5 Slotted opto switch

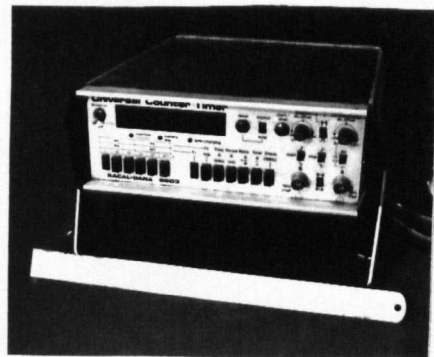


Plate 3.6 Universal counter timer 9903

3.2.7 Universal Counter Timer 9903

The counter timer (Plate 3.6) was initially used to measure the hammer velocities for the small scale impact tests. It has a frequency range from 10 to 50MHz and screen format of seven digits in-line. Any time interval from 100nsec to 28 hours can be measured by selecting appropriate range unit. In our case it measured time intervals of about 20msec (which later gave us the average velocity between two triggering points). The timer itself was triggered by two microswitches the first of which starts the timer and the second stops it. The time was then simply read from the screen.

3.2.8 D.C. Power Supply

D.C. bench power supplies (Plate 3.7) were mainly used to supply a constant DC voltage to the displacement transducers. The coarse and fine controls allow output voltage to be varied between zero and maximum voltage (20 or 30 volts D.C.). The supply stability is about 10,000 times better than the stability of the ordinary mains supply. In most of the cases displacement transducers used a 10V supply.

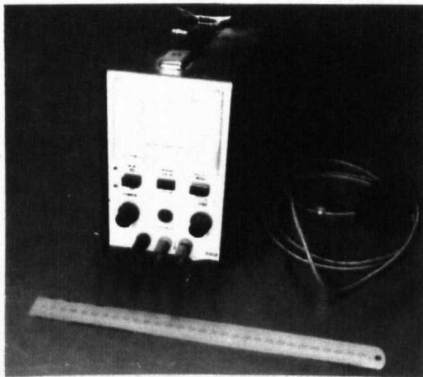


Plate 3.7 D.C. Bench Power Supply

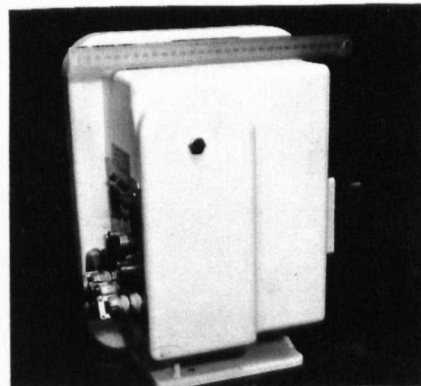


Plate 3.8 Photec IV - High Speed Camera

3.2.9 Photec IV - 16mm High Speed Camera

A rotating prism high speed camera, Plate 3.8, was used to film the damage on some of the small scale impact and impulse tests. When recording in full frame mode the speed can vary from 100 to 10,000 pictures per second (pps) but half frame and quarter frame shutters are also available and these increase the speed by two and four times respectively. The camera can accommodate from 30 to 150m of 16mm film. Very importantly the camera has an internal lighting source that marks the edge of the film with a mark at every millisecond. Two cables are provided with the camera. The Y-cord is used to connect the camera to the event - synchroniser and the remote cord is used for starting the camera. The event-synchroniser can be set to start an electrically controlled event, a blast or impact in our case, at any preselected point on the film. It was powered by a 15 volt 2A DC power supply and the amount of film set to pass before

triggering the event is set on the control panel of the camera. Illumination of the specimen becomes of major importance when the camera runs in the fastest mode so we used 8000W of light positioned very close to the specimen.

In our case a half frame shutter was used so framing rates of up to 10,000 half frames per second were used to record the events. Ilford 400ASA HP5-plus Type 782, 30.5m long 16mm wide high speed films produced images of very high quality. After processing, the high speed films were analysed with the Vanguard instrumentation motion analyser projector which allows the freezing of single frames and up to 15 times enlargement of the picture and can run the film at variable speed.

3.2.10 Reynolds FS-10 Firing System

The firing system, Plate 3.9, was used to generate and deliver an electrical pulse to fire the detonator and thus the charge itself. It consists of a control unit, which provides low charging voltage to the firing module and ensures a safe and reliable operation, and a firing module, which provides an input voltage of 3000 volts to the detonator lasting for about 0.2 μ sec. Peak output current is about 1000 Amps.

All the charges were initiated by the L2A1 detonators which had operational time of about 50 μ sec.

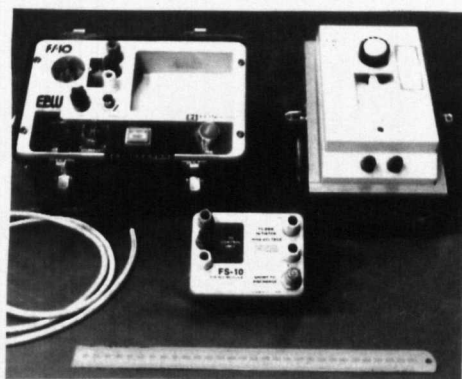


Plate 3.9 F.S.10 - Firing System

3.2.11 Kulite Pressure Transducer - HKM-375-1000

Kulite miniature pressure transducers of two different types were used for all explosion overpressure measurement. They are both made as fully active four arm Wheatstone bridges that utilise either a metal (Kulite HKM-375-1,000) or a silicon (Kulite HKS-375-15,000) diaphragm that deforms under the blast pressure and has a piezo resistive sensor as its sensing element. Both were of a sealed type operational mode with rated pressures of 68.95 bar and 1034.25 bar respectively. The natural frequency of the metal diaphragm was 275kHz and of the silicon diaphragm was 700kHz. This were both very satisfactory. The sampling rates used were up to 1MHz. They were both usually powered with 5V DC and infinite resolution output signals were later amplified from 100 to 2500 times. As can be seen from Plate 3.10, 9.5mm thread allows very easy installation of the gauge and on all occasions they were mounted in steel holders facing the blast wave.

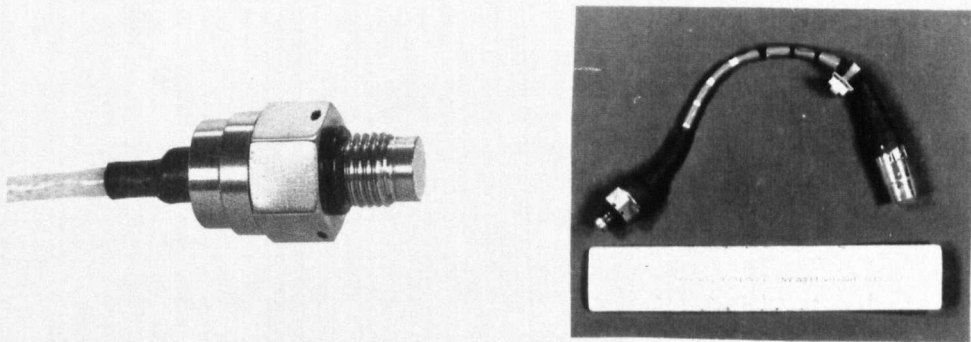
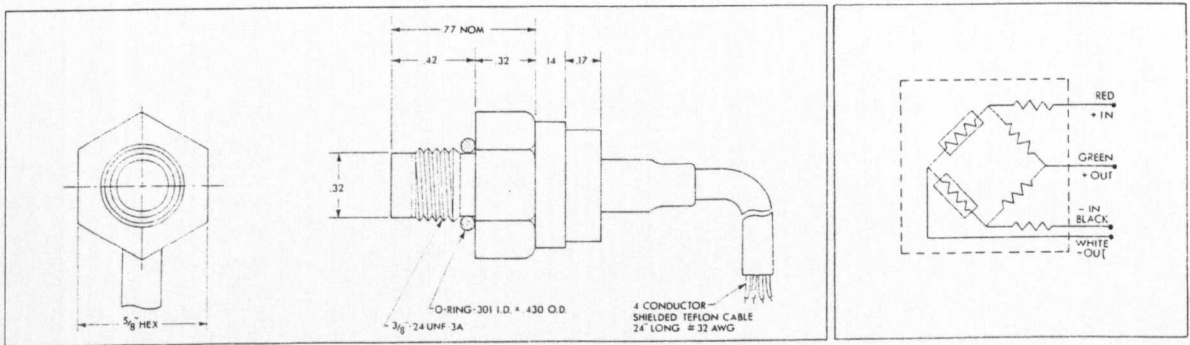


Plate 3.10 HKM-375-1000-Kulite pressure transducer

Both gauges, were supplied with the calibration factors, but were also statically calibrated and typical results are given in Fig. 3.17.

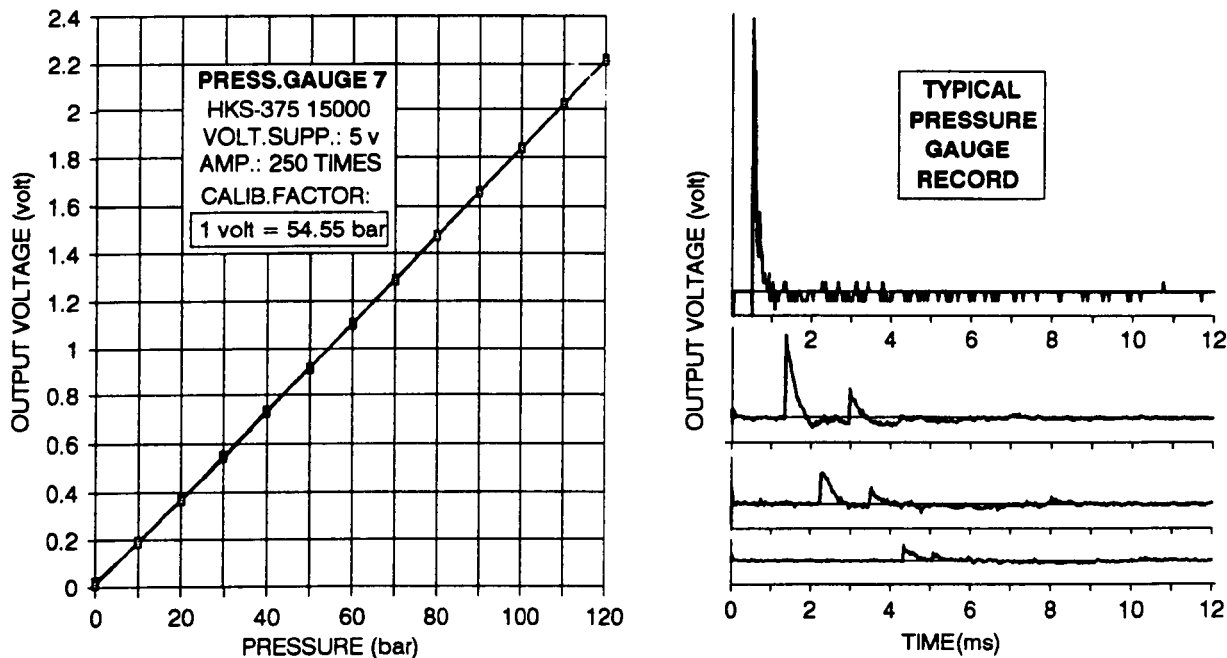


Fig. 3.17 Pressure gauge calibration and test results

The gauge with the metal diaphragm produced much better and more consistent results and some of the typical traces are shown in Fig. 3.17.

3.2.12 Hycam - K 2001 R - 16 mm High Speed Camera

This camera, Plate 3.11, was used in the initial phase of the work for filming the small scale specimens under impact load. It had a film capacity of about 30m and a variable frame rate of 100 to 8500 full frame pictures per second (pps). The camera allowed event synchronisation and the event synchroniser itself provided the triggering of the major event to occur at a preselected point on the film. The frame rate was controlled by varying the input voltage to the camera motor by a variable transformer. The timing light was set to give 1,000 marks on the film per second in order to confirm the set framing rate.

In our case the camera was set for about 4,000 pps (voltage 110-150V) and illumination was provided by 2,000W cine lights which were placed at about 400mm from the specimen.



Plate 3.11 16mm HYCAM camera

3.3 Test arrangements

3.3.1 Support conditions

Most of the specimens tested in these investigations had supports that can be classified as fully fixed supports but in the initial phase of the research some tests on the small scale specimens were performed on supports which were free to rotate, but on which all vertical lifting and sliding of two edges of the slab was prevented. Also during the testing programme it was observed that the formation of the shear plug in the central region of the specimen had a great influence on the behaviour of the slabs so it was felt useful to do some tests in which that shear plug region would be predefined by placing an additional set of inner supports and consequently some of the small scale specimens were tested in that way, Fig. 3.19.

The widely accepted scaling principles require the support condition for the large scale specimens to be an enlarged version (in our case 2.5 linear scaling factor) of the small size supports and this rule was followed.

3.3.1.1 Free supports

This type of support was used in the initial phase of the research when testing the small slabs S1 to S8, S17 and S18 (impact tests) and for SE1 to SE4 (impulse tests). As can be seen

from Fig. 3.18 this kind of support prevents the ends of the specimen from moving vertically in either direction but allows a certain degree of rotation on all four edges out of which two had a freedom of horizontal movement in both directions on rollers. The other two edges were placed on unmovable rollers welded to the frame. In the case of the explosive tests it was felt necessary to remove the top face rollers and replace them with rubber pads.

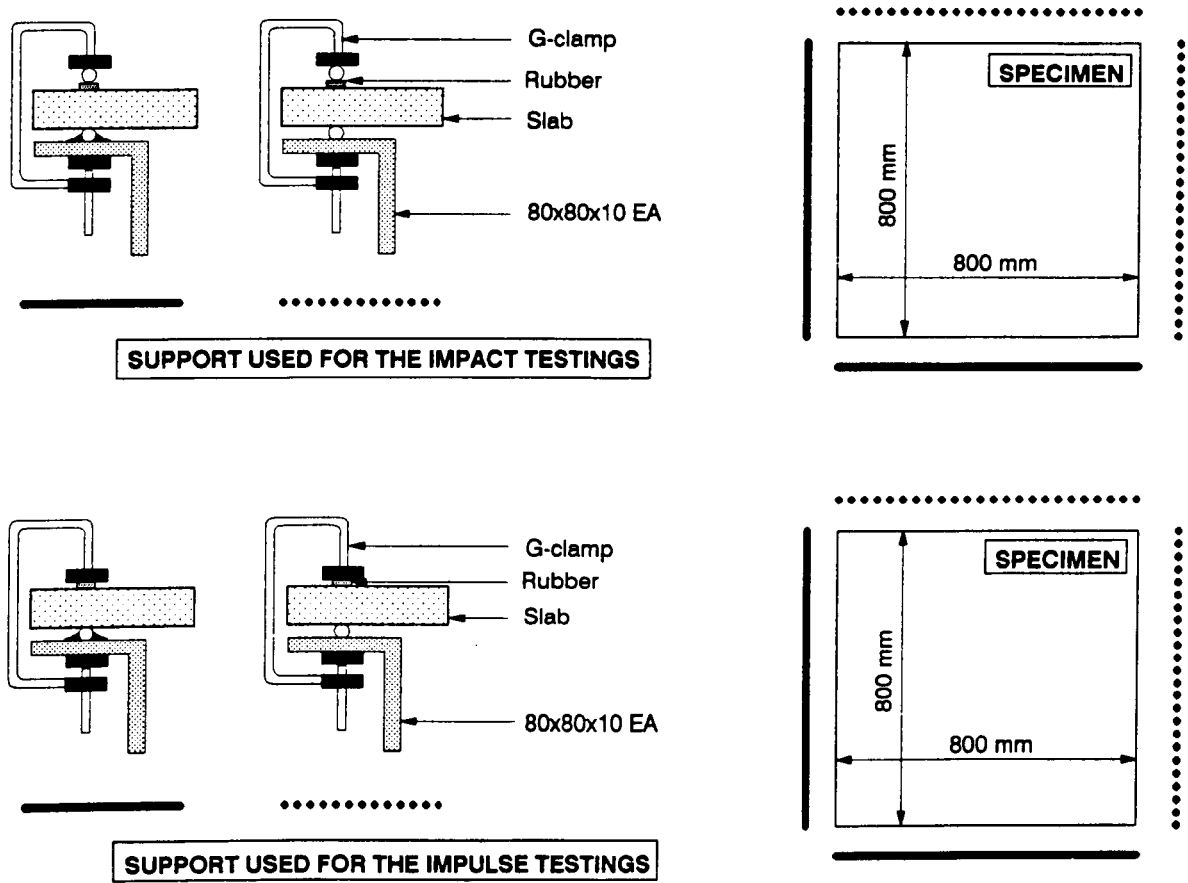


Fig. 3.18 Free supports

3.3.1.2 Inner supports

Inner supports together with fixed outside supports were used in the small slab impulse tests SE7 and SE8 and in the small slab static tests SS3 to SS5. In all cases they were finely adjusted before the test so that they were just touching the slabs while the slab itself was still mostly supported by the outside fixed supports. In both types the touching area of the support was 80mm all around.

Inner supports are shown in Fig. 3.19.

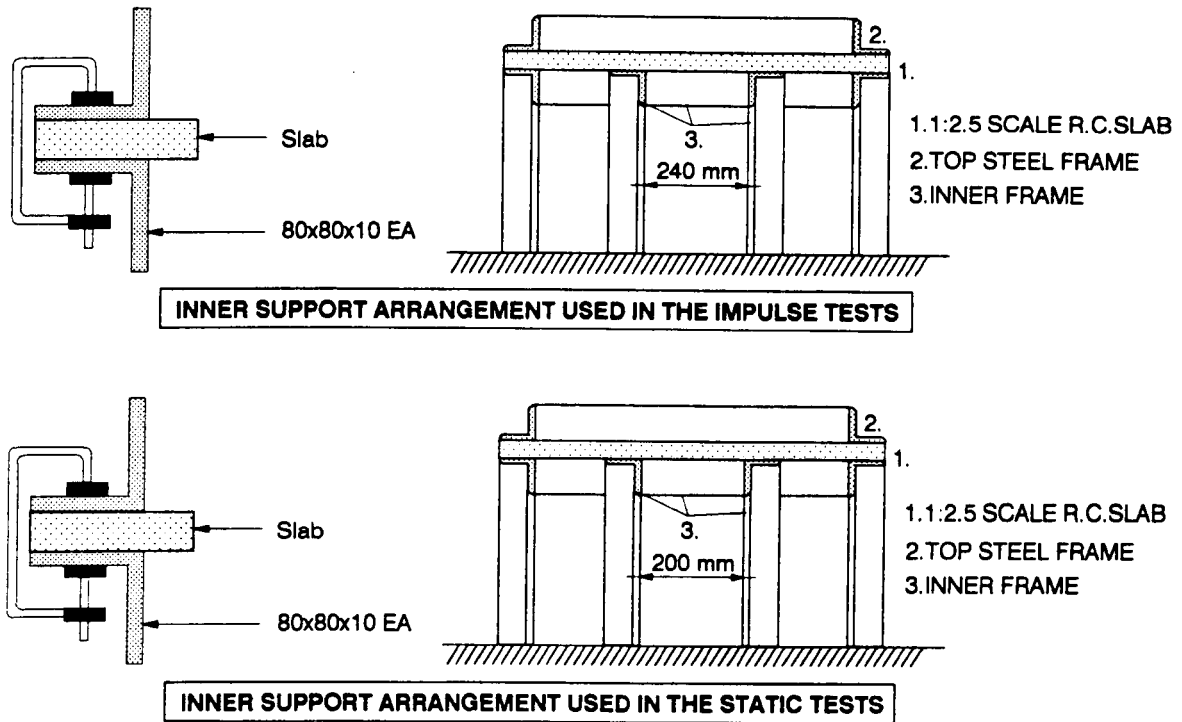


Fig. 3.19 Inner supports

3.3.1.3 Fixed supports

This type of support was used for most of the small scale specimens (SE5, SE6, SE10 to SE19 - impulse tests, S9 to S16 and S19 - impact test and also SS1 and SS2 - static tests) and for all large scale specimens. Scaling rules were also carefully fulfilled so that for the small scale slabs the supported area was 80mm on all sides and for the large size specimens it was 200mm. In both cases fixity was provided by clamping the upper and lower beams together.

In the case of the small slabs, G-clamps were strongly hand-tightened while for the large slabs bolts were also hand-tightened with the appropriate size spanner.

The main feature of the fixed supports, Fig. 3.20 is that they prevent almost all rotation of the slab and vertical and horizontal movement in the support region. All four sides of the slab were fixed in the same way.

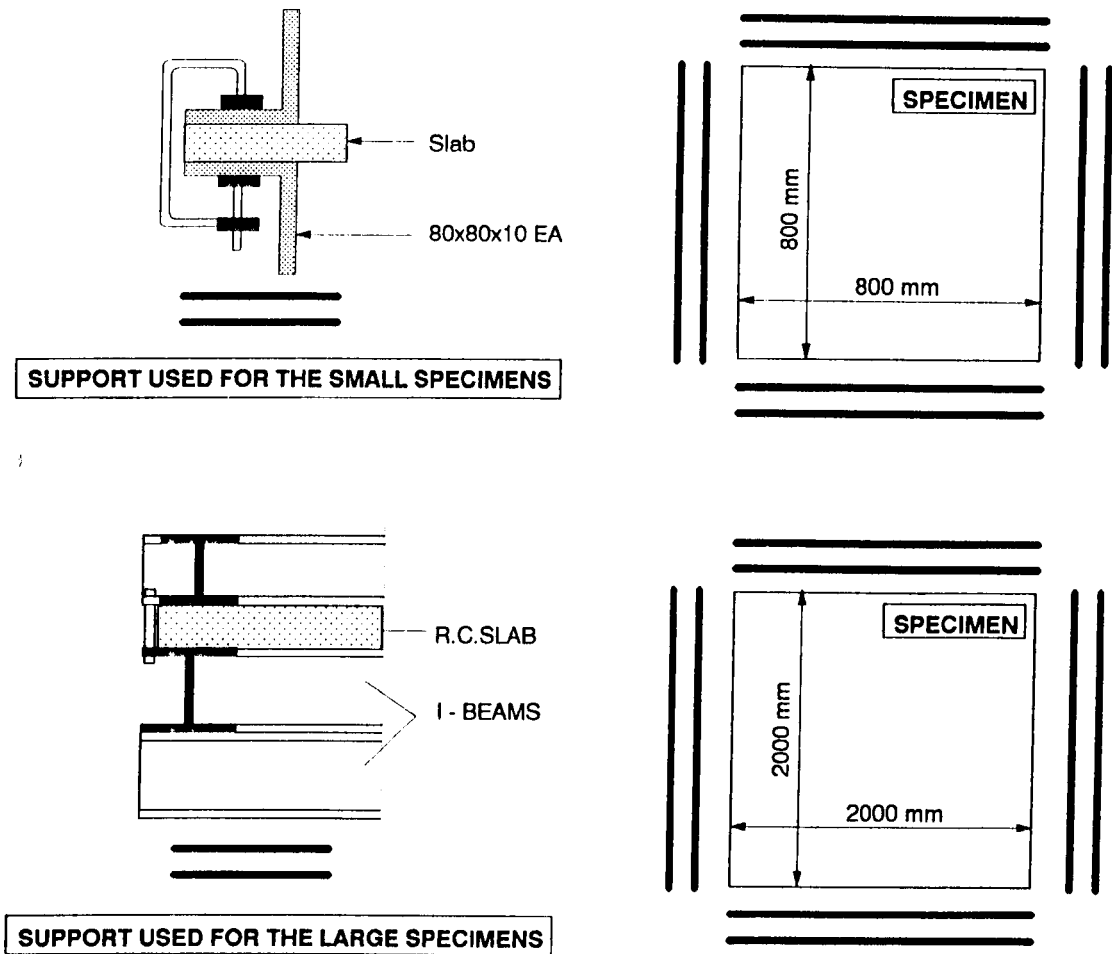


Fig. 3.20 Fixed supports

3.3.2 Loading conditions

The load vs time relation is of crucial importance in understanding the response of the structure to dynamic loading. Great attention has been paid to produce uniformity in the application of both types of dynamic load.

The use of model and prototype specimens requires the application of the scaling laws to the loading functions applied to the specimens. Available sources indicate that the two dimensional linear scaling of the load transmitter (pressure bar in the case of impact) and cube root scaling laws in the case of impulse, represent the minimal scaling requirements that can provide any consistency between the specimen response from two different sizes. In addition the impulse testing arenas should have similar features for both scales. The following sections provide detailed information about the loads to which the slabs were exposed.

3.3.2.1 Impact test

Impact loads were produced by a free falling cylindrically shaped hammer. Both size specimens were tested in the same specially designed and built drop hammer rig (Fig. 3.21). It consists of a steel frame supported on the roof of the laboratory which guides the dolly carrying the hammer. To operate the system the hammer is first lifted to the required drop height by a dolly which holds the hammer by its top plate. The dolly has four wheels which ride along two vertical rails and keep the dolly and the hammer in the vertical position as they are lifted by the lifting winch, or as they fall. During lifting, the dolly is raised carrying the hammer, until it engages with a solenoid operated bomb release (opening time about 50msec). Once the dolly is released, both it and the hammer fall at the same velocity but when the hammer hits the pressure bar and comes to a halt before rebounding, the dolly continues to fall until it is stopped by a set of buffers. Since there was no means of stopping the hammer hitting the specimen again after rebound, the whole impact event actually consists of not one but several impacts with a significant decrease in power for each successive impact. The frequency of repeat impacts was low enough for them to be clearly distinguished in the pressure bar records.

The velocities obtained in this rig are up to 99% of free fall velocity. A maximum drop height of 3.5m is available for the hammer. The impact of the dolly on the frame is transmitted directly to the roof by the guide rails and the attached buffer plate supported by the roof structure of the laboratory. Consequently there is no real possibility of any of the stress waves produced in the frame of the drop hammer reaching the slab or the instrumentation attached to it, since there is no contact between the two. The slab response to the impact is produced by the hammer impacting a load cell which rests freely on the slab. Slabs of up to 3.5m x 3.5m can be easily tested in this drop hammer since the frame is supported on the roof above.

The hammer is restricted in diameter but can easily be changed in mass by simply using hammers of different lengths. Also the simple cylindrical shape of the hammer means that stress waves in the hammer can be more easily analysed enabling the impact force to be measured more accurately by electrical resistance strain gauges bonded to the static load cell.

For the small size slabs, a 33.7kg, 200mm diameter and 131mm long hammer was employed while for the large slabs a 70kg, 272mm long and 150kg, 583mm long hammers were used.

DROP HAMMER, C.E.D.U.S. LABORATORY, BUXTON

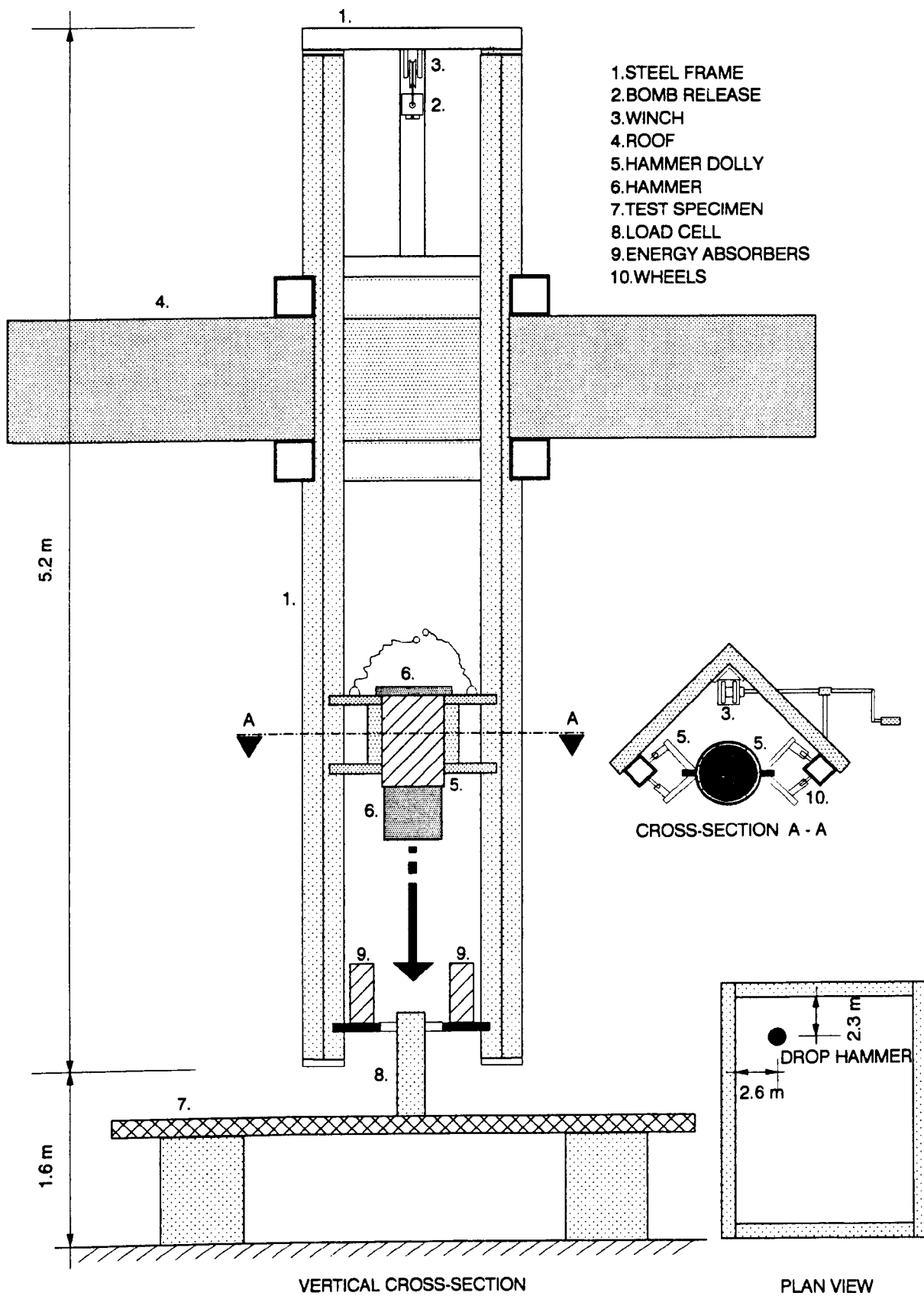


Fig. 3.21 Drop hammer test rig

For both types of slab specimen the load from the impacting hammer was transferred to the specimen through a mild steel 500mm long load cell. In the case of the small slabs its diameter was 50mm while for the large slab scaling factor of 2.5 was used so the diameter was 125mm. Both bars were equipped with electrical resistance strain gauges which were used to record the stress waves produced by the impact. Section 3.3.3.1 gives the details of the instrumentation on the load cell.

Two different types of impact were produced. In the so called hard impact the hammer struck directly onto the pressure bar (or load cell) while soft impact was obtained by placing a 25mm thick rubber on the top of the pressure bar to serve as a buffer between it and the falling hammer. For both sizes of slab the diameter of the rubber pad corresponded to the diameter of the pressure bar.

3.3.2.2 Impulse tests

All explosive tests were performed in blast cells at the laboratories for Civil Engineering Dynamics, University of Sheffield, CEDUS. Since the main objective of the research was to determine the behaviour of the slabs to blast from close range explosive charges it was decided that its standoff distance to the specimen should be in the region of 500mm to 200mm for the large specimens and from 250mm to 50mm for the small slabs. In all cases standoffs were measured as a clear spacing between the charge and the specimen. All the tests were, because of the amount of explosive involved, performed in open blast cells and very strict safety procedures were adhered to.

3.3.2.2.1 Test arena

Both small and large scale slab specimens were tested outdoors in the open roof test chambers. The small scale slabs were tested in a chamber built of concrete blocks that was 2m wide, 5m long and 2.5m high with a concrete floor and no roof. Large scale slabs were tested in the open space at the rear of one of the R.C. bunkers. The space at ground level, was about 5.43m long and 2.9m wide with side walls about 3.8m high at the top.

The 1:2.5 scale testing site is shown in Plate 3.12.



Plate 3.12 1:2.5 Scale impulse test site

3.3.2.2.2 Explosive charge

The explosive used in the impulse tests was plastic explosive PE4 which had mass density of 1590kg/m^3 , detonation velocity of 8189m/sec , detonation pressure of $2.68 \times 10^7\text{kN/m}^2$ and mass specific energy of 5111kJ/kg^2 which gives it a TNT equivalent of 1.13.

Apart from a few initial tests on the small scale slabs where the charge was cylindrical in shape, all charges were of hemispherical shape with the spherical side of the charge facing the specimen.

They were all hand made from 454g explosive sticks that were compacted in to the specially made steel moulds, so producing a charge of uniform shape and consistent density. The L2A1 detonators were placed in to a pre-formed 10mm deep hole in the centre of the flat side of

the charge in all tests and then held in place by insulation tape. In all tests the charges were initiated from the side furthest from the specimen.

The large scale charge was chosen to be 1300g since the large blast cell has been proved for that amount of explosive. The diameter of the hemispherical charge was 142.5mm.

The scaling law for explosions is based on geometrical similarity and the explosive charges and distances from the specimen were scaled according to the cube root scaling laws.

Cube root scaling indicates that a charge of mass $M_1 = 1300\text{g}$ will produce the same peak overpressure and shock wave velocity at a distance R_1 from the charge, as a scaled charge of mass M_2 of the same explosive type and shape at range R_2 when:

$$\frac{R_1}{\sqrt[3]{M_1}} = \frac{R_2}{\sqrt[3]{M_2}}$$

So the scale factor is:

$$\frac{R_1}{R_2} = \sqrt[3]{\frac{M_1}{M_2}}$$

and for: $\frac{R_1}{R_2} = 2.5$ and $M_1 = 1300\text{g}$ then:

$$M_2 = \frac{1300}{2.5^3} = 83\text{g}$$

For practical reasons (the same size detonator was used for both scales), the model charge was actually $M_2 = 78\text{g}$ and it had a diameter of 57mm,. Although the scaled charges gave the same peak pressure and shock wave velocity at scaled distances, the positive duration and impulse produced by the larger charge are 2.5 times greater than corresponding values produced by the smaller charge at scaled distances.

3.3.2.3 Static test

In all five statically tested small scale slabs, loading was done by the displacement control screw jack type loading machine. Loading rates were kept well within the static region at $15\text{N/mm}^2/\text{min}$. The load was applied to the specimens through the Novotech type 50kN load cell placed on top of the spherical seat under which there was a 50mm diameter x 50mm long mild steel cylinder. The purpose of this transmitting cylinder was to provide the same area of loading

of the specimen as in the impact tests. The static test loading arrangement used for the SS1 and SS2 slabs is shown in Fig. 3.22.

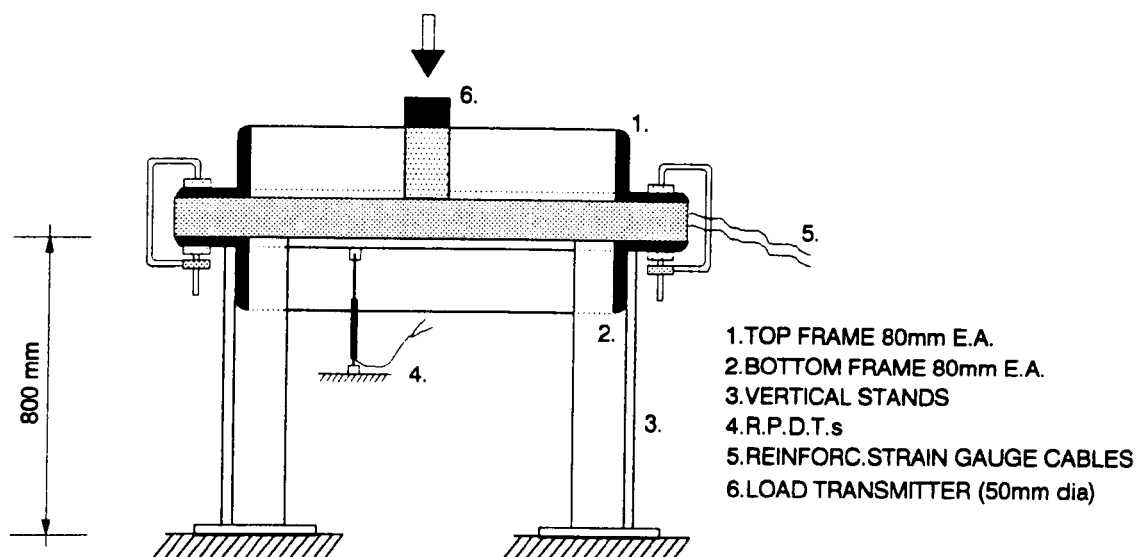


Fig. 3.22 Static test loading arrangement

3.3.3 Specimen response record

A very important feature of any experimental research is the ability to record the behaviour of the test specimen in every aspect which can more precisely determine and explain its response. Testing in the field of dynamic response, particularly under impact and impulse loading, has been additionally complicated because of the very transient nature of the event which complicates the problem with additional unknowns.

Measurements of the response of the specimen taken in this investigation can broadly be separated as measurements prior to the loading (hammer velocity, static concrete characteristics), during the loading (force-time relations, pressure-time relations, displacement of the specimen, reinforcement strain and filming of the areas of interest) and post test assessment of the specimen (crack marking and photographing, overall assessment of the state of the specimen etc.).

Most of the measurements immediately prior to and during loading are, because of the very short time duration and the nature of the load, very complicated and require great knowledge of the instrumentation and its features. In addition to this, test settings in most of the cases require

some prediction not only of the specimen response in physical terms (deflection, strain, force, etc.) but also of the duration of the event and synchronisation (filming at 10,000 p.p.s. on 30m long film for example). Obviously none of these parameters can be readjusted during the test itself. Further problems are caused by the need to safely protect the usually very expensive equipment which is particularly complicated in the case of blast loading.

Finally the selection of the equipment that can be used, and its usage, is closely related to the amount of money available, to the amount of already existing equipment and its condition and usefulness and very importantly to the time available. All measurements and recordings of the specimens' response taken in this work represent a compromise between all above mentioned aspects and they are described in the following pages.

3.3.3.1 Impact load measurements

The previous sections and Fig. 3.21 show that the impact load was produced by the falling drop hammer impacting a stationary mild steel pressure bar with the end in direct contact with the specimen. The main purpose of the bar was to measure the strain-time relations for the bar produced by the hammer hitting it which can later give the force applied to the specimen.

The pressure bars used for both large and small specimens were round bars and that used for the large specimens had a diameter of 125mm. For the small specimens the diameter was 50mm. The length of the pressure bar was 500mm for both scales of specimen. The voltage output from a Wheatstone bridge with electrical resistance strain gauges, (section 2.2.3, ERSG Kyowa KFC-5-C1-11, bonded by CC-15A adhesive), was measured and calibrated to give load.

Both pressure bars were equipped with one strain gauge station consisting of four ERSG arranged on opposite ends of orthogonal bar diameters in order to cancel bending strains. The gauges were connected into the active arms of a full Wheatstone Bridge as shown in Fig. 3.23. Dummy gauges were bonded to short steel bars of the same diameter as the pressure bars. The instrumentation arrangement for both pressure bars is also given in Fig. 3.23.

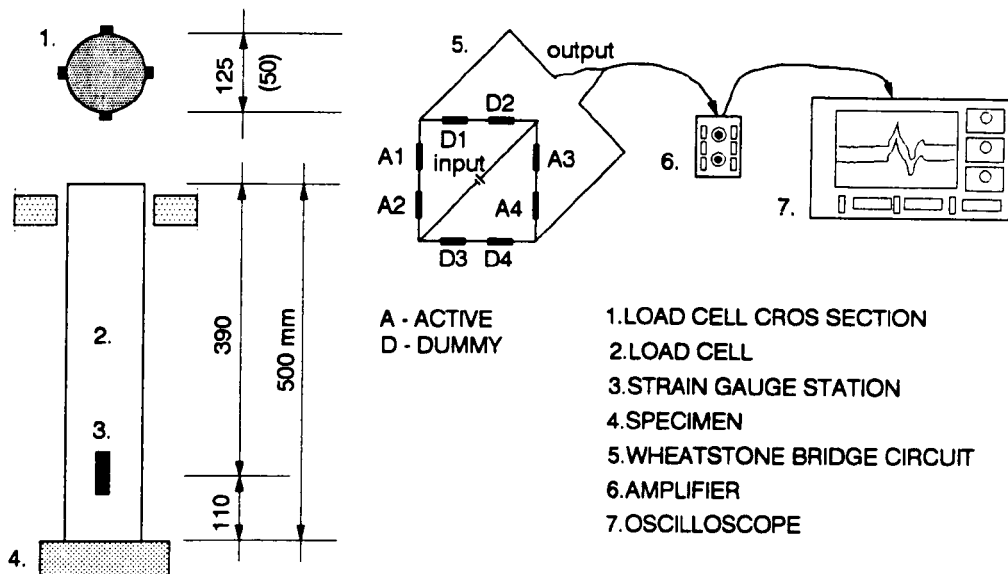


Fig. 3.23 Pressure bar set-up and strain gauge station arrangement

A static load cell calibration was done for both bars in an Amsler loading machine. For the small scale pressure bar the multiplying (calibration) factor is $1V = 161.3kN$ using a bridge supply of 5V and 500 times amplification.

The results of the static load calibration for the large scale pressure bar are given in Fig. 3.24 The calibration factor is $1V = 2067.7 kN$ using the 5V bridge supply and 250 times amplification

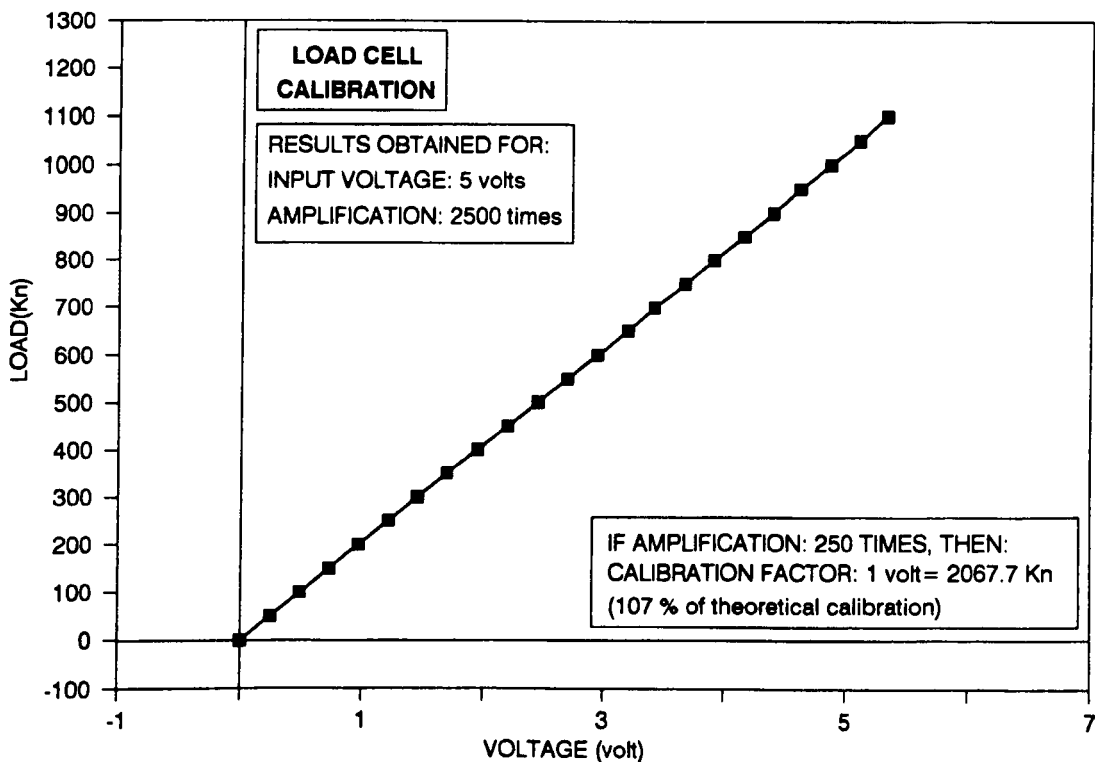


Fig. 3.24 1:1 Scale pressure bar - static calibration results

In addition to the static load calibration, a theoretical calibration has been done for both pressure bars, using the Wheatstone Bridge equation:

$$\Delta E = V \cdot \frac{r}{(1+r)^2} \left(\frac{\Delta R_1}{R_1} - \frac{\Delta R_2}{R_2} + \frac{\Delta R_3}{R_3} - \frac{\Delta R_4}{R_4} \right)$$

where: ΔE - output voltage (volts) from the unbalanced bridge

V - supply voltage (volts)

$R_1 = R_2 = R_3 = R_4$ - arm resistance (ohms)

ΔR - change to arm resistance as a result of strain ϵ

$$r = \frac{R_2}{R_1} = 1$$

$$\frac{\Delta R_1}{R_1} = \frac{\Delta R_3}{R_3} = S_g \cdot \epsilon$$

S_g - gauge factor (given as 2.08)

$$\frac{\Delta R_2}{R_2} = \frac{\Delta R_4}{R_4} = 0 \text{ (because } R_2 \text{ and } R_4 \text{ are dummy gauges)}$$

Since:

$$\epsilon = \frac{\sigma}{E} = \frac{P}{A \times E}$$

where A = cross-section of the bar and for the large pressure bar:

$$A = \frac{(125)^2 \times \pi}{4} = 12271.8 \text{ mm}^2, \text{ and } E = 204,000 \text{ N/mm}^2$$

for $P = 1 \text{ kN}$, strain should be:

$$\epsilon = \frac{1000}{12271.8 \times 204,000} = 0.3994 \times 10^{-6}$$

then:

$$\Delta E = 5 \times \frac{1}{(1+1)^2} \times 2 \times 2.08 \times 0.3994 \times 10^{-6}$$

$$\Delta E = 2.07688 \cdot 10^{-6} \text{ Volt/kN}$$

For amplification 250 times:

$$\Delta E = 250 \times 2.07688 \times 10^{-6} = 0.51922 \times 10^{-3} \text{ Volt/kN}$$

and $1 \text{ kN} = 0.51922 \text{ mv}$ or $1 \text{ Volt} = 1925, 96 \text{ kN}$

For the case of the small bar the theoretical calibration gave a value of $1 \text{ V} = 152.63 \text{ kN}$

(for the same amplification and voltage).

All results presented further in the text were calculated using experimentally obtained calibration factors.

3.3.3.2 Hammer velocity measurements

In the drop-hammer impact tests the velocity measurements were obtained in two different ways. On the first eight small scale specimens two microswitches (section 3.2.5) were mounted as shown in Fig. 3.25 and connected to a Racal timer (section 3.2.7) which recorded the period of time for the hammer to travel between them.

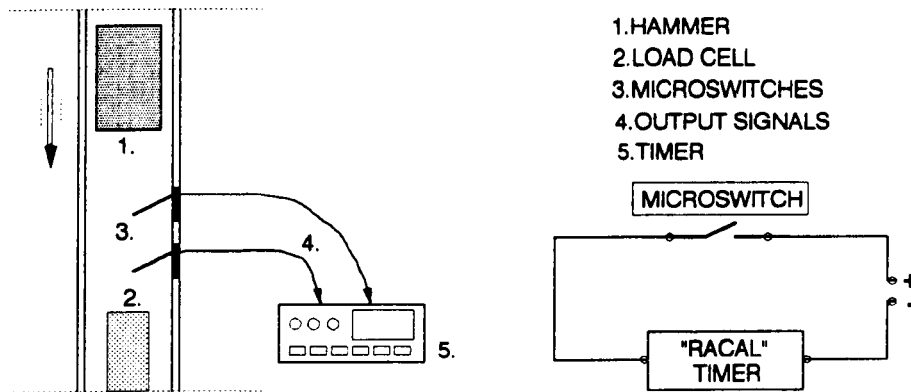


Fig. 3.25 Arrangement for measuring drop-hammer velocity by microswitches

For the 11 remaining small scale slabs and for all large scale specimens, a "comb" was attached to the hammer dolly and this passed through opto switches (section 3.2.6) attached to the rig as shown in Fig. 3.26.

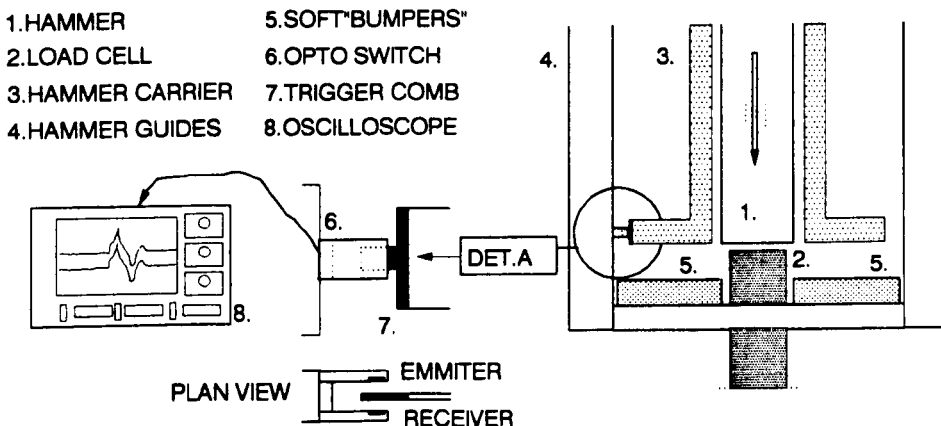


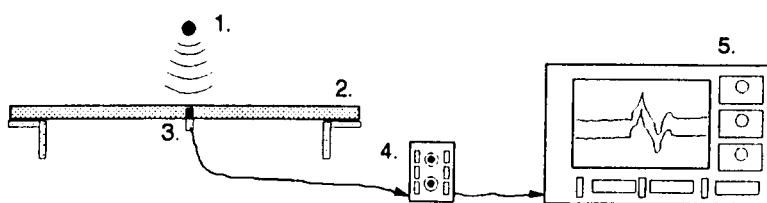
Fig. 3.26 Arrangement for measuring drop-hammer velocity by opto-switches

The velocity was then obtained by measuring the time for the comb teeth to go through them. The whole event was recorded on a digital oscilloscope and later analysed to give the velocity.

The velocity of the hammer was found to be well above 90% of the theoretical free fall velocity in all tests.

3.3.3.3 Blast pressure measurements

In all the tests, Kulite type pressure gauges (section 3.2.11) were employed and usually powered with 10 volts D.C. and amplified from 100 to 2500 times. The connection circuit is shown in Fig. 3.27.



PRESSURE GAUGE DESCRIPTION:

1.CHARGE	TYPE: "KULITE" HKS(or HKM) 375 SERIES
2.STEEL PLATE	PRESSURE RANGE: max.10.000 psi = 689.5 bar
3.PRESSURE GAUGE	ELECTRICAL EXCITATION: 5 volt D.C.
4.AMPLIFIER	FULL SCALE OUTPUT: 100 m volt (nominal)
5.OSCILLOSCOPE	IF AMPLIFICATION A=100 times THEN 1 volt = 68.95 bar

Fig. 3.27 Instrumentation for pressure measurement

The main problem in the evaluation of the blast pressure imposed onto the slab specimens was that the blast pressure gauges could not be placed between the charge and the slab but were placed at 500mm on the other side of the charge and so were exposed to the pressure from the flat side when the slab was exposed to pressure from the hemispherical side of the charge. For this reason a series of tests was conducted in which pressure-time histories from the spherical side were recorded. Two different test set ups were used and they are shown in Fig. 3.28. The pressure measured from the flat side of the charge during the main tests gave some comparison between the loadings in order to see if they were consistent.

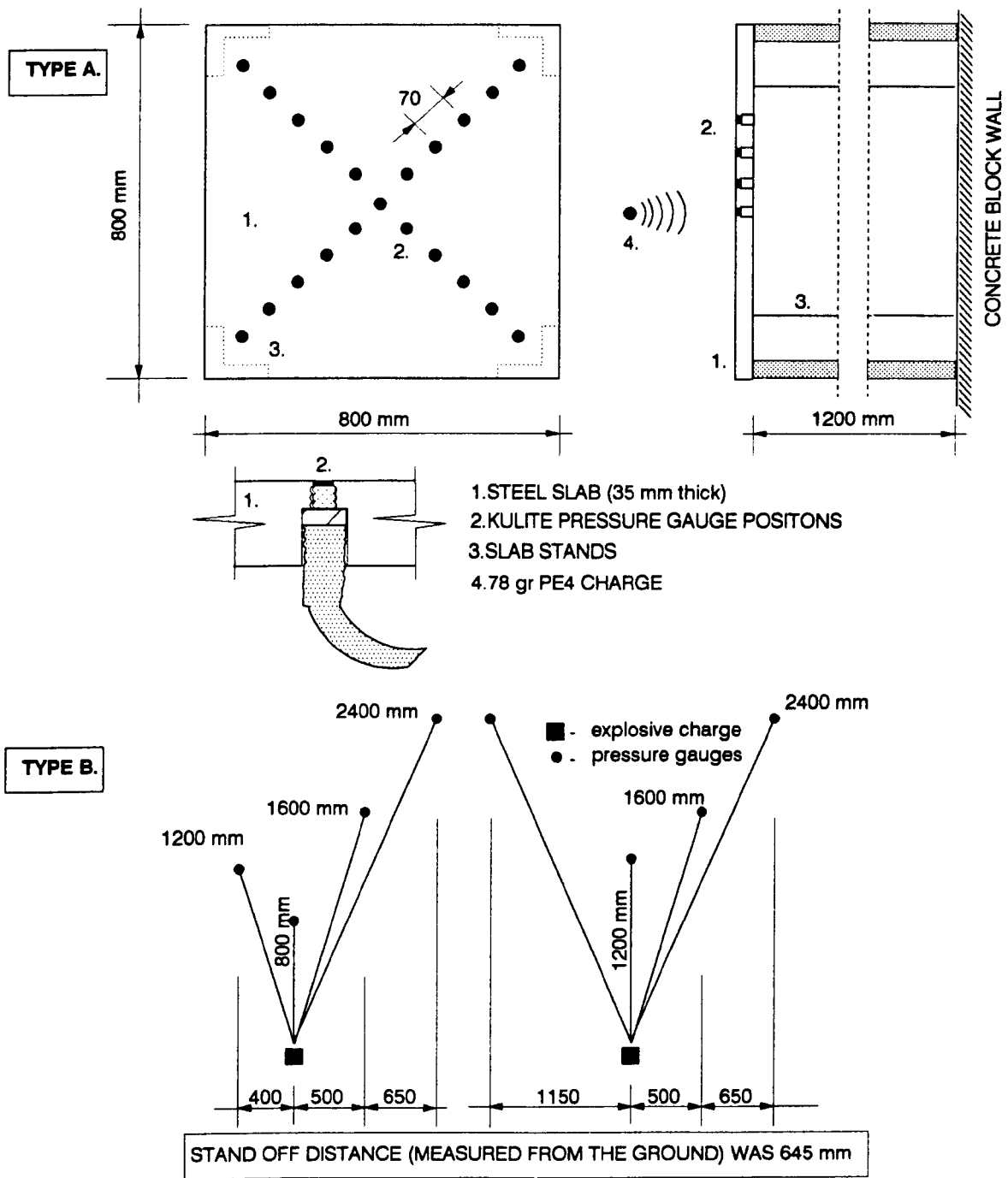


Fig. 3.28 Pressure test set-up

3.3.3.4 Reinforcement strain measurement

For each of the impact and impulsive tests, the two bottom layer bars, one in each direction, were equipped with electrical resistance strain gauges placed at the midspan point of the bars. Before bonding the electrical resistance gauges, the reinforcement was carefully cleaned of rust and a small area about the size of the gauge was ground smooth. The strain gauges were

glued to the bars, using gauge adhesive type CC-15A. Wires were then soldered to the gauge terminals and the leads were covered with an adhesive and lined heat shield which did not allow any contact between the gauges and the surrounding concrete.

The gauges were type Kyowa KFC-10-C1-11 (section 3.2.3) connected into a Wheatstone Bridge circuit as shown in Fig. 3.29.

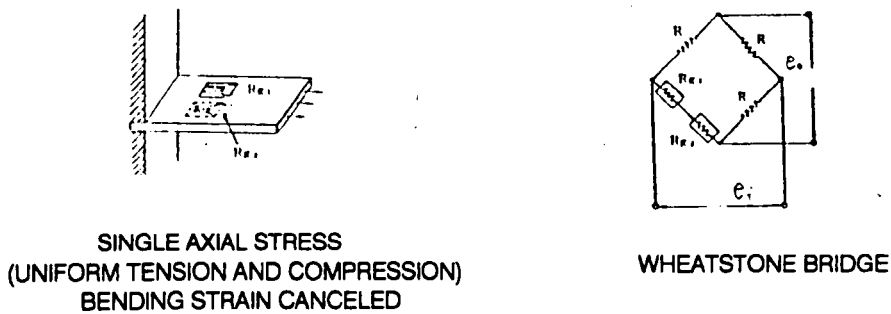


Fig. 3.29 Wheatstone bridge circuitry for measuring the strain in the reinforcement

The gauges were calibrated using the manufacturers gauge factor in the Wheatstone Bridge equation. For this type of Wheatstone bridge the relation between the output voltage from the system and the strain ϵ_o is given as:

$$e_o = \frac{1}{4} \cdot K_s \cdot \epsilon_o \cdot e_i \cdot A$$

where: K_s - gauge factor (given as 2.15 by the gauge manufacturer)

e_i - input voltage

A - amplification of the signal

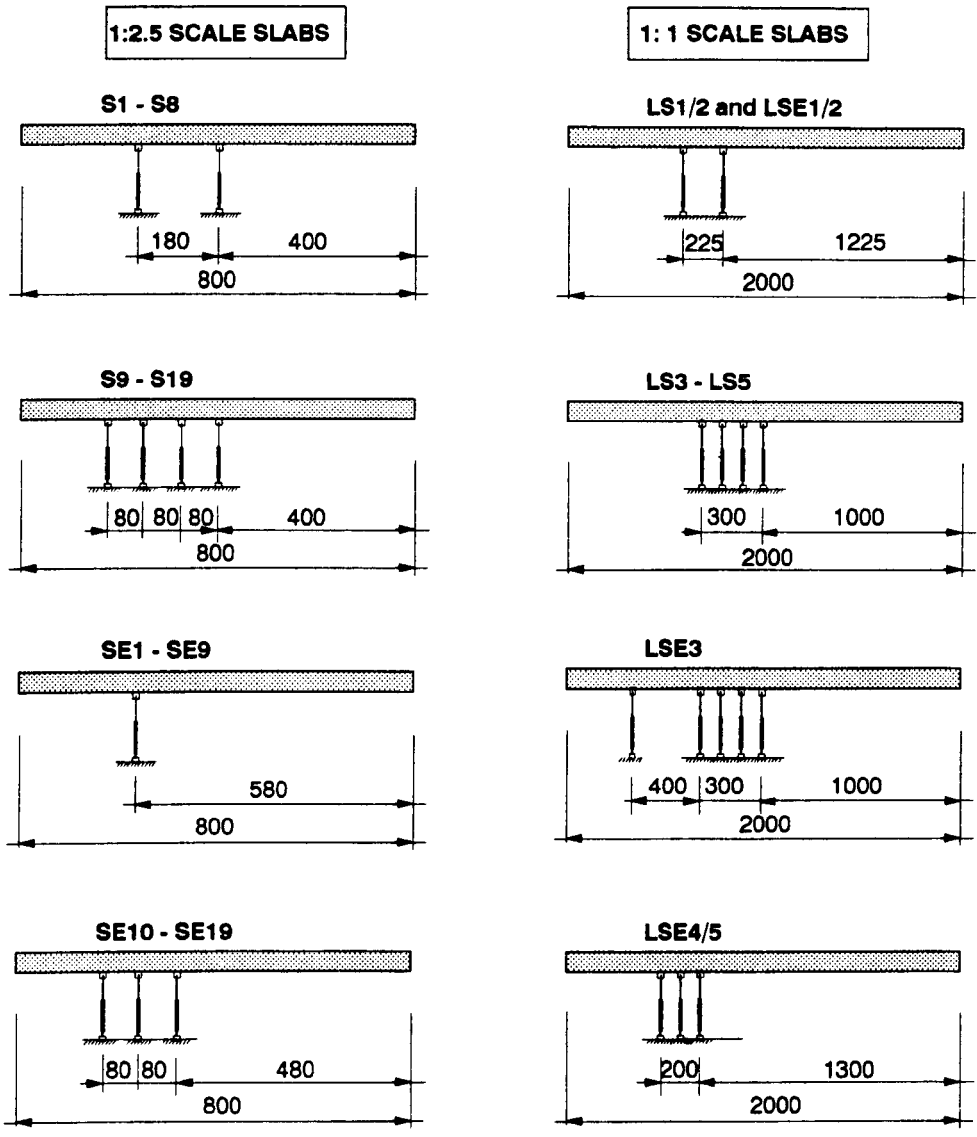
for: $A = 100$ times and $e_i = 4$ volts

$$e_o = 215\epsilon_o$$

so: 1 volt = 0.0046512 strains.

3.3.3.5 Deflection measurements

The deflection measurements were taken by rectilinear potentiometer displacement transducers (RPDT) (section 3.2.1) which were attached to the specimens at the positions shown in Fig. 3.30. In the case of the impact and impulse tests they were all placed along one centre line of the specimen but the positions of the transducers for the static tests SS1/2, SS3-SS5, are along both centre lines and one diagonal as shown in Fig. 3.30.



STATIC TESTS

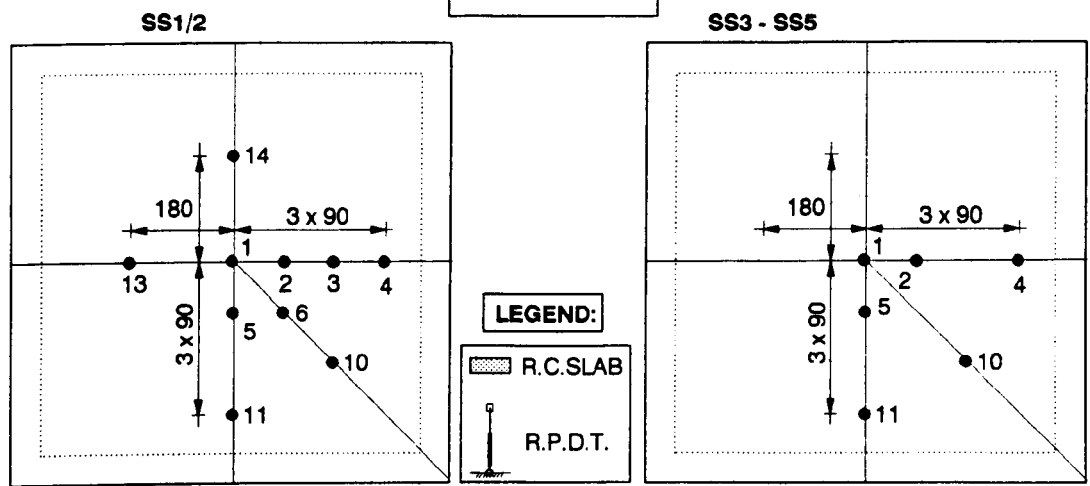


Fig. 3.30 RPDT positions

The RPDT's were connected to the specimen through special fixings (Plate 3.13) that kept the contact between the slab and the RPDT in upward and downward movement and allowed rotational movement of the RPDT. These fixings were screwed onto a threaded rod fixed to the central reinforcing rod at mid and quarter span. The fixing was simply a nut slipped onto the bar and the nut had a short length of threaded rod brazed onto it. When ready made welded reinforcement meshes were used, the fixings were tightened onto the threaded bar which was strongly wired to the reinforcement.

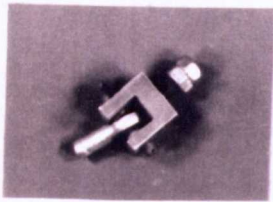


Plate 3.13 RPDT slab fixing

With this connection, the RPDT measured the deflection of the reinforcement layer, and not the lower surface of the concrete slab. This was a necessary arrangement because the concrete usually spalled away beneath the point of dynamic loading.

In all the tests displacement transducers were connected to 10 volt powered circuits as shown in Fig. 3.31

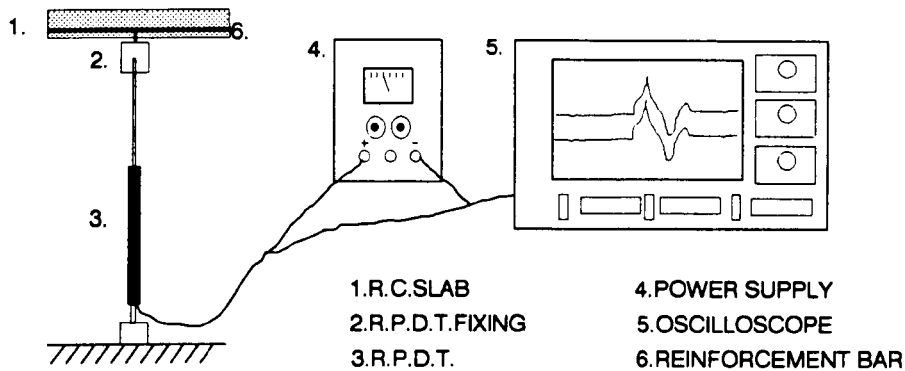


Fig. 3.31 Instrumentation for deflection measurements

3.3.3.6 High speed filming

High speed filming was used on almost all small scale specimens. Two different cameras, Hycam K-2001R (section 3.2.12) and Photec IV (section 3.2.9) were usually set to run at up to 10,000 p.p.s. As mentioned earlier (section 3.1.3.5) on all small scale slab specimens, meshes were drawn before the test with squares of 36mm x 36mm, starting from the central line. In all cases when the Photec IV High speed camera was employed a half frame shutter was used and the size and position of the area that was filmed is approximately shown in Fig. 3.32.

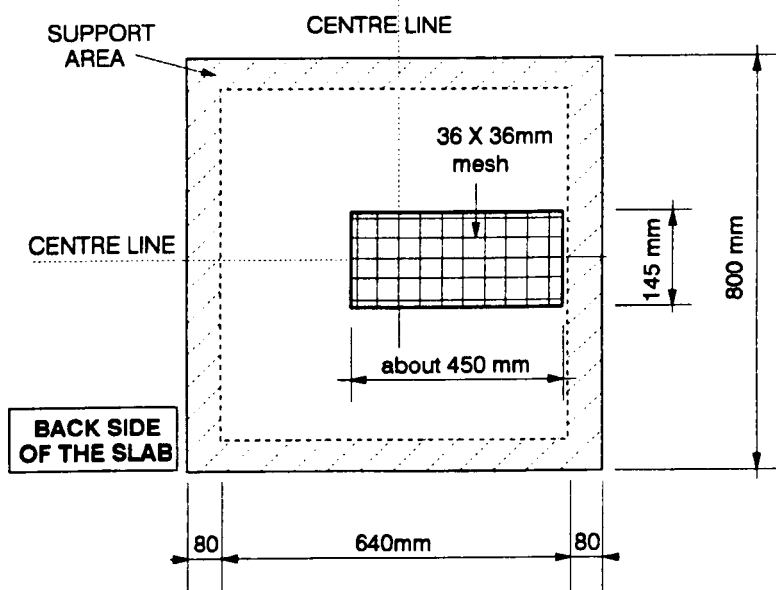


Fig. 3.32 The area that was filmed by the High Speed Camera

In the case of the impact test, since the specimen had to be kept horizontal, filming was done through the 45° inclined mirror placed just under the specimen while the camera was at about 1.5m distance from it securely fixed to the floor. The mirror itself was positioned and held in such a way that it rested on the floor and did not touch the drop hammer rig and consequently

did not vibrate during the impact. In the initial phase of the impulse testing of the small scale slabs the arrangement with the 45° mirror was again employed but it proved to be unreliable since the mirror was very difficult to protect. To overcome this problem a new rig was designed and built in which the slab was held vertically and the camera placed at about 2.5m behind the wall filming through the protected port hole. The camera arrangements are shown in Fig. 3.3.3.

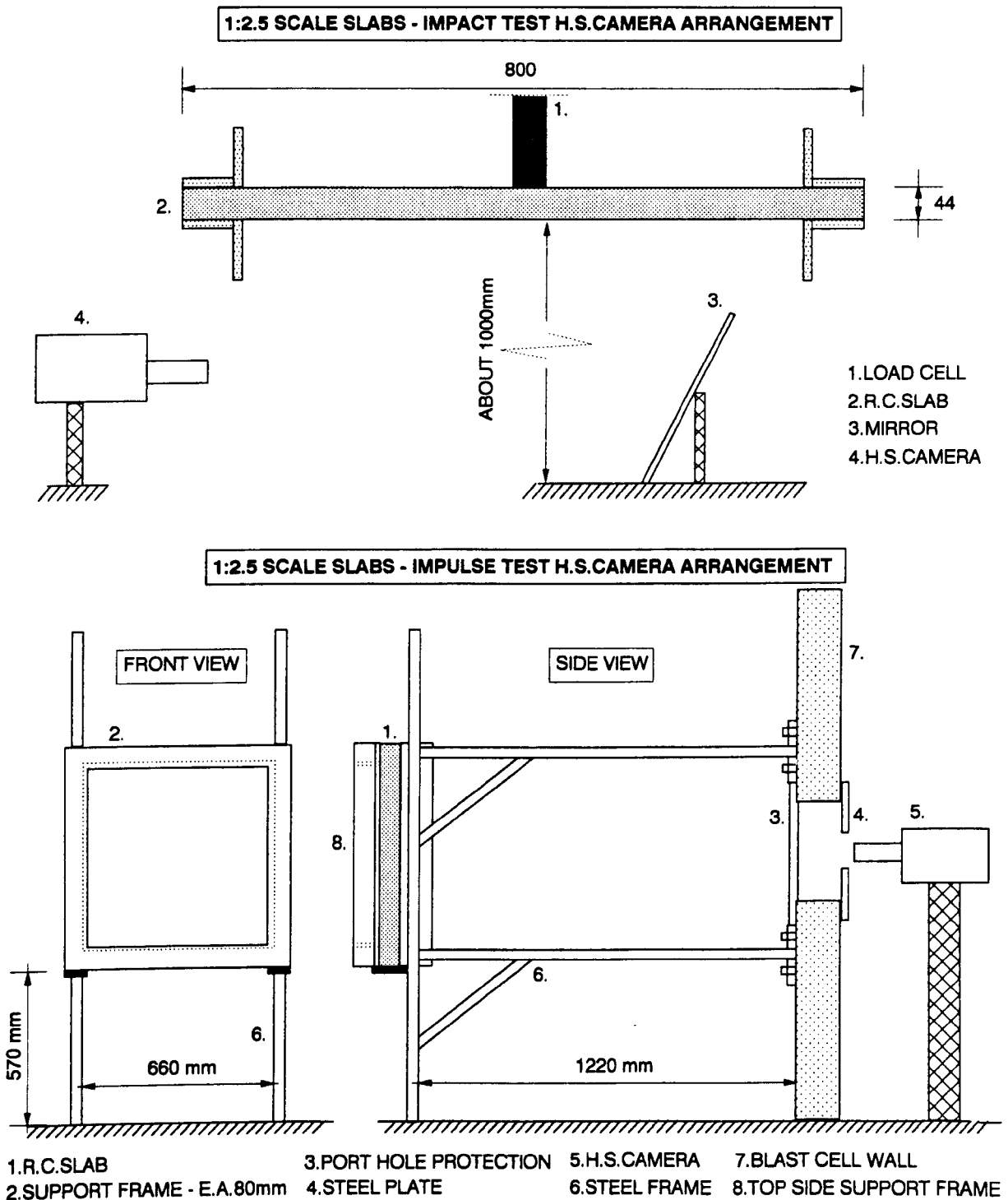


Fig. 3.33 High speed camera arrangements

3.3.3.7 After test damage assessment

After the test, specimens were carefully removed from the supports and all the visible cracks were marked by tracing along them. Since the smallest cracks were not visible by the naked eye a 6 times magnifying glass was used to find and mark these cracks. Specimens were later photographed and stored.

3.3.4 Test set-up procedure and event synchronisation

The transient nature of the events and extensive usage of electronic instrumentation, made the whole process of testing very time consuming and complex to set up. Some aspects of these complexities are described on the following pages and they highlight the need for a properly designed approach to testing.

3.3.4.1 Impact test

The impact test arrangement for small scale slabs is shown in Plate 3.14.

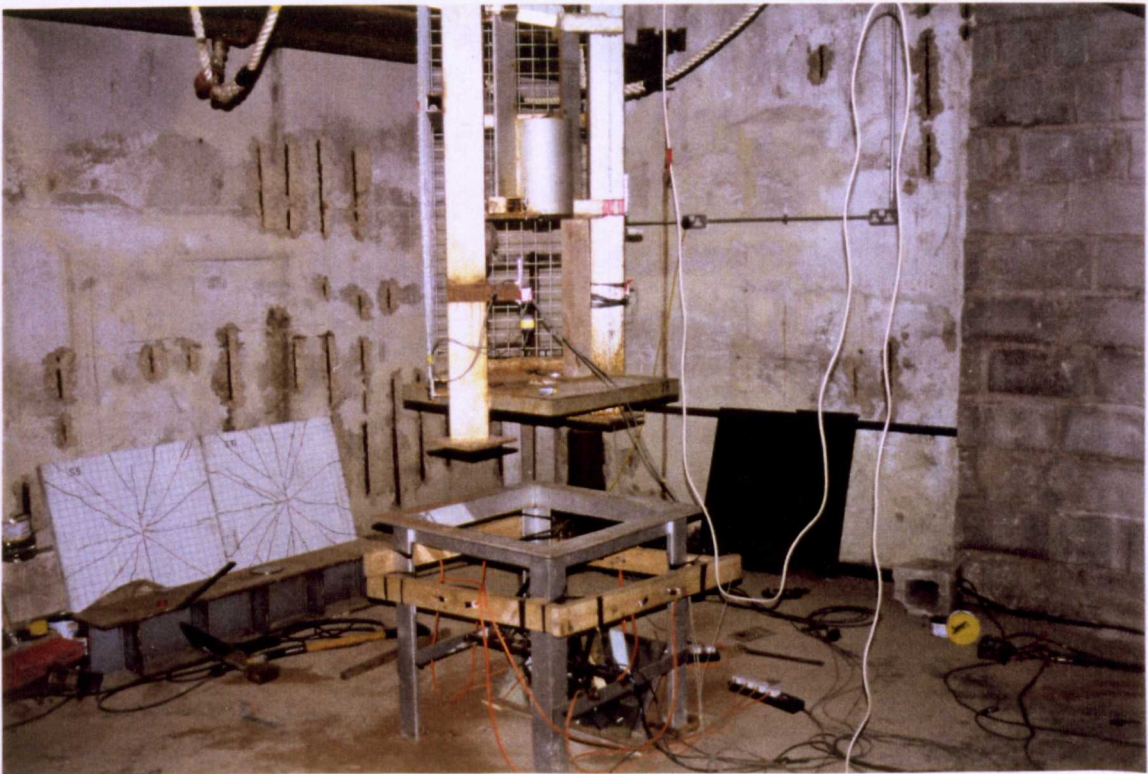


Plate 3.14 Small scale slab impact test set up

The test procedures were as follows and will be explained for the more complicated case of the small scale tests:

1. R.C. slab placed onto the support rig.
2. Top support frame positioned and G clamps tightened.
3. Displacement transducers connected to the threaded bars on the lower surface of the slab.
4. Load cell positioned at the centre of the slab.
5. Dolly buffers placed on the sides of the load cell.
6. Mirror placed underneath the slab.
7. High speed camera positioned.
8. Electrical resistance of the strain gauges on the reinforcement and load cell checked.

The next step was to connect the instrumentation and it was done in the following order:

- (a) The required number of digital storage oscilloscopes were placed on the instrumentation bench at a short distance from the rig and properly connected to the I.E.E.E. socket on the P.C. so the data can later be transferred to the computer.
- (b) The required number of D.C. stabilised power supplies, amplifiers, batteries and dummy strain gauge boxes placed close to the rig.
- (c) Displacement transducer output cables were connected into the connection box and powered by the required voltage (usually 10 volts) from the D.C. power supply. BNC end output cables were connected to the required number of storage channels and oscilloscope settings (data capture rate, voltage capacity, trigger mode, trigger window, position of the traces etc.) adjusted to the required positions. Finally the RPDT's were checked by moving the stroke to its ultimate position.
- (d) The output cables from the electrical resistance strain gauges on the reinforcing bars were connected with the inactive "dummy" gauges with which they made a fully active, four arm Wheatstone bridge. Output cables from the bridge were then connected to the bridge amplifiers to power the bridge and amplify the signal. They were then set to the right modes (amplification, power supply, etc.)

and lastly the bridge circuits were finely balanced on the amplifier and if more course adjustment was needed, also on the dummy boxes. The amplifier output cables were connected to the digital storage oscilloscope and were then set to run in the required mode.

- (e) The electrical resistance strain gauges mounted on the load cell were connected to the oscilloscopes in the same way as the reinforcement gauges. Activity in the load cell was checked by tapping the top with a hammer.
- (f) The velocity rig opto switches were powered by two D.C. power supplies one of which powered the infra red emitters and the other the sensors. They were then connected to the oscilloscope occupying usually two channels (one for each station). Afterwards the rig was checked by running the trigger "comb" through the opto switches so causing the breakage of the electric circuitry. The bottom set of opto switches, which was usually 10mm above the load cell, was also used to trigger the recording of displacements, load and reinforcement strains.
- (g) The High Speed camera was electrically connected to the solenoid that operated the hammer release so that after the film had accelerated to the required speed, it would then trigger the solenoid and release the hammer. The camera also had an electrical input signal from the additional microswitch placed just above the load cell which operated the special timing light which then marked the beginning of the event on the film. The camera was then focused and tested with a dummy film run in the same way as it would operate in the test. Finally the new film was loaded, the camera speed decided and the trigger length of the film set.
- (h) Finally all oscilloscopes were connected into the same triggering circuitry and the whole triggering process tried again.
- (i) The drop hammer was then lifted to the required height in the dolly and before the 8000W lights were switched on, the balancing for the strain gauge circuitry was checked again. The whole event was triggered by switching the camera on.

Once the camera is set to run the events were synchronised as follows:

After operating the bomb release, the dolly and hammer fell at up to 99% of free fall velocity. Just above the load cell the dolly comb passes through the opto switches so measuring

the velocity and triggering the oscilloscopes that record the displacement, strains in the reinforcement and stress waves through the pressure bar. At almost the same height (10mm above load cell) the dolly switches the microswitch so operating the timing light of the camera marking the beginning of the event on the high speed film which by this time runs through the camera at constant speed. After the hammer hits the load cell and freely rebounds, the dolly continues downwards until stopped by the set of buffers effectively damping its impact on the rest of the rig.

The 8000W lights were then turned off, the film unloaded and the stored data transferred to a P.C.

3.3.4.2 Impulse test

The instrumentation of the slabs in the impulse test is in most respects identical to that of the slabs in the impact tests and the test procedures were very similar. For most of the impulse tests a pressure gauge was placed 500mm behind the charge so providing a check on blast pressure consistency between tests.

The impulse test arrangements for both sizes of specimen are shown in Plates 3.15 and Plate 3.16.

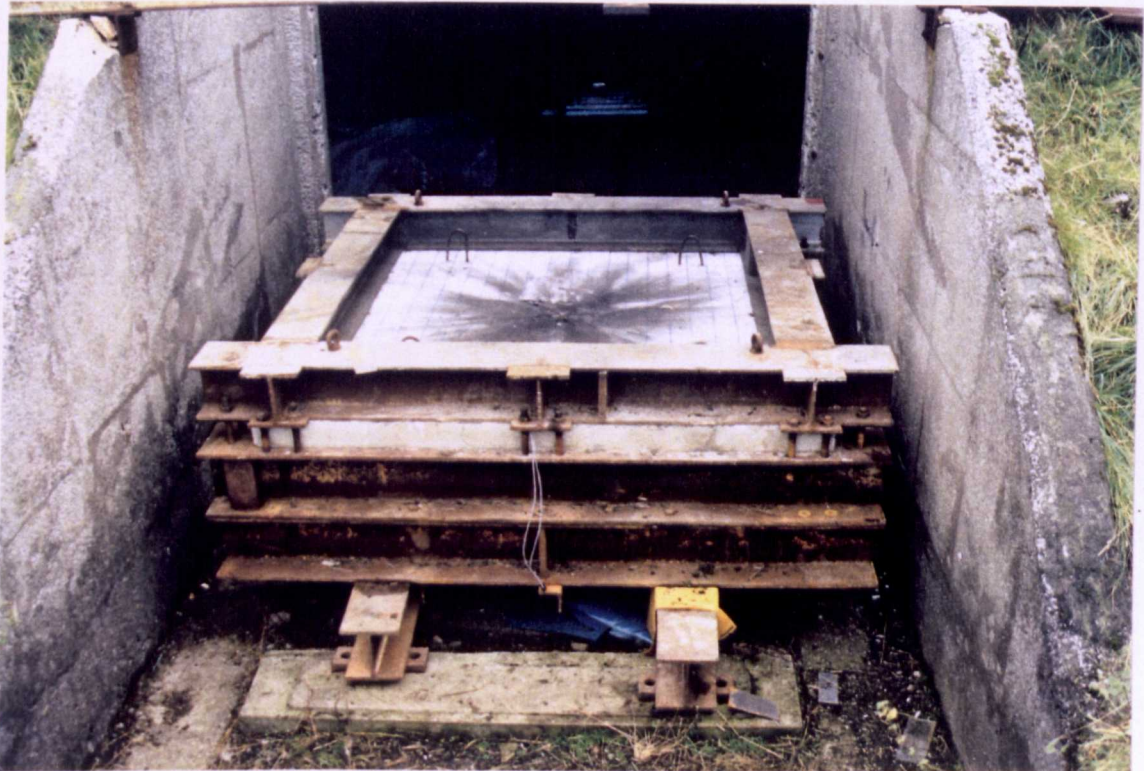


Plate 3.15 Large scale slab impulse test set up

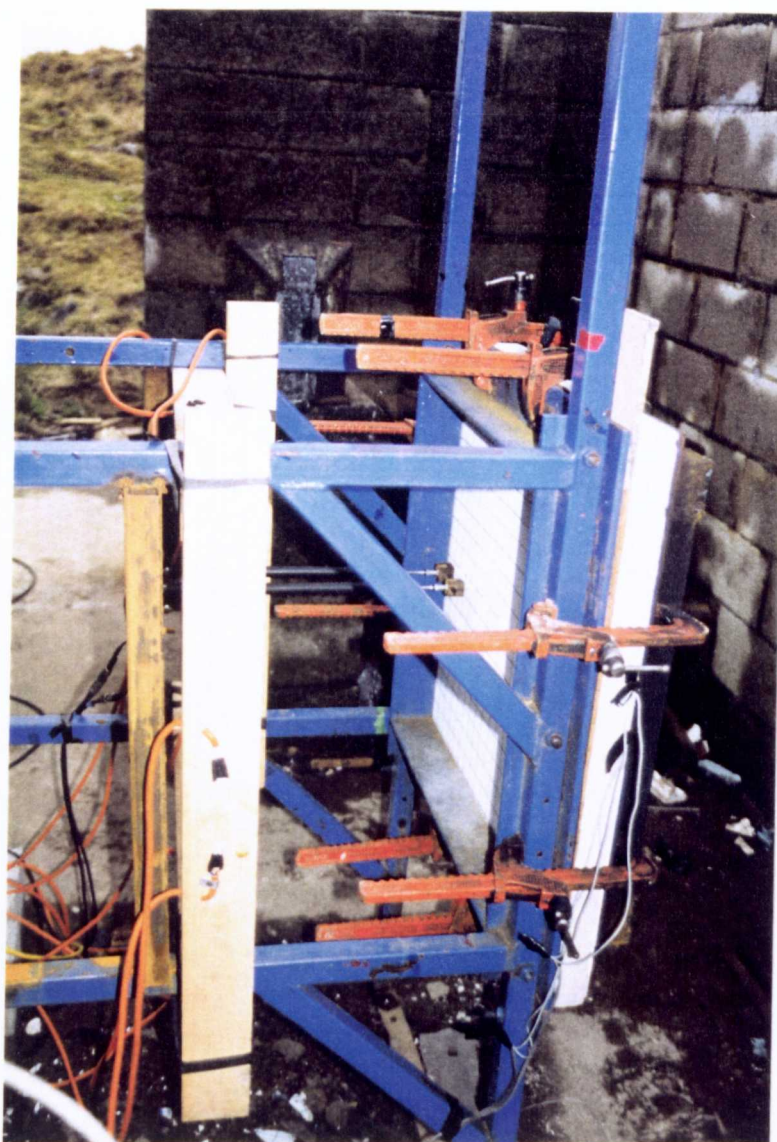


Plate 3.16 Small scale slab impulse test set up

Triggering of the explosive event is also produced by the high speed camera after the film had accelerated to the required speed. The same trigger was used for the storage oscilloscopes and consequently the initial point of the records corresponds to the initiation of the detonator.

3.3.5 Experimental programme and variables

The main experimental program consisted of impact tests on 19 small scale and 5 large scale slabs and the same number of impulse tests. Static testing was carried out on 5 small scale slab specimens. Additional tests were carried out on the materials used for the production of the slabs and to determine blast pressure-time relations at different points on the slab. The whole of the testing programme is schematically shown in Fig. 3.34.

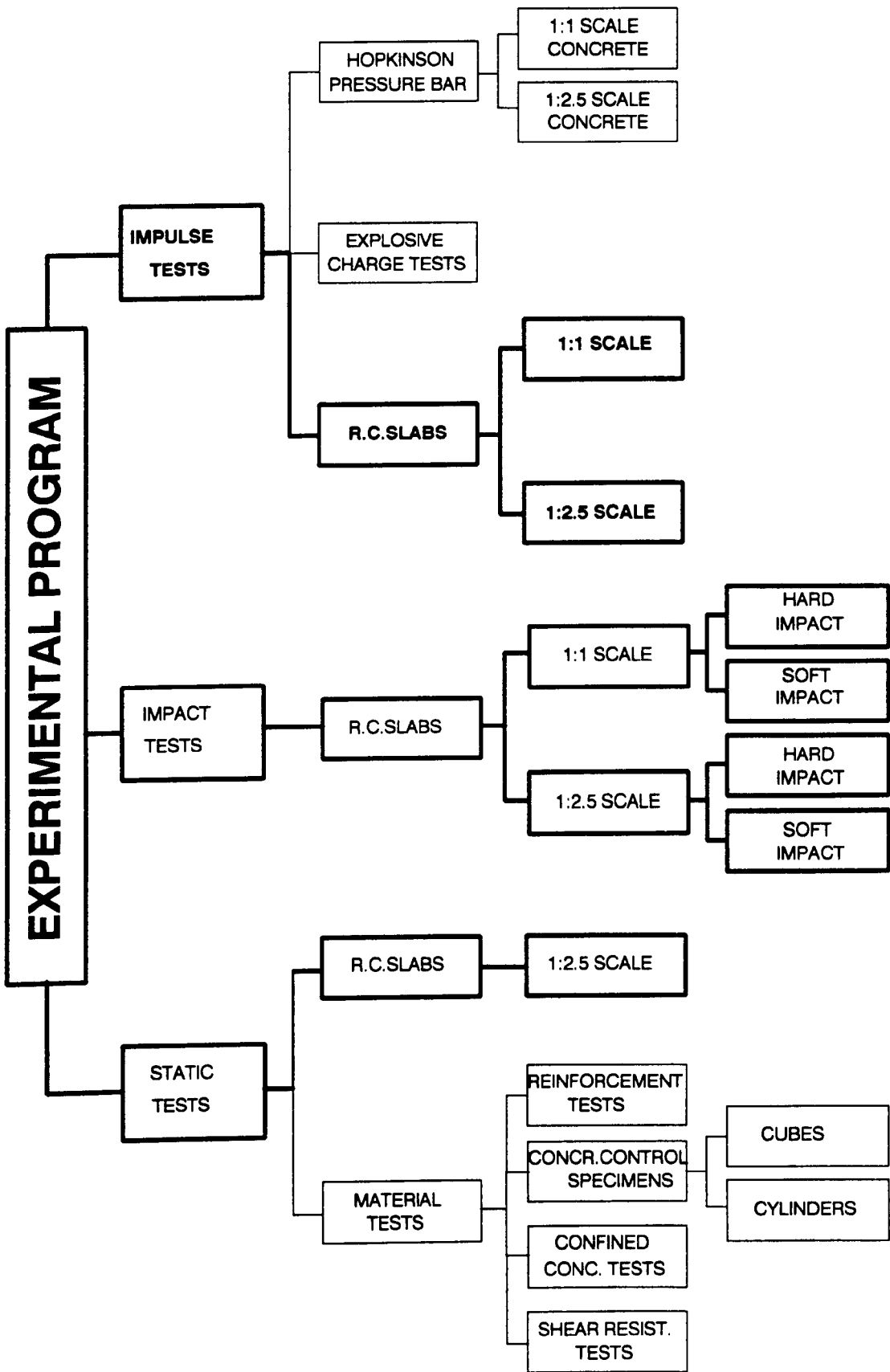


Fig. 3.34 Testing programme

In the initial phase of the work the variables for the small scale specimens were: amount of reinforcement, support conditions and loading function but in later tests the variable was limited to the loading function only. For the main test series the loading function was varied by the type of impact (soft and hard) and the height of drop for the impact test and the standoff distance of the charge for the impulse testing.

For large scale tests the loading function was also the main variable and it was changed in the same way as for the small scale specimens.

All variables for each individual test are given on test sheets in Appendices - Test Results.

CHAPTER 4

EXPERIMENTAL RESULTS

4.0 Introduction

This chapter gives a more detailed view of the results obtained from the impact and impulse tests carried out on the specimens described in previous sections and also explains the way in which certain test variables were used. The chapter should be read in conjunction with Appendices A1 to A3, B1 to B3 and C1, "Test Results", which contain almost all the results obtained during the course of the research programme.

As explained in Chapter 3 many parameters, like displacements, reinforcement strains, loading functions, damage filming and crack patterns, were monitored. Consequently there is a large database of results, many of which will be presented subsequently.

The static compressive and tensile strength of the concrete used are presented in section 3.1.2.1.2, Table 3.4.

4.1 Impact tests

Two major types of impact test were performed in this research. These can be described as soft and hard impact (section 3.3.2.1). The hard impact was produced by the falling hammer hitting the pressure bar that rested on the slab, while in the case of soft impact a rubber pad was placed on the top of the pressure bar so producing the damping effect.

4.1.1 1:2.5 Scale slabs

In total 19 small scale slabs were tested. In the initial phase of the work the main variable was the amount of the reinforcement in the tensile zone of the slab while later it was kept constant at 0.28%. The main variables were the impact energy, rise time and the duration of the load and the values of all variables are given in Table 4.1.

The reinforcement percentages given in Table 4.1. represent those at the under side of the slab. Slab No. S7 was the only slab tested twice and the loading conditions were kept identical for both tests. Slab S19 was the only one without any central reinforcement. Whilst slabs S1 - S8 had only tensile zone reinforcement, slabs S9 to S19 also had compression zone reinforcement in the area 200mm to the edges (section 3.1.1) On all 19 slabs a steel hammer, of mass 33.7kg was used.

Two different support types were used and they are given in sections 3.3.1.1 to 3.3.1.3.

SLAB NO.	DROP HEIGHT (m)	TYPE OF IMPACT	REINFORCEMENT %		SUPPORT TYPE
			UPPER LAYER	LOWER LAYER	
S1	1.85	hard	3.73	2.90	Free
S2	1.85	hard	3.73	2.90	Free
S3	1.85	hard	2.39	2.01	Free
S4	1.85	hard	2.39	2.01	Free
S5	1.85	hard	1.25	1.05	Free
S6	1.85	hard	1.25	1.05	Free
S7	1.85	soft	1.25	1.05	Free
S8	1.85	soft	1.25	1.05	Free
S9	1.50	soft	0.29	0.27	Fixed
S10	2.00	soft	0.29	0.27	Fixed
S11	2.50	soft	0.29	0.27	Fixed
S12	3.00	soft	0.29	0.27	Fixed
S13	1.50	hard	0.29	0.27	Fixed
S14	0.50	hard	0.29	0.27	Fixed
S15	1.00	hard	0.29	0.27	Fixed
S16	0.75	hard	0.29	0.27	Fixed
S17	1.85	soft	0.29	0.27	Free
S18	2.00	soft	0.29	0.27	Free
S19	1.50	soft	none	none	Fixed

Table 4.1 Small scale impact tests - test variables

4.1.1.1 Pressure bar records and velocity measurement

The force produced by the impact on the 1:2.5 scale slabs was measured on the pressure bar (Section 3.3.3.1, Fig. 3.23) using electrical resistance strain gauges placed 110mm from that end of the bar which rested on the slab. For all the hard impact tests, (Slabs S1 - S6 and S13 - S16) the peak force of impact was of the same order of magnitude and varied from 105.66kN to 378.39kN but under soft impact, the peak force was much lower and varied between 29.38kN and 50.45kN. Under hard impact, the rise time to the maximum force and the duration of the pulse, are much shorter than under soft impact. It can be observed that the amount of reinforcement in the slab did not influence the peak force or the duration of the pulse. The peak forces, hammer velocities, rise times and the loading rates for all the specimens are given in Table 4.2. Typical load time records for these two kinds of impact are shown in Fig. 4.1 and Fig 4.2.

SLAB NO.	HAMMER VELOCITY AT IMPACT m/sec	PERCENTAGE OF FREE FALL VELOCITY %	MAXIMUM FORCE kN	RISE TIME msec	LOAD RATE kN/msec
S1	5.51	91.47	-	0.10	-
S2	5.94	98.63	105.66	0.10	1.06 x 10 ⁶
S3	5.67	94.03	166.03	0.146	1.14 x 10 ⁶
S4	5.76	95.56	140.87	0.146	0.97 x 10 ⁶
S5	5.73	95.05	133.28	0.097	1.37 x 10 ⁶
S6	5.63	93.52	169.05	0.146	1.16 x 10 ⁶
S7 - Two impacts	-(5.96)	-(98.98)	29.1,(31.2)	2.1,(2.3)	14.2,(13.3)
S8	5.77	95.73	33.21	2.34	14.19
S9	5.19	95.76	37.84	1.63	23.21
S10	5.94	94.89	39.94	1.60	24.96
S11	6.59	94.14	44.15	2.20	20.07
S12	7.21	94.00	50.45	1.80	28.03
S13	5.17	95.39	378.39	0.10	3.78 x 10 ⁶
S14	2.97	94.89	115.62	0.13	0.89 x 10 ⁶
S15	4.30	97.29	119.82	0.10	1.20 x 10 ⁶
S16	3.73	97.14	140.85	0.15	0.94 x 10 ⁶
S17	5.85	97.18	-	-	-
S18	6.06	96.81	34.69	2.15	16.13
S19	5.23	96.49	43.09	2.53	17.03

Table 4.2 Small scale slabs - force time records

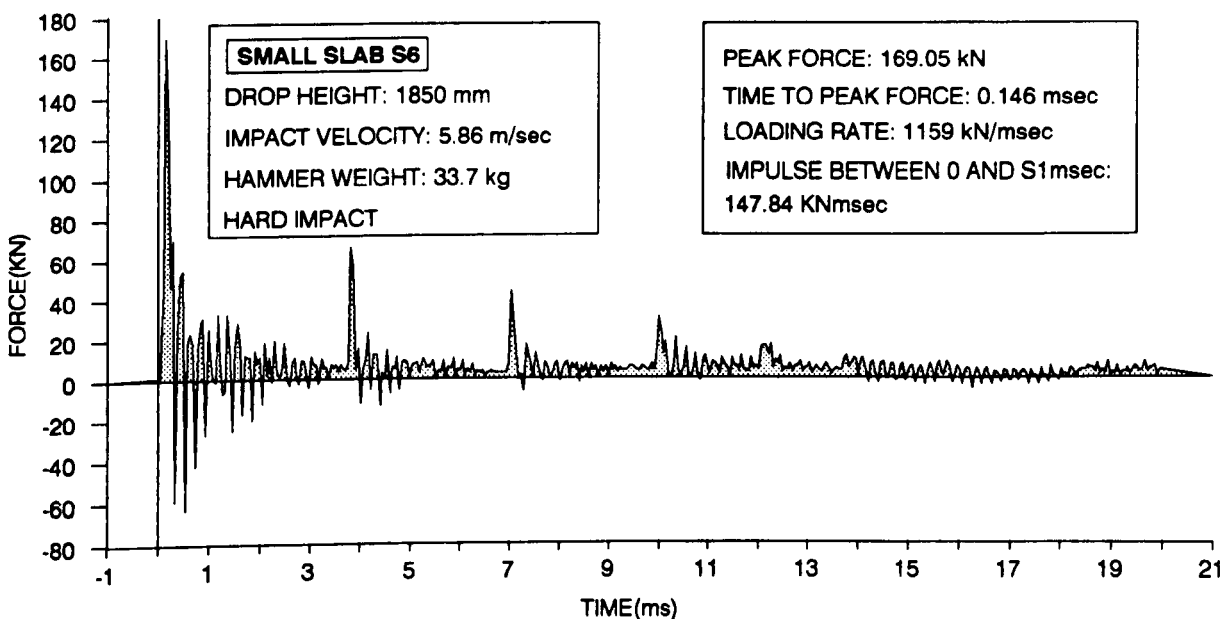


Fig. 4.1 Small scale slab, hard impact test, typical force vs time record

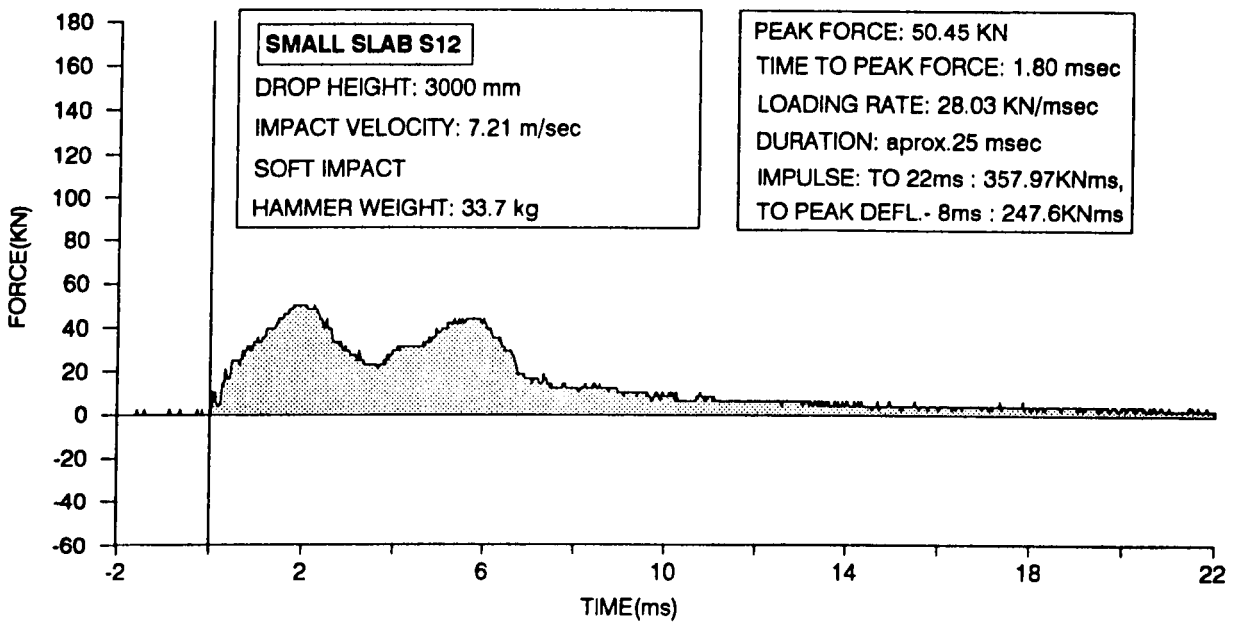


Fig. 4.2 Small scale slab, soft impact test, typical pressure bar record

The impact velocities were obtained by extrapolation of the velocities measured about 10mm above the impact point.

4.1.1.2 Displacement record

Under concentrated impact loads two different types of deflection occurred. The deflection just under the point of impact load was the deflection of a local area and consisted of movement of the punching cone itself, relative to the remainder of the specimen, and of movement of that area as a part of the subsequent overall flexural response of the slab. Overall deflection of the remaining part of the slab was caused by the load transfer from the impact zone and was largely dependent on whether or not local punching failure occurred. In these tests the local deflection was measured by the RPDT's (section 3.3.3.5) which were attached to the soffit of the slab under the impact point and close to it. The RPDTs outside the punch zone gave the deflection of the remainder of the slab. For the first three slabs (S1, S2 and S3) midspan deflections were measured with RPDTs which were simply glued to the bottom surface of the slab. This proved to be unreliable as the glued joint did not survive the impact. For the remaining tests the RPDTs were always attached directly to the reinforcement, as shown in Plate 3.13, section 3.3.3.5 and so were prevented from falling off the specimen during the tests.

The punching resistance of the small scale slabs S1 - S6 was greatly exceeded and the ratio between midspan and quarter span point deflections was very high. In the case of small

scale slabs S7 and S8, exposed to soft impact, that ratio was much lower because the resistance was either not reached or was only just reached (Slab S8). The slabs with a higher percentage of reinforcement had the least maximum recorded deflection at midspan under the impact point but showed no obvious changes in the peak deflection at quarter span point.

In the final phase of the work (slabs S9 to S19) the number of RPDTs was increased to up to 4 and consequently the deflection profile of the slab could be estimated more reliable.

A typical result for the deflection vs time record in impact tests is given in Fig. 4.3.

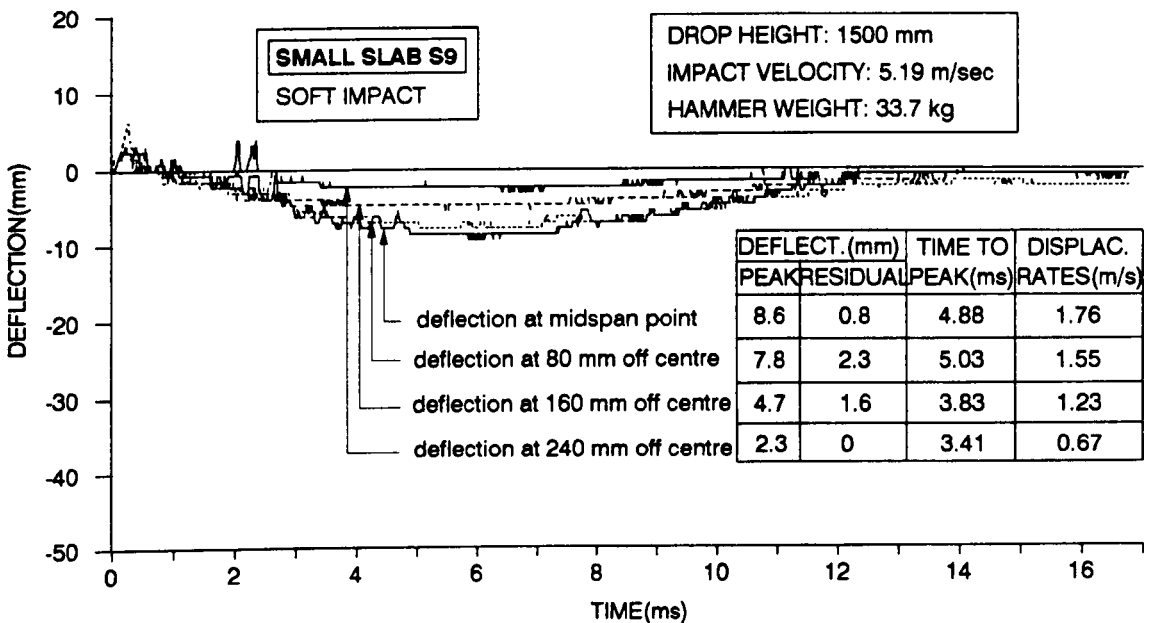


Fig. 4.3 Small scale slab, soft impact test - typical deflection vs time record

4.1.1.3 Reinforcement strain record

The reinforcement strain at the midspan point was monitored for the tensile zone bars in both directions. Being placed just under the actual impact point of the loading, the electrical resistance strain gauges (section 3.3.3.4) did not always survive for very long after the load application, particularly in the cases when punching failure occurred. However, even when the record was incomplete, it did give the strain rates for the local area of the slab under the impact loading. Typical strain vs time traces are of two different types. The first type is for gauges which survived the impact, shown on Fig. 4.4. The other type of record, when gauges did not survive, is shown in Fig. 4.5.

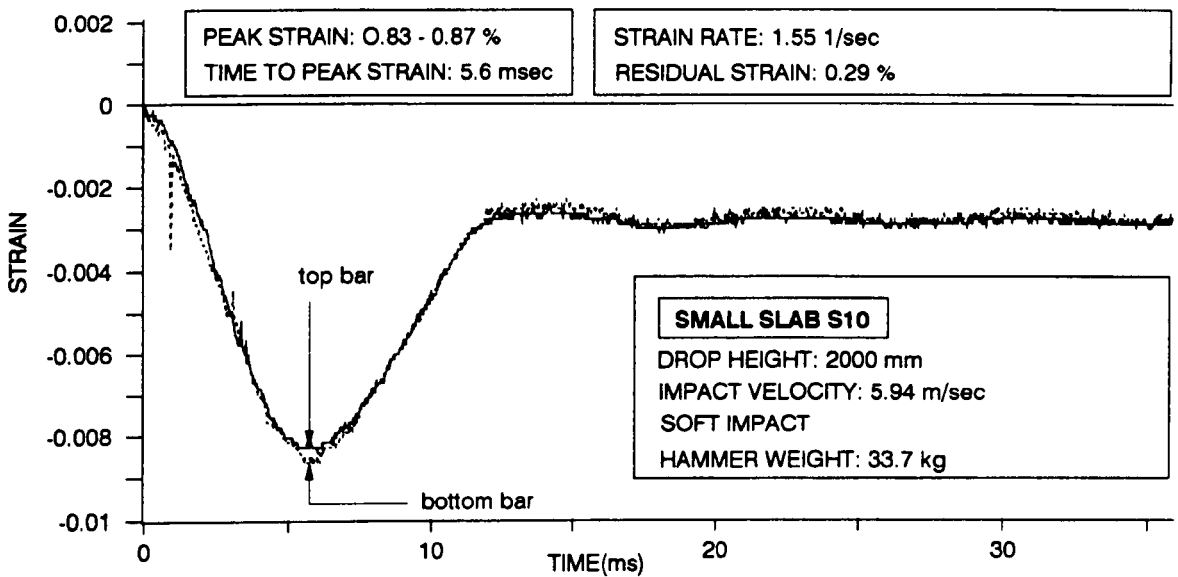


Fig. 4.4 Small scale impact test - full reinforcement strain record

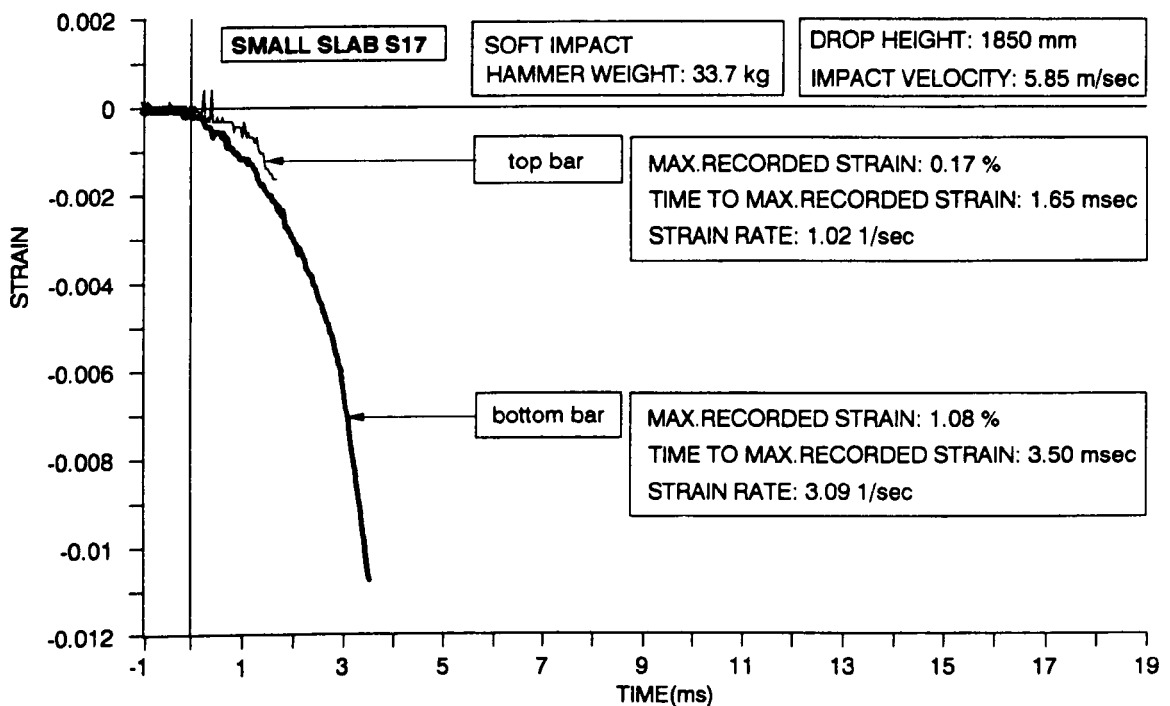


Fig. 4.5 Small scale impact test - partial reinforcement strain record

All available reinforcement strain records are presented in Table 4.3. Strain rates are given as the average strain rate to the peak strain or to the failure of the gauge, if the peak was not recorded. In cases of hard impact, the strain in the reinforcement first showed changes at 125-150 μ sec after impact, while in the case of soft impact that time varied between about 275 μ sec and 600 μ sec.

SLAB	TENSILE ZONE BARS	STRAIN RATE (1/sec)	RECORDED TIME (msec)	ADDITIONAL AVAILABLE INFORMATION
	GAUGE			
S1	Upper	-	-	Not recorded
	Lower	-	-	Not recorded
S2	Upper	0.226	3.80	Gauge broken at 0.1% strain , uniform strain rate
	Lower	2.489	3.80	Gauge broken at 1.17% strain, two zones of strain rate
S3	Upper	2.032	3.15	Gauge broken at 0.64% strain, uniform strain rate
	Lower	1.787	2.07	Gauge broken at 0.37% strain, uniform strain rate
S4	Upper	0.550	2.88	Gauge broken at 0.16% strain, uniform strain rate
	Lower	0.758	1.98	Gauge broken at 0.15% strain, uniform strain rate
S5	Upper	2.050	3.22	Gauge broken at 0.66% strain, two zones of strain rate
	Lower	3.004	2.83	Gauge broken at 0.85% strain, two zones of strain rate
S6	Upper	3.208	2.12	Gauge broken at 0.68% strain, two zones of strain rate
	Lower	2.969	2.29	Gauge broken at 0.68% strain, two zones of strain rate
S7	Upper	-	-	Not recorded
	Lower	-	-	Not recorded
S8	Upper	0.635	4.88	Gauge broken at 0.31% strain, uniform strain rate
	Lower	2.404	3.91	Gauge broken at 1.17% strain, two zones of strain rate
S9	Upper	1.157	12.60	Peak strain was 0.65%
	Lower	2.46	12.60	Peak strain was 1.17%, sudden recovery to 0.96%
S10	Upper	1.54	35.92	Peak strain was 0.83%, residual strain about 0.23%
	Lower	1.55	35.92	Peak strain was 0.82%, residual strain about 0.23%
S11	Upper	1.71	11.60	Peak strain was 0.78%, two zones of strain rate
	Lower	2.46	8.95	Peak strain was 1.18%, two zones of strain rate
S12	Upper	1.26	8.5	Peak strain was 0.42%
	Lower	2.60	7.45	Peak strain was 0.72%
S13	Upper	2.62	3.23	Gauge broken at 0.02% - after recovery
	Lower	1.81	2.60	Gauge broken at 0.47%
S14	Upper	1.15	34.25	Peak strain was 0.41%, residual strain about 0.12%
	Lower	-	-	Not recorded
S15	Upper	0.85	2.23	Gauge broken at 0.19%
	Lower	1.12	2.58	Gauge broken at 0.29%
S16	Upper	1.26	35.93	Peak strain 0.46%, residual strain about 0.10%
	Lower	1.31	35.93	Peak strain 0.52%, residual strain about 0.19%
S17	Upper	1.02	1.65	Gauge broken at 0.17%
	Lower	3.09	3.50	Gauge broken at 1.08%
S18	Upper	1.57	36.43	Peak strain 0.69%
	Lower	2.66	3.88	Gauge broken at 1.03%
S19	No central reinforcement			

Table 4.3 Small scale impact tests - Reinforcement strain record

4.1.1.4 High speed films

As described in sections 3.3.3.6 the underside of the slabs was photographed at filming rates of up to 9,000 pictures per second (p.p.s.). Details from the successful trials are given in Table 4.4.

SLAB NUMBER	FILM RATE (p.p.s.)	INTER-FRAME TIME (μ sec)	APPROXIMATE RECORDED TIME AFTER IMPACT (msec)	CAMERA TYPE	SHUTTER SIZE
S2	5090	196.46	30	Hycam	Full frame
S4	3843	260.21	25	Hycam	Full frame
S5	4418	226.35	20	Hycam	Full frame
S6	4470	223.74	35	Hycam	Full frame
S12	6242	160.21	500	Photec IV	Half frame
S13	8739	114.43	400	Photec IV	Half frame
S17	6278	159.28	500	Photec IV	Half frame

Table 4.4 Small scale impact test - High speed film details

Typical frames taken with the full and half frame shutters are shown and explained in more detail in Fig. 4.6.

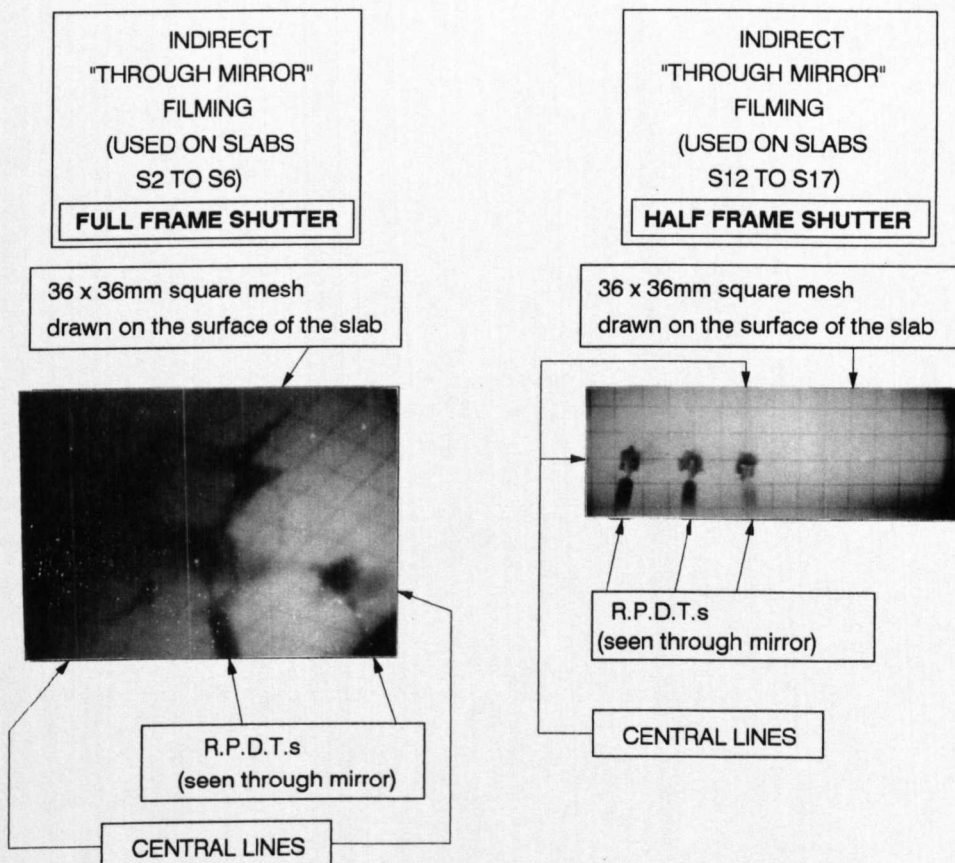


Fig. 4.6 Typical 16mm Frame details - Impact test

Some typical sequences of failure for both soft and hard impacts are shown below, Fig. 4.7.

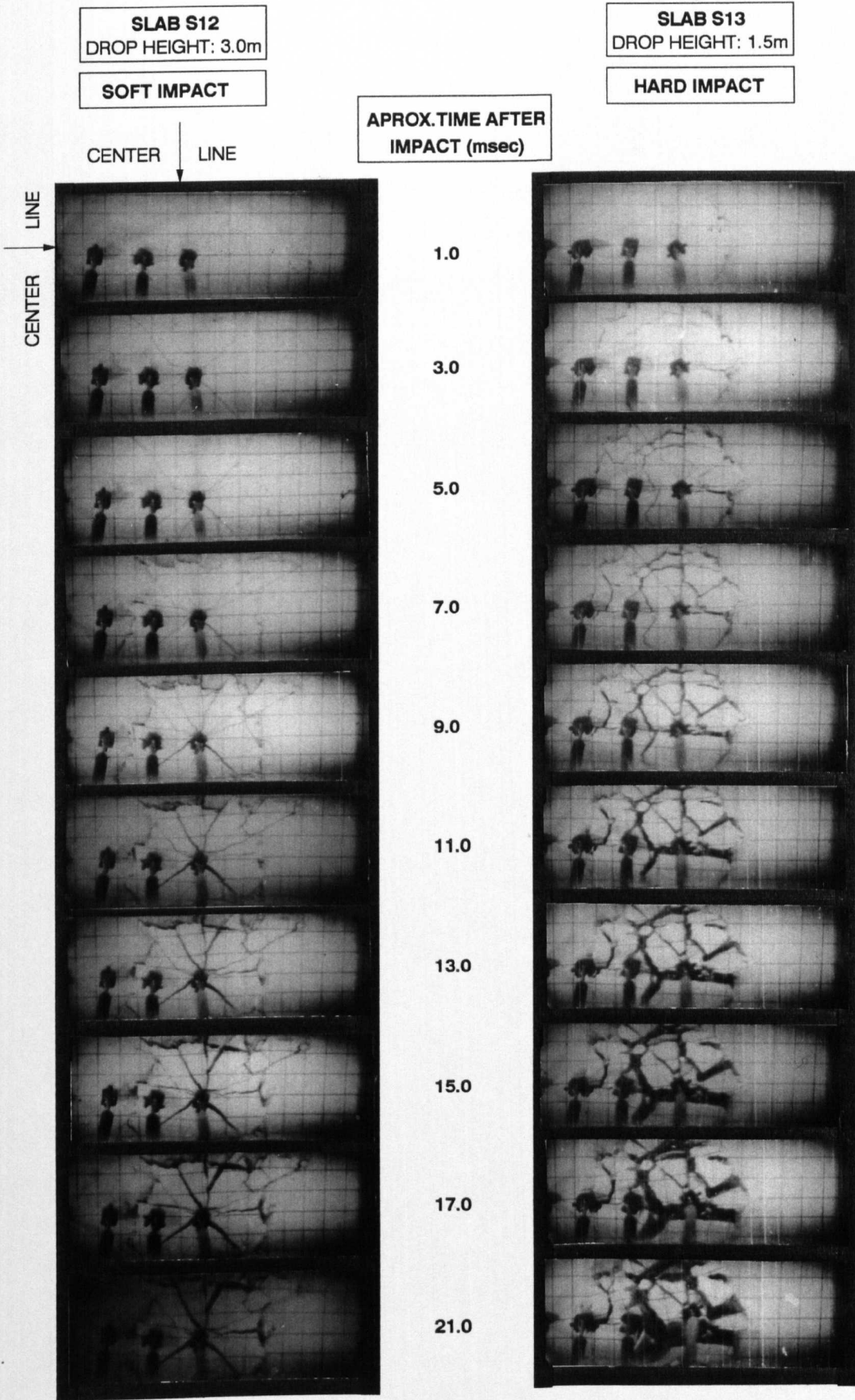


Fig. 4.7 Failure propagation for hard and soft impact tests

4.1.1.5 Crack patterns and slab cross-sections

After the test all visible cracks were marked after inspecting the slabs using a 6 X magnification magnifying glass (section 3.3.3.7). Clear differences between the crack patterns produced by soft and hard impact tests can be established, the most pronounced difference being the number of surface cracks.

On some of the specimens the cracks were marked in two phases. In the first phase the most pronounced cracks were marked whilst the smaller and more difficult to observe were marked in a more careful inspection during a second phase.

Some typical first and second phase crack patterns for both soft and hard impact are shown in Fig. 4.8 and 4.9.

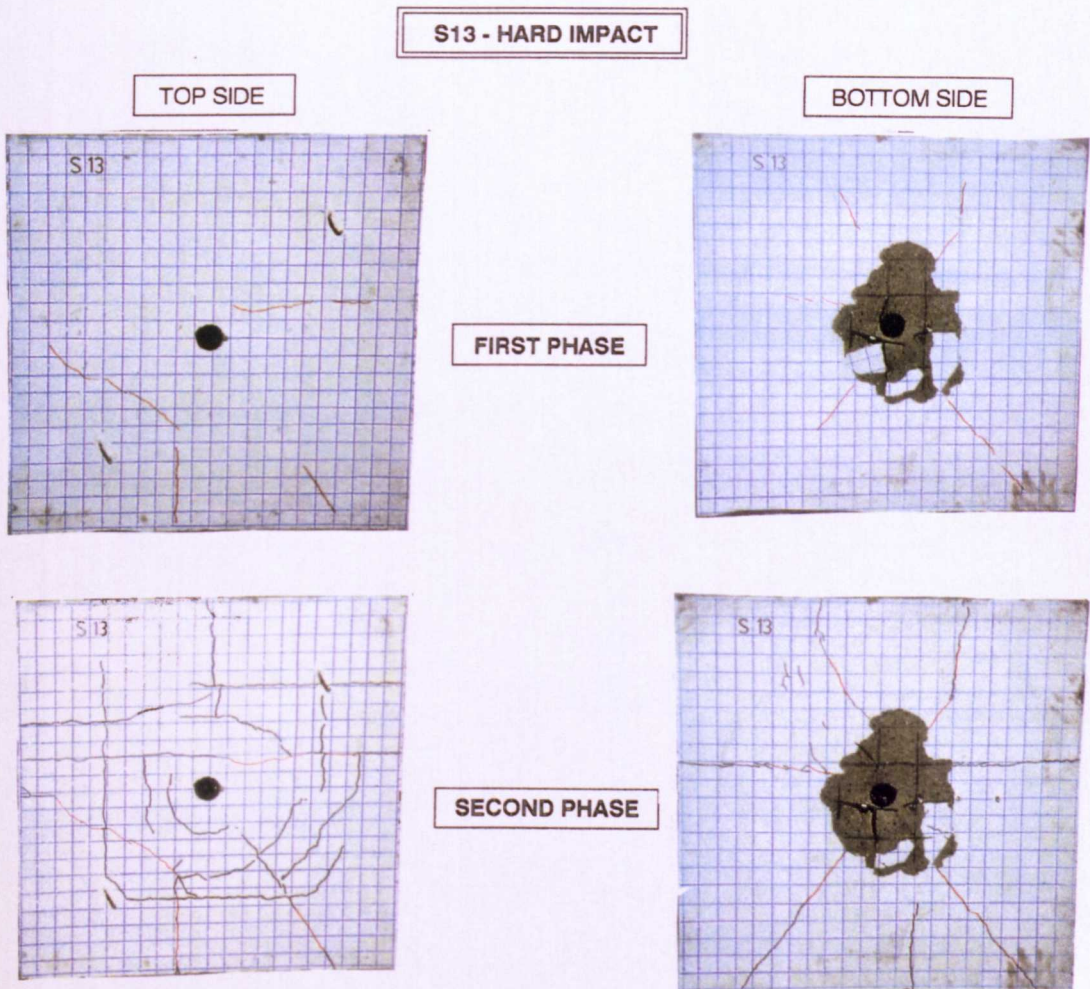


Fig. 4.8 Small scale slabs - hard impact tests - crack patterns

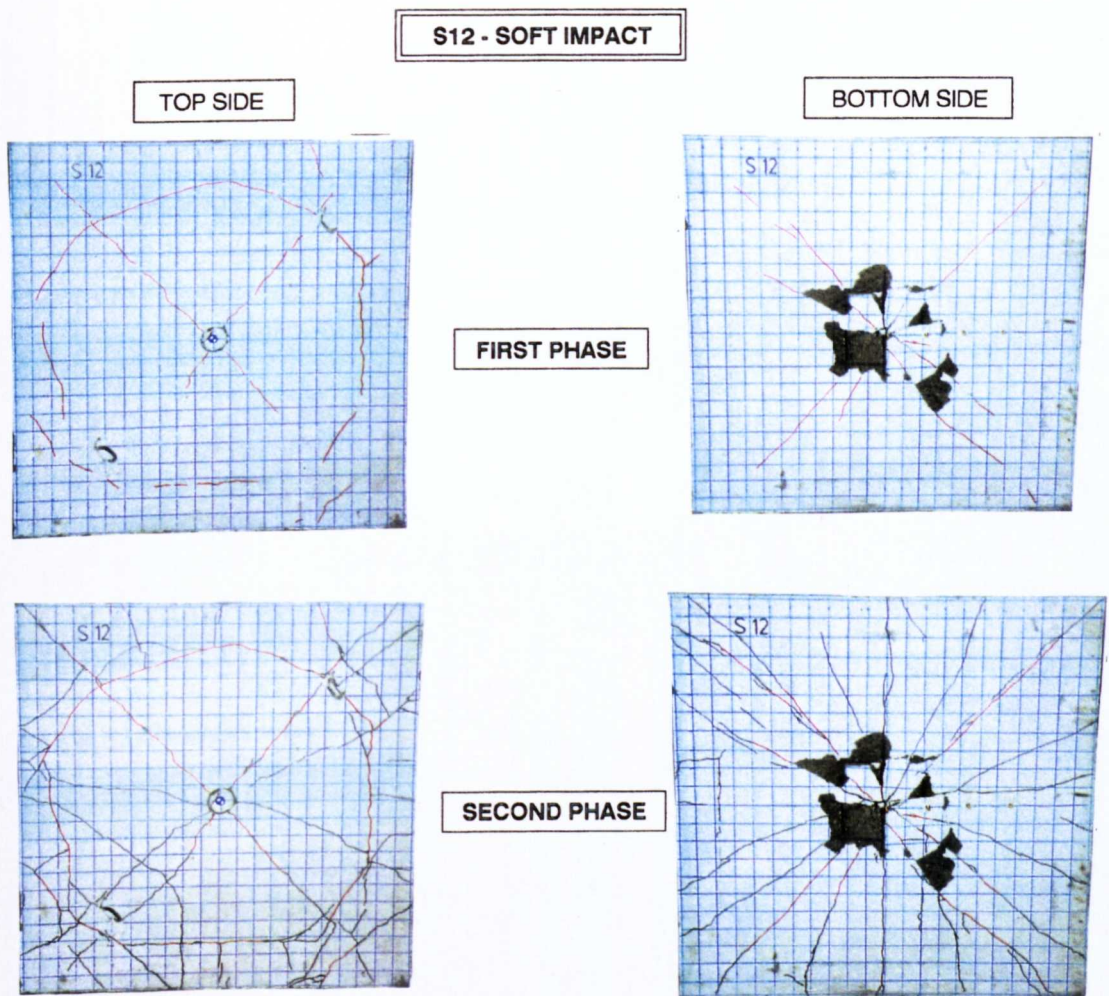


Fig. 4.9 Small scale slabs - soft impact tests - crack patterns

After the impact tests, some typical cracked slabs were carefully cut along the centre line in order to monitor cracks on the cross-section. Typical examples are shown in Fig. 4.10 for hard impact and in Fig. 4.11 for soft impact.

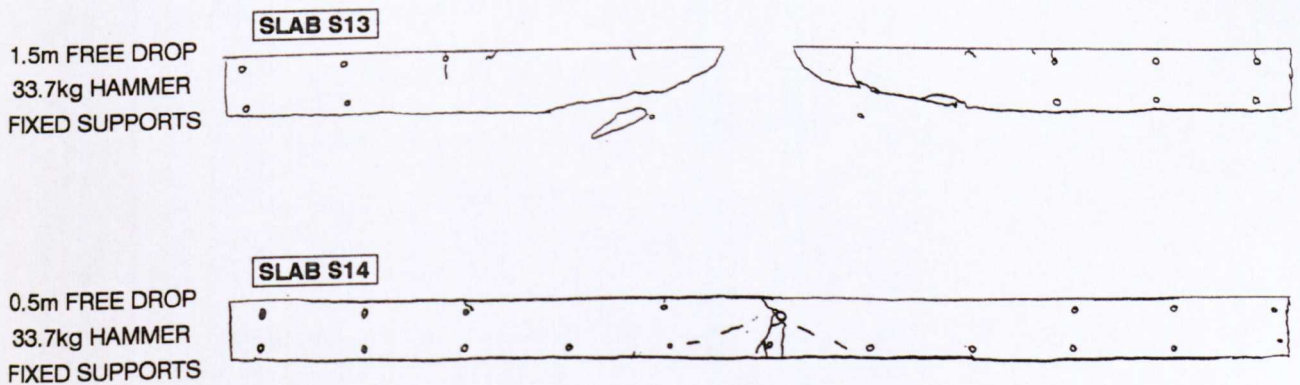


Fig. 4.10 Small scale slabs - hard impact test - cross-sections

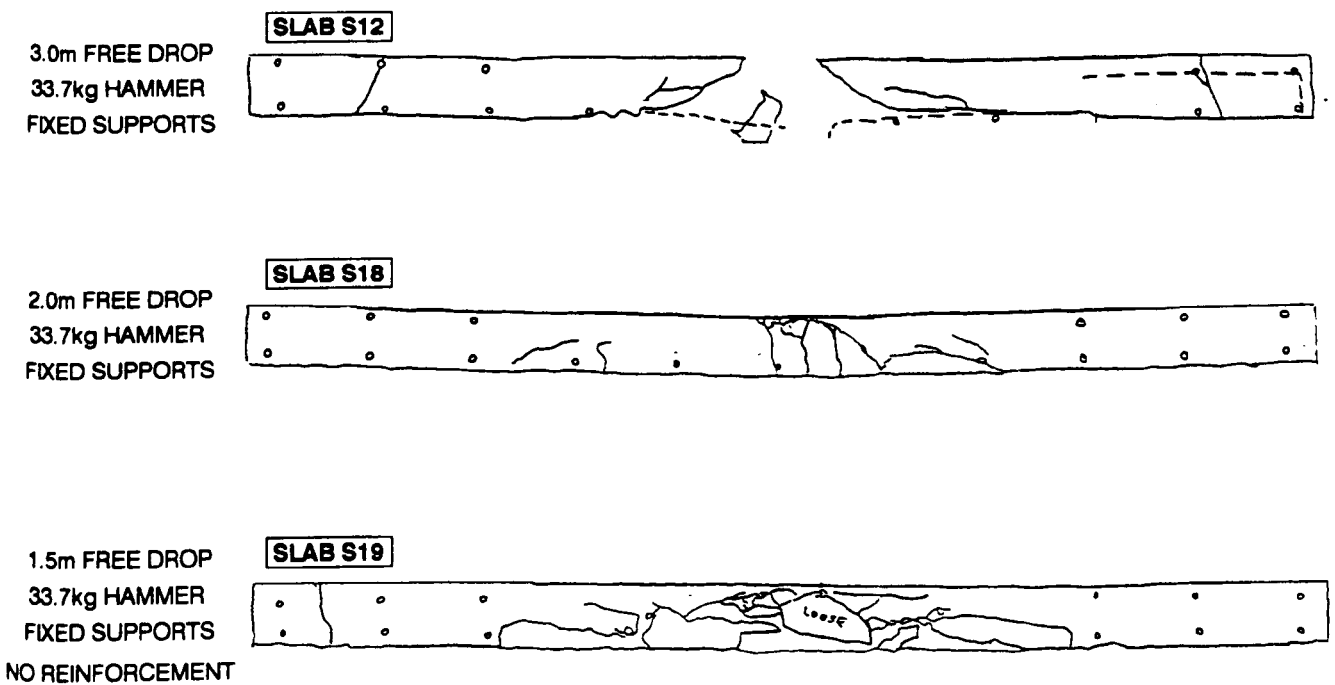


Fig. 4.11 Small scale slabs - soft impact test - cross-sections

4.1.2 1:1 Scale slabs

The testing programme consisted of tests on five full scale slabs. Slab LS5 was exposed to soft impact while the remaining four were subjected to hard impacts. In all five tests the same support conditions were employed (section 3.3.1.3), and the load was always applied through the 125mm dia, 500mm long load cell, (section 3.3.2.1). The reinforcement was as given in Fig. 3.1. Slab LS1 was the only slab to be tested twice (with a 70kg hammer) while the remaining four slabs were tested with a 150kg hammer. All five slabs were equipped with strain gauges to monitor midspan reinforcement strains and displacement transducers were placed at up to four positions. Recording of the stress waves caused by the falling hammer hitting the load cell were taken from the load cell itself (section 3.3.3.1). Velocity of the hammer was monitored as explained in section 3.3.3.2. After the tests, cracks were marked and photographs of the crack patterns taken.

The main test variables were the amount of impact energy and the force duration applied to the specimens. These were achieved by changing the impact velocity and by placing a rubber pad in between the hammer and the load cell in order to extend the duration of the load and reduce

its peaks. The only other variable was the amount of reinforcement, although an effort was made to keep the bar spacing constant. All the test variables are given in Table 4.5.

SLAB NO.	REINFORCEMENT		IMPACT TYPE	DROP HEIGHT (m)	HAMMER SIZE (kg)
	TOP LAYER	BOTTOM LAYER			
LS1	1.2% each way	1.2% each way	Hard	3.22(two impacts)	70
LS2	1.2% each way	1.2% each way	Hard	3.22	150
LS3	0.41% each way	0.41% each way	Hard	2.5	150
LS4	0.41% each way	0.41% each way	Hard	3.22	150
LS5	0.41% each way	0.41% each way	Soft	2.5	150

Table 4.5 Full scale slabs - impact test - test details

Slabs LS3 to LS5 were designed without central region reinforcement (500mm x 500mm) in the top side of the specimen. Reinforcement percentages were kept the same for both directions in all five slabs.

The following sections will give an insight into some of the typical results obtained from the tests. All available test results together with the test details are presented in Appendix A1.

4.1.2.1 Pressure bar and velocity record

In all cases load was applied to the specimen over a 12,265mm² circular area defined by the diameter of the load cell. Impact velocities varied between 6.99 - 7.93m/sec which represented up to 99.8% of the free fall velocities. The duration of the pulse was in the case of slab LS5, prolonged by a placing a 25mm thick 125mm dia. rubber pad in between the falling hammer and the load cell and so producing a soft impact. Some of the additional test details are given in Table 4.6.

As expected there was a clear distinction between soft and hard impact. The peak loads in the load vs time function for hard impact were up to six times greater and the load duration was about 15 times shorter than in case of soft impact. The differences can easily be seen from the typical results for both cases presented in Fig.4.12 (hard impact) and Fig.4.13 (soft impact). The impulse value given in Fig.4.13 is calculated to the time of 13msec. Since the peak displacement of this slab occurred at about 12msec, the impulse at that time had a value of 1019.2kN msec.

SLAB NO.	IMPACT VELOCITY m/s	% OF FREE FALL VELOCITY (%)	PEAK LOAD (kN)	TIME TO REACH PEAK LOAD (msec)	LOADING RATE (kN/msec)
LS1, First impact	-	-	1090.39	0.005	19818.0
LS1, Second impact	7.71	97.0	1046.77	0.10	10467.0
LS2	7.79	98.0	3028.86	0.11	27535.0
LS3	6.93	99.0	2059.80	0.06	34330.0
LS4	7.93	99.7	1485.76	0.08	18572.0
LS5	6.99	99.8	256.63	1.66	154.60

Table 4.6 Full scale slab - impact test - load function results

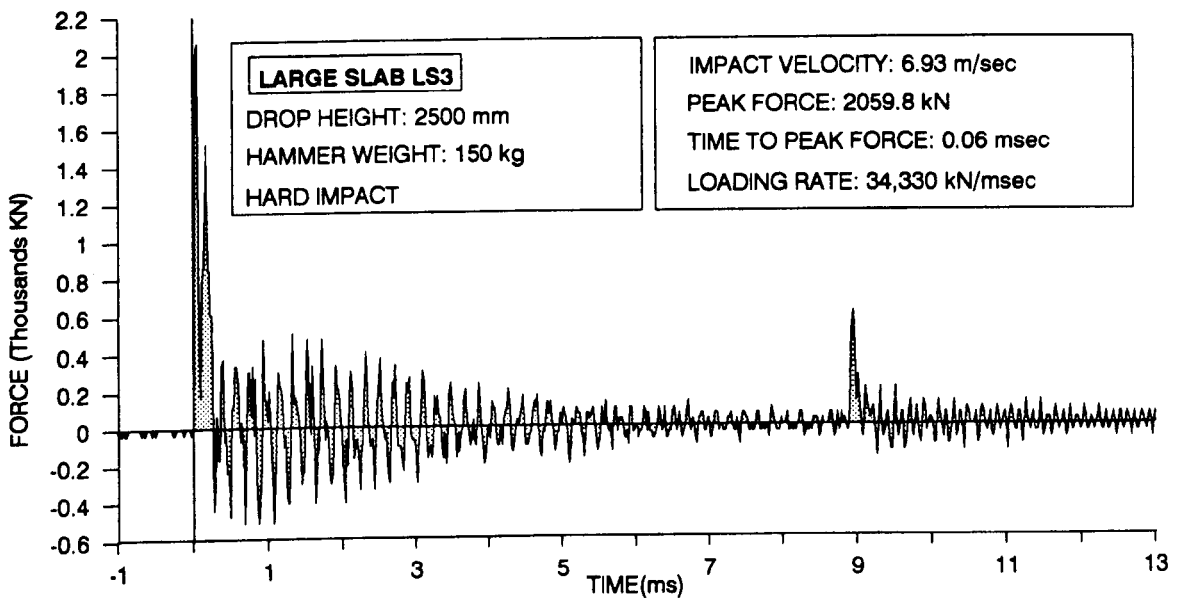


Fig. 4.12 Full scale slab - hard impact test - typical load-time record

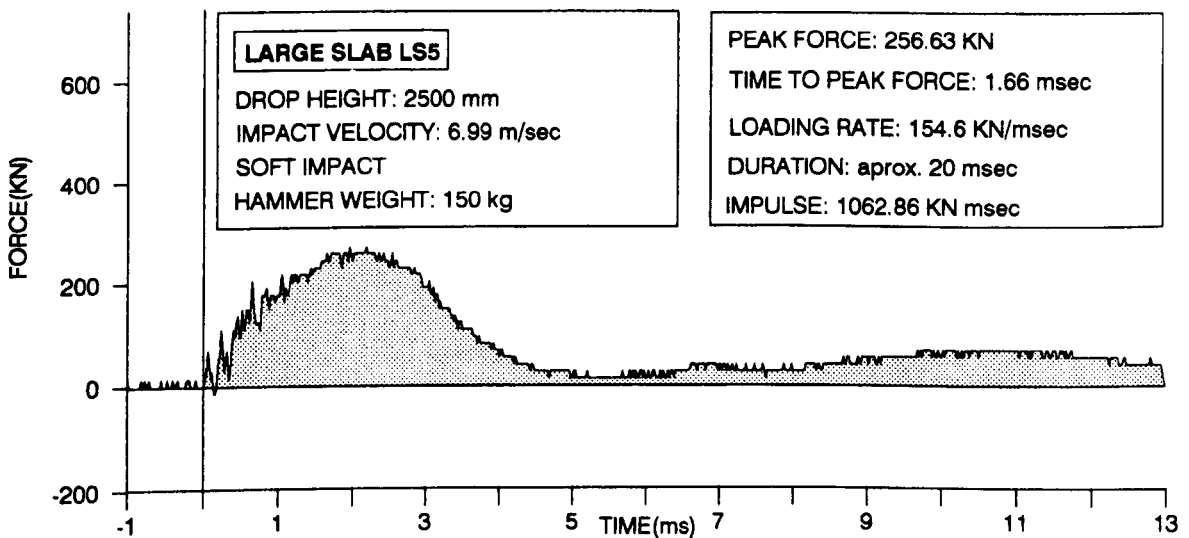


Fig. 4.13 Full scale slab - soft impact test - typical load time record

4.1.2.2 Displacement record

On all five specimens displacement measurements (section 3.3.3.5) were taken at up to four positions by the RPDTs (section 3.2.1) connected to the bottom reinforcement of the slab. Displacement transducer positions for each of these tests are given in Fig. 3.30. In the case of hard impact movement of the slab soffit usually commenced at about 0.25msec after the impact while in the case of soft impact it commenced later, at 0.80msec. Some typical results for both soft and hard impact deflections vs time are presented in Fig. 4.14 and Fig. 4.15.

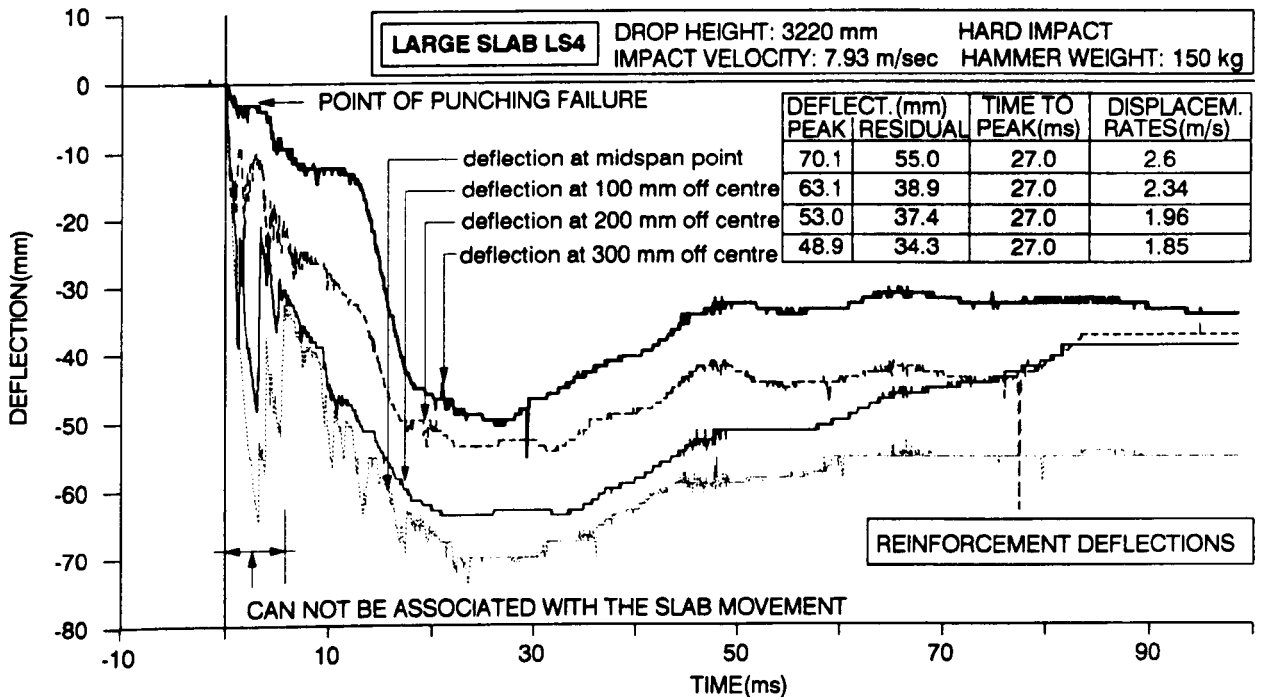


Fig. 4.14 Full scale slabs - hard impact test - typical displacement vs time record

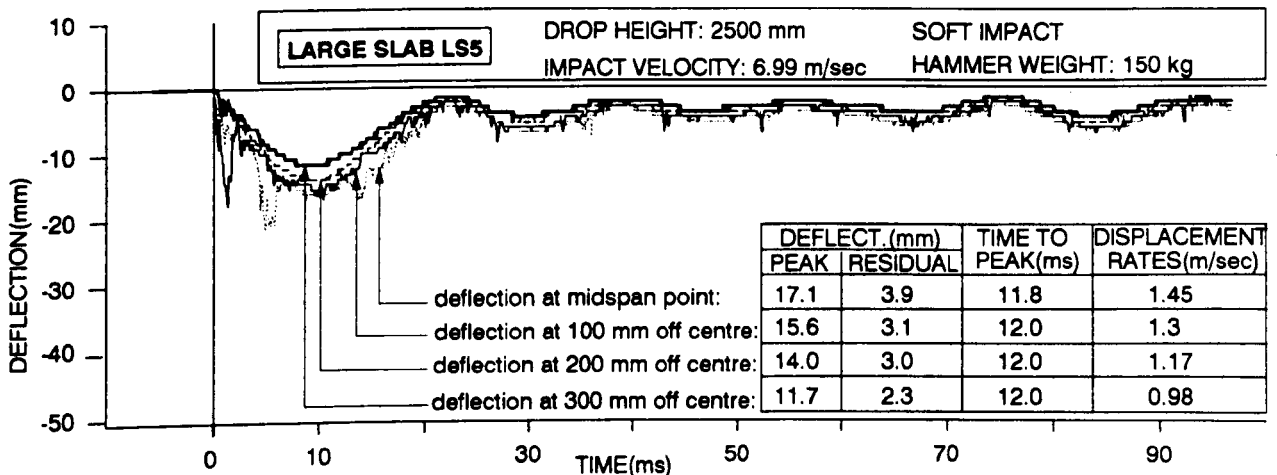


Fig. 4.15 Full scale slabs - soft impact test - typical displacement vs time record

A brief description of the results is given in Table 4.7.

SLAB	DISPLACEMENT RECORD DETAILS
LS1	Displacement was recorded for the first impact only, at 225mm and 450mm off centre. At 225mm off centre the peak was 6.8mm and it was reached after 4.2msec giving a deflection rate of 1.63m/sec. At 450mm off centre the peak was 3.1mm, reached after 1.35msec - deflection rate 2.3m/sec. Almost full recovery in both cases was reached at 13.1msec so producing recovery rates of 0.77m/sec and 0.35m/sec for 225 off centre and 450mm off centre positions respectively. Residual displacements were not very clear and were almost identical for both positions - about 1.5mm.
LS2	Displacement was again taken at two positions. At 225mm off centre the peak deflection was 11.2mm and was reached after 8.9msec, deflection rate 1.26m/sec. About 80msec of the record was obtained so residual displacement can only be estimated as about 4.5mm. At 450mm off centre, peak displacement of 4.9mm was reached after 8.9msec giving a displacement rate of 0.56m/sec. The first natural period appeared to be 22msec and the residual deflection is estimated as 1mm.
LS3	This slab failed in the central region and as in the previous cases, RPDTs were connected to the bottom reinforcement. The initial 3.7msec of the trace was very noisy and has not been taken into account. Measurements were taken at midspan, 100mm and 200mm from the centre. The peak of the midspan deflection was 42mm reached after 11.8msec producing a deflection rate of 3.56m/sec. It appears that after 19msec the punching resistance of the slab was reached and another peak deflection appeared at 30msec. After this time the reinforcement started to recover. The 100mm off centre peak displacement was 38.1mm, it was difficult to distinguish it from the failure point and almost no elastic recovery of the reinforcement occurred. The 200mm off centre peak displacement was 13mm, reached after 10msec implying a deflection rate of 1.3m/sec. The second peak, probably caused by the shear failure, occurred at 29msec. In all three cases residual displacements of the bottom reinforcement were difficult to estimate.
LS4	Although this slab also had a central area punching failure, displacements were very consistent but peaks generally did not correspond with the natural period of the slab but to the time of punching failure and the movement of the bottom reinforcement associated with it. Peak displacement at midspan, 100, 200 and 300mm off centre happen almost at the same time (27msec), and these were 70.1mm, 63.1mm, 13.0mm and 49.3mm respectively, so implying the maximum deflection rate of 2.6m/sec. Full recovery occurred at 52msec and the residual displacements of the reinforcement are estimated as 55mm, 38.9mm, 37.4mm and 34.3mm for the central, 100mm, 200mm and 300mm off centre transducers respectively.
LS5	This was the only slab that was tested in soft impact conditions. Displacements were measured at the same positions as for the slab LS4. Peaks were reached at 11.8msec, and these were 17.1mm 15.6mm 14mm and 11.7mm for the central, 100, 200 and 300mm off centre transducers respectively. Full recovery was reached 26msec after the impact with the residual deflections being estimated as 3.9mm, 3.1mm, 3mm and 2.3mm respectively, reached at about 95msec after the impact.

Table 4.7 Full scale slabs - Impact test - Displacement record details

4.1.2.3 Strain record

Reinforcement strains (section 3.3.3.4) were, as in all other cases taken at the midspan point from the bars in both directions. In all cases strain records closely resembled the displacement record indicating that most of the reinforcement strain was produced by flexural displacement of the slab and not by in-plane deformation. Table 4.8 gives some details about these records.

SLAB	STRAIN RECORD							
	TOP BAR				BOTTOM BAR			
	PEAK VALUE (strain) %	TIME TO PEAK (msec)	STRAIN RATE (sec ⁻¹)	RESID. STRAIN (strain) %	PEAK VALUE (strain) %	TIME TO PEAK (msec)	STRAIN RATE (sec ⁻¹)	RESID. STRAIN (strain) %
LS1-1st	0.07	4.2	0.17	0.01	0.08	4.2	0.19	0.02
LS1-2nd	0.08	5.1	0.15	0.01	0.09	5.5	0.16	-
LS2	0.14	8.0	0.18	0.02	0.16	8.0	0.20	0.04
LS5	0.25	8.8	0.28	0.03	0.29	9.2	0.31	0.09

Table 4.8 Full scale slabs - impact test - strain record

In the case of the hard impact tests straining of the reinforcement usually started at about 400µsec after the impact whilst in the case of the in soft impact tests it started at about 700µsec after the impact. Fig. 4.16 and Fig. 4.17 represent typical strain vs time results for both hard and soft impact tests respectively.

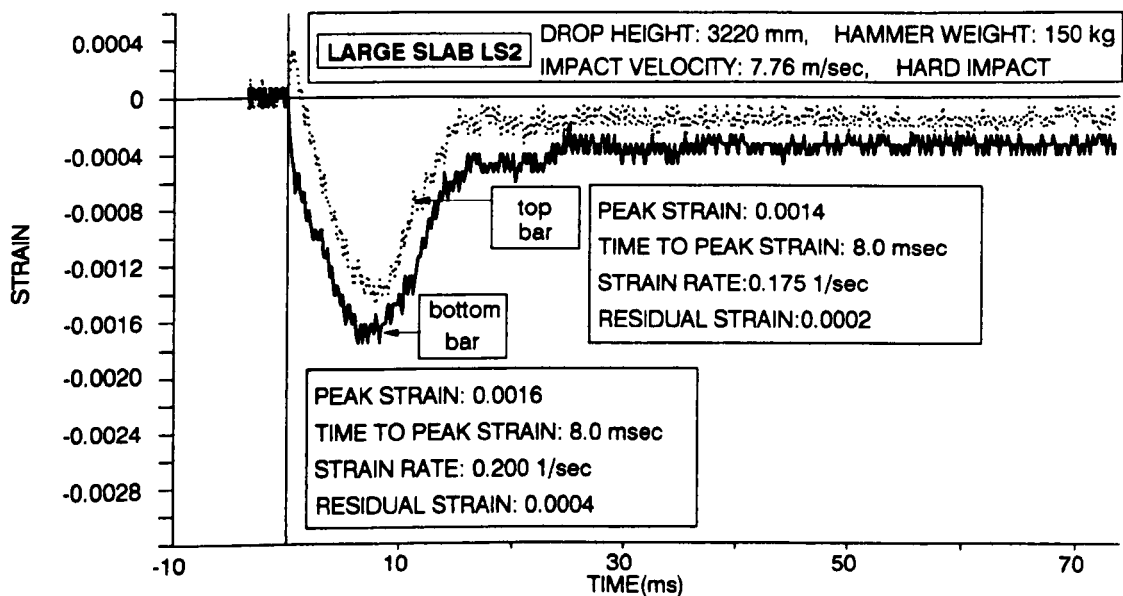


Fig. 4.16 Full scale slabs - hard impact test - typical strain record

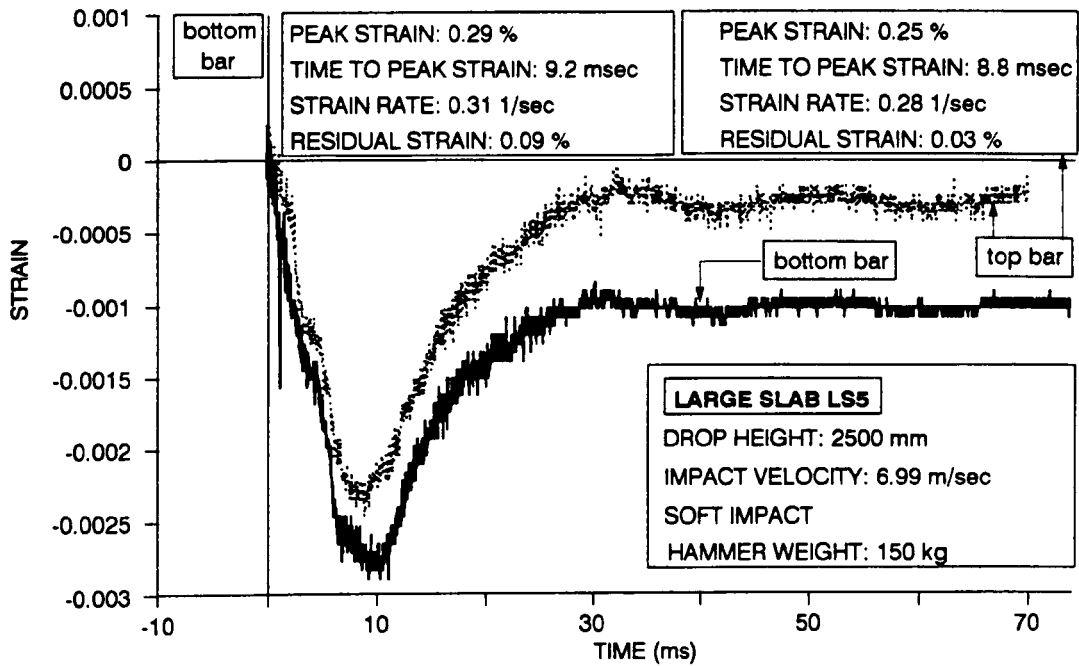


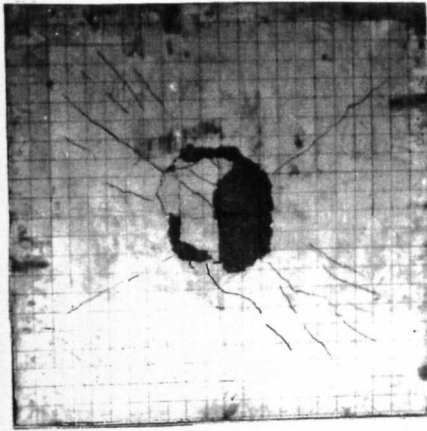
Fig. 4.17 Full scale slabs - soft impact test - typical strain record

4.1.2.4 Crack pattern

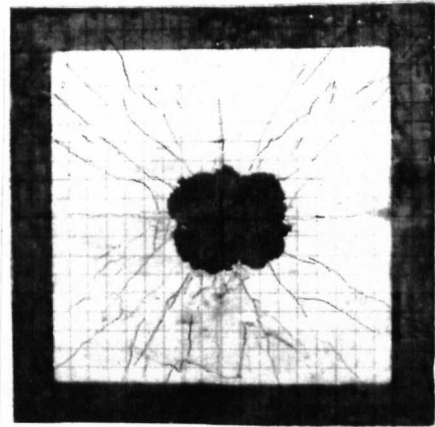
Crack patterns greatly depended on the type of failure that occurred. In cases when the slabs suffered punching failure (LS3 and LS4) the cracks were few in number, implying that most of the energy was used in producing the hole. In the three remaining cases it was very obvious that a flexural response was taking place, so producing much more cracking. The crack pattern was very much the same as on the small scale slabs. This appears to verify the scaling laws employed in this research.

Crack patterns of the bottom sides of all five slabs that were tested are shown in Fig. 4.18.

LS1 - DROP HEIGHTS 3220 mm



LS2 - DROP HEIGHT 3220 mm



SOFT IMPACT

LS3 - DROP HEIGHT 2550 mm

LS4 - DROP HEIGHT 3220 mm

LS5 - DROP HEIGHT 2500 mm

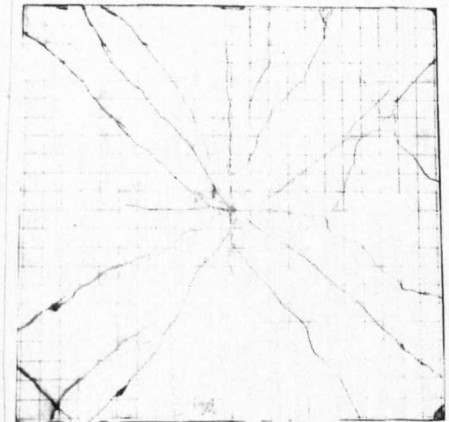
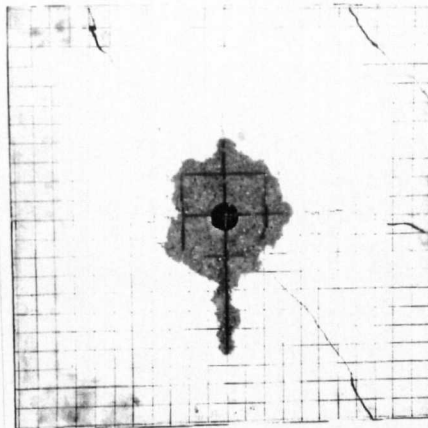
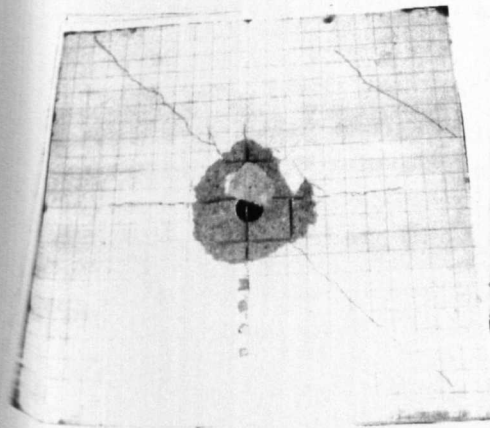


Fig. 4.18 Large scale slabs - impact tests - crack patterns

4.1.3 Conclusions

Soft and hard impact tests on both small and large scale specimens produced results which were closely related to the main characteristics of the impact loading function. In the small scale hard impact tests loading rates of up to $3.78 \cdot 10^6$ kN/msec produced displacement rates of up to 2.0m/sec and strain rates of up to 3.2sec^{-1} . Large scale slabs were tested at loading rates of up to 34×10^3 kN/msec, reinforcement strain rates of up to 0.3sec^{-1} and deflection rates of up to 3.56m/sec were observed. In most of the slabs punching failure occurred with the formation of a hole almost equal to the diameter of the pressure bar on the top side of the specimen, followed by

cratering on the bottom side. Crack patterns indicated that the specimens, apart from absorbing energy in the punching failure mechanism, absorbed some of the energy flexurally. The main indicators of the flexural response of the specimens were the cracks that propagated towards the corners of the slabs, corresponding to the yield lines produced in slabs under static loading.

The soft impact test produced loading rates of 28kN/msec, deflection rates of up to 2.1m/sec and strain rates of up to $3.1/\text{sec}^{-1}$ for the small scale slabs, and 155kN/msec, 1.45m/sec and 0.31sec^{-1} respectively for the large scale slabs. The response of the specimens to soft impact was governed by the combination of the punching (shear) resistance and by the overall flexural response. The duration of the load was the main reason for ensuring that the punching or local response of the specimen did not have such a dominant role as for the hard impact tests. Instead, the overall response of the structure was much more pronounced. It was characterised by the deflection profile of the specimen which clearly indicated a first mode of vibration response, and by a very dense mesh of diagonal cracks forming a static like yield-line crack pattern.

The overall shape of the damage, the failure mechanisms, the crack patterns, and direct comparison between the recorded strains and 2.5 times linear scaling between displacements appear to validate the modelling considerations that were employed.

4.2 Impulse tests

The main test results were obtained from the specimens exposed to the curved side of the hemispherical charge. In all tests the main variable was the pressure loading function (section 3.3.2.2), altered by changing the standoff distance.

4.2.1 1:2.5 Scale slabs

The testing programme on the small scale slabs consisted of 19 specimens. The main variables were the amount of tensile zone reinforcement and the blast pressure function. Initially the reinforcement was varied around the balanced section percentage (section 3.1.1) where as in later tests (slabs SE9 - SE19) the bottom reinforcement was kept constant at 0.28%. Slabs SE1 and SE2 did not have any top reinforcement whilst slab SE9 did not have any top or bottom

central zone reinforcement. Slabs SE10 to SE19 had top zone reinforcement only in a 200mm wide strip around the edges. The loading function was mainly varied by changing the charge standoff distance, the charge size was kept constant at 78g of PE4. Tests on slabs SE1 - SE4 used a cylindrically shaped charge while tests on the remaining 15 slabs used a hemispherical charge.

All the test variables are given in Table 4.9.

SLAB NO	SHAPE OF THE CHARGE	SIDE OF THE CHARGE FACING THE SPECIMEN	POSITION OF THE CHARGE	STANDOFF DISTANCE (mm)	BOTTOM REINFORCE.		SUPPORT
					Xway	Yway	
SE1	cylindrical	parallel	central	650 and 100	3.73	2.90	Free
SE2	cylindrical	parallel	central	<50	3.73	2.90	Free
SE3	cylindrical	parallel	central	50	2.39	2.01	Free
SE4	cylindrical	parallel	central	100	2.39	2.01	Free
SE5	hemispherical	spherical	central	100	1.25	1.05	Fixed
SE6	hemispherical	flat	central	100	1.25	1.05	Fixed
SE7	hemispherical	spherical	central	100	1.25	1.05	Internal
SE8	hemispherical	flat	central	50	1.25	1.05	Internal
SE9	hemispherical	spherical	central	100	none	none	Fixed
SE10	hemispherical	spherical	central	250	0.29	0.27	Fixed
SE11	hemispherical	spherical	central	200	0.29	0.27	Fixed
SE12	hemispherical	spherical	central	150	0.29	0.27	Fixed
SE13	hemispherical	spherical	central	125	0.29	0.27	Fixed
SE14	hemispherical	spherical	central	100	0.29	0.27	Fixed
SE15	hemispherical	spherical	central	75	0.29	0.27	Fixed
SE16	hemispherical	spherical	central	60	0.29	0.27	Fixed
SE17	hemispherical	spherical	central	50	0.29	0.27	Fixed
SE18	hemispherical	spherical	off centre	200	0.29	0.27	Fixed
SE19	hemispherical	spherical	off centre	100	0.29	0.27	Fixed

Table 4.9 Small slabs - Impulse tests - Test details

The charge was centrally placed in all slabs except slabs SE18 and SE19 where the charge was placed 283mm off centre along a diagonal. In the case of tests on slabs SE6 and SE8 the flat side of the hemispherical charge was positioned facing the slab.

4.2.1.1 Blast pressure records

The way in which the blast pressure measurements were taken is given in section 3.3.3.3. The influence of the charge shape and orientation was investigated using 78g-PE4 explosive charges of three different shapes and orientations to a blast pressure gauge. The cylindrical charge was placed with its longitudinal axis parallel to the gauge, the hemispherical charge had the curved or flat side facing the gauge which was always on the axis central and perpendicular to the flat side. Typical results for all three types are given in Figs. 4.19, 4.20 and 4.21 and in Table 4.10. In all of them the zero time has been taken as a time of a charge initiation.

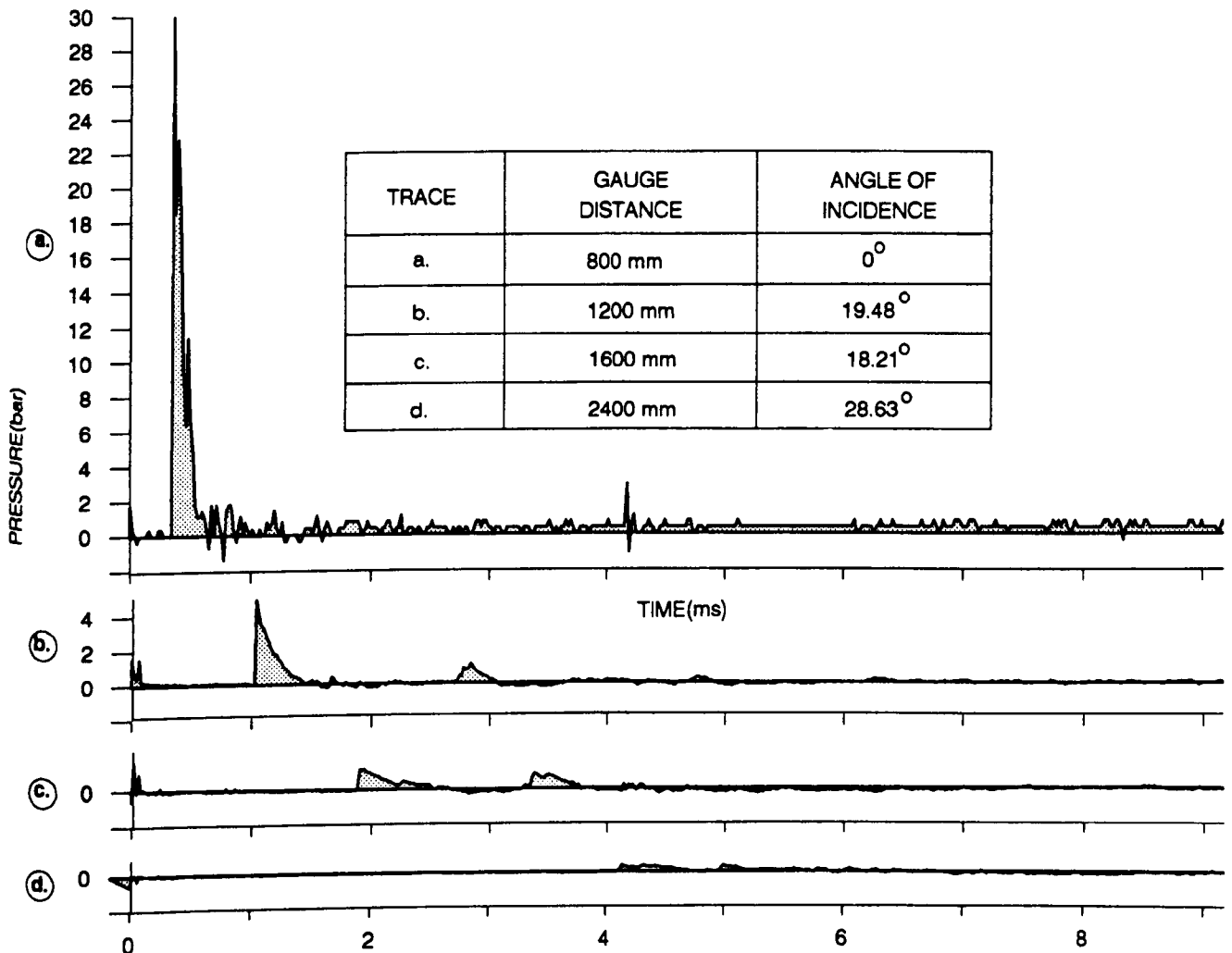


Fig. 4.19 Typical pressure-time record for the 78g PE4 hemispherical charge, flat side

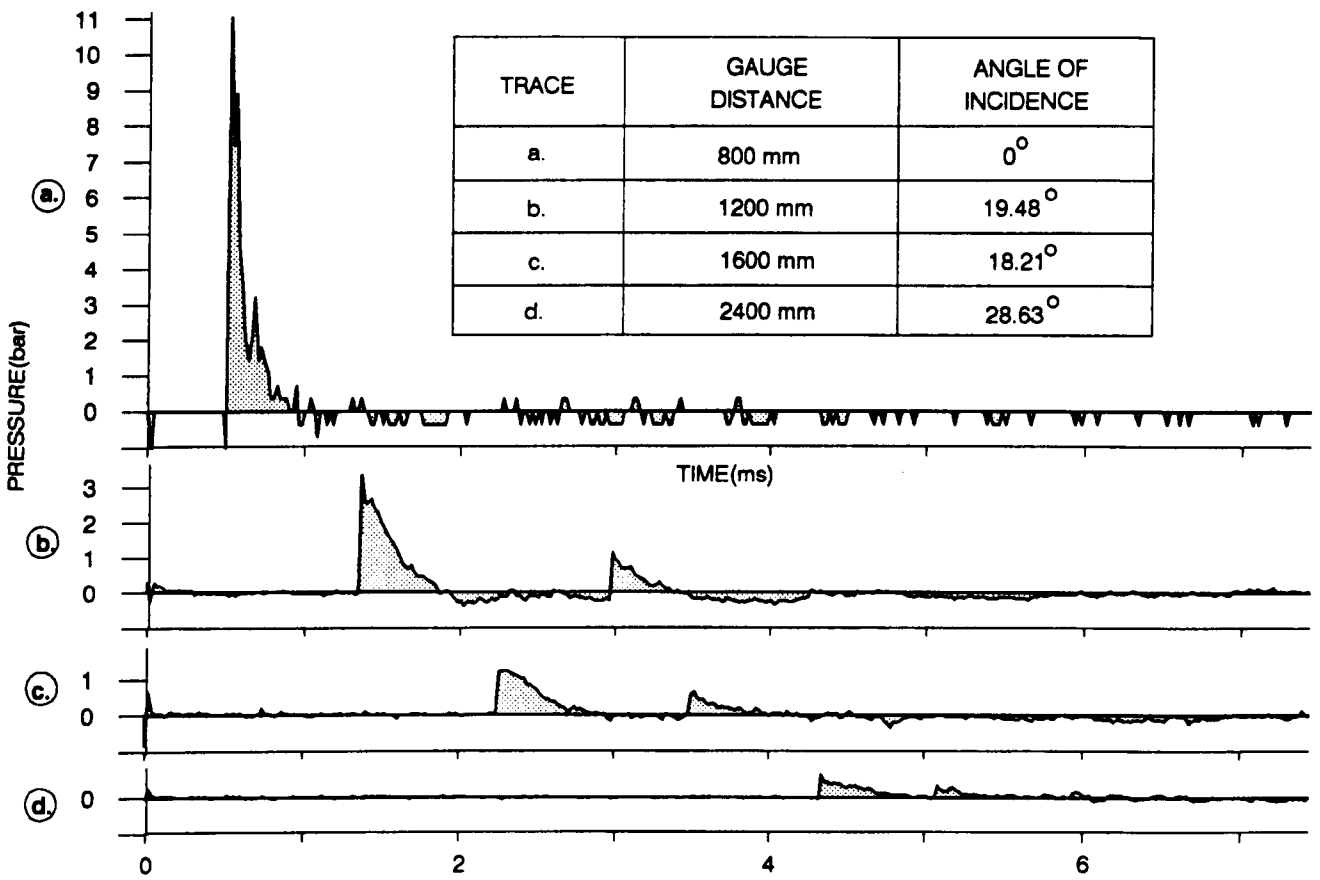


Fig. 4.20 Typical pressure-time record for the 78g PE4 hemispherical charge curved side facing the gauges

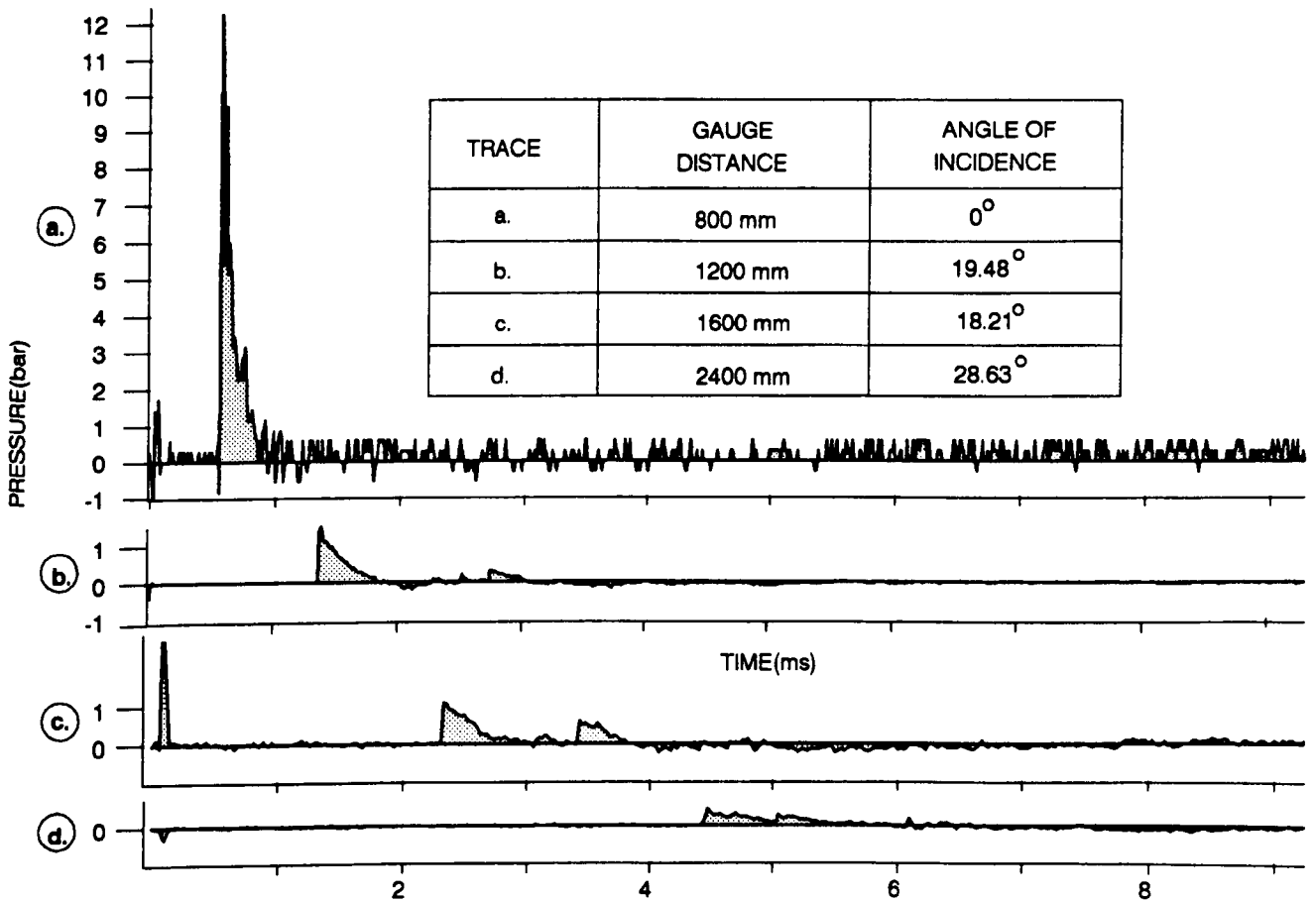


Fig. 4.21 Typical pressure-time record for the 78g PE4 cylindrical charge

	CHARGE STANDOFF FROM (m)	PULSE ARRIVAL TIME (msec)	PEAK PRESSURE (bar)	DURATION OF IMPULSE (ms)	SPECIFIC IMPULSE (bar msec)
CYLINDRICAL CHARGE	0.8	0.56	12.26	0.36	1.14
	1.2	1.38	1.54	0.50	0.27
	1.6	2.32	1.07	0.70	0.26
	2.4	4.42	0.44	1.53	0.21
HEMISPHERICAL CHARGE CURVED SIDE FACING THE GAUGE	0.8	0.52	11.05	0.44	0.95
	1.2	1.36	3.35	0.50	0.63
	1.6	2.20	1.25	0.76	0.37
	2.4	4.34	0.63	0.58	0.13
HEMISPHERICAL CHARGE FLAT SIDE FACING THE GAUGE	0.8	0.36	29.94	0.28	2.40
	1.2	1.04	4.88	0.52	0.64
	1.6	1.90	1.14	0.78	0.30
	2.4	4.12	0.37	1.76	0.22

Table 4.10 Blast pressure test results for the cylindrical and hemispherical 78g PE4 charge

As expected different shapes, orientation and positions of the charge gave different results. For instance, for a charge standoff of 0.8m when the flat side of the hemispherical charge faced the gauge, the peak pressure was much higher (29.94 bar) than for a hemispherical charge of the same mass of explosive but with the spherical side facing the gauge (11.05 bar), or for a cylindrical charge of the same mass (12.26 bar). The duration of the impulse varied inversely with the peak pressure so the impulse of the shortest duration was produced when the flat side of the hemispherical charge faced the gauge.

A hemispherical charge with the curved side facing the specimen was used on 13 out of 19 slabs and additional tests with this type of charge were carried out to establish the spatial distribution of pressure across the surface of the slab (Fig. 3.28). Some typical results are presented in Fig. 4.22 and Fig. 4.23.

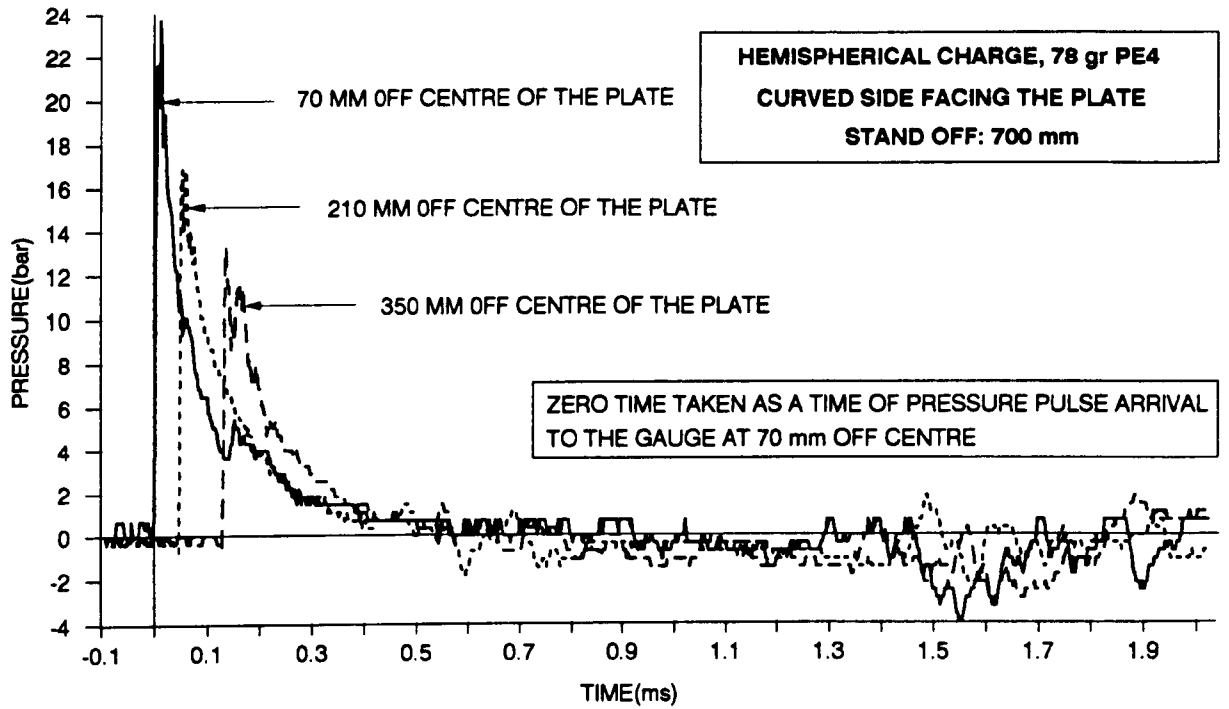


Fig. 4.22 Spatial pressure distribution from the 78g PE4 hemispherical charge - curved side facing the gauges

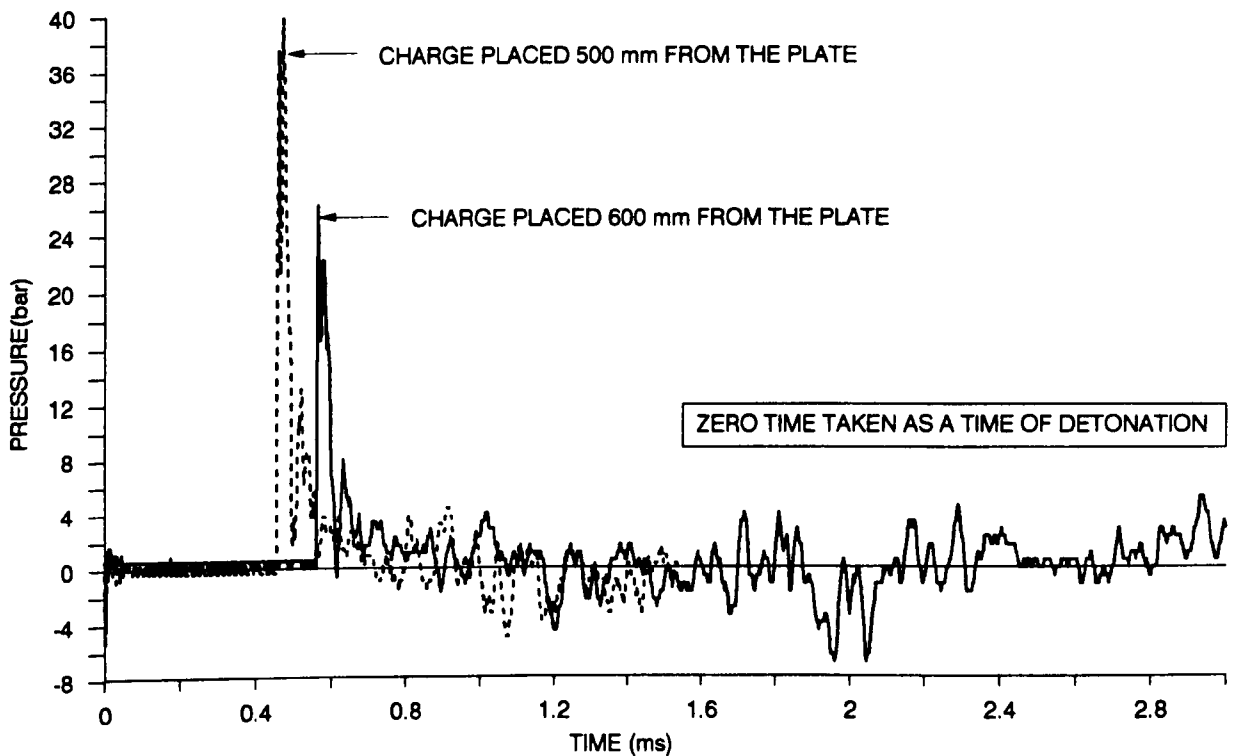


Fig. 4.23 Blast pressures taken at 420mm off centre of the plate from the curved side of the 78g PE4 hemispherical charge

4.2.1.2 Displacement record

Peak deflections on the small scale slabs were recorded between 3 and 5msec after the slab displacement began. Displacement rates were at up to 2.2m/sec and the rates of recovery

were about half of this value. The slabs containing greater reinforcement percentages, slabs SE5 - SE9, had peak upward displacements almost identical to the downward displacements which can be associated with the greater amount of energy being stored in the reinforcement. Slabs with smaller reinforcement percentages, and of discontinued top reinforcement (slabs SE9 - SE19, section 3.1.1), had a lower upward displacement above the initial position of the slab, which indicates that the top reinforcement was storing the energy which caused upward movement in previous cases. The deflections of the perforated slabs were almost the same under different blast pressure loading, indicating that as soon as the slab was perforated a constant value of energy from the blast pulse was transferred to the remainder of the slab.

Slabs with greater reinforcement percentages showed almost no residual deflection but there was a permanent deformation of the reinforcement in the punching zone. The small scale slabs, SE7 and SE8, had an inner support 200mm from the centre and showed almost no downward movement, but there was an upward movement shown on the RPDT records of almost the same order of magnitude as for the slabs without inner supports. These inner supports were not designed to hold the slab down.

Some of the displacement vs time traces showed electrical noise in about the first 3msec of the record which obscured the true displacement record. A typical trace without electrical noise is shown in Fig. 4.24 and a typical trace with noise is shown in Fig. 4.25.

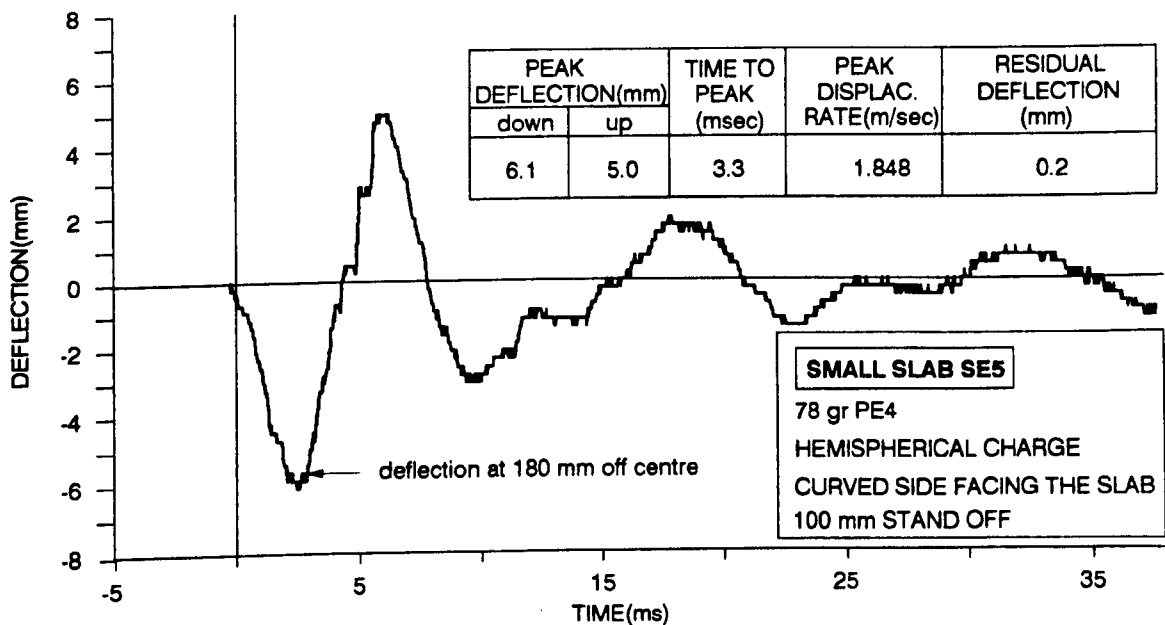
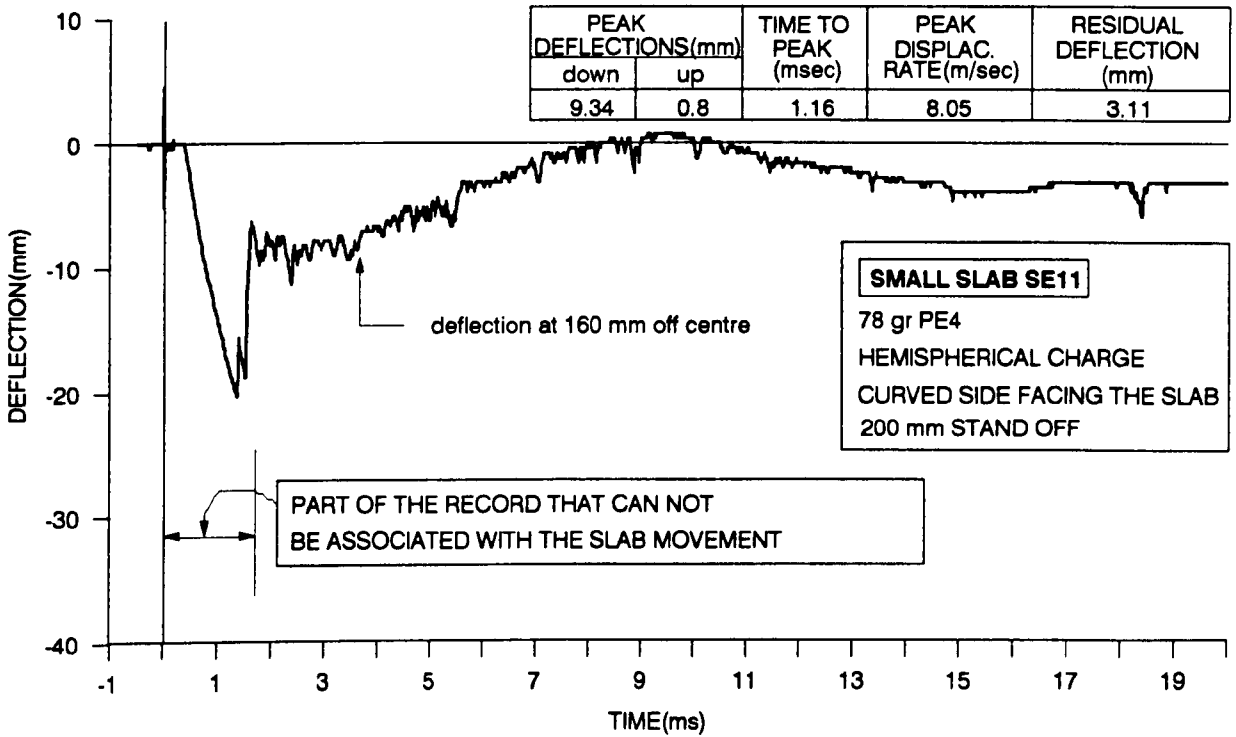


Fig. 4.24 Small slabs - impulse test - typical deflection vs time record



4.25 Small slabs - Impulse test - Example of deflection record with electrical disturbance

4.2.1.3 Reinforcement strain record

The typical reinforcement strain vs time record obtained from the small scale slabs tested by explosive is shown in Fig. 4.26.

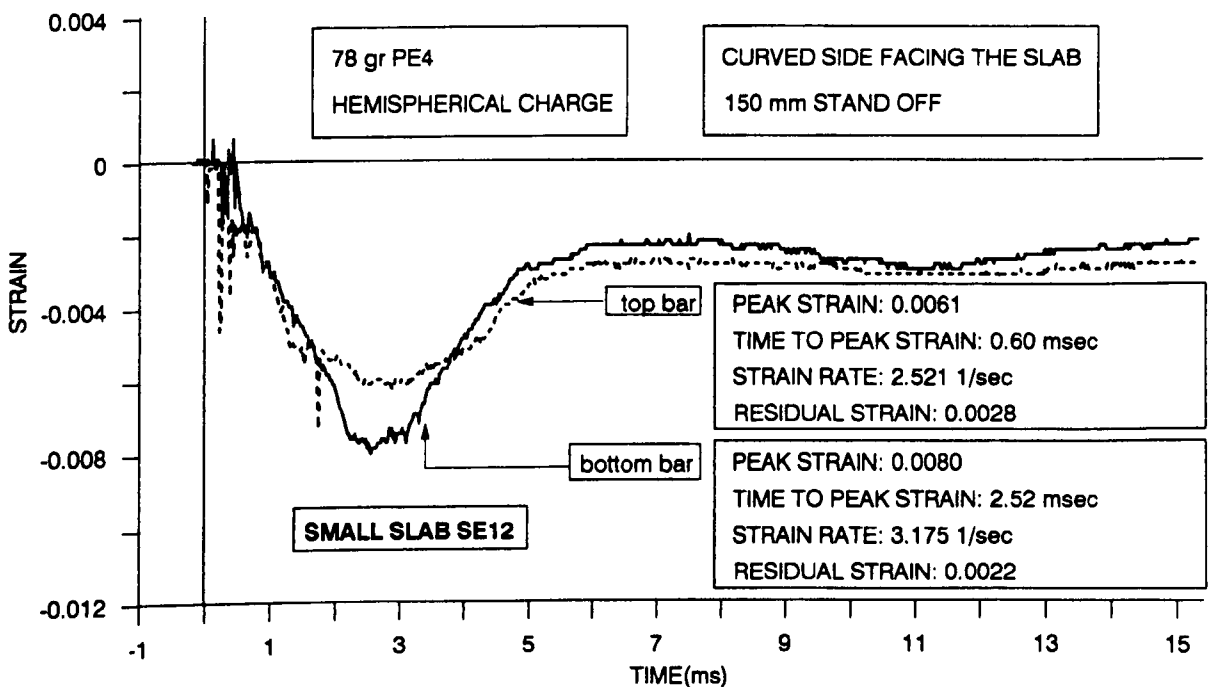


Fig. 4.26 Small slab - Impulse test - Typical reinforcement strain record

The strain rates obtained from the small slabs tested explosively were of the same order of magnitude as those in the impact tests, varying from 1.53sec^{-1} to 10.11sec^{-1}

Details of all the test results are shown in Table 4.11. The column labelled "Time to peak or recorded time" gives either the time when the peak was reached or the overall time of recording in cases when the peak strain was not recorded. Consequently the column labelled "Peak value or max recorded strain" gives either real peaks or maximum recorded strain before the failure of the gauge.

SLAB No	TENSILE ZONE REINFORCEMENT	PEAK VALUE OR MAX RECORDED STRAIN (strain)	TIME TO PEAK OR RECORDED TIME (msec)	STRAIN RATE (sec^{-1})	RESIDUAL STRAIN (strain)
	GAUGE STATION POSITION				
SE4	top bar	0.0018	1.20	1.500	0.000
	bottom bar	0.0041	2.28	1.798	0.001
SE5	top bar	0.0085	1.95	4.359	-
	bottom bar	0.0131	1.90	6.895	-
SE6	top bar	0.0036	2.35	1.532	-
	bottom bar	0.0045	2.17	2.074	-
SE7	bottom bar	0.003	0.96	3.125	-
SE9	No central zone reinforcement				
SE10	top bar	0.0045	2.40	0.185	0.0009
SE11	bottom bar	0.0120	2.60	4.615	0.0062
SE12	top bar	0.0061	2.42	2.521	0.0028
	bottom bar	0.0080	2.52	3.175	0.0022
SE13	bottom bar	0.0136	1.62	8.395	-
SE14	bottom bar	0.0078	2.32	3.362	0.0024
SE15	top bar	0.0061	0.60	10.117	-
	bottom bar	0.0080	0.80	10.000	-
SE16	top bar	0.0201	1.64	12.256	-
SE17	top bar	0.0022	0.12	18.333	-
	bottom bar	0.0255	0.32	17.188	-
SE18	top bar	0.0027	1.70	1.588	0.0005
	bottom bar	0.0036	1.92	1.875	0.0006
SE19	top bar	0.0035	2.21	1.584	0.0008
	bottom bar	0.0054	2.14	2.523	0.0016

Table 4.11 Small slabs - Impulse tests - Strain record

As in the case of the impact tests sometimes the gauge was broken before the end of the test and a typical example is shown in Fig. 4.27.

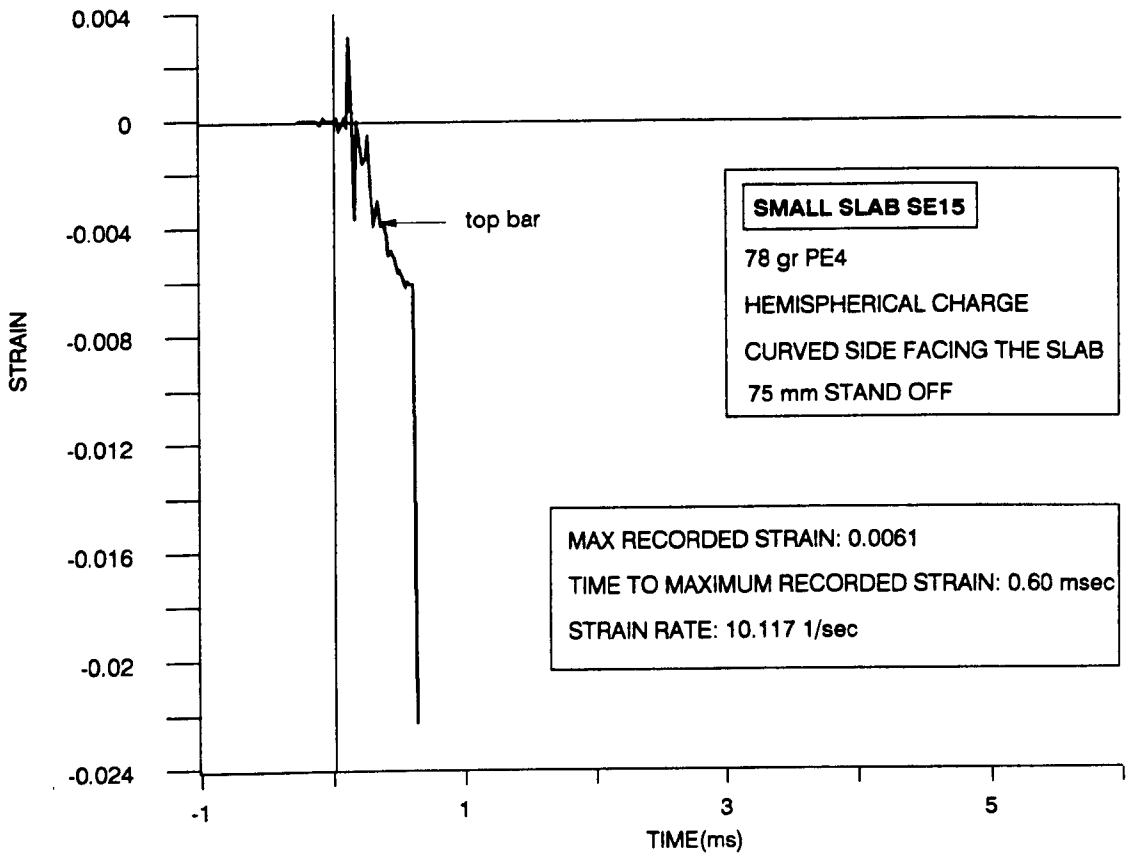


Fig. 4.27 Small slabs - Impulse test - Partial strain gauge record

4.2.1.4 High speed films

Small scale explosively tested slabs were filmed with the High Speed Motion Camera (section 3.2.9) as described in section 3.3.3.6. The soffit of the slab was viewed either directly by the camera or after reflection in a mirror at 45°. Typical single frames by each method are shown in Fig. 4.28.

Although all small scale specimens were filmed the very uncertain timing and triggering of the events meant that only the trials presented in Table 4.12 produced clear films. In all cases a half frame shutter was used.

Typical frames taken from film No. SE15 are presented in Fig. 4.29.

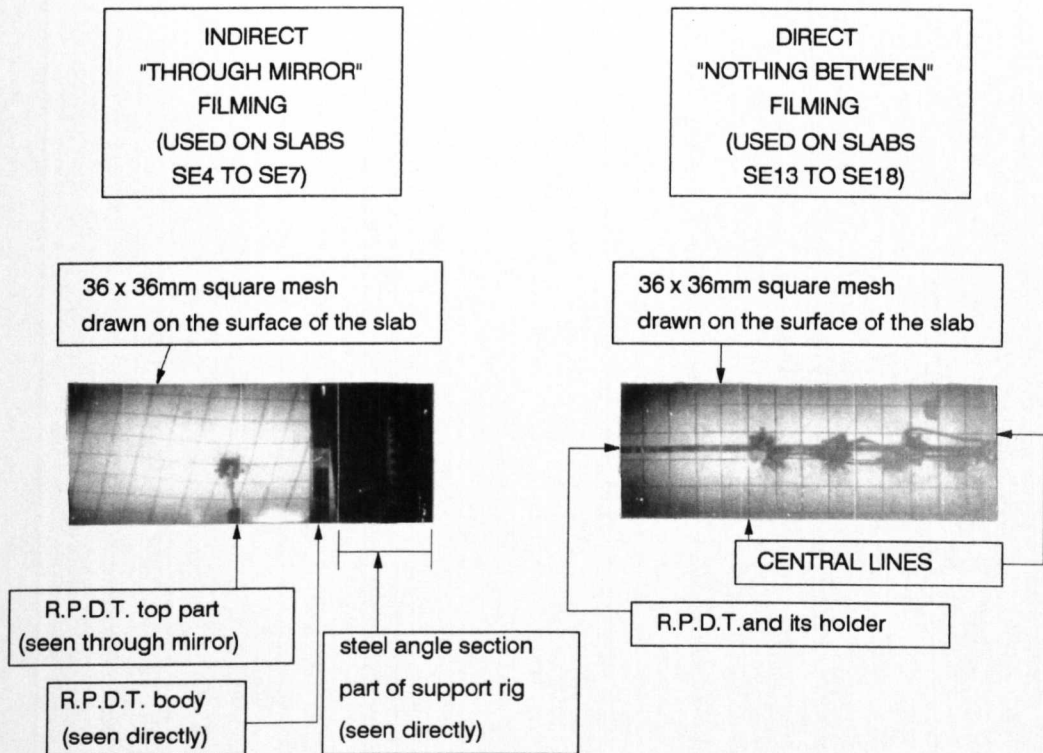


Fig. 4.28 16mm Film frame details- Blast impulse tests

SLAB NUMBER	FILM RATE (p.p.s.)	INTER-FRAME TIME (μ sec)	APPROXIMATE RECORDED TIME AFTER THE BLAST (msec)	FILMING MODE
SE4	~ 6000	~ 170	~ 15	MIRROR
SE5	6158	162.38	15	MIRROR
SE6	6200	161.29	5	MIRROR
SE7	8212	121.76	25	MIRROR
SE13	~ 10,000	~ 100	~ 20	DIRECT
SE14	10,437	95.81	25	DIRECT
SE15	10,525	95.01	15	DIRECT
SE17	10,672	93.70	25	DIRECT
SE18	10,500	95.24	20	DIRECT

Table 4.12 Small slabs - Impulse tests - High speed film details

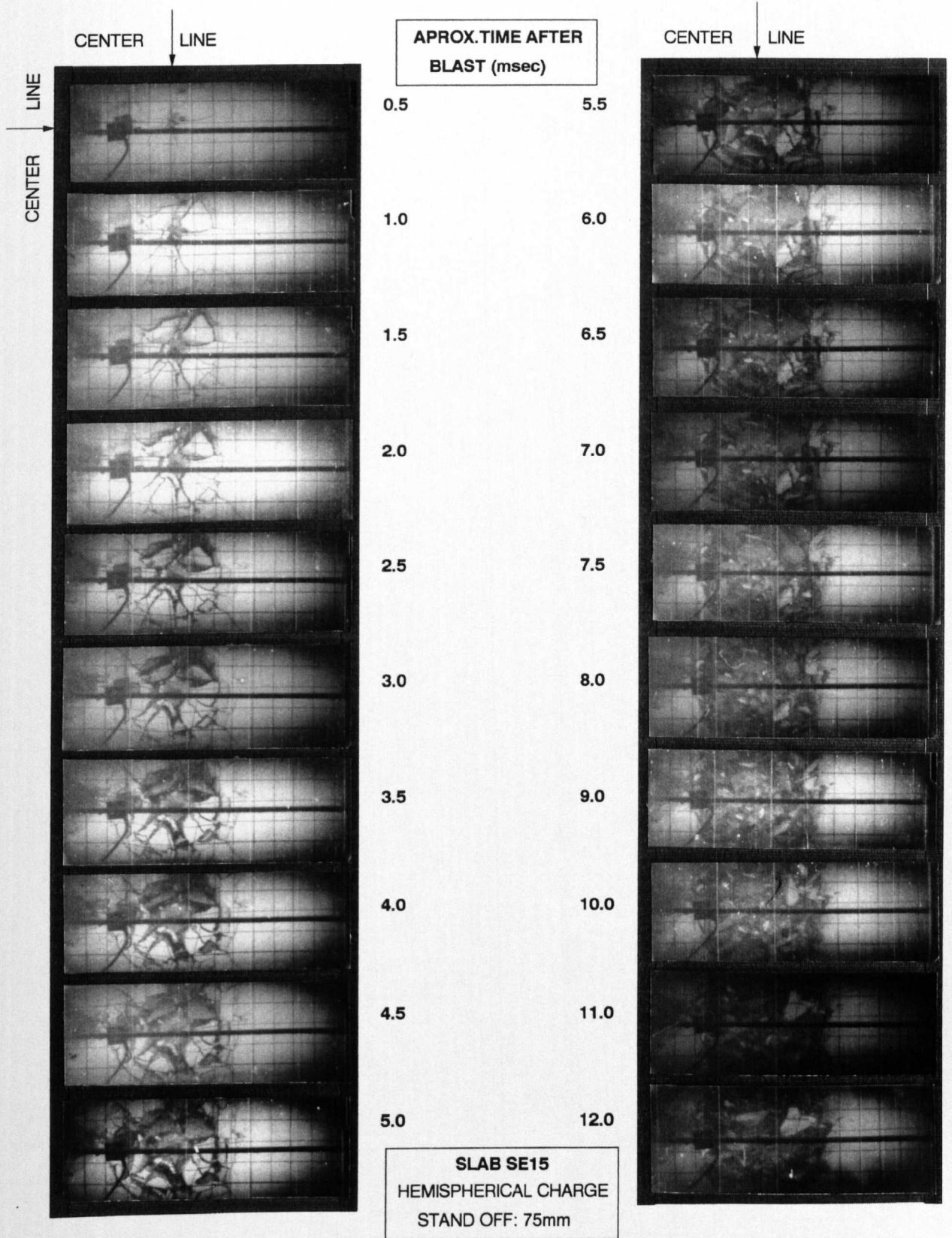


Fig. 4.29 Small slab SE15 - Blast Impulse Test - Typical frames taken from the high speed film

4.2.1.5 Crack patterns and slab cross sections

The best examples of crack patterns on the soffit or back surface of the slabs are shown in Fig. 4.30, slabs SE10 to SE17, where the standoff was gradually reduced from 250mm to 50mm.

SMALL SCALE IMPULSE TESTS - CRACK PATTERNS ON BACK FACES

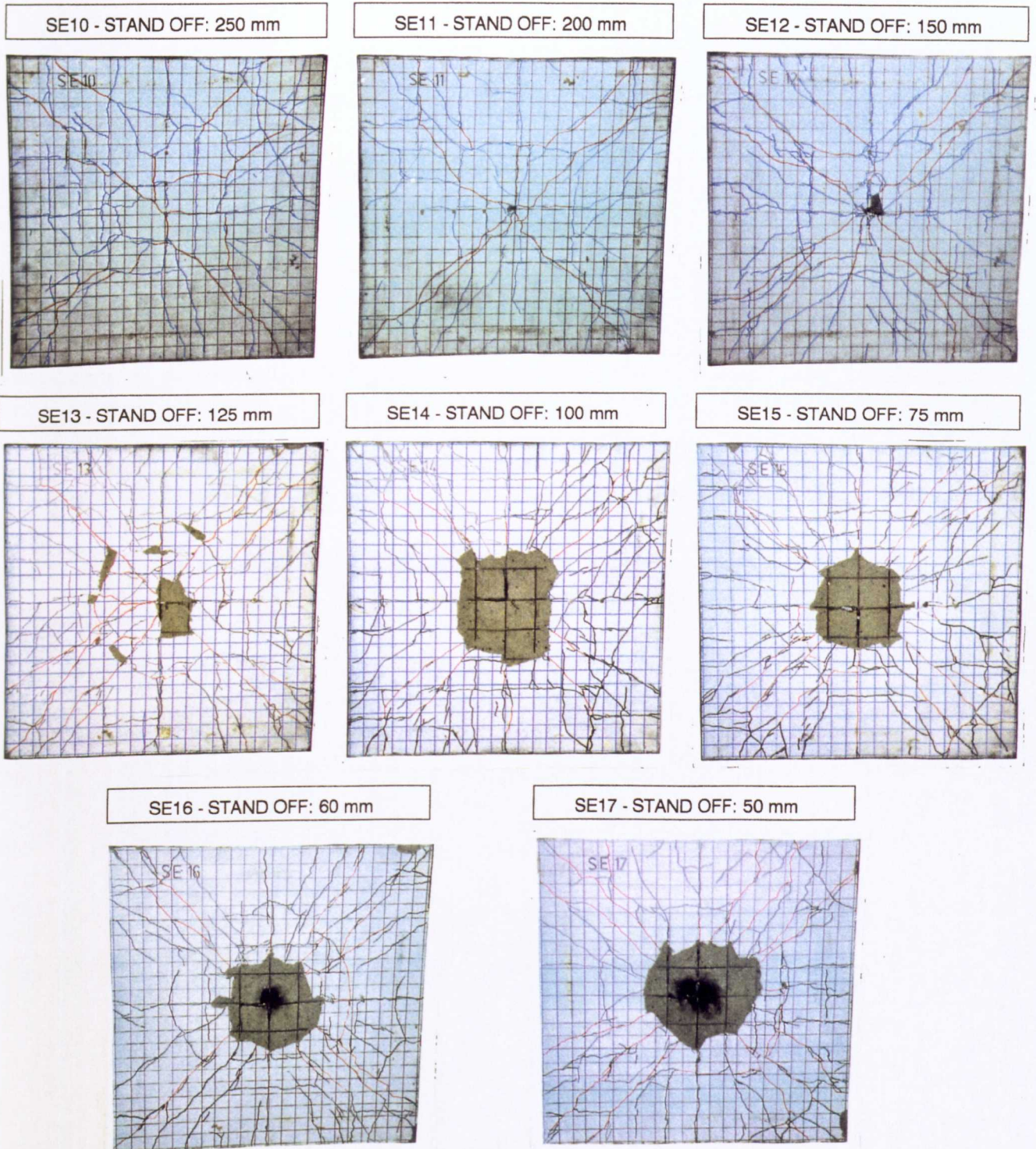


Fig. 4.30 Small slabs - Impulse test - Crack patterns

The crack patterns observed in the case of the explosively tested small scale slabs were remarkably consistent between the tests, with crack patterns changing in an easily identifiable way as a result of changing the charge standoff distance.

All of the slabs exposed to a centrally placed charge exhibited similar crack patterns. The exceptions were slabs SE7 and SE8 which had an intermediate support and showed a different crack pattern. The type of damage suffered by the back face or soffit of these slabs was similar to those slabs exposed to a soft impact. Apart from the diagonal cracks which extended to the slab corners, there were cracks just under the reinforcement bars and running along the lengths of the reinforcement bars. These were due to the local stress increase caused by the reduction in area of concrete.

The local damage produced on the slabs immediately under the charge consisted of scabbing on the back face, cratering on the front face, and cracks defining a punching cone which was cracked and partly displaced by the blast pressure, causing some deformation of the reinforcement within the cone. The area of local damage is mainly dependent on the amount of energy delivered to the slab; this was determined by the charge shape, orientation and standoff distance to the slab as well as by the size and spacing of the reinforcement.

As in the case of the impact tests, some typical slabs were carefully cut along the central line in order to monitor cracks on the cross section. They are all shown in Fig. 4.31.

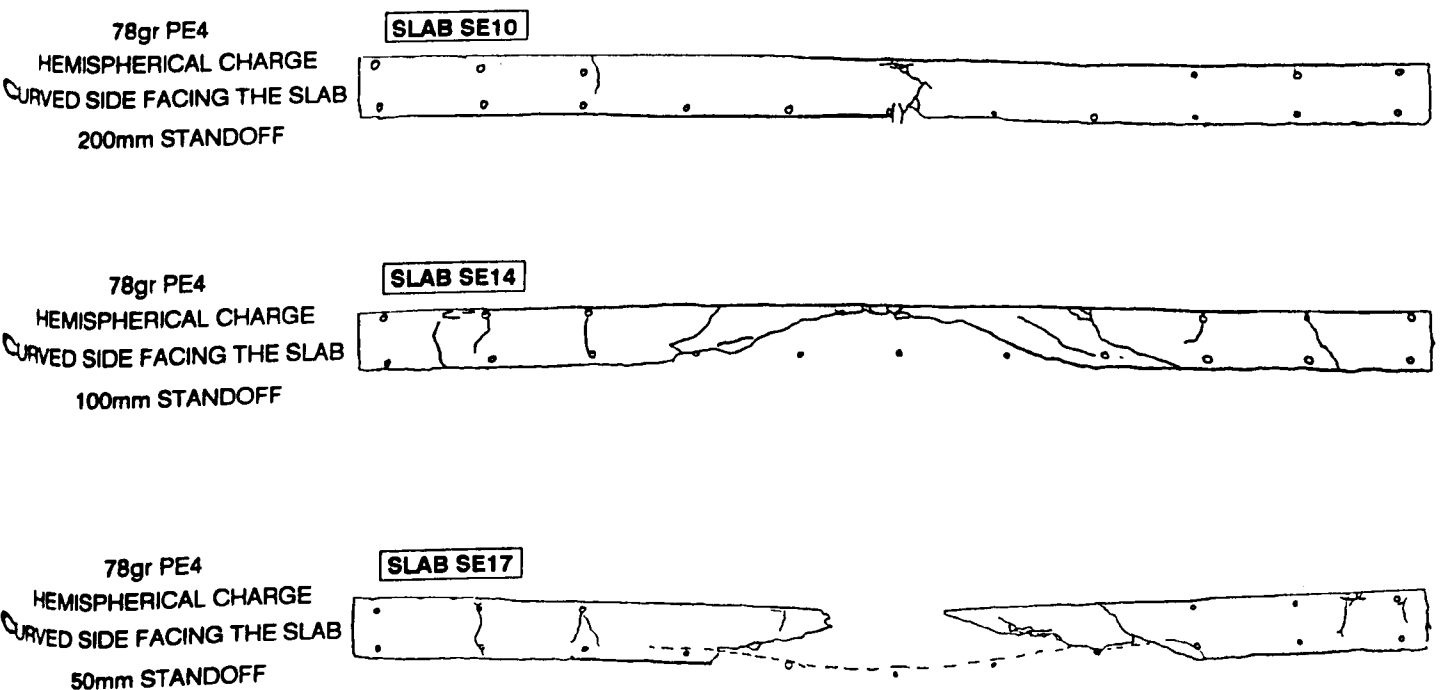


Fig. 4.31 Small slabs - Impulse tests - cross-sections

The top surface of the slabs had two main types of crack. These were circumferential cracks around the centre of the slab and radial cracks running from the centre of the slab. Both types of crack formed to the edges of the slab in some tests but the circular cracks were dominant in the case of slabs containing top reinforcement, and the radial cracks were dominant in the case of slabs without top reinforcement.

4.2.2 1:1 Scale slabs

In total five full scale slabs were blast tested using a standard 1300g PE4 hemispherical explosive charge with the curved side facing the slab. Slab LSE1 was the only slab tested twice with standoffs of 350mm and 250mm. The main variables were the amount of reinforcement and the loading function. The loading function was varied by changing the standoff distance only. All test variables are given in Table 4.13.

SLAB	REINFORCEMENT		CHARGE STANDOFF DISTANCE (m)
	COMPRESSION ZONE LAYER	TENSILE ZONE LAYER	
LSE1	1.2% each way	1.2% each way	350 + 250
LSE2	1.2% each way	1.2% each way	250
LSE3	0.41% each way	0.41% each way	500
LSE4	0.41% each way	0.41% each way	300
LSE5	0.41% each way	0.41% each way	200

Table 4.13 Full scale slabs - Impulse tests - Test details

Slabs LSE3 to LSE5 were designed without top reinforcement in an area of 500 x 500mm in the centre of the specimen. All the available test results are presented in Appendix B1 - Test Results

4.2.2.1 Displacement record

Displacement measurements were taken as explained in section 3.3.3.5. Transducer positions for each of five tests are given in Fig. 3.30 and a brief description of the results is presented in Table 4.14.

SLAB	DISPLACEMENT RECORD DETAILS
LSE1	<p>The slab was tested twice and deflections were taken at 225mm and 450mm from the centre in both cases. In the first test, peak displacements of 26.3mm and 18.8mm for 225mm and 450mm off centre positions respectively were reached at 6msec after the blast. The average deflection rate for the 225mm off centre RPDT was 4.4m/sec and the recovery rate was 3.4m/sec. The peak upward deflection was the same in both positions - 9.8mm. The transient displacement lasted for 110msec after the blast and both residual deflections were about 3mm. The second test on the same slab produced larger deflections. The peaks were 33.8mm and 25.6mm for the 225mm and 450mm off centre transducers respectively. The deflection rate at the 225mm off centre transducer was 5.7m/sec while the peaks were reached at 5.9msec. Again the peak upward deflection for both positions were almost the same - 19.6mm while the residual displacements could only be estimated as being about 4mm.</p>
LSE2	<p>Peak deflections for the 225mm and 450mm off centre transducer were 31.9mm and 20mm respectively. The average deflection rate was 5.7m/sec while the peaks were reached at 5.6msec after the blast. Upward displacements were 9.4mm and 7.8mm respectively. Residual deflections were 6mm and 5mm. Although the final crack pattern indicated the formation of a shear plug, the deflection record did not show any apparent brittle failure that could be associated with the plug formation.</p>
LSE3	<p>Deflections were taken at midspan, 100mm, 200mm, 300mm and 700mm off centre and the peaks were 52.2mm, 45.2mm, 38.9mm, 33.5mm and 7.1mm respectively. The midspan transducer gave an average deflection rate of 7.0m/sec but after 7.4msec the signal ended abruptly and it was not clear whether a peak was actually reached. As expected the lighter reinforcement of this slab caused much larger deflections than on the previous two slabs although the standoff distance was greater.</p> <p>There was almost no upward deflection above the initial position of the slab. The maximum average recovery rate was 4.5m/sec. Residual deflections can only be estimated as 10.9mm, 10.1mm and 9.3mm for 100mm, 200mm and 300mm from the centre transducers.</p>
LSE4	<p>No deflection record was taken.</p>
LSE5	<p>Deflections were taken at 300mm, 400mm and 500mm off centre and the peaks were 38.2mm, 32.7mm and 23.4mm respectively and they occurred 7.5msec after the detonation. The maximum average deflection rate was 5.1m/sec. The second period peaks were recorded 6.0msec after the blast and they were 17.9mm, 14.8mm and 9.3mm respectively. The record lasted for 110msec after the blast and residual displacements were estimated as 16.4mm, 13.2mm and 8.6mm respectively.</p>

Table 4.14 - Full scale slabs - Impulse test - Displacement vs time record details

Typical deflection vs time trace is shown in Fig. 4.32.

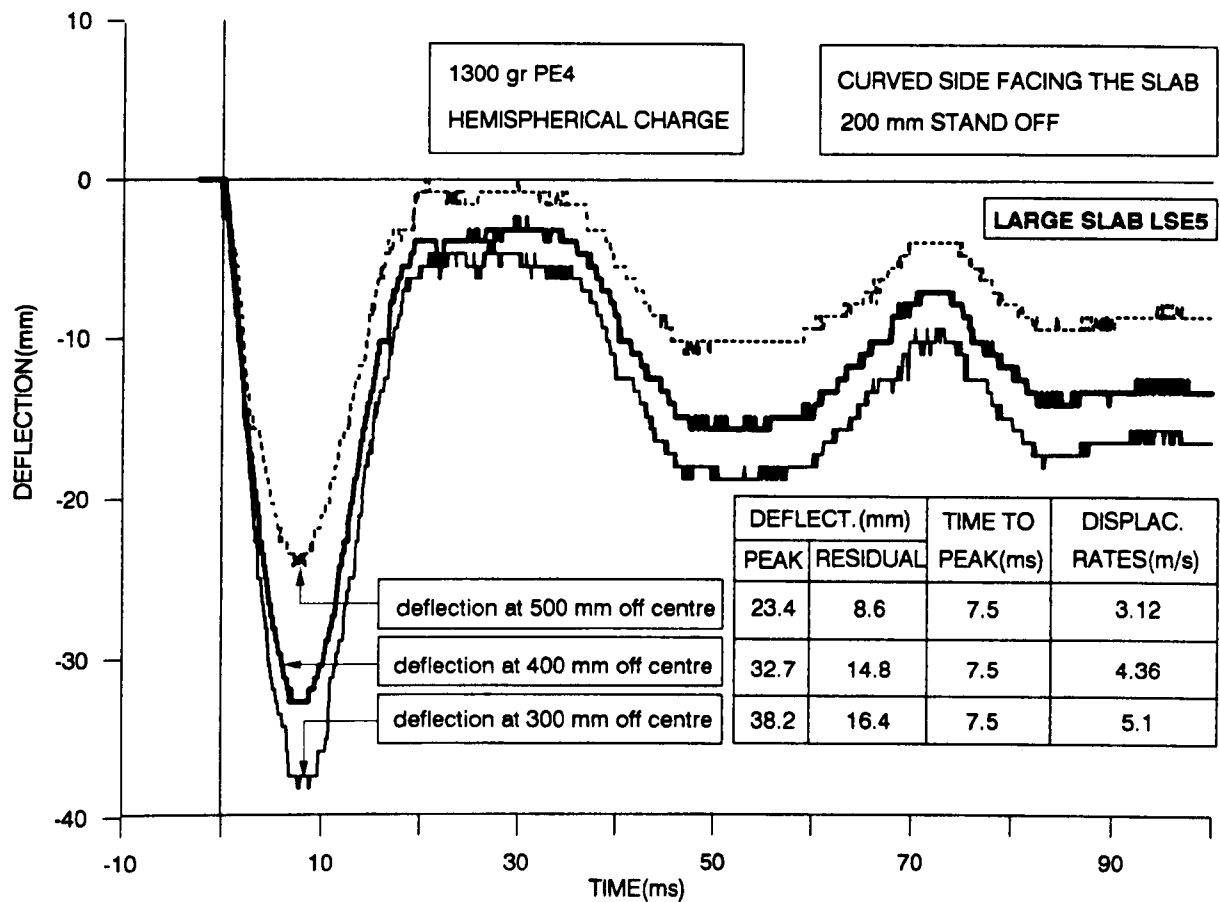


Fig. 4.32 Full scale slab - Impulse test - Typical displacement record

4.2.2.3 Strain record

Reinforcement strains were measured as explained in section 3.3.3.4. The maximum strain rate measured in these tests was 2.61sec^{-1} .

Table 4.15 gives additional details about the strain records taken from the large scale slabs.

SLAB	BAR POSITION	RECORDED TIME (msec)	STRAIN RATE (sec^{-1})	PEAK RECORDED STRAIN
LSE1 - two shots	top	40,(10)	1.43,(2.61)	0.0114,(0.0219)
LSE2	bottom	40	0.58	0.0042
LSE3	top	75	0.29	0.0044
LSE5	top	10	2.18	0.0194
	bottom	22	-	0.0225

Table 4.15 Reinforcement strain record details, large scale explosive tests

It is interesting to note that the peak strains cannot be directly related to the standoff distance. For example slab LSE1 tested with an explosive charge at 350mm standoff, had a greater peak strain than LSE2 where the standoff was only 250mm. The explanation could be associated with the spatial distribution of the pressure produced by the hemispherical charge and by the local straining.

A typical record of the strains in the reinforcement for the large slabs tested by explosive is given in Fig. 4.33.

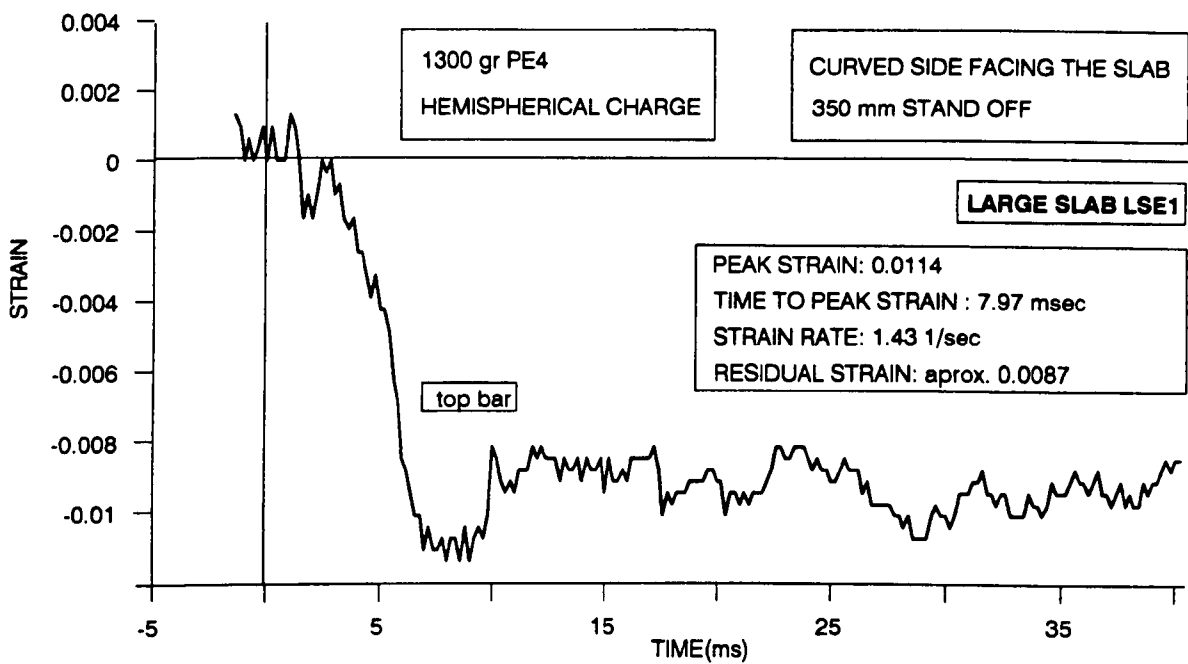


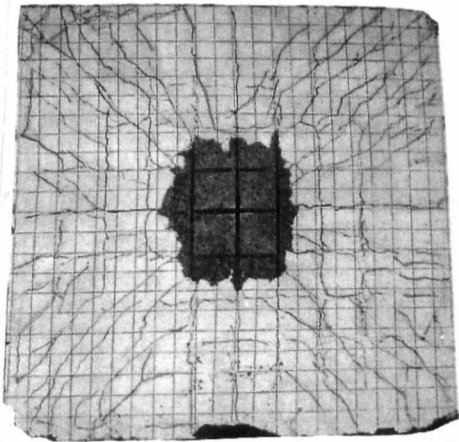
Fig. 4.33 Full scale slab - Impulse test - Typical reinforcement strain record

4.2.2.4 Crack patterns

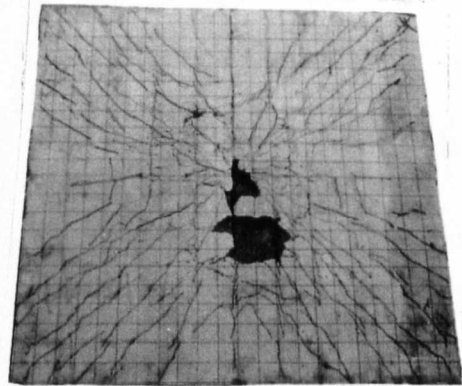
The crack patterns closely resemble those obtained in the small scale tests. The density of cracking is again very high with most of the cracks occurring on the back face of the slabs and propagating towards the corners of the slab. The front face crack pattern is similar to the back face pattern although there are additional circular cracks around the centre of the slab.

Back face crack patterns of all five specimens are given in Fig. 4.34.

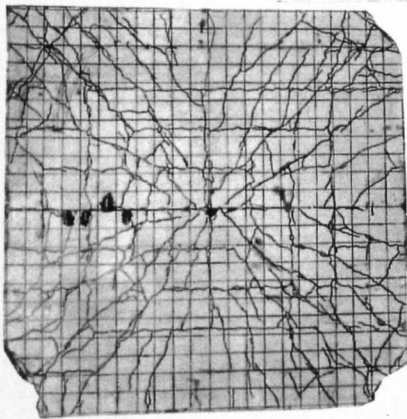
LSE1 - STAND OFF 350 + 250 mm



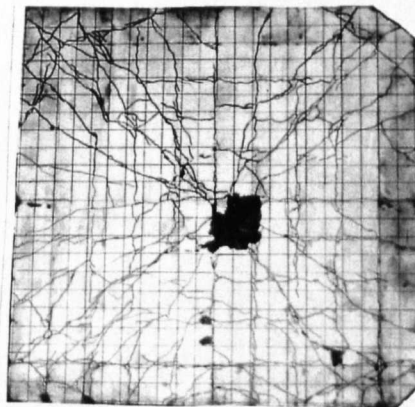
LSE2 - STAND OFF 250 mm



LSE3 - STAND OFF 500 mm



LSE4 - STAND OFF 300 mm



LSE5 - STAND OFF 200 mm

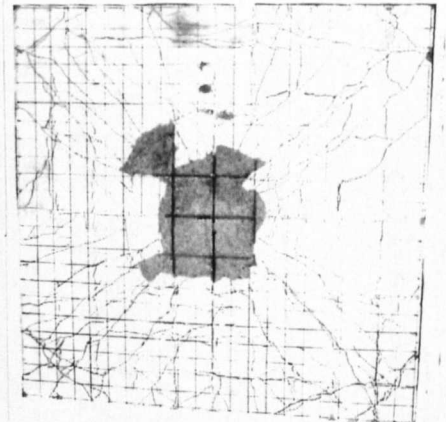


Fig. 4.34 Large scale slabs - Impulse tests - Crack patterns

4.2.3 Conclusions

The characteristics of the loading function seem to determine the slab behaviour in both impulse and impact tests. The main characteristics of the blast pressure-time history are given as the peak pressure and duration of the positive phase of impulse. Very similar crack patterns were observed in the case of the large and small scale slabs. The consistency of the change to the crack pattern under different pressure functions underline the possibility of establishing exact response mechanism to cover the behaviour of R.C. slabs under these extreme conditions. The impulse tests presented here produced reinforcement strain rates of up to 2.61sec^{-1} and displacement rates

of up to 8.0m/sec. The shear resistance of the central area of the slab is very important in determining the mode of response, and it is clear that even close standoff charges, cannot be represented by a point load but should be represented as a load distributed over a central region which expands and governs the response not only of the structure as a whole, but also of the local area directly exposed to the greatest load. The best proof of the above is given in the slab cross-sections that show cracking much further from the central area than the boundaries of the punch zone. The most important response characteristics together with the general shape of the damage justifies the modelling laws employed in the work.

CHAPTER 5

DISCUSSION

5.1 Introduction

Impact loading is a more simple form of dynamic loading which has time variation but not the spatial variation that occurs with blast loading from close-in explosive charges.

All the impact tests in this work were conducted primarily in order to give a better understanding of the blast-impulse behaviour of RC slabs as the ultimate case of dynamic loading. The following discussion analyses slab behaviour under blast loading and the behaviour under impact loading is compared with that under blast loading to show the difference in the slab response due to spatial variation of blast pressure and the rate of loading.

Shear failure planes perpendicular to the plane of the slab have been reported in the impact and blast literature but these are almost always close to the supports. This type of failure

has been described as direct shear and the failure criteria is determined from a direct shear resistance to shear slip function, along an actual or potential crack, *Ross and Krawinkler, (1985)*. It would seem for the present experiments, that the direct shear failure resistance when blast pressure is applied to a local region of a reinforced concrete slab, is too high for this to be the dominant shear failure mode. The more critical shear failure mechanism is that likely to be initiated by diagonal tension cracking which forms a shear plug, but before this plug can be displaced, the concrete is fragmented by compression forces.

The failure planes observed here were always closer to the epicentre than to the support and their angle to the slab surface plane was never greater than 35°.

5.1.1 Loading function

In the tests reported in Chapter 4, the blast pressure loading function has been generated by a close range explosion, but the load distribution can not be approximated as a time varying or transient point load. There are clear differences in the local response of the slabs exposed to impact, where the point load is transient at a fixed location, and blast loading where the load is transient but there is also a spatial distribution of the pressure function as important as its magnitude and duration. In impulse tests the amount of cracking furthest from the epicentre is greater than for the impact tests. The most probable reason is that although the charge was close to the target there was a large amount of distributed pressure over the slab surface.

Explaining and quantifying the blast pressure function is a necessary requirement for understanding the response of the structure. In most of the tests carried out in this work, the spherical side of a hemispherical charge faced the specimen and it was initiated from the centre of the flat side.

5.1.1.1 Calculation of Blast Loading Function

The blast pulse that produces the dynamic pressure on the slab was quantified using both experimentally obtained measurements, which are described in section 4.2.1.1. and the theoretical approach of *Henrych, (1979)*.

The velocity of detonation of the plastic explosive PE4 used in this research, was about 8000m/sec and the shock wave initiated by the explosion will travel at close range distances, at about 7500m/sec (*Henrych, 1979*). Standoff distances used in this research were 250mm to 50mm for the 1:2.5 scale and 500mm to 200mm for the 1:1 scale slabs. Consequently the shock wave reaches the specimen after $7\mu\text{sec}$ to $33\mu\text{sec}$ in the case of the 1:2.5 scale slabs and after $27\mu\text{sec}$ to $67\mu\text{sec}$ in the case of the 1:1 scale slabs.

The shock front propagates in all directions from the charge but the "shock front vectors" that produce forces perpendicular to the slab are of greatest importance to the structural response. For example the shock front vectors from a charge at 500mm standoff will reach the 1:1 scale slab, at points 1m from the centre of the slab in about $150\mu\text{sec}$ and will act on the structure at an angle of 26.5° . The vertical component of force will then be much reduced due to obliquity and travel distance.

When the shock front reaches the structure, the overpressure produces a compressive stress wave propagating into the structure. Internal reflections of that stress wave will produce tensile stresses. These can produce some form of local fracture before there is any flexure of the slab.

If we denote the angle of incidence between the shock front vector and the line perpendicular to the slab surface as α , Fig. 5.1,

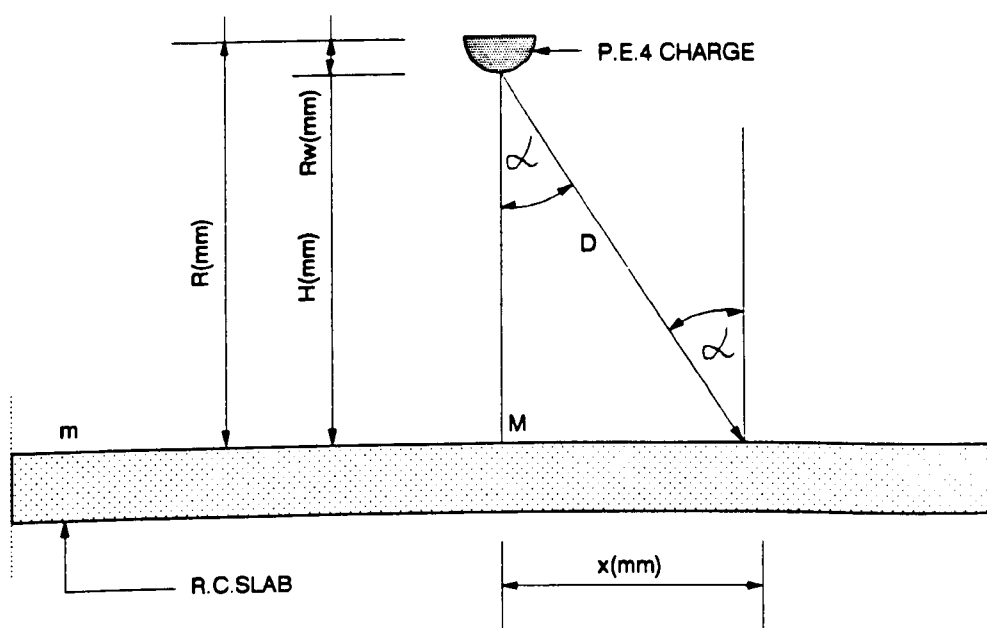


Fig. 5.1 Loading function

then *Henrych, (1979)*, gives the peak theoretical pressure $P_{(m)}$ at any point defined by α , as:

$$P_{(m)} = P_{\text{det}} \cdot \left(\frac{R_w}{R} \right)^A \cdot \cos^2 \alpha$$

where P_{det} is the detonation pressure of a spherical, flat or cylindrical charge of radius R_w and standoff distance R . The parameter A is determined by the shape of the charge and is 2 for a spherical charge and 3 for a hemispherical charge with the flat side towards the slab.

Transient pressure distribution $P(t)$ is given by:

$$P(t) = P_{(m)} \cdot \left(1 - \frac{t}{\tau} \right)^A$$

If we consider a hemispherical charge initiated from the centre of the flat side as being similar to a spherical charge initiated from the centre of the sphere then the above relations can be directly implemented using $A = 2$. Since $R_w = 28.5\text{mm}$ and 71.25mm for the 1:2.5 scale and 1:1 scale tests respectively and P_{det} is 26.8kN/mm^2 then the loading function can be written for the 1:2.5 scale 78g PE4 charge as:

$$P(t) = P_{\text{det}} \cdot \left(\frac{R_w}{R} \right)^A \cdot \cos^2 \alpha \cdot \left(1 - \frac{t}{\tau} \right)^A,$$

where t represents the time measured from the arrival of the blast front at the slab and τ is the positive duration of the pressure pulse. It is clear that τ will be dependent on the standoff distance of the charge and the position on the slab. It was therefore decided to relate τ to the charge inclined distance $D(\text{mm})$, Fig.5.1. The values for τ can be obtained experimentally and theoretically. For charge inclined distances of up to 560mm, which are of the greatest interest, (1:2.5 scale slabs), the test results showed that the positive duration of the pulse was an almost linear function of the distance D . For calculation purposes τ has been taken as:

$$\tau_{(\text{in } \mu \text{ sec})} = K \cdot D_{(\text{in mm})}$$

where $K = 0.715$

It must be noted from Fig 5.1 that charge inclined distances of up to 560mm correspond to standoffs of up to 391mm.

It was experimentally established that the positive duration of the blast pressure pulse for the smaller charge placed at 300mm standoff was about 200µsec and this has been chosen as a maximum for calculation purposes.

Direct implementation of the Henrych relations gives results which do not compare well with the experimentally obtained results because no allowance is given for different pressure arrival times at different slab points. Instead an instantaneous pressure rise is assumed across the slab. This problem can be resolved by simply calculating pressures for each point taking pressure arrival time as zero time for that particular point but still relating it to the arrival time of the blast pulse at the centre of the slab. Peak pressures calculated using Henrych's values for A do not correspond to the experimentally measured ones. This may be due to the fact that the Henrych values for A refer to the spherical and cylindrical charges while values for hemispherical charges are applicable only to the flat side of the charge.

The values measured in these tests are the vertical components of the pressure on the slab but the Henrych calculations give full pressure values. After corrections the pressure function is:

$$P(t) = P_{det} \cdot \left(\frac{R_w}{R}\right)^{2.65} \cdot \cos^3 \alpha \cdot \left(1 - \frac{t-L}{\tau}\right)$$

where: $L = \frac{D-H}{V}$, $V = 7.5mm/\mu\text{sec}$ and $\frac{D-H}{V}$ represent the delay which occurs due to the late arrival of the pressure at different points across the slab. The value of 2.65 for A has been chosen as the best fit to the available experimental results.

The apparent difference in the pressure arrival time can be related to inconsistencies in the bursting time of the L2A1 charge detonators which is about 50µsec.

The pressures on the 1:2.5 scale slab, calculated from the equations above, are given in Figs. 5.2 to 5.7. They compare relatively well with experimentally obtained results when calculation is done at every 2mm of the slab. A LOTUS 123 spreadsheet has been used to both calculate and draw the traces in these figures.

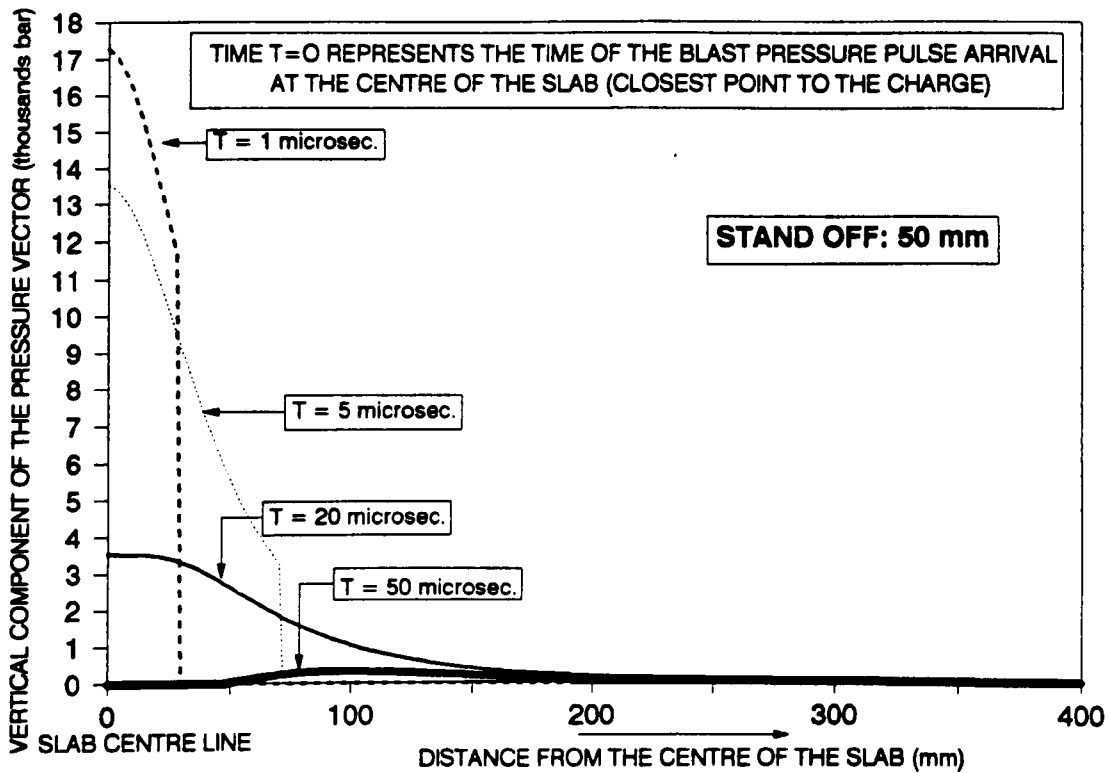


Fig. 5.2 Pressure vs. time profile for 78g PE4 charge according to Henrych (1979) - 50mm standoff

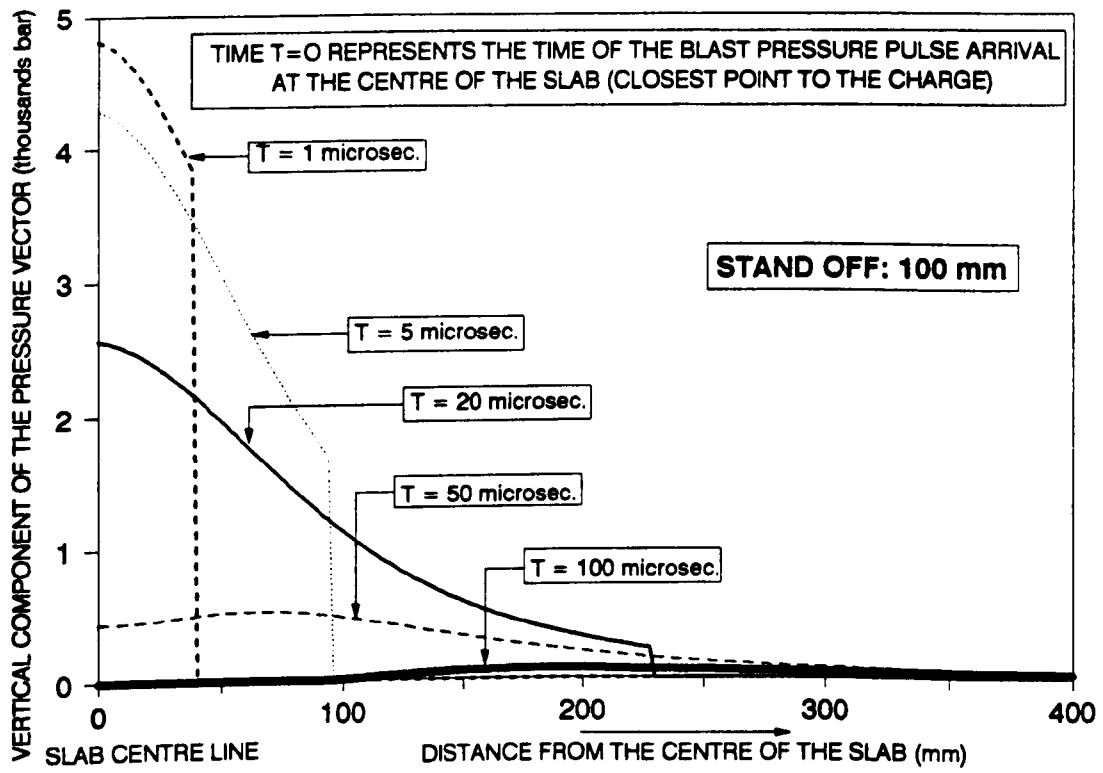


Fig. 5.3 Pressure vs. time profile for 78g PE4 according to Henrych (1979) - 100mm standoff

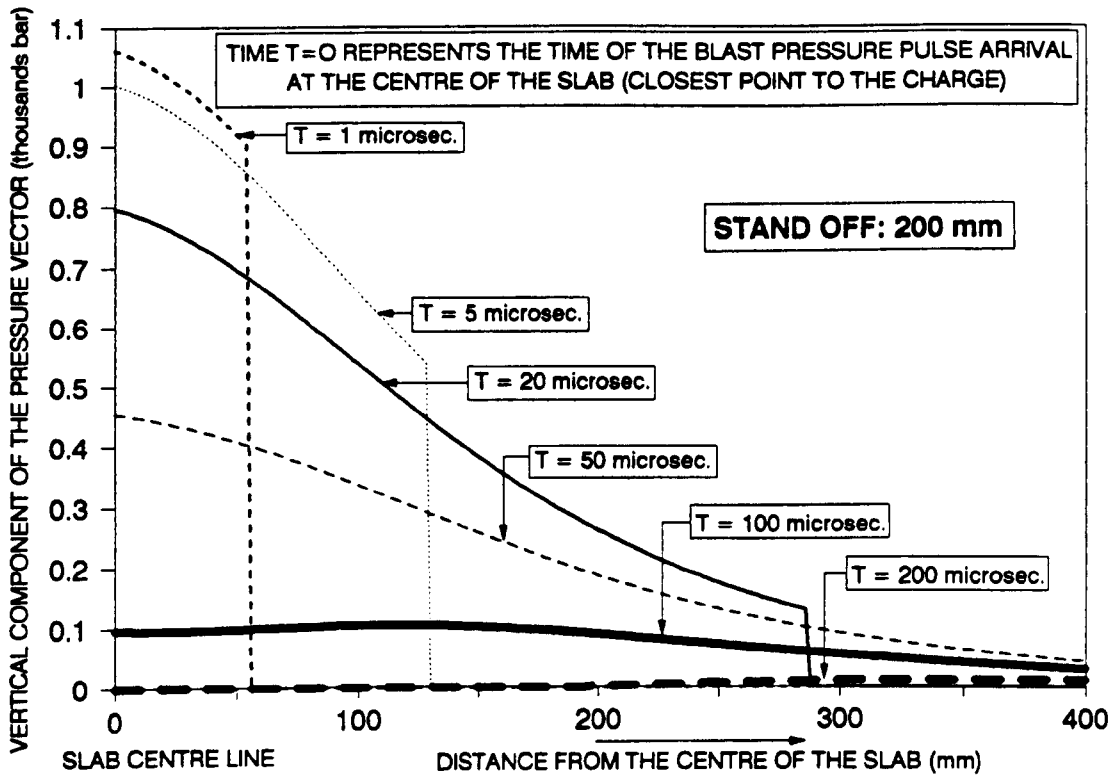


Fig. 5.4 Pressure vs. time profile for 78g PE4 charge according to Henrych (1979) - 200mm standoff

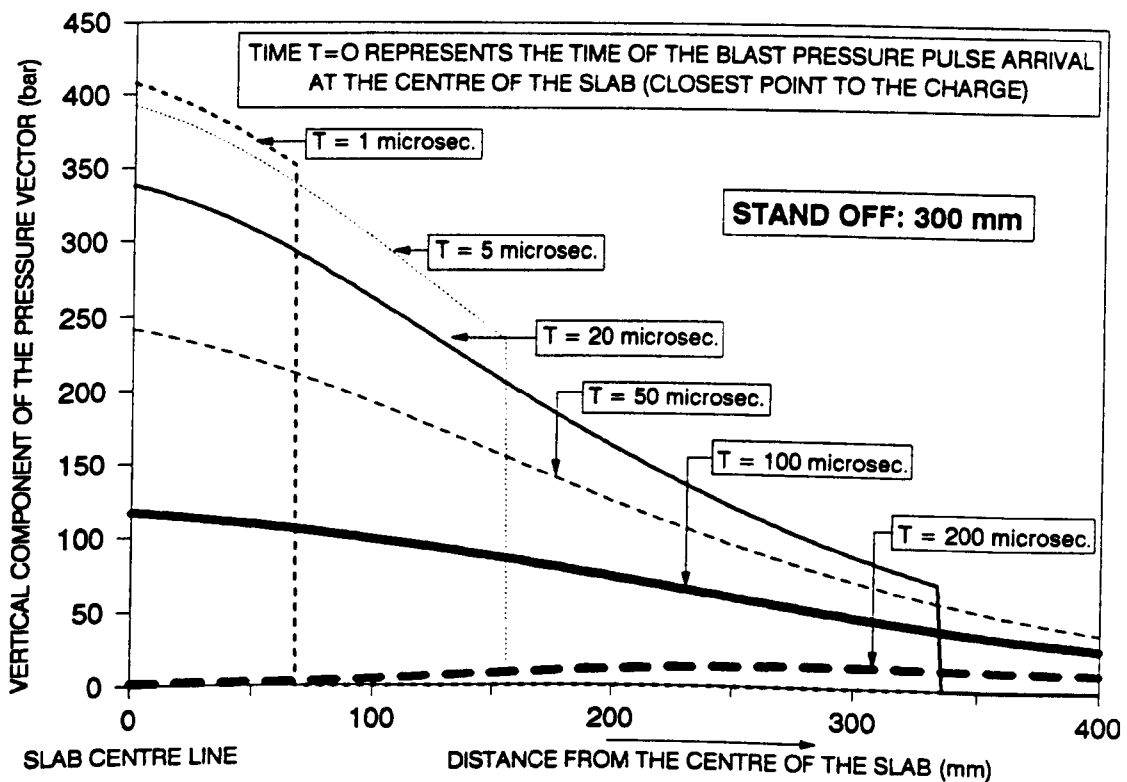


Fig. 5.5 Pressure vs. time profile for 78g PE4 charge according to Henrych (1979) - 300mm standoff

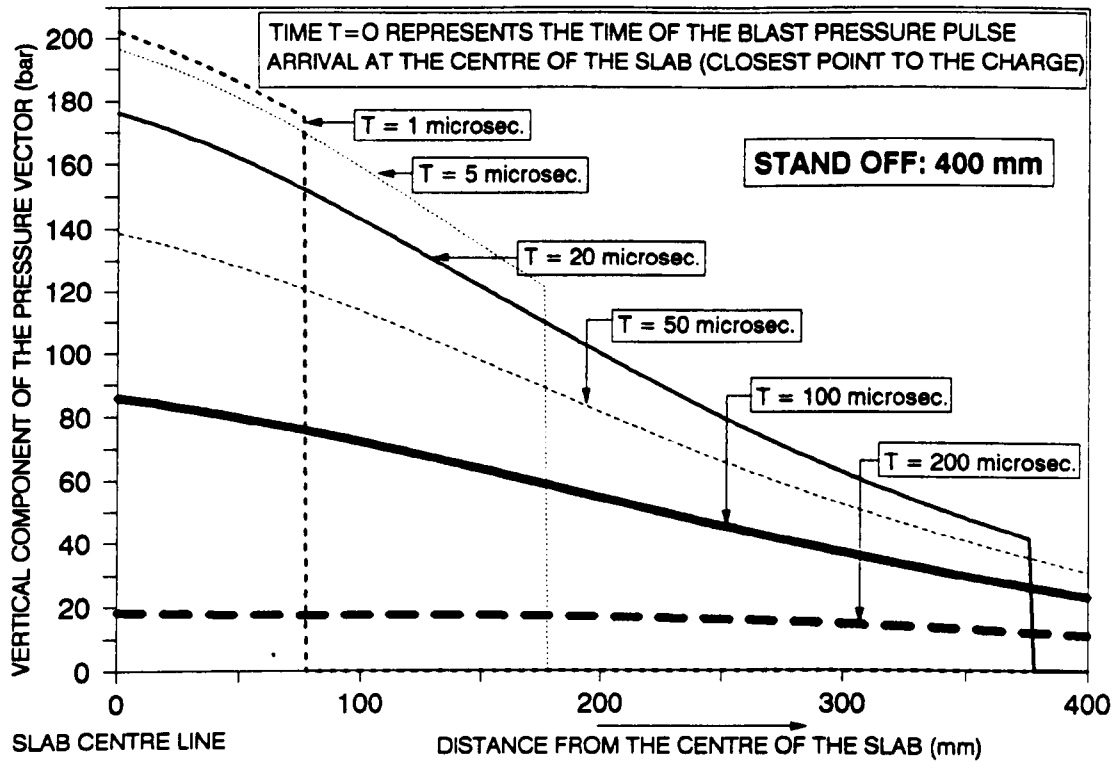


Fig. 5.6 Pressure vs. time profile for 78g PE4 charge according to Henrych (1979) - 400mm standoff

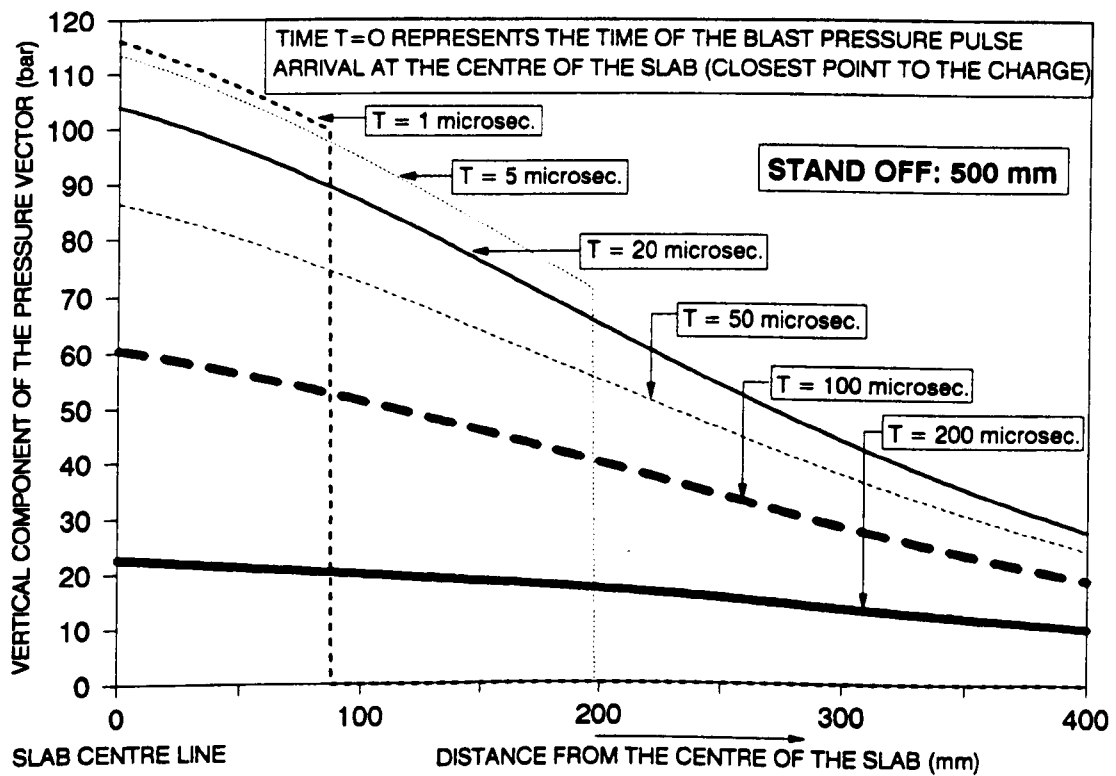


Fig. 5.7 Pressure vs time profile for 78g PE4 charge according to Henrych (1979) - 500mm standoff

A comparison between the measured and calculated results is given in Table 5.1. Since the positive duration τ of the calculated pressure functions was chosen to more or less equal the experimentally measured results, it is not given in the table. The arrival time of the pressure pulse at a point on the slab must not be confused with the time of the pressure pulse arrival at the closest point on the slab which, if presented in the table, would vary because of the different bursting times for L2A1 detonators.

STANDOFF (mm)	DISTANCE TO THE EPICENTRE (mm)	PEAK PRESSURES	
		MEASURED VALUE (bar)	CALCULATED VALUE (bar)
600	420	26	21.2
500	0	100 to 140	116.14
400	0	180 to 280	202.2
400	350	45 to 55	48.8
300	0	290 to 320	407.9
300	350	35	63.6
200	350	40 to 52	74.2
100	350	55	57.8

Table 5.1 Comparison of measured with calculated pressures

It can be seen in the Table that all the calculated pressures have the same order of magnitude as the measured pressures and most are within 10% of the measured values. The blast function is not always so consistent.

5.1.1.2 Attenuation of the loading function and inertia

The loading function characteristics depend on the energy absorption capacity of the slab and on the dynamic attenuation characteristics of the material causing stress wave attenuation and vibration damping.

Krauthammer, (1986), approximates that the damping ratio can be up to 40% for a rapidly applied dynamic load. In the local, stress wave dominated region, damping represents the internal friction of the material. In flexural response it represents the energy lost from internal damage of the concrete and dowel action of the bending reinforcement.

Inertial forces on the specimen oppose the initial slab downward movement and contribute to the formation of an area of local response and the start of the flexural response of the slab. The slab inertia also contributes to the establishment of three dimensional stress state which increases the concrete's apparent strength, section 5.1.2. The inertia of the fractured zone of concrete at the epicentre at peak displacement causes further damage of the scab region of the slab.

5.1.2 Dynamic character of material behaviour

The R.C. slab constitutive material characteristics are sensitive to strain rates. The quantitative change of mechanical properties of the steel and concrete have been presented in Chapter 2, and the reasons for the change of these parameters will be discussed here.

It is obvious from the experimental results that the failure pattern at different loading rates is not exactly the same. In impact and blast loading a great amount of energy is introduced into the specimen in a very short period of time. Load transfer may not develop under dynamic load as under static load because the parts of the system that show the lowest resistance to failure may not have enough time to respond. In the case of concrete the weakest link is the cement aggregate bond and cracks propagating through these regions would require a lower amount of energy than crack propagating through the aggregate particles. Static load allows time for the failure paths of lowest energy requirements to be activated (*Zielinsky et al,1981*), but the rapid change in stress under dynamic loading does not allow time for cracks to form preferentially through the weakest regions of the concrete. This necessarily leads to a greater amount of aggregate particle fracture Fig. 5.8 and Fig. 5.9 and consequent increase in fracture energy absorbed in failure under dynamic loading, so increasing the apparent resistance of the material. This indicates that the higher strength and deformation of concrete under dynamic loading can be explained by crack development through zones of higher resistance and a much greater amount of micro and macro cracking in the whole region than under static loading. It is a function therefore, of the heterogeneous nature of concrete which allows alternative fracture modes to occur.

Steel also exhibits changes of mechanical properties with strain rate but since it is more homogenous than concrete, the strain rate enhancement cannot be entirely due to the heterogeneity of the materials.

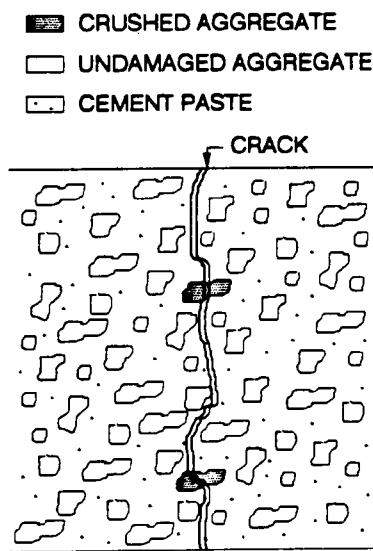


Fig. 5.8 Static type concrete failure

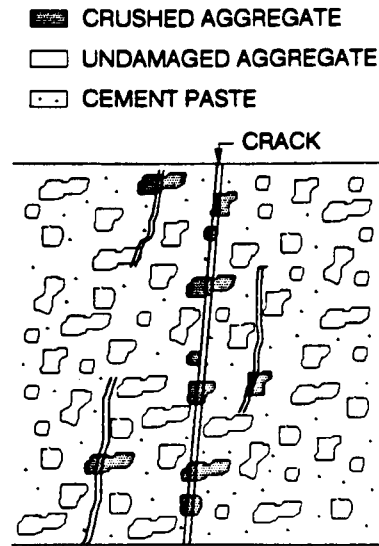


Fig. 5.9 Dynamic type concrete failure

Sheridan et al, (1989), considered the influence of radial inertial confinement introduced into the specimen by the speed of loading which does not permit the structure to develop lateral strains. This confinement in a three dimensional stress state ultimately leads to an increase of compressive strength compared to the uniaxial state. This three dimensional stress state also leads to a much greater density of internal and external, surface cracks under dynamic loading so increasing the energy required to produce the failure as discussed above and also reported by *Zielinsky and Reinhardt, (1982)*.

Relations that govern the apparent increase in dynamic compressive and tensile strength of concrete and dynamic tensile strength of steel are given in sections 2.2.1.2, 2.2.1.3 and 2.2.2.

The Hopkinson Pressure Bar tests carried out in this research show up to 2.5 times increase of concrete dynamic compressive strength compared to static values (section 3.1.2.1). The increase in tensile strength can be even greater but was not investigated experimentally in this research. The strain rates used in this research were up to 10^6 times greater in the dynamic than in the static tests.

5.1.3 Dual nature of the slab response

In a static test on RC slabs, resistance mechanisms can usually be described as shear or flexural, and failure follows response of the whole slab. A combination between the two effects

can also be present but shear-flexure failure occurs often after considerable flexural deflection of the member. With impact and impulsive load from close range explosive charges, different failure mechanisms occur in the time scale of events, and evidence of local and overall failure mechanisms can be found in the shape, location and characteristics of the damage caused to the specimen. In coupling local and overall failure mechanisms the transfer of energy to the specimen and the partition of energy between them, becomes a major question. Local response of the specimen is determined by spalling and scabbing mechanisms and by dynamic shear resistance. It starts long before the overall response of the structure which is defined as a flexural response and limited by the specimen's natural period of vibration. The energy absorbed in flexure will depend on the amount of energy transmitted to the rest of the specimen from the shear plug boundaries of the local damage and that absorbed by the dynamic shear resistance of the specimen. When perforation of the slab occurs before the end of the shock pulse, some of the energy will be removed as the missile or blast pressure exits through the hole in the slab.

Local response is basically characterised by the development of a central "shear plug" with all damage and deformation being localised, usually around the point on the slab closest to the explosive charge or impact point. Overall flexural response is a global response whose main effects are the formation of failure lines similar to the yield lines characteristic of a static failure mode, and permanent displacement of the rest of the slab.

The following sections of this chapter will mainly deal with these phenomena.

5.2 Local response

When an explosion occurs near to the surface of a R.C. slab, then the blast pressures are first applied very locally at the point on the slab closest to the charge, the epicentre, and then vary with distances and time across the slab surface because of the significant curvature of the blast wave front, section 5.1.1. As a result the response of the slab can usually be separated into a local and overall response which occur at different times. The local response, often produces a shear plug around the epicentral axis, but could also produce shear failure at the slab supports. This response includes, in addition to shear some or all of the following fractures which occur very shortly after the first application of pressure:

- (i) The formation of radial and circumferential cracks centred on the epicentre of the blast but with most cracks on the surface of the slab away from the charge.
- (ii) The formation of craters on both faces of the slab near the epicentre, with associated deformation or even fracture of the steel reinforcement within the boundaries of these craters.
- (iii) The perforation of the slab near the epicentre.

The circumferential cracking on the surface of the slab around the epicentre may be associated with the formation of a spall crater on the front face and a scab crater on the rear face or may be the surface intersection of through-thickness cracks which form the frustum of a cone coaxial with the epicentral axis of the blast. This cone has often been described as a local punching shear failure surface, usually characterised by multiple inclined cracking.

5.2.1 Formation of an area of local response

An area of local response for RC slabs will be formed only for impact and close range explosive charges where there is a large curvature on the shock front. For far range charges, the curvature of the shock front will be small when it reaches the surface of the slab. The slab is then loaded with a uniformly distributed, though time varying pressure and any shear fractures would be confined to the local region adjacent to the supports.

Rapidly applied high magnitude loads from close range explosive charges or impact, may result in an area of local response in which the behaviour of the structural element does not depend upon the distance from the supports unless the epicentre or impact point is close to the support. The local response of this area has no apparent relation to the overall response of the rest of the slab because local response starts before there is any overall deflection of the total slab. Span of the damaged area is relatively small and has a high probability of not overlapping with the supports. There may be stress wave reflections from the slab boundaries including supports and this is discussed in later sections and section 2.3.1.

When the duration of the load is much lower than the natural period of specimen vibration then almost all local response takes place in only a fraction of the time required for the specimen's full response.

The main features of local response are localised slab cracking and crushing resulting in shear failures and in top and bottom slab cratering or even perforation, followed by the local bending of the reinforcement.

Information about the local response of the slabs to impact and blast loading was obtained from deflection measurements, high speed films taken during the tests and photographs and cross sections of the specimens taken after the tests. Some typical results are presented in Chapter 4 and are commented upon in more detail below.

5.2.1.1 High speed films

The initial stage of local response of slab SE15 to an explosive charge at 75mm standoff was characterised by the formation of radial or fan shaped cracks on the underside of the slab, propagating from the centre of the slab. These cracks start to form by around 100 μ sec after detonation. The visible length of the longest crack after 190 μ sec was about 147mm measured from the centre of the slab.

In addition to these radial cracks, a set of circular cracks was formed around the epicentre on the underside of the slab early in the response, in a region about 20mm radius from the centre. This was followed by extensive surface cracking inside that circle.

Another set of circular cracks forming a shear plug, with a radius of about 126mm on the back face of the slab and close to the future scab region, was completely established by around 860 μ sec after the detonation. In about 1.8msec after detonation the area of local response was fully defined within the circular cracks. Inside that area extensive fan shaped cracking occurred and disintegration was starting to take place. New cracks began to propagate, being initiated at the circular crack that borders the area of a scab.

The process that characterised the formation of the local damage in slab SE17 was very similar to that one observed on Slab SE15, the main difference being that slab SE17 was perforated. Extensive radial cracking on slab S17 first occurred inside the circular crack at about 25mm radius from the epicentre. About 655 μ sec later further circular cracks became visible at about 80mm radius from the epicentre. The establishment of the full circular crack around the epicentre took another 200 μ sec and the local scab area was then clearly established.

Slab SE13, explosively loaded, did not have any significant scabbing but it was observed that the initiation of fan shaped cracks was almost 3msec before any visible circular cracks, at about 125mm from the centre, became obvious. Although the circular cracks closed when the slab recovered, the fan shaped cracks remained open throughout the event and were combined with the scabbing that was observed after the test.

Slab SE14 also explosively loaded, had diagonal cracking inside the area of the future scab before the circular cracks around that area became visible. These fan shaped cracks formed about 800 μ sec before the circular cracks and the area of the scab was of square shape with sides about 250mm long. The boundaries of the square were parallel to the reinforcement.

In soft impact test S12, the time difference between the initiation of the diagonal and the circular cracks inside the scab area was about 4.16msec with the diagonal cracks occurring first. The overall time needed for the formation of the scab area was about 6msec from the impact.

Slab S13 was exposed to a hard impact and was fully perforated by the impact hammer. In this case the formation of radial cracks happened much later than the initiation of the first circular cracks that were formed at a radius of about 100mm from the impact point. The time difference between the two was approximately 1.6msec. After another 1.6msec the circular crack was fully developed while the fan shaped ones were still in the process of forming.

Slab S17 was exposed to a soft impact and had no visible damage associated with local response of the specimen.

High speed photography was attempted for all the slabs. Those from the impacted Slabs S2 to S6 were of poor quality, but it could be seen that on Slab S2 circular cracks occurred before the radial cracks inside the shear plug area. On Slab S5 and Slab S6 the formation of both types of crack seemed to be almost simultaneous.

The formation of a well defined cracked area of a circular shape can be caused by at least two different mechanisms. The concentric rings of identical pressures as the blast wave produced by the explosion of the hemispherical charge, spread across the slab, gave a load function that had radially varying intensities. This is contributed to further by the curvature of the initial blast front. The other reason may be related to the rate of loading which necessitates the shortest paths of stress relaxation. The circle has the smallest length of circumferential line of all geometrical areas so the first cracks will most likely be initiated along that line.

It is observed from the high speed films, that the boundaries of the local damage are formed early in time and that most of the further damage then forms within that area. The cracks that define the local area are then a limit on the size of the punching shear cone and the energy confined within this area is unable to fracture the surrounding concrete. Typical crack velocities observed from the high speed films were between 420 and 770m/sec.

5.2.1.2 Stress wave theory approach

Stress wave theory is a useful tool for a qualitative and quantitative understanding of radial and circumferential tensile cracking, cratering and through-thickness shear cone cracking near the epicentre, which are all fractures characteristic of the local deformation. Predicting the fracture pattern from a stress wave analysis of the blast loaded slabs requires a model of the pressure variation with time and distance on the slab and the rate dependent properties of the concrete.

The incident pulse imposed on the specimen is of the same shape as the pulse produced by the blast. The shape of the positive overpressure pulse can be approximated as triangular with an instantaneous rise to peak pressure and a uniform decay to atmospheric pressure, Fig. 5.10 shown by the dotted line.

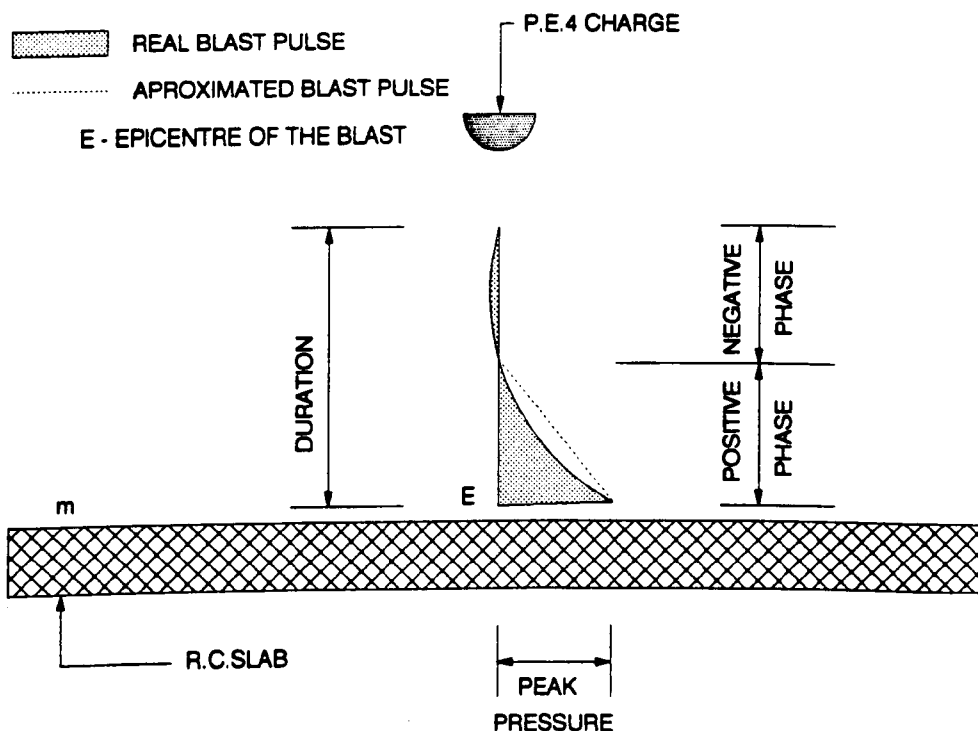


Fig. 5.10 Shape of the incident pulse

The compressive pulse in the concrete slab, initiated at the time of contact of the shock front with the front of the slab, produces the initial blast shock whose quantitative characteristics are given by the equations in section 5.1.1. As the compression wave propagates in to the slab, its characteristic parameters may change as the concrete fractures when the magnitude of the stress is greater than the compressive strength of the concrete.

The fracturing is a process of disintegration or pulverisation of the concrete with the destruction of the aggregate/cement matrix bond, leaving only frictional forces between the particles. This fracturing will absorb considerable energy from that supplied by the shock pulse. In the case when no damage occurs to the concrete on the front face of the slab, the compressive pulse propagates further into the specimen without causing any local damage and its magnitude and energy are reduced by the divergence of the expanding wave.

The alteration in the pulse shape produced by divergence and the different impedances of air voids, cement matrix, aggregates and steel produces attenuation and dispersion that are also the result of different velocities of propagation for the different frequency components of the compressive pulse. The plastic portion of the stress wave will always be slower than the elastic portion which precedes it because of the greater elastic modulus.

The amplitude of the stress wave also decreases as it propagates because of heat energy losses and because of damping in the material through which it travels (*Sheridan, 1987*).

The stress wave energy absorbed in deforming the affected areas of the structure will be small for elastic deformations but plastic deformations and fracture absorb considerably more. The changes produced by the heterogeneity of the concrete are relatively small.

When the compression pulse reaches the free boundary of the slab, the bottom surface, it is reflected as a tensile wave (Fig. 5.11 (a) to (c)). The whole of the pulse is reflected and the boundary regions then experience a period of combination of the incident compressive wave and the reflected tensile wave. If the pulse has a triangular shape then net tensile stresses occur immediately and the maximum occurs at a half pulse length from the boundary (Fig. 5.11 (d)). Tensile failure will start at the point where the net tensile stress exceeds the tensile strength of the concrete. This is generally about 10% of the compressive strength of concrete but the strain rate enhancement of tensile strength is greater than that of the compressive strength.

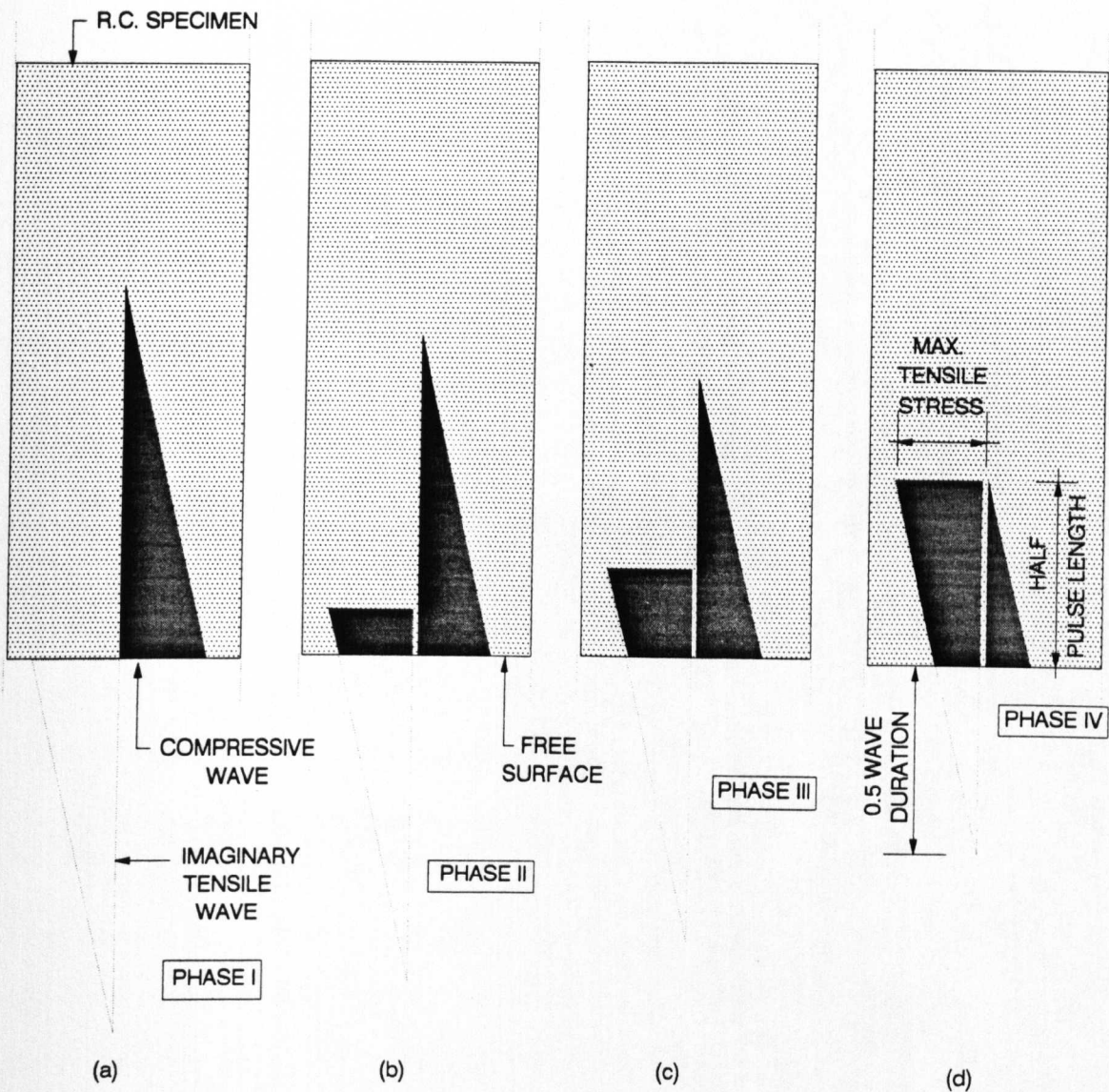


Fig. 5.11 Stress wave reflection

For plane waves the tensile failure will occur parallel to the free surface and a certain amount of energy will be consumed in forming the new free surface. Several cracks can occur as the residual compressive pulse reflects at the new free surface as a tensile pulse and propagates into the slab. In the process of forming the crack a certain amount of energy will be trapped between the crack faces or the crack and the boundary of the slab, and it will trap momentum in the cracked part of concrete referred to as the scab. The velocity of scab ejection then depends upon the shape and the magnitude of the reflected stress wave and the velocity of the scab can be considerable. By observing flying particle velocity, ejected from the back of the R.C. slab, *McVay, (1987)*, reported velocities in the order of 5 to 53 m/sec. A single crack plane will be formed when the tensile strength of concrete is greater than 50% but less than 100% of the peak tensile stress.

For incident compressive waves of larger amplitudes, tensile failure will be reached sooner and the scab thickness will be smaller but multiple scabs may occur depending on the shape of the pulse.

If the rise time of the shock front is assumed to be zero then the thickness of the scabbing layers, for the triangular incident pulse, will be equal.

Scabbing could also be influenced by the velocity of the slab movement or deflection rate. **Kropatscheck, (1983)**, predicts that if the deflection velocity becomes greater than 15m/sec, the momentum will become significant and the concrete layer, or scab will be blown out.

The speed of elastic wave propagation through the concrete is of the order of 3400m/sec and the compressive pressure pulse will reach the free surface of the small scale slab used in the research described here in about 13µsec, and the top face around the epicentre has already experienced the full magnitude of the compressive pressure pulse. The duration of the pulse that reaches the free, bottom surface of the slab depends on the initial shape and size of the pulse and any attenuation or dispersion that has occurred.

Most of the changes to the stress pulse reaching the free surface are caused by compressive failure in the top layer of concrete and by divergence of the stress pulse in the slab. The stress wave produced by the 78gr explosive charge at 50mm standoff exhibits greater changes due to fracture of the concrete while the stress wave from the charge at 250mm standoff changes more due to divergence since it causes little damage to the concrete. Estimation of these effects which distort the pulse is of great importance.

Divergence causes the magnitude of the stresses to decrease as the stress wave expands since the energy is spread over a greater volume of concrete. Fig. 5.12.

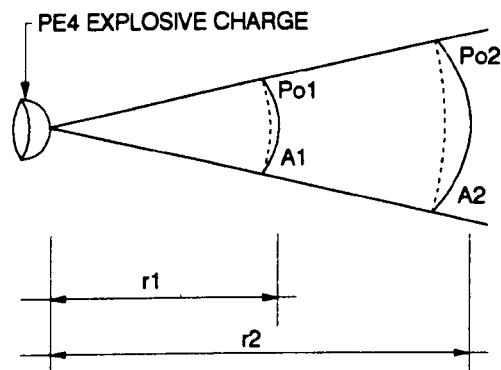


Fig. 5.12 Divergence of the stress wave

If we assume that the curved side of the hemispherical charge has a spherically expanding stress wave then neglecting losses, the sum of the energy of the wave at any distance must be equal, It can be concluded that the amplitude of the stress wave will be inversely proportional to the surface area of the sphere whose origin is at the stress wave initiation point. So:

$$A_1 \cdot P_{O1} = A_2 \cdot P_{O2}$$

$$P_{O2} = \frac{A_1}{A_2} \cdot P_{O1}$$

If we take P_{O1} to be the peak overpressure at any point on the R.C. slab and $A_{1/2}$ as the area to which the stress wave has propagated, then the magnitude of the pressure will decrease at distance r_2 to:

$$P_{O2} = \frac{P_{O1}}{A_2}$$

This would imply a dramatic decrease in the magnitude of the stress wave which is not true because the pressure is not actually applied at one point only and the consequent resultant stress magnitude represents the sum of the magnitudes of stresses generated across the whole slab. The solution to the problem lies in numerical integration across the whole slab surface.

It is much more complicated to calculate the losses due to cratering and cracking of concrete.

If only scabbing takes place, Fig. 5.13.,

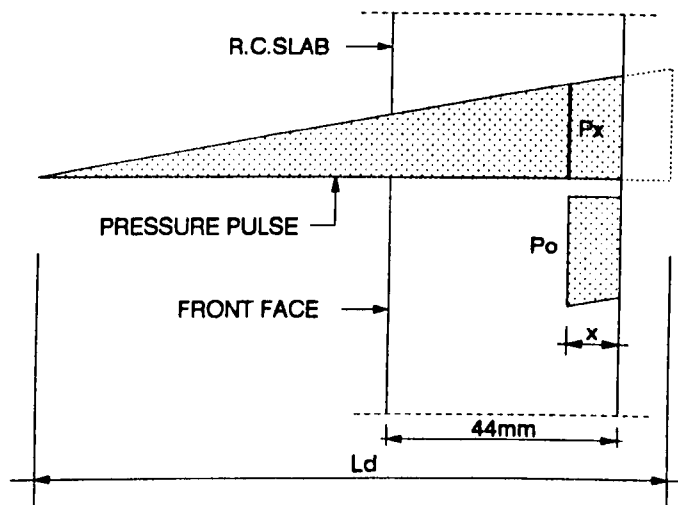


Fig. 5.13 Scab thickness

or in other words, the dynamic compressive strength was not exceeded, then the scabbing thickness can be easily computed, providing the pressure pulse characteristics and dynamic tensile strength of concrete are known.

Attenuation due to divergence may be taken as 10%, *Kropatscheck, (1983)*. It can be seen from Fig. 5.13 that at the scab thickness x the net stress will be equal to the ultimate dynamic tensile strength of concrete which can be estimated to be about 2.5 times greater than the static strength at these strain rates.

$$f_{dt} = P_o - P_x$$

where: f_{dt} - dynamic tensile strength of concrete, taken as 10N/mm²

P_o - peak overpressure (N/mm²) - peak amplitude of stress pulse

P_x - corresponding overpressure at distance of scab thickness (N/mm²) - corresponding amplitude of stress pulse.

If the pressure wave has a triangular shape P_x can be calculated as:

$$P_x = \frac{P_o \cdot (L_d - 2x)}{L_d}$$

where L_d represents the length of the pulse:

$$L_d = T_d \cdot V$$

where T_d is the positive duration of the pressure pulse in msec while V is longitudinal velocity of concrete 3400mm/msec. Then:

$$x = \frac{L_d \cdot f_{dt}}{2P_o}$$

If we consider slab SE15 under blast loading where the calculated peak pressure at the epicentre, which was at the midspan point, was 846.31N/mm² and the positive duration was 0.05362msec then $L_d = 182.3$ mm and after allowing for 10% attenuation due to divergence of the stress wave, the scabbing thickness x can be calculated as $x = 2.39$ mm. Subsequent layers of the scab will be formed in the same way and will be of the same thickness since the rise time for the pressure pulse was assumed to be zero.

5.2.2 Development of cracking within the area of local response

Once the boundary of local response has been established by the circular crack, there are limits on the size of the future scab and the length of radial cracking from the centre of the shear plug since further damage mostly happens inside that boundary.

High Speed photography of Slabs SE15 and SE17 show very clearly the pattern of scab disintegration under explosive blast loading. The circular crack formed at about 20mm radius from the epicentre, limited the area of the scab that will fail first, Fig. 5.14 (Zone A) and it appeared to have completely disintegrated randomly and fractured into very small pieces.

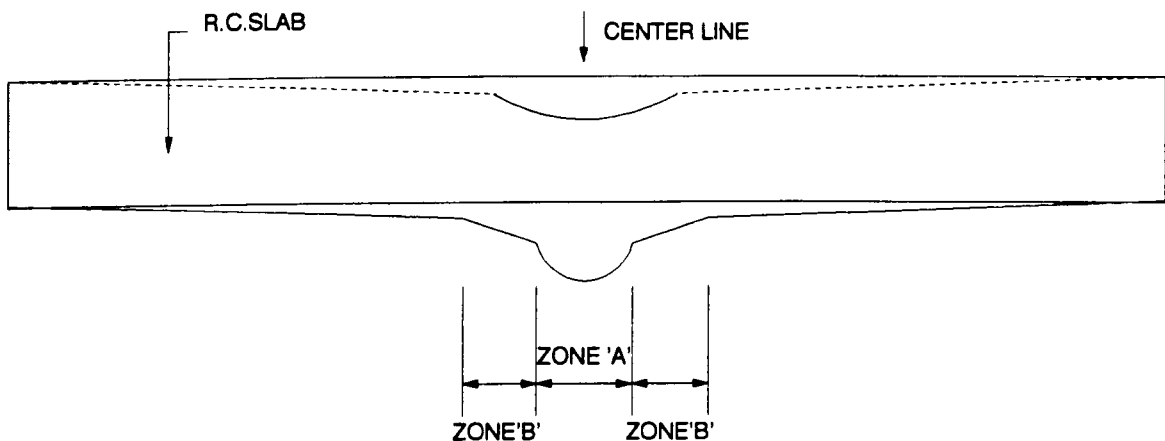


Fig. 5.14 Development of area of local response

The outside ring (zone B) cracked and fractured into almost equal ring segments, Fig. 5.15. These two zones approximately correspond to the size of the future scab region.

Radial cracks almost always propagated just to the circular cracks of the shear plug so giving the impression that the concrete within the circular crack deformed as a dome supported on the edges of the shear plug in a local flexural deformation. An alternative explanation of these radial cracks is that they are due to hoop stresses associated with an outwardly propagating compression pulse. In slab SE17 with a charge standoff of 50mm, there is more than just one Zone B ring, indicating larger stresses at greater distances from the epicentre.

In the case of soft impact the cracking inside the circular crack boundary was in many respects similar to the cracking due to blast loading but a Zone A was not observed, Slab S12. In

the case of hard impact slabs, radial cracks from the epicentre were formed after the formation of an initial circular crack but were not symmetrically arranged. The failure was more characteristic of a direct shear failure than it was in either soft impact or blast.

R.C.SLAB
BACK SIDE

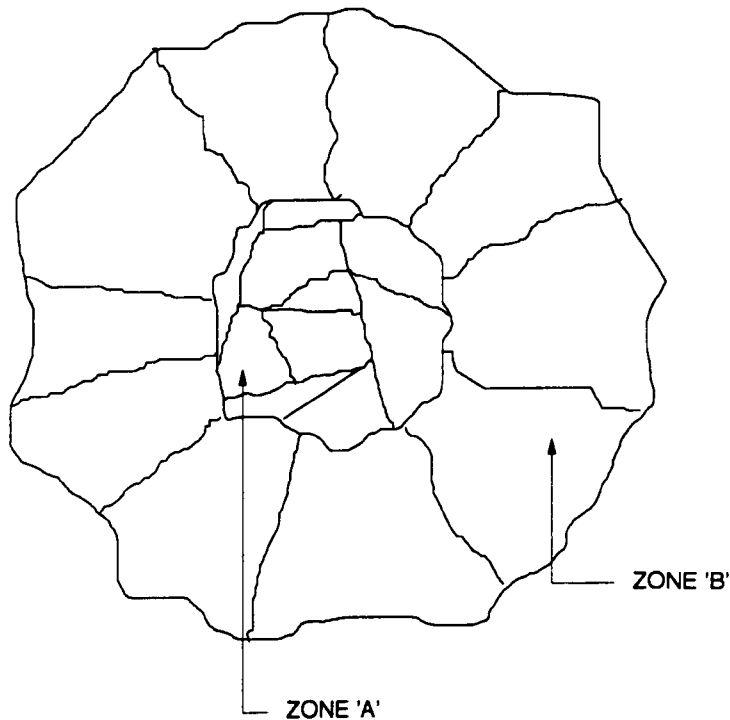


Fig.5.15 Symmetrical segmentation of the outer ring (ring B) and random segmentation of the inner ring (ring A)

The high speed films showed that the cracks did not propagate in a continuous manner with time but stop and start for microseconds periods. This could be explained by local increases in cracking resistance due to, for instance, a concentration of aggregate particles, or by the time needed for the stress to increase following stress relaxation due to the previous cracking.

Flexural strain of the reinforcement in the cases of close range blast loading or impact on the RC slabs is caused by local or overall bending of the reinforcement, and axial strain caused by longitudinal stress wave propagation and axial deformation. Bending of the bars occurs in both

the local and overall deformation modes and in punching shear. When the punch zone is moving downwards relative to the rest of the slab, there is local stretching of the bars.

In some of the tests the reinforcement strain records can be divided into two regions: initial response which lasts about 2msec and is characterised by a lower strain rate of values up to 0.8sec^{-1} , and the later response with much higher strain rates of up to 9.1sec^{-1} . It is expected that these can be related to the movement of the punching cone and dowel action of the reinforcement.

5.2.3 Ultimate state conditions in the area of local response and failure

The ultimate limit state conditions for local response are: cracking and cratering in the area around the epicentre on both faces of the slab, and possible perforation. In the case of impact loading penetration might also sometimes occur without perforation. All these phenomena are mostly the product of the stress wave propagation through the slab but certain local damage may also occur as the result of overall deflection of the specimen. Consequently the final shape of the local area occurred very early in the slab response with some further damage occurring much later, during the overall flexural response of the slab. The total time needed for the slab to completely respond to the dynamic loads can be estimated from the deflection vs time records and it was almost equal for both impact and blast tests. For the 1:2.5 scale slabs it was up to 60msec while for the 1:1 scale slabs it lasted up to 150msec. The deflection vs time traces of the central area of the slab could have given a good indication of the local failure since any sudden increase in displacement would have indicated local failure. The deflection transducers were however, usually connected to the slab reinforcement since connections to the concrete surface often failed or the concrete scabbed. This meant that the instant of local failure was not always easily distinguished.

5.2.3.1 Spalling, scabbing and perforation of the slab

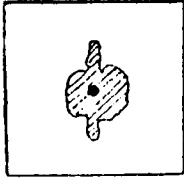
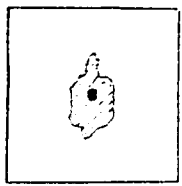
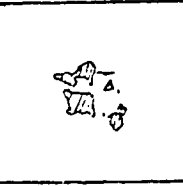
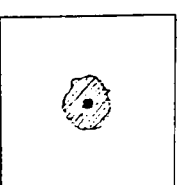
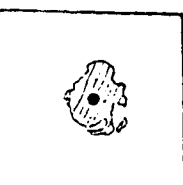
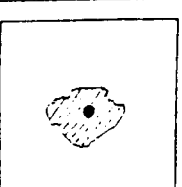
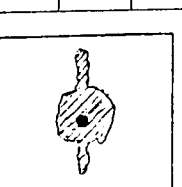
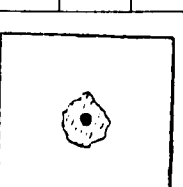
The high speed films were used to analyse the formation and initial development of local response. The ultimate state of local response was obscured on the film by dust and flying particles of concrete. Consequently the final state of local damage was determined by post test

inspection and photographs, Appendix A1 to B2 and by cross sectioning the slab, sections 4.1.1.5 and 4.1.2.5. Tables 5.2 and 5.3 give the details of the local area damage in impact tests. In these tables SCAB (cm²) gives the area of the scab and " % OF SLAB" gives the percentage of the slab surface area covered by the scab. The area of scab on bottom face crater formed by impact on the 1:2.5 scale slabs varied between zero and 11%. The largest scab occurred on the slab that had the highest percentage of reinforcement and the smallest reinforcement bar spacing, slab S1. This was probably because the reinforcement formed a plane of weakness in the slab and the cover concrete was more easily displaced. The slab S2 had a greater impact velocity and this slab had a smaller size scab than on slab S1.

The scab size could not directly relate to either the amount of reinforcement nor the impact energy. On slabs S1, S2, S5 and S6 the scab area produced by the impact also included an area of cover concrete displaced around the edges of the true scab. This cover concrete cracked and was broken away by extensive bending displacement of the reinforcing bars under the impact point. Slabs S8, S11 and S12 have well formed scab areas produced by impact but the tables give the area of concrete actually removed from the slab surface.

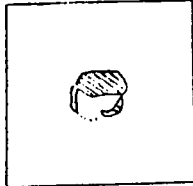
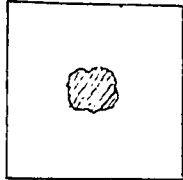
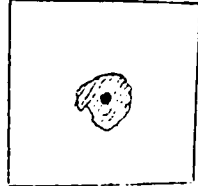
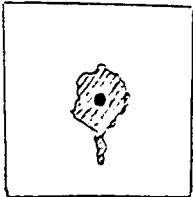
None of the impact tested slabs suffered top face spalling even when perforation occurred.

The percentage of back face surface area that failed in the 1:1 scale slabs varied between zero and 7.5%.

SLAB No	LOADING CONDITIONS	DAMAGE ON THE SLAB BOTTOM SIDE			SLAB No	LOADING CONDITIONS	DAMAGE ON THE SLAB BOTTOM SIDE			SLAB No	LOADING CONDITIONS	DAMAGE ON THE SLAB BOTTOM SIDE					
		SCAB (cm ²)	% OF SLAB	HOLE			SCAB (cm ²)	% OF SLAB	HOLE			SCAB (cm ²)	% OF SLAB	HOLE			
S1	33.7kg hammer hard impact drop height: 1.85 m impact velocity: 5.51 m/sec		704.1	11.0	✓	S6	33.7kg hammer hard impact drop height: 1.85 m impact velocity: 5.63 m/sec		694.8	10.9	✓	S11	33.7kg hammer soft impact drop height: 2.5 m impact velocity: 6.59 m/sec		233.2	3.6	-----
S2	33.7kg hammer hard impact drop height: 1.85 m impact velocity: 5.94 m/sec		514.8	8.0	✓	S7	33.7kg hammer soft impact drop height: 1.85 m impact velocity: 5.96 m/sec	NO SCAB	-----	-----	-----	S12	33.7kg hammer soft impact drop height: 3.0 m impact velocity: 7.21 m/sec		292.9	4.6	-----
S3	33.7kg hammer hard impact drop height: 1.85 m impact velocity: 5.67 m/sec		404.6	6.3	✓	S8	33.7kg hammer soft impact drop height: 1.85 m impact velocity: 5.77 m/sec		180.7	2.8	-----	S13	33.7kg hammer hard impact drop height: 1.5 m impact velocity: 5.17 m/sec		615.6	9.6	-----
S4	33.7kg hammer hard impact drop height: 1.85 m impact velocity: 5.76 m/sec		574.7	9.0	✓	S9	33.7kg hammer soft impact drop height: 1.5 m impact velocity: 5.19 m/sec	NO SCAB	-----	-----	-----	S14	33.7kg hammer hard impact drop height: 0.5 m impact velocity: 2.97 m/sec	NO SCAB	-----	-----	-----
S5	33.7kg hammer hard impact drop height: 1.85 m impact velocity: 5.73 m/sec		678.7	10.6	✓	S10	33.7kg hammer soft impact drop height: 2.0 m impact velocity: 5.94 m/sec	NO SCAB	-----	-----	-----	S15	33.7kg hammer hard impact drop height: 1.0 m impact velocity: 4.3 m/sec		391.3	6.1	-----

**Table 5.2 Details of slab bottom face damage - 1:2.5 scale impact tests
Slabs S1 to S15**

S L A B No	LOADING CONDITIONS	DAMAGE ON THE SLAB BOTTOM SIDE		
		SCAB (cm ²)	% OF SLAB	HOLE
S16	33.7kg hammer hard impact	NO SCAB		
	drop height: 0.75 m			
	impact velocity: 3.73 m/sec			
		-----	-----	-----
S17	33.7kg hammer soft impact	NO SCAB		
	drop height: 1.85 m			
	impact velocity: 5.85 m/sec			
		-----	-----	-----
S18	33.7kg hammer soft impact	NO SCAB		
	drop height: 2.0 m			
	impact velocity: 6.06 m/sec			
		-----	-----	-----
S19	33.7kg hammer soft impact	NO SCAB		
	drop height: 1.5 m			
	impact velocity: 5.23 m/sec			
		-----	-----	-----

S L A B No	LOADING CONDITIONS	DAMAGE ON THE SLAB BOTTOM SIDE		
		SCAB (cm ²)	% OF SLAB	HOLE
LS1	70 kg hammer hard impact			
	drop height: 2 x 3.22m			
	impact velocity: 7.71 m/sec			
		16,716	4.2	-----
LS2	150 kg hammer hard impact			
	drop height: 3.22 m			
	impact velocity: 7.79 m/sec			
		23255	5.8	-----
LS3	150kg hammer hard impact			
	drop height: 2.5 m			
	impact velocity: 6.93 m/sec			
		24791	6.2	✓
LS4	150 kg hammer hard impact			
	drop height: 3.22 m			
	impact velocity: 7.93 m/sec			
		30133	7.5	✓
LS5	150 kg hammer soft impact	NO SCAB		
	drop height: 2.5 m			
	impact velocity: 6.99 m/sec			
		-----	-----	-----

**Table 5.3 Details of slab bottom face damage - 1:2.5 scale impact tests
Slabs S16 to S19 and 1:1 scale slabs LS1 to LS5**

On the impact face of slabs S1 to S6, S13 and S15, the pressure bar had penetrated leaving a small indentation with vertical walls. The depth of the pressure bar penetration was up to 10mm and this must have absorbed a significant part of the impact energy. Below the pressure bar indentation was the shear plug with inclined walls at 10° to 30° and considerable cracking outside these boundaries, sometimes at up to 45° inclination, Fig 5.16.

In impact tests all of the punched holes had approximately the same size diameter, which was 10% larger than the hammer diameter i.e.50mm.

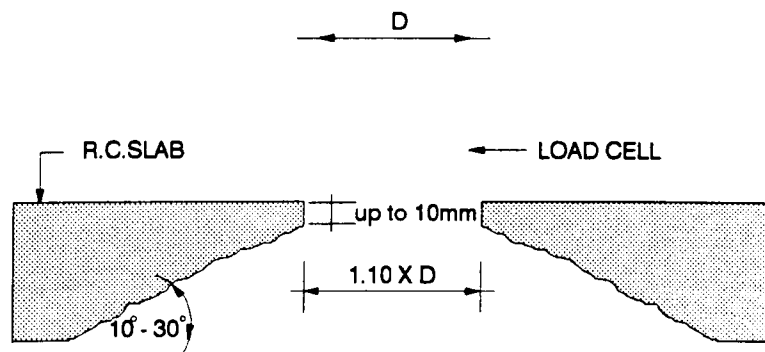
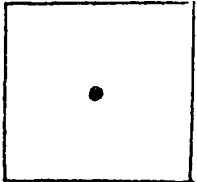
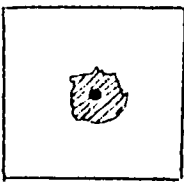
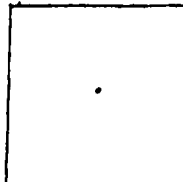
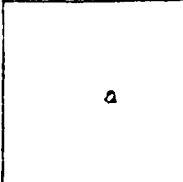
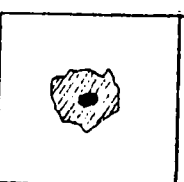
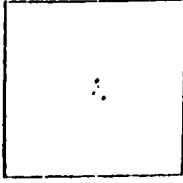
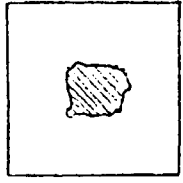
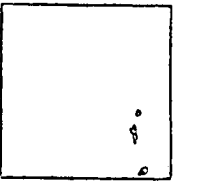
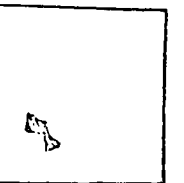
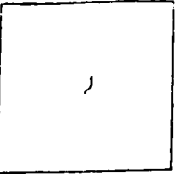
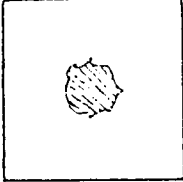


Fig. 5.16 Typical impact punched hole

Tables 5.4 and 5.5 give the details of the shape and the size of front and back face damage on the blast loaded small scale slabs.

The blast impulse tests usually produced damage on both slab faces. In all cases the bottom face crater, the scab, is much greater than the front face crater, the spall. In most cases perforation was followed by the spall (slabs SE2, SE8, SE16 and SE17) but cylindrical charges produced perforated holes only and no spall (Slabs SE2 and SE3). Damage produced on the slab back face by either a cylindrical or a hemispherical charge of the same mass was almost identical, slabs SE4 and SE5, although slab SE4 had a greater reinforcement percentage. This is consistent with observations about the peak overpressures from different charge shapes, given in section 4.2.1.1.

Percentages given in Tables 5.2 to 5.5 for the scab and spall areas also include the hole.

S L A B No	LOADING CONDITIONS	DAMAGE DESCRIPTION								S L A B No	LOADING CONDITIONS	DAMAGE DESCRIPTION									
		SLAB TOP SIDE				SLAB BOTTOM SIDE						SLAB TOP SIDE				SLAB BOTTOM SIDE					
		SPALL (cm ²)	% OF SLAB	HOLE (cm ²)	% OF SLAB	SCAB (cm ²)	% OF SLAB	HOLE (cm ²)	% OF SLAB			SPALL (cm ²)	% OF SLAB	HOLE (cm ²)	% OF SLAB	SCAB (cm ²)	% OF SLAB	HOLE (cm ²)	% OF SLAB		
SE11	78 grams PE4 hemispherical charge curved side facing the slab stand off: 200 mm	NO SPALL				NO SCAB				SE16	78 grams PE4 hemispherical charge curved side facing the slab stand off: 60 mm			37.9	0.6	28.4	0.4	482.1	7.5	18.9	0.3
SE12	78 grams PE4 hemispherical charge curved side facing the slab stand off: 150 mm			17.4	0.3	SE17	78 grams PE4 hemispherical charge curved side facing the slab stand off: 50 mm			42.4	0.7	31.8	0.5	619.5	9.7	35.1	0.5				
SE13	78 grams PE4 hemispherical charge curved side facing the slab stand off: 125 mm			19.1	0.3	183.2	2.9	SE18	78 grams PE4 hemispherical charge curved side facing the slab stand off: 200 mm	NO SPALL				NO SCAB							
SE14	78 grams PE4 hemispherical charge curved side facing the slab stand off: 100 mm			639.4	10.0	SE19	78 grams PE4 hemispherical charge curved side facing the slab stand off: 100 mm			9.9	0.2	99.6	1.6								
SE15	78 grams PE4 hemispherical charge curved side facing the slab stand off: 75 mm			438.6	6.9																

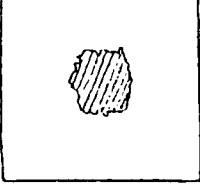
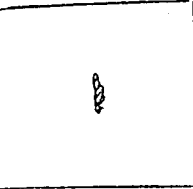
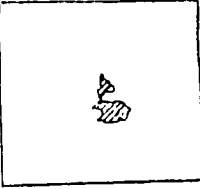
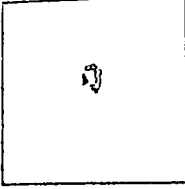
**Table 5.5 Details of slabs top and bottom face damage - 1:2.5
Scale Impulse tests - Slabs SE11 to SE19**

The greatest area of spall occurred on slabs SE7 (1.4%) and SE8 (3.1%) which both had inner supports, section 3.3.1.2. Slab SE5 was identical to slab SE7 but did not have inner supports and had no spall. The maximum size spall produced on a slab without inner supports where slab perforation did not occur was 0.3%, slab SE13. It appears that a slab will have to be perforated to produce spall greater than this. The maximum size of the hole in a slab exposed to a hemispherical charge and not supported by inner supports, was obtained in slab SE17 and was about 0.5% of the total surface area. It is important to note that slab top side damage, spall and hole is closely related to the shape of the charge but not so much to the pressure characteristics of a particular charge. For example, on slabs SE12 to SE15 which were identical apart from a slight difference in concrete strength there was no consistency between the peak overpressure characteristics such as peaks, positive duration and impulse, and the spall size.

The back face damage produced by a cylindrical charge is greater than that produced by a hemispherical charge of the same mass, as seen from the results on slabs SE3 and SE17 for example. The hole is almost 3 times larger in slab SE3 than in slab SE17. The size of the scab can not be related to slab perforation as in spalling. For example scabs on slabs SE7 and SE8 are almost the same size but only SE8 has been perforated. Scabs on these two slabs are almost the same size as the free surface inside the internal supports.

It appears that the scab size depends on the characteristics of the blast pressure function if the almost identical slabs SE10 to SE17 are compared. The scab size is directly proportional to peak overpressures and impulse and inversely proportional to duration of the pulse. The maximum scab area is about 11.2% of the surface area of the slab which is very close to the value obtained in the impact tests. Both values can be related to the size of the charge and impact loading area respectively.

As for impact loading, the maximum size of the bottom face cratering on 1:1 scale explosively tested slabs was relatively smaller than for the 1:2.5 scale slabs and it was 8.3%, Table 5.6.

S L A B No	LOADING CONDITIONS	DAMAGE DESCRIPTION							
		SLAB TOP SIDE				SLAB BOTTOM SIDE			
		SPALL (cm ²)	% OF SLAB	HOLE (cm ²)	% OF SLAB	SCAB (cm ²)	% OF SLAB	HOLE (cm ²)	% OF SLAB
LSE1	1300gms PE4 hemispherical charge								
	curved side facing the slab								
	stand off: 350+250	1647	0.4	-----	-----	32794	8.2	-----	-----
LSE2	1300gms PE4 hemispherical charge								
	curved side facing the slab								
	stand off: 250 mm	2865	0.7	-----	-----	8239	2.1	-----	-----
LSE3	1300gms PE4 hemispherical charge	NO SPALL				NO SCAB			
	curved side facing the slab								
	stand off: 500 mm	-----	-----	-----	-----	-----	-----	-----	-----
LSE4	1300gms PE4 hemispherical charge	NO SPALL							
	curved side facing the slab								
	stand off: 300 mm	-----	-----	-----	-----	6999	1.8	-----	-----
LSE5	1300gms PE4 hemispherical charge								
	curved side facing the slab								
	stand off: 200 mm	1789	0.4	-----	-----	33333	38.3	-----	-----

**Table 5.6 Details of slab's top and bottom face damage
1:1 Scale Impulse tests - Slabs LSE1 to LSE5**

Slab LSE1 which was tested twice at standoffs of 350 and 250mm, had a significantly larger scab than SE2, tested only once at 250mm standoff. This indicates that although slab LSE1 did not appear to have any permanent damage from the first test at 350mm standoff, its resistance must have been reduced before the second test. Spall sizes were maximum at 0.7% of the slab area but are not consistent with the pressure function, e.g. LSE2 and LSE5. None of the 1:1 scale slabs that were tested by explosive were perforated.

In almost all slabs, even the most lightly reinforced, the bottom reinforcing bars were deformed locally in bending over a length which always exceeded the width of the hole in the perforated slabs. There was no significant change in the reinforcement curvature across the deformed length and this indicates that the doming effect which influenced the early local response had no effect on the final shape of the reinforcement. This means that most of the doming was of elastic nature. Before any shear slip took place it was apparent that some of the concrete above the bottom bar reinforcement had been fragmented by the high compressive stress applied by the blast pressure.

Those slabs in which the blast pressures perforated the slab, produced a hole with very steep sides where sometimes the scab and spall intersected.

The shape of the punched hole can be of two different types. Type A, Fig. 5.17 has a

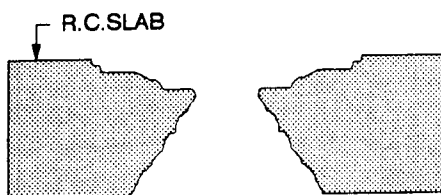


Fig. 5.17 Punched hole Type A

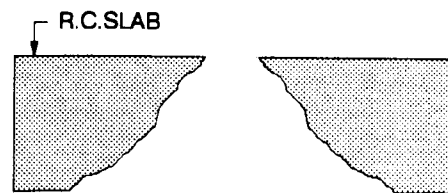


Fig. 5.18 Punched hole Type B

hole that consists of cratering from both slab faces which indicates that both the tensile (bottom side crater) and the compressive (top side crater) dynamic strength of the concrete were exceeded so the intersection of the failure planes helped in the formation of the hole through the slab. In the second case, Type B, Fig. 5.18 only the tensile strength of concrete was exceeded or the size of area where the compression failure (pulverisation) of concrete occurred was smaller than the area of tensile failure.

Although *TMP-5-855-1, (1986)*, suggests that type A action occurs when the top side crater depth, or spall, is approximately equal to one-third of the slab thickness, our tests could not confirm that prediction because in no case was the front spall so deep.

5.2.3.2 Prediction of the damage

Predictions of the damage to R.C. slabs usually concentrates on the damage in the area of local response which is related to the characteristics of the charge and the thickness of the slab. The following predictions are given for the case of blast loading only.

Hader, (1983), gives a relation between the slab thickness t , standoff distance r and cube root of the TNT equivalent of explosive weight W for bare explosive charges and the type of damage caused by the combination of those three, Fig. 5.19

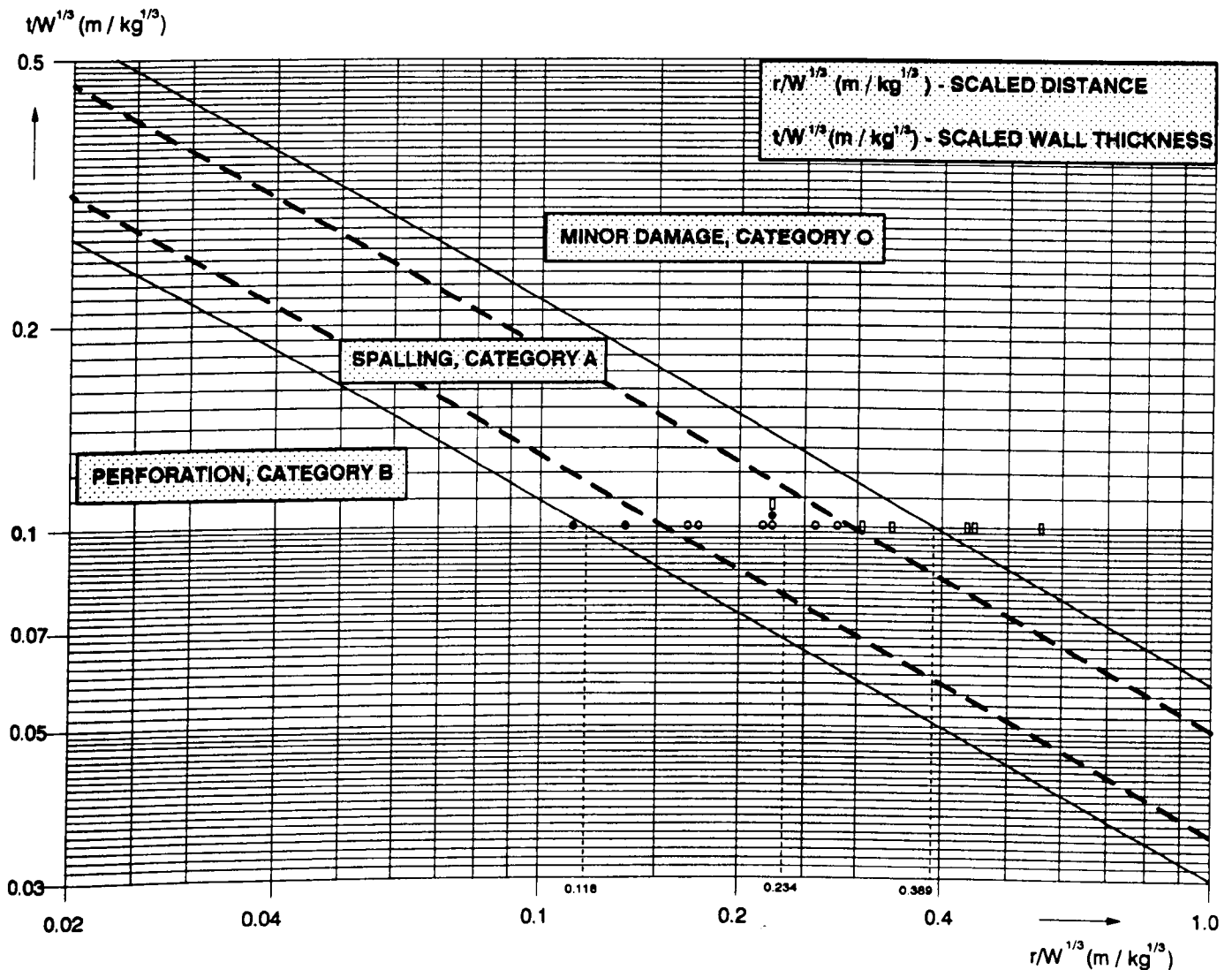


Fig. 5.19 Estimate of the slab damage

	UNITS\SLAB	SE1	SE2	SE3	SE4	SE5	SE6	SE7	SE8	SE9	SE10	SE11	SE12
r	m	0.61+0.1	0.050	0.050	0.100	0.100	0.100	0.100	0.050	0.100	0.250	0.200	0.150
$r / W^{\frac{1}{3}}$	$m / kg^{\frac{1}{3}}$	1.37+0.22	0.1124	0.1124	0.2247	0.2247	0.2247	0.2247	0.1124	0.2247	0.5617	0.4494	0.3371
Estimated damage category		O + A	B	B	A	A	A	A	B	B	O	O	O
	UNITS\SLAB	SE13	SE14	SE15	SE16	SE17	SE18	SE19	LSE1	LSE2	LSE3	LSE4	LSE5
r	m	0.125	0.100	0.075	0.060	0.050	0.200	0.100	0.35+0.25	0.25	0.500	0.300	0.200
$r / W^{\frac{1}{3}}$	$m / kg^{\frac{1}{3}}$	0.2809	0.2247	0.1685	0.1348	0.1124	0.4494	0.2247	0.31+0.22	0.2200	0.4398	0.2639	0.1759
Estimated damage category		A	A	A	B	B	O	O	O+A	A	O	A	A

Table 5.7 Values for Fig. 5.19

Table 5.7 gives the values for $r/W^{1/3}$ and the estimated damage category for both the 1:1 and 1:2.5 scale tests carried out in this research. For 1:2.5 scale slabs $t/W^{1/3}$ is 0.103 while for 1:1 scale slabs it is 0.101.

All the damage is divided into categories O, A and B. The categories O and A represent minor damage and scabbing, respectively. The category B represents the most severe damage and all cases of perforations would fall into this category. It is interesting to note that this classification does not take into account the relative position of the charge to the specimen so central and off centre blasts are treated equally and support effects are ignored.

In this case the term "spalling" has been used in reference to the back face damage. The slabs which were perforated in this research are marked with the black circles on Fig 5.19 while the most severe scabs (slabs SE4 to SE7, SE13 to SE15 and LSE1,LSE2,LSE4 and LSE5) are marked by empty circles. Minor or no damage is marked by empty squares. It can be seen that the Hader predictions more or less agree with the damage observed on the slab specimens tested in this research. All the 1:2.5 scale slabs were tested by a 78g charge at different standoff distances. The energy equivalence of 1kg of PE4 is 1.13kg of TNT, and it can be concluded that any standoff of up to 173mm should have produced minor or no damage, standoffs between 173 and 52.5mm would produce considerable scabbing, and standoffs below 52.5mm were expected to produce perforation of the slab. Tests in this research showed that the perforation prediction is optimistic while the prediction of the minor damage depends on the subjective estimate of the damage. If all scabs of less than 1.7% of the surface area are considered as minor damage then a new relation can be established to more precisely describe the damage on the slabs tested in this research project.

Although *Hader, (1983)*, did not give analytical functions for the lines on Fig 5.19 it can be shown that the boundary between perforation and scabbing was calculated according to:

$$y = K \cdot x + \beta \quad \text{or:}$$

$$\log \frac{t}{W^{1/3}} = -K \cdot \log \frac{r}{W^{1/3}} + \beta$$

where: $K = 0.224548$ and $\beta = -1.522878$

The boundary line between scabbing (or "spalling") and "minor damage" has the same shape and value for K but $\beta = -1.219$.

The new boundaries to satisfy the present test results have the same shape but different values of β . For the "perforation line" $\beta = -1.462274$ and for the "minor damage" line $\beta = -1.3023$.

To find the depth t of an R.C. slab to satisfy any design requirement the following procedure can be adopted. For example if t is chosen as:

$$t \geq W^{0.33} \cdot 10^{-K \cdot \log \frac{r}{W^{0.33}} + \beta}$$

and for $\beta = -1.462274$ the explosive charge of weight W placed at distance r from the target slab, will not perforate it. If $\beta = -1.3023$ then W will cause only minor damage at the back sides of the target i.e. scabs smaller than 1.7% of surface area. Units for t and r are metres while W is in kgs of TNT.

The new lines are shown in Fig. 5.19 with a thick dotted line. Values in between these two lines would still indicate substantial scabbing on the back face of a concrete slab with normal amounts of reinforcement. Fig. 5.19 indicates that slabs with no reinforcement, such as SE9 and slabs with unusual span to depth ratios, such as SE8 with inner supports, had damage which did not conform to the Hader or the new lines. These two cases correspond to value $r/W^{1/3} = 0.234$, Fig. 5.19.

Kinney and Graham, (1985), relate the thickness of the concrete wall r (m) and the charge size W (explosion yield in kilograms TNT) needed for perforation, as:

$$W = \beta \cdot r^3$$

where β is a breaching coefficient. It is thought that this relation is developed for contact charges only but this will be considered here for the close range charges used in the present research. For reinforced concrete β has a value of 27kg TNT/m³. By applying the 1.13 equivalence factor for PE4 to TNT (Section 2.5.2) the charge needed to perforate a 1:2.5 scale slab, W is 0.2g of PE4, since r , the slab thickness, is 0.044m. For the 1:1 scale slabs, where $r = 0.11$ m, W required is 31.8g of PE4. Since these present tests had $W = 78$ g for the 1:2.5 scale slabs and perforation was achieved only from the 60mm standoff or closer, it can be estimated that this relation greatly underestimates the breaching resistance of concrete.

McVay, (1987), predicts that a scab would appear only when the scaled distance was less than $0.6\text{m/kg}^{0.33}$ but he does not give exact details about the slab thickness and the charge shape.

Kropatscheck, (1983), gave a "damage classification" graph for both cased and uncased charges. The relation that covers the uncased charges is identical to the one provided by Hader, (1983), where r represents the standoff distance (m), t is the slab thickness (m) and w is the charge weight (kg), Fig. 5.20.

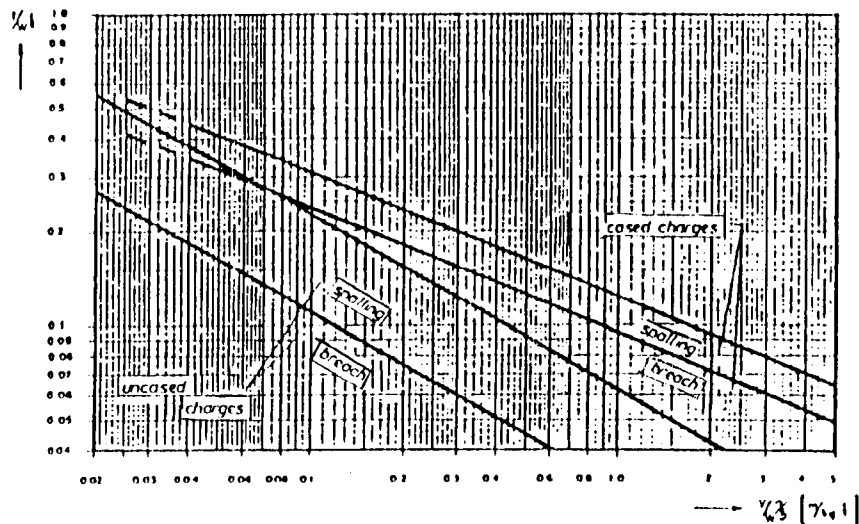


Fig. 5.20 Damage Classification (Kropatscheck, 1983)

Pressure needed to pulverise the top face concrete can be estimated from the tests SE12 which had standoff 150mm and forces were just large enough to produce a small spall. Calculated epicentre peak pressure for 150mm standoff is about 2300 bar.

5.2.4 Load transfer from the area of local response to the rest of the slab

Not all the energy transmitted by the explosion can be absorbed by the very fast local response. Part of the remaining energy will be given to the rest of the slab by the load transfer between these two regions.

Impact load transfer to the rest of the slab depends entirely on the shear strength of the section, but RC slabs are frequently designed without any shear reinforcement. The displacement

of the cone of concrete formed on the epicentral axis of a R.C. slab is resisted in shear by reinforcement dowel action, aggregate interlock and the concrete compression zone shear.

Under static loading inclined shear cracks do not propagate through the full depth of the slab or form instantaneously but with rapidly applied dynamic loads, punching shear cracks almost instantly go through the full depth of the section and as a result the compression zone shear resistance does not exist except possibly at the very beginning of the load transfer.

Once the cracks on the boundary of the shear plug are formed then load transfer to the rest of the slab depends on aggregate interlock and dowel action. The load transfer plays a dominant role in the overall flexural response of the slab and also in the continuing response of the local area.

The mechanisms that resist shear movement of the punching cone and as a result transfer forces to the rest of the slab are given in Fig. 5.21.

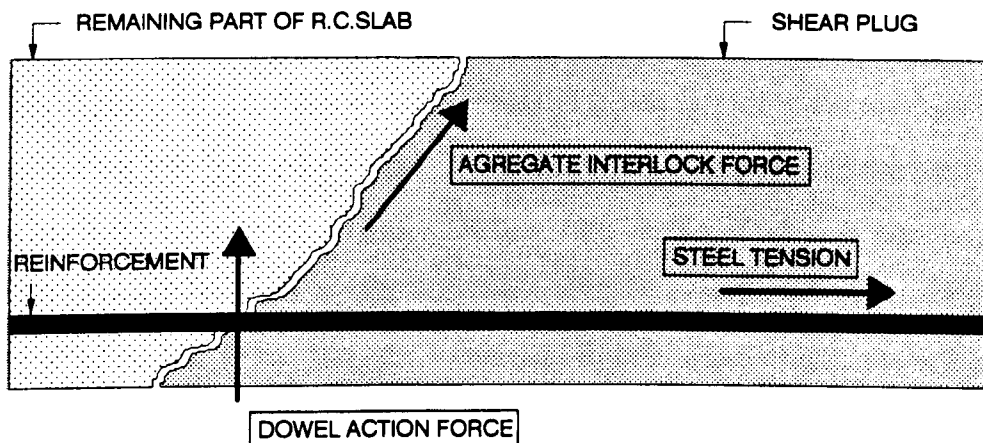


Fig. 5.21 Load transfer from the area of local response

In the early stages, when vertical displacements of the shear plug are small, aggregate interlock may carry about 90% of the overall force as in the case of static loading, and the remaining 10% would then be carried by the dowel action. When larger displacements occur and extensive cracking has almost disintegrated the shear plug, the influence of the aggregate interlock decreases because the gap between the shear faces is much larger and most of the resistance is through the dowel action of the longitudinal reinforcement. It can be estimated that this change of

the predominant load transfer mechanism will be completed when the shear gap exceeds the size of the largest aggregate particle. At this stage there is breaking of the concrete cover, from the reinforcing bars and the high speed photography indicates that this is a later event. *Reinhardt and Walraven, (1982)*, report that the crack opening path, the ratio of crack width or shear gap to shear displacement, for reinforced concrete subjected to static shear loading was not influenced by a variation of the reinforcement ratio between 0.2 and 3.4%. In the present dynamic tests the reinforcement ratio was within these limits.

5.3 Overall response of the slab

Overall flexural movement of the slab follows the localised response that was discussed in section 5.2 for slabs exposed to very localised dynamic loads. Stress waves are of major importance in determining the local response but are less significant than the inertial forces in the overall response. The overall flexural response takes place after the local response and is determined by the peak load or impulse, depending upon the duration relative to the natural period of oscillation of the specimen. The overall response of a slab is mainly characterised by the existence of multiple diagonal cracks typical of yield line rotation, reverse yield lines and cracks formed close to and parallel with the supports and across the corners of two way spanning slabs. The cracks that appear in the specimen will be analysed in the next section.

The local damage to the slab, the inertia due to high accelerations, the spatial and temporal variation of the dynamic load and the dynamic enhancement of the material properties, may all affect the overall flexure of a R.C. slabs under locally applied dynamic loads and produce results which differ markedly from static loading. All damage produces a change in the mass, resistance and stiffness parameters of a member. The possible reduction in some of these parameters before the slab acquires the transient deflection profile, could significantly change the maximum deflections from those determined for undamaged slab.

Some typical deflection - time profiles of the slabs under explosive blast, impact and static loading are given in Figs. 5.22 to 5.31 and show the difference in overall deflected shape of the slabs.

5.3.1 Crack type analysis

The cracking seen on the high speed films has been discussed in the section on local response. This section deals in more detail with the cracks and the crack patterns found after the test on the top and bottom surfaces and central cross sections of the slabs. Although not all the crack types discussed here appear on every single specimen, most specimens show very similar crack patterns.

5.3.1.1 Top surface cracks

Slab S12, Plate 5.1, and Slab SE5, Plate 5.2, exposed to hemispherical charge, (100mm standoff) are typical of the top surface cracking that occurred from impact and blast loading, respectively.

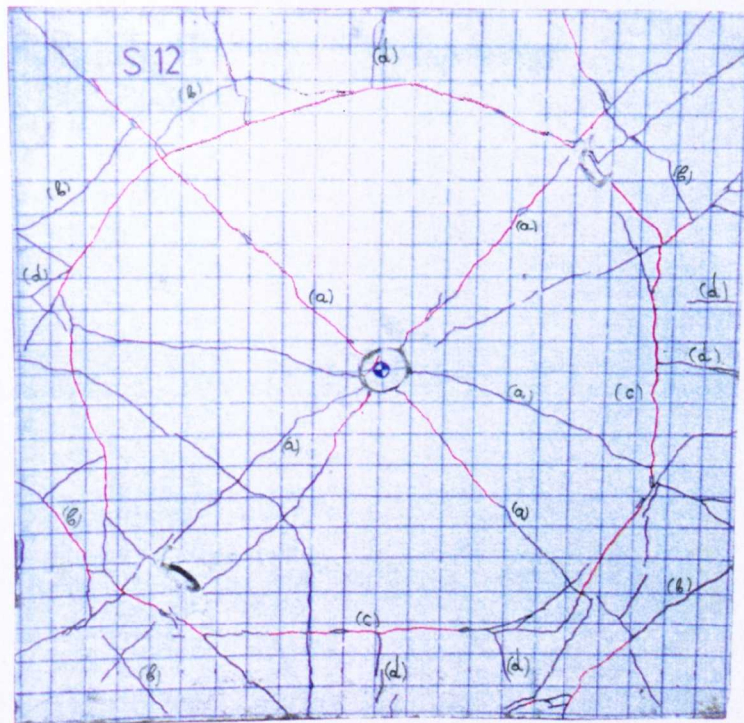


Plate 5.1 Top face of Slab S12, 1:2.5 scale - soft impact test, 3.0m drop

Although Slab SE5 had a much denser crack pattern than Slab S12, both slabs had more or less the same pattern and types of crack.

The **radial cracks (a)** that propagate from impact point on Slab S12 and from about 50-100mm from the blast epicentre on Slab SE5, are produced either by flexure or by hoop stress

perpendicular to radial compression. They are similar to the yield lines that occur on the back of R.C. slabs in static tests and show some rotation along these lines. They are reverse yield lines with a multiplicity of cracks as a result of the oscillations of the slab and clamping of the support area.

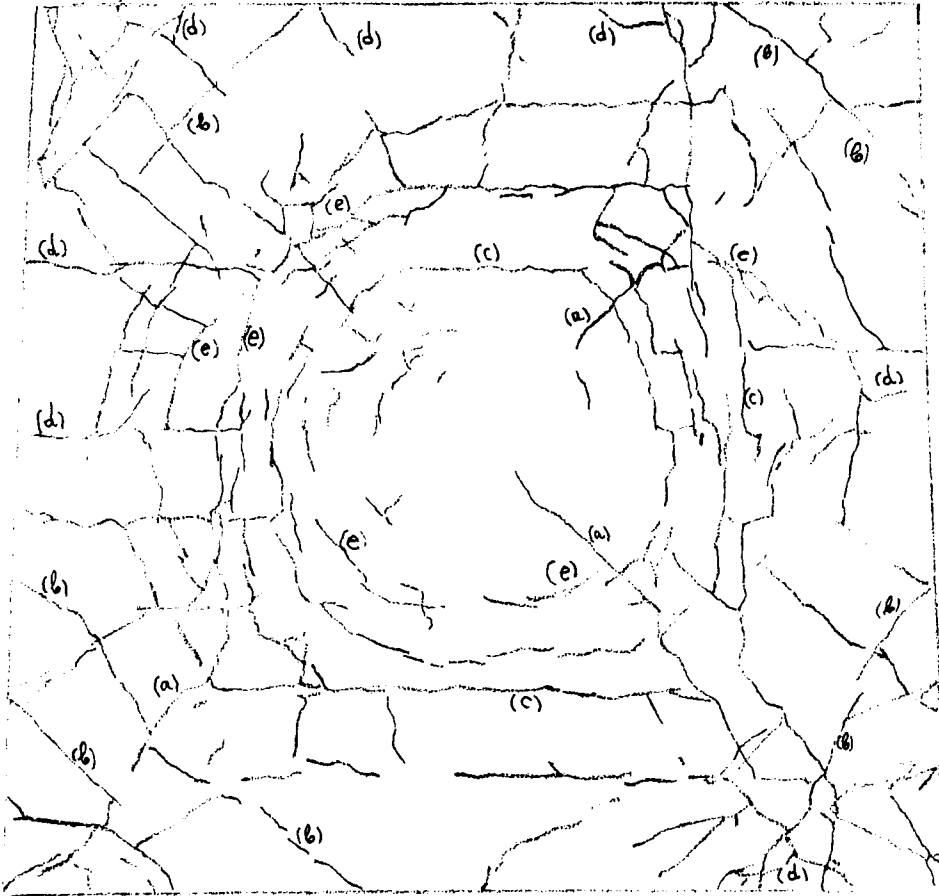


Plate 5.2 Top face of SE5, 1:2.5 scale - hemispherical charge, 100mm standoff

The corner cracks (b) that produce a symmetrical pattern in all four corners may be caused by membrane stress waves or by flexure during the overall deformation of the slab at the time of maximum downwards movement.

Formation of these corner cracks by concentration and amplification of the radiating compression wave occurs when the membrane stress waves move into each corner of the slab. Tensile reflections from the adjacent slab sides interact and so amplify the tensile stresses which become greater than the tensile resistance of the concrete, *Johnson, (1972)*.

The maximum downwards movement of the slab happens much later and could also produce corner cracks.

Some of the corner cracks do not extend completely across the corner, see Plate 5.2 and since some of them appear to originate from the flexural yield lines, they must have been formed after the yield lines. Consequently, corner cracks that originate from the yield lines are clearly not produced by membrane stress waves but by the flexural movement of the slab.

"Reinforcement" cracks (c) propagate along some of the longitudinal reinforcement bars, and are due to an increase in transverse flexural stress increased by the reduction in the area of concrete or to bond forces between concrete and reinforcement. These cracks never propagate deeply into the slab.

Short length cracks (d) appear in the support area of the slab as shown in Plates 5.1 and 5.2 and are very similar to the corner cracks. These are probably caused by multiple reflections of stress waves from the top and bottom beam support arrangement and by concentrations of stress due to non uniform fixity of the supports.

Circular cracks (e) around the blast epicentre may be associated with possible spall formation or may be the surface intersection of through-thickness cracks which form the frustum of the punching cone coaxial with the epicentral axis of the blast. Those furthest from the epicentre may be related to the "doming" of the epicentral area on the back face, and so associated with the flexural response.

Much greater overall density of the front face cracking in impulse than in either type of impact test is the best indication of the influence of dynamic pressure distribution that follows even close range explosion.

5.3.1.2 Bottom surface cracks

Slab S12, Plate 5.3 - impact tested and slab SE16 Plate 5.4 - explosively tested at a standoff distance of 60mm, have bottom surface cracking typical of impact and blast loaded slabs produced by both flexural and local response of the slab.

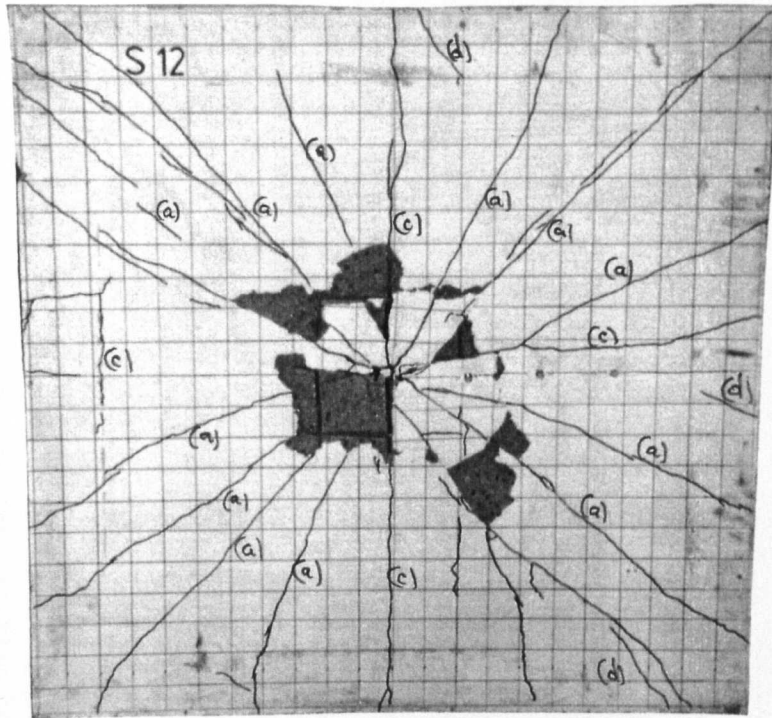


Plate 5.3 Bottom face of Slab S12 - soft impact test - 3.0m drop

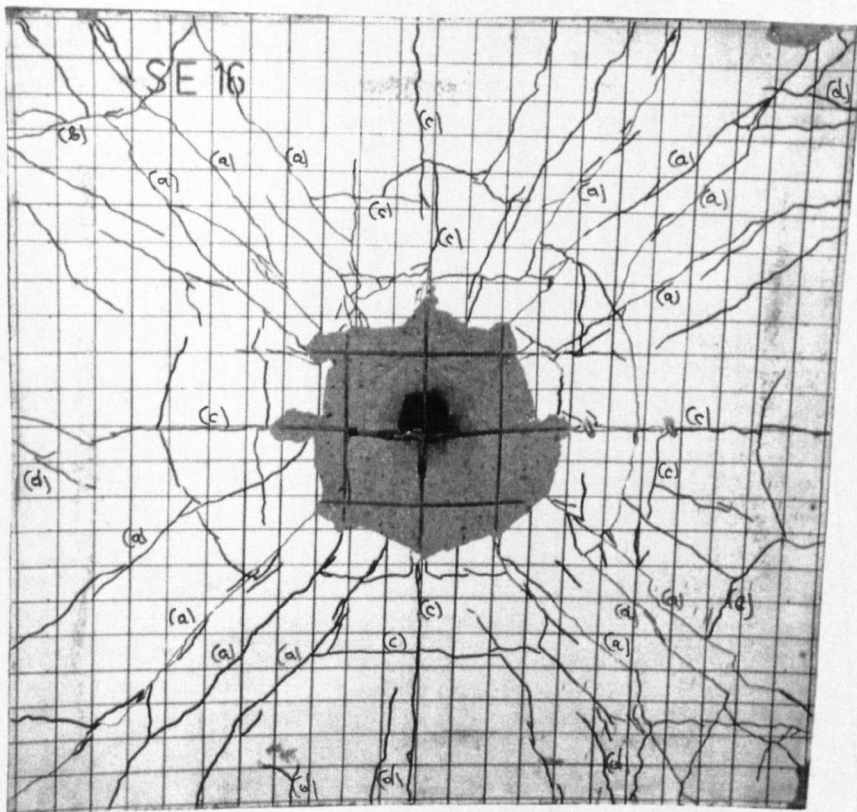


Plate 5.4 Bottom face of Slab SE16 - hemispherical charge - 60mm standoff

The most obvious cracks are the **multiple diagonal cracks (a)** typical of yield line formation, and they are present in all cases of impact and blast test although the absence of residual deflection after some of the tests might indicate that plastic rotation along the yield lines did not occur. They are obviously part of the flexural - overall response of the specimen although the high speed films indicated that their initiation may be closely related to the initial formation of the area of local response and doming that occurs in that region.

The greater density of yield line cracks that occur in soft impact and impulse tests than in hard impact tests, clearly indicates that the major part of the impact energy was absorbed in these parallel cracks. Since the length of the pulse in the soft impact was much longer than in the hard impact, the energy was used mainly for flexural displacement of the slab instead of in local punching at the impact point.

In addition there are cracks **across the corners (b)**, **along the reinforcement (c)** and **short length support cracks (d)** which are similar to those appearing on the front surface.

Circular cracks outside the scab zone could be related to the formation of the shear plug but since they are usually not so close to the epicentre, could also be caused by a plastic hinge as the centre of the slab "domes". Not all the crack types are present in every test but appear in some of them and are typical of the deformation mechanisms.

Plates 5.5 and 5.6 show the larger and smaller size cracks on slab SE17, respectively.

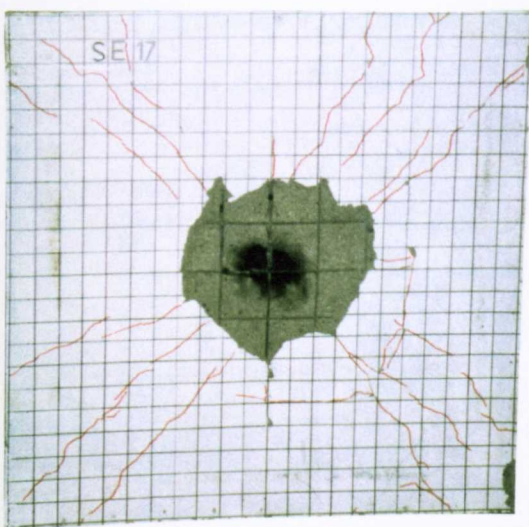


Plate 5.5 Slab SE17 Larger size cracks

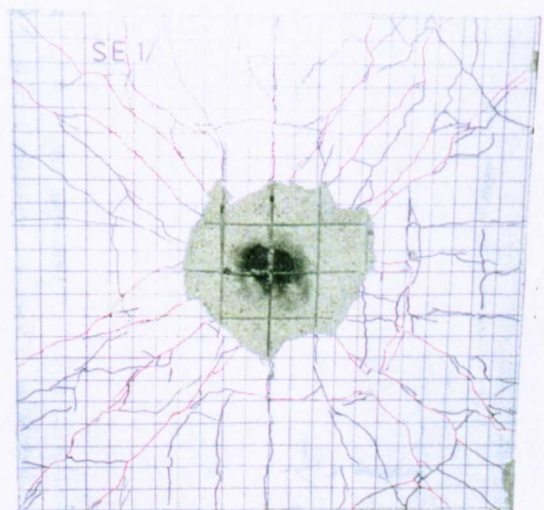


Plate 5.6 Slab SE17 Smaller size cracks

Larger size cracks are mainly those in a radial direction from the centre which suggests that flexural behaviour of the slab is very dominant and that rotations along the diagonal yield

lines were significant. Smaller size cracks in a radial direction are usually further from the yield lines region. The "reinforcement" cracks, corner cracks, support cracks and circular cracks are of a smaller size and do not go deeply into the concrete.

Under static loading the cracks which are first initiated develop to the failure that represents the ultimate response of the slab. The larger flexural cracks indicate a different pattern of behaviour for dynamic tests. Local failure in dynamic tests occurs first but does not develop into the ultimate slab response since it is usually followed by a progressive flexural failure.

5.3.1.3 Cross sectional cracks

Some concrete slabs were sawn along a centre line parallel to the sides to reveal the cracks on the cross sections and these are shown in Figs. 4.10, 4.11 and 4.31. It can be seen that in the epicentral region, the shear plug exists in the form of a conical frustum formed by inclined cracking through the thickness of the slab. These are shear cracks and their inclination is related to the load rise time, duration, and magnitude as well as the depth of the specimen and material characteristics.

In the hard impact tests almost all the damage is concentrated in the area close to the impact point, even in the cases where perforation occurred. The shear planes were almost vertical in this case, and additional bottom face scabbing was a result of movement of the reinforcement. Soft impact and particularly blast tests, produced a different pattern of cross sectional cracks. Apart from the inclined cracks close to the epicentre, additional inclined, through depth cracks are formed almost all the way to the support region and are produced by flexure. In the case of blast loading they also result from pressure distribution across the slab.

Horizontal cross sectional cracks are the produced by the scabbing mechanism, and are explained in section 5.2.1.

5.3.2 Deflection analysis

The initial deflected shape of R.C. slabs when exposed to a very fast locally applied load is very different from that of slabs under static loading. Because of the inertia forces produced by the slab acceleration, the deflected shape of the slab is a combination of different modes. Figs.

5.24 to 5.31 from the impact and blast impulse tests show the deflection profiles that were measured in the present research. Deflection profiles of the static tested slabs are given in Figs. 5.22 and 5.23.

For soft impact and blast impulse tests the measured deflections show the whole slab deforming to a continuous shape but in the hard impact the deflection inside the central region is much greater than in the rest of the slab.

Slabs SE5 and SE6 had top reinforcement and a higher percentage of bottom reinforcement than slab SE14 and had a greater flexural resistance and lower displacement under the same loading. Overall flexural resistance under these extreme load conditions, is closely related to the static flexural resistance of the R.C. slab.

The peak deflection at midspan in static tests SS1 and SS2 were 7mm and 6.7mm which were about 1% of the span length. Slab S10 with soft impact did not have a punching or flexural failure and although there was no residual deflection the peak midspan transient displacement was up to 22% greater than in static test on identical slab. This indicates greater strain in the dynamic test than the ultimate strain produced in static test. In the impact test on slab LS11, the peak flexural displacement coincided with a punching failure but was almost double the peak displacement in the static test, 12.5mm. Even the displacement at 160mm from the centre was greater than ultimate midspan displacement in the static test and yet the slab fully recovered and came to rest with zero residual displacement. Similar effects were also observed in the hard impact tests. In all impact tests the loaded area was the end of the 50mm diameter pressure bar. Deflections measured in the blast impulse tests show even greater increases in peak deflection compared with static and impact ultimate values. Slab SE10 had no residual deflection after a peak deflection of 14.4mm, at 80mm off centre, and in slab SE11 the peak deflection was 17.9mm.

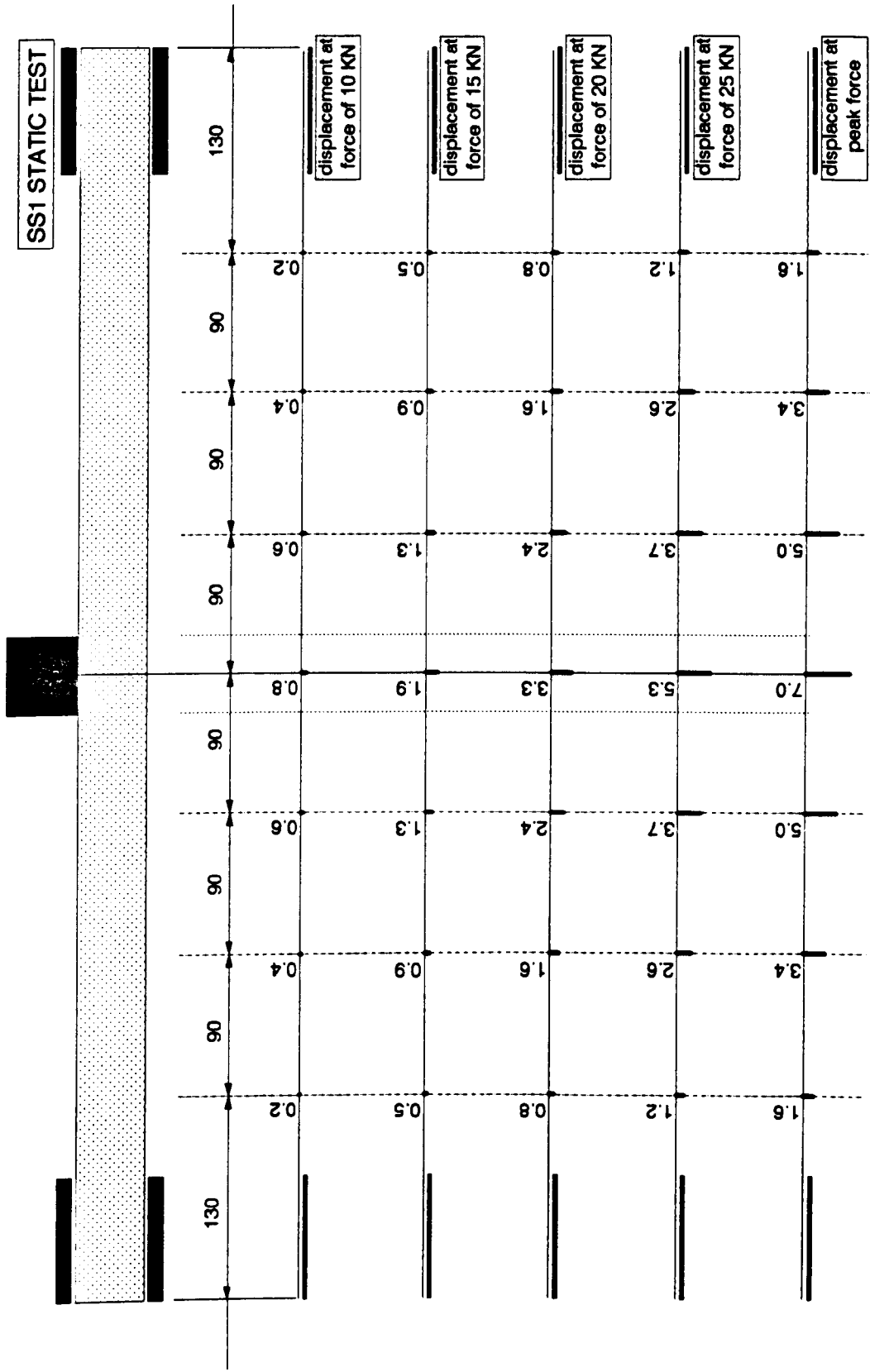


Fig. 5.22 Deflection profiles of small slab SS1 - static test

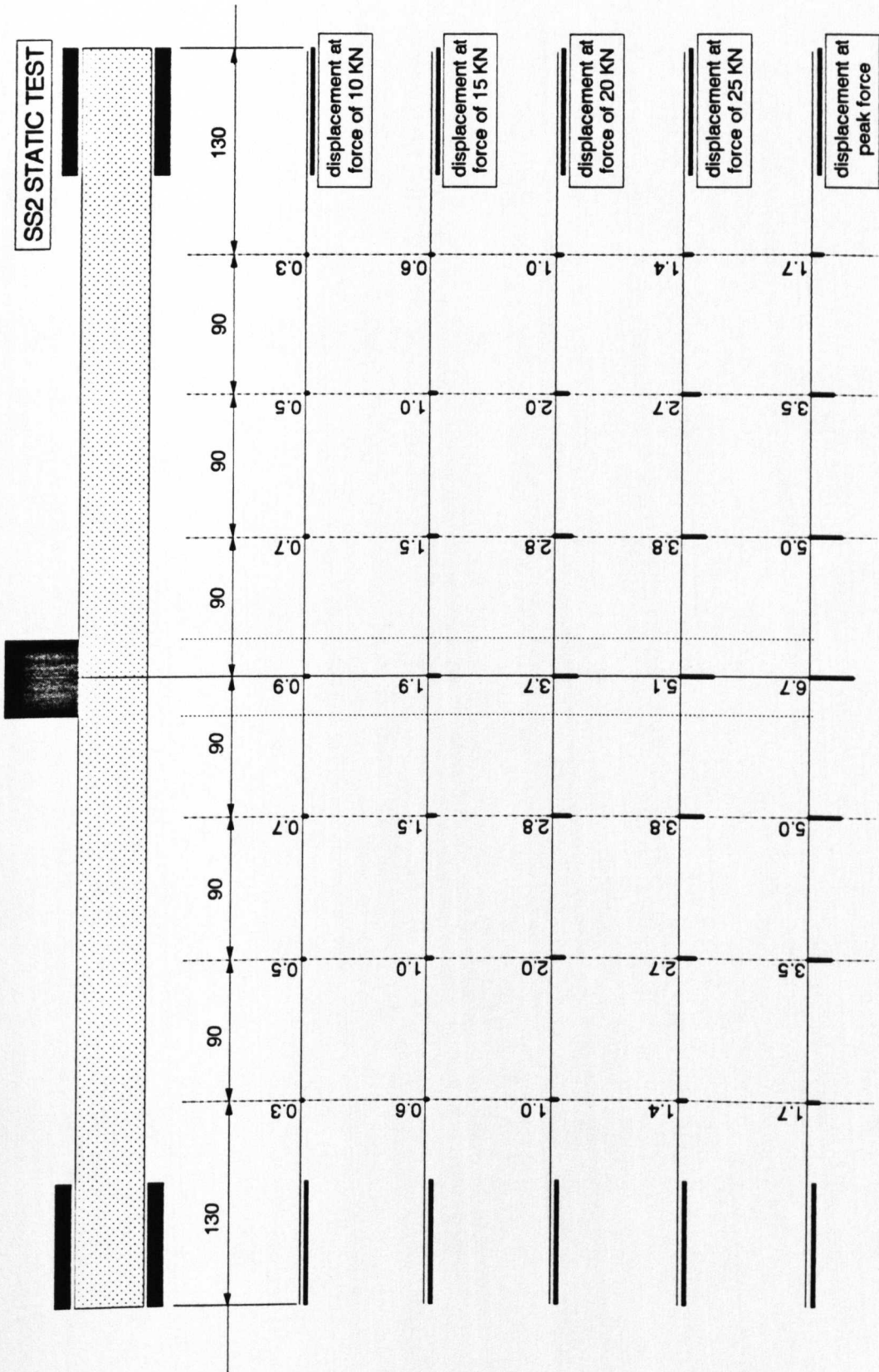


Fig. 5.23 Deflection profiles of small slab SS2 - static test

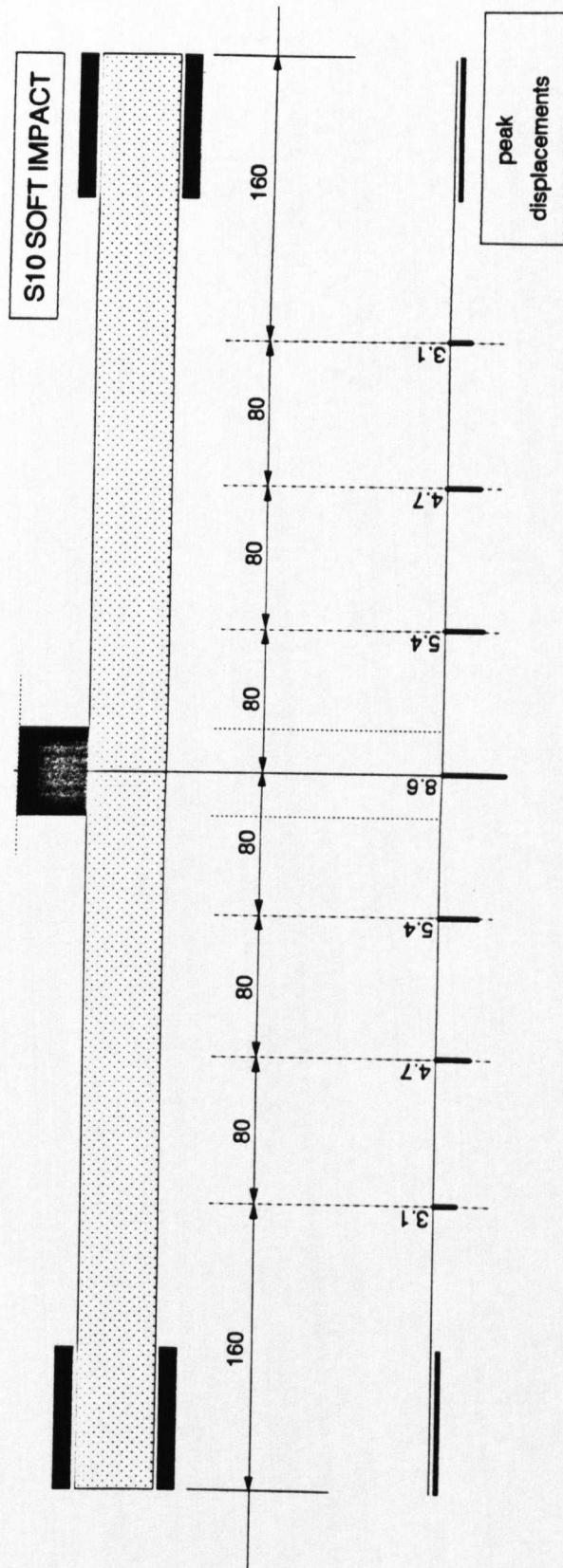


Fig. 5.24 Deflection profile of small slab S10 - soft impact

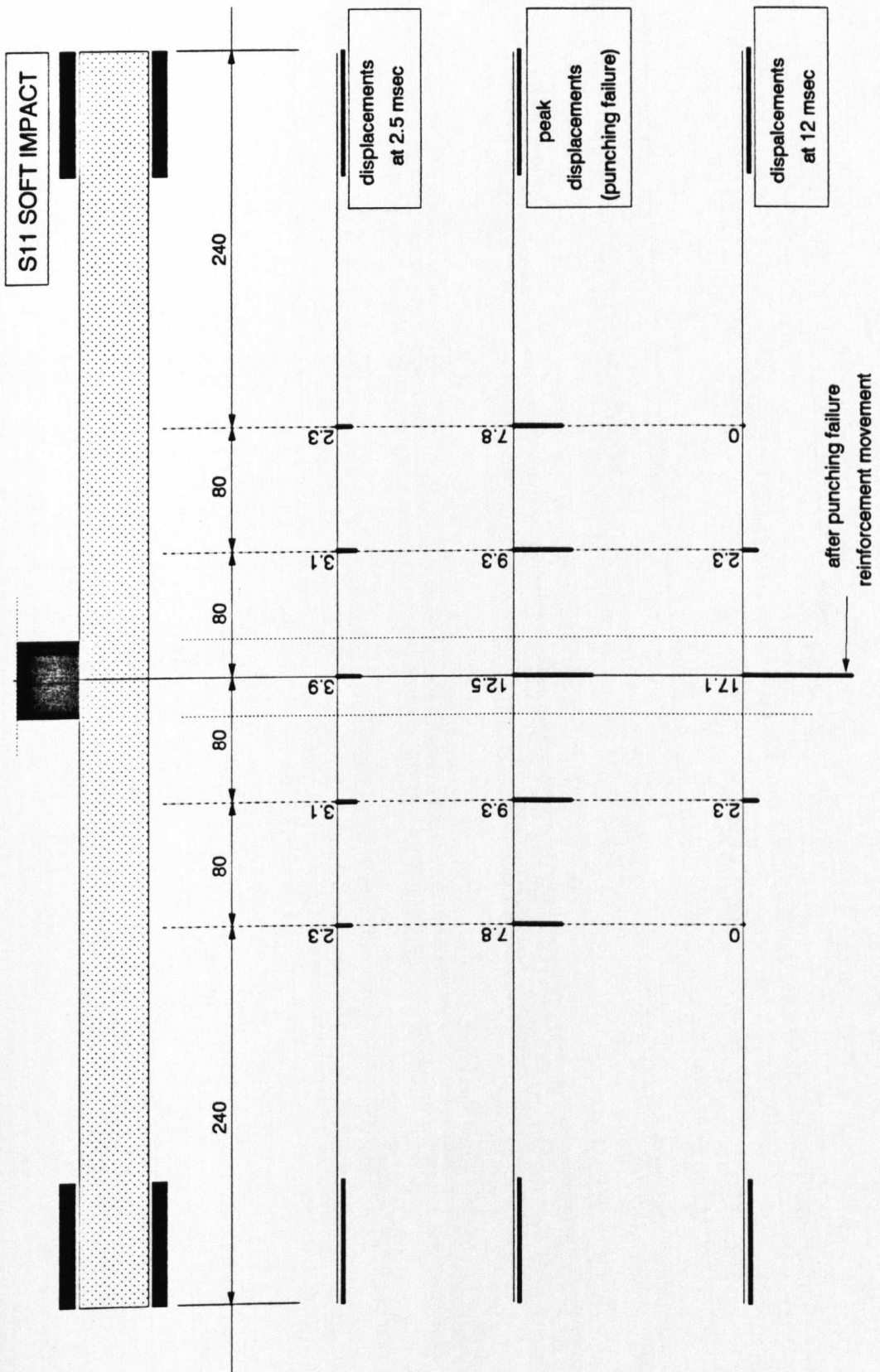


Fig. 5.25 Deflection profiles of small slab S11 - soft impact

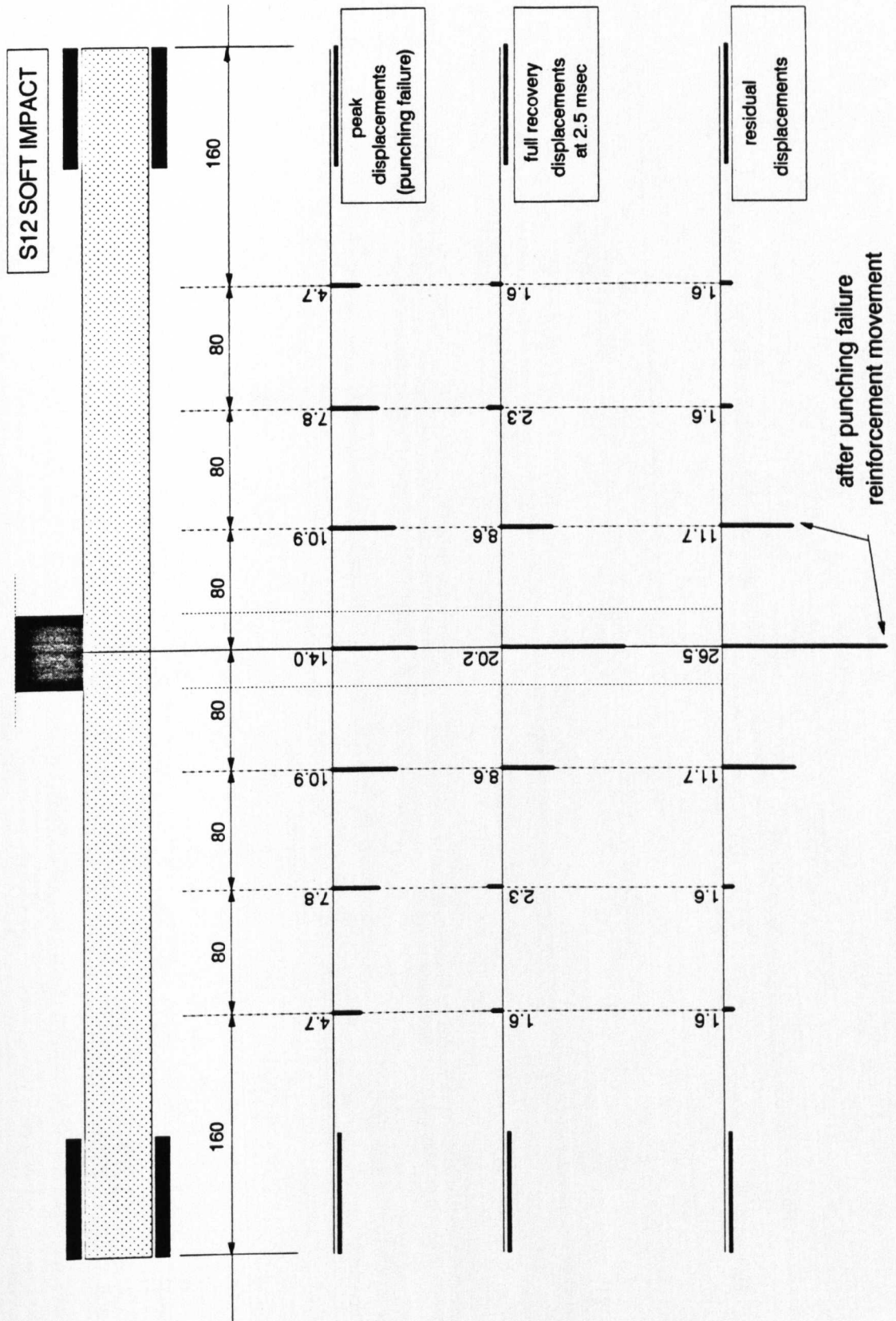


Fig. 5.26 Deflection profiles of small slab S12 - soft impact

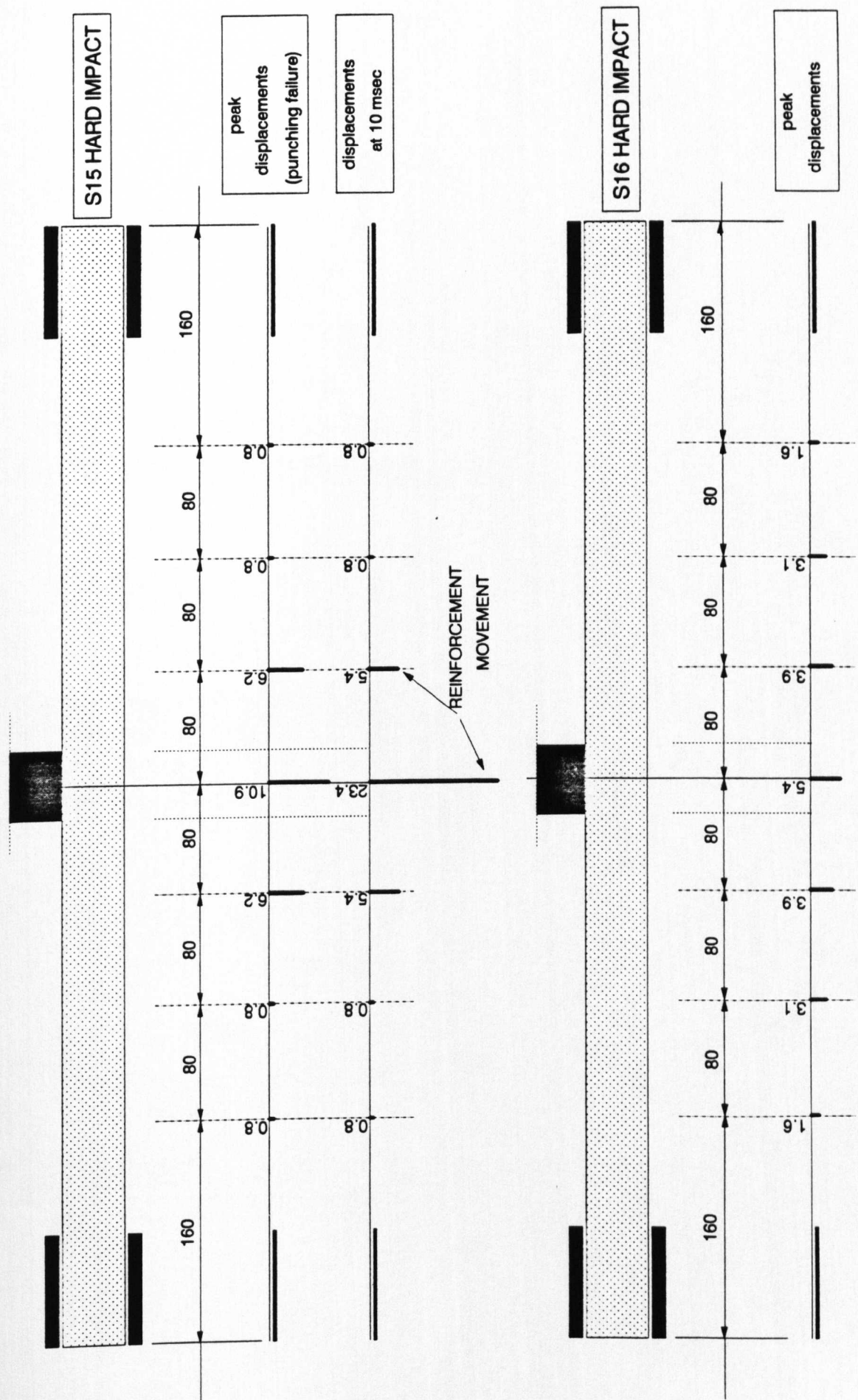


Fig. 5.27 Deflection profiles of small slabs S15 and S16 - hard impact

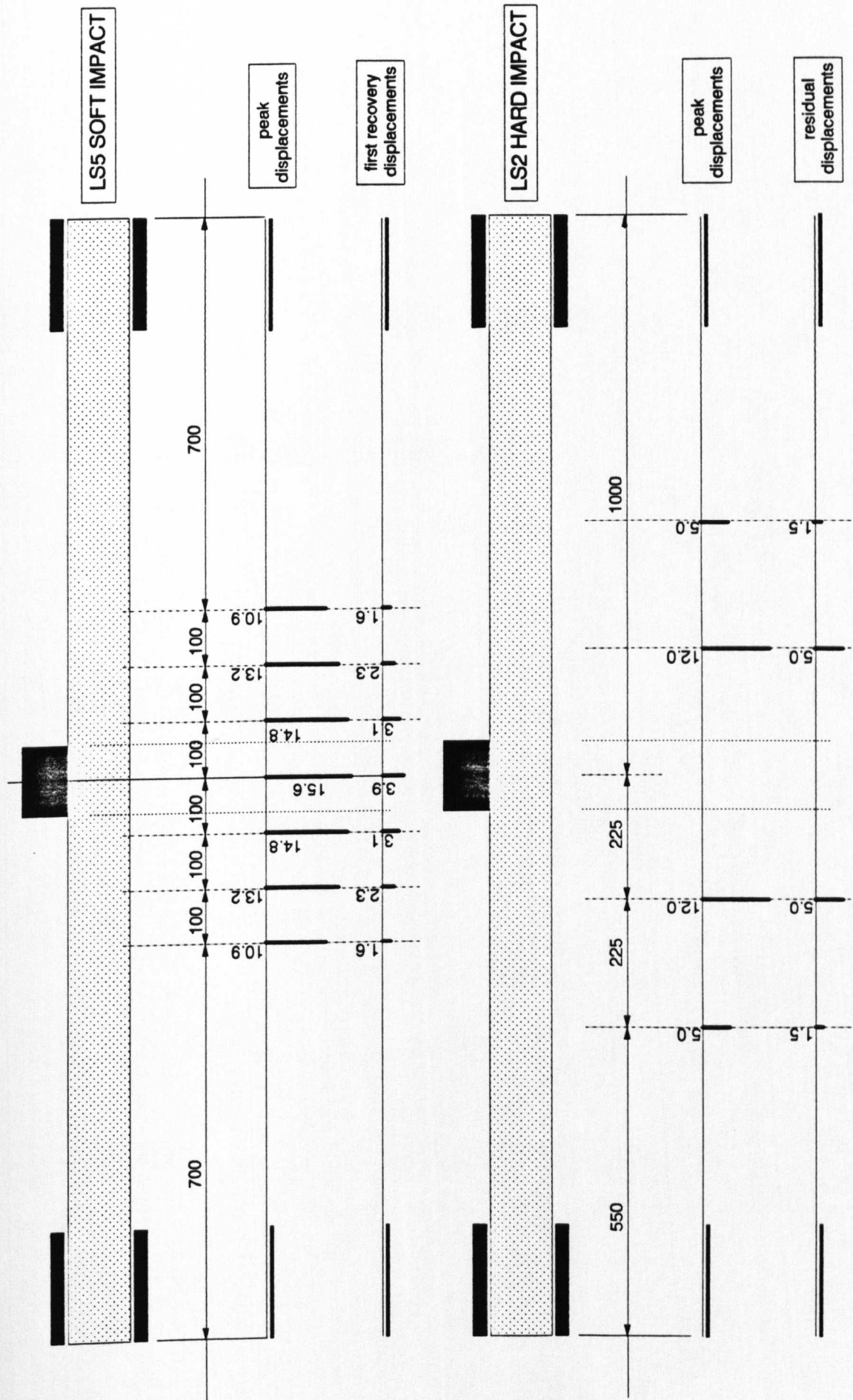


Fig. 5.28 Deflection profiles of large slab LS5 - soft impact and LS2 - hard impact

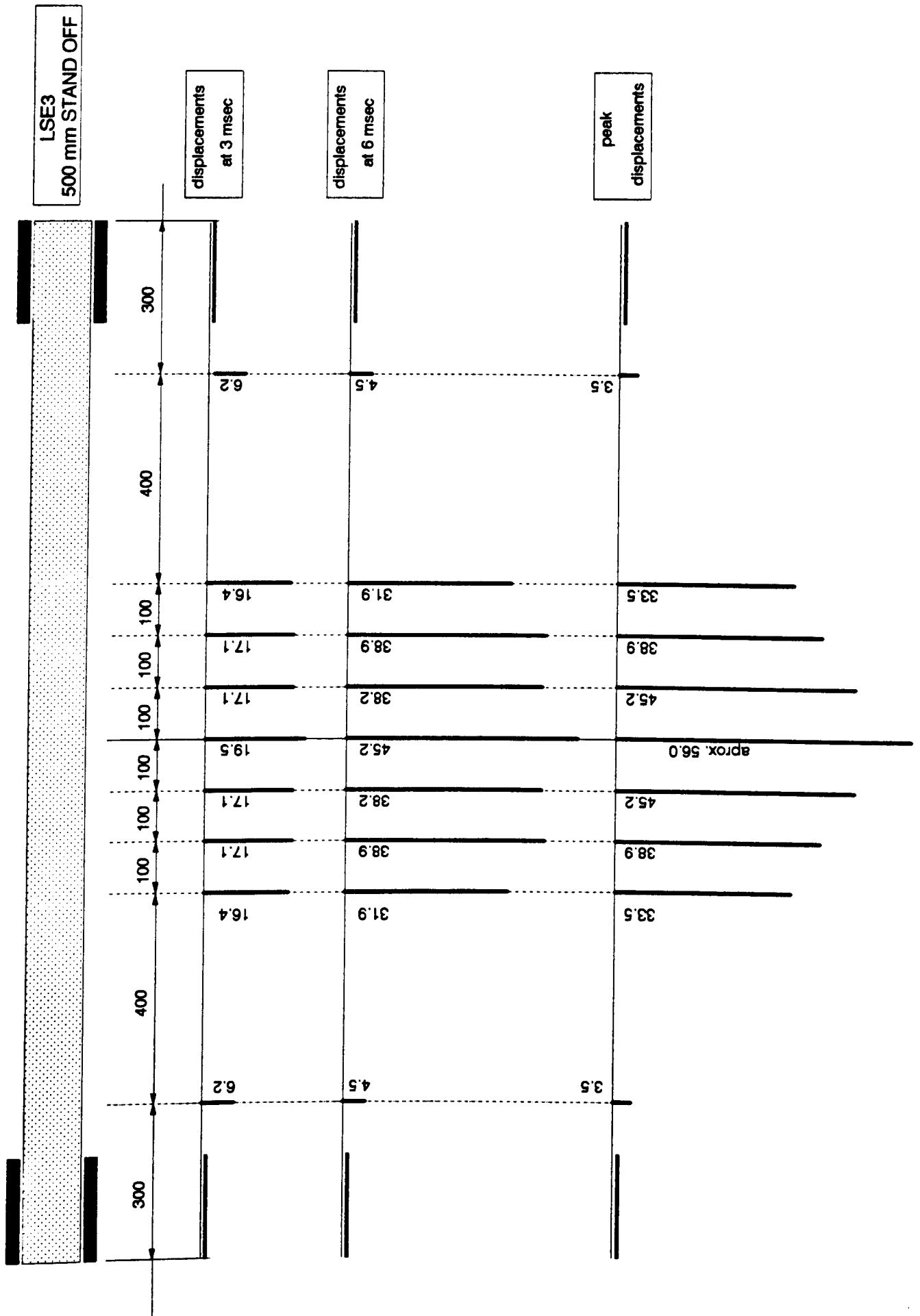


Fig. 5.30 Deflection profiles of large slab LSE3 - blast loading test

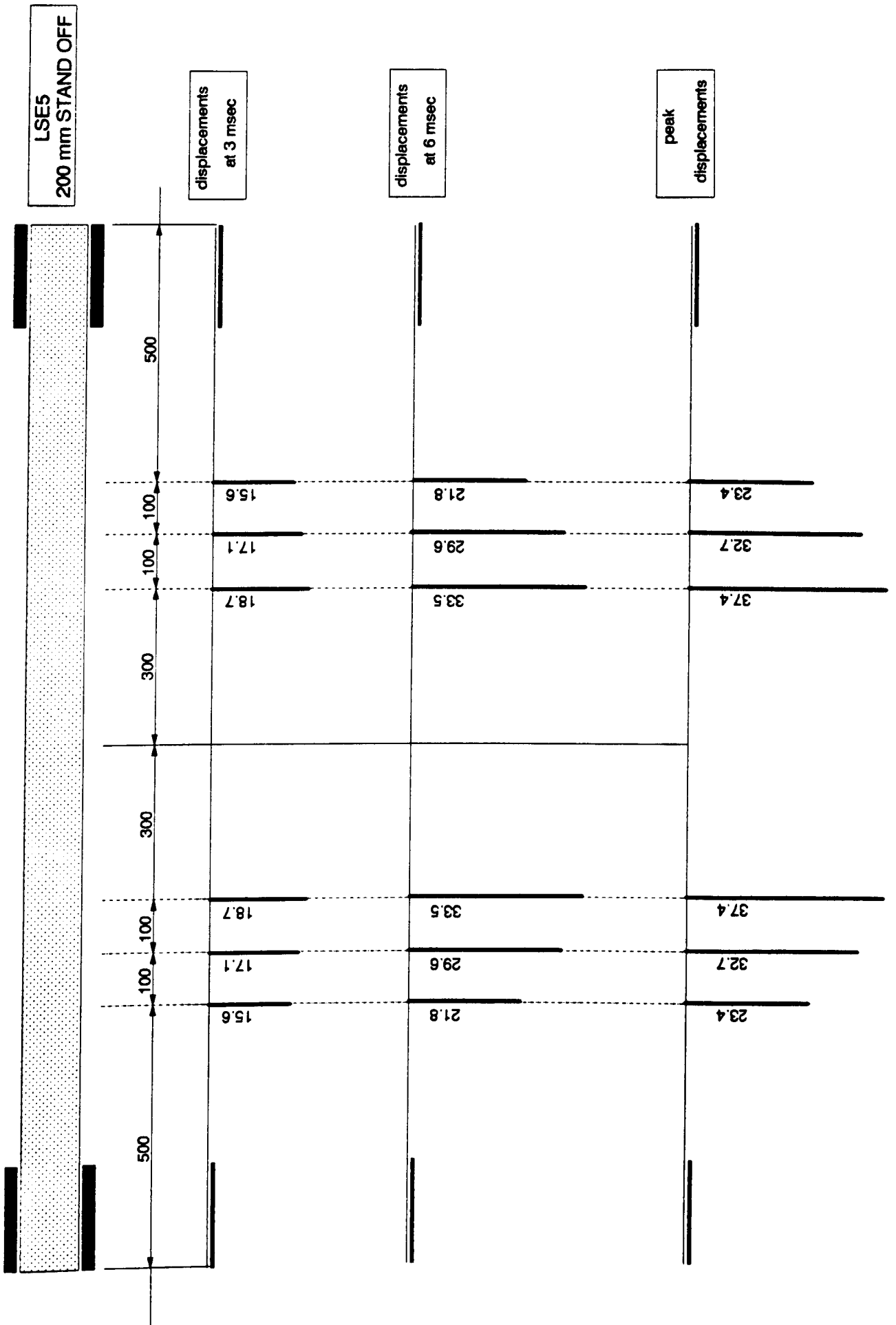


Fig. 5.31 Deflection profiles of large slab LSE5 - blast loading test

The displacement curve has significant curvature changes at between 100mm and 280mm, from the impact point or the epicentre of the slab. These curvature changes indicate higher vibration modes. Between the points of curvature change, the axis of the slab is almost linear. Third mode deformation was clearly observed on Slab SE12 at the time of the peak upward movement of the slab, Fig. 5.26.

The restraint to lateral movement at the supports along of the slab induces membrane forces in the slab. Initially, the membrane action is compressive but later it becomes tensile. *Tankreto, (1991)*, concludes that the tensile membrane action takes effect "well beyond 12° support rotation".

5.3.3 Energy considerations due to close range explosion

The total energy E given to the reinforced concrete slab by an explosive charge is given by:

$$E = \frac{I^2}{2M}$$

where I - total impulse from the blast pressure - time record.

M - effective mass of the slab

Some of this energy will be absorbed in plastic work producing permanent damage of the slab in the form of scabbing, spalling, cracking, residual displacement and perforation, some of the energy will be absorbed in elastic flexural deformation and reinforcement strains and some will be absorbed in vibration and stress wave damping.

5.4 Connection between local and flexural response

The local response and the overall flexural movement of the slabs are often separated for analysis but the damage due to local response may alter the overall response. The timescale difference associated with local and flexural response is the main reason for employing a decoupled approach, but inertia and the finite disintegration speed of concrete mean that the two

forms of response can overlap, not only in the time scale but also in the loading function and in the reduction of effective flexural mass due to local disintegration at the centre of the slab.

The loading function on the whole slab depends in part on the transfer of load from the central plug. This depends on aggregate interlock and dowel action and has been discussed in section 5.2.7. In addition the amount and the nature of the local damage determines the amount of energy that remains to produce the overall deformation. Slab SE13 had a greater charge standoff and the peak flexure shape of that slab, Fig 5.29, indicates that the peak flexural movement outside the local response region is greater than for Slab SE17. The perforation of Slab SE17 meant that a much greater amount of energy was spent on the production of the hole and the associated permanent local deformation so leaving very little energy for the overall flexural response.

The time scale of events indicates that because of the much earlier formation of the local damage, overall response can be decoupled but the final disintegration of local area, however, happens significantly later, and it may not be complete at the start of the overall response. The importance of this can be evaluated by considering static loading response where additional deformation occurs beyond the peak load but in dynamic loading even the additional load might still be resisted even after the failure of part of the structure, so causing secondary flexural damage on a slab that has already failed.

Reduction of the effective flexural mass of the slab due to disintegration of the central shear plug of concrete is important in the vibration response and in the reduction of inertia but the loss of mass is only a small percentage. Final disengagement of the concrete from this central region would complete the localised response and only after this disengagement does the response of the specimen become fully flexural.

Inertial effects on the slab can be considered to produce effective supports close to the point of loading at the initial stages of the response when they may be important for the local response of the slab. At later stages these effective supports move outward from the epicentre and may become moving plastic hinges as explained by the Symond's analysis, *(Watson, 1991)*.

The amount of energy absorbed in local response also influences the overall deformed shape. The full scale impact tested slabs that did not have punching failure, do have a greater relative displacement than the 1:2.5 scale tests that were perforated.

The small scale impulse tests have produced results that show great consistency between the tests. Tests SE10 to SE12 show mainly flexural response of the slab (standoffs 250mm, 200mm and 150mm), but by moving the charge closer to the specimen the response is both flexural and localised punching shear with the soffit cracks indicating more steeply inclined walls to the punch zone, particularly for slabs SE16 and SE17, standoffs 60mm and 50mm respectively.

5.5 Time sequence of events in the blast impulse loading of R.C. slabs

- (1) The FS-10 firing system sends a 3000 volt electrical signal to the charge detonator. This signal lasts for about $0.2\mu\text{sec}$ and was taken as a reference time for the rest of the event.
- (2) The L2A1 electrical detonator receives the FS-10 signal and then detonates but detonation time for this type of detonator is not consistent, so detonation occurred up to $50\mu\text{sec}$ after receiving the FS-10 signal.
- (3) Detonation of the PE4 explosive charge was at velocity of about 8000m/sec and so the full scale 1300g charge detonated in about $9.1\mu\text{sec}$ and the 1:2.5 scale charge in about $3.6\mu\text{sec}$.
- (4) At close ranges the shock wave in air will travel at about 7500m/sec and it will reach the slab in about 6.7 to $33.3\mu\text{sec}$ for the 1:2.5 scale tests and between 26.6 and $66.6\mu\text{sec}$ for the 1:1 scale tests, depending on the standoff distance (section 5.1.1). If the charge is at 75mm standoff as for slab SE15, the blast wave arrives at 13.5 to $63.5\mu\text{sec}$ after the FS-10 signal.
- (5) Curvature of the blast pressure front causes a variation in the time of blast arrival for different parts of the slab. For instance, on slab SE15, at the furthest part of the slab 565.7mm diagonally off the centre, the blast wave arrives about $65.4\mu\text{sec}$ later than at the epicentre and the dynamic pressure loading of this slab will commence between $13.5\mu\text{sec}$ and $128.9\mu\text{sec}$ after initiation of the detonator. If the longitudinal stress pulse velocity in concrete is taken as 3400m/sec then the stress wave from the epicentre has travelled about 222.36mm through the concrete before all of the slab has been loaded and could have been reflected about 5 times from the free surfaces of the slab.

- (6) Once the shock front impacts the slab it will continue to propagate through the concrete, expanding radially from the point of impact, Fig. 5.32. If the dynamic compressive strength and forces of cohesion of the concrete on the upper face have been exceeded, then the concrete will start to pulverise and crater to form a spall on the top surface. This would reduce the energy of the initial shock and could remove the plastic wave. A plastic wave travels more slowly than the elastic wave and always has an elastic precursor.

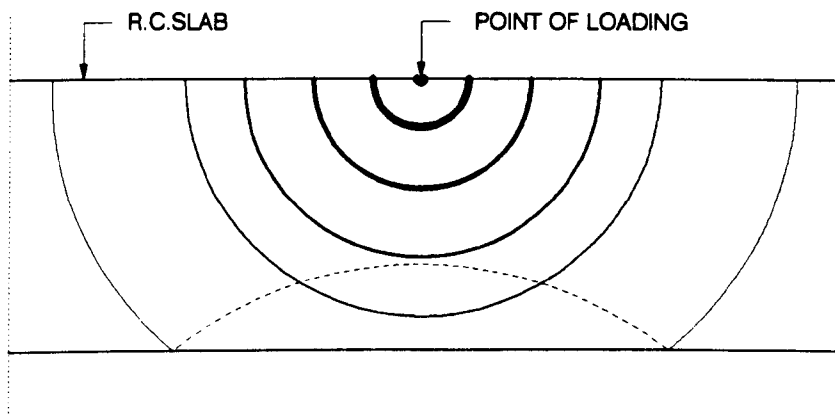


Fig. 5.32 Radial expansion of the stress wave

The shortest time for the elastic pulse to reach the free boundary immediately below the epicentre is $12.9\mu\text{sec}$ for the case of 1:2.5 scale slab. After this time the compressive stress wave will reflect so becoming a tensile wave (section 5.2.1).

- (7) High speed photography first shows radial cracking starting from the epicentre on the back face of the slab. At about the same time a circular crack was formed at about 20mm radius from the centre. The mechanism of crack formation was discussed in section 5.2.2.
- (8) The front of the compressive stress wave will reflect as tensile stress from the back side of the slab and travel towards the front surface before the rest of compressive pulse has reached the back face because of the relatively long overpressure duration time. In addition, an oblique incidence will cause the compressive pulse to reflect as a shear pulse. The net stress level between the three pulses will determine the state of the concrete. Net tensile stresses are important because the initial compressive stress failed to crush the concrete and all further failure will be tensile.
- (9) Displacement of the shear plug begins once the through thickness cracks are formed and this changes the nature of the load transfer to the rest of the slab through aggregate

interlock and dowel action (Section 5.2.4). Gradually, the force transfer changes to dowel action only which can influence the flexural response of the rest of the slab and also increase the size of the scab.

- (10) Deflection of the slab begins at 0.25 to 0.8msec and 0.1 to 0.6msec after the load application for the 1:1 scale and 1:2.5 scale tests respectively and. The furthest point of the slab can be loaded by 1.1msec in the case of 1:1 scale slab since the duration of the pressure pulse increases with distance. Consequently deflection is affected not only by the load transfer from the epicentral area but also by the vertical components of the blast pressure function.

The forces causing flexural deflections are shown in Fig. 5.33. Compressive (F_C) and tensile (F_T) membrane action forces act at different times but they both increase the slab resistance to blast loading.

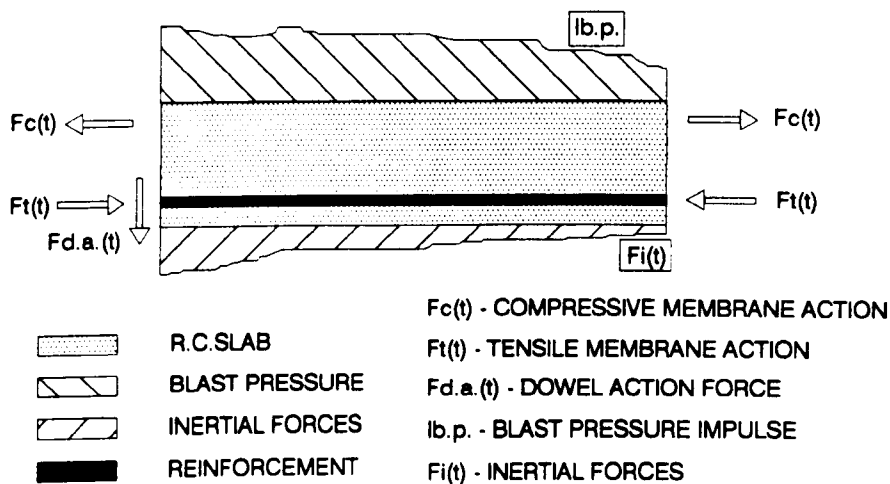


Fig. 5.33 Flexural mechanism forces

- (11) Straining of the reinforcement begins at about the same time as deflections at the centre of the slab and so the initial strains are entirely due to local flexuring of the specimen and only later may include effects of overall bending or in-plane straining due to stress waves and membrane forces.
- (12) Times of peak displacement can be seen from displacement - time records, Appendix B1 and B2. At this time the yield lines and "reinforcement" cracks have been formed. High deflection rates produce intense inertial forces, particularly near the epicentre, and later,

the inertial forces may pull concrete off the reinforcement and greatly increase the size of the scab.

5.6 Modelling

In the scaling laws, the strain-rate effects and gravity effects are assumed negligible. The following sections make a comparison between damage and displacements on the full and small scale slabs.

5.6.1 Local damage

The damage is quantitatively very similar at both scales. The same pattern of spall and scab damage was produced and the quantifiable damage on slabs of two different scales compare well. In both cases the spalls are very minor and the scabs are extensive and the same kind of circumferential and radial cracking around the epicentre indicates similar failure mechanisms. The similarity of loading and cross section characteristics allows comparison between the damage on the large slab LSE5 and small slab SE15, both subjected to explosive blast. Neither of them was perforated, the spall was slightly larger on LSE5 and the scab percentages are within 1.4%. The top and bottom face local cracking is almost identical. Slab SE16 had a same charge as SE15, only 15mm closer to the slab but produced a different failure mechanism and perforation.

5.6.2 Overall flexural damage

Yield line patterns dominate the shape of flexurally produced damage at both scales. The same types of cracks (section 5.3.1) appear on the slab surfaces at both scales indicating the existence of identical response patterns at both scales.

The scaling of local and overall damage of the slab was more successful then scaling of slab displacements or reinforcement strains.

5.6.3 Displacement record

The three dimensional linear scaling used in this research meant that measured displacements were also scaled at scaled distances, i.e. distances on the smaller scale slab are multiplied by the scaling factor - in our case 2.5. Table 5.8 gives a comparison between some of the results.

BLAST IMPULSE TESTS		RELATI. DIFFER. (%)
1:1 SCALE RC SLABS	1:2.5 SCALE RC SLABS	
<p>LSE - 1st shot Charge standoff :350mm Displacement :at 225mm off centre: 26.3mm, at 450mm off centre: 18.8mm. These positions correspond to 90 and 180mm off centre on 1:2.5 scale slabs, respec.</p>	<p>Scaled standoff distance : 140mm SE12 - standoff distance : 150mm : Displacements : at 80mm off centre : ~ 21mm at 160mm off centre: ~ 13mm at 240mm off centre : ~ 7mm Estimated displacement at 90mm : ~20mm Estimated displacement at 180mm : ~ 11.5mm</p>	-
<p>Reinforcement ratio of slab SE12 was significantly smaller than on LSE1 and the small slab had the top reinforcement discontinued at the centre. Results are not directly comparable.</p>		
<p>LSE2 Charge standoff:250mm Displacement : at 225mm off centre = 31.9mm at 450mm off centre = 20mm</p>	<p>Scaled standoff distance : 100mm SE5 - standoff distance : 100mm Displacement at 180mm off centre : 6.3mm Scaled displacement at 180mm off centre : $6.3 \times 2.5 = 15.75\text{mm}$ Relative difference in displacements R.D. = $\frac{15.75}{20} = 0.788$</p>	21.2%
<p>LSE3 Charge standoff = 500mm Displacements : at the centre : 52.2mm at 100mm off centre : 45.2mm at 200mm off centre : 38.9mm at 300mm off centre : 33.5mm at 700mm off centre : 7.1mm These positions correspond to : centre, 40, 80, 120 and 280mm off centre on 1:2.5 scale slabs, res.</p>	<p>Scaled standoff distance : 200mm SE11 - standoff distance : 200mm</p>	
	<p>Displacement at 80mm off centre : ~ 19mm</p>	22.1%
	<p>Displacement at 160mm off centre : ~ 11mm</p>	11.9%
	<p>Estimated displacement at 110mm : 15mm Displacement at 240mm off centre : ~ 8mm</p>	
<p>LSE5 Charge standoff = 200mm at 300mm off centre : 38.2mm at 400mm off centre : 32.7mm at 500mm off centre : 23.4mm These positions correspond to : 120mm, 160mm and 200mm off centre on 1:2.5 scale slabs</p>	<p>Scaled standoff distance: 80mm SE15 - standoff distance : 75mm Displacements at 80mm off centre : ~ 18mm Estimated displacement at 120mm : 15mm</p>	1.9%
	<p>Displacement at 180mm : ~ 12mm</p>	8.3%

Table 5.8 Blast Impulse Tests, displacement scaling

These results show that when overall flexural response was dominant, as in slabs LSE5 and SE15, there was much better scaling than in cases when local response was dominant.

CHAPTER 6

CONCLUSIONS

The following conclusions can be drawn from the work described in this thesis:

6.1 Modelling

- (a) Manufacturing and testing problems together with the cost of full scale specimens make the use of model specimens extremely beneficial providing the results and behaviour can be compared to real structures.
- (b) The modelling laws employed in this research are widely used for structural dynamic modelling neglecting the existence of gravitational forces. Neglect of strain rate effects is more important and can affect the final result.

(c) The displacements obtained on small scale specimens are expected to be 2.5 times smaller than on the full scale specimens for the scaled loading and support conditions. Results from some of the related specimens are shown in Table 5.8, section 5.6.3. The ratios of displacement on 1:1 scale slabs and on 1:2.5 scale slabs magnified by 2.5, vary between 87.9% and 98.9%.

(d) The local and overall damage was almost identical in appearance for both sizes of slab which indicates a similarity of the failure mechanisms.

6.2 Instrumentation

(a) Impact hammer velocity measurement using microswitches can give a maximum error of 2.3% of the average velocity obtained in the tests, section 3.2.5. Using opto-schmidts the maximum error is a function of the capture rate of the oscilloscope and is therefore negligible in comparison with the hammer velocity.

(b) Limitations on the velocity of the R.P.D.T. stroke, recommended for movements of up to 1m/sec, caused errors in some of the displacement - time results, section 4.2.1.2, particularly for the early parts of the slab movements that had much greater displacement rates, Appendix B3.

(c) High speed filming is a useful method of assessing failure mechanism. Filming at rates up to 10,000 pps in the blast loading tests produced a minimum of 150 frames or about 15msec of the film on which the visibility was very clear.

(d) To precisely measure the crack velocity from the high speed films the magnification has to be increased and so the film area is reduced. The film speed has to be increased to cover about 1mm of crack extension on every frame i.e. filming rates of up to 1,000,000 pps. This is possible using a rotating mirror camera but was not tried in these tests.

(e) Direct filming gives much better pictures than filming through a mirror, but this was not possible with the slabs horizontal so the last 10 slabs at 1:2.5 scale were tested vertically.

(f) Blast pressure gauges with a metal diaphragm produced much better results than those with a silicon diaphragm. The amount of electrical noise from the metal diaphragm gauges was very minor.

(g) The digital storage oscilloscope is a well established device for capturing and storing electrical output from transducers recording fast events. Only a limited amount of data can be stored and there is a need to compromise between the frequency of sampling and the length of record required. Inconsistent and unreliable levels of electrical signal needed to trigger the scopes sometimes caused premature signalling with a consequent loss of results.

6.3 Dynamic properties of materials and the blast loading function

(a) The Hopkinson Pressure bar tests gave 2.5-3 times greater compressive strengths for concrete specimens when the strain rates were up to 10^9 times greater than in static tests. The ultimate dynamic compressive strengths varied between 90N/mm^2 and 114N/mm^2 for 1:1 scale - macroconcrete and between 103N/mm^2 and 142N/mm^2 for 1:2.5 scale - microconcrete. The peak strain rates were up to $1.46 \times 10^3\text{sec}^{-1}$ and $2.29 \times 10^3\text{sec}^{-1}$, respectively.

(b) The peak strain rates in the epicentral zone of the slab in impact test varied between 0.3sec^{-1} and 3.2sec^{-1} . In explosive blast tests they varied between 0.2sec^{-1} and 18.3sec^{-1} .

(c) The much greater amount of cracking observed in dynamic compared to static tests, Appendices A, B and C, indicates that under dynamic loading the cracks follow shorter paths requiring higher energies and propagate too fast to benefit from stress relief and there is lateral confinement of concrete, induced by inertia forces in the dynamic tests, which introduces a three dimensional state of stress. These factors contribute to the increase in the dynamic strength of the concrete.

(d) *Henrych's, (1979)*, pressure vs. time vs. distance relations given for spherical and cylindrical charges were adjusted for hemispherical charges and they then correspond to the

measurements made from the tests, Table 5.1. All the calculated pressures have the same order of magnitude and most of them are within 10% of the measured pressures.

The pressure gauges were placed to measure the vertical component of the pressure at various points across the surface of the slab and the calculated pressure profiles for 78gr hemispherical charges placed at stand-offs 50 to 500mm are given in Figs.5.2 to 5.7. The blast pressures exerted on the slab by the curved side of hemispherical charge can be calculated according to:

$$P(t) = P_{det} \cdot \left(\frac{R_w}{R} \right)^{2.65} \cdot \cos^3 \alpha \cdot \left(1 - \frac{t-L}{\tau} \right)$$

which is described further in section 5.1.1.1.

(e) Peak loading rates in explosive tests can be estimated from the calculated values of the pressure function and they are of the order of 17,000bar/microsec.

(f) The peak impact loading rates were 3.8×10^6 KN/msec for 1:2.5 scale slabs and 34×10^3 KN/msec for 1:1 scale slabs.

6.4 Local response

(a) As soon as the shock front from an explosion reaches the structure, some of the top face concrete in the epicentral zone of the slab may be cratered. Later the back face may scab and the slab may be perforated.

(b) None of the impact tested slabs had top face cratering even when there was full penetration.

(c) In the explosive tests the cratering producing a spall is produced by the compressive and shear stress on the top face of the concrete but unlike hemispherical charges, none of the cylindrical PE4 charges produced a spall even when the slab was perforated.

(d) Slabs SE7 and SE8 had inner supports, and this appeared to influence the spall formation since they both had larger spall sizes with a surface area up to 3.1% of the slab surface, than other

slabs without the inner supports where the maximum spall size was 0.3% for no perforation and 0.5% when there was perforation.

(e) The spalls produced by charge stand-offs of 150 to 75mm were almost identical in surface area.

(f) A scab is produced by a compressive stress wave reflected as tension and the trapped momentum which depends on particle velocity. Additional scab damage is produced by the displacement rate of the concrete at the time of peak deflection. Hence the scab size depends on both local response and on overall flexural response, which influences displacement rate.

(g) The scab size was related to the reinforcement percentages as shown in Figs. 5.4 and 5.5, slabs SE5 and SE14. This is due in part to the fact that greater amounts of reinforcement reduce the area of concrete connecting the cover to the core concrete.

(h) In the case of impact loading, the scab covered up to 11% of the slab area.

(i) In the case of explosive blast loading the scab size was directly related to peak overpressures or impulse for stand-offs of up to 100mm but for the closer placed charges that was not the case.

(j) The maximum scab produced in the explosive blast tests was also about 11% of the slab area.

(k) Given the scaled stand off distance and scaled slab thickness, scab size and perforation can be predicted, as shown in section 5.2.1.2.

(l) If the slab thickness:

$$t > W^{\frac{1}{3}} \cdot 10^{-K \cdot \log \frac{r}{W^{\frac{1}{3}}} + \beta}$$

where: W - explosive weight in kgs of TNT

r - charge standoff in m

$K = 0.224548$ and

$\beta = -1.462274$

then perforation will not occur. If $\beta = -1.3023$, then a minor scab will be produced.

(m) Kinney and Graham's (1985), relation for breaching resistance of concrete greatly underestimates its actual breaching resistance, section 5.2.3.2.

(n) A way of calculating the scab layer thickness on a slab under explosive tests is presented in section 5.2.1.2., Fig. 5.13 and is based on a comparison between the ultimate dynamic strength of concrete and the peak amplitude of the attenuated stress pulse.

(o) The impact hammer produced an indentation in the slabs about 10% larger than the area of the impact hammer and about 10mm deep. The inclination of the shear plug was up to 30° to the vertical.

(p) Whether the slab will be perforated or not depends on the peak load and rise time and not on the impulse delivered to the R.C. slab. For example slab S12 received an impulse larger than slab S15 but unlike SE15 was not perforated.

(q) Cylindrical charges produced no top face cratering and a Type B hole, but hemispherical charges produced both top and bottom face cratering and Type A holes, Figs. 5.17 and 5.18.

(r) The maximum size of the punched hole in the blast tests was 0.5% of the surface area.

(s) The bottom reinforcing bars in slabs tested with an explosive charge were always deformed locally in bending over a length which slightly exceeded the size of the hole.

(t) In both impact and blast tests the first cracks become visible 2 to 100 microsec after the load application.

(u) The visible cracks on blast tested slabs occurred in the following order:

(1) Radial cracks were initiated at the epicentre of the slab immediately after the blast, in less than 100μ sec and had a length after 190μ sec of about 147mm.

(2) The inner circular crack formed at about 10mm radius from the centre of the slab appeared at the same time as the radial crack.

- (3) The outer circular crack formed at about 80 to 130mm radius was established by up to 800 μ sec after the blast.
- (v) The area that was limited by the inner circular crack disintegrated randomly, while the area inside the outer circular crack fractured into almost symmetrical ring segments, Fig.5.15.
- (w) Typical crack velocities observed from the high speed films were between 420m/sec and 770m/sec.
- (x) The visible cracks on slabs under soft impact were similar to those on blast loaded slabs but the outer circular crack happened much later, at up to 5msec after the radial cracks.
- (y) The hard impacts produced radial cracks up to 1.6msec after the initiation of the first circular crack.

6.5. Overall flexural response

- (a) The overall flexural response began after the beginning but, often before the end of the local response, as can be seen from the high speed films, Appendices A3 and B3.
- (b) Overall flexural response is influenced by continuing externally applied pressure and by the mechanism of load transfer from the edges of the area of local response.
- (c) Load transfers from the area of local response to the rest of the slab mainly by aggregate interlock and dowel action.
- (d) The overall flexural displacement depends on the amount of energy remaining after local response but can not be related to the amount of local damage since greater local damage does not necessarily mean greater flexural movement in overall response.
- (e) The main indicators of overall flexural response are yield lines that propagate towards the corners of the slab.
- (f) Deflection histories under static and dynamic loading are very different. Under the blast and impact loading ultimate deflections are much greater but the slab showed considerable recovery of deflection even in the case of full perforation of the slab, Figs 5.22 to 5.31.

- (g) The soft impact and blast loading produced significant deflections across the whole slab span but hard impact only produced deflection within the local response zone.
- (h) The beginning of the local response is governed by the stress waves but, at the time of the peak overall displacement, momentum is dominant and combines with scab formation and displacement produced by stress waves earlier in time.
- (i) The peak deflection rates in explosion tests were 7.0m/sec and 8.0m/sec for the 1:2.5 and 1:1 scale tests, respectively. In impact tests they were 2.0m/sec and 3.6m/sec, respectively.

CHAPTER 7

FUTURE WORK

Most of the tests reported here were conducted with the hemispherical charge and only a few slabs were exposed to a cylindrical charge. Even the small number of these tests showed the great differences that occur in specimen behaviour due to different shape of the charge. It is suggested that more of the future tests be conducted with the spherical and cylindrical charge which would assist in understanding the influence of the charge shape on the response of the structure. A comprehensive charge test programme would also contribute in further validation of the pressure vs time vs distance relations for the hemispherical charge that are presented in section 5.1.1. Further attempts to measure blast pressure spatial and transient distribution for hemispherical charges placed at 50 - 250mm (small scale) and 500 - 200mm (full scale) standoffs should constitute a part of that programme. Also testing of charges of other shapes that can be initiated either from the top or from the centre and observing the differences, and comparison to the results observed from the hemispherical charge initiated either from the flat or spherical side would provide further information on the nature of both local and overall R.C. slab response.

Displacement records reported here do not fully cover displacements of the slab, particularly in the area of the local response. An attempt should be made to measure reinforcement displacement immediately under that area in order to get better deflection vs time profile of the whole slab. This should be tried even in cases when perforation of the slab is expected.

Tensile strength of concrete is much more strain rate sensitive than compressive strength. Ratio of static values of these two parameters does not apply in cases of dynamic loading. The Hopkinson Bar techniques has been successfully used to get dynamic compressive strengths of concrete. The same approach can also be used for obtaining values for the dynamic tensile strength.

Three dimensional confinement, which is introduced into concrete as a result of the high speed loading, can significantly change the apparent dynamic strength of the structure. The stress histories at different places can be monitored by using stress gauges. They should be embedded into concrete during the casting in a way which will not affect the resistance of the slab.

Fixed support arrangement used for the present investigation can not fully represent the fixity provided in real structures. Fixity of the support I sections was applied through the high strength bolts so producing non uniform spread of forces across the support area. Surface areas of support and slab that are in contact are not ideally flat and smooth. Problems related to fully fixed support conditions could partly be overcome by casting them together with the specimen, Fig. 7.1, so providing contact as in a real structure. The size of support should be such so as not to interfere with the response of the slab. The whole element can then be clamped by using the similar support arrangement to that which was used in this investigation.

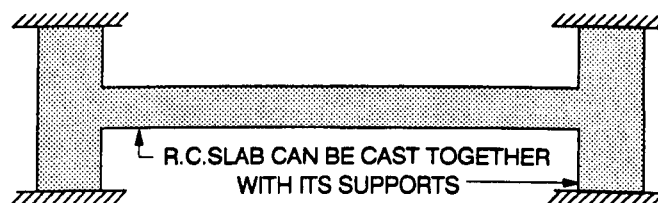


Fig. 7.1 Fixed supports

Almost the whole of the testing programme was conducted on slabs that had the same reinforcement bar spacing. Reinforcement spacing may play an important role, particularly in local response and it was decided to keep it constant in order to avoid introducing additional parameters into the study. Testing of the specimens with different reinforcement spacing might establish its possible influence on both local and overall response of R.C. slabs.

Dynamic force transfer from the area of local response to the rest of the slab plays an important role in slab response to impulsive loading. Aggregate interlock mechanism transfers most of the force before the shear slip becomes too great. Towards the end of force transfer the dowel action will play a much greater role than at the beginning of the process. Dynamic tests on aggregate interlock/dowel action test specimens would be useful to establish a better transferred force-time relation. They can be performed on the same kind of specimens as in the case of static loading or on specimens that more resemble R.C. slab configuration.

High speed filming of the soffit of the slab proved to be very reliable for accessing the damage mechanism in the area of local response. High speed filming of the diagonal-yield line zones of the specimen would help to get a better relation between the formation of the area of local response and overall flexural R.C. slab response. In order to prove that the time sequence of the failure mechanism is identical in both 1:1 and 1:2.5 scale it would be useful to film full scale specimens with the High Speed camera.

REFERENCES

- ABDEL-ROHMAN, M. and SAWAN, J. (1985)**, "Impact effect on RC slabs: Analytical approach", ASCE Journal of Structural Engineering, Vol. 111, No. 7, July 1985, pp. 1590-1601.
- AMERICAN ARMY TECHNICAL MANUAL TM - 5 - 855 - 1, (1986)**, "Fundamentals of protective design for conventional weapons", American Army, Washington, USA, 1986.
- ATCHLEY, B.L. and HOWARD, L.F., (1967)**, "Strength and energy absorption capabilities of plain concrete under dynamic and static loadings", American Concrete Institute Journal, Vol. 64, No. 11, 1967. pp. 745-756
- BAKER, W. E., (1973)**, "Explosions in Air", University of Texas Press, Austin and London, 1973.
- BANGASH, M.Y.H., (1993)**, "Impact and Explosion, Analysis and Design", Blackwell Scientific Publications, London, 1993.
- BENTUR, A., MINDESS, S. and BANTHIA, N.P., (1986)**, "The behaviour of concrete under impact loading: Experimental procedures and method of analysis", Materials and Structures, Vol. 19, No. 113, 1986, pp. 371-378.
- BIGGS, J. M., (1964)**, "Introduction to structural dynamics", McGraw-Hill Book Company, London, 1964.
- BS 1881** "Methods of testing concrete", British Standard Institutions, London, 1983.
- BS 4483** "Steel fabric for the reinforcement of concrete", British Standard Institutions, London, 1985.
- BS 8110** "Structural use of concrete", British Standard Institutions, London, 1985.
- CEB BULLETIN D'INFORMATION, No. 187, (1988)**, "Concrete structures under impact and impulsive loading", Group of authors. 1988.
- CERNICA, J.H. and CHARIGNON, M.J., (1963)**, "Ultimate static and impulse loading of reinforced concrete beams", American Concrete Institute Journal, Vol. 60, No. 9, Sept 1963, pp. 1219-1228.
- COOK, M. A., (1958)**, "The Science of High Explosives", Reinhold Publishing Corp., New York, 1958.
- DRAGOSAVIC, M. and BEUWEL, A., (1974)**, "Punching shear", HERON, Delft University of Technology, The Netherlands, Vol. 20, No. 2, 1974.
- EIBL, J., (1987)**, "Design of concrete structures to resist accidental impact", The Structural Engineer, Vol. 65A, No. 1, Jan 1987, pp. 27-33.
- FERTIS, D.G. (1975)**, "Dynamics and vibrations of structures", John Wiley and Sons, London, 1975.
- GOLDSMITH, W., (1960)**, "Impact" Richard Clay and Company, Ltd, England, 1960.
- GOLDSMITH, W., POLIVKA, M. and YANG, T., (1966)**, "Dynamic behaviour of concrete", Experimental Mechanics, Vol. 6, Feb 1966, pp. 65-79.
- GOPALARATNAM, V.S., SHAH, S.P. and JOHN, R., (1984)**, "A modified instrumented Charpy test for cement-based composites", Experimental Mechanics, Vol. 24, No. 2, June 1984, pp. 102-111.
- GREEN, H., (1964)**, "Impact strength of concrete", Journal of the Institution of Civil Engineers, Vol. 28, 1964, pp. 383-396.
- HADER, H., (1983)**, "Effects of bare and cased explosive charges on reinforced concrete walls", from "Proceedings of the First International Symposium of Interaction of non-nuclear munitions with structures", Colorado, U.S.A., 10 - 13 May, 1983, pp. 221-226.
- HENRYCH, J., (1979)**, "The Dynamics Of Explosion and its use", Elsevier Scientific Publishing Company, Oxford, 1979.
- HERTER, J., LIMBERGER, E. and BRANDES, K., (1985)**, "Experimental and Numerical Investigation of Reinforced Concrete Structural Members Subjected to Impact Load", from "Design of Concrete Structures", Proceedings of seminar organised by Institution of Structural Engineers Informal Study Group - Model Analysis as a Design Tool, Watford, November 1984. Elsevier Applied Science Publisher, London, 1985, pp. 168-178.
- HUGHES, B.P., and WATSON, A.J., (1978)**, "Compressive strength and ultimate strain of concrete under impact loading", Magazine of Concrete Research, Vol. 30, No. 105, Dec 1978, pp. 189-199.

- HUGHES, B.P. and GREGORY, R., (1972),** "Concrete subjected to high rates of loading in compression", Magazine of Concrete Research, Vol. 24, No. 78, March 1972, pp. 25-36.
- JOHN, R. and SHAH, S.P., (1986),** "Fracture of Concrete subjected to impact loading" Cement, Concrete and Aggregates, Vol. 8, No. 1, Summer 1986, pp.24-32.
- JOHNSON, W. , (1972),** "Impact Strength of Materials" Edward Arnold, London, 1972.
- KHAWANDI, A.A., (1991),** "Impact response of prestressed concrete", PhD thesis, University of Sheffield, 1991.
- KIGER, S.A. and HYDE,D.W., (1987),** "Flexural response of reinforced concrete structures to conventional weapons", from "Proceedings of the Third International Symposium of Interaction of non-nuclear munitions with structures", Mannheim, Germany, April, 1987, pp. N42-N53.
- KINNEY, G. F. and GRAHAM, K. J., (1985),** "Explosive Shocks in Air", Springer-Verlag, N. York 1985.
- KOLSKY, H., (1963),** "Stress Waves in Solids", Dover Publications, New York, 1963.
- KRAUTHAMMER, T., (1991),** "Modified Analysis of Reinforced Concrete Structures under Impulsive Loads", from "Proceedings of the 5th International Symposium on the Interaction of Conventional munitions with Protective Structures", Mannheim, Germany, April 1991, pp. 54-67.
- KRAUTHAMMER, T., (1991),** "Fracture Mechanics Model for Concrete under High Loading Rates", from "Proceedings of the 5th International Symposium on the Interaction of Conventional munitions with Protective Structures", Mannheim, Germany, April 1991, pp. 267-275.
- KRAUTHAMMER, T., BAZEOS, N. and HOLMQUIST, T.J., (1986),** "Modified SDOF analysis of RC box-type structures", ASCE Journal of Structural Engineering, Vol. 112, No. 4, April 1986, pp. 726-744.
- KROPATSCHECK, M.O., (1993),** "Tests and evaluation of close-in detonations", from "Proceedings of the First International Symposium of Interaction of non-nuclear munitions with structures", Colorado, U.S.A., 10 - 13 May, 1983, pp. 227-236.
- MAINSTONE, R.J., (1975),** "Properties of materials at high rates of straining or loading", Materials and Structures, Vol. 8, No. 44, March/April 1975, pp. 102-115.
- McVAY, M.K., (1987),** "Spalling of concrete from nearby detonation", from "Proceedings of the Third International Symposium of Interaction of non-nuclear munitions with structures", Mannheim, Germany, 1987, pp. N3-N17.
- NEW CIVIL ENGINEER,** publication of the I.C.E. London, 22.2.1990
- NILSSON, L., SAHLIN, S., (1982),** "Impact of a Steel Rod on a Reinforced Concrete Slab" , from "Dynamic Modelling of Concrete Structures", Proceedings of ACI Annual Convention, Las Vegas, USA, March 1980 and ACI Fall Convention, San Juan, Puerto Rico, Sept. 1980, ACI, Detroit, 1982, pp. 165-187
- NOOR, F.A. and BOSWELL, L.F., (1992),** "Small scale modelling of concrete structures", Elsevier Applied Science, London, 1992.
- NORRIS et al, (1960),** "Structural design for dynamic loads" McGraw-Hill Book Company, N.York, 1960.
- OH, B.H., (1987),** "Behaviour of concrete under dynamic tensile loads", American Concrete Institute Journal, Jan/Feb 1987, pp. 8-13.
- PARK, R., (1964),** "Ultimate strength of rectangular concrete slabs under short-term uniform loading with edges restrained against lateral movement", Journal of Institution of Civil Engineers, June 1964, pp. 125-149.
- PETROVIC, B., (1985),**"Odabrana poglavlja iz zemljotresnog gradjevinarstva", IRO Gradjevinska knjiga, Beograd, Yugoslavia, 1985.
- POPOV, E.P., (1976),** "Mechanics of Materials" Prentice-hall, Inc., New Jersey, U.S.A., 1976.
- REINHARDT, H.W., (1982),** "Concrete under impact loading, tensile strength and bond", HERON, Delft University of Technology, The Netherlands, Vol. 27, No. 3, 1982.
- REINHARDT, H.W. and WALRAVEN, J.C., (1982),** "Cracks in concrete subject to shear", ASCE Journal of Structural Engineering, Vol. 108, No. ST1, Jan 1982.
- ROSS, T.J. and KRAWINKLER, H., (1985),** "Impulsive direct shear failure in RC slabs", ASCE Journal of Structural Engineering, Vol. 111, No. 8, Aug 1985, pp. 1661-1678.

SABNIS, G.M. et al, (1983), "Structural modelling and experimental techniques", Newark and Hall, Prantice-Hall, New-Jersey, USA, 1983.

SAWAN, J. and ABDEL-ROHMAN, M., (1986), "Impact effect on RC slabs: Experimental approach", ASCE Journal of Structural Engineering, Vol. 112, No. 9, Sept 1986, pp. 2057-2065.

SHERIDAN, A.J., (1987), "Response of concrete to high explosive detonation", from "Proceedings of the Third International Symposium of Interaction of non-nuclear munitions with structures", Mannheim, Germany, April, 1987, pp. 494-503.

SHERIDAN, A.J. et al, (1989), "The behaviour of concrete under explosive shock in relation to its compaction under uniaxial strain loading", from "Structures under shock and impact I", Proceedings of the First International Conference on S.U.S.I. held in Cambridge, U.K., July 1989, pp. 88-96.

SMITH, J.L. and MIAKAR, P.F., (1991), "A simplified two-dimensional methodology for predicting in structure shock for complex structures", from "Proceedings of the 5th International Symposium on the Interaction of Conventional munitions with Protective Structures", Mannheim, Germany, April 1991, pp. 478-485.

SUARIS, W. and SHAH, S.P., (1981), "Inertial effects in the instrumented impact testing of cementitious composites", Cement, Concrete and Aggregates, Vol. 3, No. 2, Winter 1981, pp77-83.

SUARIS, W. and SHAH, S.P., (1983), "Properties of Concrete subjected to Impact", ASCE Journal of Structural Engineering, Vol. 109, No. 7, July 1983, pp. 1727-1741.

TANCRETO, J.E., (1991), "Response of Reinforced Concrete Slabs to Close-in Explosive Loads", from "Proceedings of the 5th International Symposium on the Interaction of Conventional munitions with Protective Structures", Mannheim, Germany, April 1991, pp. 514.

TIMOSHENKO, S. "Strength of Materials", D. van Nostrand Company, London.

VEEN, C. and BLAAUWENDRAAD, J., (1983), "Dynamic elasto-plastic model for reinforced concrete members", HERON, Delft University of Technology, The Netherlands, Vol. 28, No. 1, 1983.

YAMAGUCHI, H., FUJIMOTO, K., (1991), "Strain Rate Effects on Dynamic Response of Reinforced Concrete Plate under Impact Loading", from "Proceedings of the 5th International Symposium on the Interaction of Conventional munitions with Protective Structures", Mannheim, Germany, April 1991, pp.317-327.

ZECH, B. and WITTMANN, F.H., (1980), "Variability and mean value of strength of concrete as function of load", American Concrete Institute Journal, Vol 77, No. 5, Sep/Oct 1980, pp. 358-362.

ZIELINSKI, A.J., (1984), "Model for tensile fracture of concrete at high rates of loading", Cement and Concrete Research, Vol. 14, No. 2, March 1984, pp. 215-222.

ZIELINSKI, A.J. and REINHARDT, H.W., (1982), "Stress-strain behaviour of concrete and mortar at high rates of tensile loading", Cement and Concrete Research, Vol. 12, No. 3, May 1982, pp. 309-319.

ZIELINSKI, A.J., REINHARDT, H.W. and KORMELING, H.A., (1981), "Experiments on concrete under uniaxial impact tensile loading", Materials and Structures, Vol. 14, No. 81, March/April 1981, pp. 163-169.

WATSON, A.J., (1991), Lectures on Structural Dynamics, Department of Civil and Structural Engineering, University of Sheffield, 1991.

WATSON, A.J., and AL-AZAWI, T.K. (1985), "Impact Resistance of reinforced concrete slabs", from "Design of Concrete Structures", Proceedings of seminar organised by Institution of Structural Engineers Informal Study Group - Model Analysis as a Design Tool, Watford, November 1984. Elsevier Applied Science Publisher, London, 1985, pp. 158-167.

WATSON, A.J. and SANDERSON, A.J. (1984), "Cratering and subcrater fractures produced by explosive shock on concrete" from "Mechanical Properties at High Rates of Strain", Proceedings of the Third Conference on the Mechanical Properties of Materials at High Rates of Strain, Oxford, April 1984, Institute of Physics, London, 1984, pp 329-336.

WATSTEIN, D., (1953), "Effect of straining rate on the compressive strength and elastic properties of concrete", American Concrete Institute Journal, Vol. 49, April 1953, pp. 729-744.

WRIGHT, S.J., (1991), "The vulnerability of reinforced concrete elements to explosive loading, PhD thesis, University of Sheffield, 1991.

IMPACT TEST RESULTS

1:1 SCALE SLABS

APPENDIX A1

IMPACT TEST

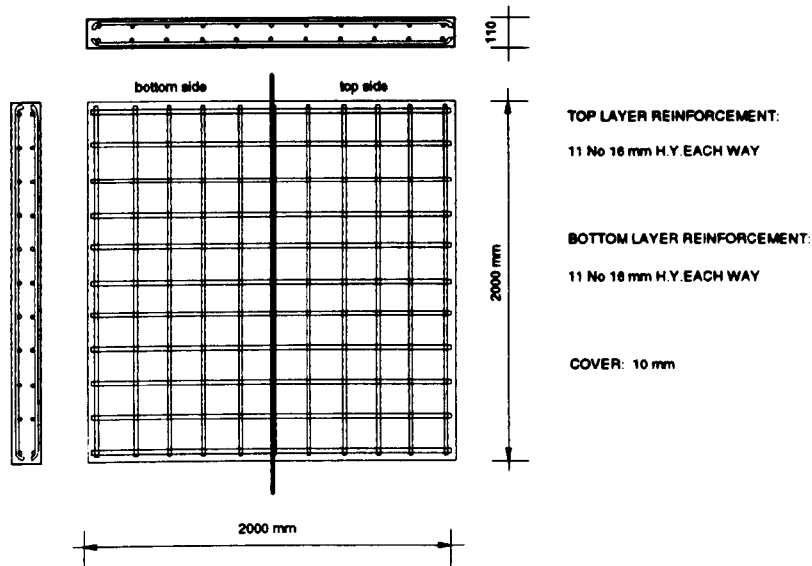
DATE: 6.06.91

LARGE SLAB LS1

AGE OF SPECIMEN: 8 days

Cube compressive strength	N/mm ²	45.0	Cylinder tensile strength	N/mm ²	3.37	Age (days)	15
---------------------------	-------------------	------	---------------------------	-------------------	------	------------	----

REINFORCEMENT:

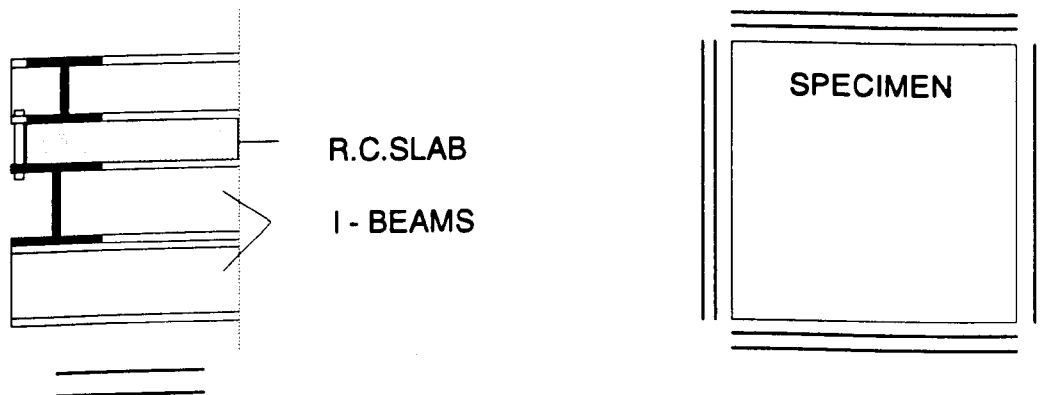


LOADING CONDITIONS

(2nd impact)

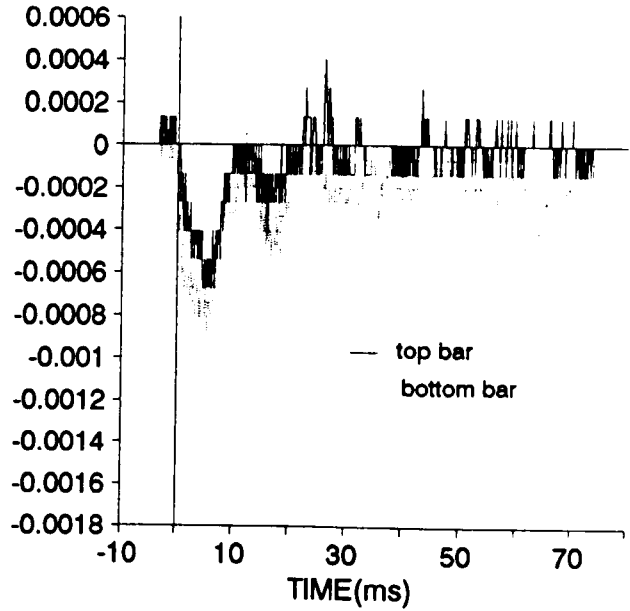
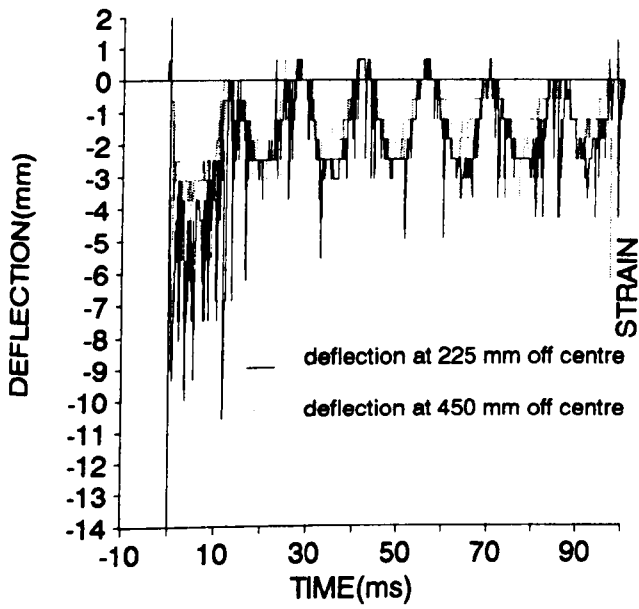
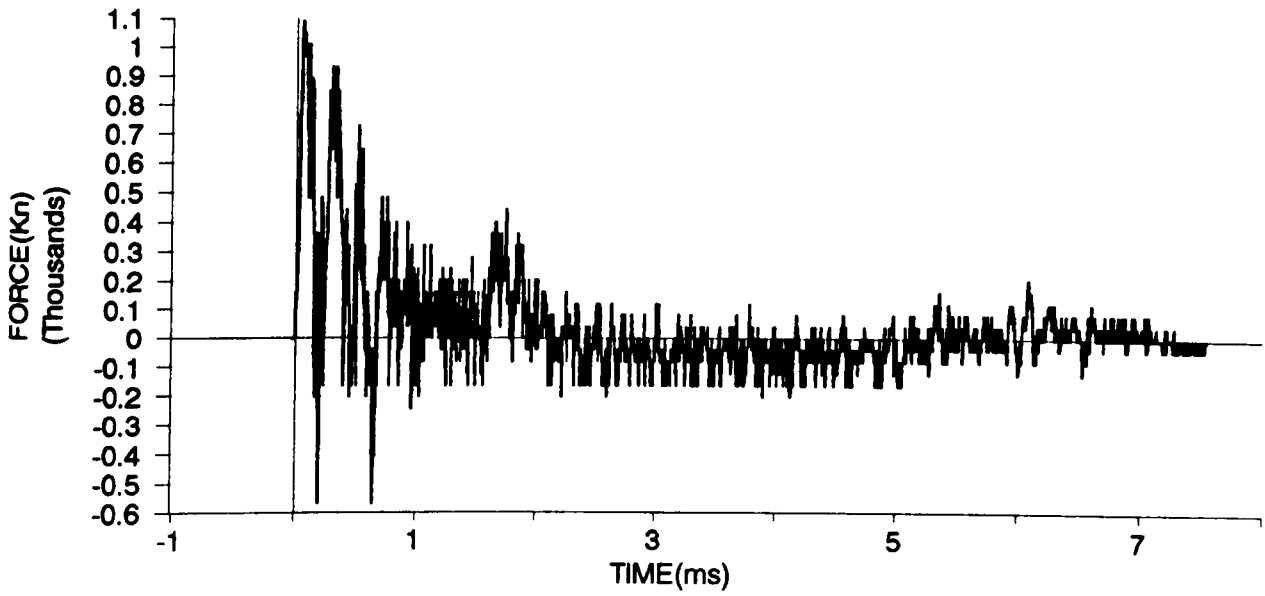
TYPE OF IMPACT	: HARD
HAMMER WEIGHT	: 70kg
HEIGHT OF DROP (ABOVE CENTRE OF SPECIMEN)	: 3220mm
IMPACT VELOCITY	: 7.71m/sec
THEORETICAL VELOCITY $V = \sqrt{2gh}$: 7.95m/sec
AREA OF THE PRESSURE BAR CROSS-SECTION	: 12,265mm ²

SUPPORTS



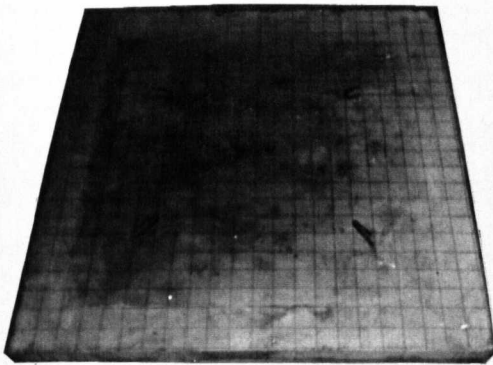
IMPACT TEST - LARGE SLAB - LS1

SHOT 1.

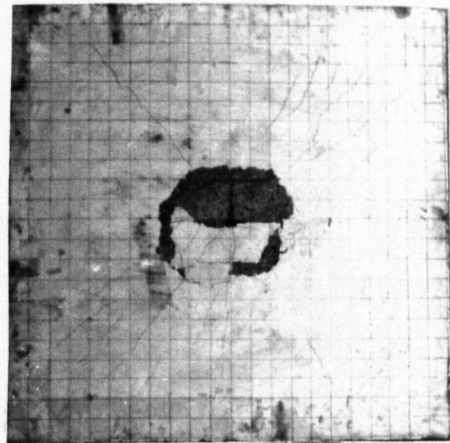


IMPACT TEST - LARGE SLAB - LS1

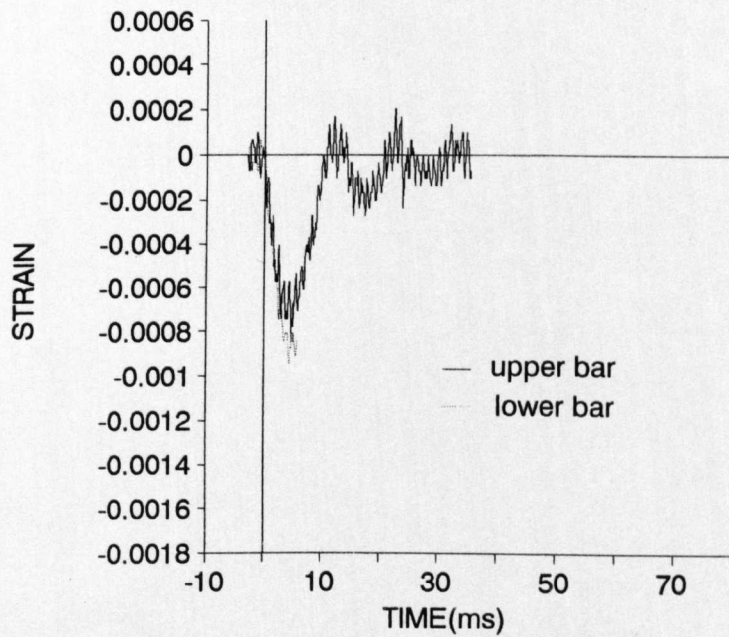
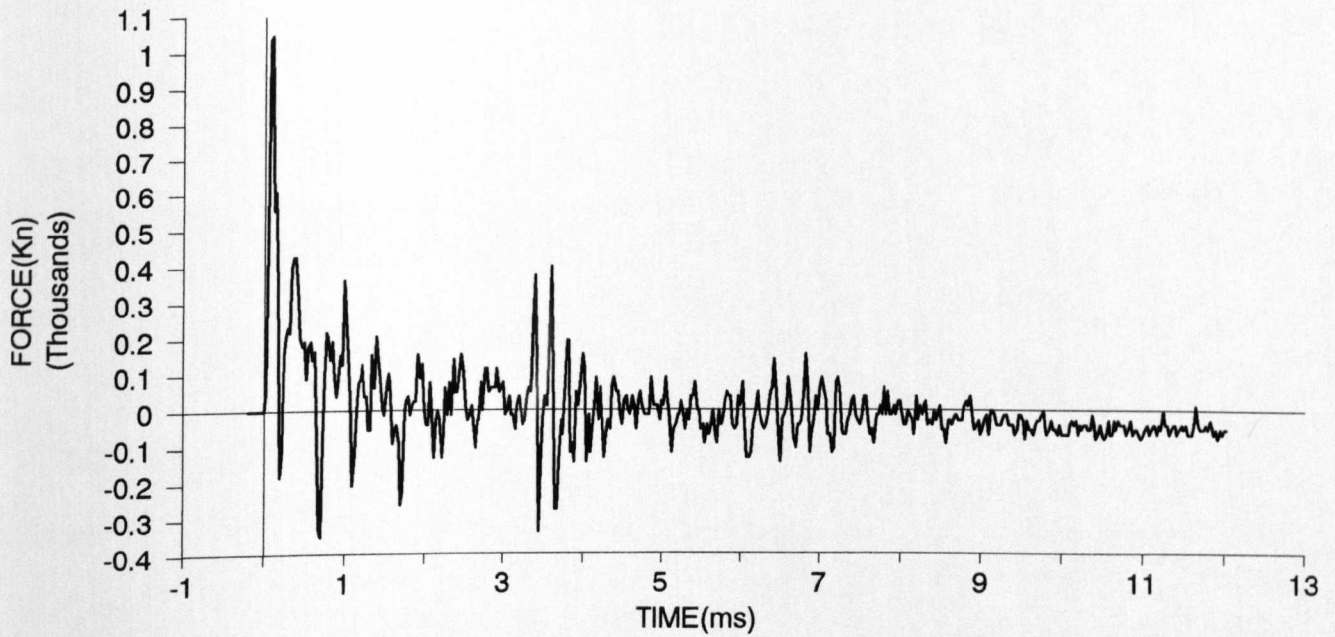
SHOT 2.



top side



bottom side



IMPACT TEST

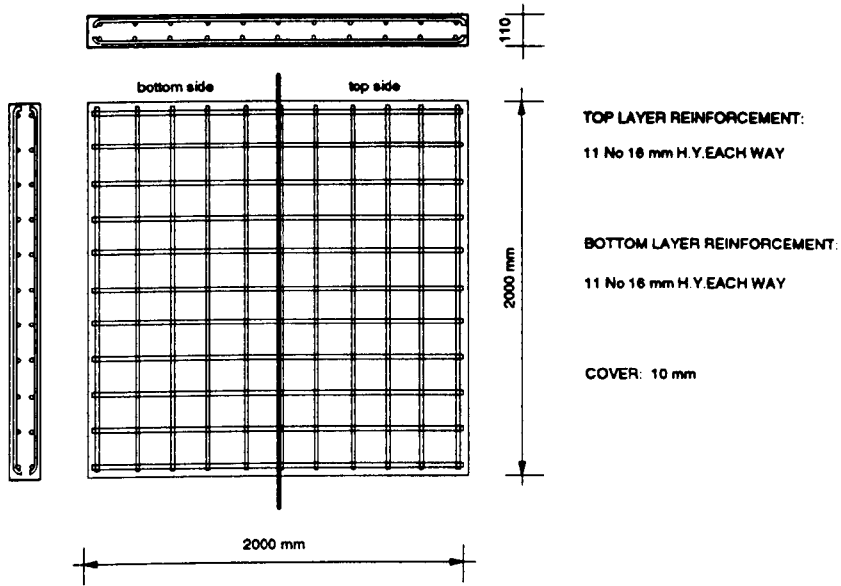
DATE: 10.07.91

LARGE SLAB LS2

AGE OF SPECIMEN: days

Cube compressive strength	N/mm ²	45.3	Cylinder tensile strength	N/mm ²	3.28	Age (days)	15
---------------------------	-------------------	------	---------------------------	-------------------	------	------------	----

REINFORCEMENT:



LOADING CONDITIONS

TYPE OF IMPACT : HARD

HAMMER WEIGHT : 150kg

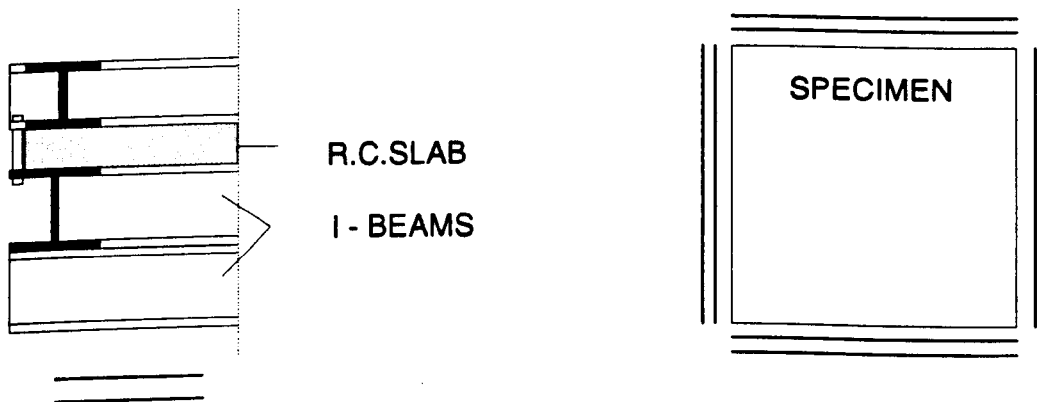
HEIGHT OF DROP (ABOVE CENTRE OF SPECIMEN) : 3220mm

IMPACT VELOCITY : 7.79m/sec

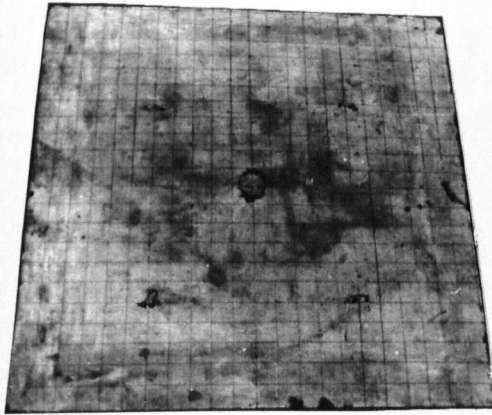
THEORETICAL VELOCITY $V = \sqrt{2gh}$: 7.95m/sec

AREA OF THE PRESSURE BAR CROSS-SECTION : 12,265mm²

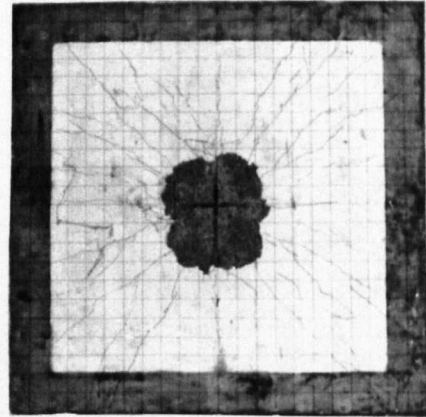
SUPPORTS



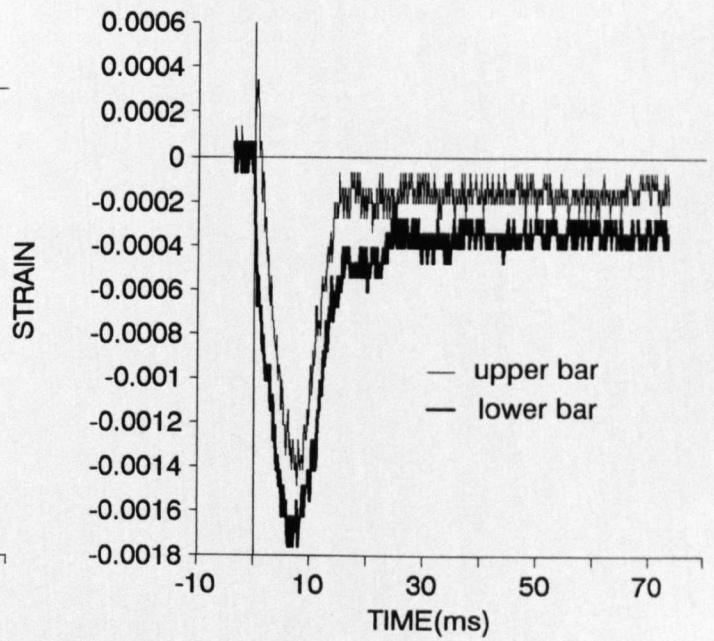
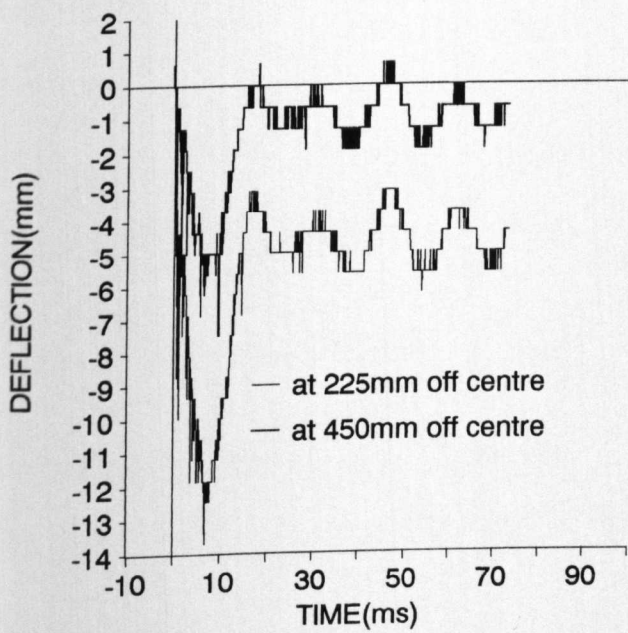
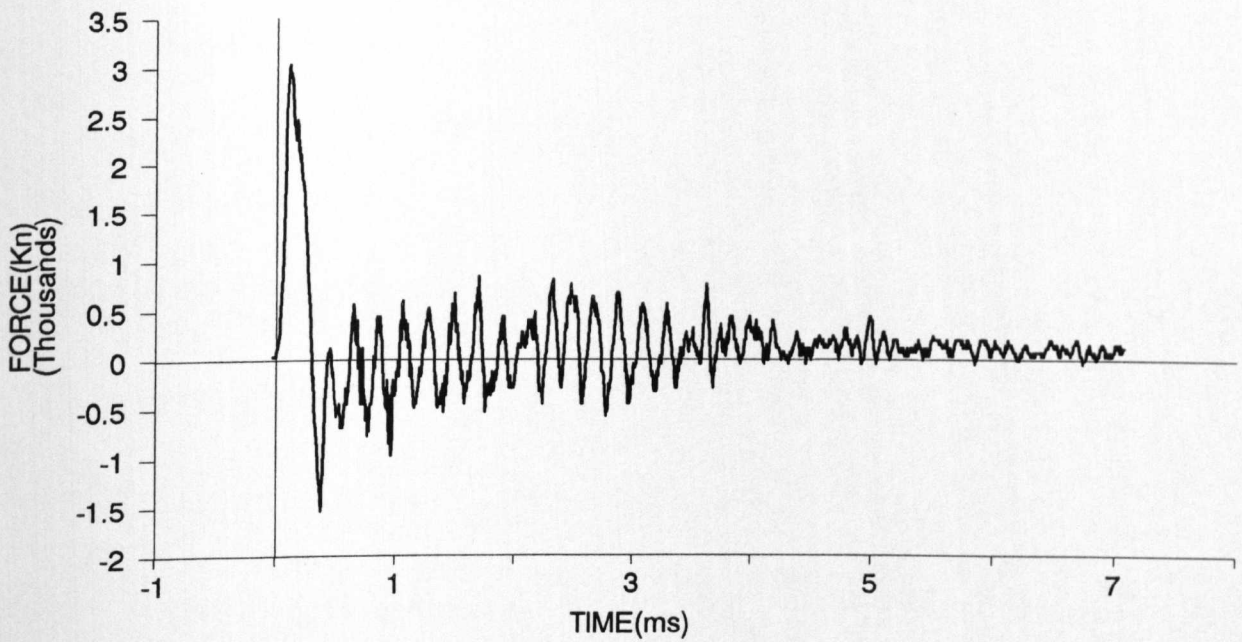
IMPACT TEST - LARGE SLAB - LS2



top side



bottom side



IMPACT TEST

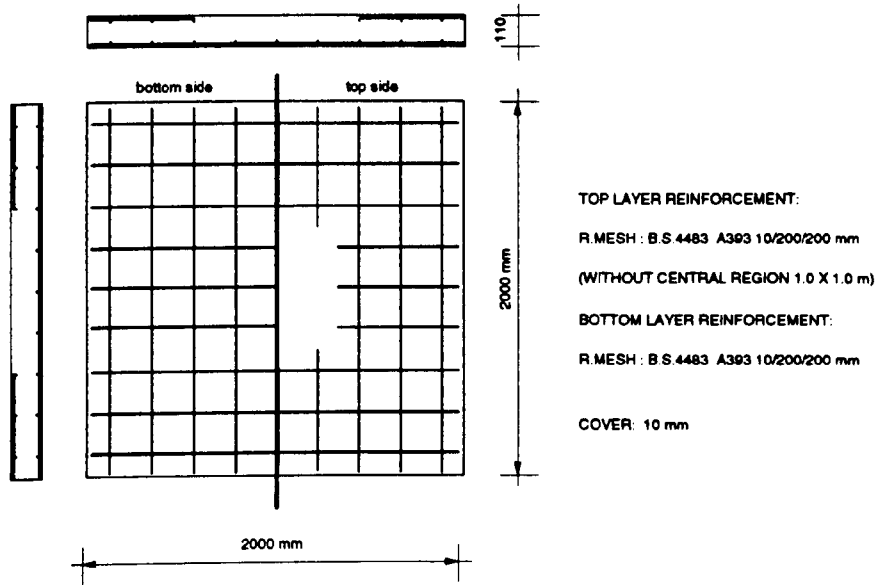
DATE: 23.07.92

LARGE SLAB LS3

AGE OF SPECIMEN: 16 days

Cube compressive strength	N/mm ²	56.0	Cylinder tensile strength	N/mm ²	3.59	Age (days)	16
---------------------------	-------------------	------	---------------------------	-------------------	------	------------	----

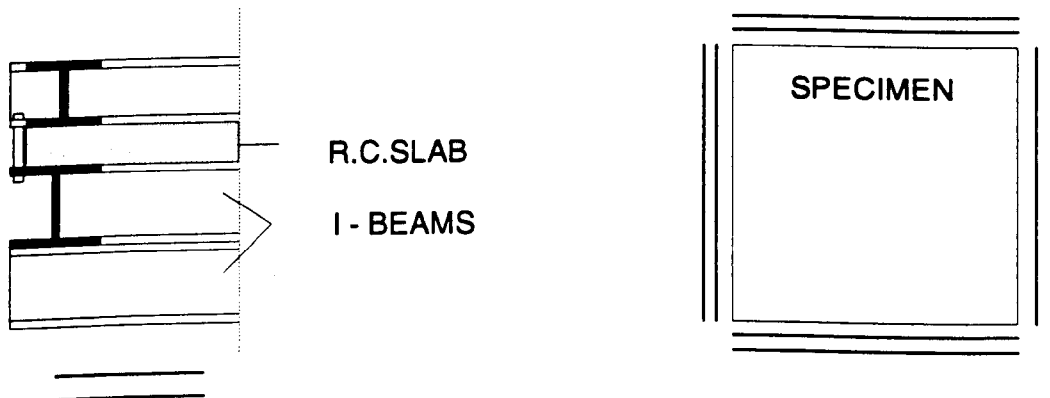
REINFORCEMENT:



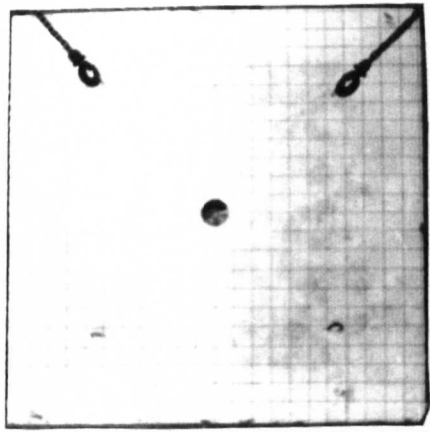
LOADING CONDITIONS

TYPE OF IMPACT : HARD
 HAMMER WEIGHT : 150kg
 HEIGHT OF DROP (ABOVE CENTRE OF SPECIMEN) : 2500mm
 IMPACT VELOCITY : 6.93m/sec
 THEORETICAL VELOCITY $V = \sqrt{2gh}$: 7.00m/sec
 AREA OF THE PRESSURE BAR CROSS-SECTION : 12,265mm²

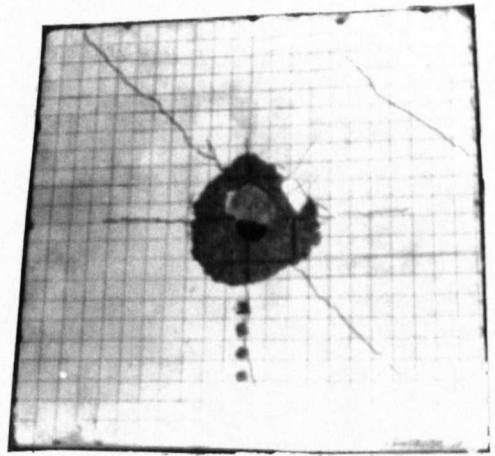
SUPPORTS



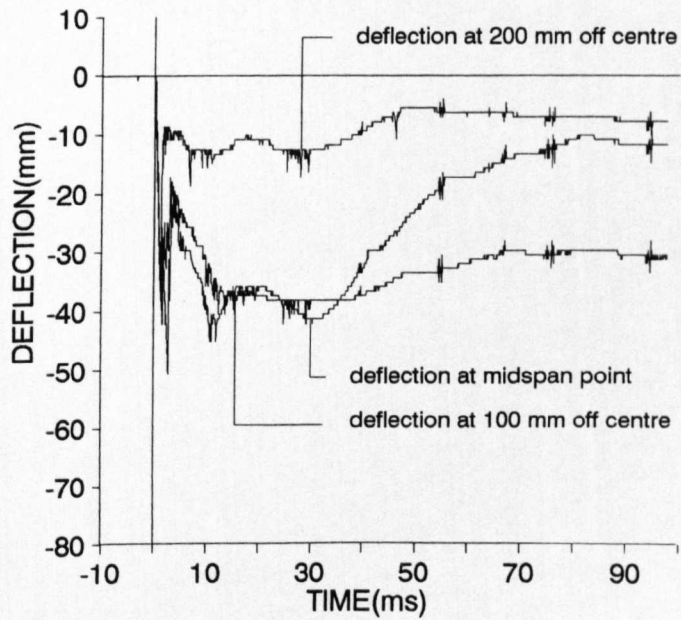
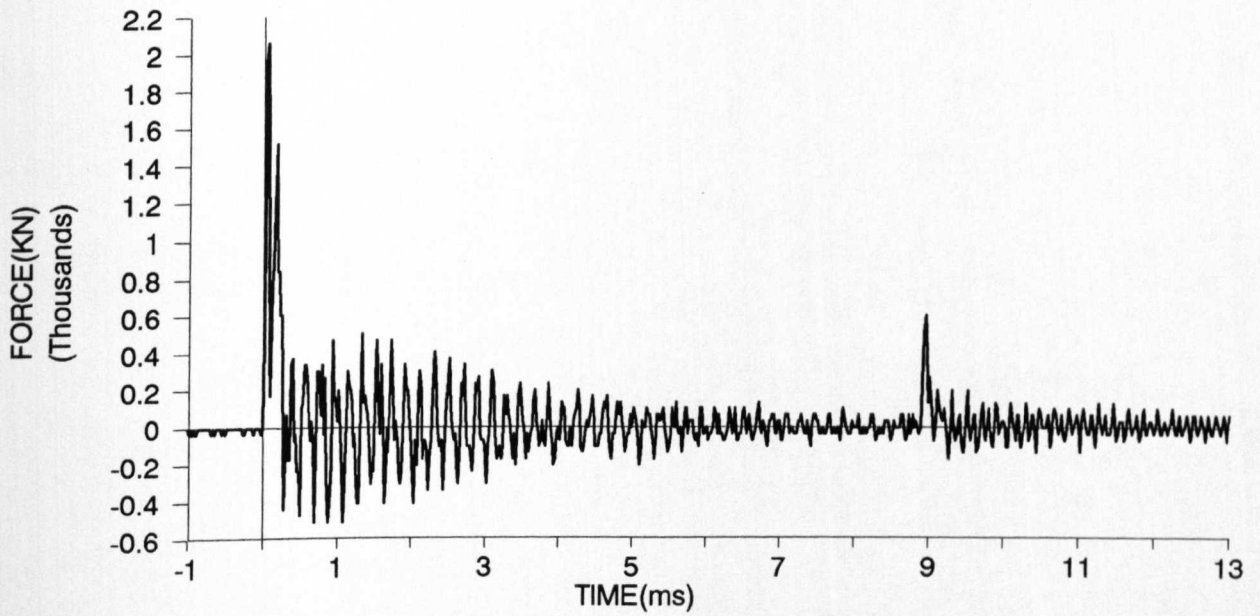
IMPACT TEST - LARGE SLAB - LS3



top side



bottom side



IMPACT TEST

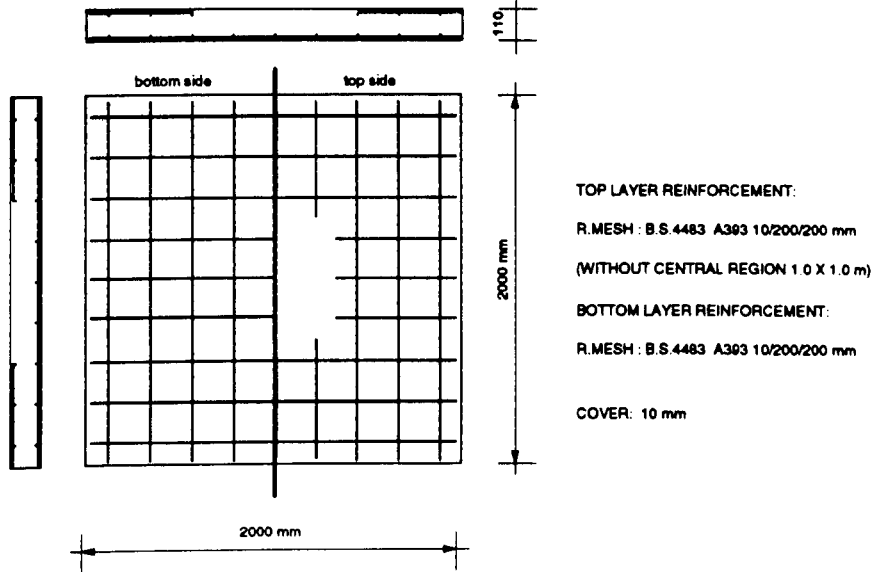
DATE: 10.08.92

LARGE SLAB LS4

AGE OF SPECIMEN: 10 days

Cube compressive strength	N/mm ²	43.9	Cylinder tensile strength	N/mm ²	3.44	Age (days)	10
---------------------------	-------------------	------	---------------------------	-------------------	------	------------	----

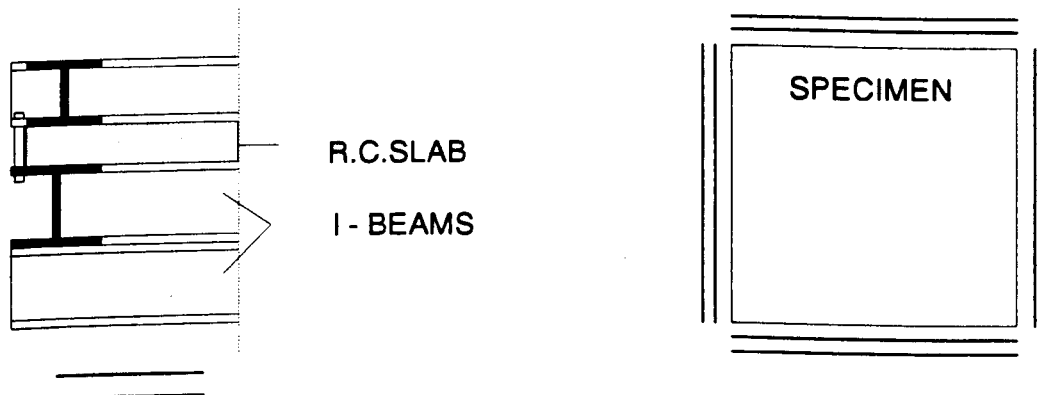
REINFORCEMENT:



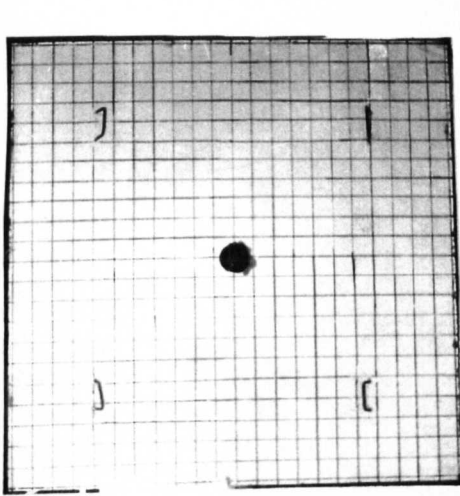
LOADING CONDITIONS

TYPE OF IMPACT	: HARD
HAMMER WEIGHT	: 150kg
HEIGHT OF DROP (ABOVE CENTRE OF SPECIMEN)	: 3220mm
IMPACT VELOCITY	: 7.93m/sec
THEORETICAL VELOCITY $V = \sqrt{2gh}$: 7.95m/sec
AREA OF THE PRESSURE BAR CROSS-SECTION	: 12,265mm ²

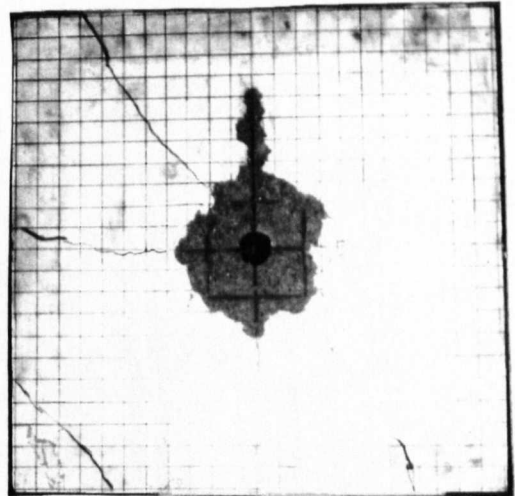
SUPPORTS



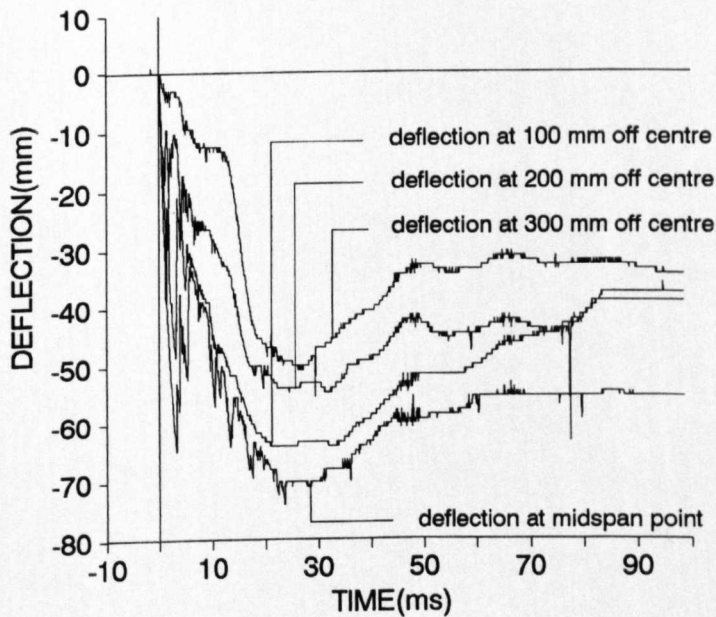
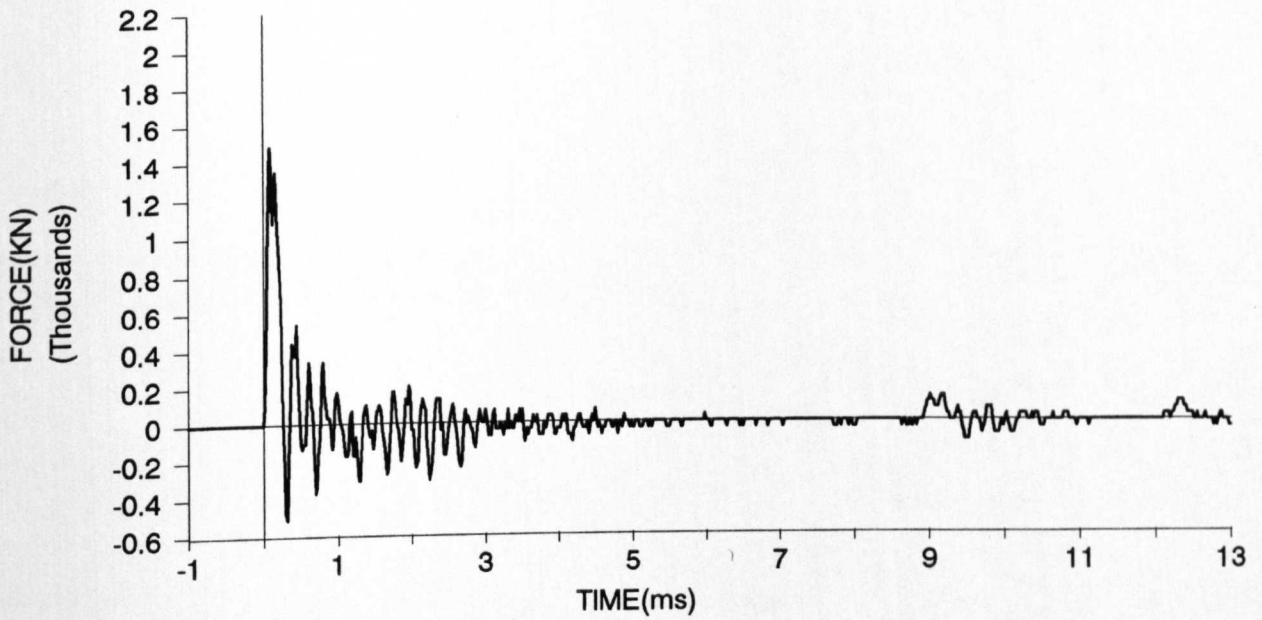
IMPACT TEST - LARGE SLAB - LS4



top side



bottom side



IMPACT TEST

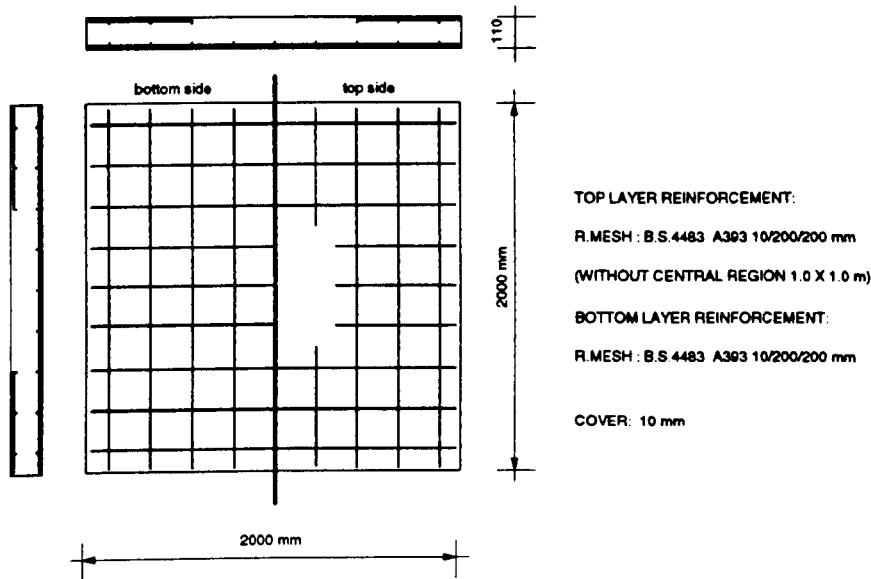
DATE: 18.8.92

LARGE SLAB LS5

AGE OF SPECIMEN: 8 days

Cube compressive strength	N/mm ²	41.9	Cylinder tensile strength	N/mm ²	3.32	Age (days)	8
---------------------------	-------------------	------	---------------------------	-------------------	------	------------	---

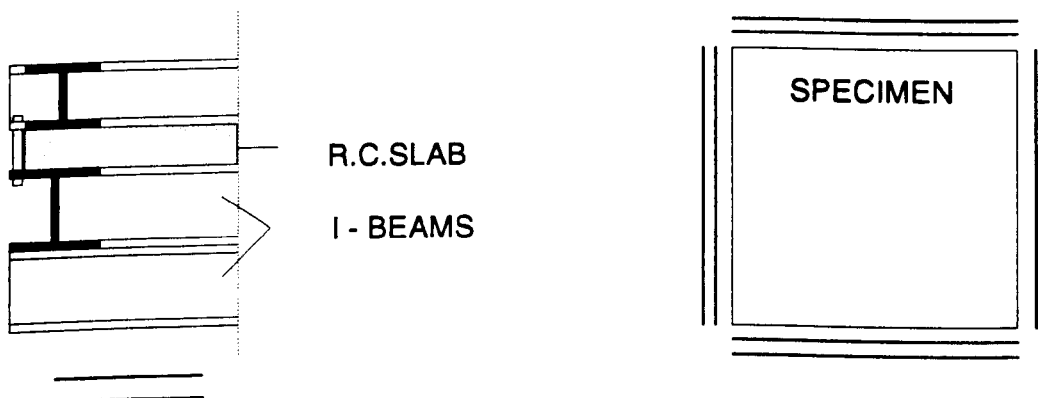
REINFORCEMENT:



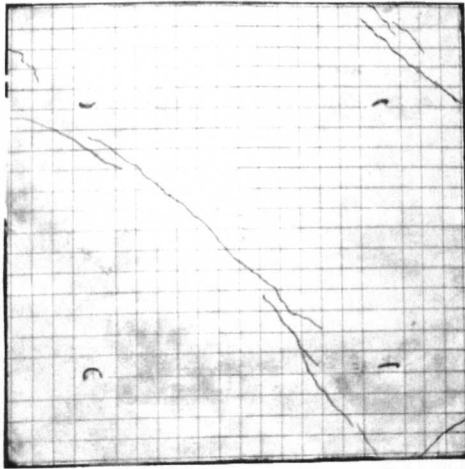
LOADING CONDITIONS

TYPE OF IMPACT	: SOFT
HAMMER WEIGHT	: 150kg
HEIGHT OF DROP (ABOVE CENTRE OF SPECIMEN)	: 2500mm
IMPACT VELOCITY	: 6.99m/sec
THEORETICAL VELOCITY $V = \sqrt{2gh}$: 7.00m/sec
AREA OF THE PRESSURE BAR CROSS-SECTION	: 12,265mm ²

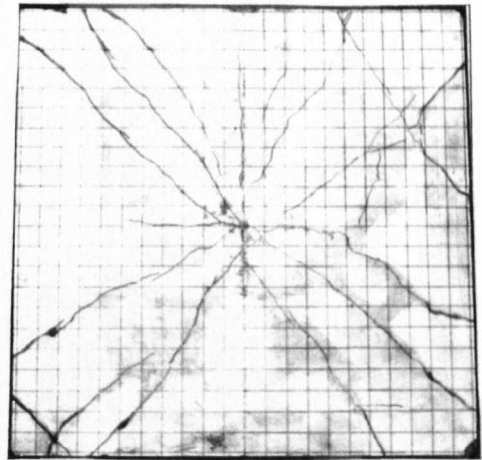
SUPPORTS



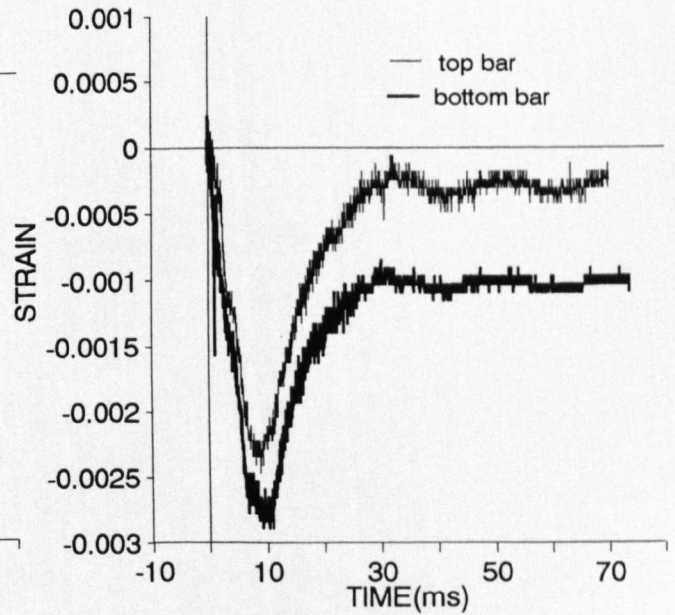
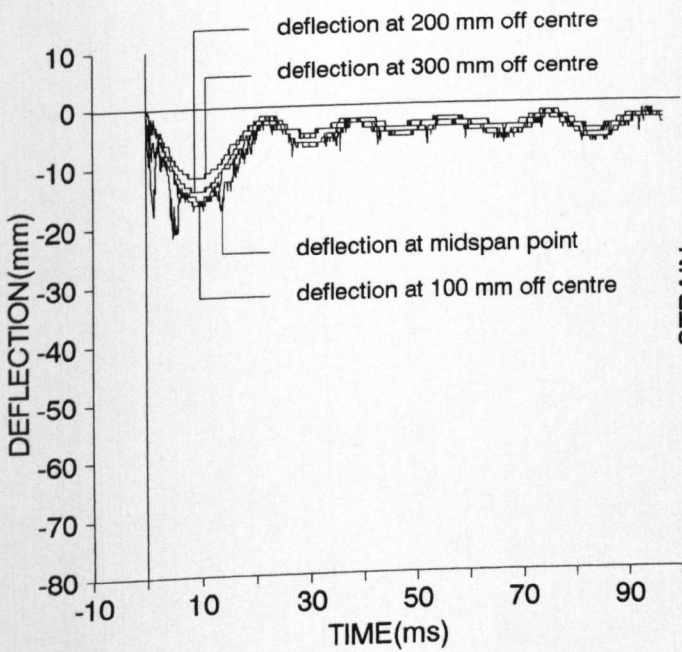
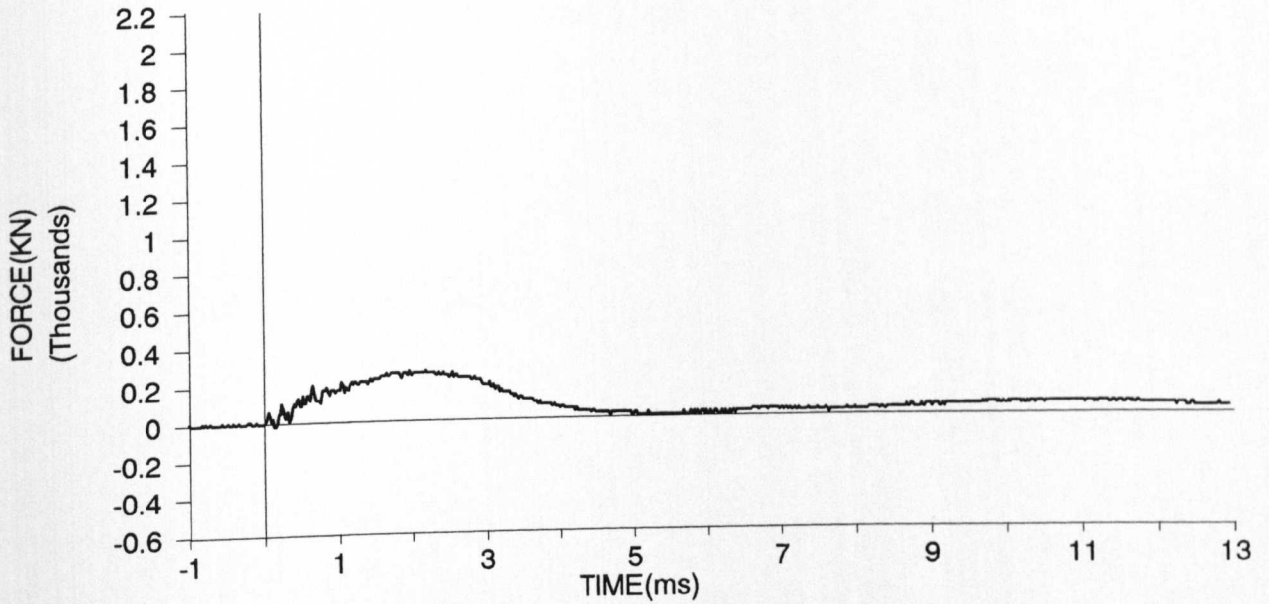
IMPACT TEST - LARGE SLAB - LS5



top side



bottom side



IMPACT TEST RESULTS

1:2.5 SCALE SLABS

APPENDIX A2

IMPACT TEST

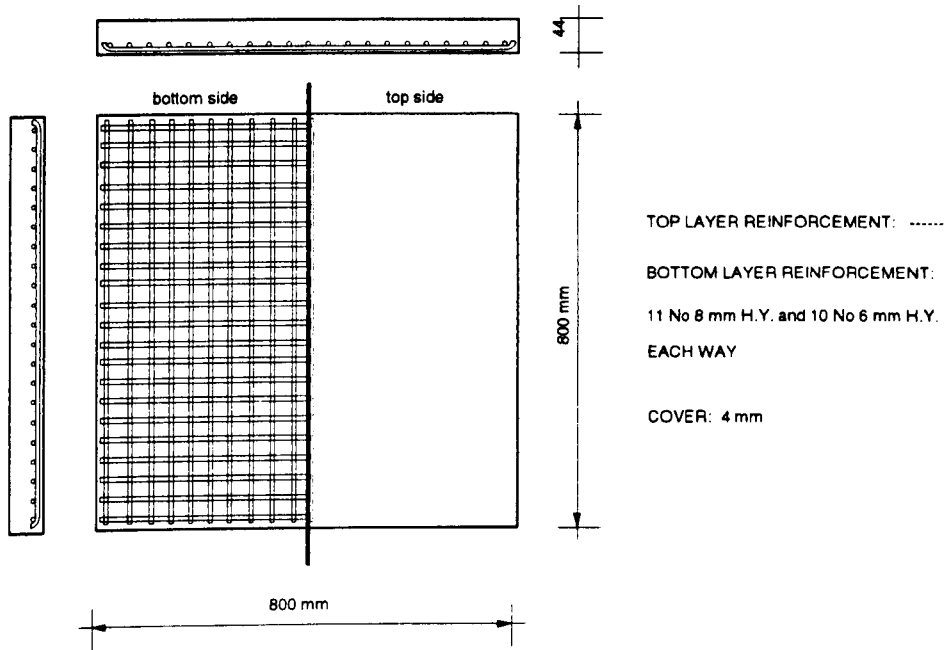
DATE: 22.05.90

SMALL SLAB S1

AGE OF SPECIMEN: 8 days

Cube compressive strength	N/mm ²	35.70	Cylinder tensile strength	N/mm ²	3.90	Age (days)	9
---------------------------	-------------------	-------	---------------------------	-------------------	------	------------	---

REINFORCEMENT:



LOADING CONDITIONS

TYPE OF IMPACT : HARD

HAMMER WEIGHT : 33.7kg

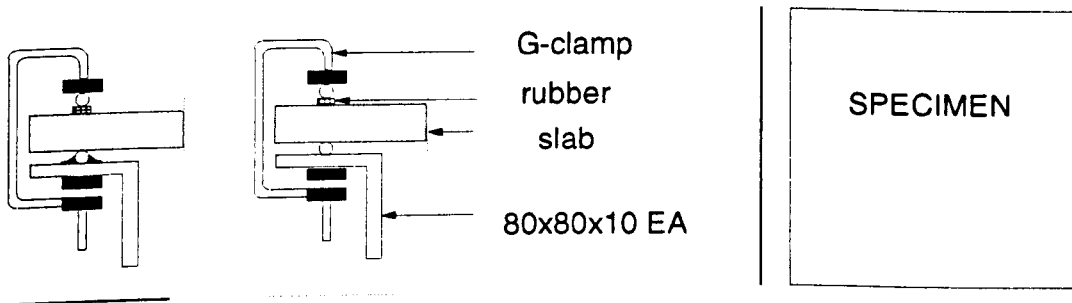
HEIGHT OF DROP (ABOVE CENTRE OF SPECIMEN) : 1850mm

IMPACT VELOCITY : 5.51m/sec

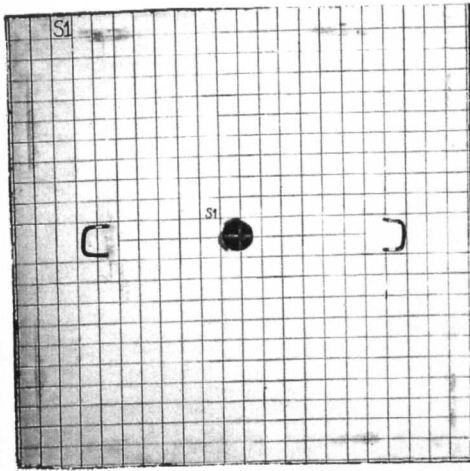
THEORETICAL VELOCITY $V = \sqrt{2gh}$: 6.02m/sec

AREA OF THE PRESSURE BAR CROSS-SECTION : 1962.5mm²

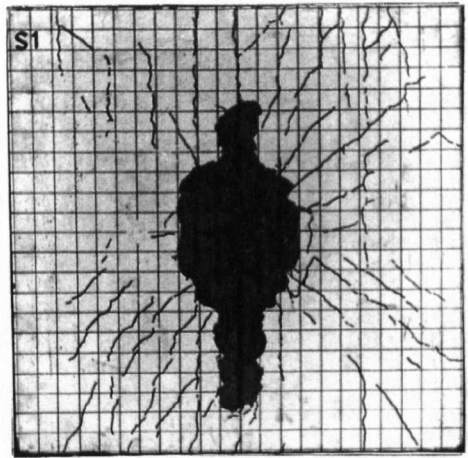
SUPPORTS



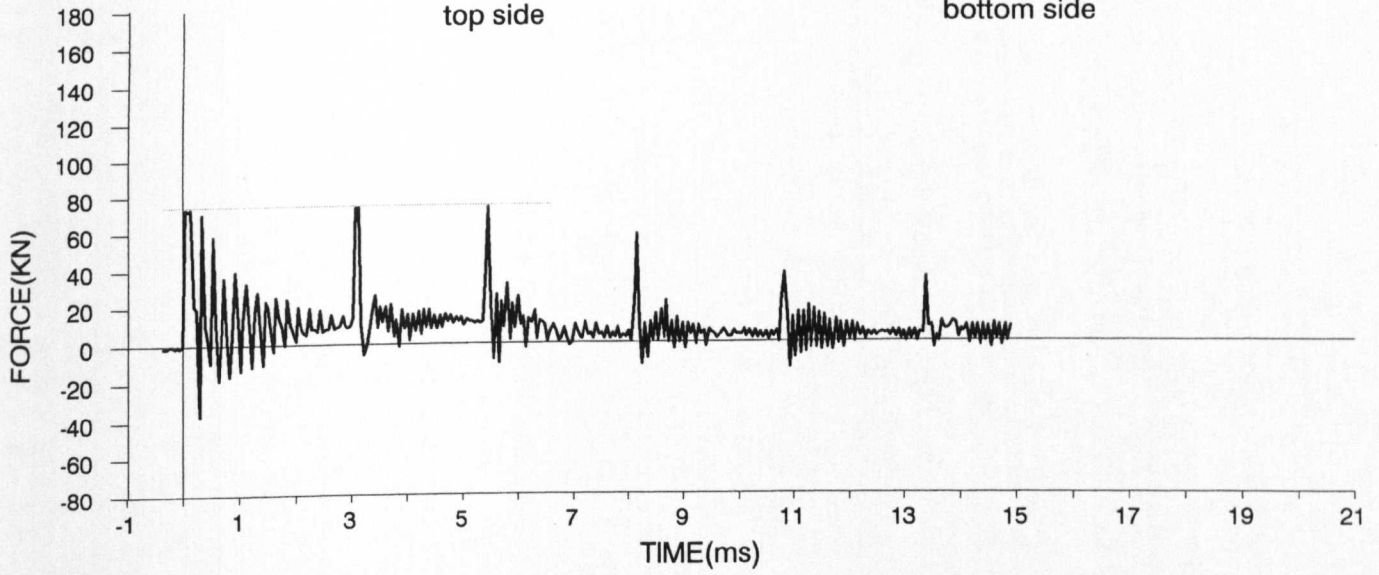
IMPACT TEST - SMALL SLAB - S1



top side



bottom side



IMPACT TEST

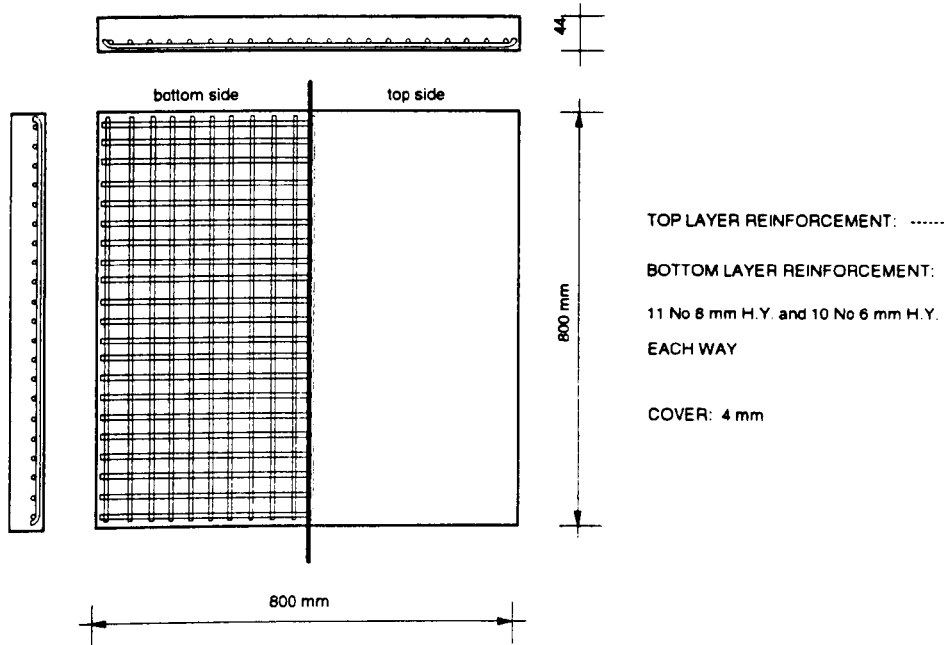
DATE: 24.05.90

SMALL SLAB S2

AGE OF SPECIMEN: 10 days

Cube compressive strength	N/mm ²	35.7	Cylinder tensile strength	N/mm ²	3.90	Age (days)	9
---------------------------	-------------------	------	---------------------------	-------------------	------	------------	---

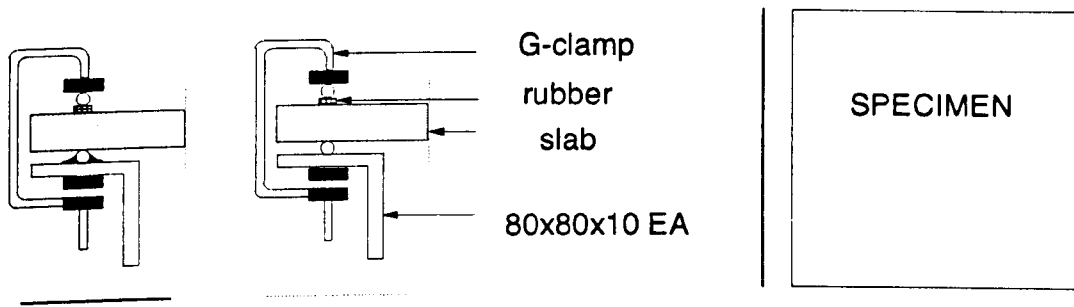
REINFORCEMENT:



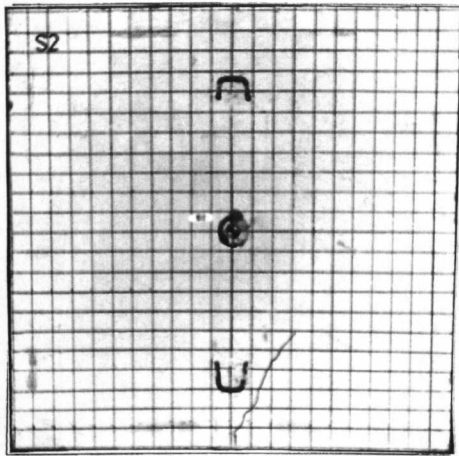
LOADING CONDITIONS

TYPE OF IMPACT	: HARD
HAMMER WEIGHT	: 33.7kg
HEIGHT OF DROP (ABOVE CENTRE OF SPECIMEN)	: 1850mm
IMPACT VELOCITY	: 5.94m/sec
THEORETICAL VELOCITY $V = \sqrt{2gh}$: 6.02m/sec
AREA OF THE PRESSURE BAR CROSS-SECTION	: 1962.5mm ²

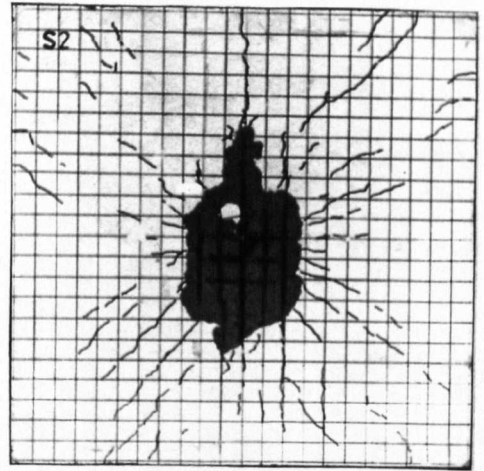
SUPPORTS



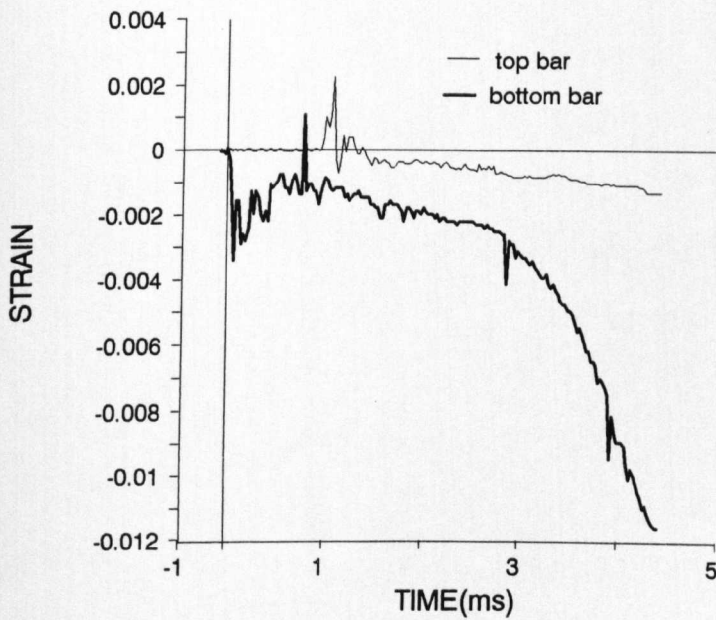
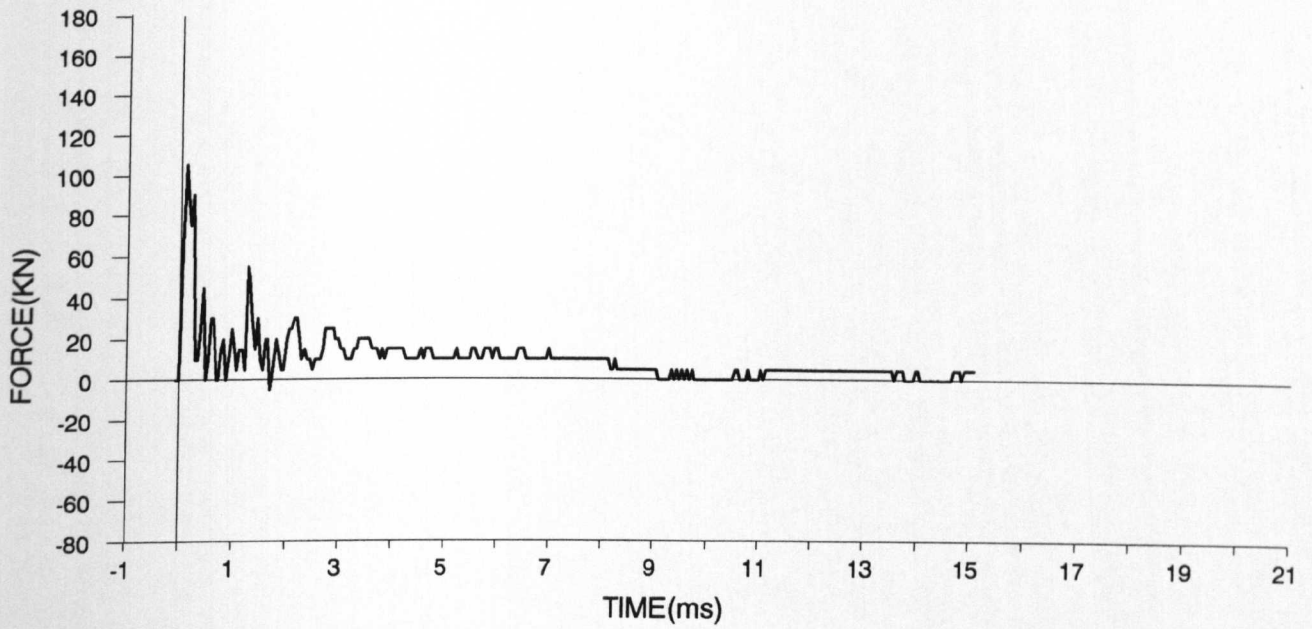
IMPACT TEST - SMALL SLAB - S2



top side



bottom side



IMPACT TEST

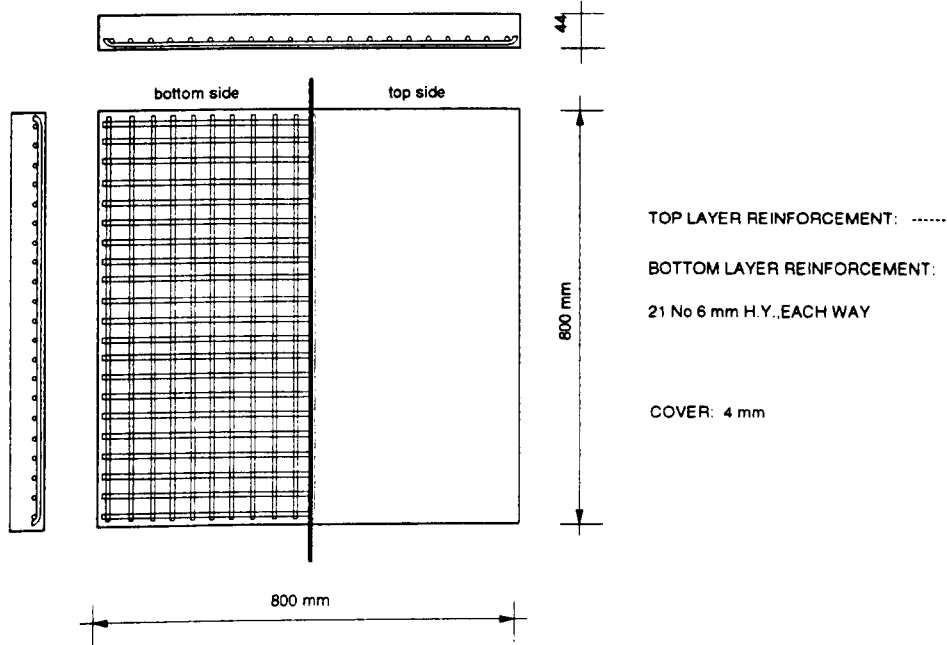
DATE: 1.06.90

SMALL SLAB S3

AGE OF SPECIMEN: 7 days

Cube compressive strength	N/mm ²	37.7	Cylinder tensile strength	N/mm ²	4.12	Age (days)	9
---------------------------	-------------------	------	---------------------------	-------------------	------	------------	---

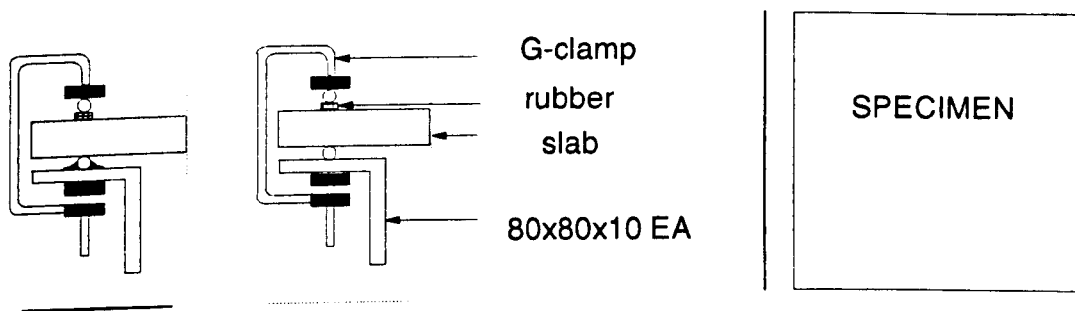
REINFORCEMENT:



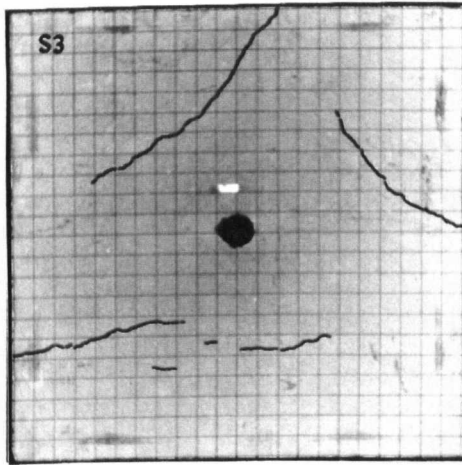
LOADING CONDITIONS

TYPE OF IMPACT	: HARD
HAMMER WEIGHT	: 33.7kg
HEIGHT OF DROP (ABOVE CENTRE OF SPECIMEN)	: 1850mm
IMPACT VELOCITY	: 5.67m/sec
THEORETICAL VELOCITY $v = \sqrt{2gh}$: 6.02m/sec
AREA OF THE PRESSURE BAR CROSS-SECTION	: 1962.5mm ²

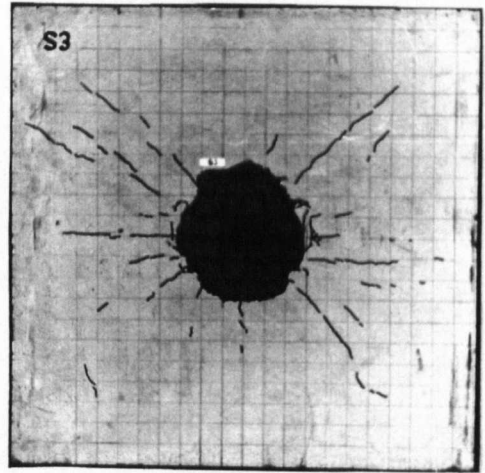
SUPPORTS



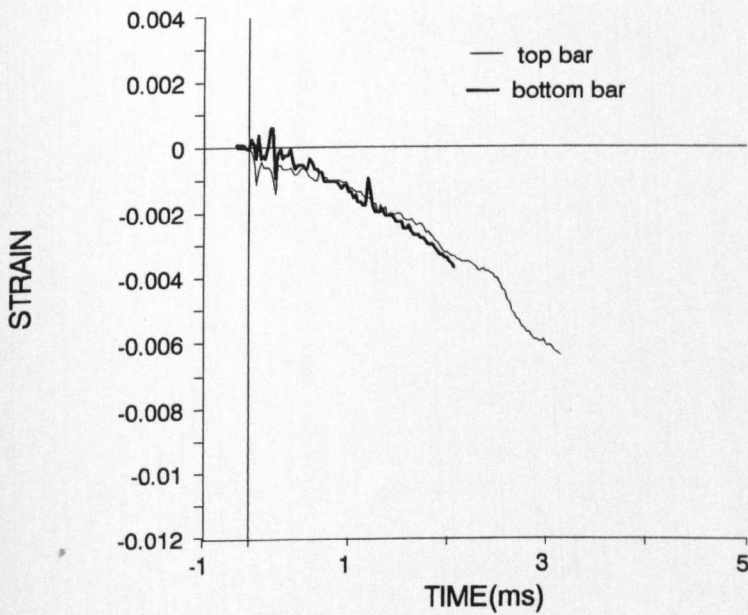
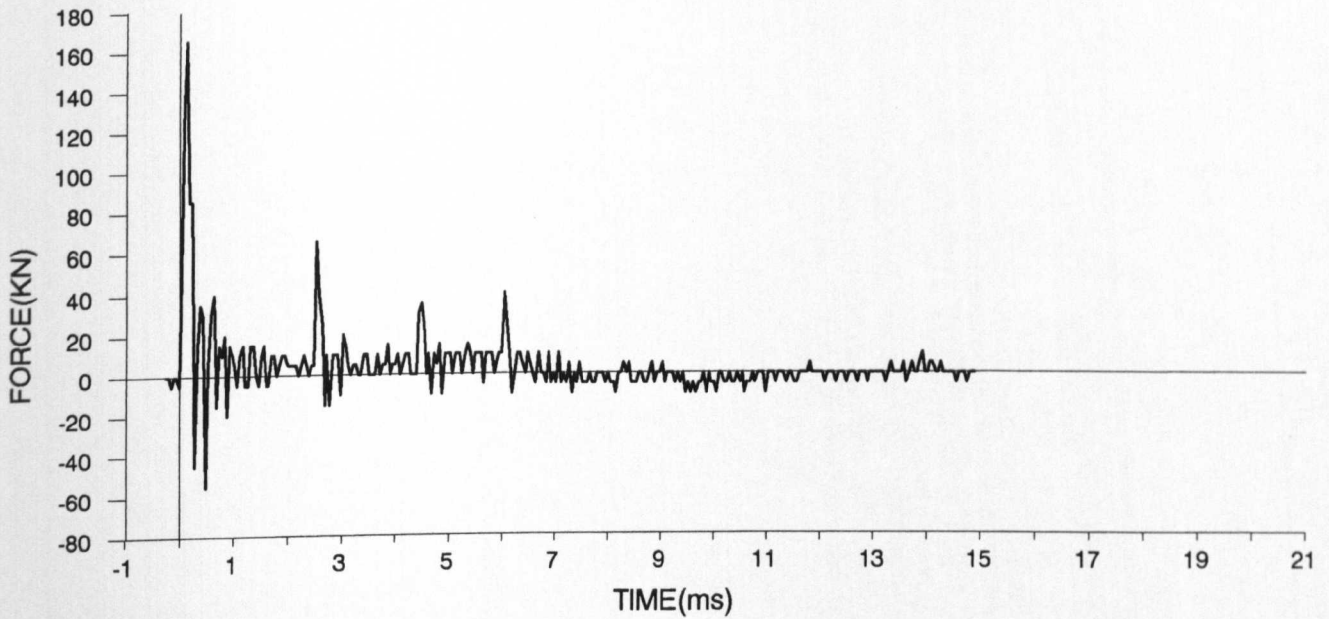
IMPACT TEST - SMALL SLAB - S3



top side



bottom side



IMPACT TEST

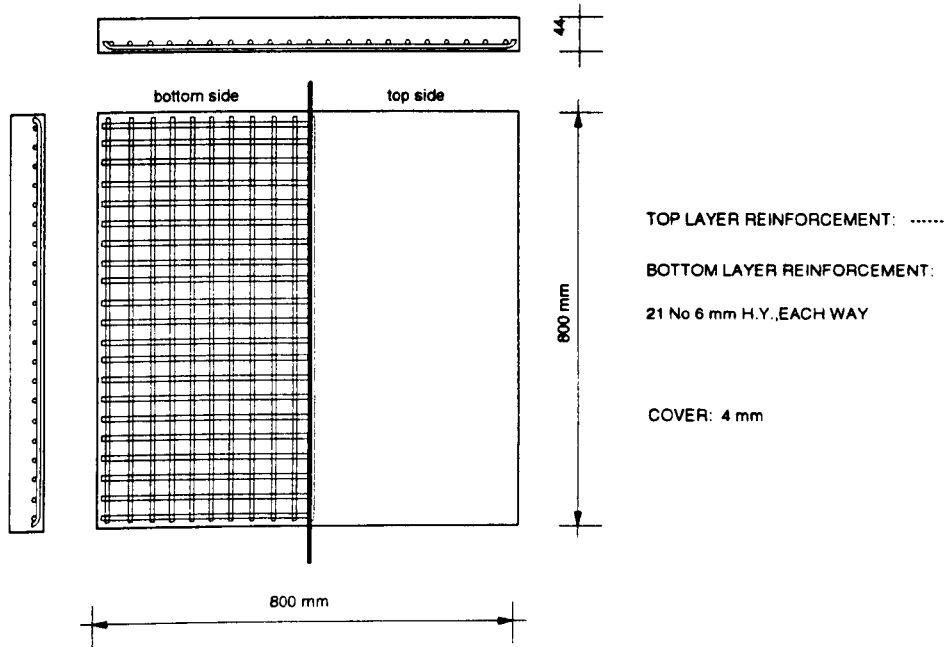
DATE: 5.06.90

SMALL SLAB S4

AGE OF SPECIMEN: 11 days

Cube compressive strength	N/mm ²	37.7	Cylinder tensile strength	N/mm ²	4.12	Age (days)	9
---------------------------	-------------------	------	---------------------------	-------------------	------	------------	---

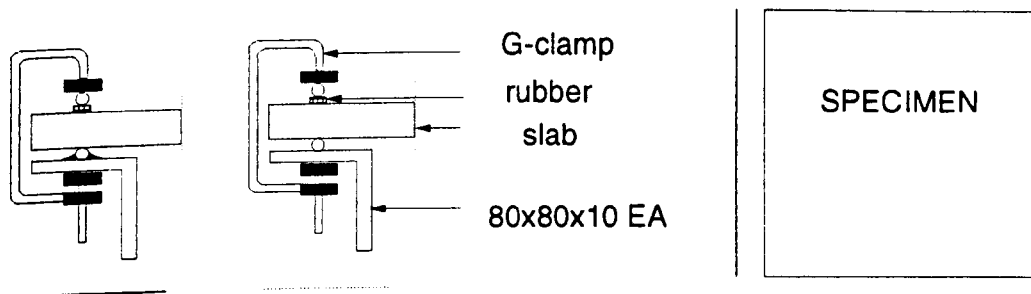
REINFORCEMENT:



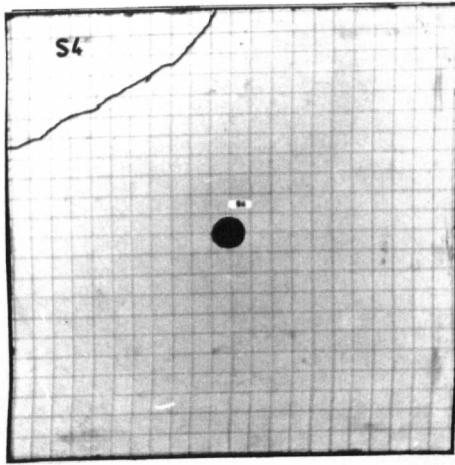
LOADING CONDITIONS

TYPE OF IMPACT	: HARD
HAMMER WEIGHT	: 33.7kg
HEIGHT OF DROP (ABOVE CENTRE OF SPECIMEN)	: 1850mm
IMPACT VELOCITY	: 5.76m/sec
THEORETICAL VELOCITY $V = \sqrt{2gh}$: 6.02m/sec
AREA OF THE PRESSURE BAR CROSS-SECTION	: 1962.5mm ²

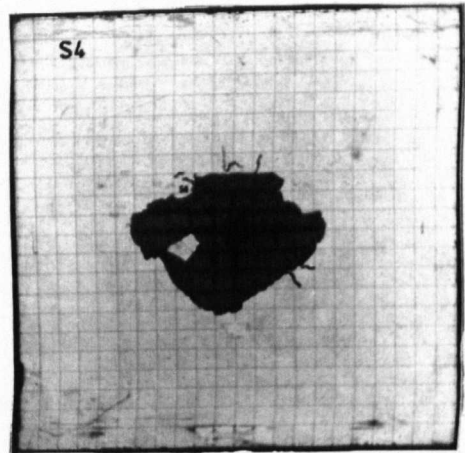
SUPPORTS



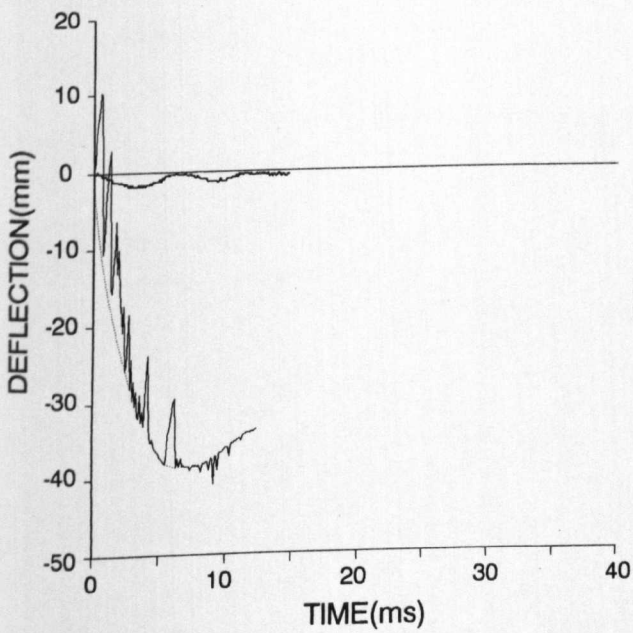
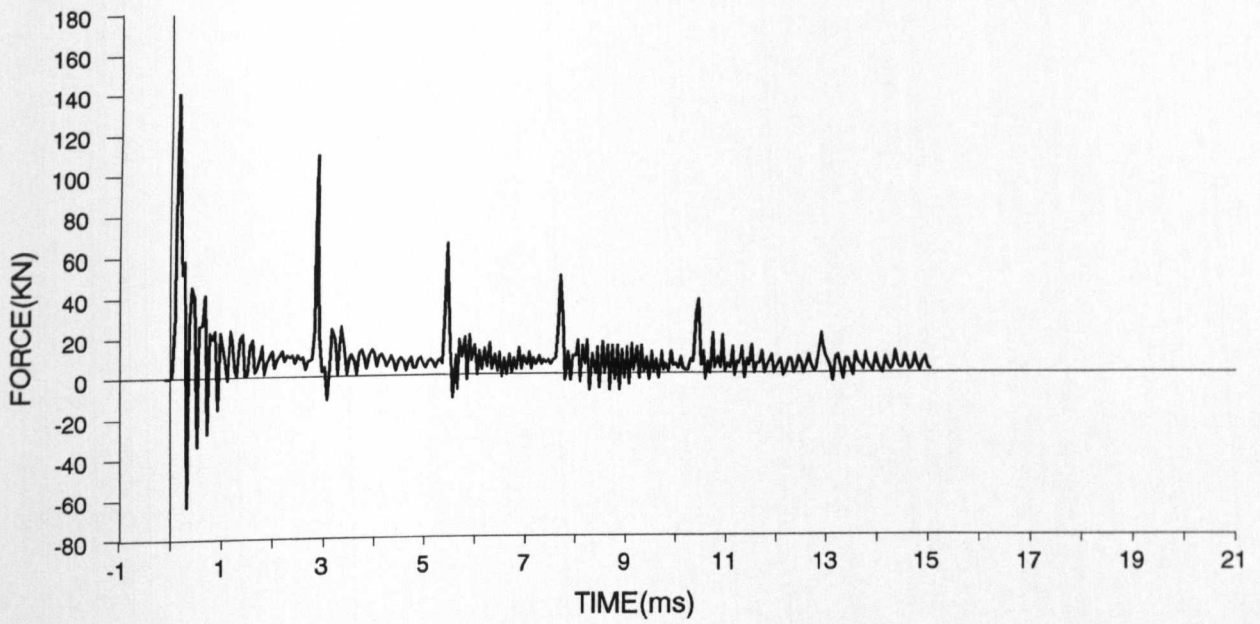
IMPACT TEST - SMALL SLAB - S4



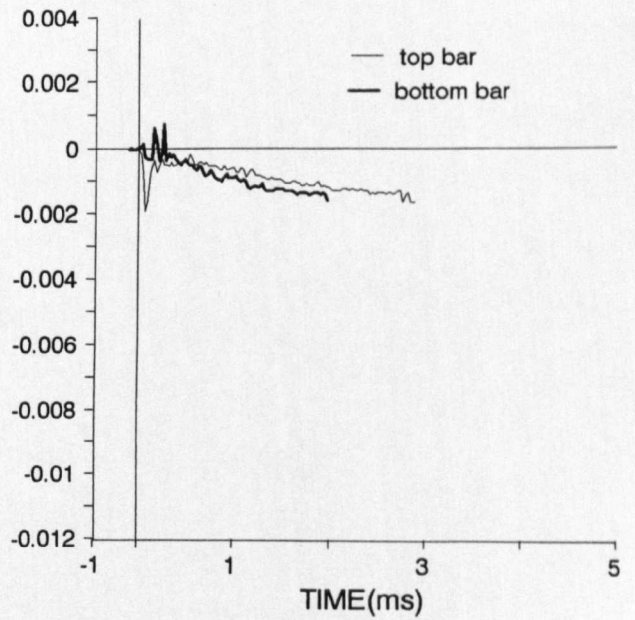
top side



bottom side



STRAIN



IMPACT TEST

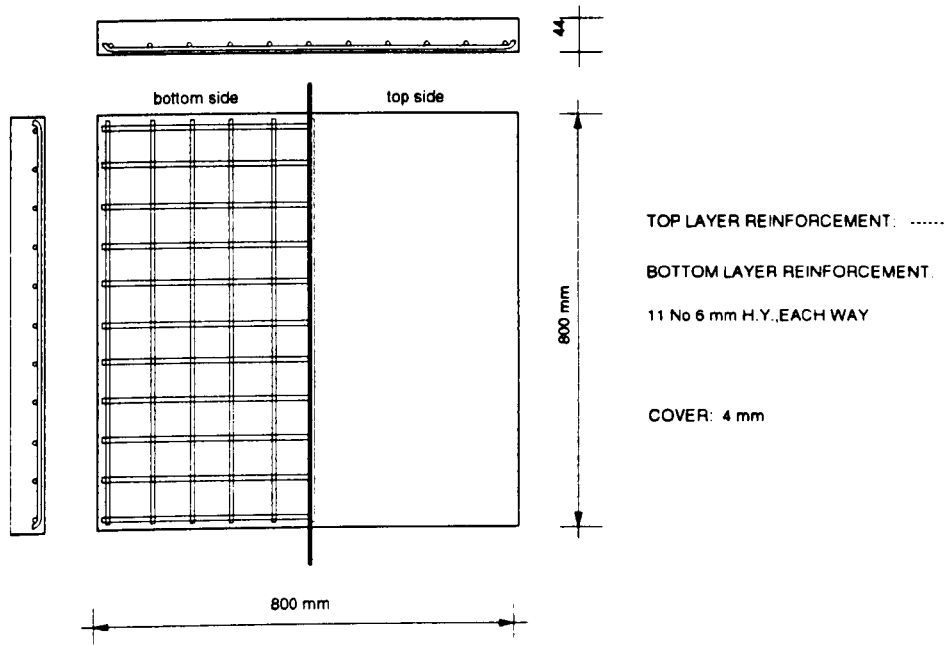
DATE: 12.06.90

SMALL SLAB S5

AGE OF SPECIMEN: 7 days

Cube compressive strength	N/mm ²	37.6	Cylinder tensile strength	N/mm ²	4.33	Age (days)	9
---------------------------	-------------------	------	---------------------------	-------------------	------	------------	---

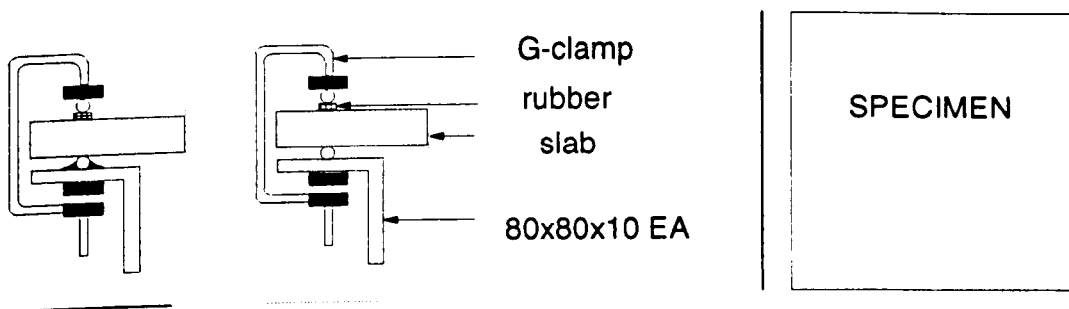
REINFORCEMENT:



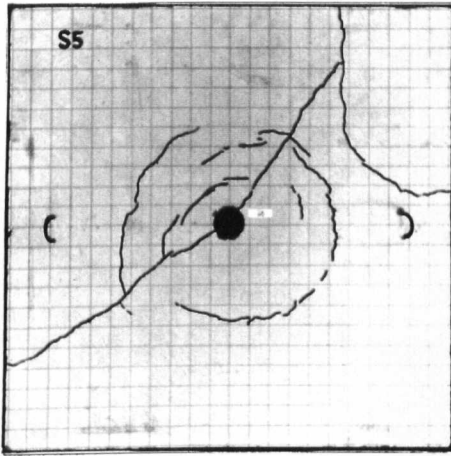
LOADING CONDITIONS

TYPE OF IMPACT	: HARD
HAMMER WEIGHT	: 33.7kg
HEIGHT OF DROP (ABOVE CENTRE OF SPECIMEN)	: 1850mm
IMPACT VELOCITY	: 5.73m/sec
THEORETICAL VELOCITY $V = \sqrt{2gh}$: 6.02m/sec
AREA OF THE PRESSURE BAR CROSS-SECTION	: 1962.5mm ²

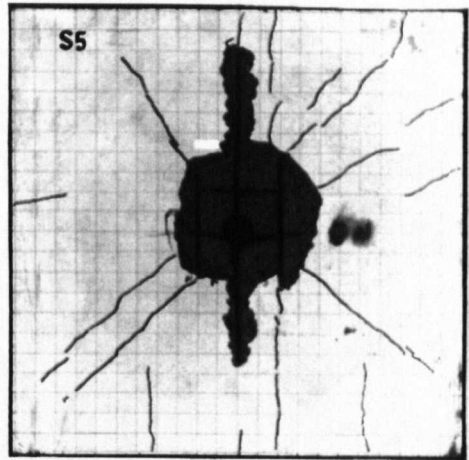
SUPPORTS



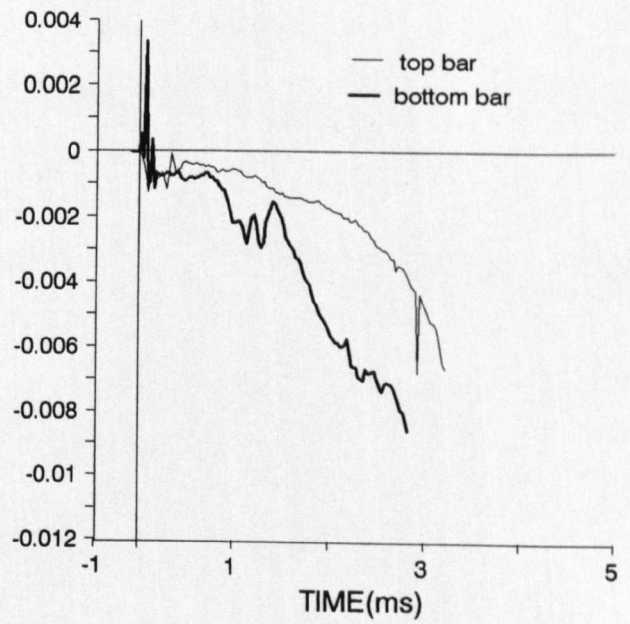
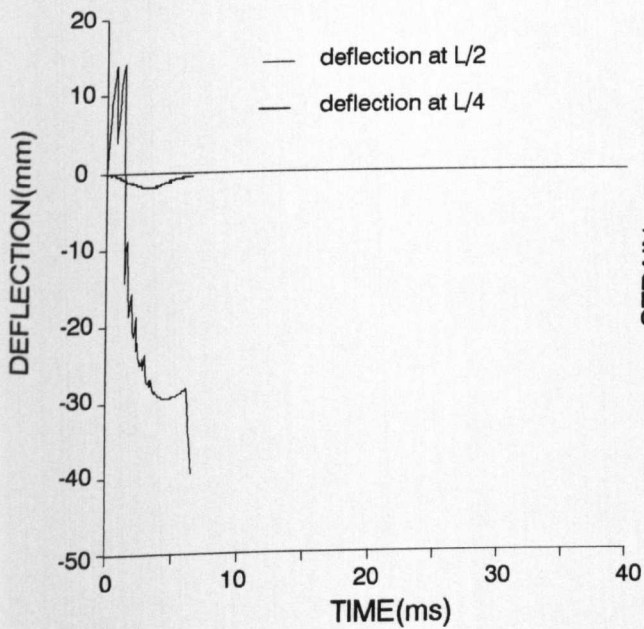
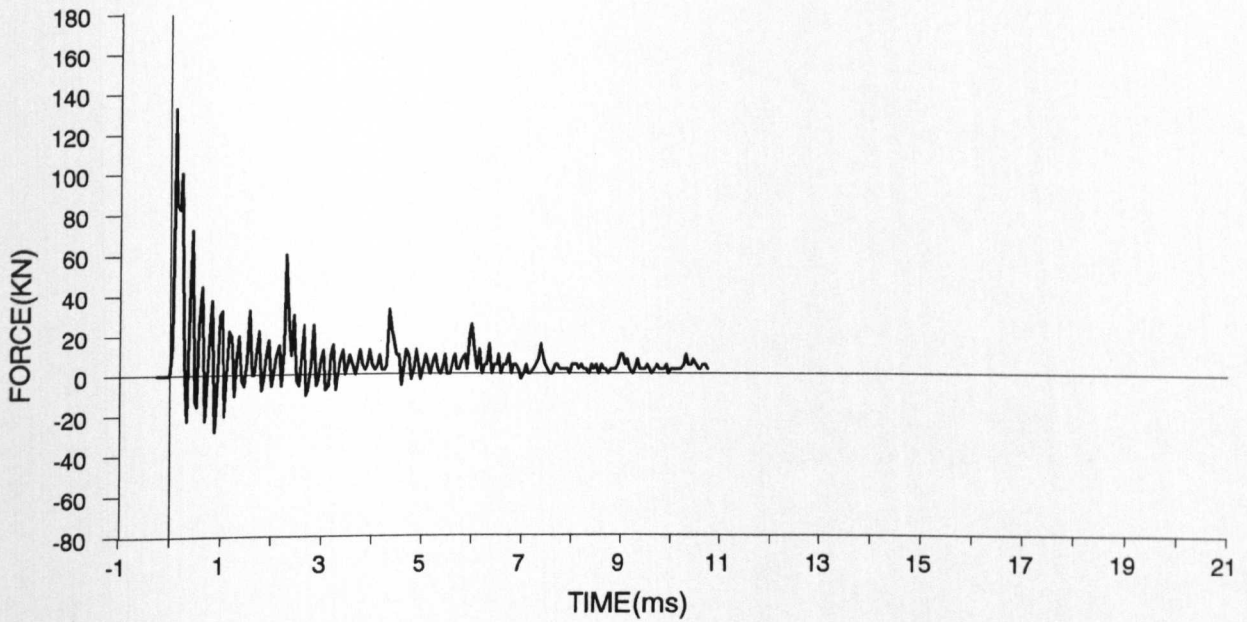
IMPACT TEST - SMALL SLAB - S5



top side



bottom side



IMPACT TEST

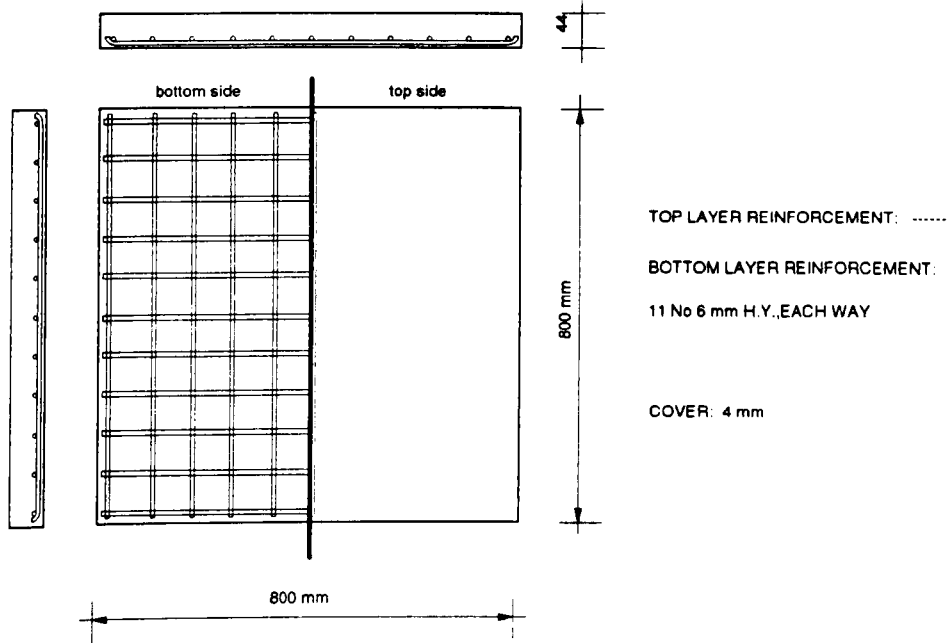
DATE: 13.06.90

SMALL SLAB S6

AGE OF SPECIMEN: 9 days

Cube compressive strength	N/mm ²	37.6	Cylinder tensile strength	N/mm ²	4.33	Age (days)	9
---------------------------	-------------------	------	---------------------------	-------------------	------	------------	---

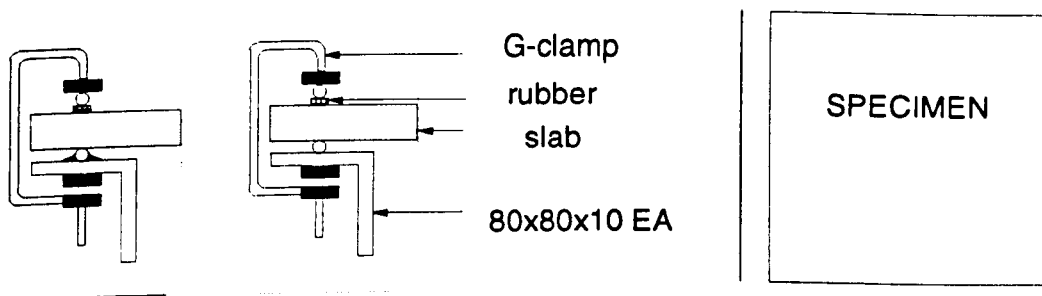
REINFORCEMENT:



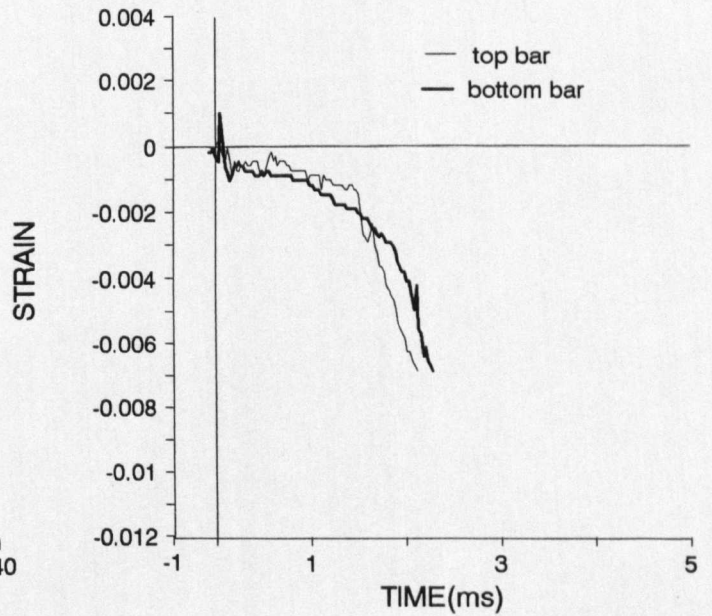
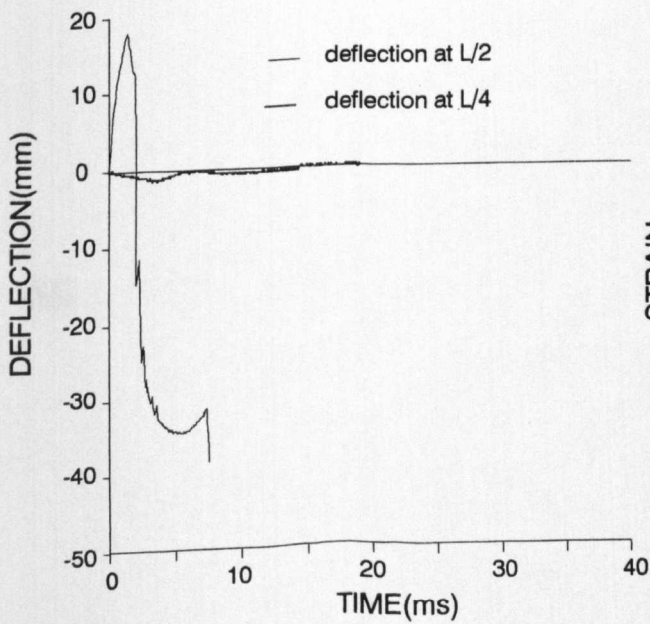
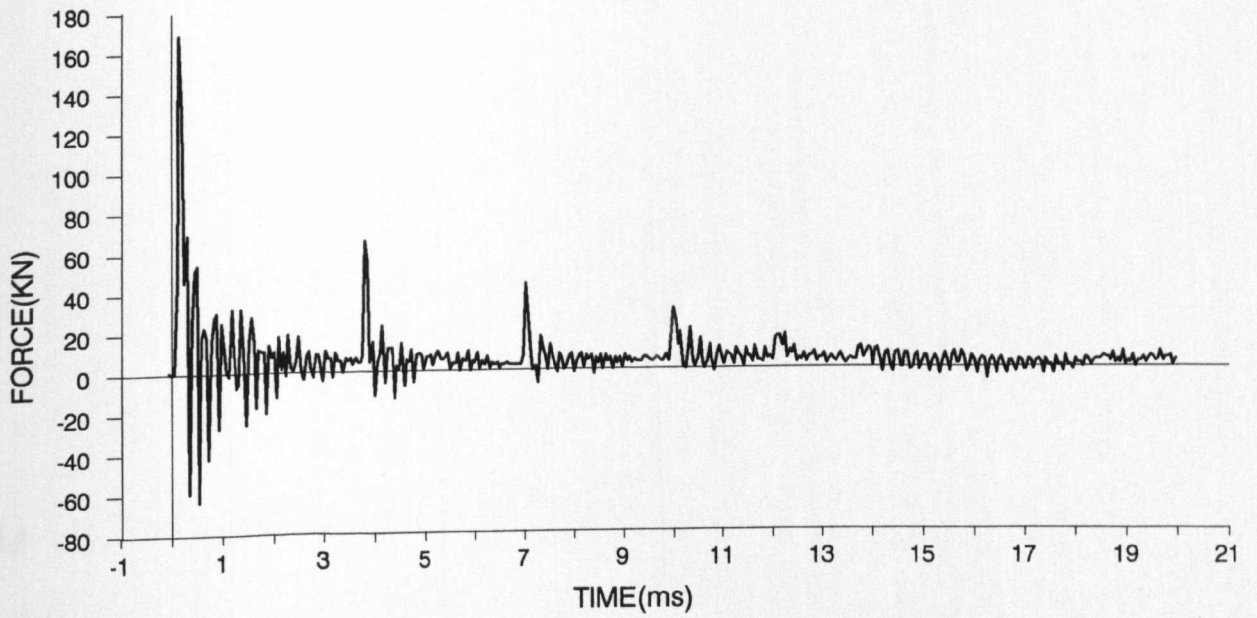
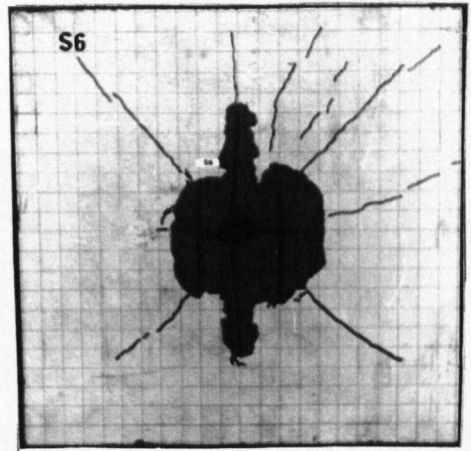
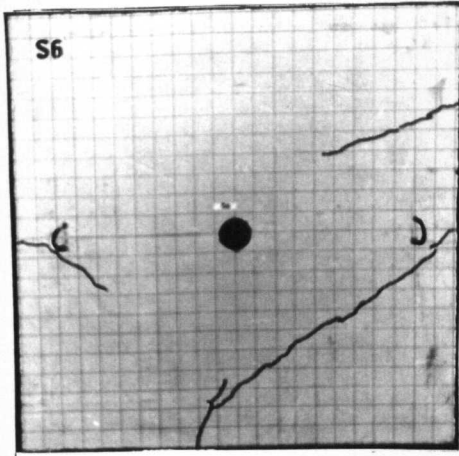
LOADING CONDITIONS

TYPE OF IMPACT	: HARD
HAMMER WEIGHT	: 33.7kg
HEIGHT OF DROP (ABOVE CENTRE OF SPECIMEN)	: 1850mm
IMPACT VELOCITY	: 5.63m/sec
THEORETICAL VELOCITY $V = \sqrt{2gh}$: 6.02m/sec
AREA OF THE PRESSURE BAR CROSS-SECTION	: 1962.5mm ²

SUPPORTS



IMPACT TEST - SMALL SLAB - S6



IMPACT TEST

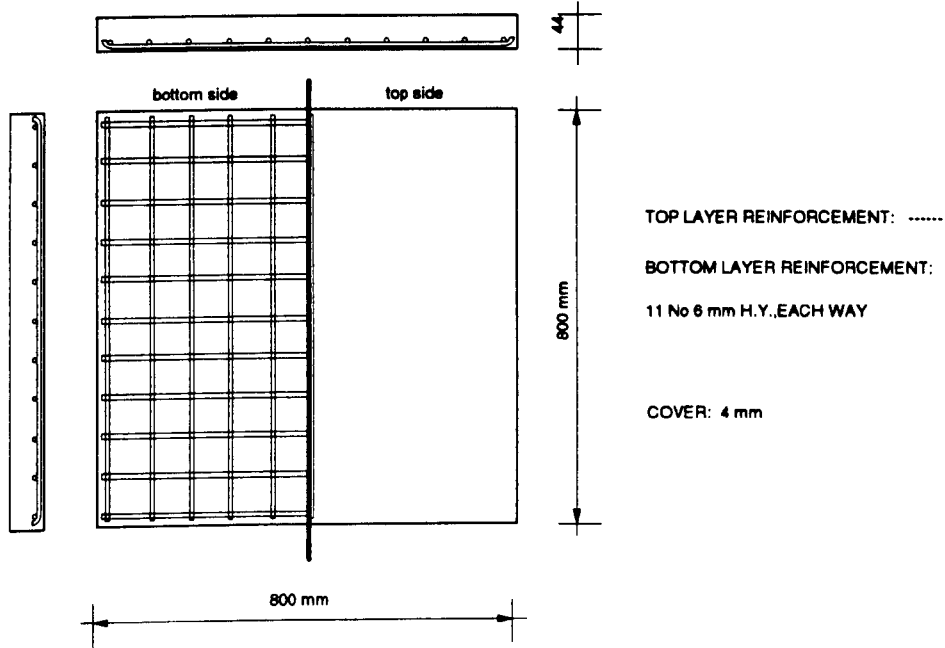
DATE: 21.06.90

SMALL SLAB S7

AGE OF SPECIMEN: 7 days

Cube compressive strength	N/mm ²	36.6	Cylinder tensile strength	N/mm ²	4.02	Age (days)	11
---------------------------	-------------------	------	---------------------------	-------------------	------	------------	----

REINFORCEMENT:

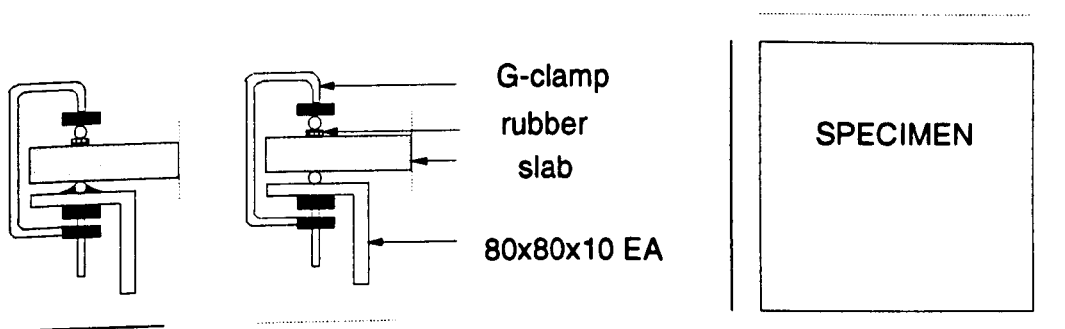


LOADING CONDITIONS

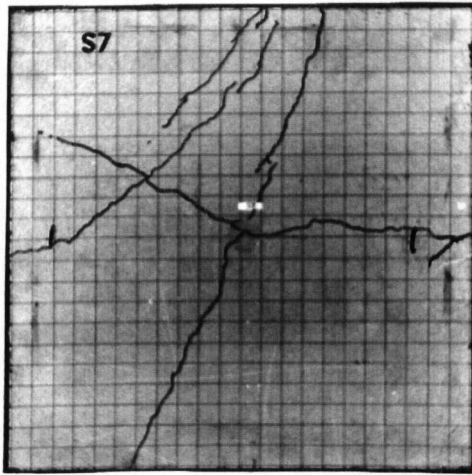
(2nd impact)

TYPE OF IMPACT	: SOFT
HAMMER WEIGHT	: 33.7kg
HEIGHT OF DROP (ABOVE CENTRE OF SPECIMEN)	: 1850mm
IMPACT VELOCITY	: 5.96m/sec
THEORETICAL VELOCITY $V = \sqrt{2gh}$: 6.02m/sec
AREA OF THE PRESSURE BAR CROSS-SECTION	: 1962.5mm ²

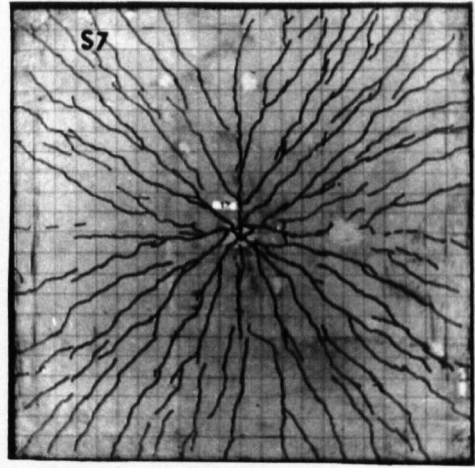
SUPPORTS



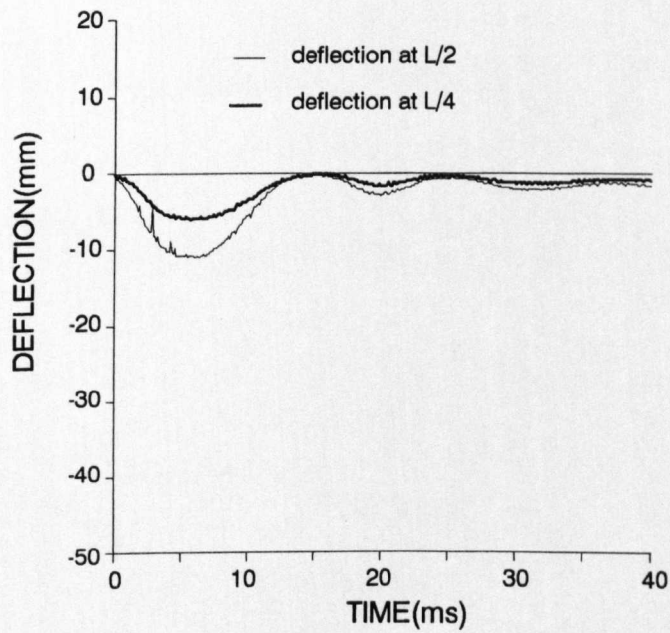
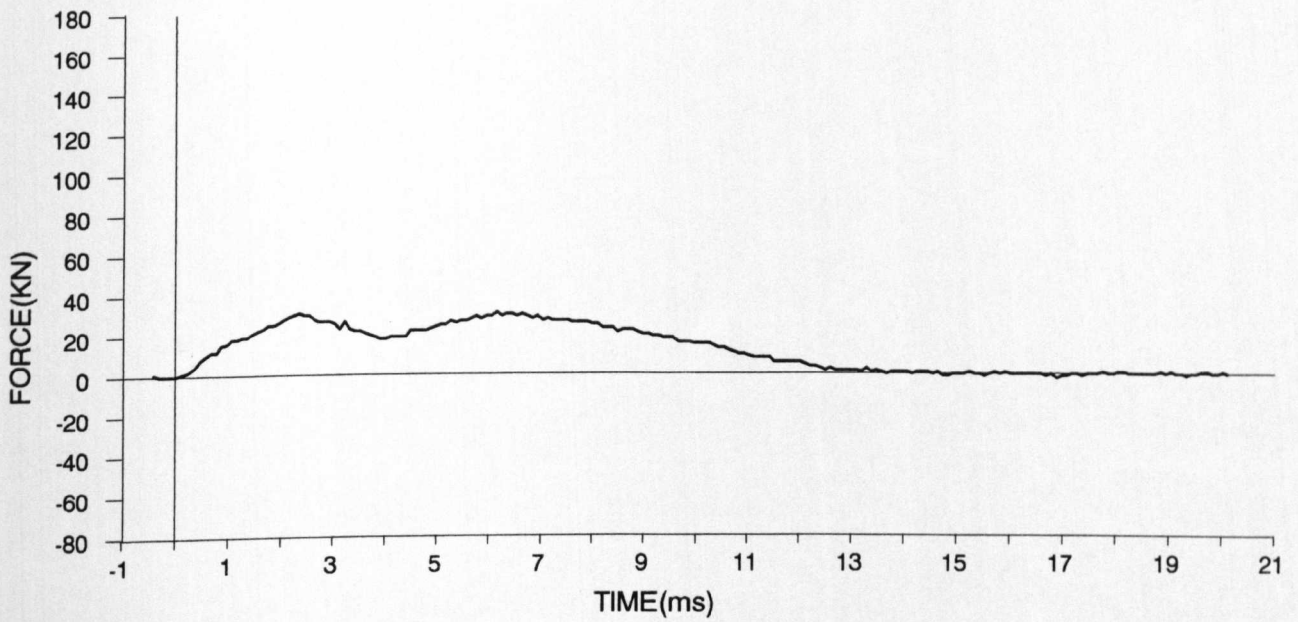
IMPACT TEST - SMALL SLAB - S7



top side



bottom side



IMPACT TEST

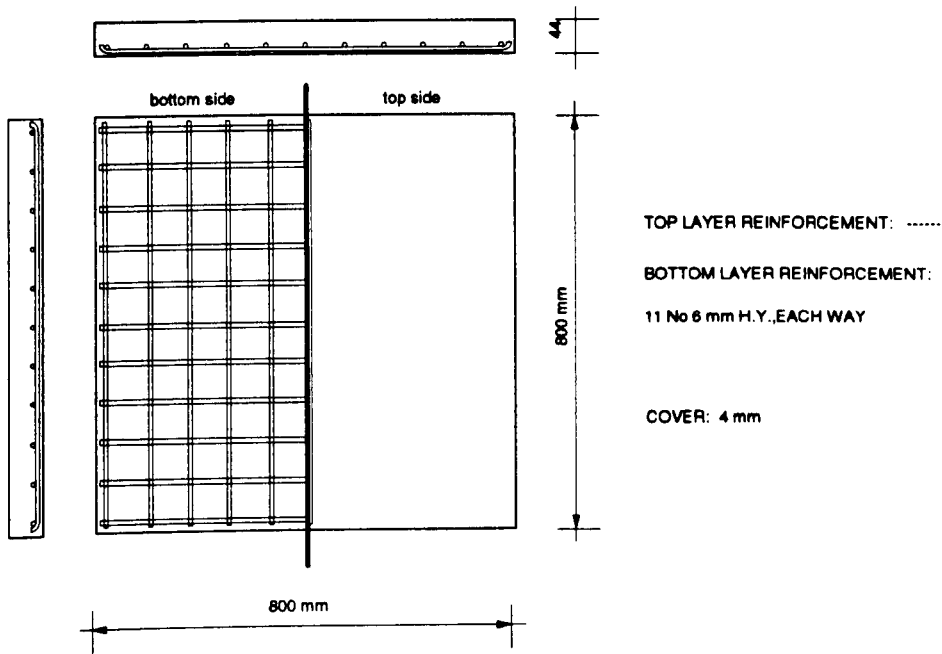
DATE: 22.06.90

SMALL SLAB S8

AGE OF SPECIMEN: 8 days

Cube compressive strength	N/mm ²	36.6	Cylinder tensile strength	N/mm ²	4.02	Age (days)	11
---------------------------	-------------------	------	---------------------------	-------------------	------	------------	----

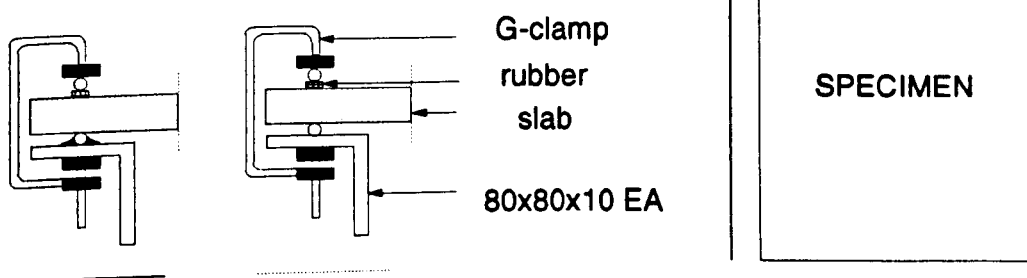
REINFORCEMENT:



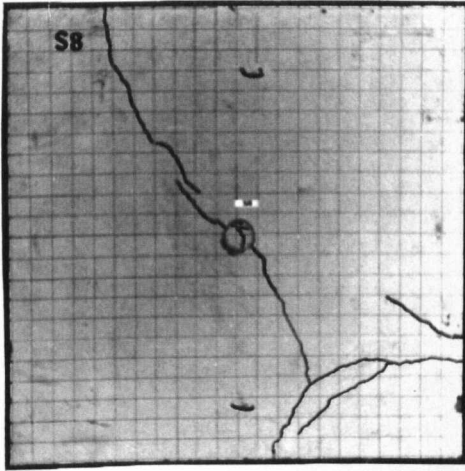
LOADING CONDITIONS

TYPE OF IMPACT	: SOFT
HAMMER WEIGHT	: 33.7kg
HEIGHT OF DROP (ABOVE CENTRE OF SPECIMEN)	: 1850mm
IMPACT VELOCITY	: 5.77m/sec
THEORETICAL VELOCITY $V = \sqrt{2gh}$: 6.02m/sec
AREA OF THE PRESSURE BAR CROSS-SECTION	: 1962.5mm ²

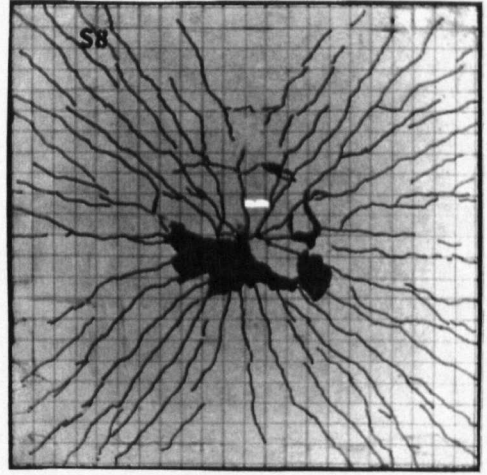
SUPPORTS



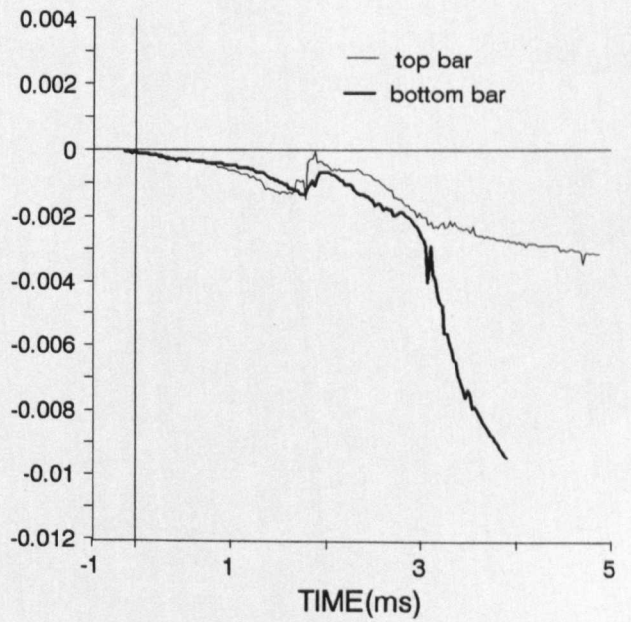
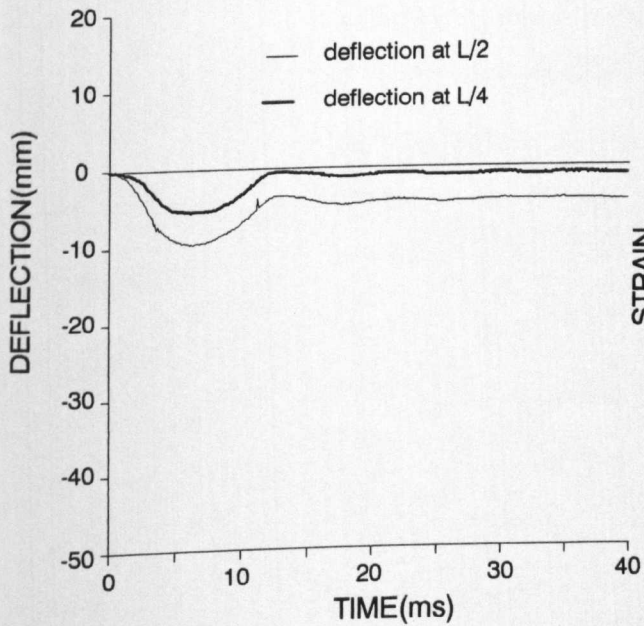
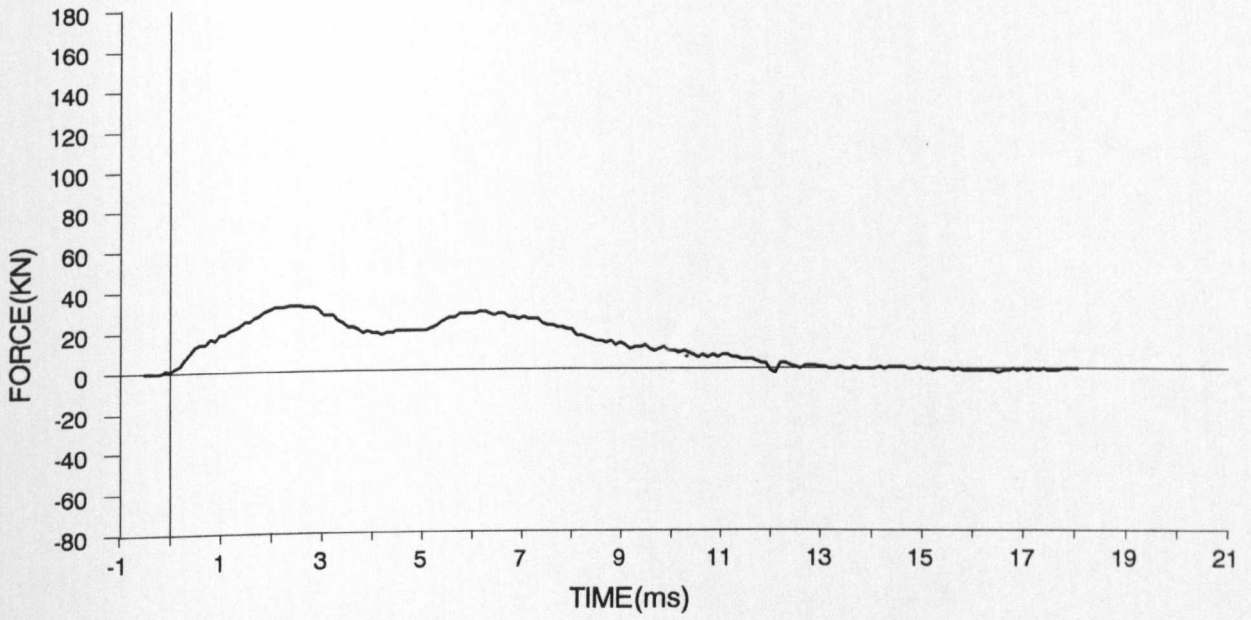
IMPACT TEST - SMALL SLAB - S8



top side



bottom side



IMPACT TEST

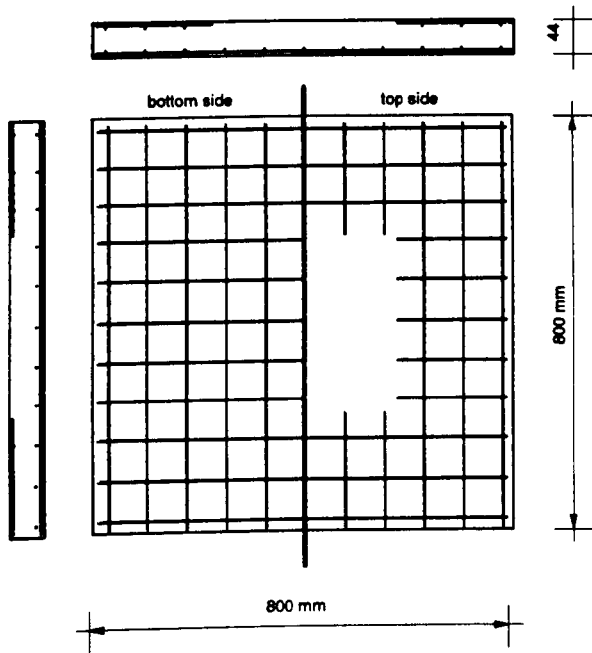
DATE: 32.01.93

SMALL SLAB S9

AGE OF SPECIMEN: 15 days

Cube compressive strength	N/mm ²	40.0	Cylinder tensile strength	N/mm ²	4.03	Age (days)	8
---------------------------	-------------------	------	---------------------------	-------------------	------	------------	---

REINFORCEMENT:

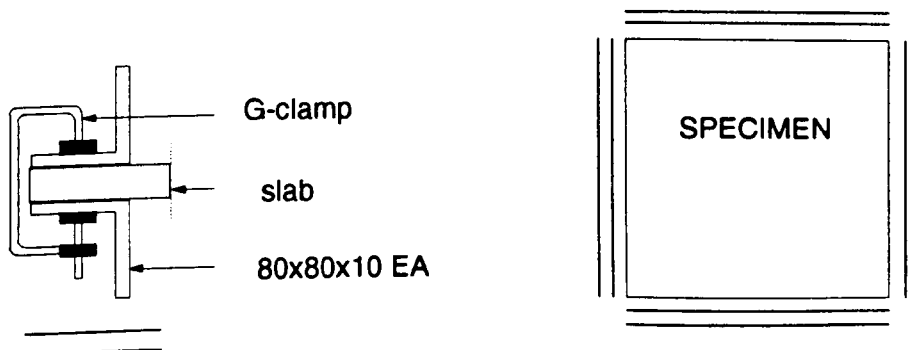


TOP LAYER REINFORCEMENT:
 R.MESH : 3.15 mm DIAM. / 76.2 mm CENTRES
 (WITHOUT CENTRAL REGION 400 X 400 mm)
 BOTTOM LAYER REINFORCEMENT:
 R.MESH : 3.15 mm DIAM. / 76.2 mm CENTRES
 COVER: 4 mm

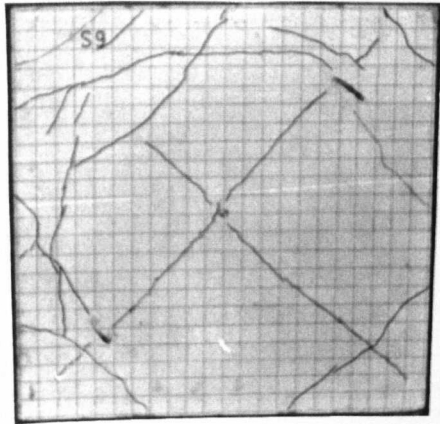
LOADING CONDITIONS

TYPE OF IMPACT : SOFT
 HAMMER WEIGHT : 33.7kg
 HEIGHT OF DROP (ABOVE CENTRE OF SPECIMEN) : 1500mm
 IMPACT VELOCITY : 5.19m/sec
 THEORETICAL VELOCITY $v = \sqrt{2gh}$: 5.42m/sec
 AREA OF THE PRESSURE BAR CROSS-SECTION : 1962.5mm²

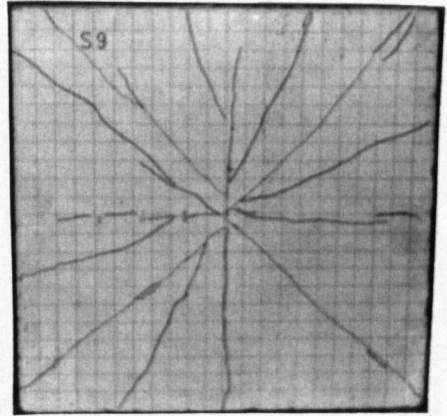
SUPPORTS



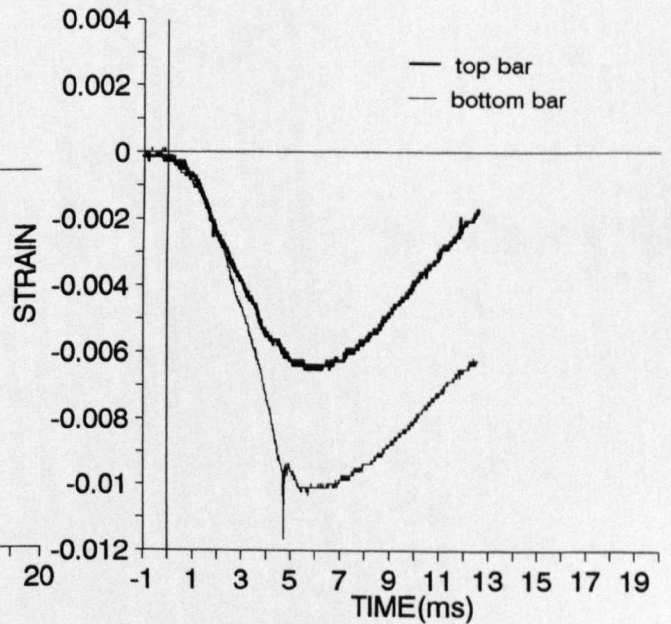
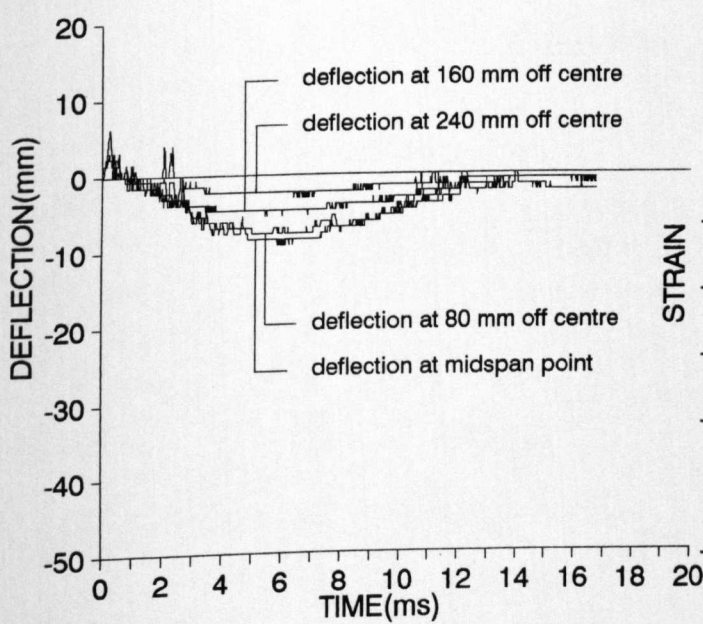
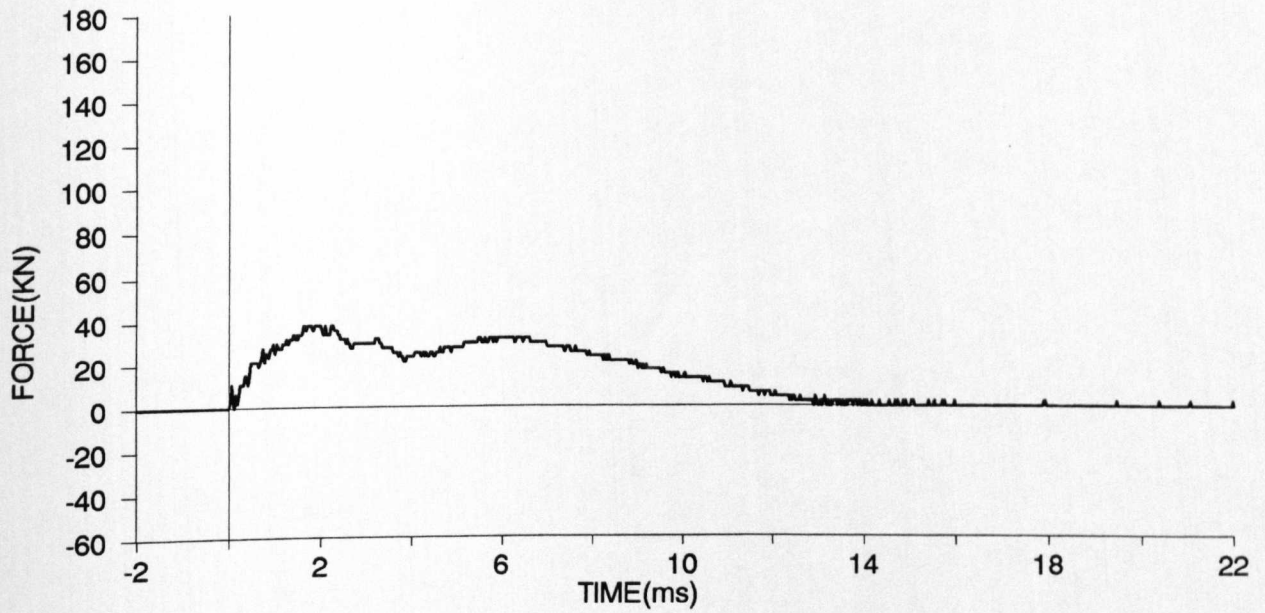
IMPACT TEST - SMALL SLAB - S9



top side



bottom side



IMPACT TEST

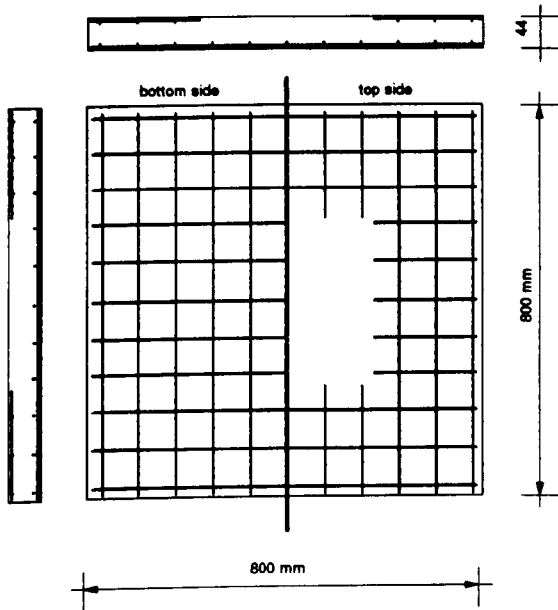
DATE: 2.02.93

SMALL SLAB S10

AGE OF SPECIMEN: 12 days

Cube compressive strength	N/mm ²	40.0	Cylinder tensile strength	N/mm ²	4.03	Age (days)	8
---------------------------	-------------------	------	---------------------------	-------------------	------	------------	---

REINFORCEMENT:



TOP LAYER REINFORCEMENT:

R.MESH : 3.15 mm DIAM. / 76.2 mm CENTRES

(WITHOUT CENTRAL REGION 400 X 400 mm)

BOTTOM LAYER REINFORCEMENT:

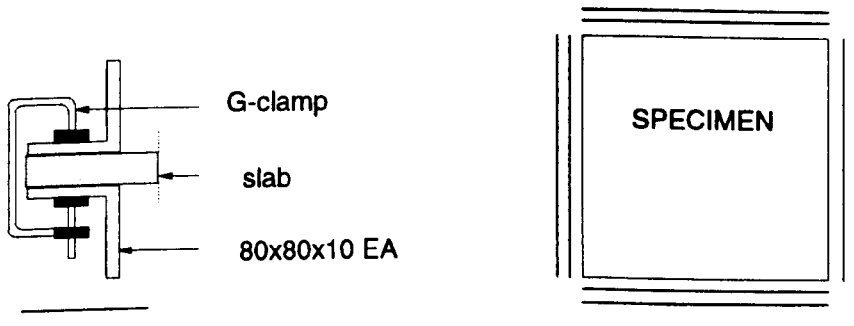
R.MESH : 3.15 mm DIAM. / 76.2 mm CENTRES

COVER: 4 mm

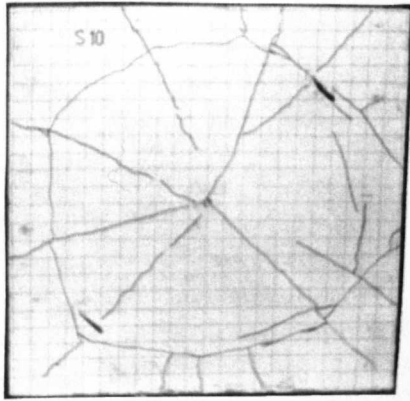
LOADING CONDITIONS

TYPE OF IMPACT	: SOFT
HAMMER WEIGHT	: 33.7kg
HEIGHT OF DROP (ABOVE CENTRE OF SPECIMEN)	: 2000mm
IMPACT VELOCITY	: 5.94m/sec
THEORETICAL VELOCITY $V = \sqrt{2gh}$: 6.26m/sec
AREA OF THE PRESSURE BAR CROSS-SECTION	: 1962.5mm ²

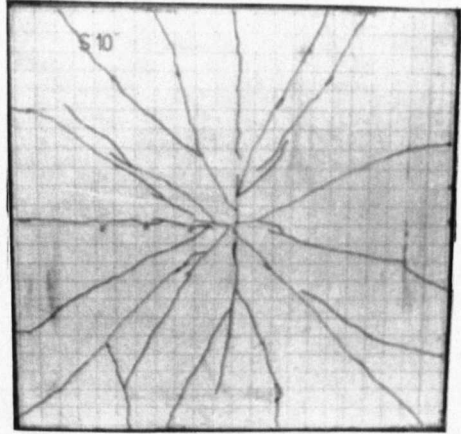
SUPPORTS



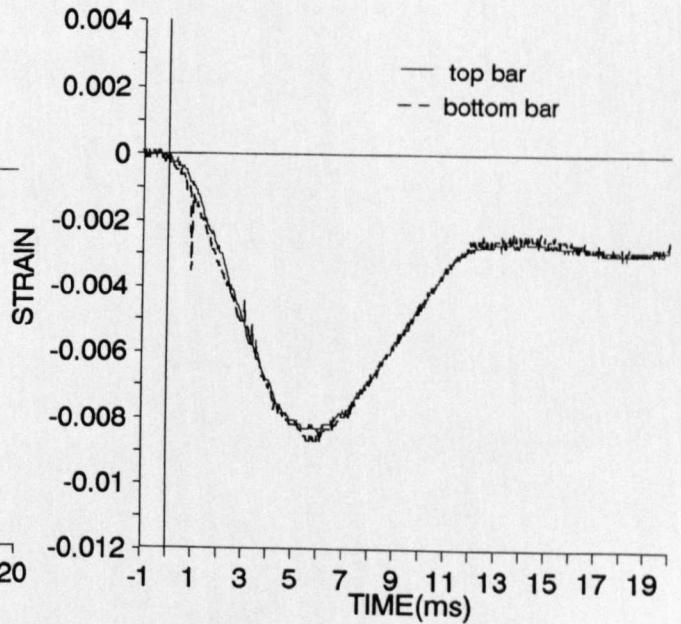
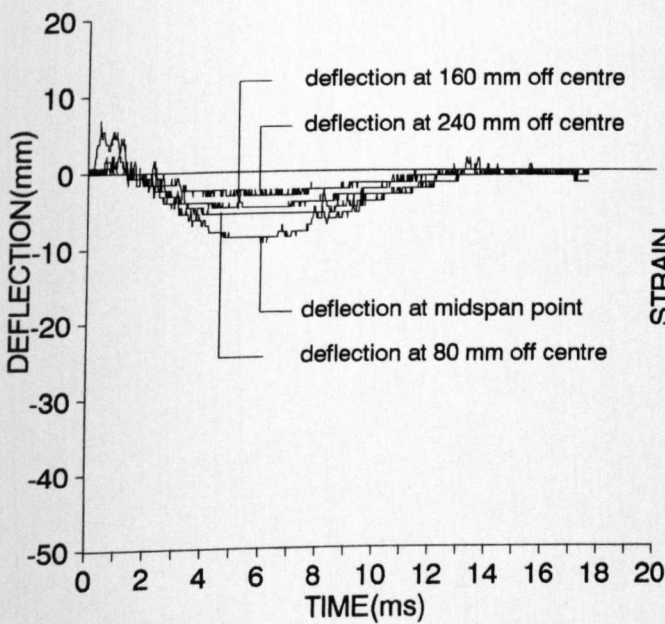
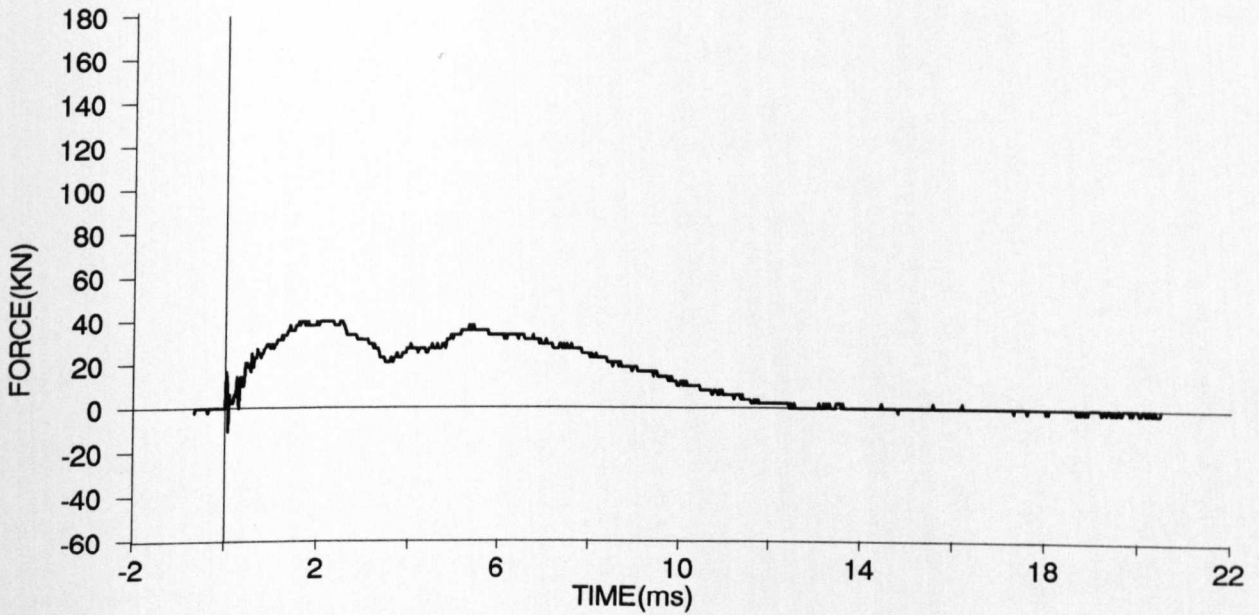
IMPACT TEST - SMALL SLAB - S10



top side



bottom side



IMPACT TEST

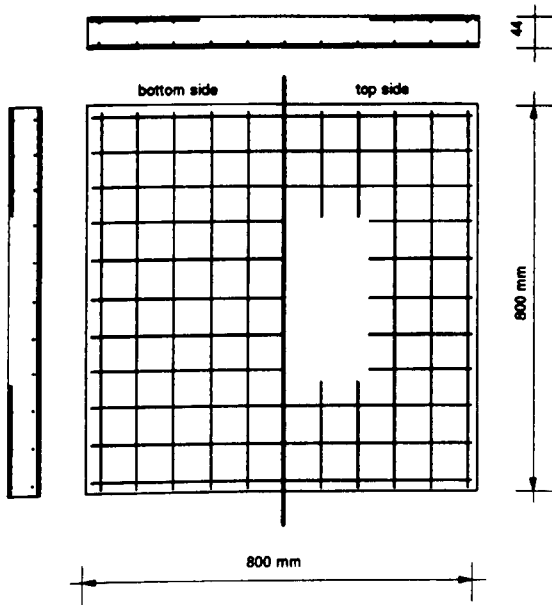
DATE: 18.02.93

SMALL SLAB S11

AGE OF SPECIMEN: 9 days

Cube compressive strength	N/mm ²	43.3	Cylinder tensile strength	N/mm ²	4.58	Age (days)	10
---------------------------	-------------------	------	---------------------------	-------------------	------	------------	----

REINFORCEMENT:



TOP LAYER REINFORCEMENT:

R.MESH : 3.15 mm DIAM. / 76.2 mm CENTRES
(WITHOUT CENTRAL REGION 400 X 400 mm)

BOTTOM LAYER REINFORCEMENT:

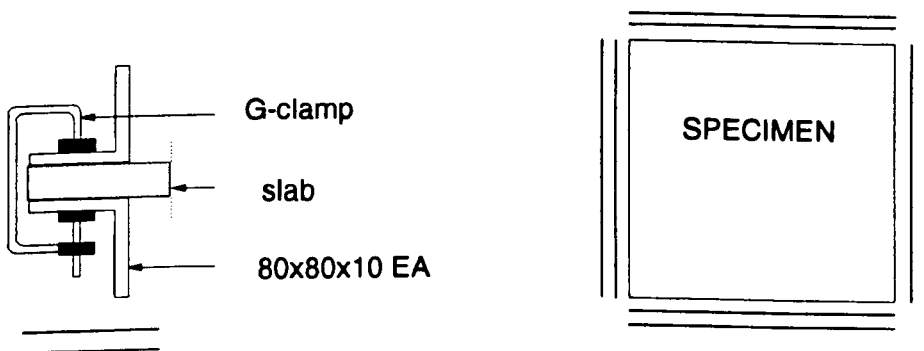
R.MESH : 3.15 mm DIAM. / 76.2 mm CENTRES

COVER: 4 mm

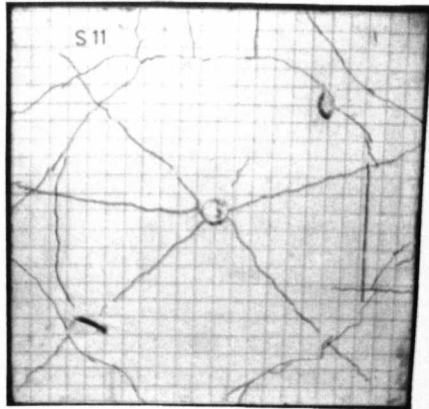
LOADING CONDITIONS

TYPE OF IMPACT	: SOFT
HAMMER WEIGHT	: 33.7kg
HEIGHT OF DROP (ABOVE CENTRE OF SPECIMEN)	: 2500mm
IMPACT VELOCITY	: 6.59m/sec
THEORETICAL VELOCITY $V = \sqrt{2gh}$: 7.00m/sec
AREA OF THE PRESSURE BAR CROSS-SECTION	: 1962.5mm ²

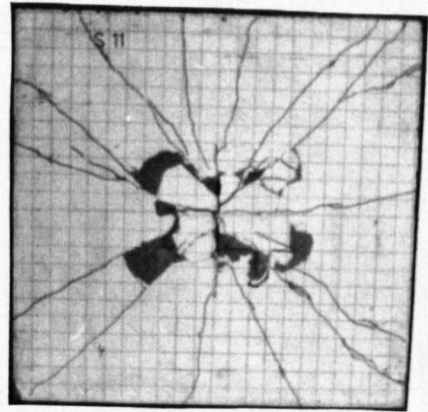
SUPPORTS



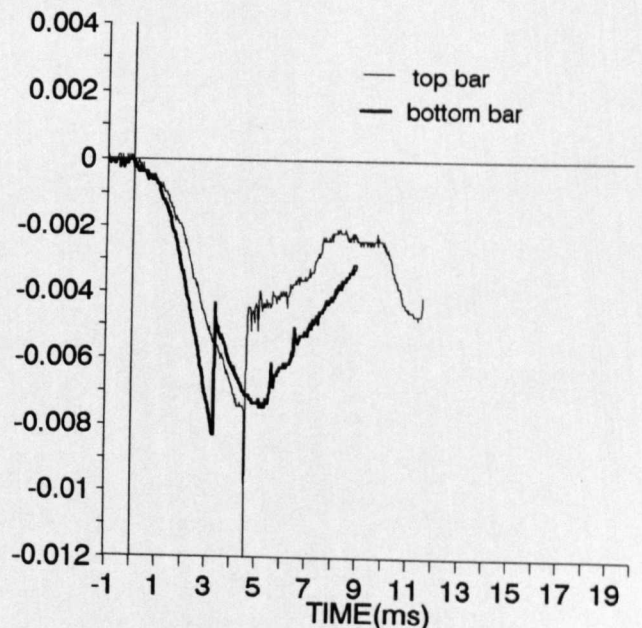
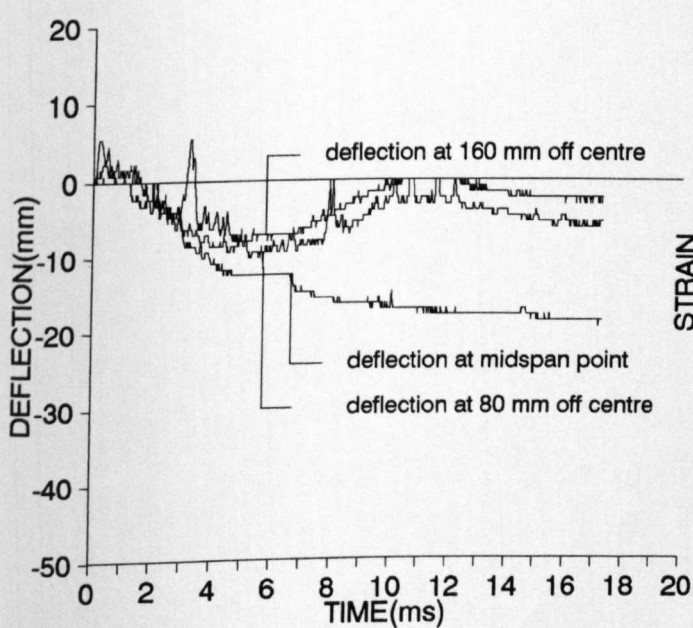
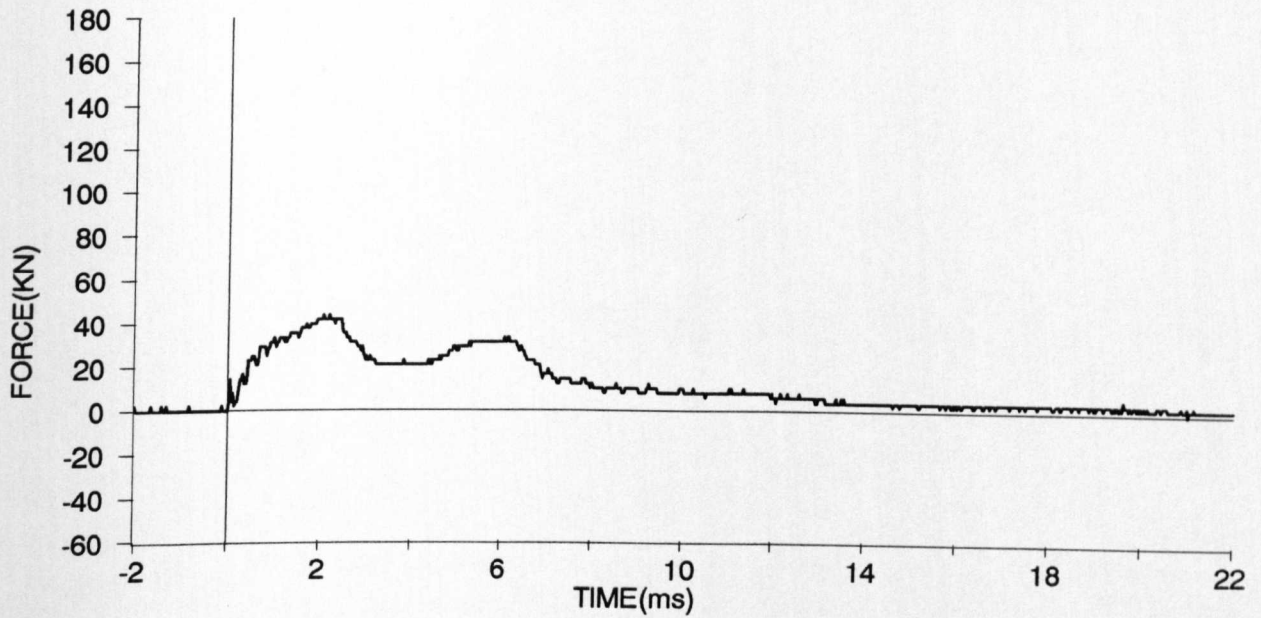
IMPACT TEST - SMALL SLAB - S11



top side



bottom side



IMPACT TEST

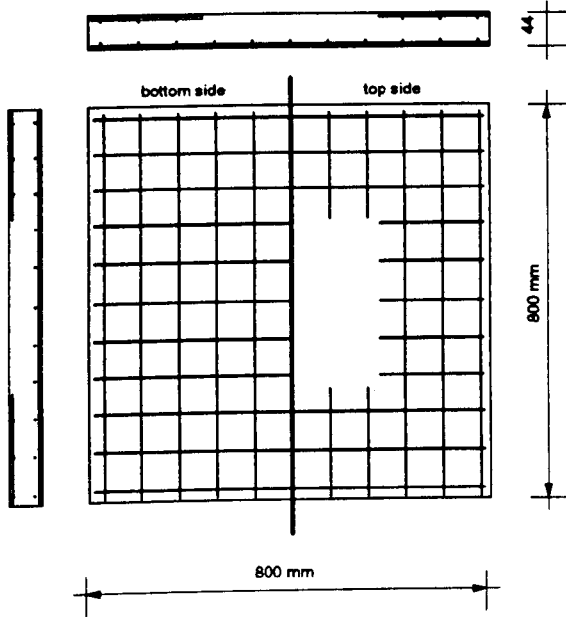
DATE: 19.02.93

SMALL SLAB S12

AGE OF SPECIMEN: 10 days

Cube compressive strength	N/mm ²	43.3	Cylinder tensile strength	N/mm ²	4.58	Age (days)	10
---------------------------	-------------------	------	---------------------------	-------------------	------	------------	----

REINFORCEMENT:



TOP LAYER REINFORCEMENT:

R.MESH : 3.15 mm DIAM. / 76.2 mm CENTRES
(WITHOUT CENTRAL REGION 400 X 400 mm)

BOTTOM LAYER REINFORCEMENT:

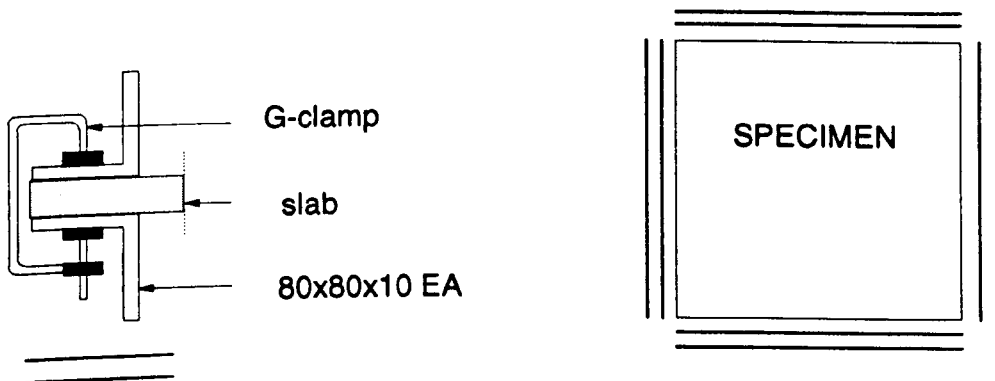
R.MESH : 3.15 mm DIAM. / 76.2 mm CENTRES

COVER: 4 mm

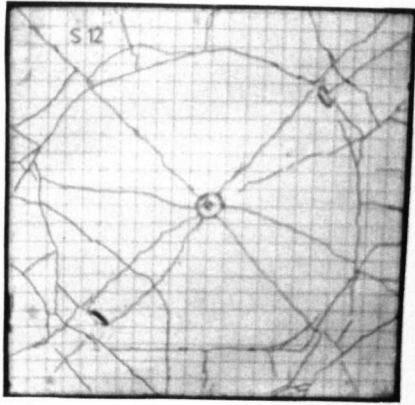
LOADING CONDITIONS

TYPE OF IMPACT	: SOFT
HAMMER WEIGHT	: 33.7kg
HEIGHT OF DROP (ABOVE CENTRE OF SPECIMEN)	: 3000mm
IMPACT VELOCITY	: 7.21m/sec
THEORETICAL VELOCITY $V = \sqrt{2gh}$: 7.67m/sec
AREA OF THE PRESSURE BAR CROSS-SECTION	: 1962.5mm ²

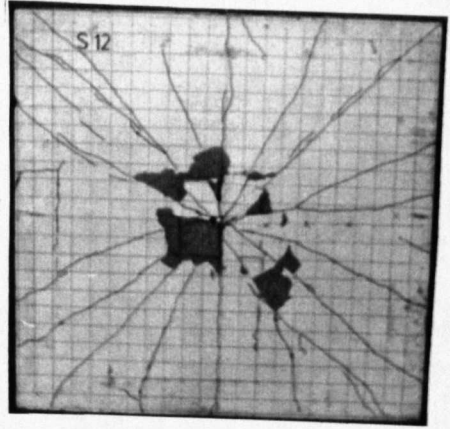
SUPPORTS



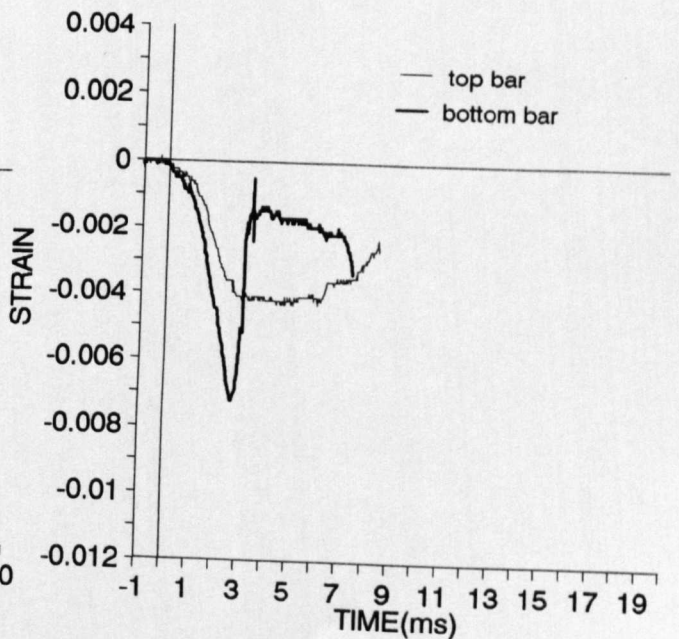
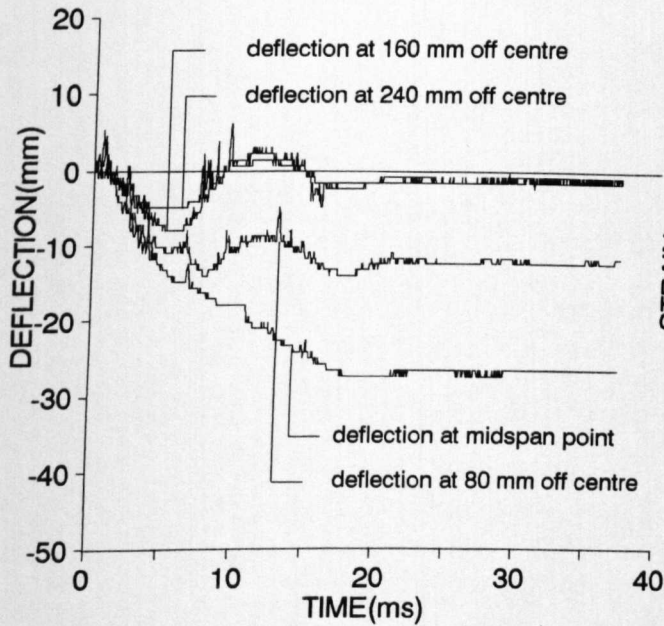
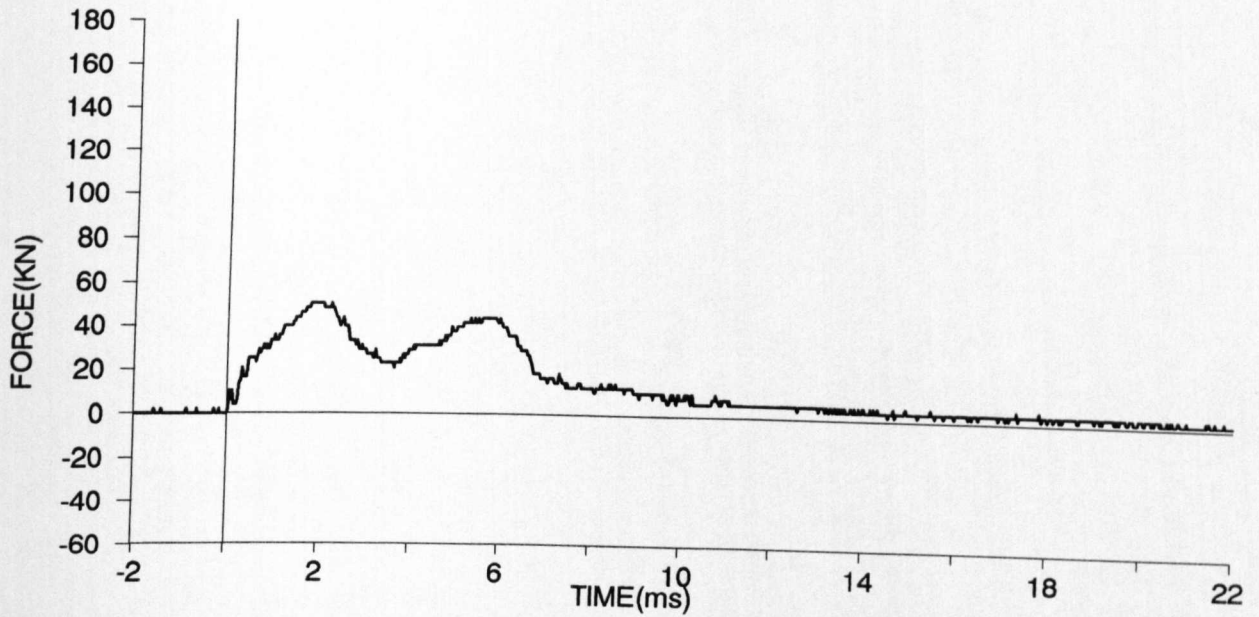
IMPACT TEST - SMALL SLAB - S12



top side



bottom side



IMPACT TEST

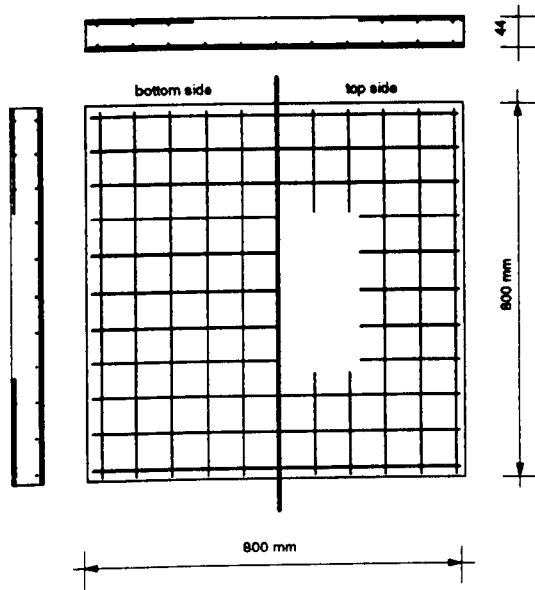
DATE: 19.02.93

SMALL SLAB S13

AGE OF SPECIMEN: 10 days

Cube compressive strength	N/mm ²	43.3	Cylinder tensile strength	N/mm ²	4.58	Age (days)	10
---------------------------	-------------------	------	---------------------------	-------------------	------	------------	----

REINFORCEMENT:



TOP LAYER REINFORCEMENT:

R.MESH : 3.15 mm DIAM. / 76.2 mm CENTRES
(WITHOUT CENTRAL REGION 400 X 400 mm)

BOTTOM LAYER REINFORCEMENT:

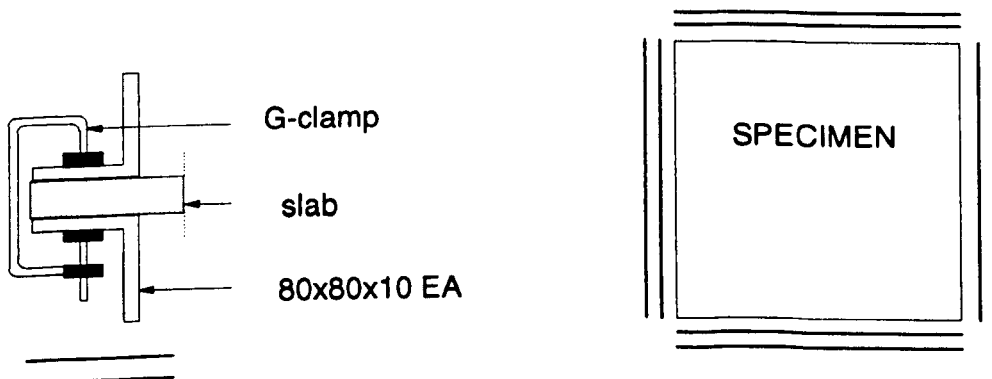
R.MESH : 3.15 mm DIAM. / 76.2 mm CENTRES

COVER: 4 mm

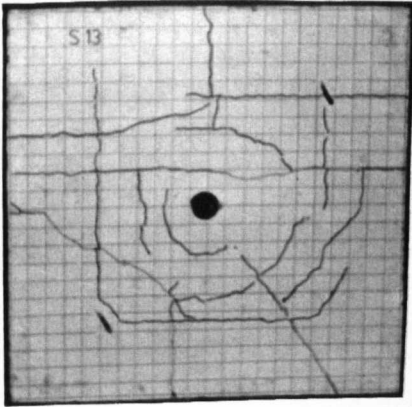
LOADING CONDITIONS

TYPE OF IMPACT	: HARD
HAMMER WEIGHT	: 33.7kg
HEIGHT OF DROP (ABOVE CENTRE OF SPECIMEN)	: 1500mm
IMPACT VELOCITY	: 5.17m/sec
THEORETICAL VELOCITY $V = \sqrt{2gh}$: 5.42m/sec
AREA OF THE PRESSURE BAR CROSS-SECTION	: 1962.5mm ²

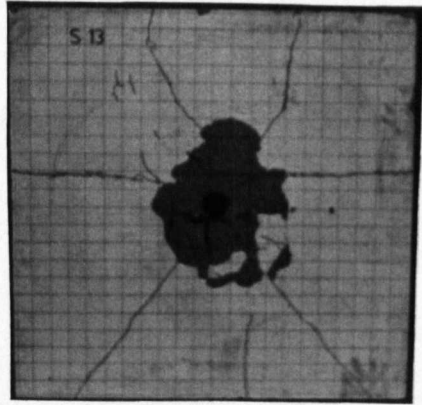
SUPPORTS



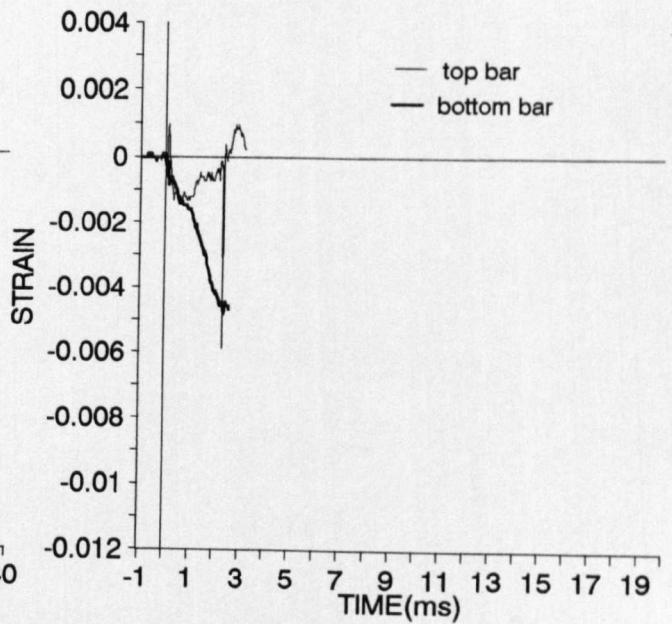
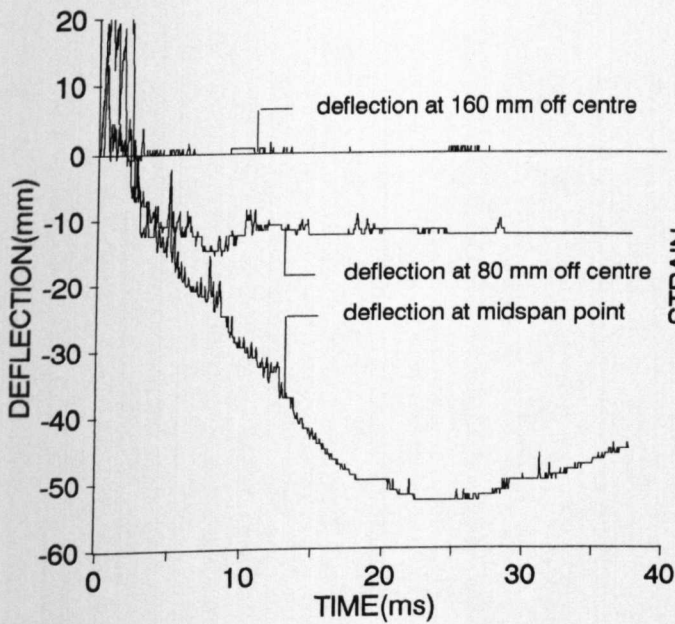
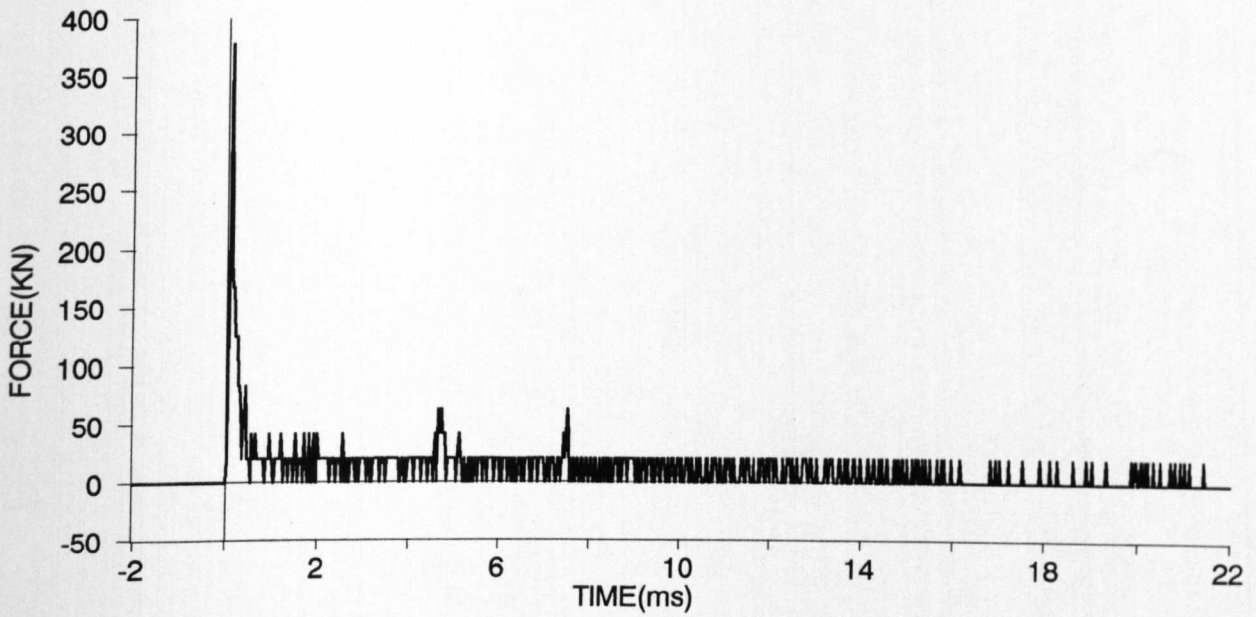
IMPACT TEST - SMALL SLAB - S13



top side



bottom side



IMPACT TEST

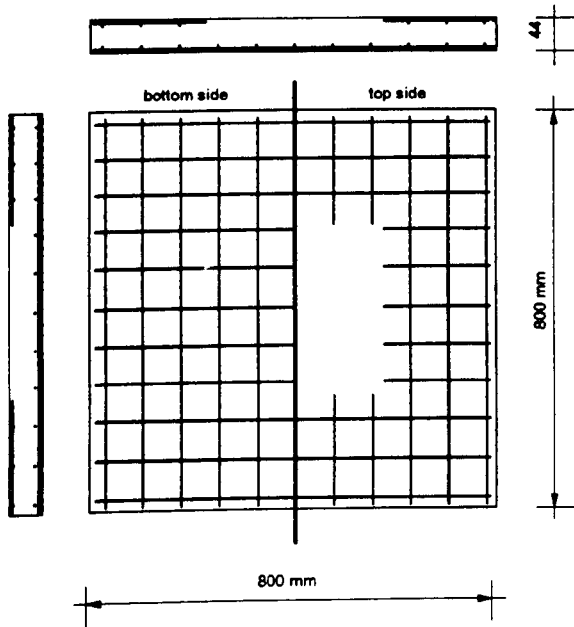
DATE: 3.03.93

SMALL SLAB S14

AGE OF SPECIMEN: 14 days

Cube compressive strength	N/mm ²	45.3	Cylinder tensile strength	N/mm ²	4.88	Age (days)	10
---------------------------	-------------------	------	---------------------------	-------------------	------	------------	----

REINFORCEMENT:



TOP LAYER REINFORCEMENT:

R.MESH : 3.15 mm DIAM. / 76.2 mm CENTRES
(WITHOUT CENTRAL REGION 400 X 400 mm)

BOTTOM LAYER REINFORCEMENT:

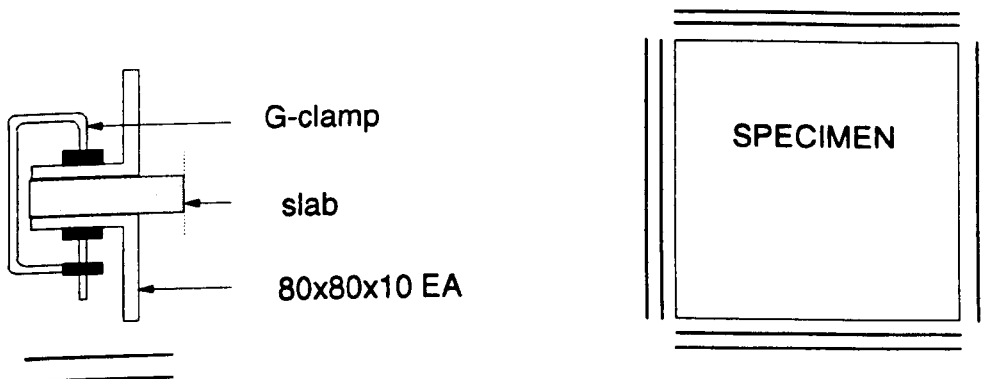
R.MESH : 3.15 mm DIAM. / 76.2 mm CENTRES

COVER: 4 mm

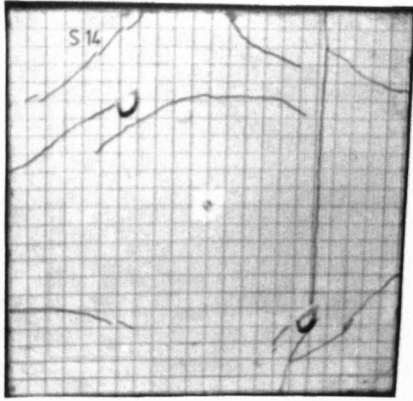
LOADING CONDITIONS

TYPE OF IMPACT	: SOFT
HAMMER WEIGHT	: 33.7kg
HEIGHT OF DROP (ABOVE CENTRE OF SPECIMEN)	: 500mm
IMPACT VELOCITY	: 2.97m/sec
THEORETICAL VELOCITY $V = \sqrt{2gh}$: 3.13m/sec
AREA OF THE PRESSURE BAR CROSS-SECTION	: 1962.5mm ²

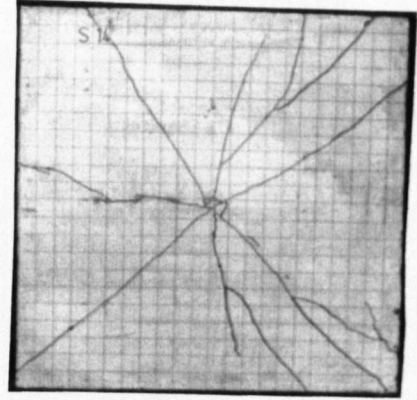
SUPPORTS



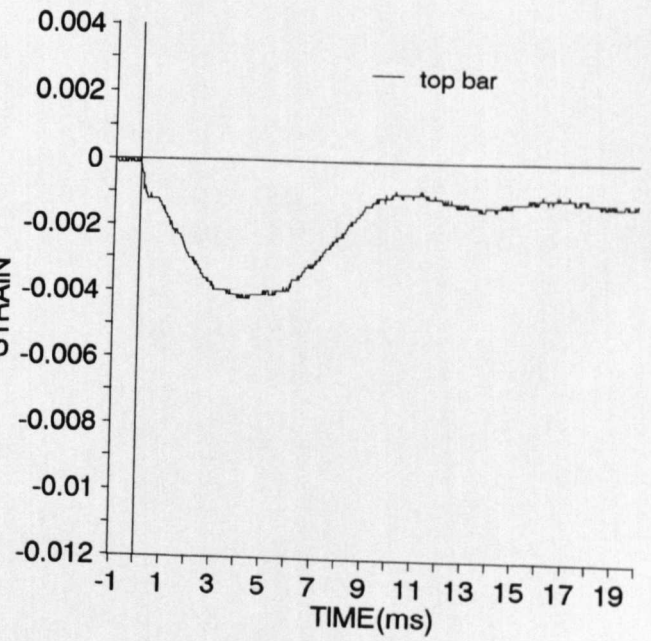
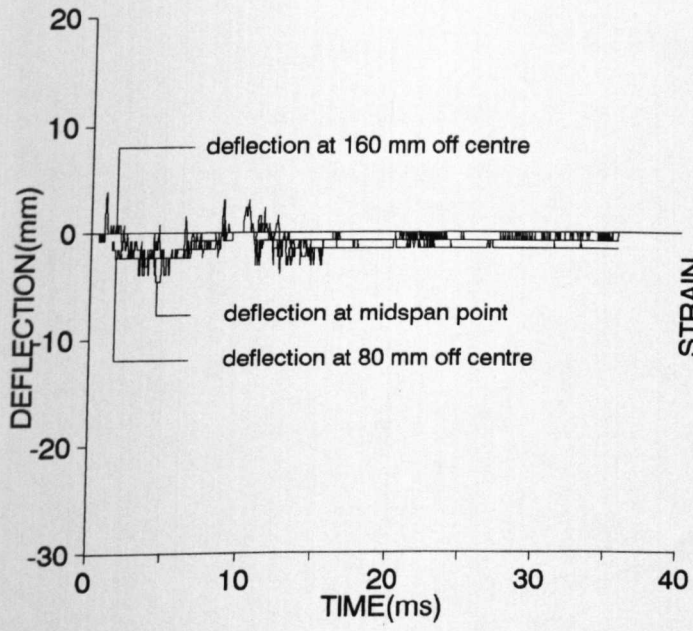
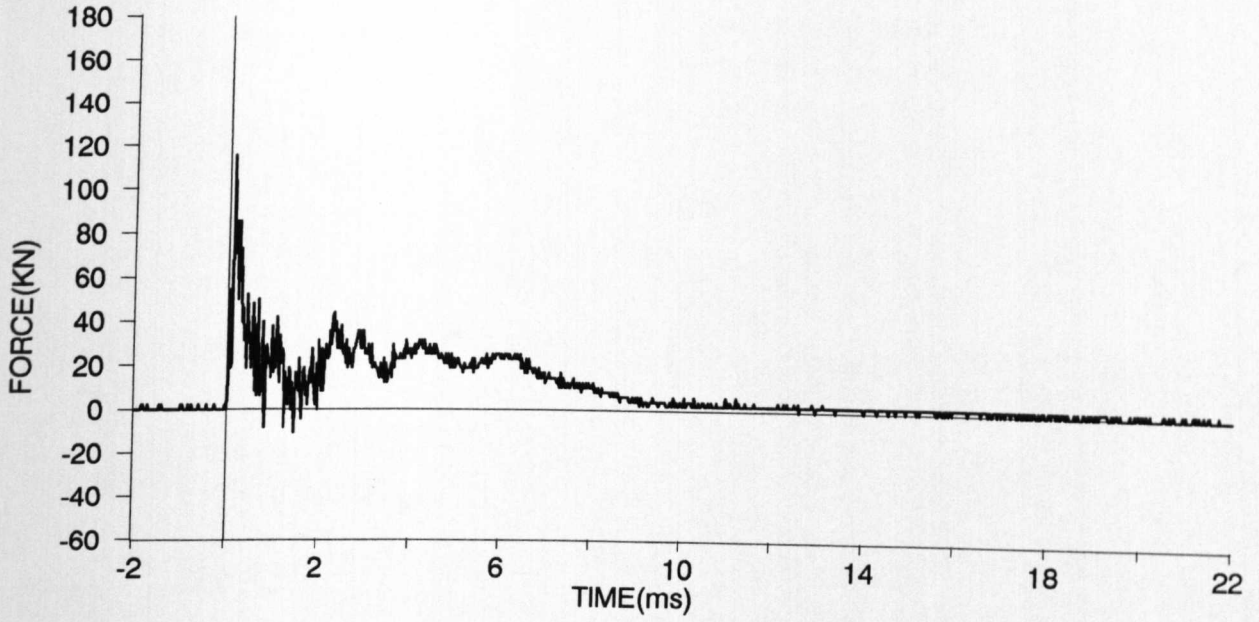
IMPACT TEST - SMALL SLAB - S14



top side



bottom side



IMPACT TEST

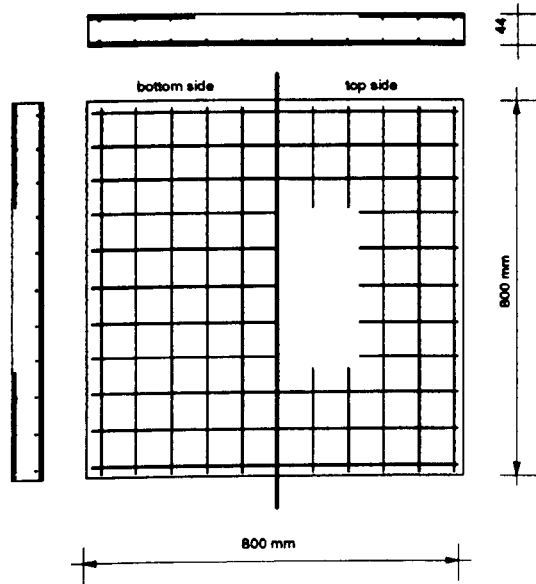
DATE: 3.03.93

SMALL SLAB S15

AGE OF SPECIMEN: 14days

Cube compressive strength	N/mm ²	45.3	Cylinder tensile strength	N/mm ²	4.88	Age (days)	10
---------------------------	-------------------	------	---------------------------	-------------------	------	------------	----

REINFORCEMENT:



TOP LAYER REINFORCEMENT:

R.MESH : 3.15 mm DIAM. / 76.2 mm CENTRES
(WITHOUT CENTRAL REGION 400 X 400 mm)

BOTTOM LAYER REINFORCEMENT:

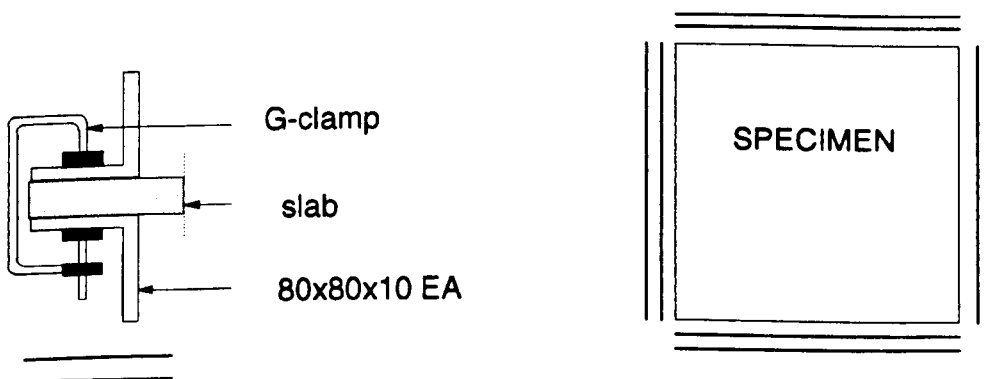
R.MESH : 3.15 mm DIAM. / 76.2 mm CENTRES

COVER: 4 mm

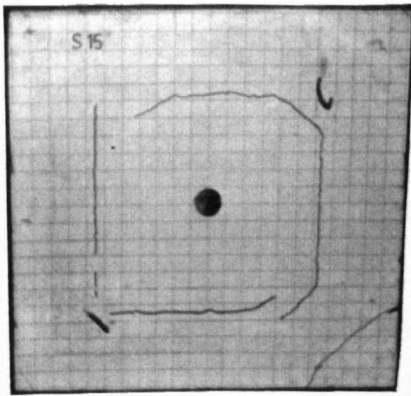
LOADING CONDITIONS

TYPE OF IMPACT	: HARD
HAMMER WEIGHT	: 33.7kg
HEIGHT OF DROP (ABOVE CENTRE OF SPECIMEN)	: 1000mm
IMPACT VELOCITY	: 4.30m/sec
THEORETICAL VELOCITY $v = \sqrt{2gh}$: 4.42m/sec
AREA OF THE PRESSURE BAR CROSS-SECTION	: 1962.5mm ²

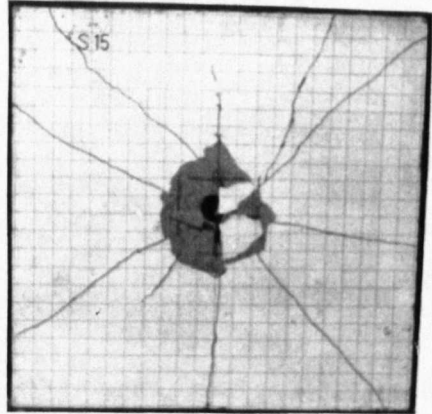
SUPPORTS



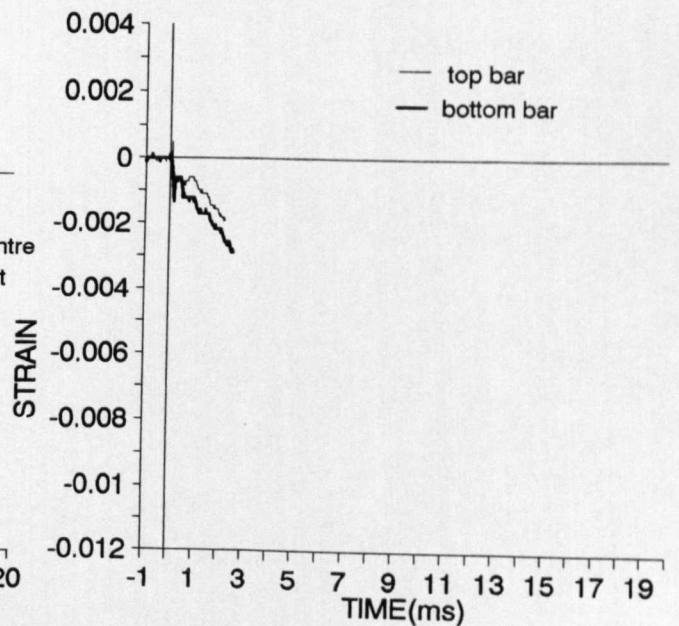
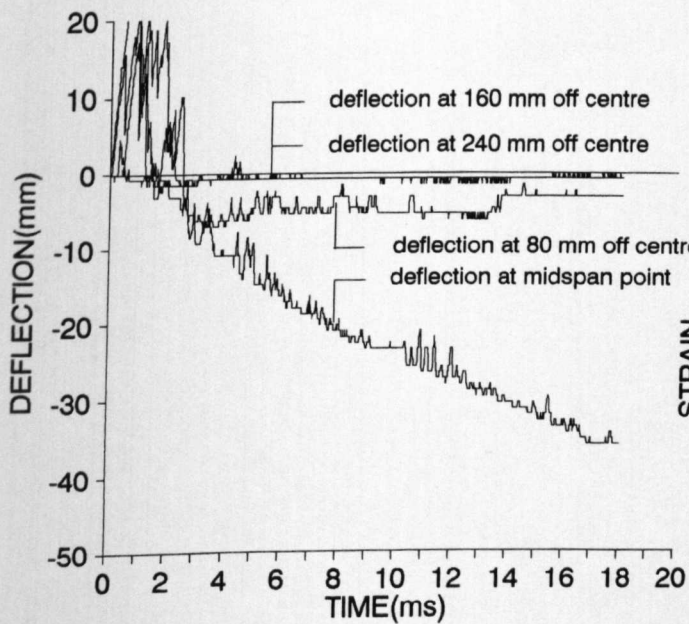
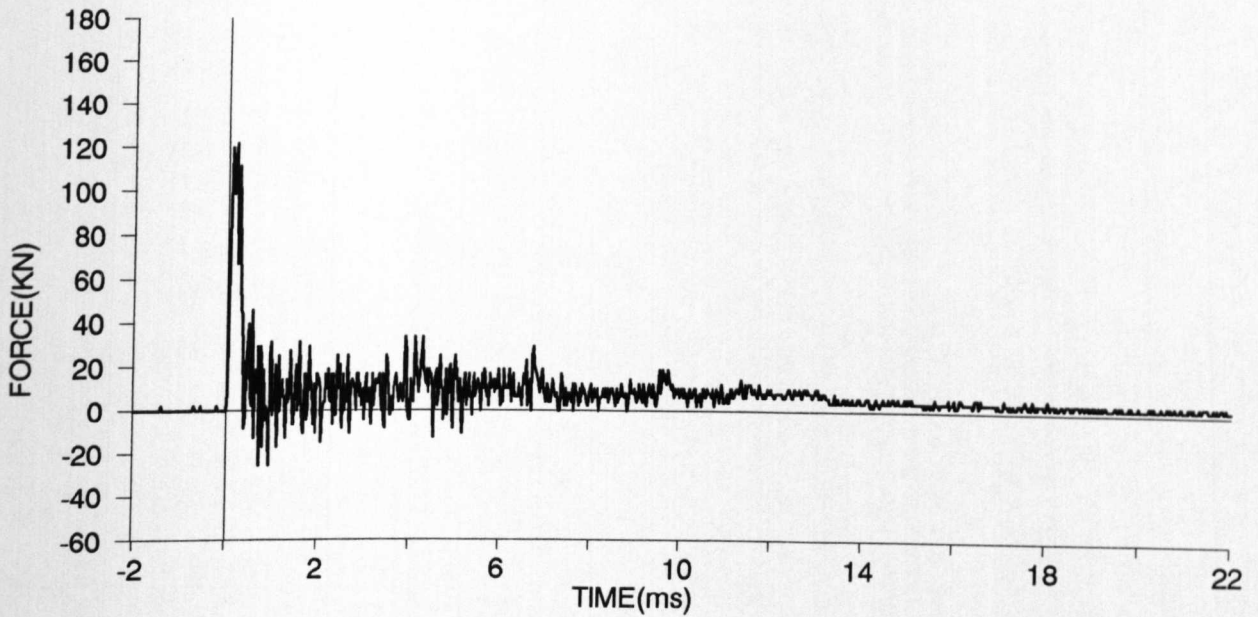
IMPACT TEST - SMALL SLAB - S15



top side



bottom side



IMPACT TEST

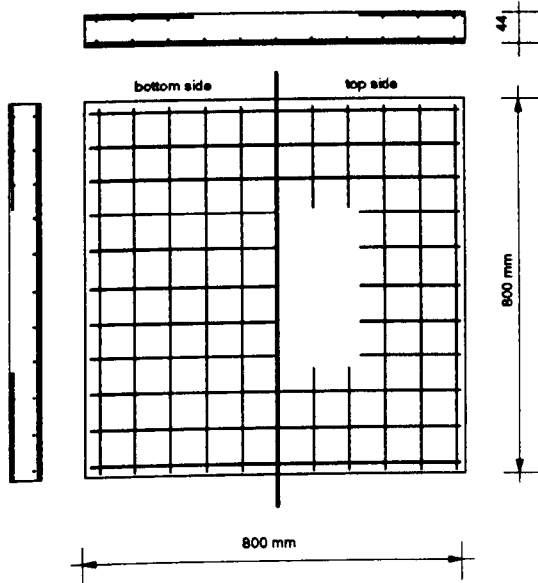
DATE: 4.03.93

SMALL SLAB S16

AGE OF SPECIMEN: 15 days

Cube compressive strength	N/mm ²	45.3	Cylinder tensile strength	N/mm ²	4.88	Age (days)	10
---------------------------	-------------------	------	---------------------------	-------------------	------	------------	----

REINFORCEMENT:

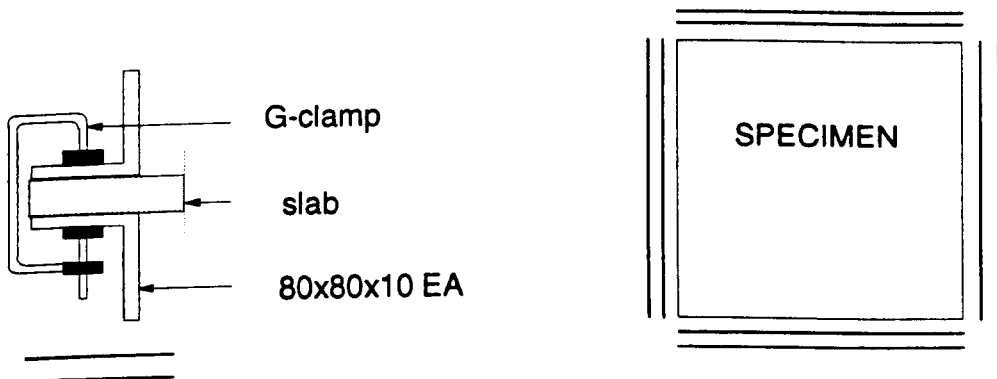


TOP LAYER REINFORCEMENT:
 R.MESH : 3.15 mm DIAM. / 76.2 mm CENTRES
 (WITHOUT CENTRAL REGION 400 X 400 mm)
 BOTTOM LAYER REINFORCEMENT:
 R.MESH : 3.15 mm DIAM. / 76.2 mm CENTRES
 COVER: 4 mm

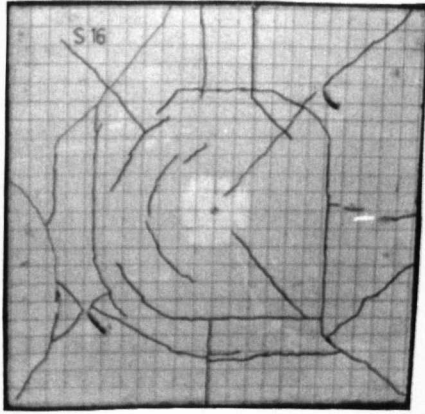
LOADING CONDITIONS

TYPE OF IMPACT : HARD
 HAMMER WEIGHT : 33.7kg
 HEIGHT OF DROP (ABOVE CENTRE OF SPECIMEN) : 750mm
 IMPACT VELOCITY : 3.73m/sec
 THEORETICAL VELOCITY $V = \sqrt{2gh}$: 3.84m/sec
 AREA OF THE PRESSURE BAR CROSS-SECTION : 1962.5mm²

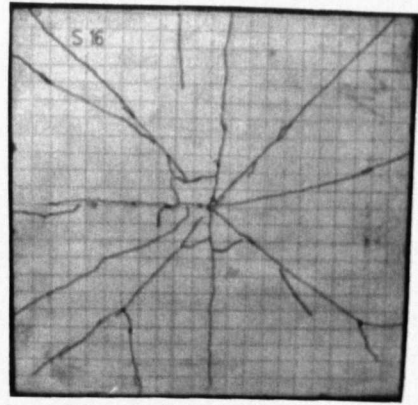
SUPPORTS



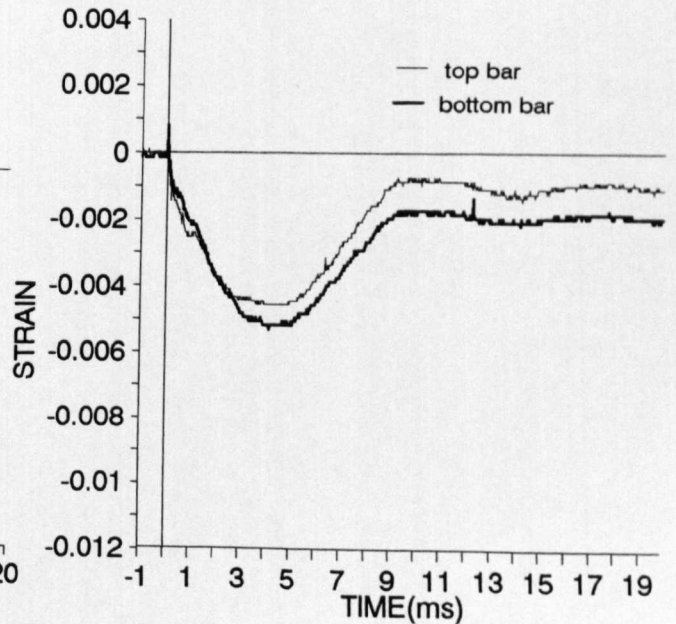
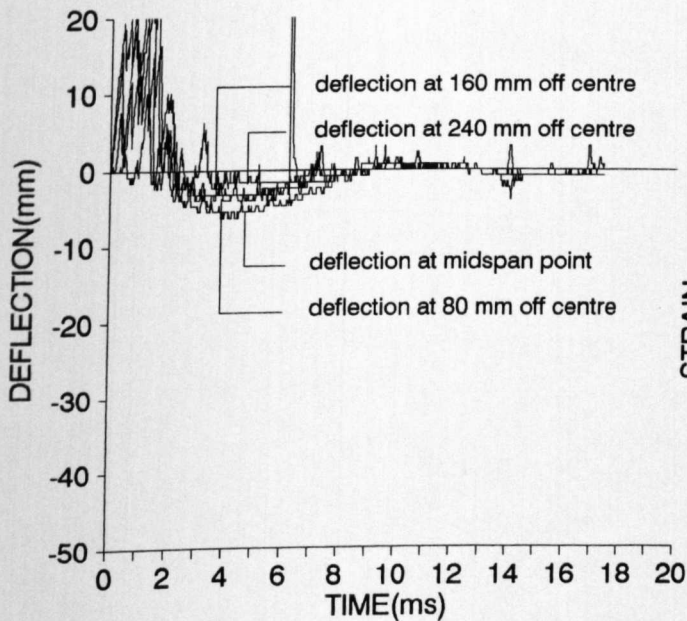
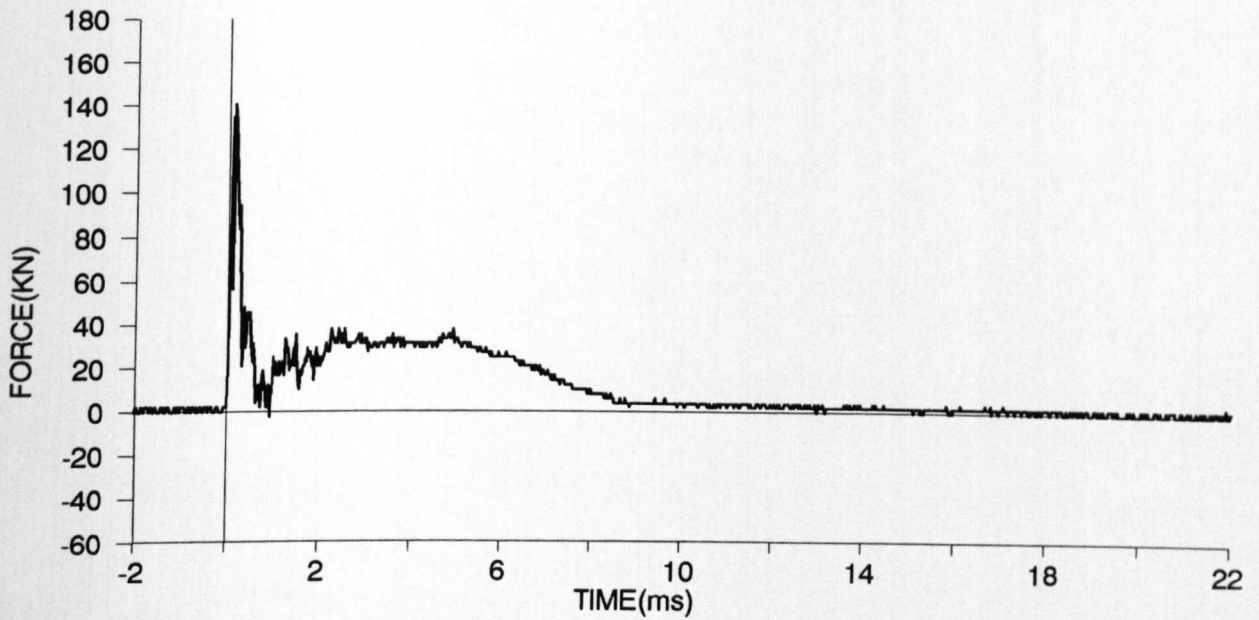
IMPACT TEST - SMALL SLAB - S16



top side



bottom side



IMPACT TEST

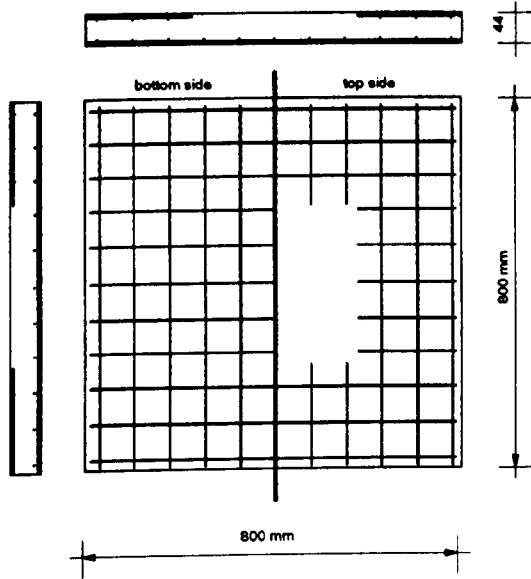
DATE: 6.03.93

SMALL SLAB S17

AGE OF SPECIMEN: 9 days

Cube compressive strength	N/mm ²	48.4	Cylinder tensile strength	N/mm ²	4.62	Age (days)	10
---------------------------	-------------------	------	---------------------------	-------------------	------	------------	----

REINFORCEMENT:



TOP LAYER REINFORCEMENT:

R.MESH : 3.15 mm DIAM. / 76.2 mm CENTRES
(WITHOUT CENTRAL REGION 400 X 400 mm)

BOTTOM LAYER REINFORCEMENT:

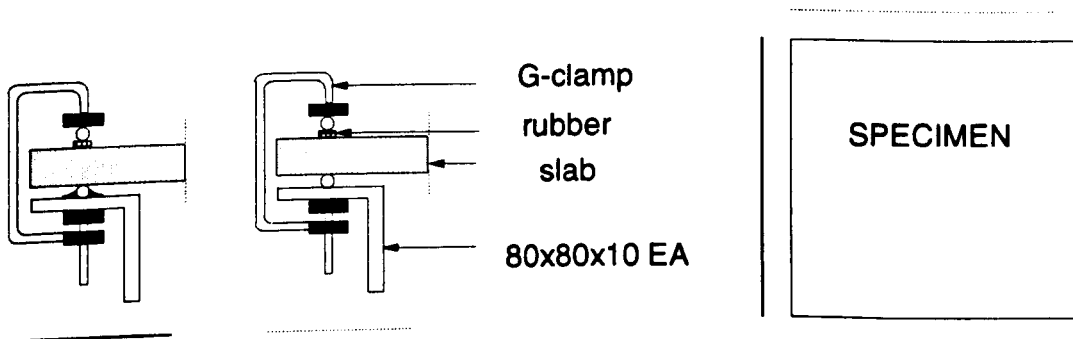
R.MESH : 3.15 mm DIAM. / 76.2 mm CENTRES

COVER: 4 mm

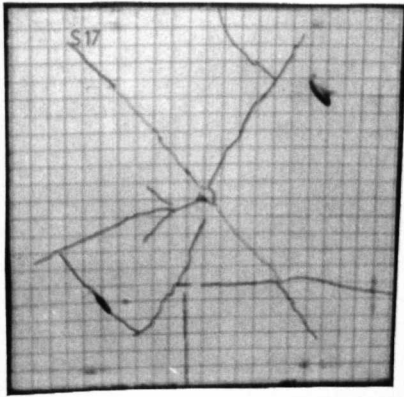
LOADING CONDITIONS

TYPE OF IMPACT : SOFT
 HAMMER WEIGHT : 33.7kg
 HEIGHT OF DROP (ABOVE CENTRE OF SPECIMEN) : 1850mm
 IMPACT VELOCITY : 5.85m/sec
 THEORETICAL VELOCITY $V = \sqrt{2gh}$: 6.02m/sec
 AREA OF THE PRESSURE BAR CROSS-SECTION : 1962.5mm²

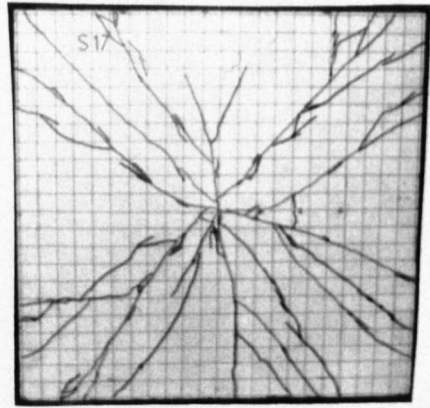
SUPPORTS



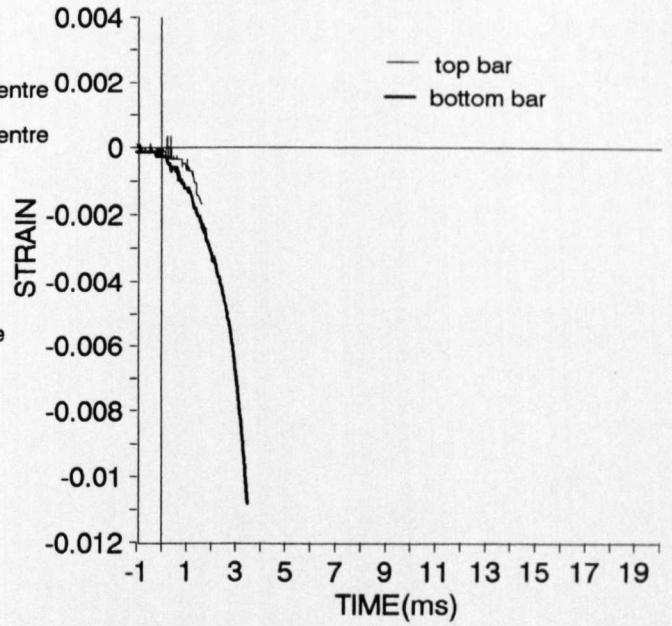
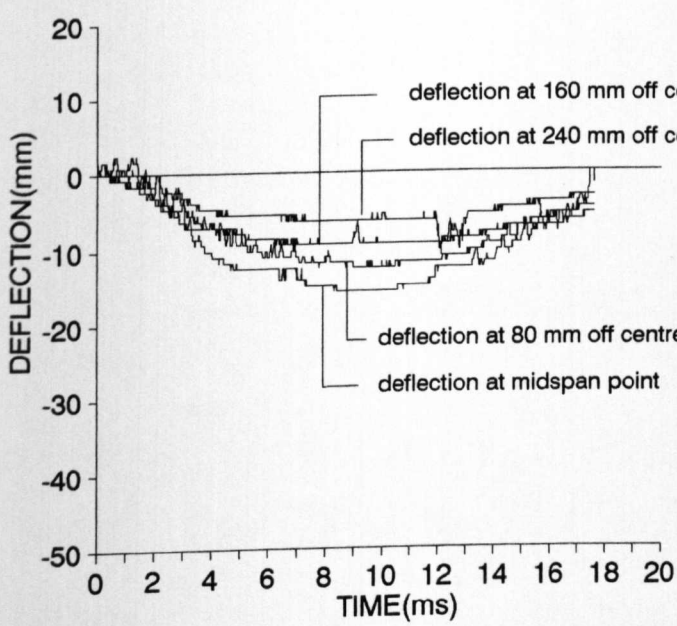
IMPACT TEST - SMALL SLAB - S17



top side



bottom side



IMPACT TEST

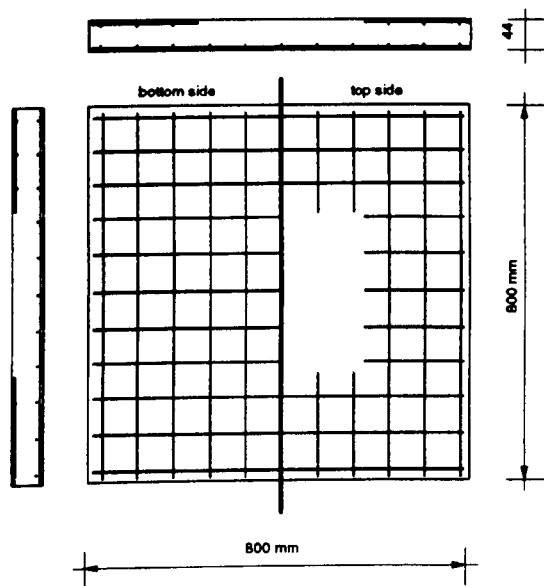
DATE: 6.03.93

SMALL SLAB S18

AGE OF SPECIMEN: 9 days

Cube compressive strength	N/mm ²	48.4	Cylinder tensile strength	N/mm ²	4.62	Age (days)	10
---------------------------	-------------------	------	---------------------------	-------------------	------	------------	----

REINFORCEMENT:

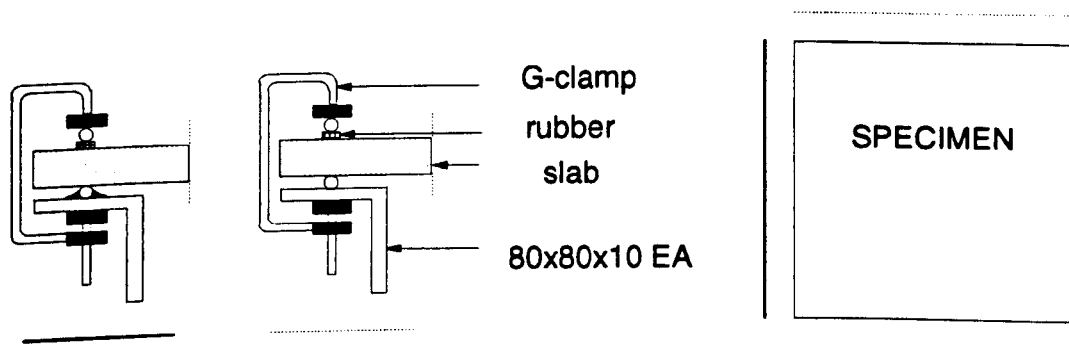


TOP LAYER REINFORCEMENT:
 R.MESH : 3.15 mm DIAM. / 76.2 mm CENTRES
 (WITHOUT CENTRAL REGION 400 X 400 mm)
 BOTTOM LAYER REINFORCEMENT:
 R.MESH : 3.15 mm DIAM. / 76.2 mm CENTRES
 COVER: 4 mm

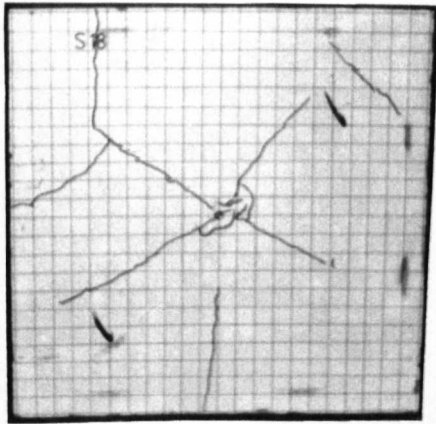
LOADING CONDITIONS

TYPE OF IMPACT : SOFT
 HAMMER WEIGHT : 33.7kg
 HEIGHT OF DROP (ABOVE CENTRE OF SPECIMEN) : 2000mm
 IMPACT VELOCITY : 6.06m/sec
 THEORETICAL VELOCITY $V = \sqrt{2gh}$: 6.26m/sec
 AREA OF THE PRESSURE BAR CROSS-SECTION : 1962.5mm²

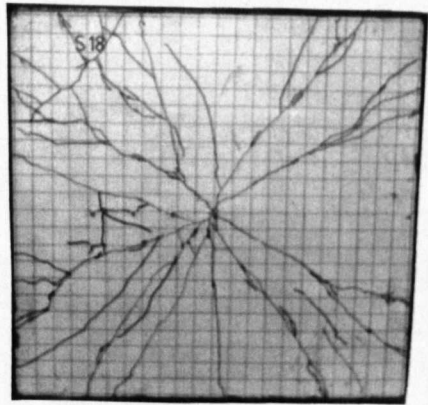
SUPPORTS



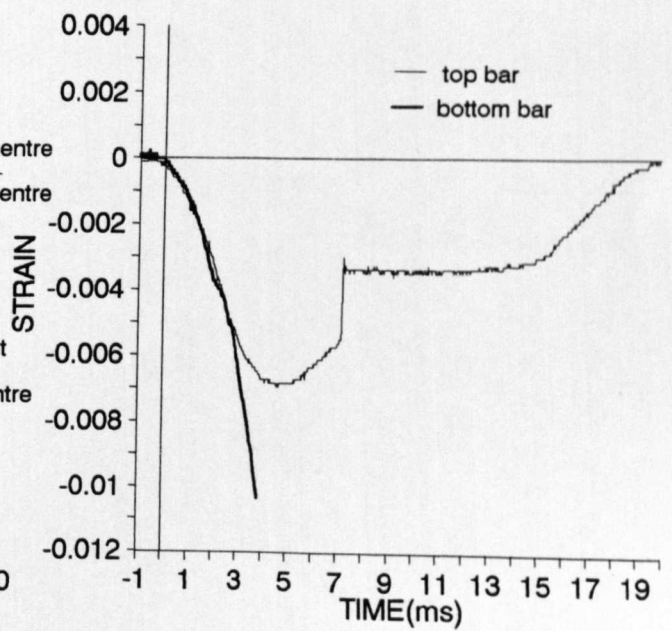
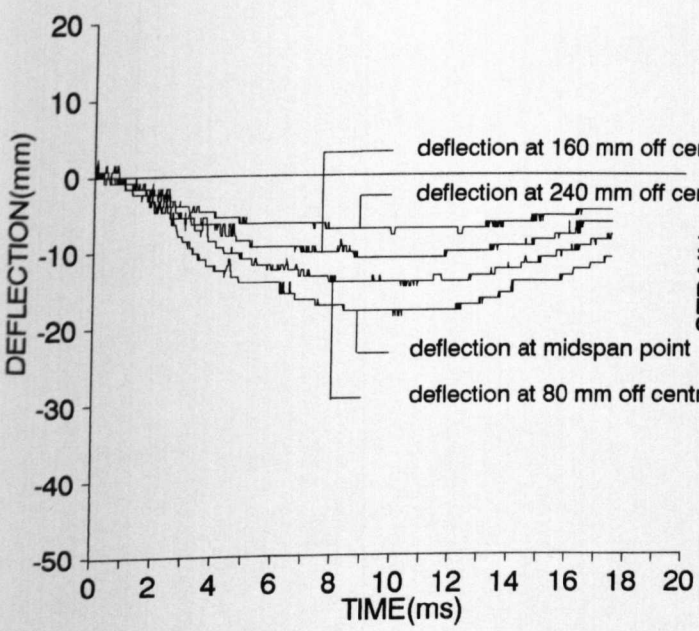
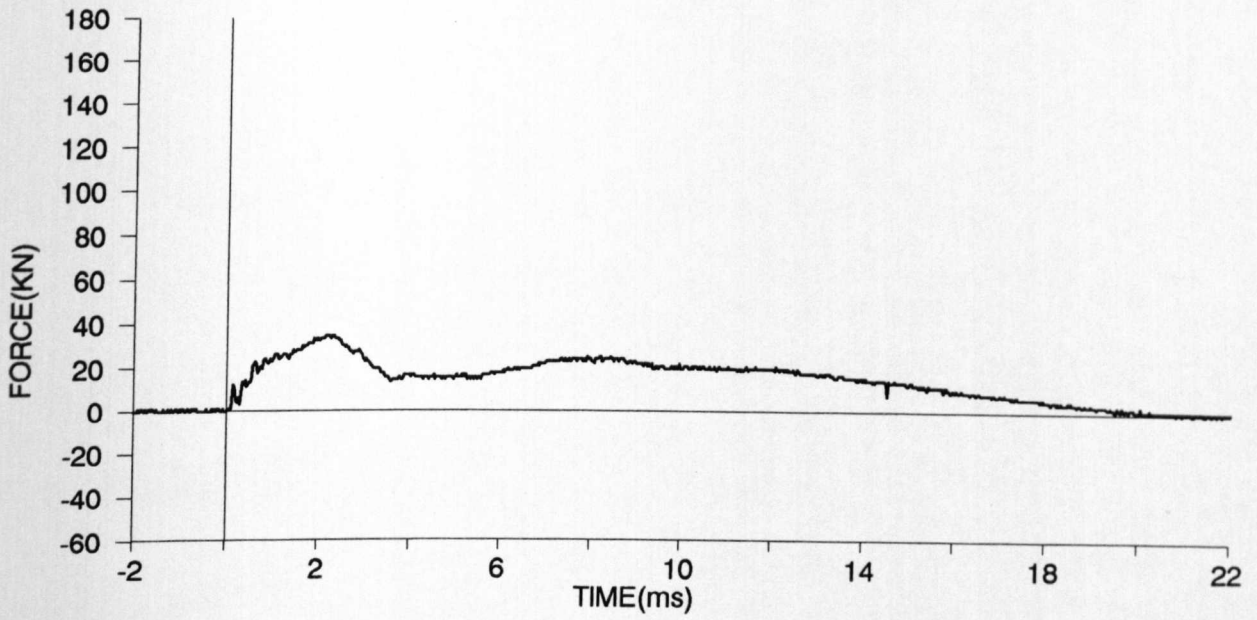
IMPACT TEST - SMALL SLAB - S18



top side



bottom side



IMPACT TEST

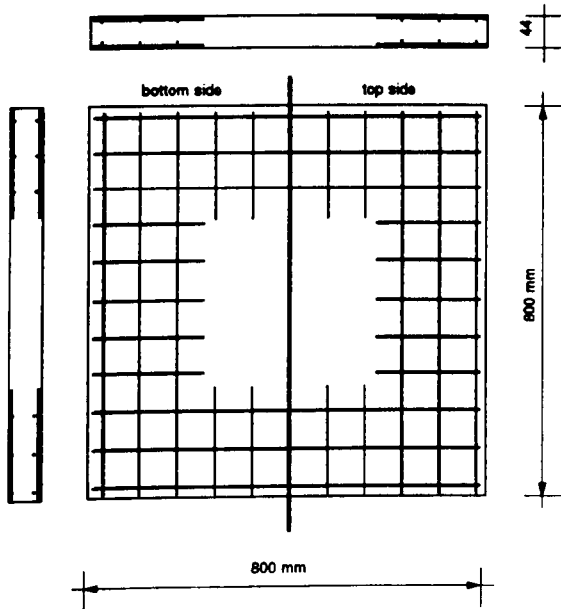
DATE: 7.03.93

SMALL SLAB S19

AGE OF SPECIMEN: 10 days

Cube compressive strength	N/mm ²	48.4	Cylinder tensile strength	N/mm ²	4.62	Age (days)	10
---------------------------	-------------------	------	---------------------------	-------------------	------	------------	----

REINFORCEMENT:



TOP LAYER REINFORCEMENT:

R.MESH : 3.15 mm DIAM. / 78.2 mm CENTRES
(WITHOUT CENTRAL REGION 400 X 400 mm)

BOTTOM LAYER REINFORCEMENT:

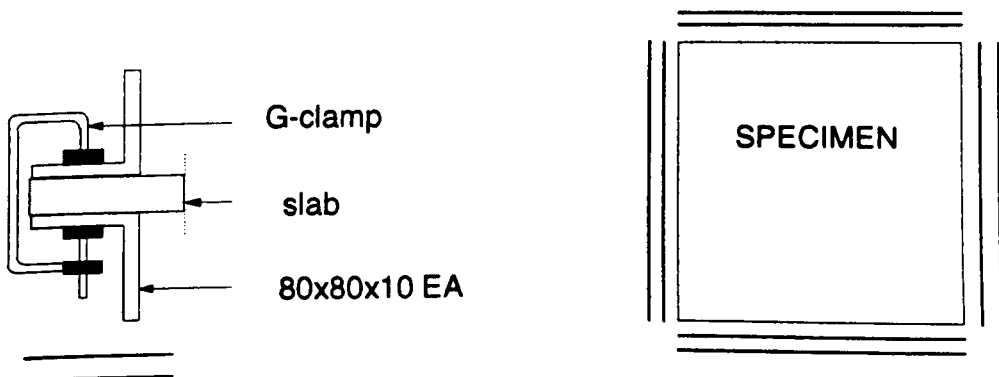
R.MESH : 3.15 mm DIAM. / 78.2 mm CENTRES
(WITHOUT CENTRAL REGION 400 X 400 mm)

COVER: 4 mm

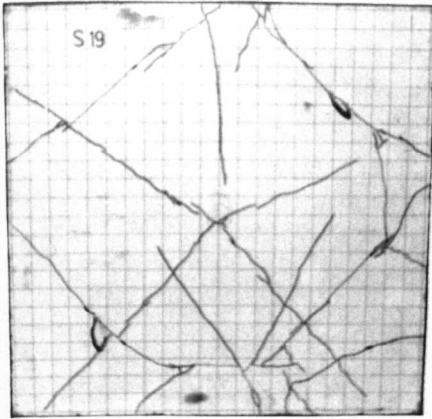
LOADING CONDITIONS

TYPE OF IMPACT	: SOFT
HAMMER WEIGHT	: 33.7kg
HEIGHT OF DROP (ABOVE CENTRE OF SPECIMEN)	: 1500mm
IMPACT VELOCITY	: 5.23m/sec
THEORETICAL VELOCITY $v = \sqrt{2gh}$: 5.42m/sec
AREA OF THE PRESSURE BAR CROSS-SECTION	: 1962.5mm ²

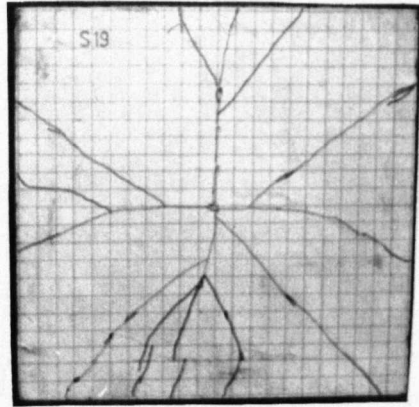
SUPPORTS



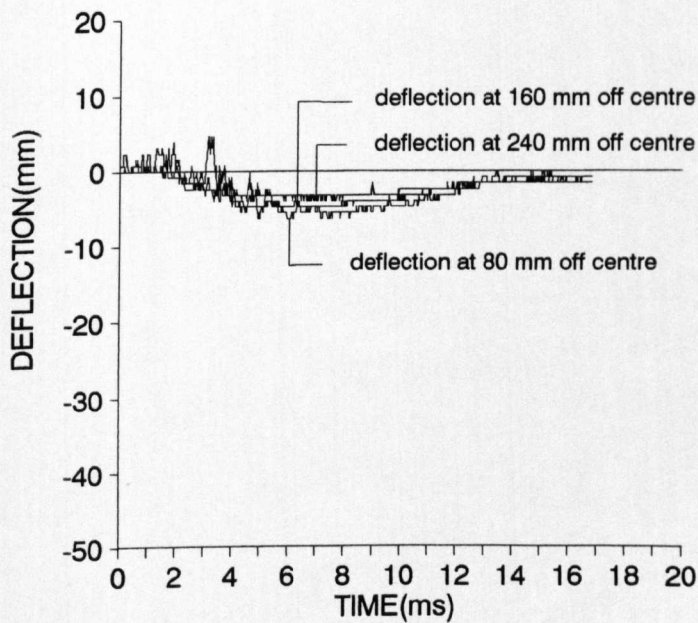
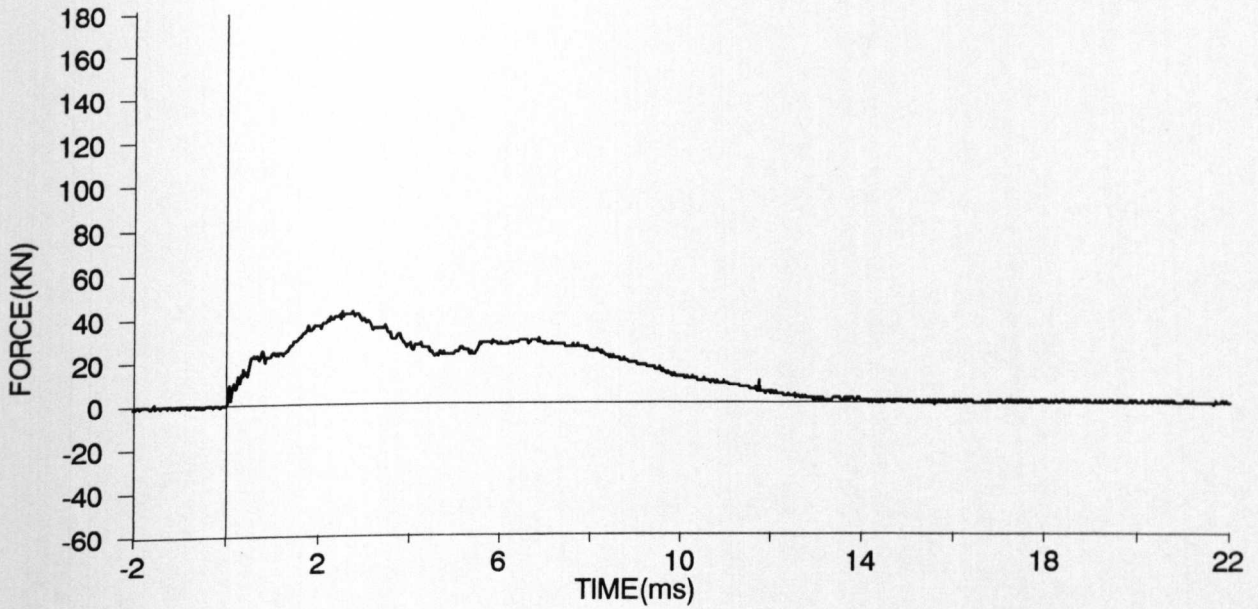
IMPACT TEST - SMALL SLAB - S19



top side



bottom side



IMPACT TESTS

HIGH SPEED FILMS

APPENDIX A3

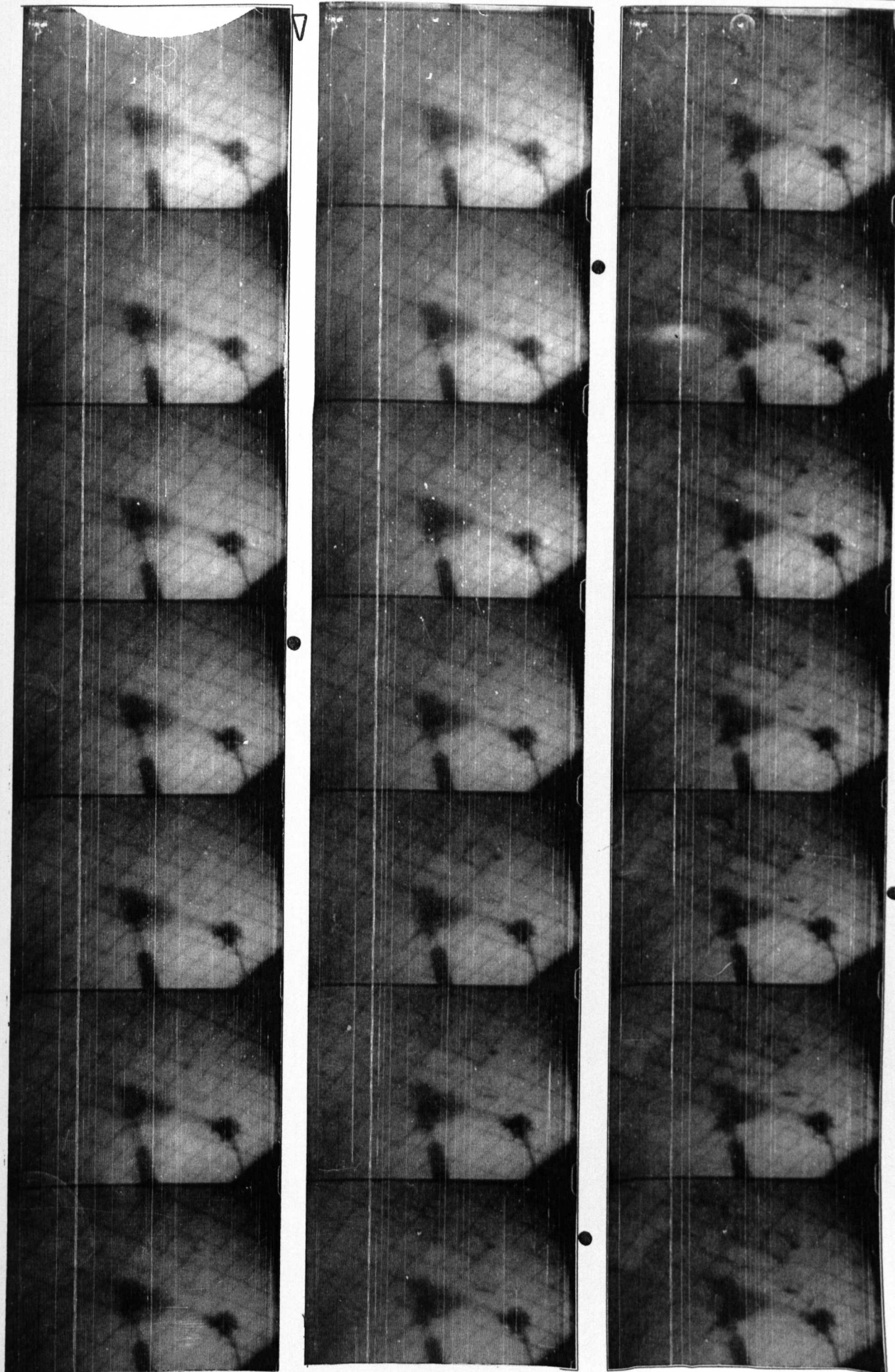
IMPACT TEST S2

INTERFRAME TIME 196.46 μ sec

▽ -3.5MSEC AFTER IMPACT

● -MSEC'S MARKER

1.



GRID SIZE : 36mm X 36mm

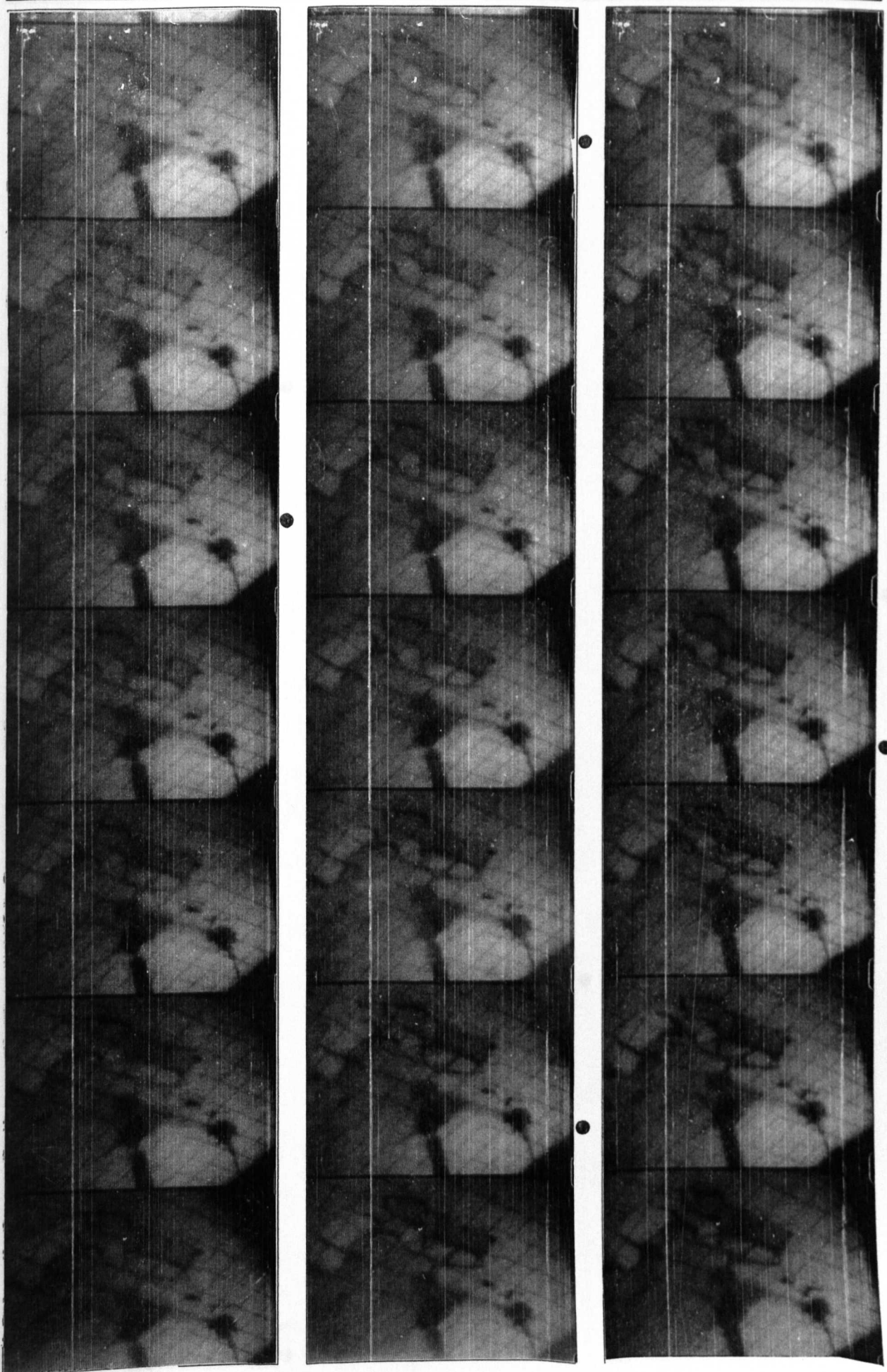
IMPACT TEST S2

INTERFRAME TIME 196.46 μ sec

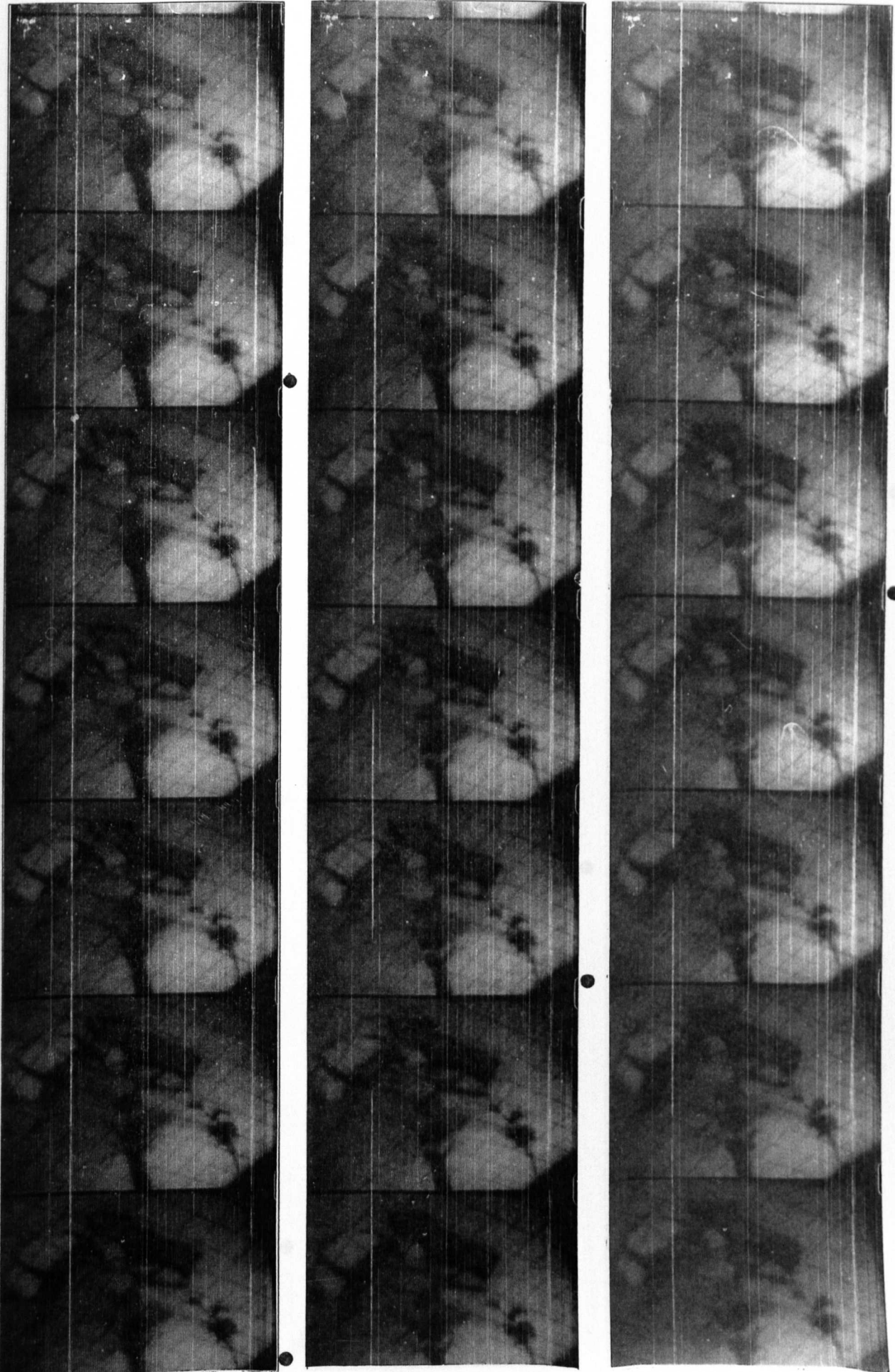
▽ -3.5MSEC AFTER IMPACT

● -MSEC'S MARKER

2.



GRID SIZE : 36mm X 36mm



GRID SIZE : 36mm X 36mm

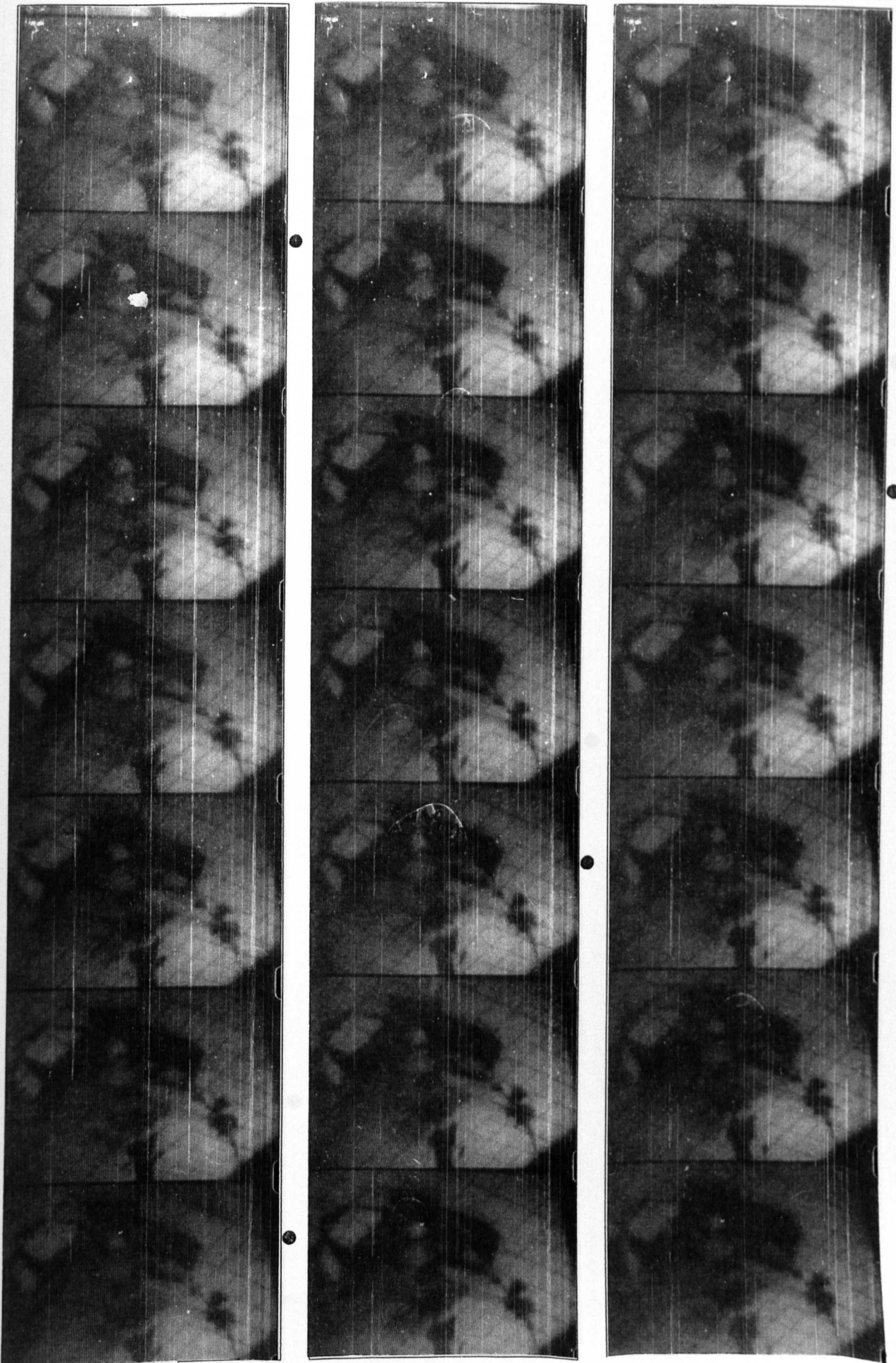
IMPACT TEST S2

INTERFRAME TIME 196.46 μ sec

∇ -3.5MSEC AFTER IMPACT

● -MSEC'S MARKER

4.



GRID SIZE : 36mm X 36mm

IMPACT TEST S2

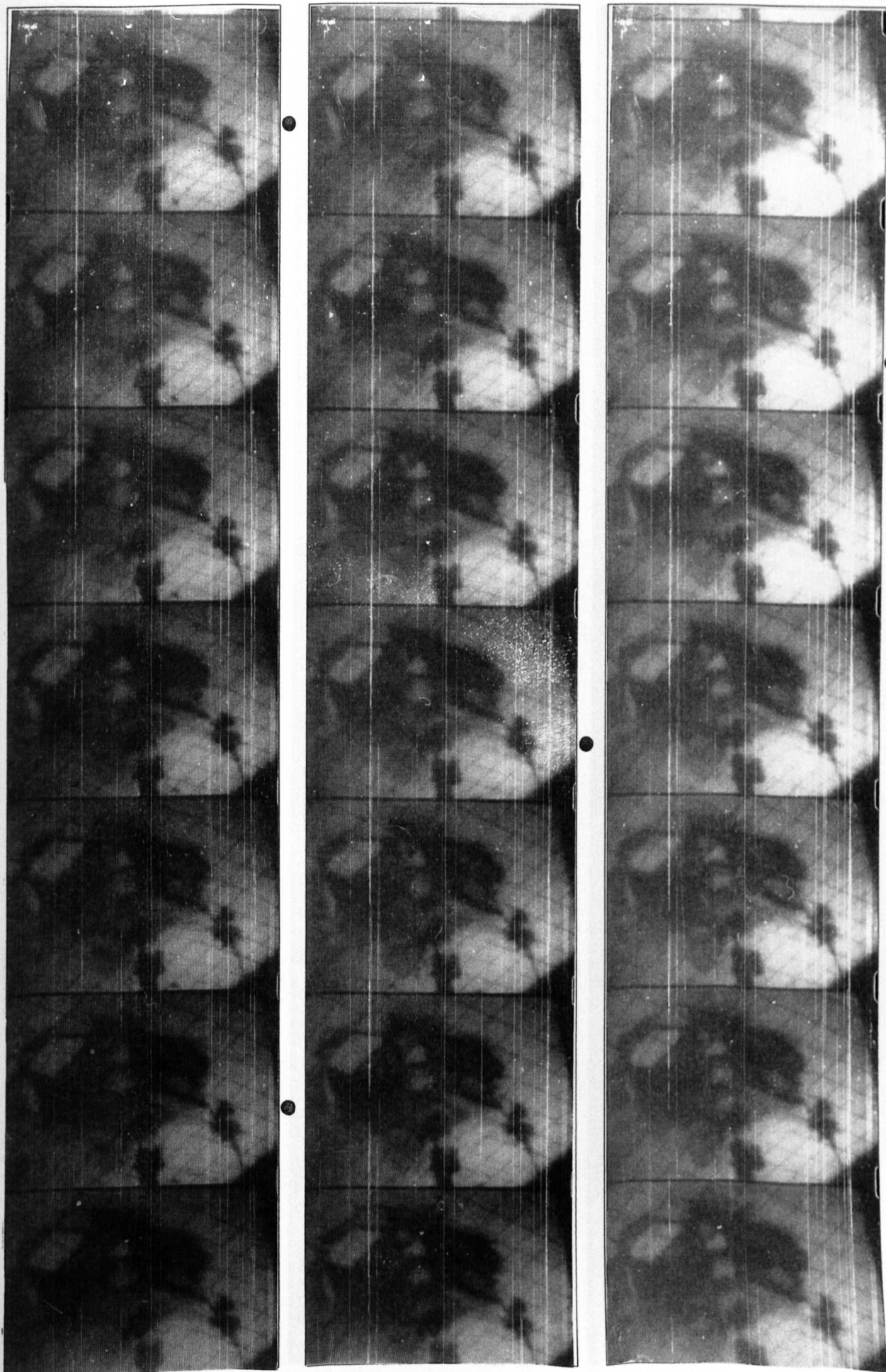
INTERFRAME TIME 196.46 μ sec



-3.5MSEC AFTER IMPACT

● -MSEC'S MARKER

5.



GRID SIZE : 36mm X 36mm

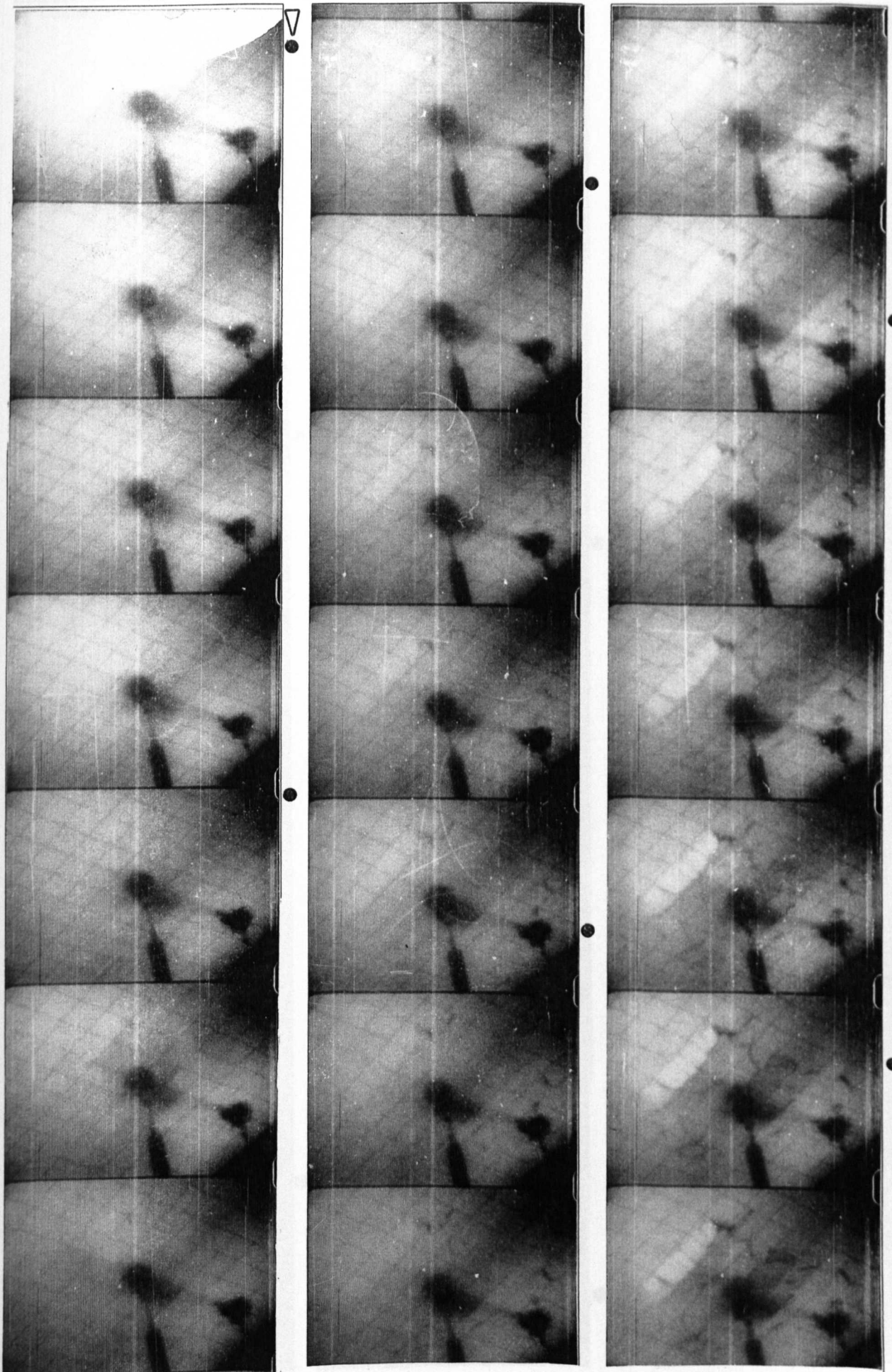
IMPACT TEST S4

INTERFRAME TIME 260.21 μ sec

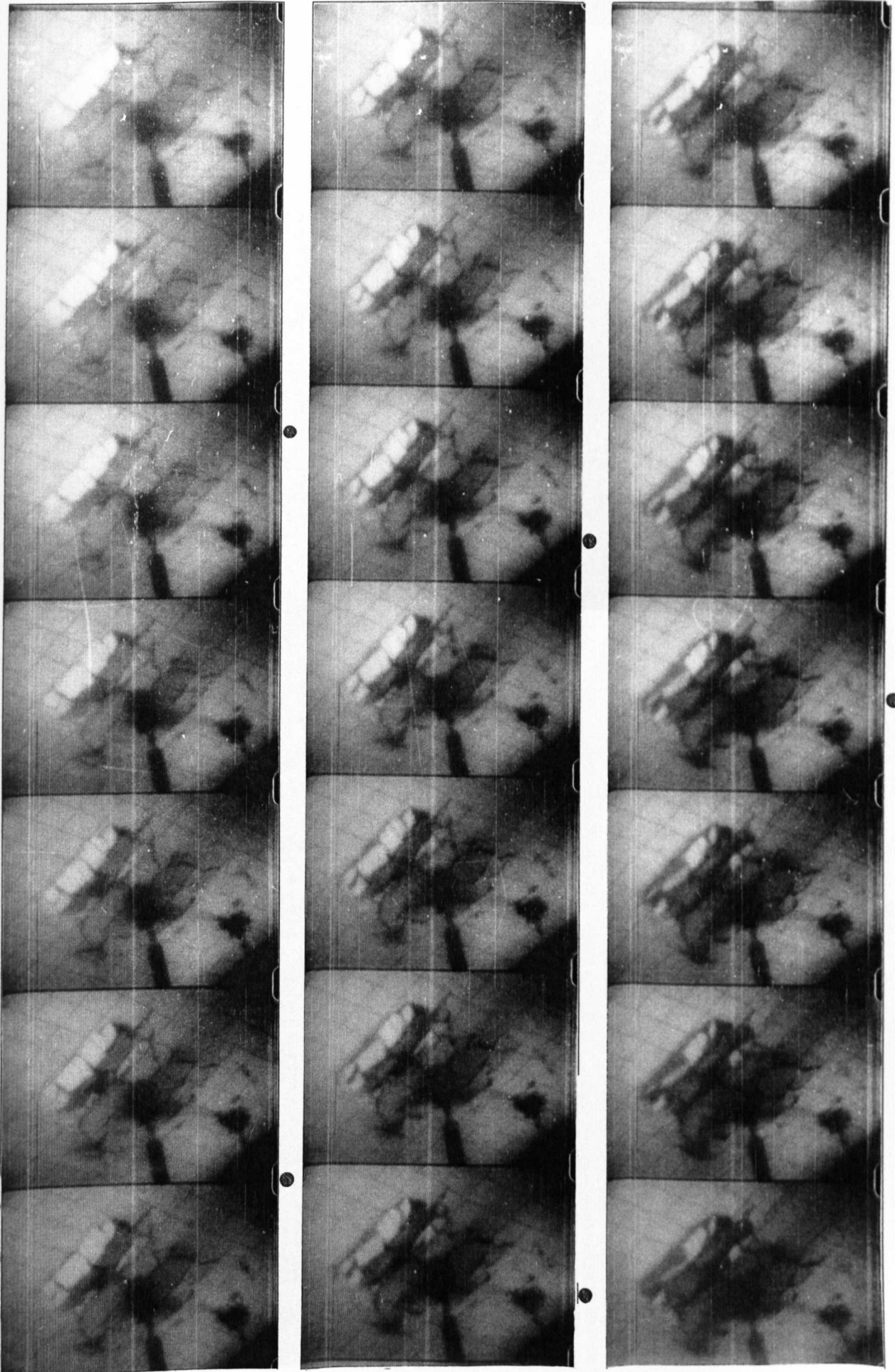
▽ -2.5MSEC AFTER IMPACT

● -MSEC'S MARKER

1.



GRID SIZE : 36mm X 36mm



GRID SIZE : 36mm X 36mm

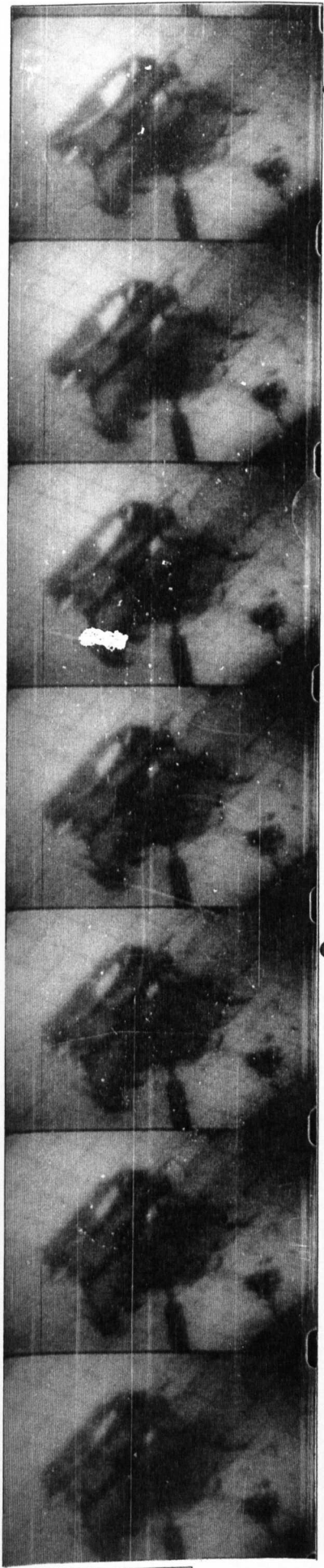
IMPACT TEST S4

INTERFRAME TIME 260.21 μ sec

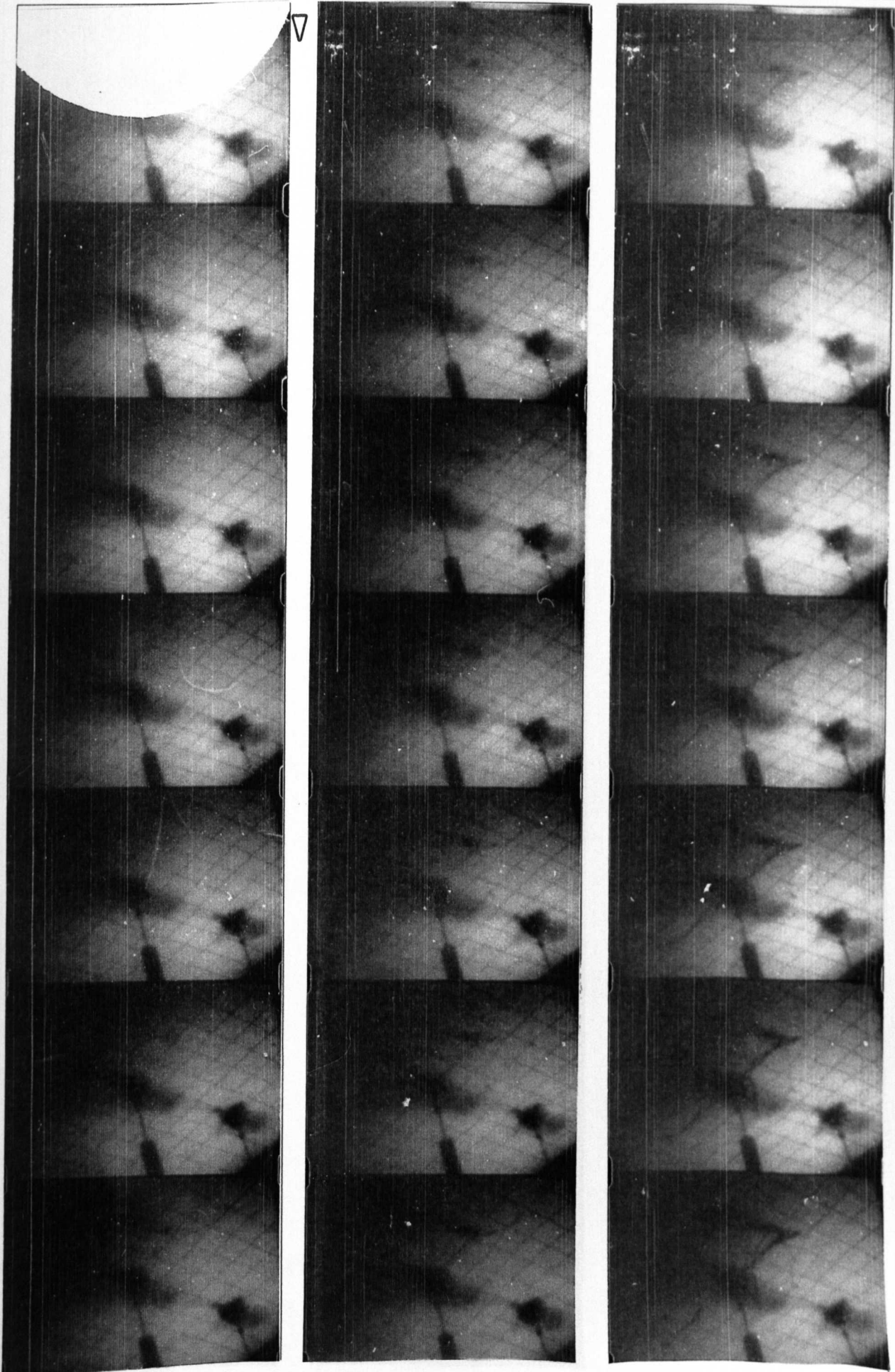
∇ -2.5MSEC AFTER IMPACT

● -MSEC'S MARKER

3.



GRID SIZE : 36mm X 36mm



GRID SIZE : 36mm X 36mm

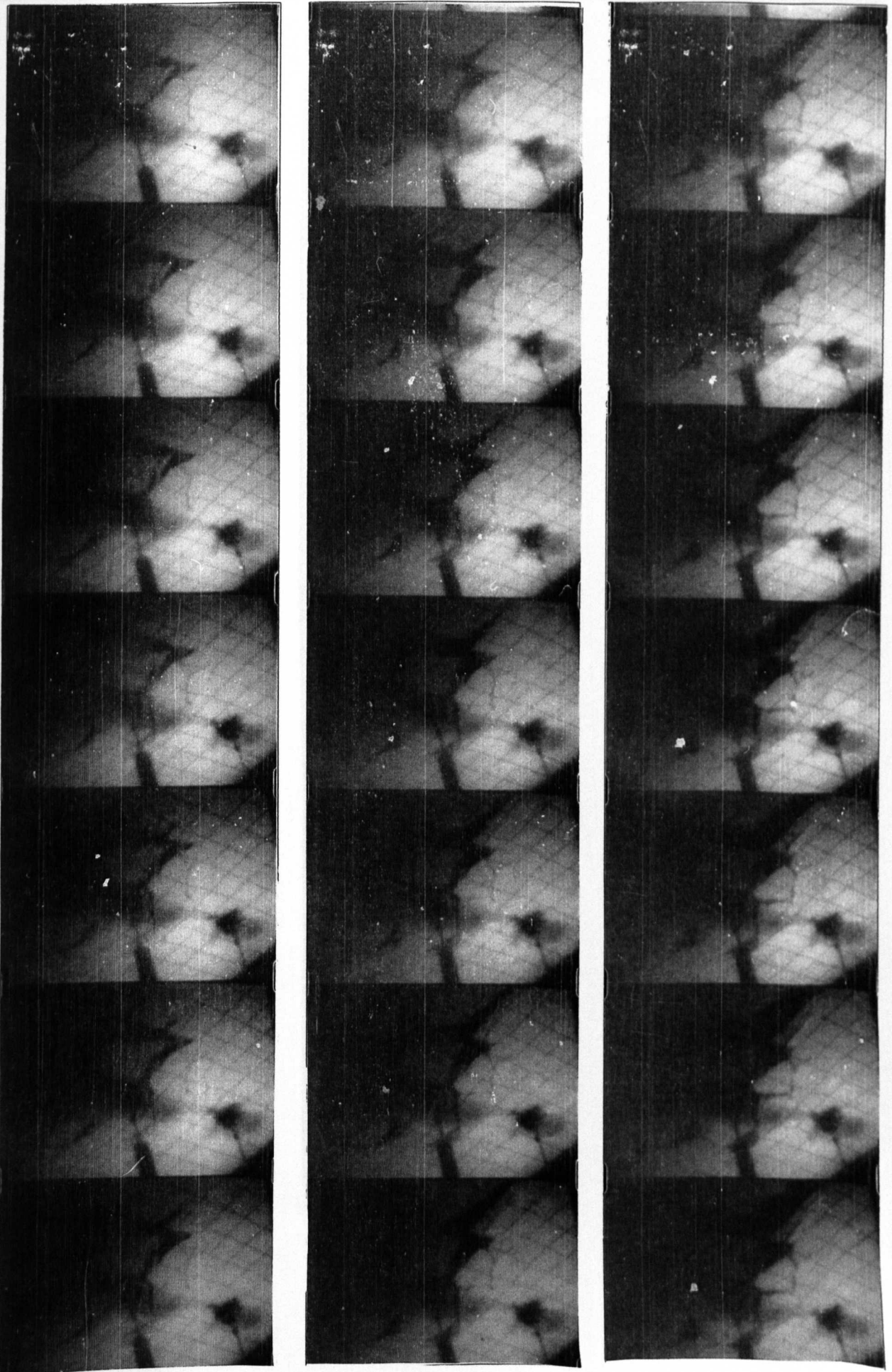
IMPACT TEST S5

INTERFRAME TIME 226.35 μ sec

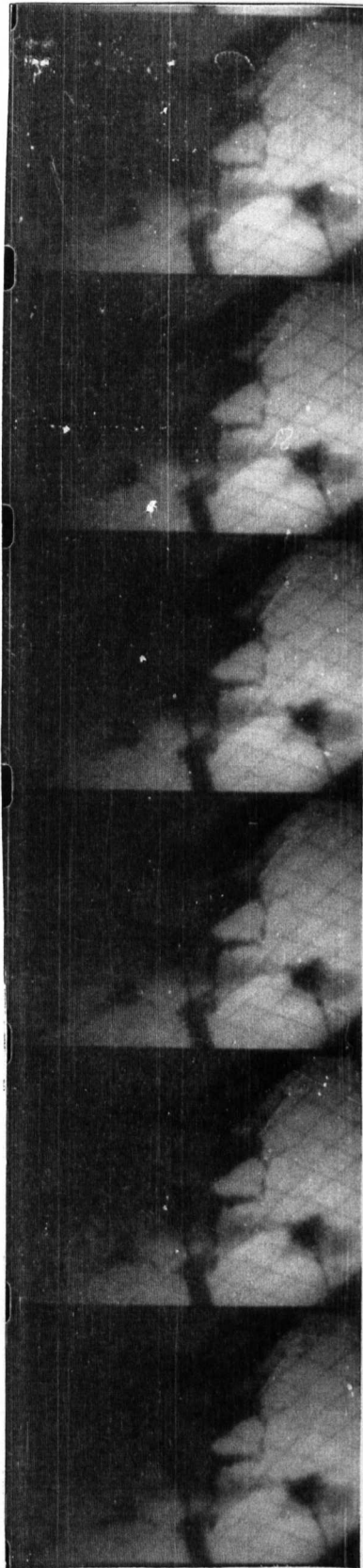
∇ -2.0MSEC AFTER IMPACT

MSEC MARKERS n.a

2.



GRID SIZE : 36mm X 36mm



GRID SIZE : 36mm X 36mm

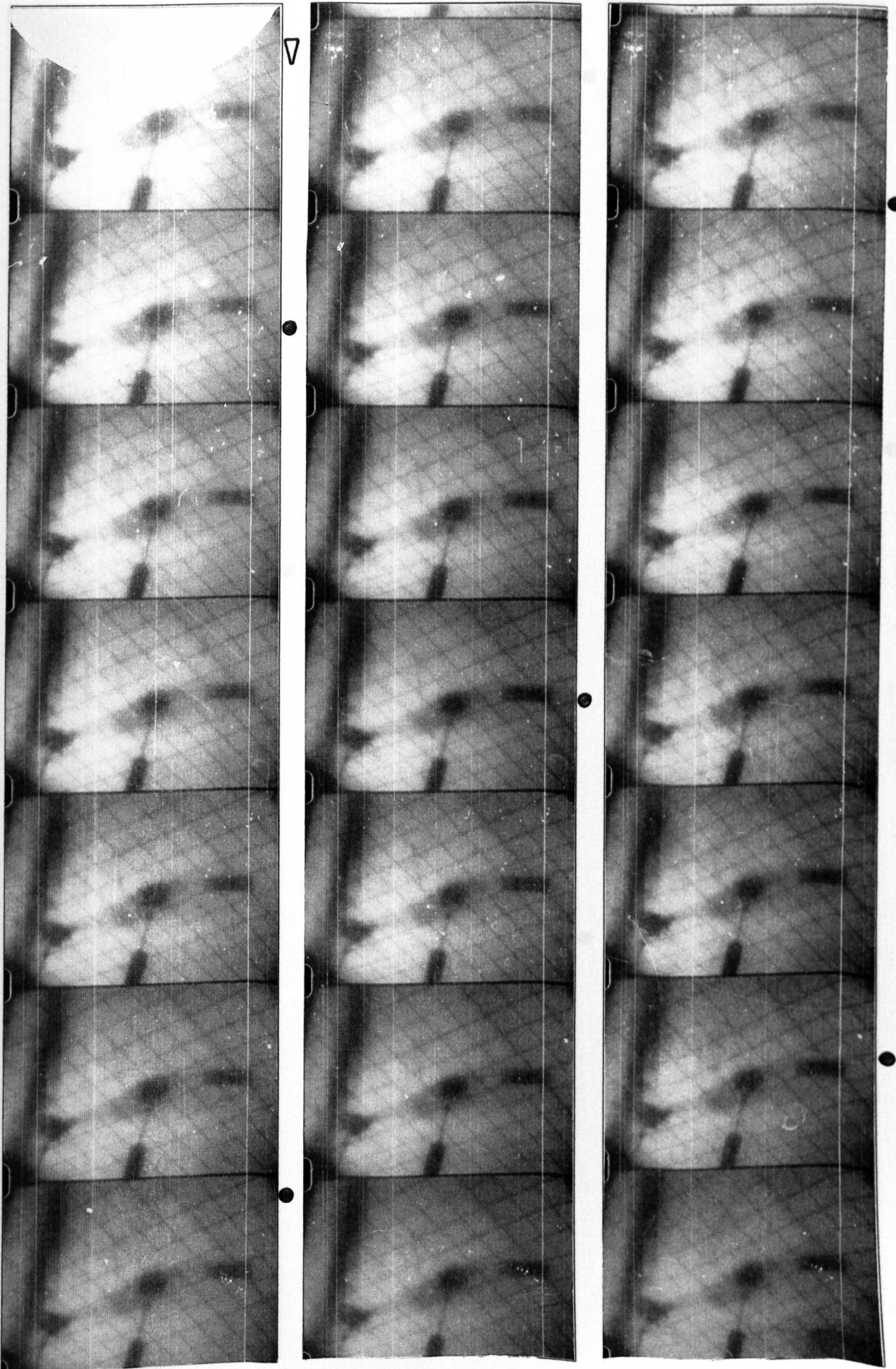
IMPACT TEST S6

INTERFRAME TIME 223.74 μ sec

∇ -IMPACT TIME

● -MSEC'S MARKER

1.



GRID SIZE : 36mm X 36mm

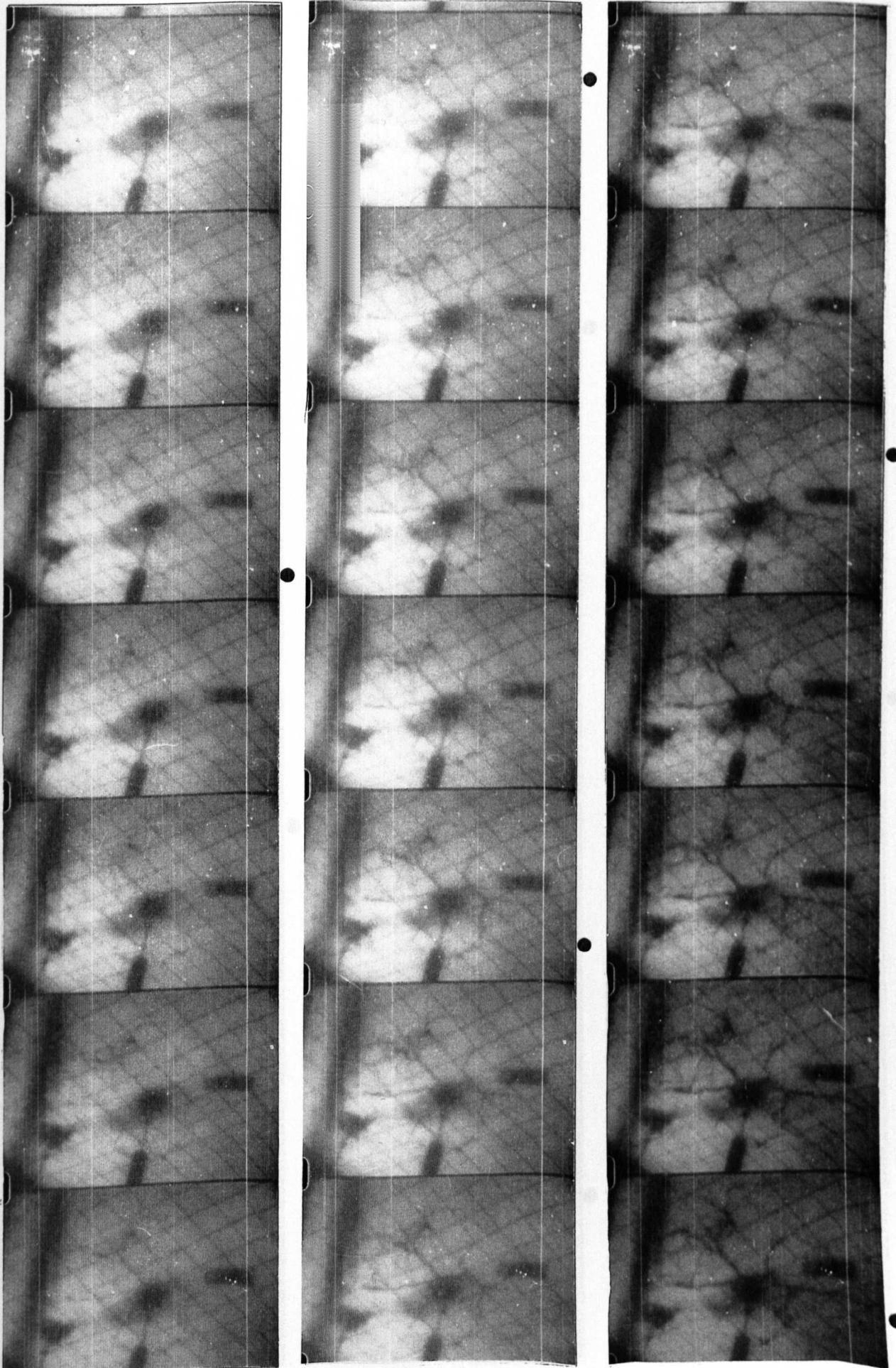
IMPACT TEST S6

INTERFRAME TIME 223.74 μ sec

▽ -IMPACT TIME

● -MSEC'S MARKER

2.



GRID SIZE : 36mm X 36mm

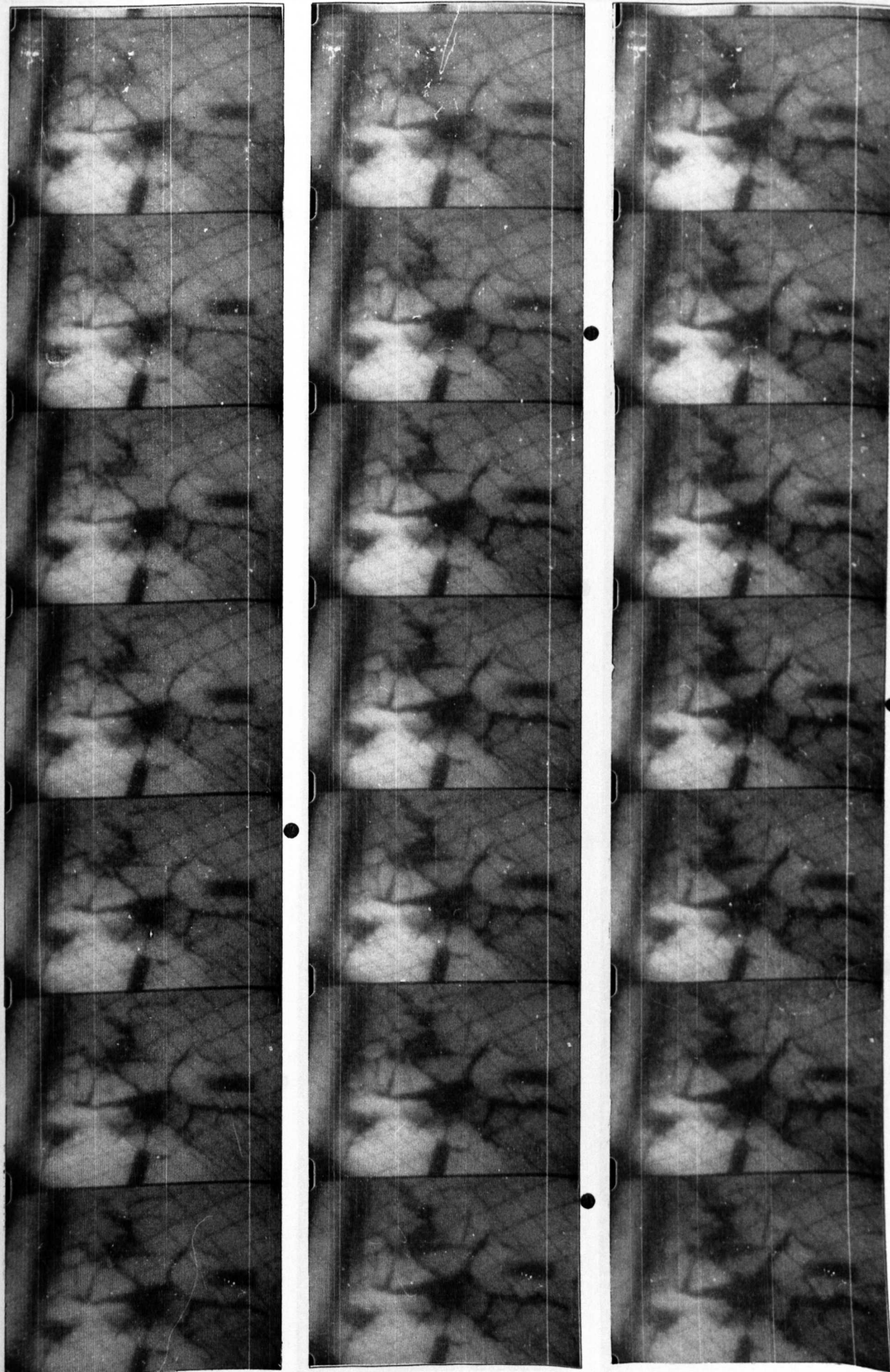
IMPACT TEST S6

INTERFRAME TIME 223.74 μ sec

∇ - IMPACT TIME

● - MSEC'S MARKER

3.



GRID SIZE : 36mm X 36mm

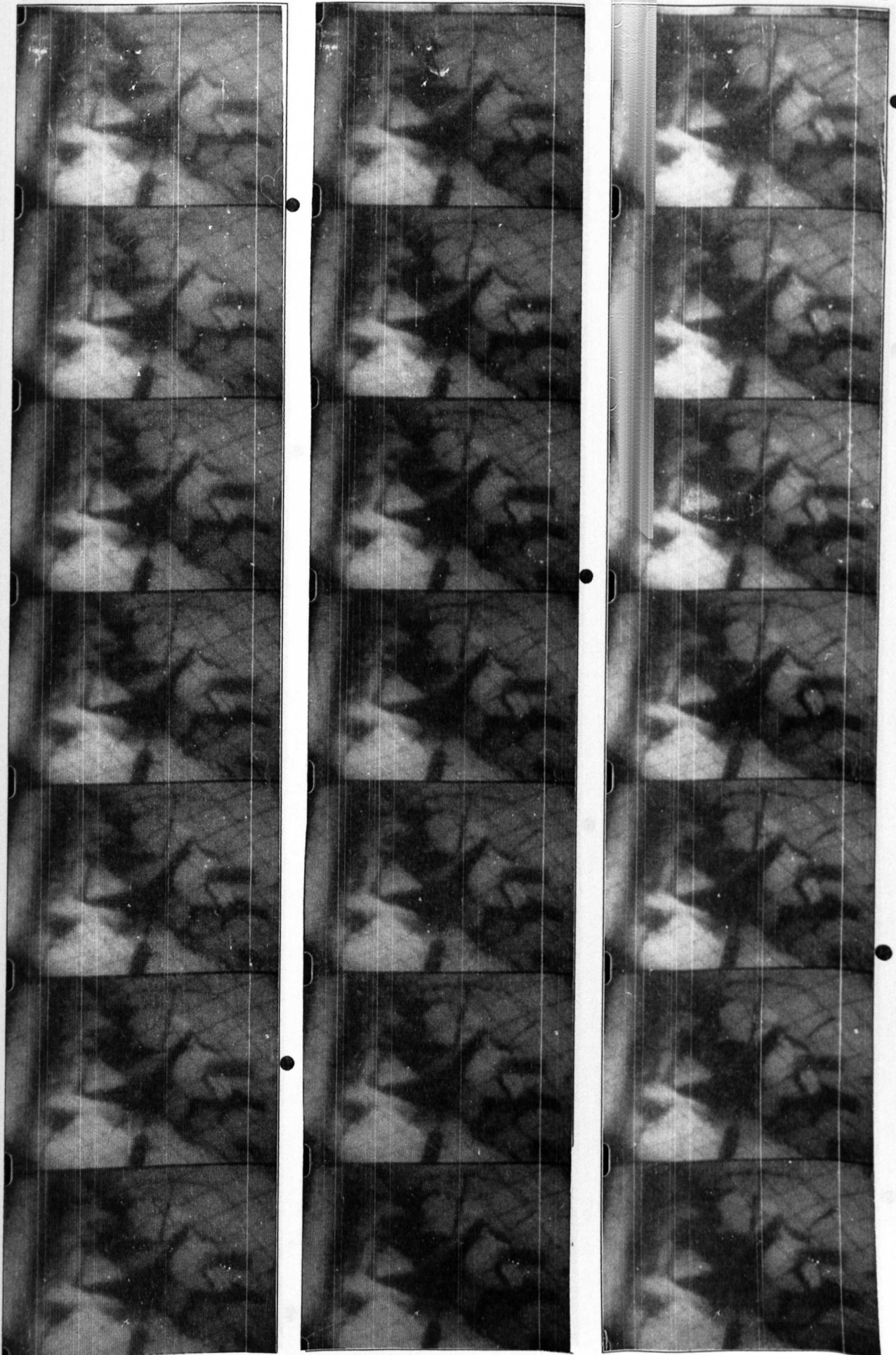
IMPACT TEST S6

INTERFRAME TIME 223.74 μ sec

∇ -IMPACT TIME

● -MSEC'S MARKER

4.



GRID SIZE : 36mm X 36mm

IMPACT TEST S6

INTERFRAME TIME 223.74 μ sec

∇ - IMPACT TIME

● - MSEC'S MARKER

5.



GRID SIZE : 36mm X 36mm

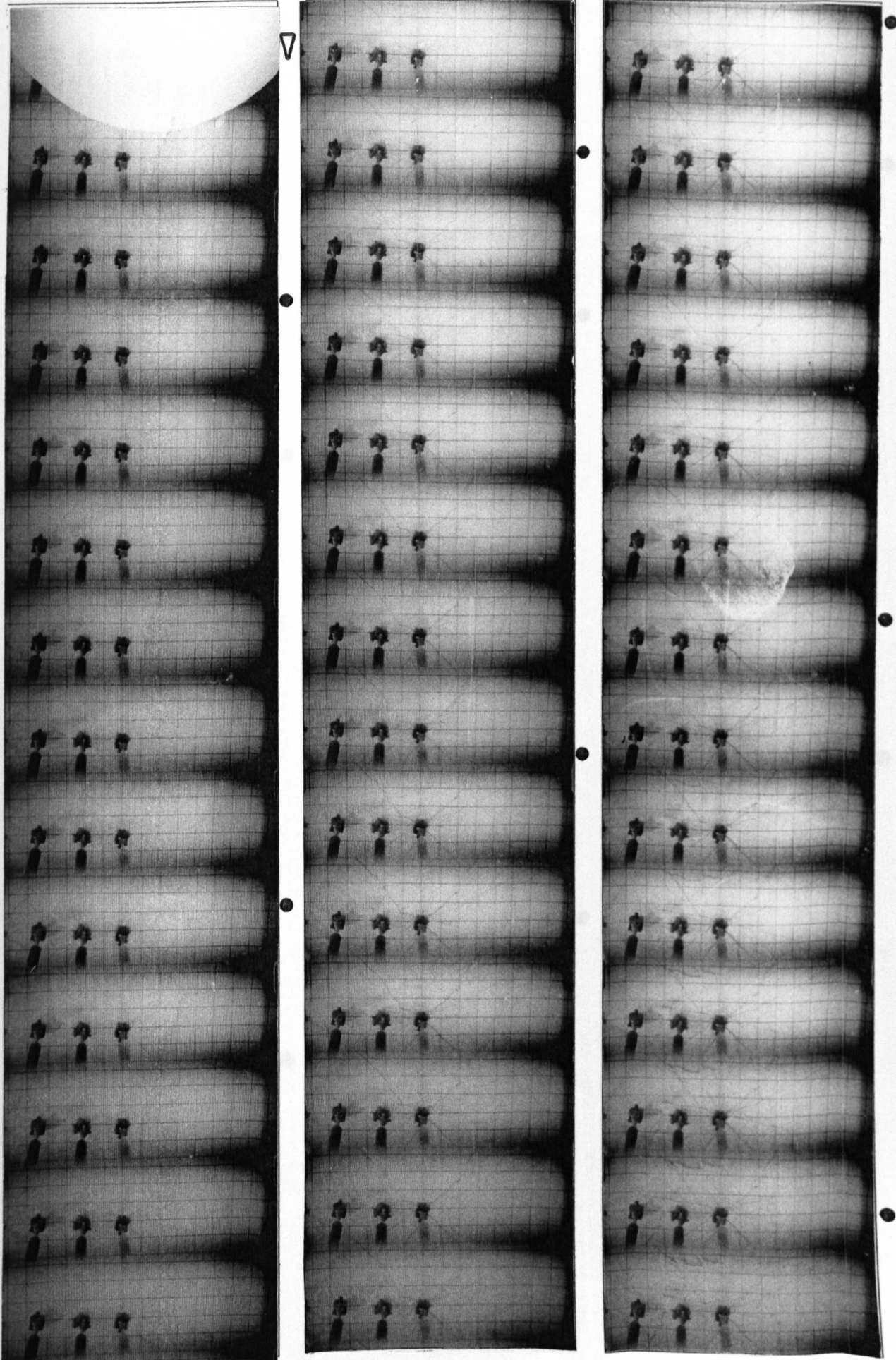
IMPACT TEST S12

INTERFRAME TIME 160.21 μ sec

▽ -IMPACT TIME

● -MSEC'S MARKER

1.



GRID SIZE : 36mm X 36mm

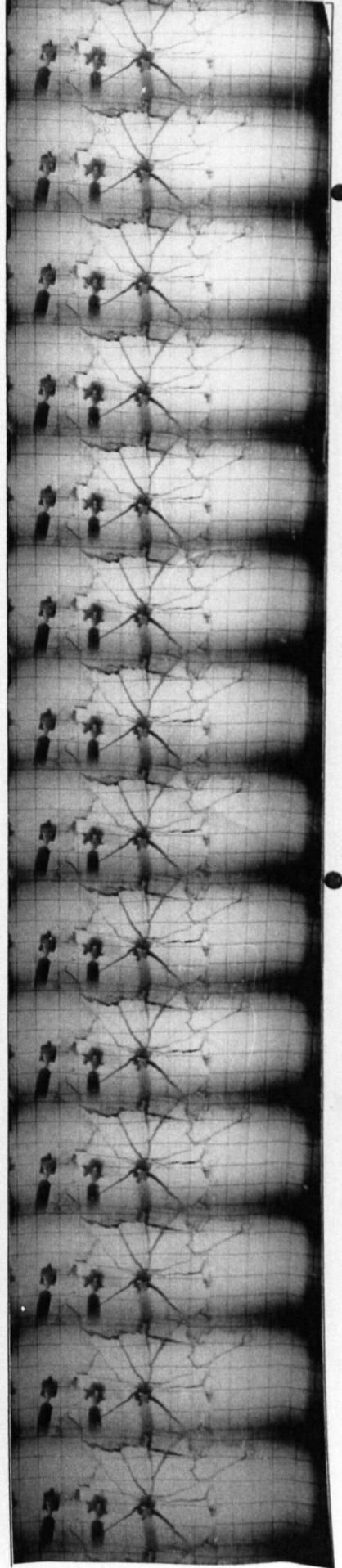
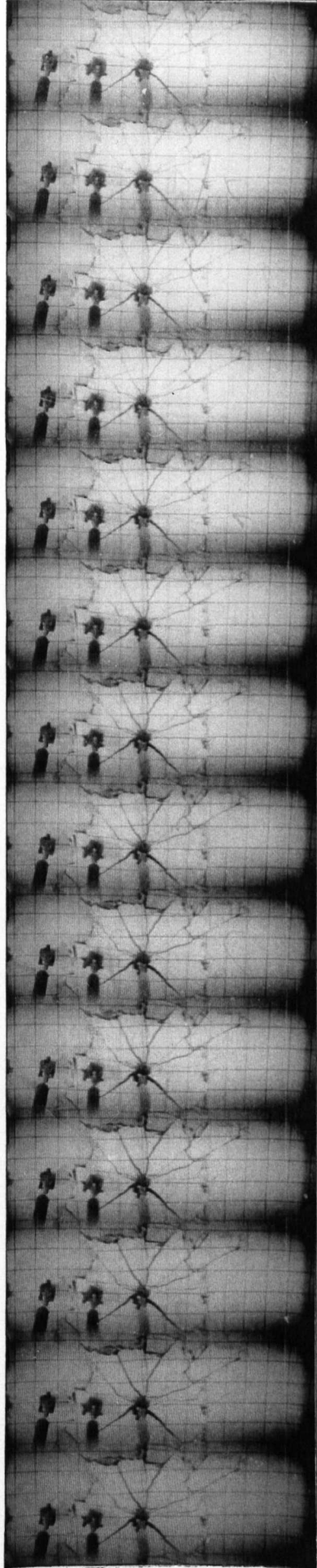
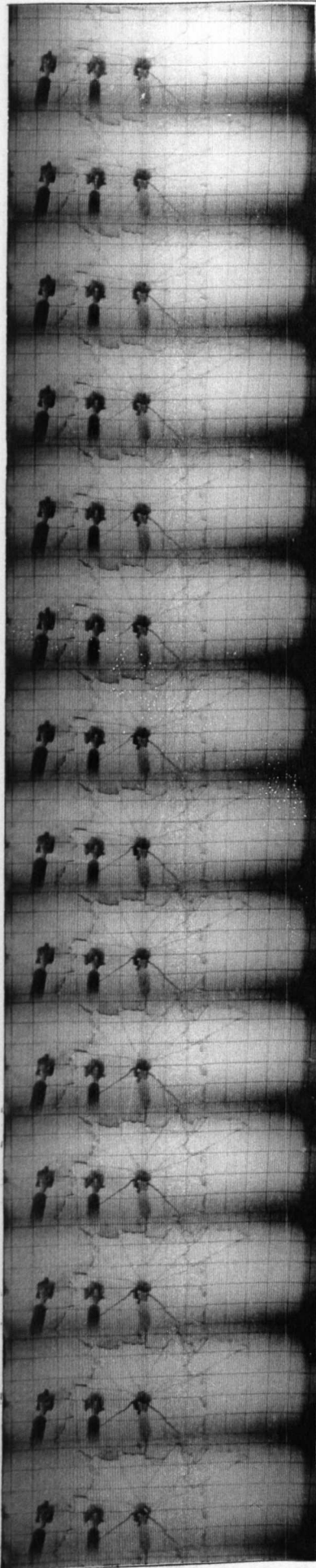
IMPACT TEST S12

INTERFRAME TIME 160.21 μ sec

∇ -IMPACT TIME

● -MSEC'S MARKER

2.



GRID SIZE : 36mm X 36mm

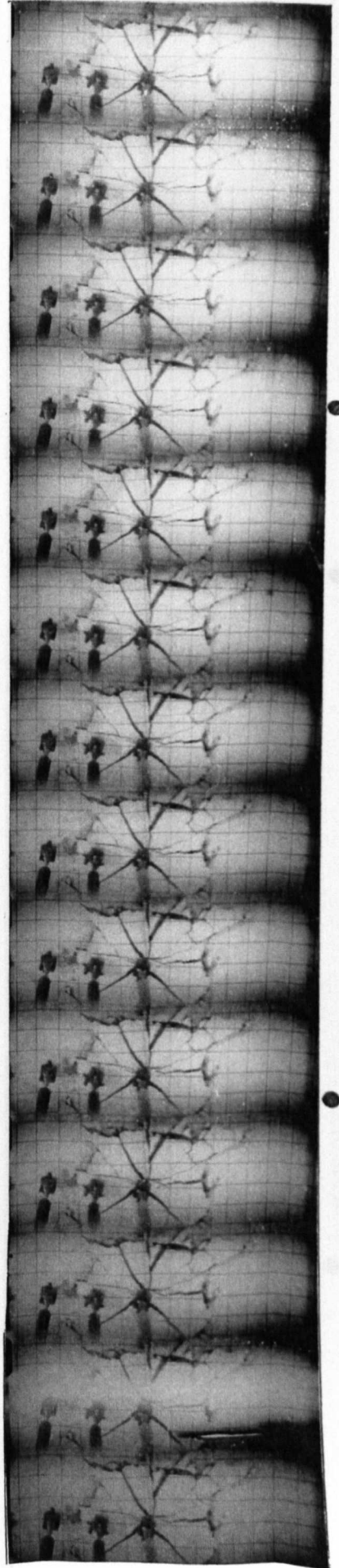
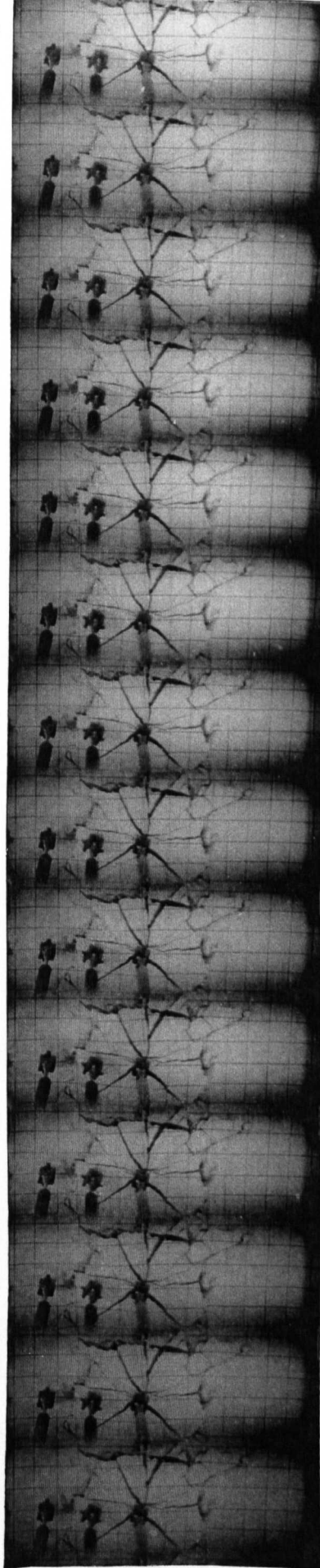
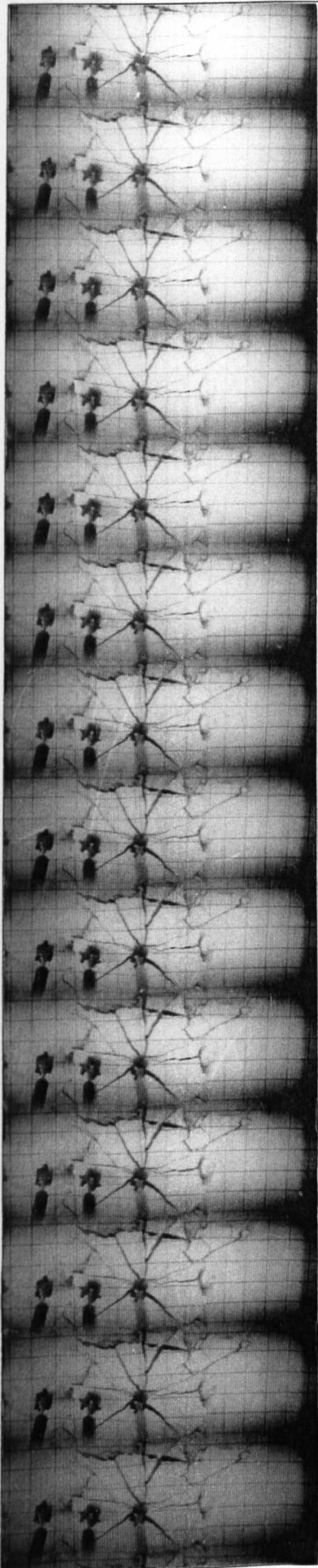
IMPACT TEST S12

INTERFRAME TIME 160.21 μ sec

∇ -IMPACT TIME

● -MSEC'S MARKER

3.



GRID SIZE : 36mm X 36mm

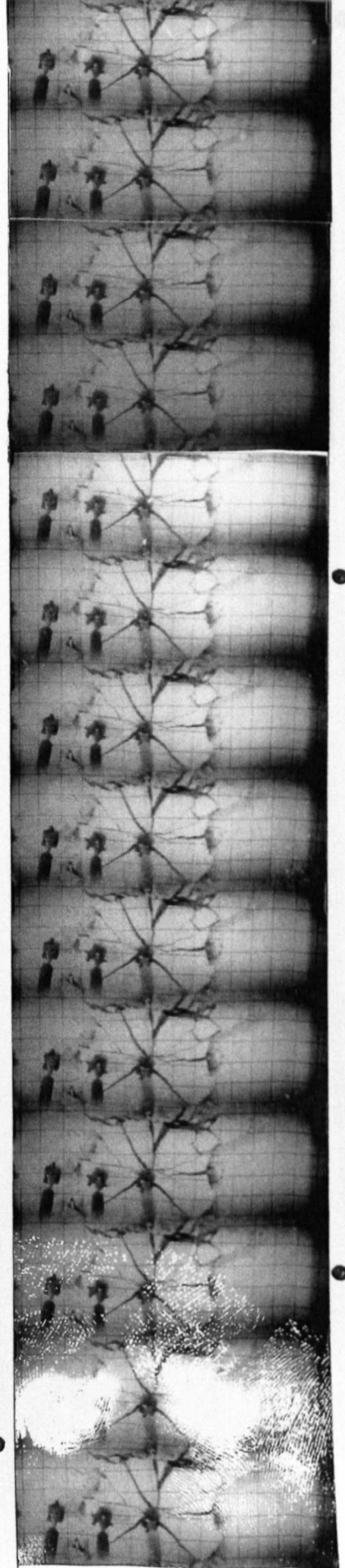
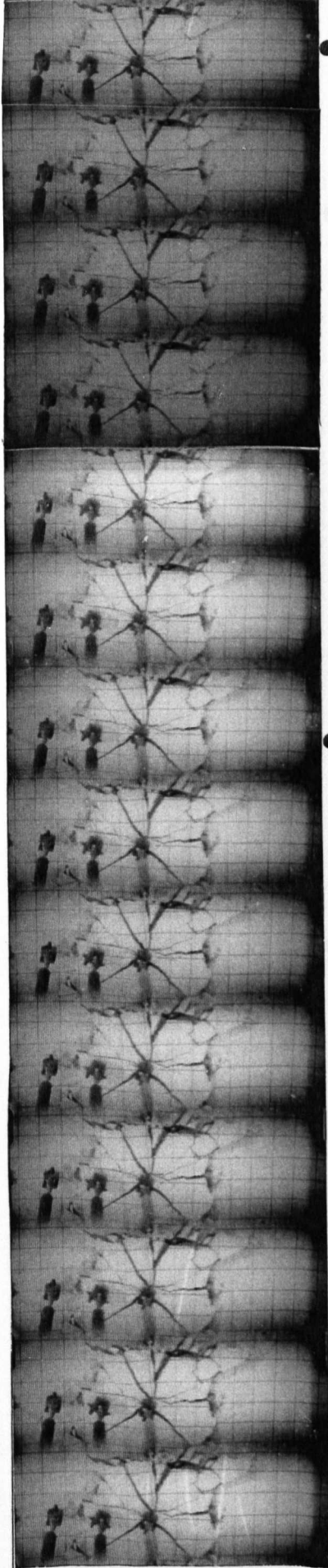
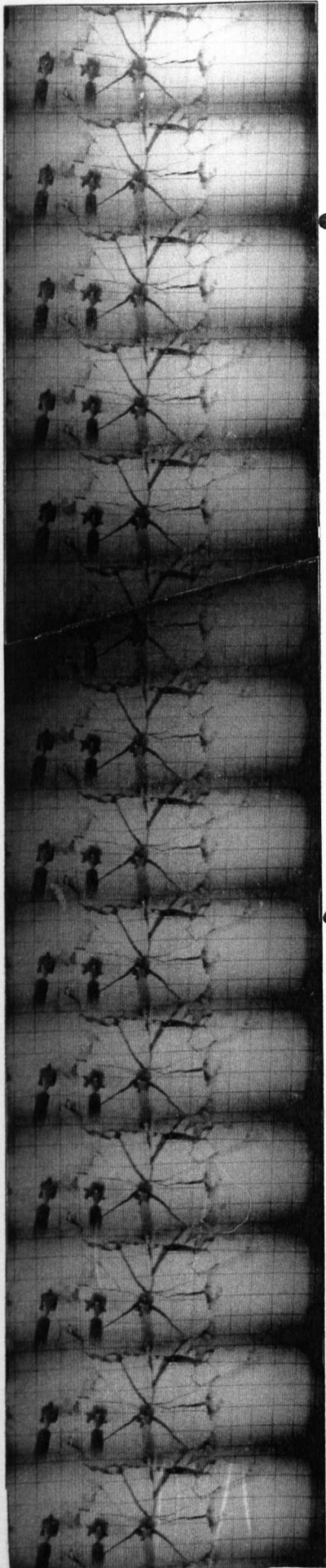
IMPACT TEST S12

INTERFRAME TIME 160.21 μ sec

∇ -IMPACT TIME

● -MSEC'S MARKER

4.



GRID SIZE : 36mm X 36mm

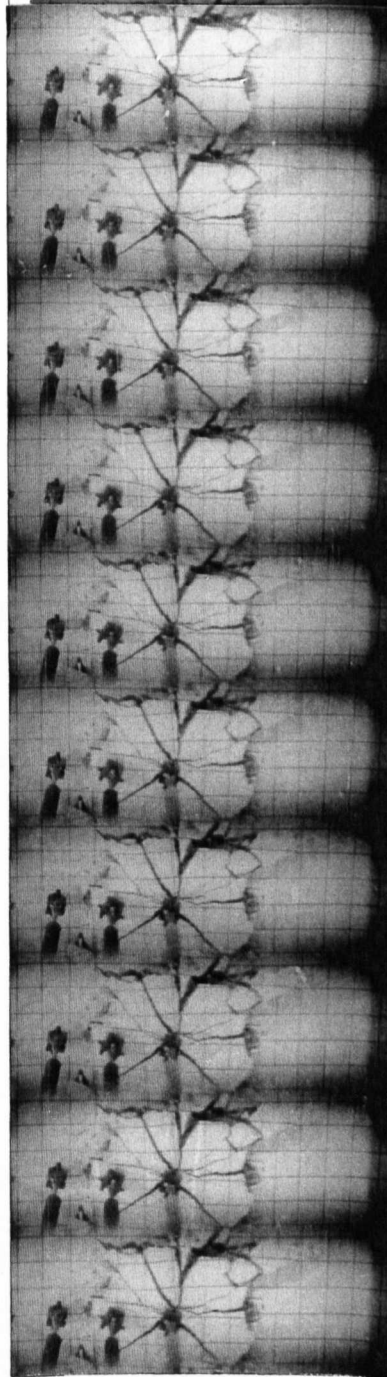
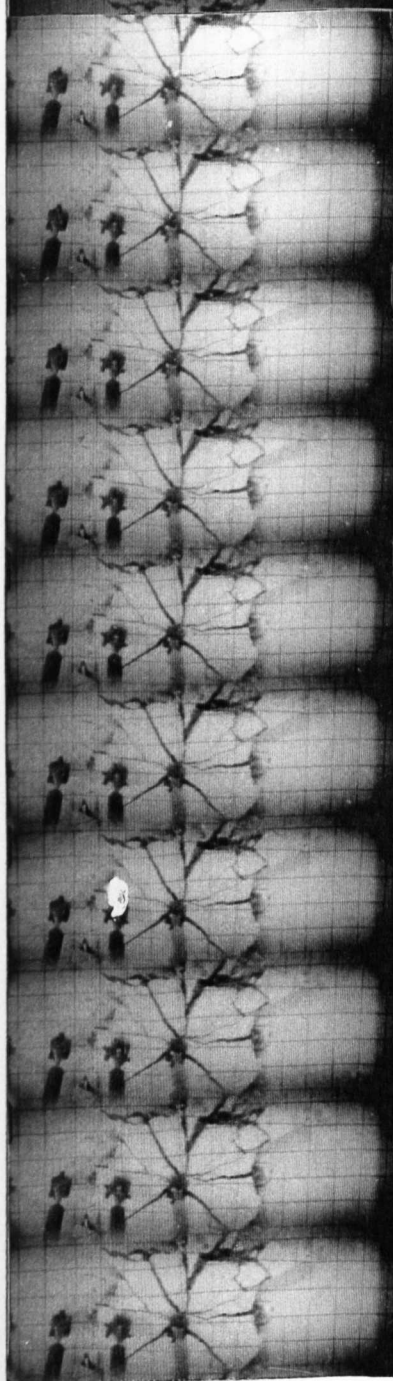
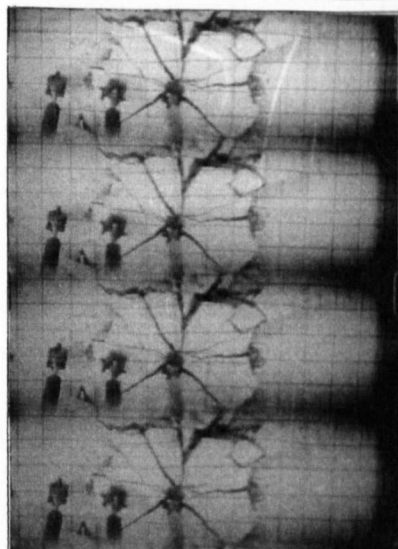
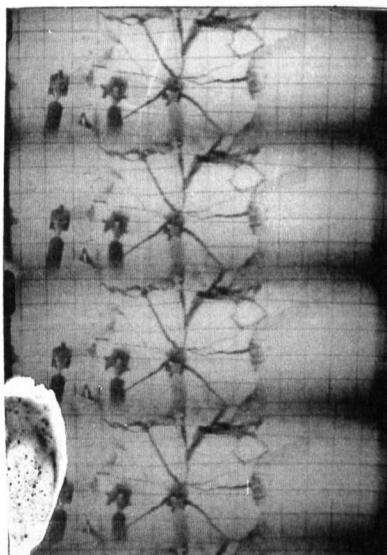
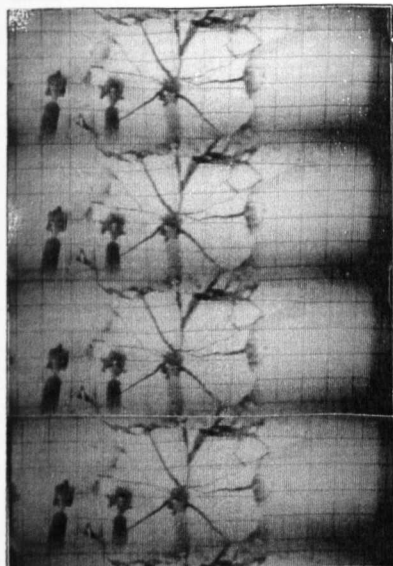
IMPACT TEST S12

INTERFRAME TIME 160.21 μ sec

∇ -IMPACT TIME

● -MSEC'S MARKER

5.



GRID SIZE : 36mm X 36mm

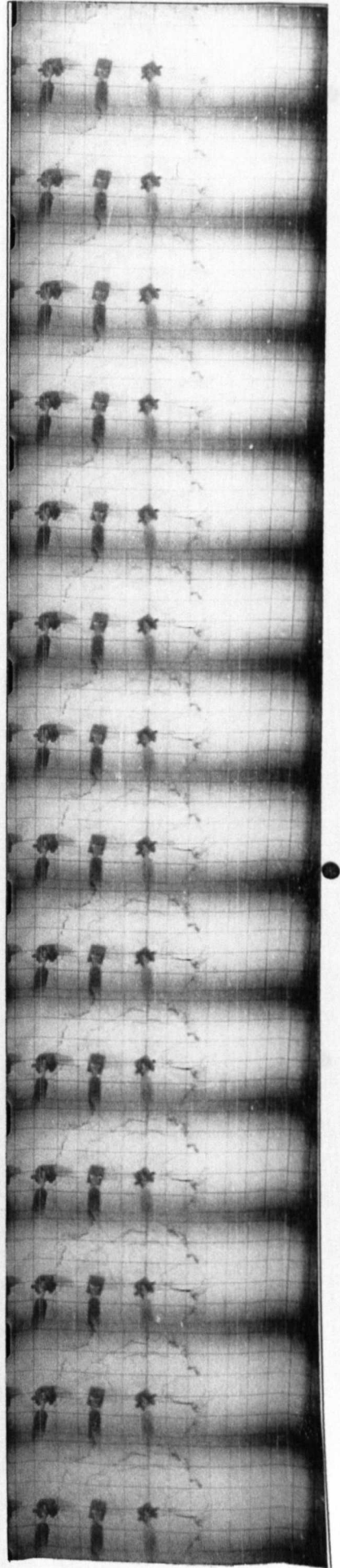
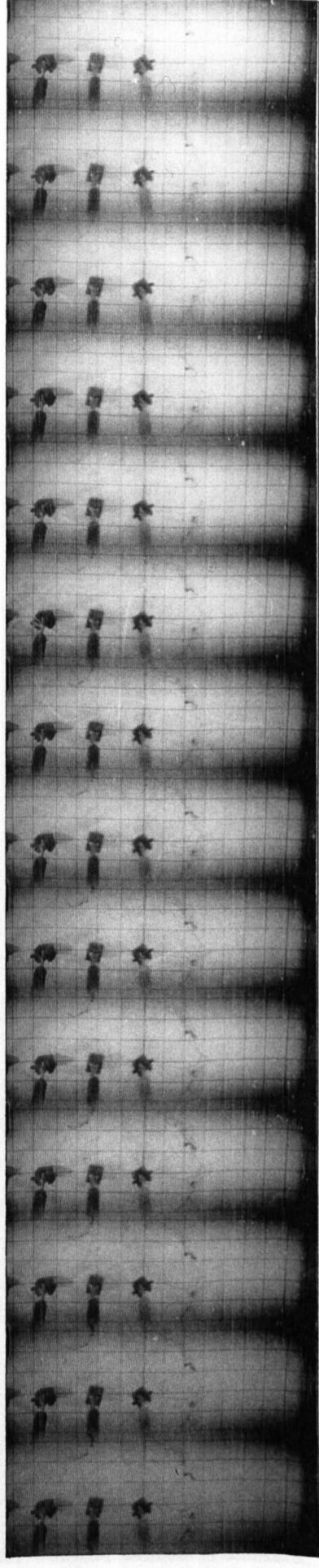
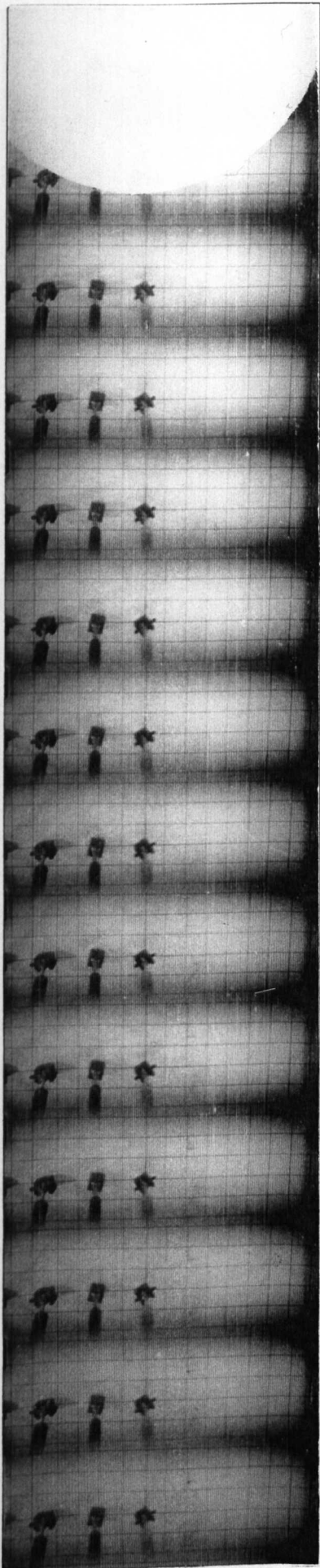
IMPACT TEST S13

INTERFRAME TIME 114.43 μ sec

∇ -IMPACT TIME

● -MSEC'S MARKER

1.



GRID SIZE : 36mm X 36mm

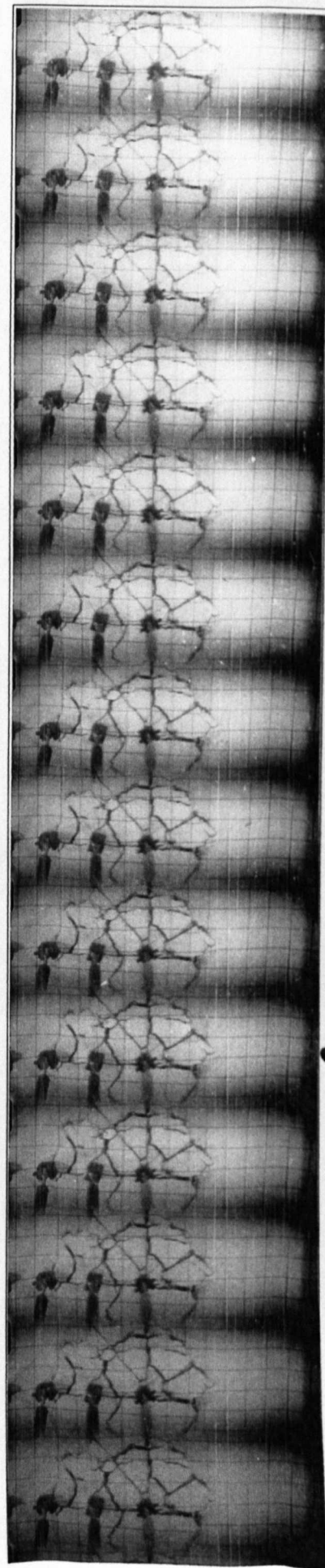
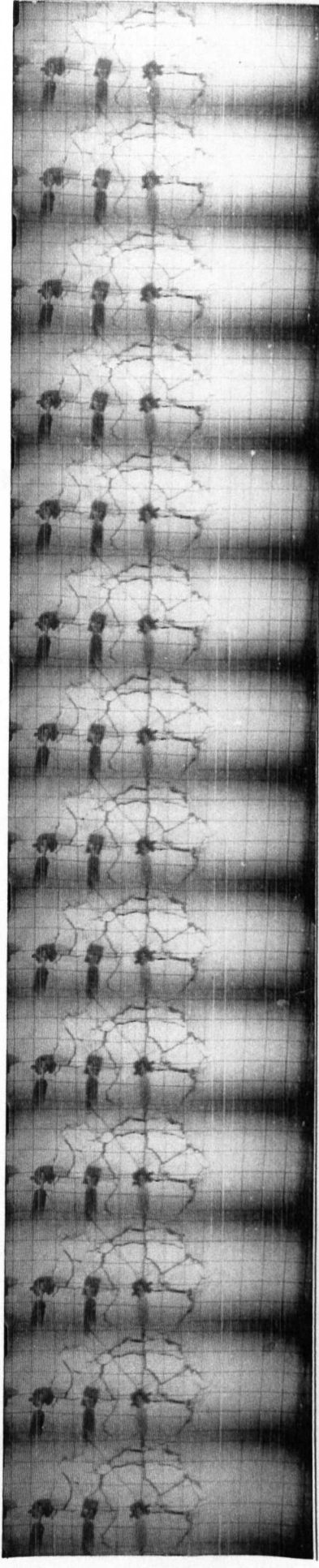
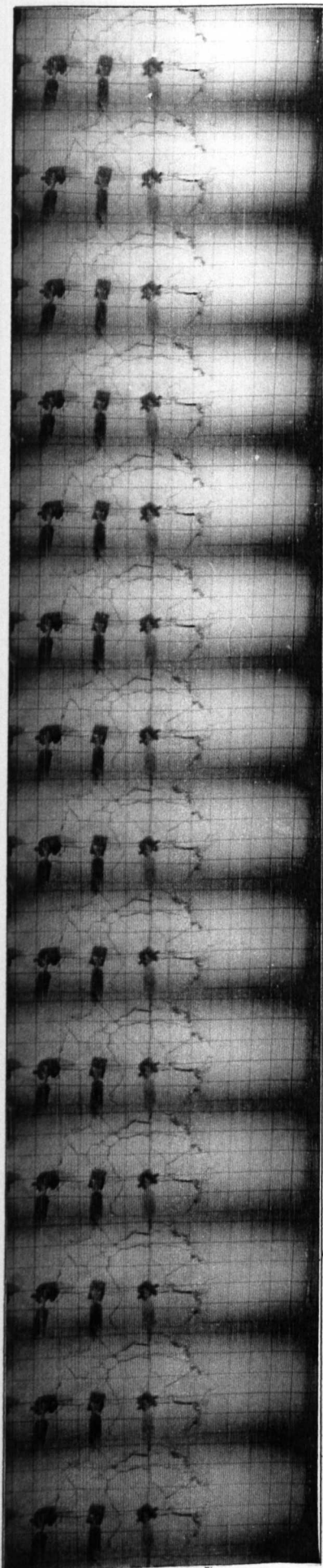
IMPACT TEST S13

INTERFRAME TIME 114.43 μ sec

▽ -IMPACT TIME

● -MSEC'S MARKER

2.



GRID SIZE : 36mm X 36mm

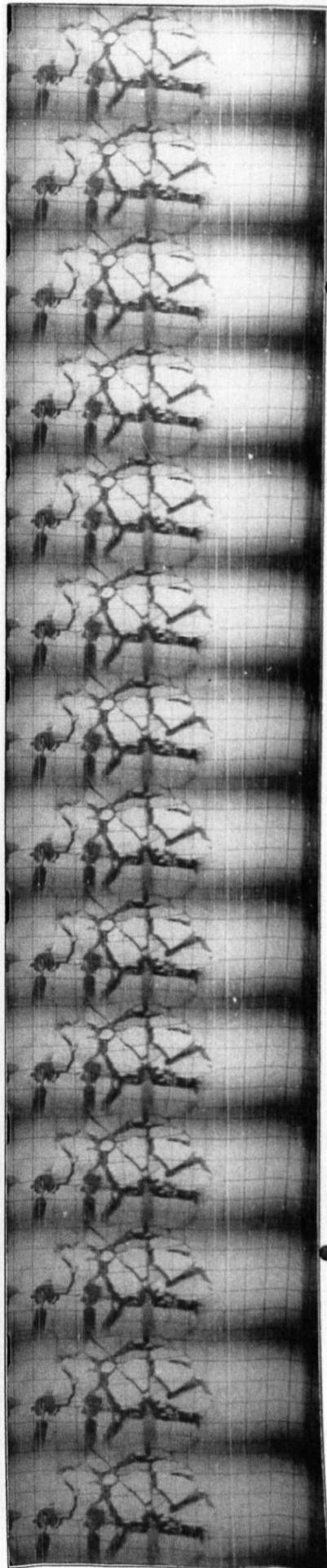
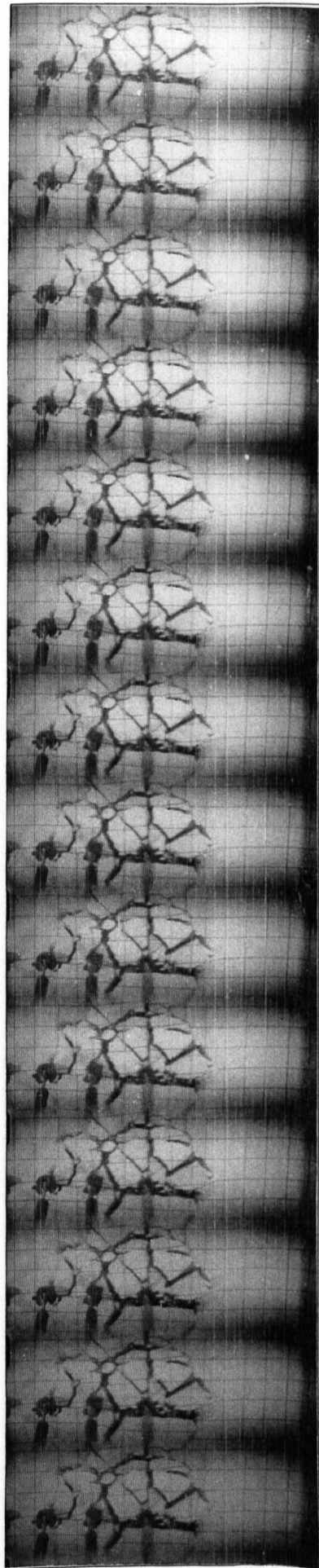
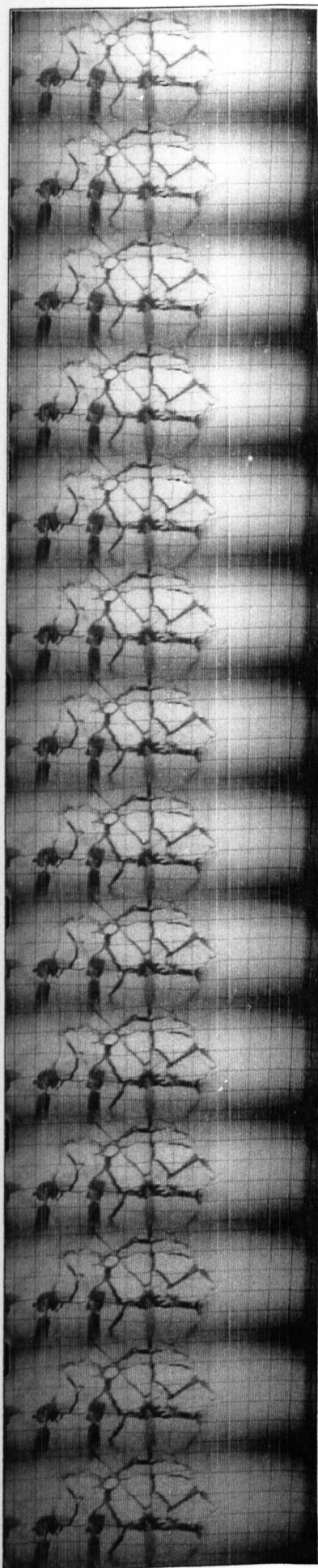
IMPACT TEST S13

INTERFRAME TIME 114.43 μ sec

∇ -IMPACT TIME

● -MSEC'S MARKER

3.



GRID SIZE : 36mm X 36mm

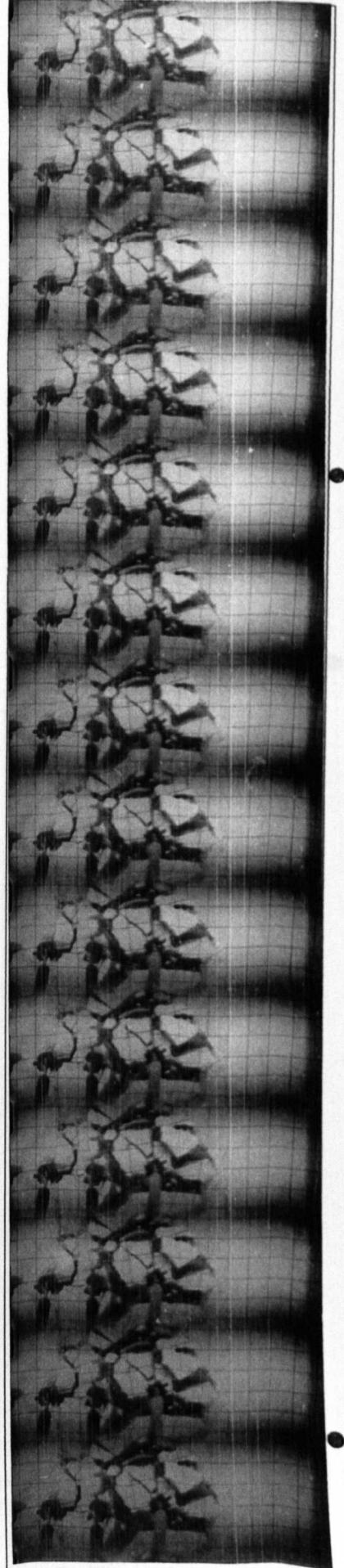
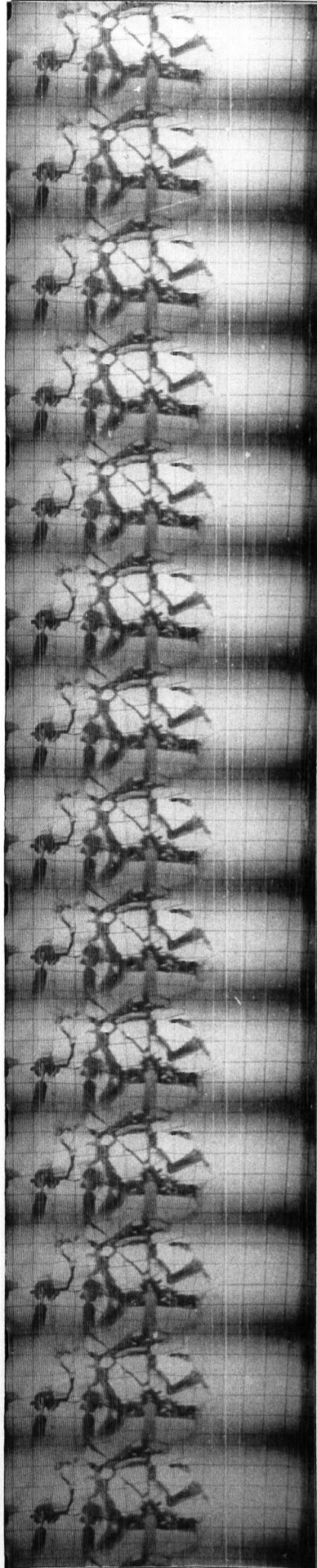
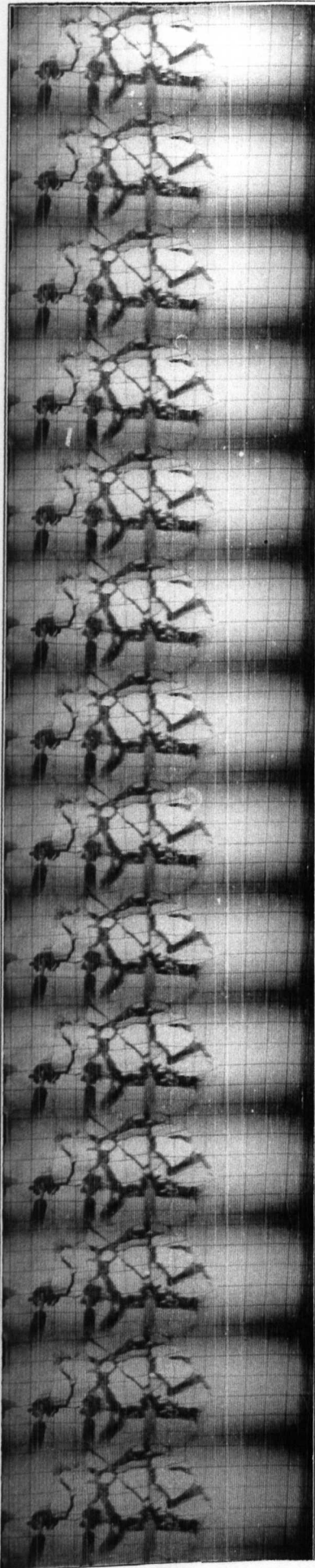
IMPACT TEST S13

INTERFRAME TIME 114.43 μ sec

∇ -IMPACT TIME

● -MSEC'S MARKER

4.



GRID SIZE : 36mm X 36mm

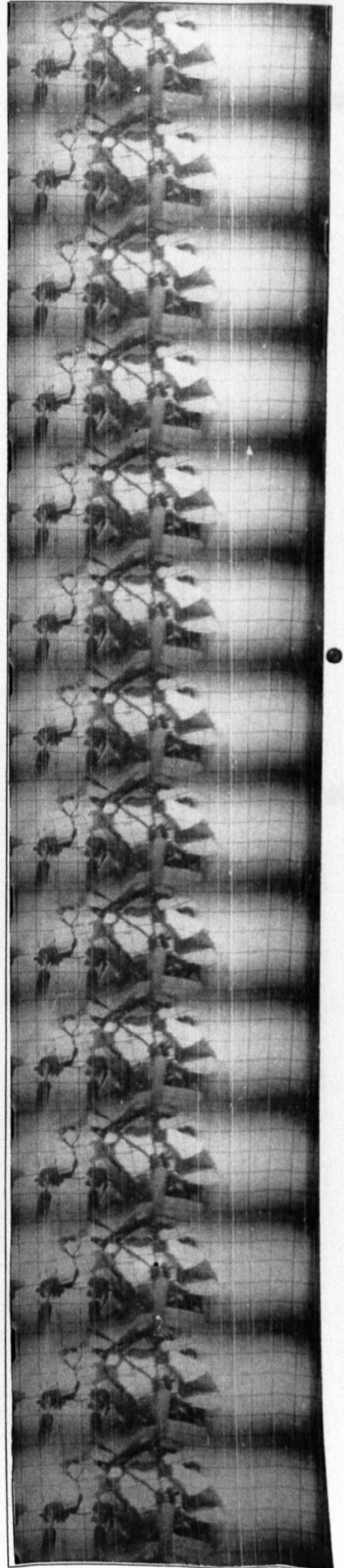
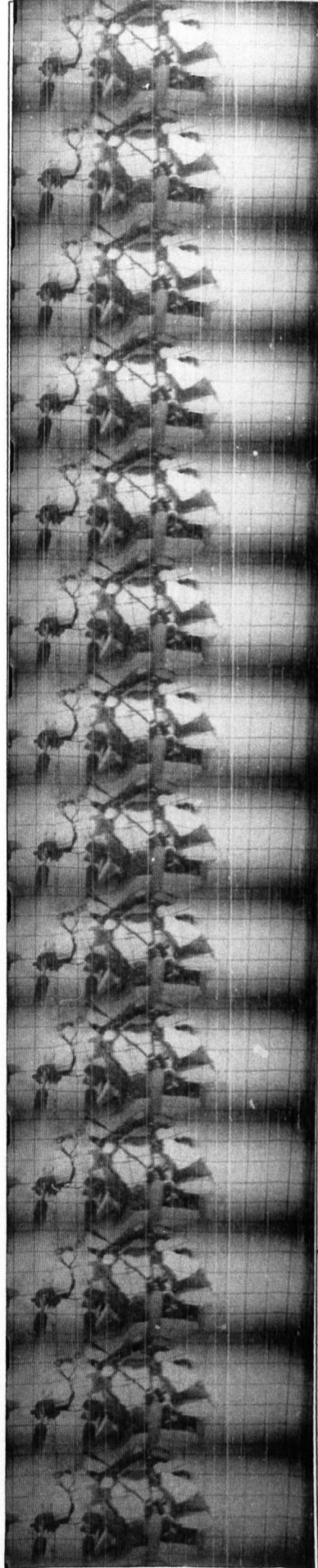
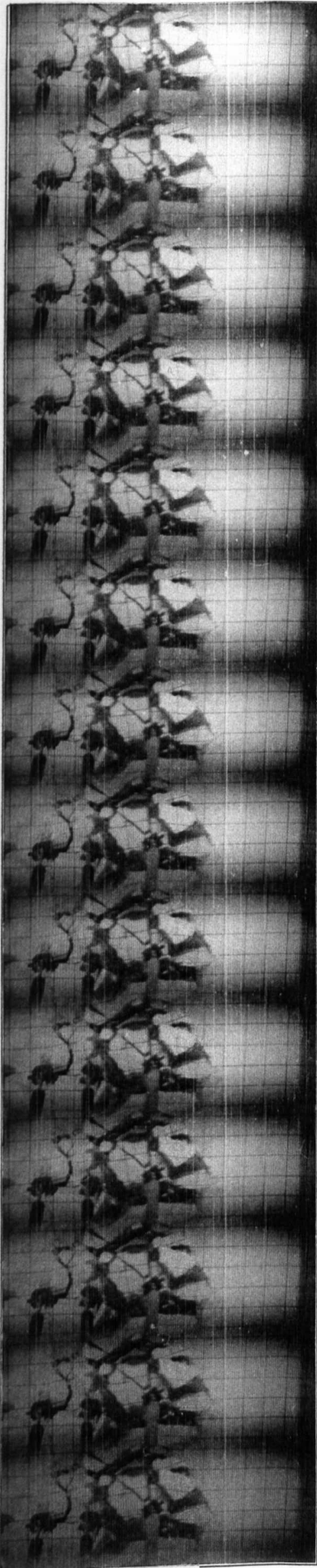
IMPACT TEST S13

INTERFRAME TIME 114.43 μ sec

∇ -IMPACT TIME

● -MSEC'S MARKER

5.



GRID SIZE : 36mm X 36mm

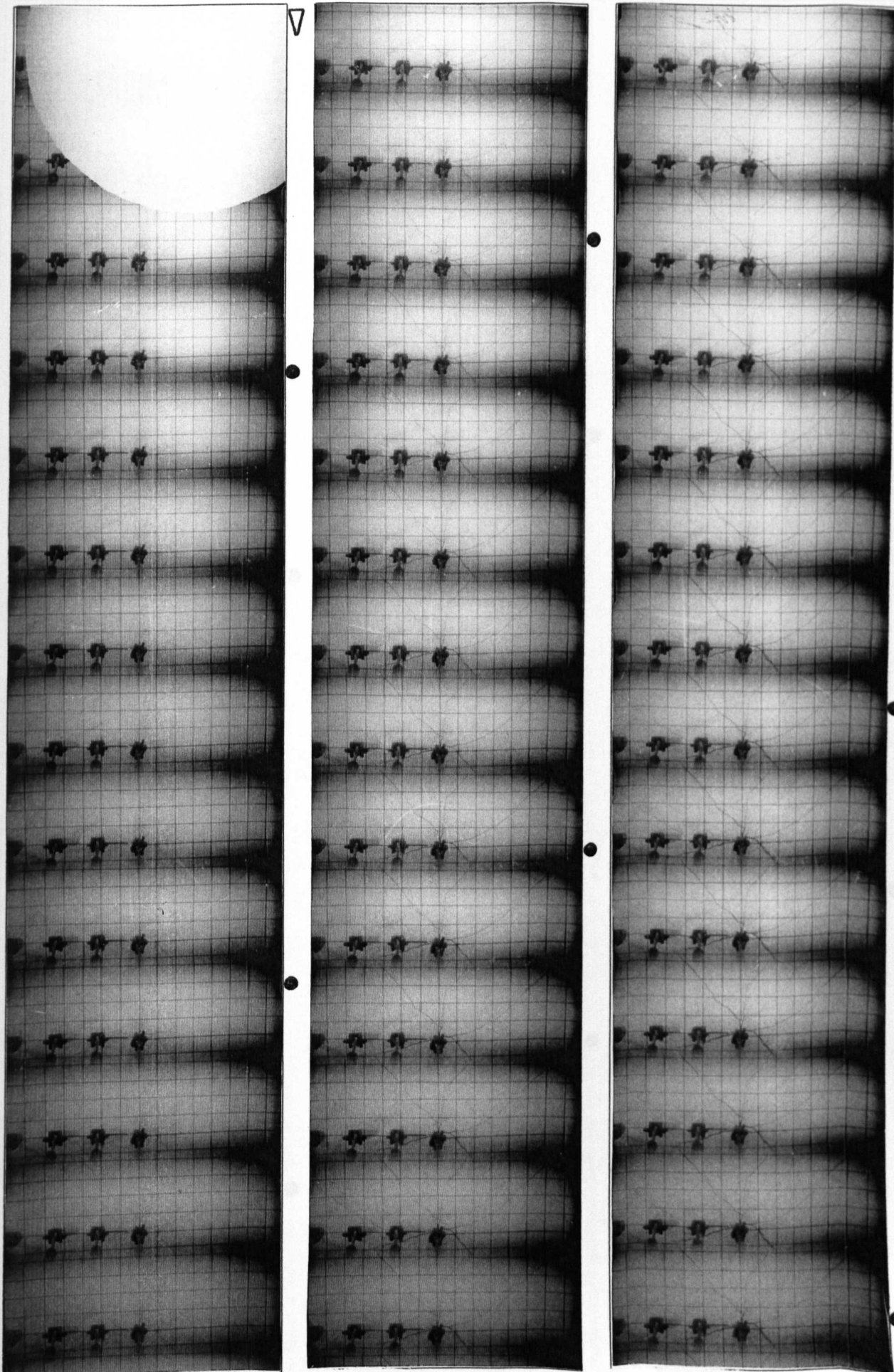
IMPACT TEST S17

INTERFRAME TIME 159.28 μ sec

▽ -IMPACT TIME

● -MSEC'S MARKER

1.



GRID SIZE : 36mm X 36mm

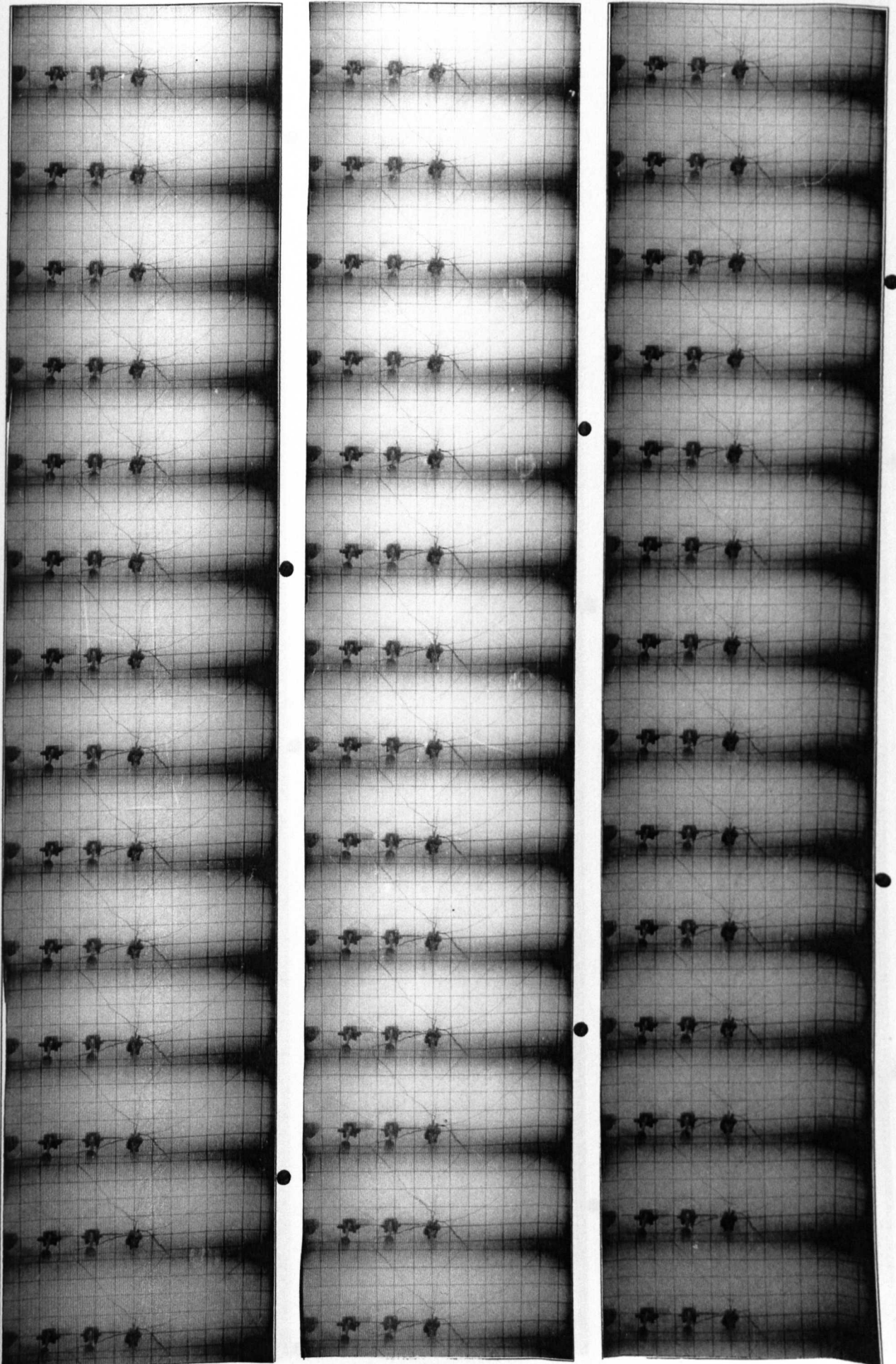
IMPACT TEST S17

INTERFRAME TIME 159.28 μ sec

▽ -IMPACT TIME

● -MSEC'S MARKER

2.



GRID SIZE : 36mm X 36mm

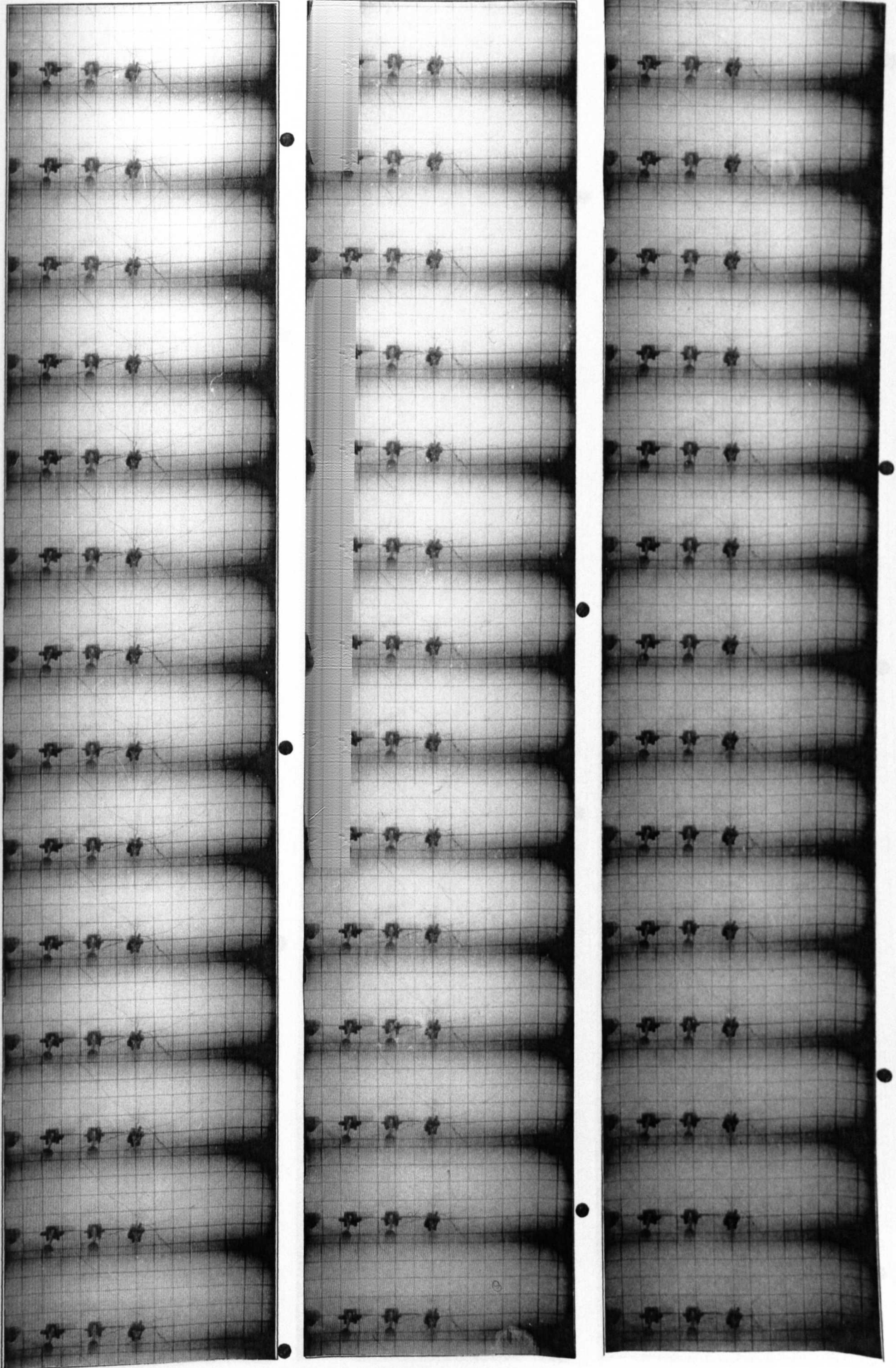
IMPACT TEST S17

INTERFRAME TIME 159.28 μ sec

▽ -IMPACT TIME

● -MSEC'S MARKER

3.



GRID SIZE : 36mm X 36mm

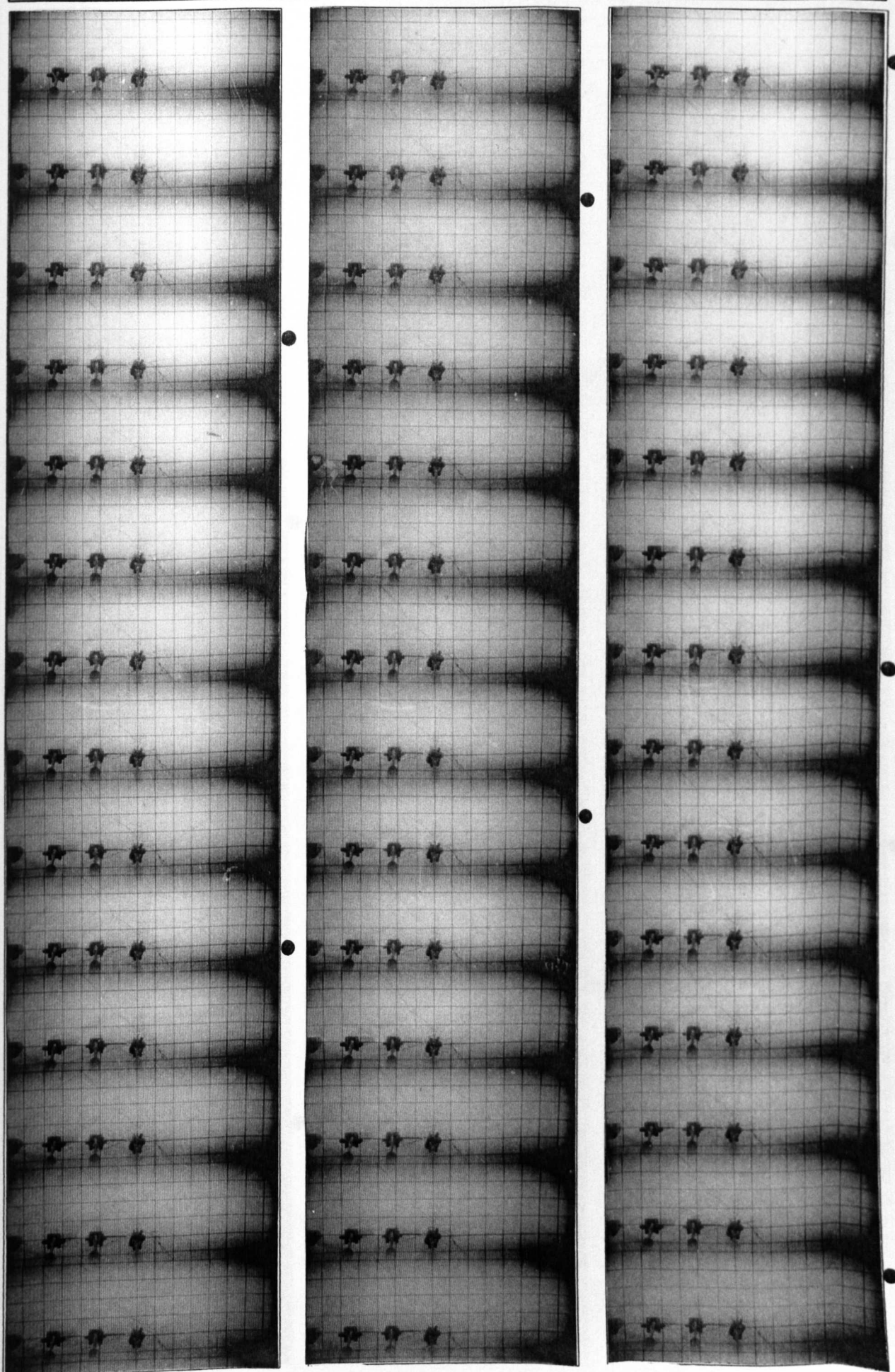
IMPACT TEST S17

INTERFRAME TIME 159.28 μ sec

∇ -IMPACT TIME

● -MSEC'S MARKER

4.



GRID SIZE : 36mm X 36mm

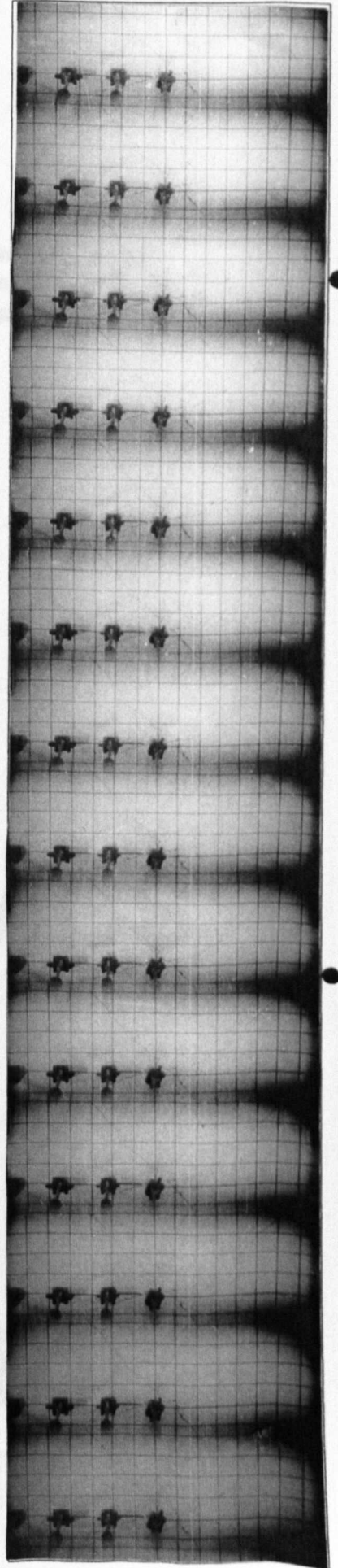
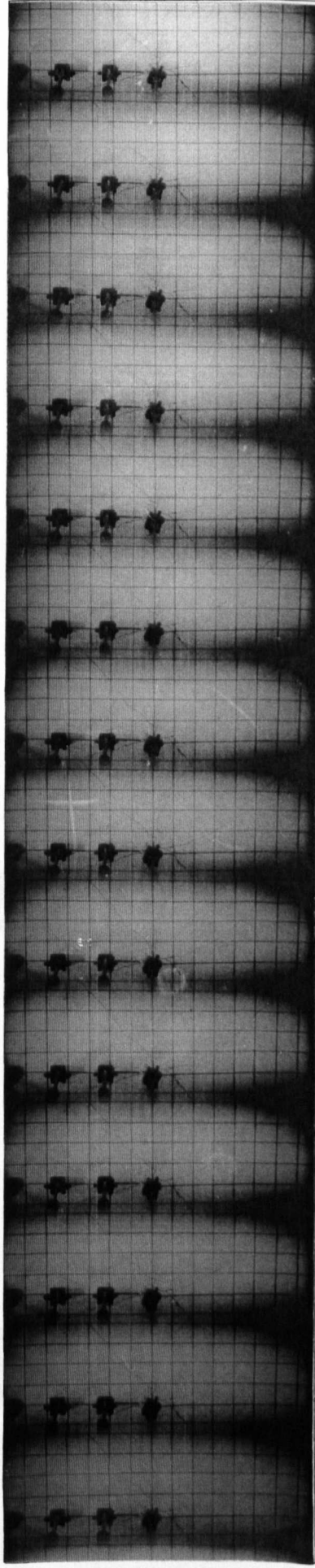
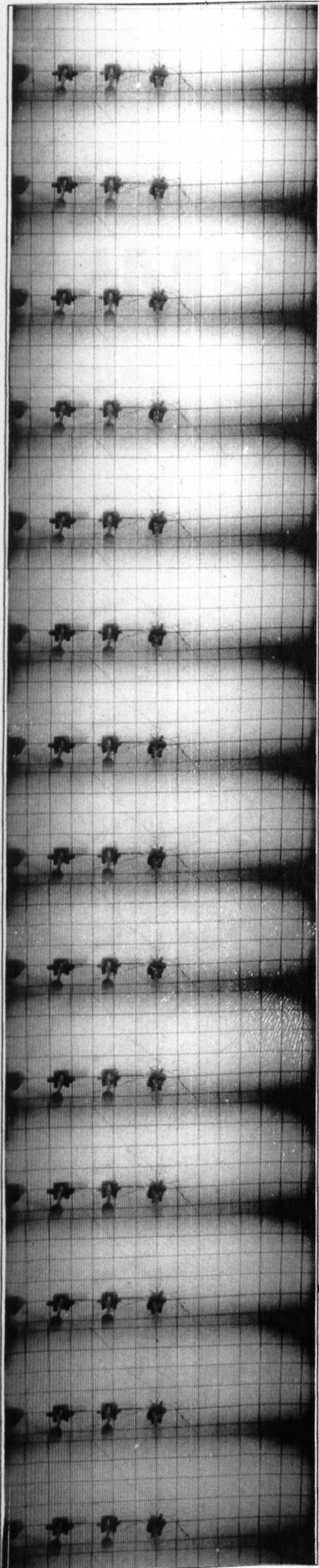
IMPACT TEST S17

INTERFRAME TIME 159.28 μ sec

▽ -IMPACT TIME

● -MSEC'S MARKER

5.



GRID SIZE : 36mm X 36mm

IMPULSE TEST RESULTS

1:1 SCALE SLABS

APPENDIX B1

IMPULSE TEST

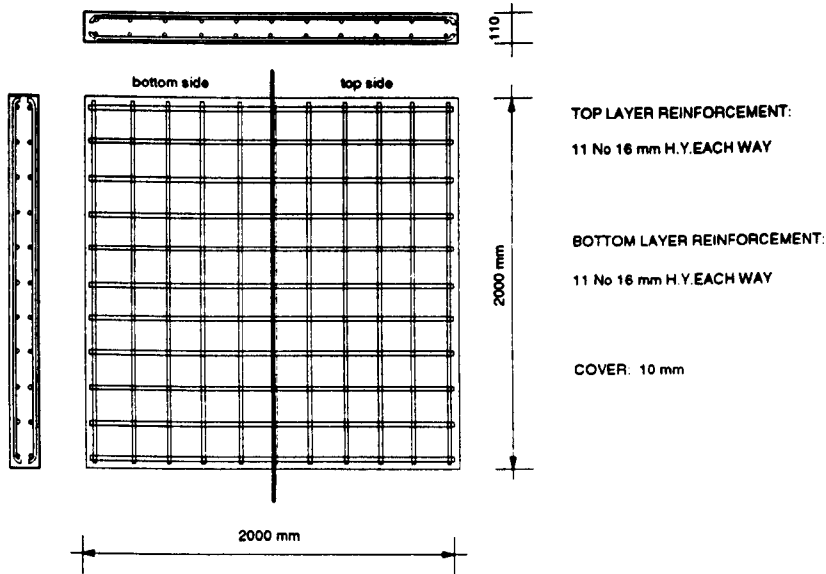
DATE: 15.01.91

LARGE SLAB LSE1

AGE OF SPECIMEN: 7 days

Cube compressive strength	N/mm ²	47.8	Cylinder tensile strength	N/mm ²	3.78	Age (days)	8
---------------------------	-------------------	------	---------------------------	-------------------	------	------------	---

REINFORCEMENT:



LOADING CONDITIONS:

(1st shot)

CHARGE WEIGHT : 1300g, PE4

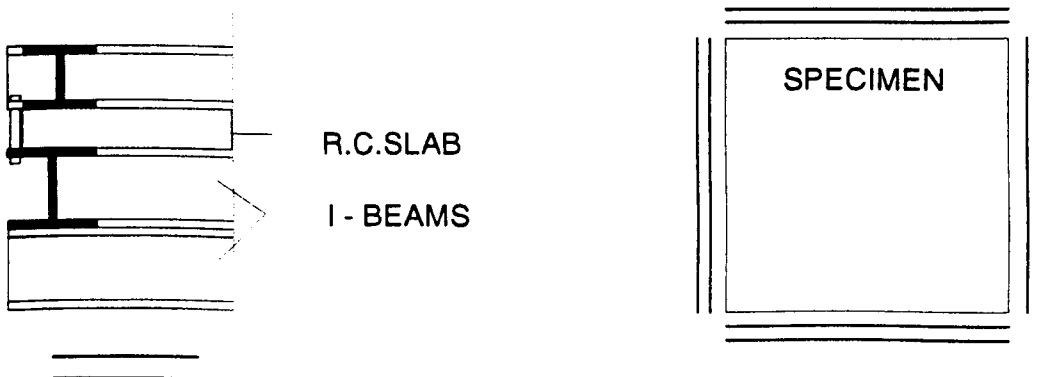
CHARGE SHAPE : Hemispherical

CHARGE DIRECTION..... : Spherical side facing the specimen

CHARGE POSITION : Central

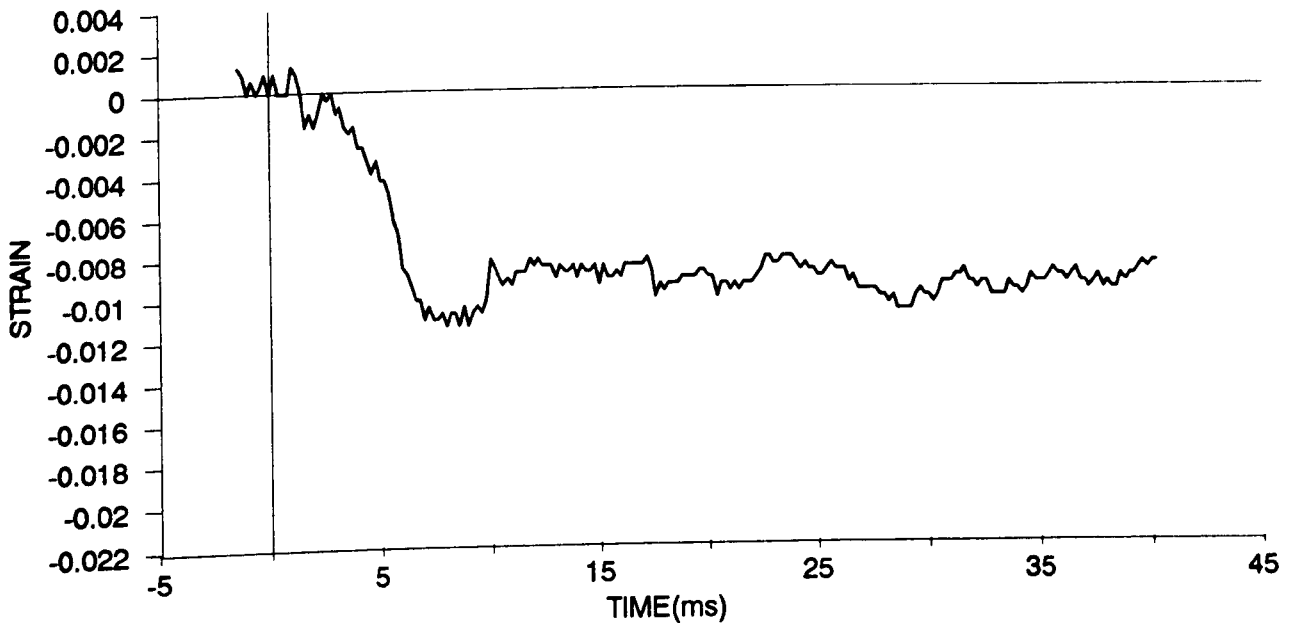
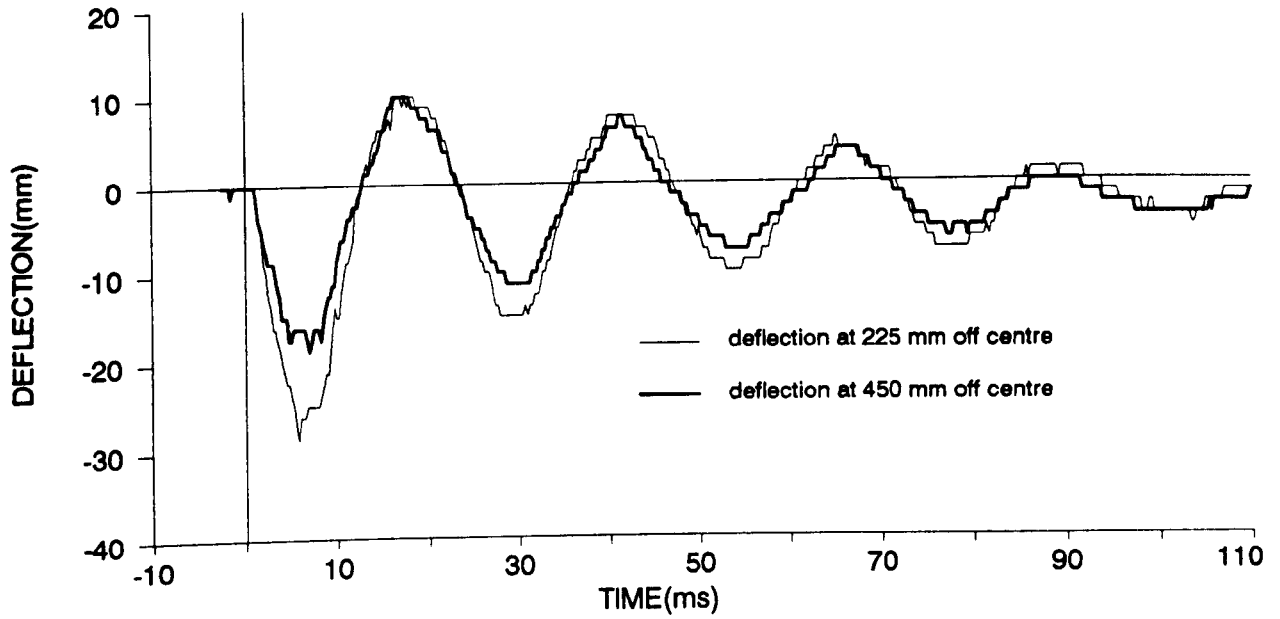
CLEAR DISTANCE TO THE CHARGE : 350mm

SUPPORTS



IMPULSE TEST - LARGE SLAB - LSE1

SHOT 1.



IMPULSE TEST

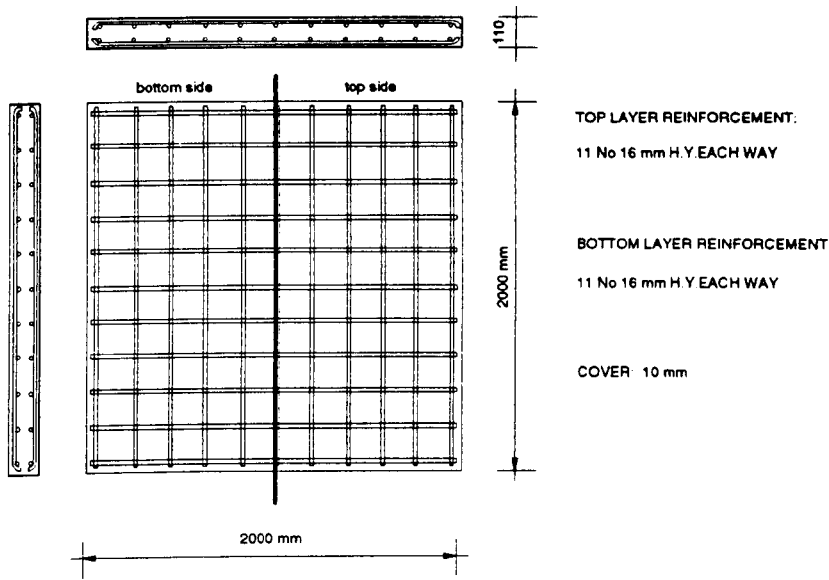
DATE: 16.01.91

LARGE SLAB LSE1

AGE OF SPECIMEN: 7 days

Cube compressive strength	N/mm ²	47.8	Cylinder tensile strength	N/mm ²	3.78	Age (days)	9
---------------------------	-------------------	------	---------------------------	-------------------	------	------------	---

REINFORCEMENT:

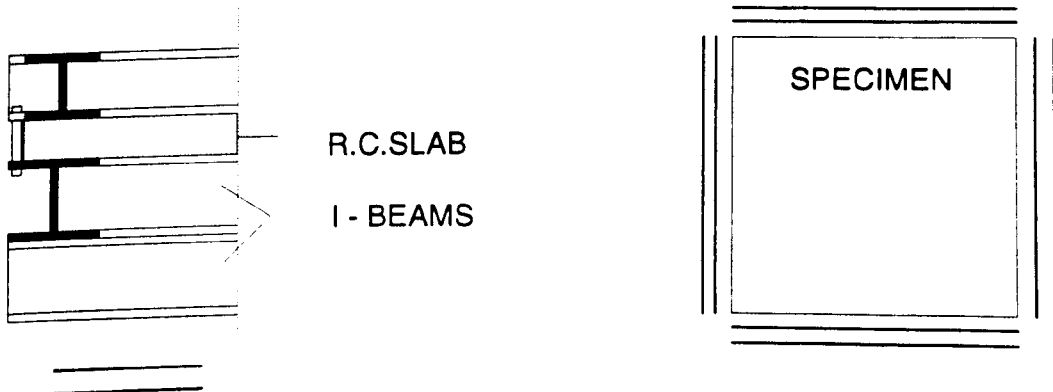


LOADING CONDITIONS:

(2nd shot)

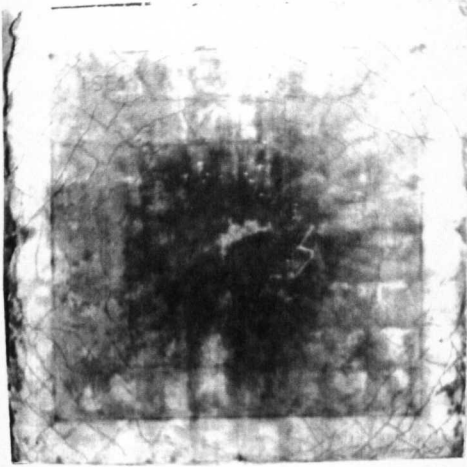
CHARGE WEIGHT : 1300g, PE4
CHARGE SHAPE : Hemispherical
CHARGE DIRECTION..... : Spherical side facing the specimen
CHARGE POSITION : Central
CLEAR DISTANCE TO THE CHARGE : 250mm

SUPPORTS

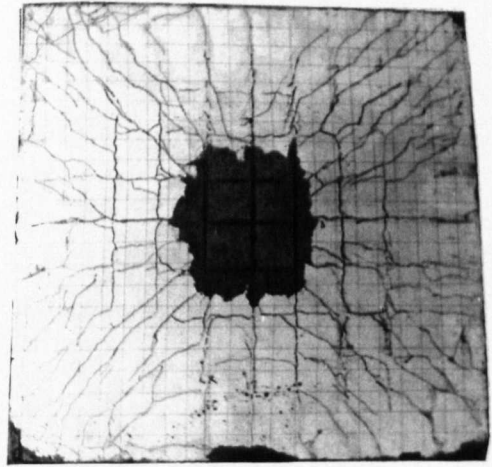


IMPULSE TEST - LARGE SLAB - LSE1

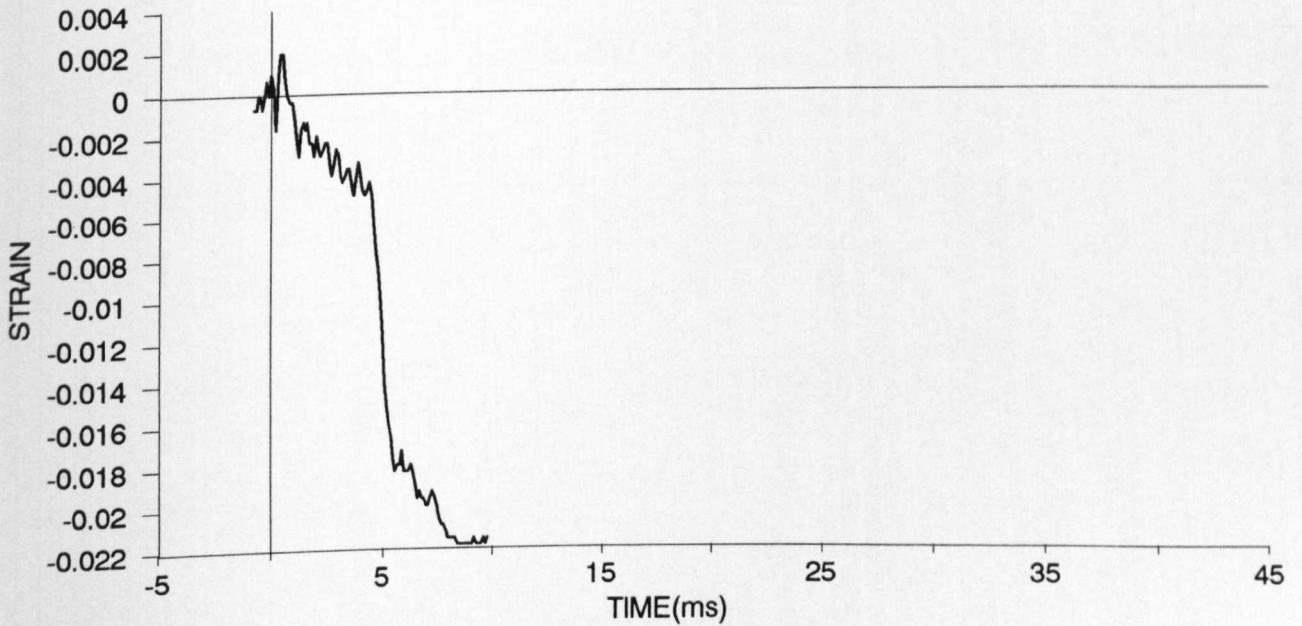
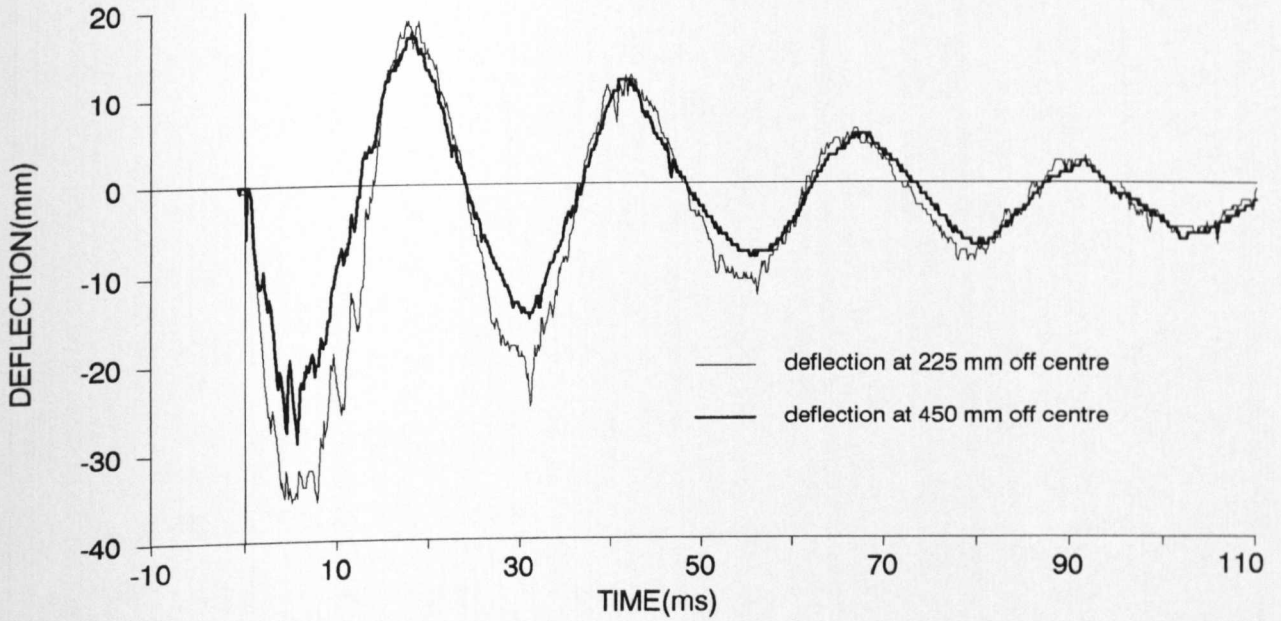
SHOT 2.



top side



bottom side



IMPULSE TEST

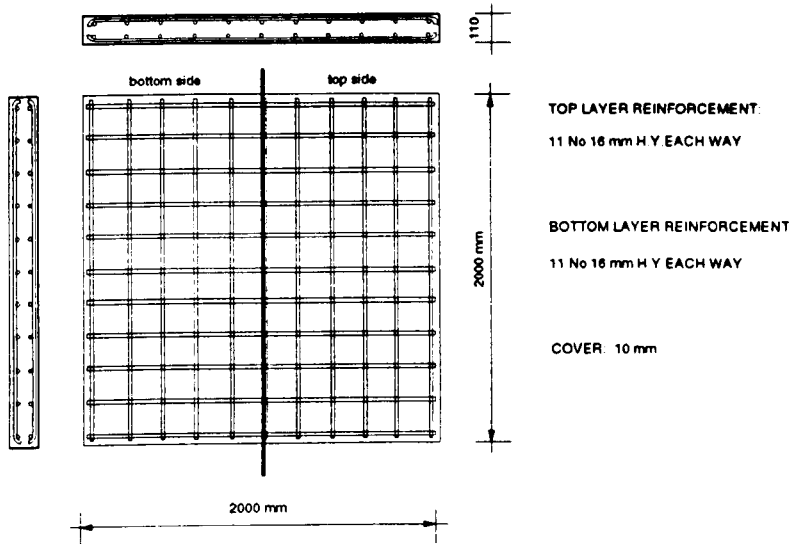
DATE: 6.03.91

LARGE SLAB LSE2

AGE OF SPECIMEN: 7 days

Cube compressive strength	N/mm ²	46.8	Cylinder tensile strength	N/mm ²	3.86	Age (days)	8
---------------------------	-------------------	------	---------------------------	-------------------	------	------------	---

REINFORCEMENT:



LOADING CONDITIONS:

CHARGE WEIGHT : 1300g, PE4

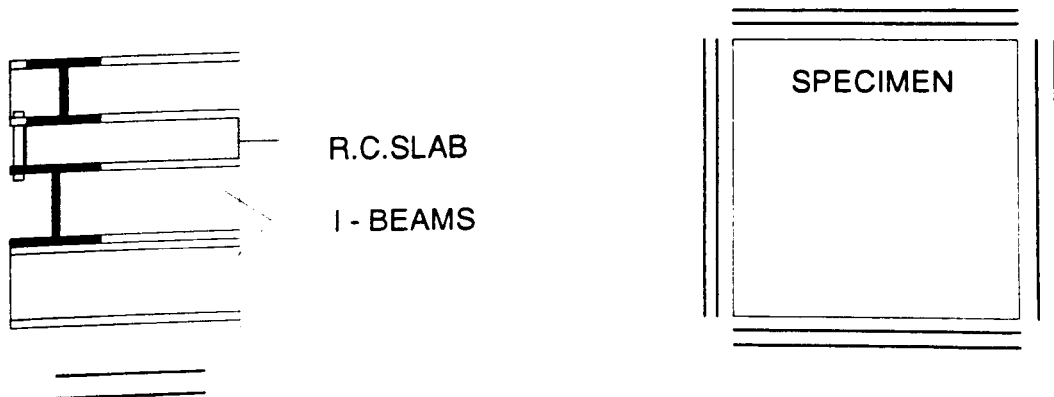
CHARGE SHAPE : Hemispherical

CHARGE DIRECTION..... : Spherical side facing the specimen

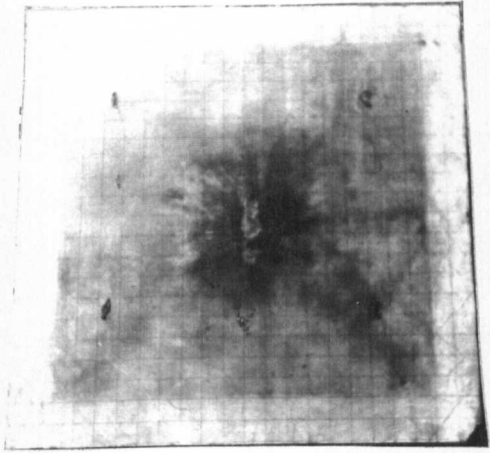
CHARGE POSITION : Central

CLEAR DISTANCE TO THE CHARGE : 250mm

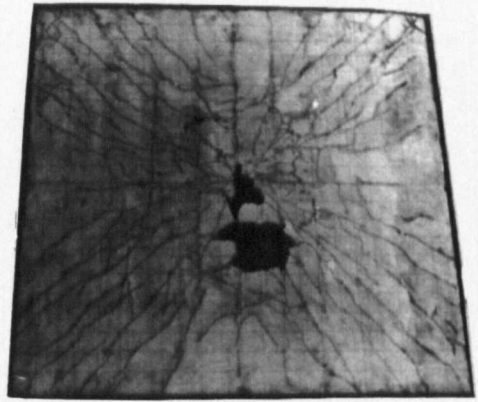
SUPPORTS



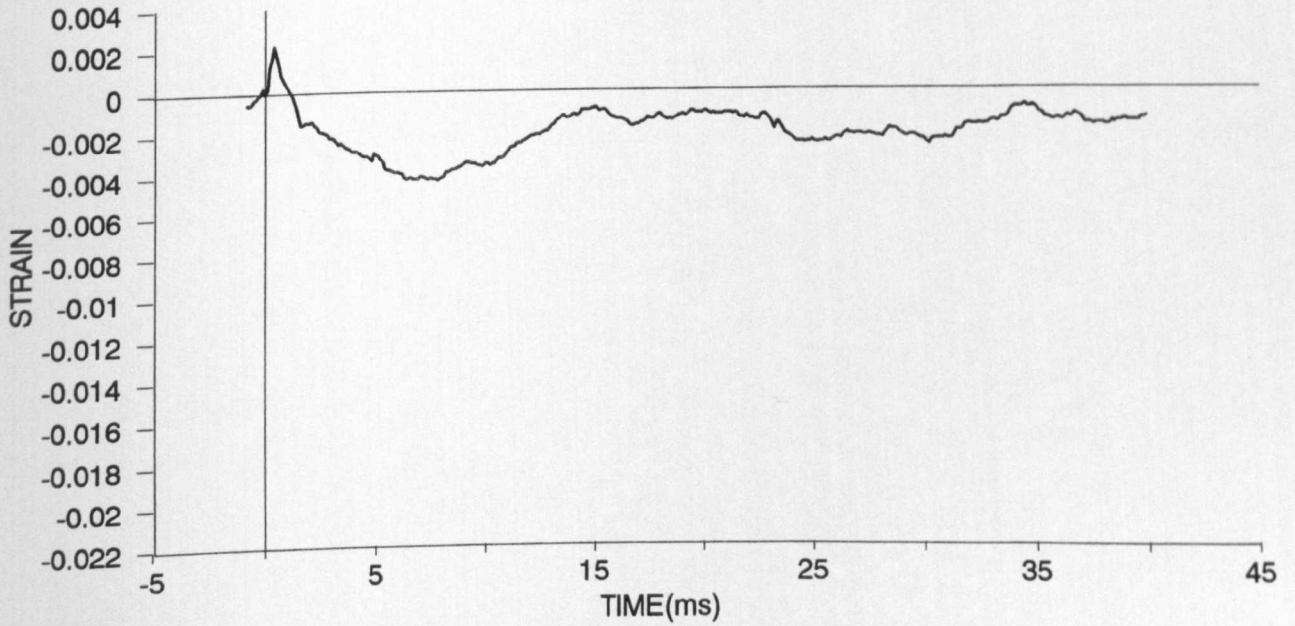
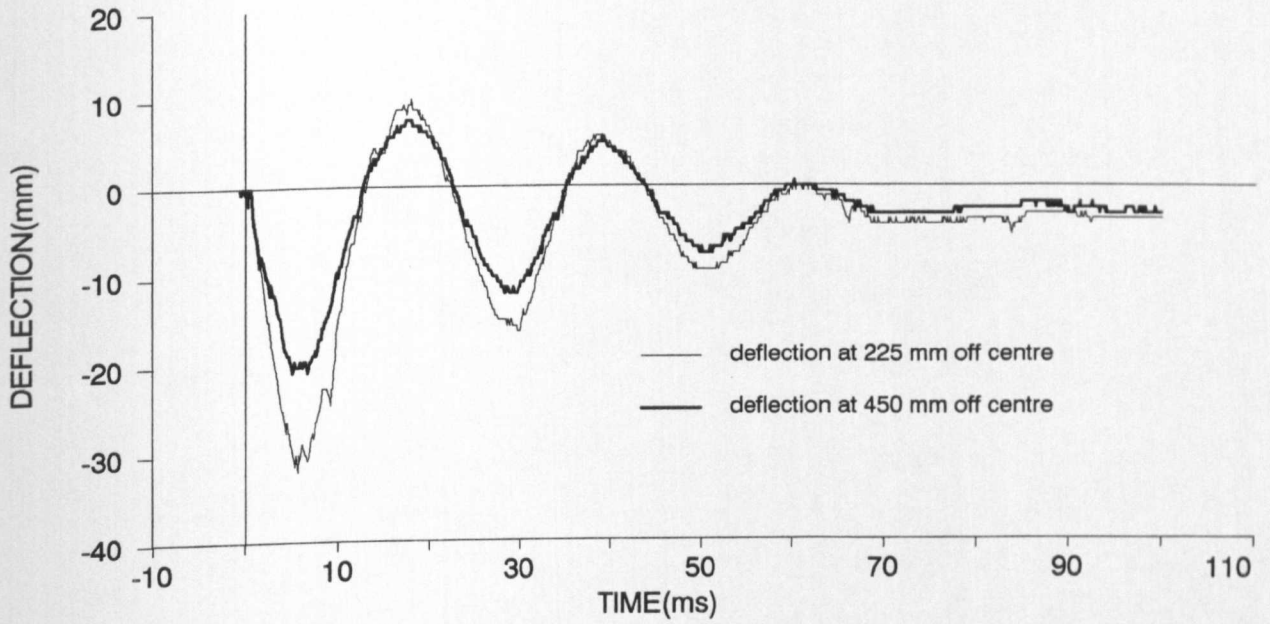
IMPULSE TEST - LARGE SLAB - LSE2



top side



bottom side



IMPULSE TEST

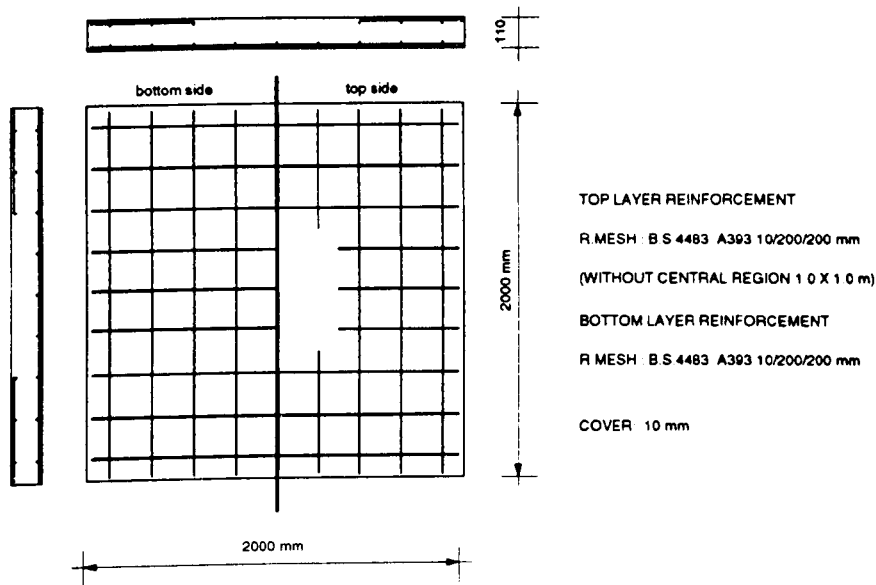
DATE: 8.09.92

LARGE SLAB LSE3

AGE OF SPECIMEN: 7 days

Cube compressive strength	N/mm ²	39.06	Cylinder tensile strength	N/mm ²	3.61	Age (days)	7
---------------------------	-------------------	-------	---------------------------	-------------------	------	------------	---

REINFORCEMENT:



LOADING CONDITIONS:

CHARGE WEIGHT : 1300g, PE4

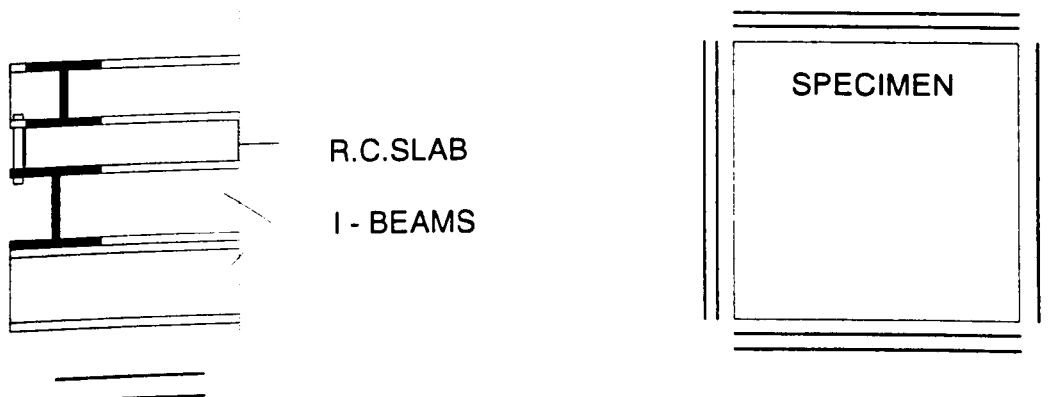
CHARGE SHAPE : Hemispherical

CHARGE DIRECTION..... : Spherical side facing the specimen

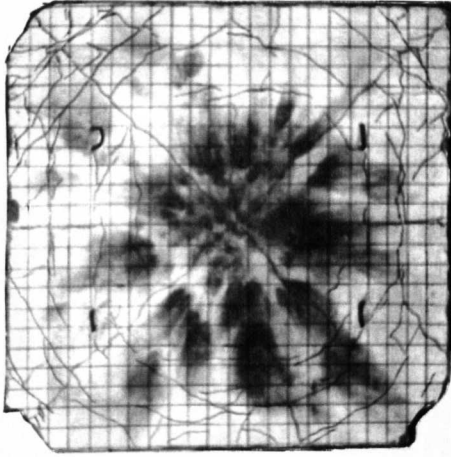
CHARGE POSITION : Central

CLEAR DISTANCE TO THE CHARGE : 500mm

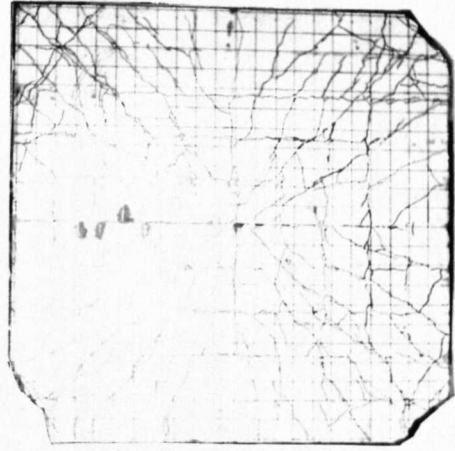
SUPPORTS



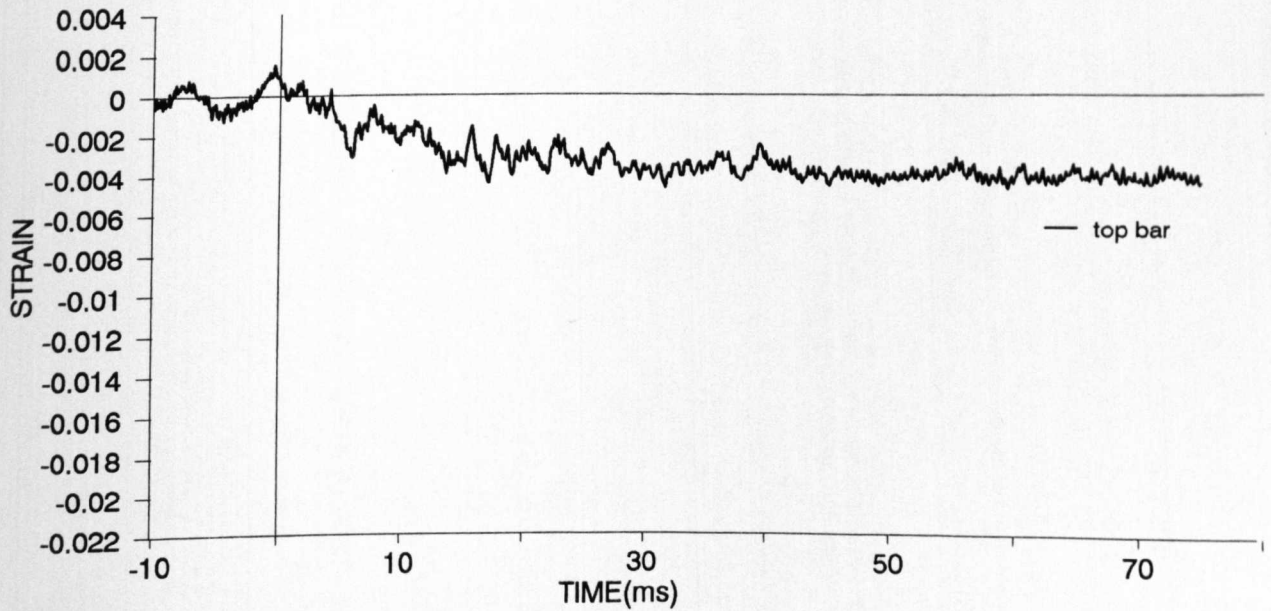
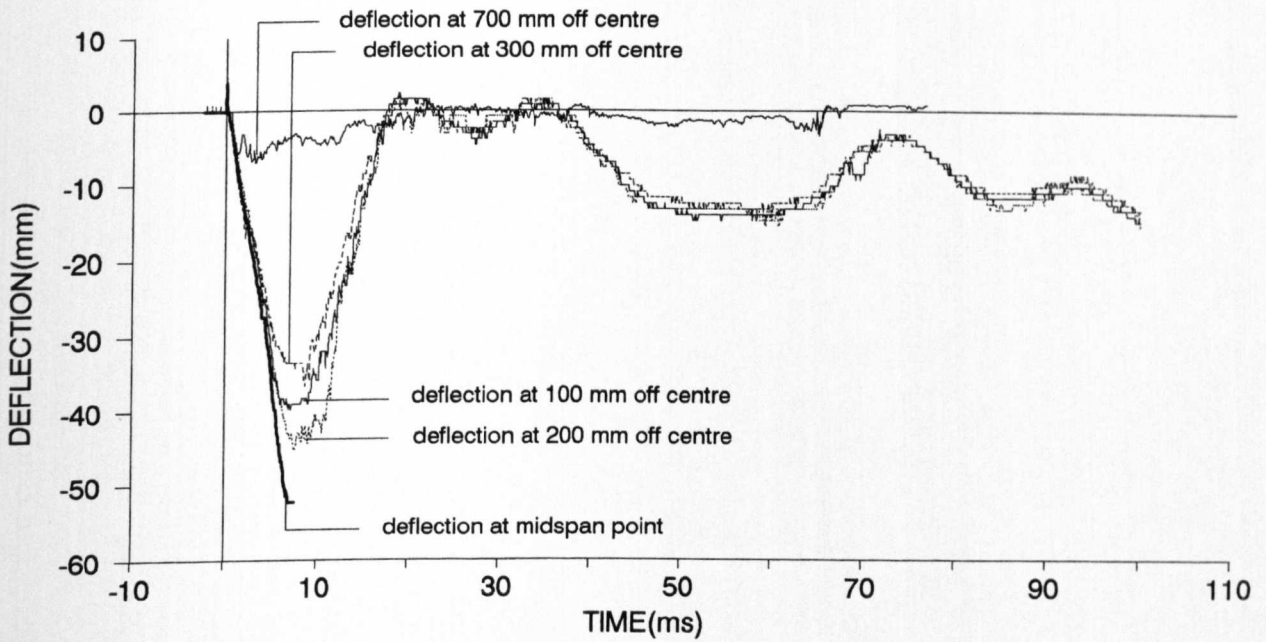
IMPULSE TEST - LARGE SLAB - LSE3



top side



bottom side



IMPULSE TEST

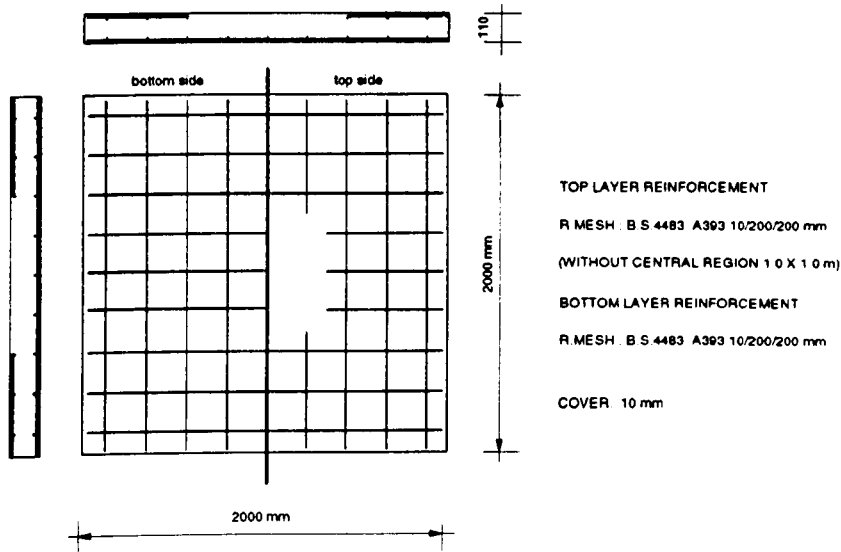
DATE: 23.09.92

LARGE SLAB LSE4

AGE OF SPECIMEN: 7 days

Cube compressive strength	N/mm ²	38.7	Cylinder tensile strength	N/mm ²	3.54	Age (days)	7
---------------------------	-------------------	------	---------------------------	-------------------	------	------------	---

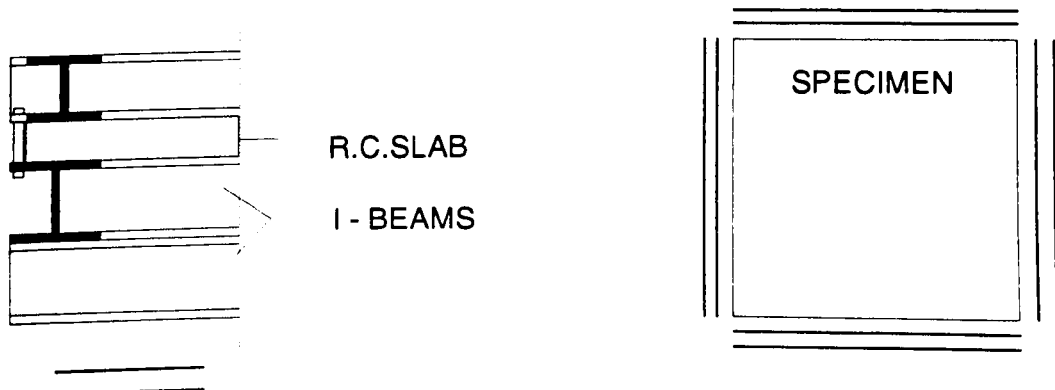
REINFORCEMENT:



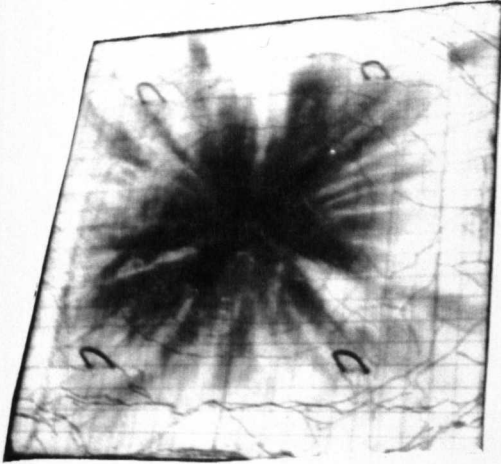
LOADING CONDITIONS:

- CHARGE WEIGHT : 1300g, PE4
CHARGE SHAPE : Hemispherical
CHARGE DIRECTION..... : Spherical side facing the specimen
CHARGE POSITION : Central
CLEAR DISTANCE TO THE CHARGE : 300mm

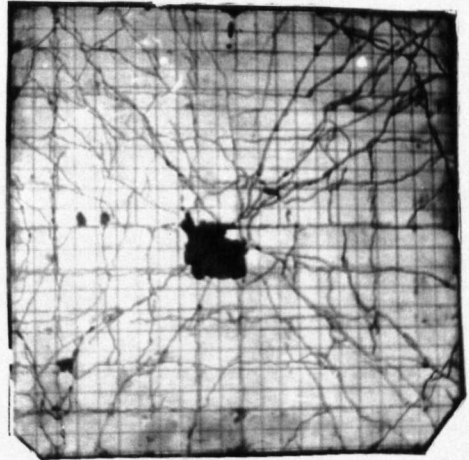
SUPPORTS



IMPULSE TEST - LARGE SLAB - LSE4



top side



bottom side

**** THE STRAIN AND DISPLACEMENT HAVE NOT BEEN RECORDED**

IMPULSE TEST

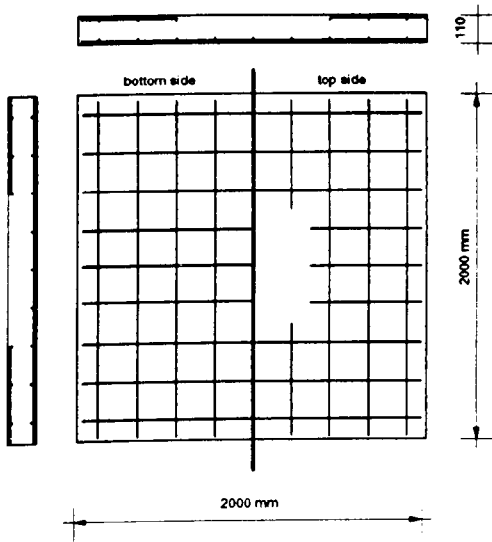
DATE: 6.10.92

LARGE SLAB LSE5

AGE OF SPECIMEN: 8 days

Cube compressive strength	N/mm ²	36.4	Cylinder tensile strength	N/mm ²	3.24	Age (days)	8
---------------------------	-------------------	------	---------------------------	-------------------	------	------------	---

REINFORCEMENT:



TOP LAYER REINFORCEMENT

R MESH : B.S. 4483 A393 10/200/200 mm
(WITHOUT CENTRAL REGION 1 0 X 1 0 m)

BOTTOM LAYER REINFORCEMENT

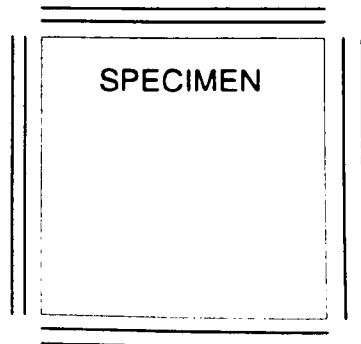
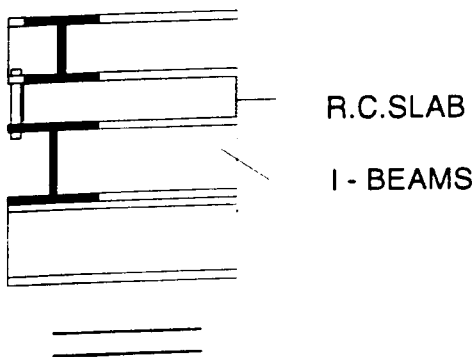
R.MESH : B.S. 4483 A393 10/200/200 mm

COVER: 10 mm

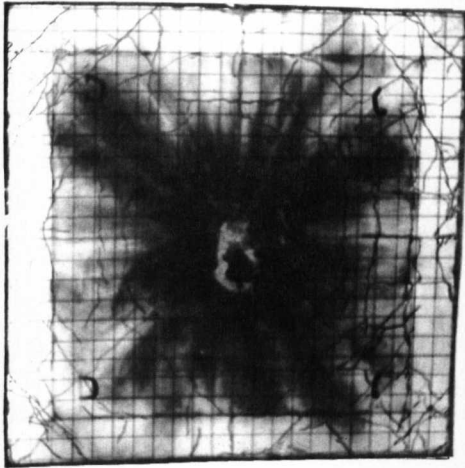
LOADING CONDITIONS:

- CHARGE WEIGHT : 1300g, PE4
- CHARGE SHAPE : Hemispherical
- CHARGE DIRECTION..... : Spherical side facing the specimen
- CHARGE POSITION : Central
- CLEAR DISTANCE TO THE CHARGE : 200mm

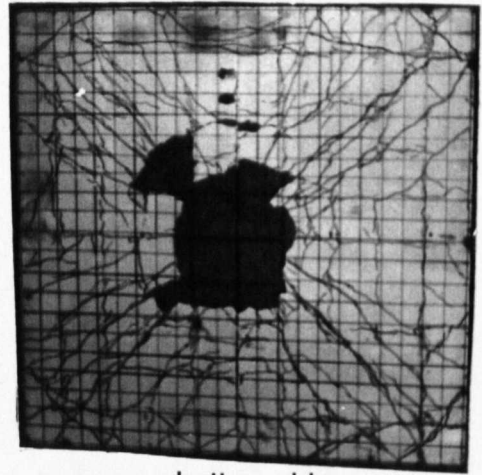
SUPPORTS



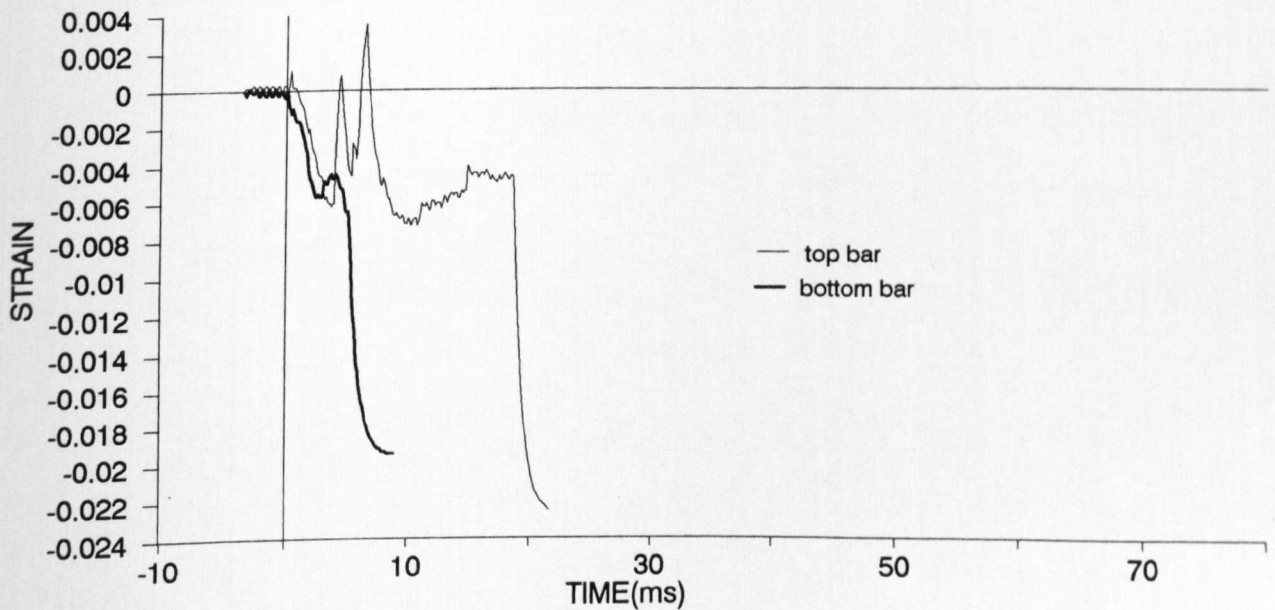
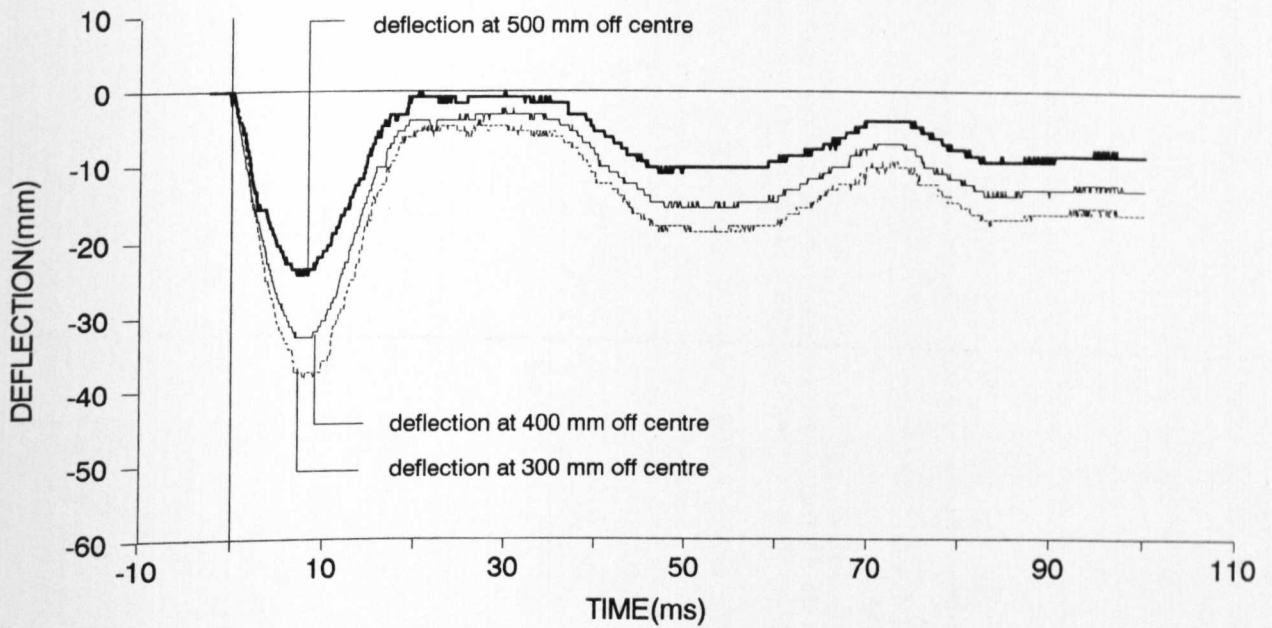
IMPULSE TEST - LARGE SLAB - LSE5



top side



bottom side



IMPULSE TEST RESULTS

1:2.5 SCALE SLABS

APPENDIX B2

IMPULSE TEST

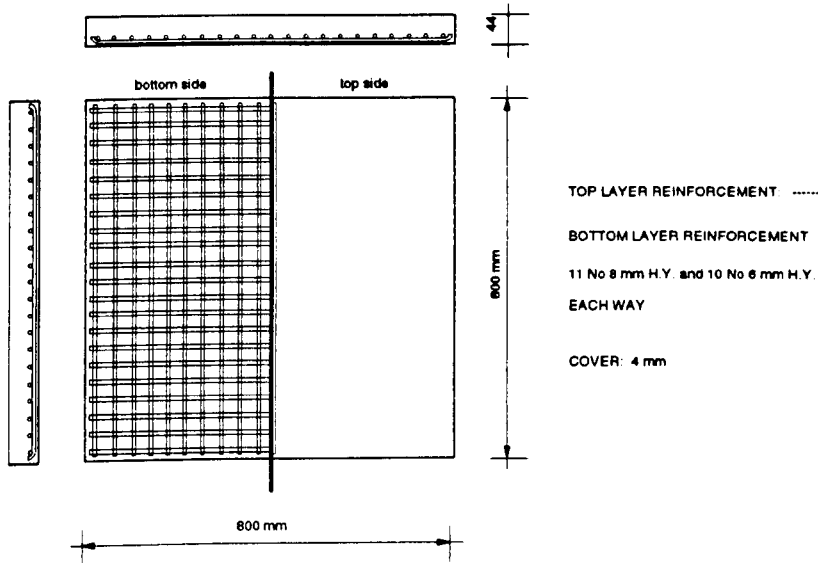
DATE: 26.07.90

SMALL SLAB SE1

AGE OF SPECIMEN: 8 days

Cube compressive strength	N/mm ²	47.7	Cylinder tensile strength	N/mm ²	4.55	Age (days)	14
---------------------------	-------------------	------	---------------------------	-------------------	------	------------	----

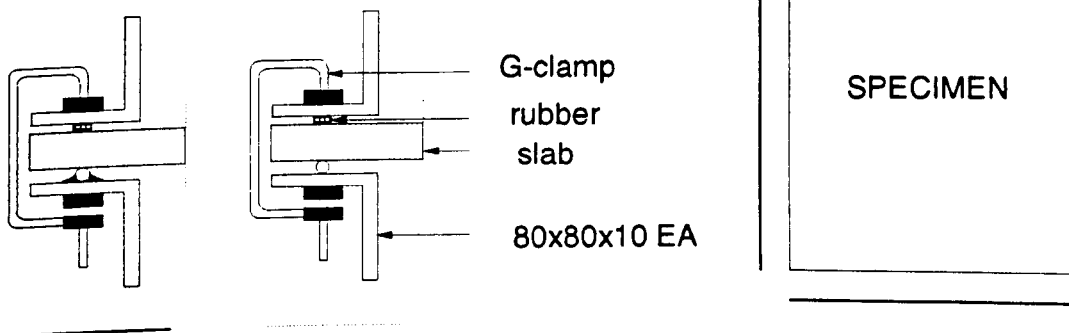
REINFORCEMENT:



LOADING CONDITIONS:

- CHARGE WEIGHT : 78g, PE4
- CHARGE SHAPE : Cylindrical
- CHARGE DIRECTION..... : Parallel to the specimen
- CHARGE POSITION : Central
- CLEAR DISTANCE TO THE CHARGE..... : 650mm 1st and 100mm 2nd shot

SUPPORTS:



IMPULSE TEST

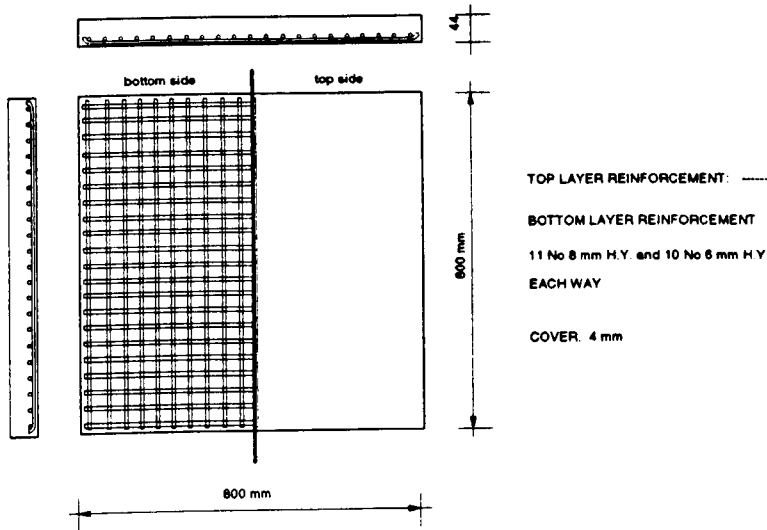
DATE: 27.07.90

SMALL SLAB SE2

AGE OF SPECIMEN: 9 days

Cube compressive strength	N/mm ²	47.7	Cylinder tensile strength	N/mm ²	4.55	Age (days)	14
---------------------------	-------------------	------	---------------------------	-------------------	------	------------	----

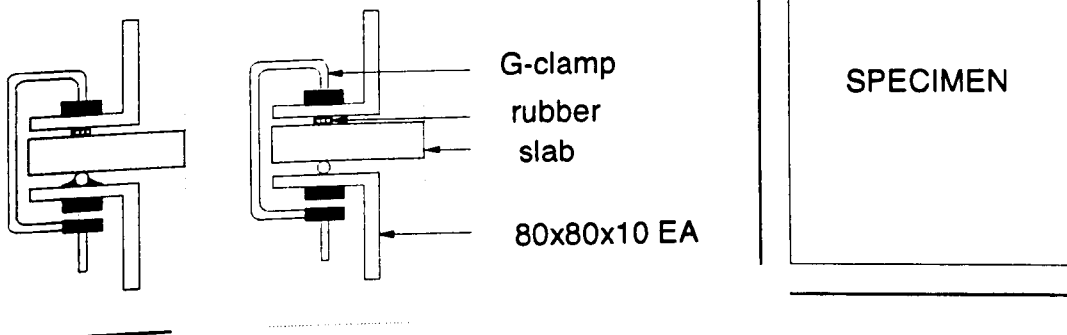
REINFORCEMENT:



LOADING CONDITIONS:

- CHARGE WEIGHT : 78g, PE4
- CHARGE SHAPE : Cylindrical
- CHARGE DIRECTION..... : Parallel to the specimen
- CHARGE POSITION : Central
- CLEAR DISTANCE TO THE CHARGE..... : < 50mm

SUPPORTS:



IMPULSE TEST

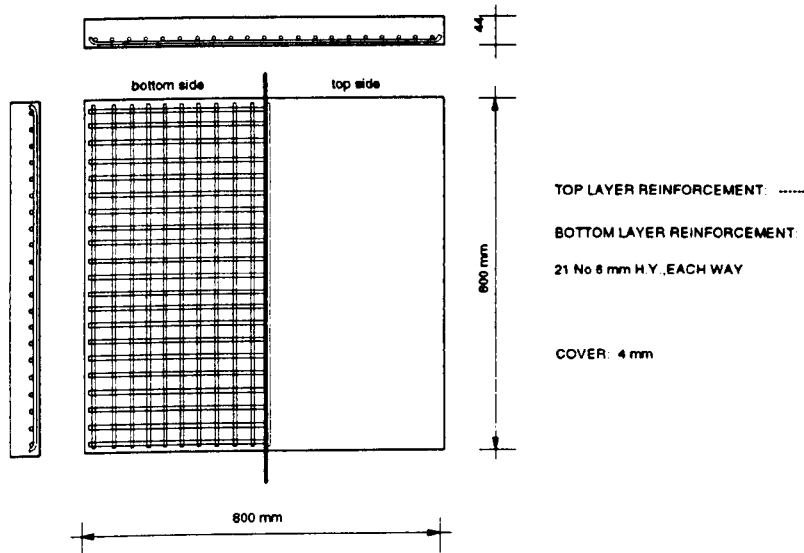
DATE: 13.09.90

SMALL SLAB SE3

AGE OF SPECIMEN: 7 days

Cube compressive strength	N/mm ²	43.3	Cylinder tensile strength	N/mm ²	3.69	Age (days)	11
---------------------------	-------------------	------	---------------------------	-------------------	------	------------	----

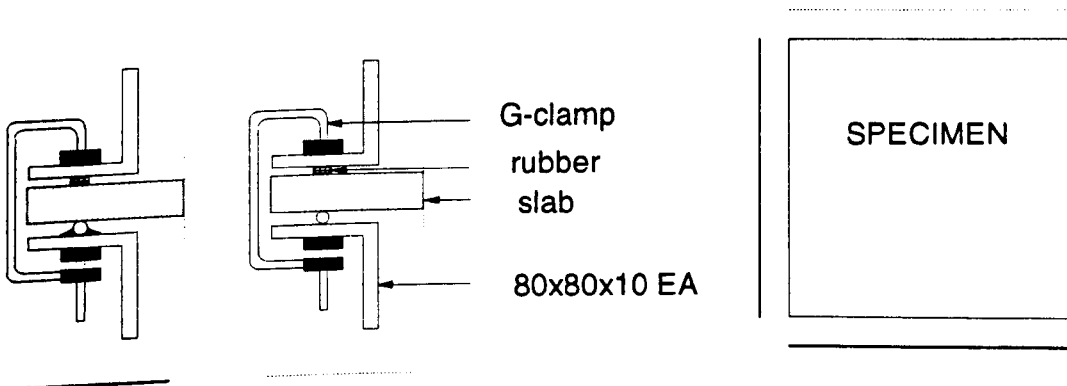
REINFORCEMENT:



LOADING CONDITIONS:

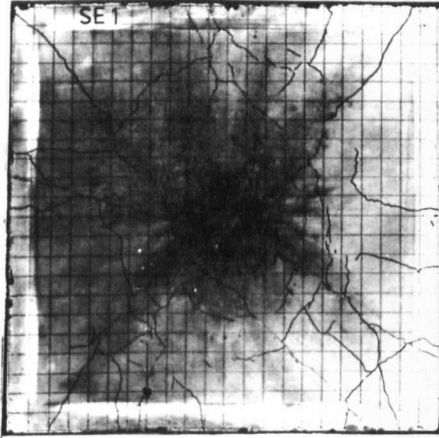
CHARGE WEIGHT : 78g, PE4
 CHARGE SHAPE : Cylindrical
 CHARGE DIRECTION..... : Parallel to the specimen
 CHARGE POSITION : Central
 CLEAR DISTANCE TO THE CHARGE..... : 50mm

SUPPORTS:

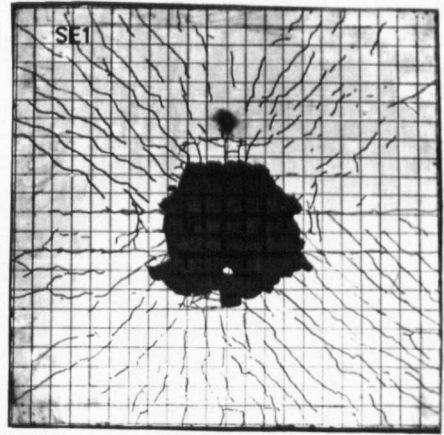


IMPULSE TEST - SMALL SLABS

SE1

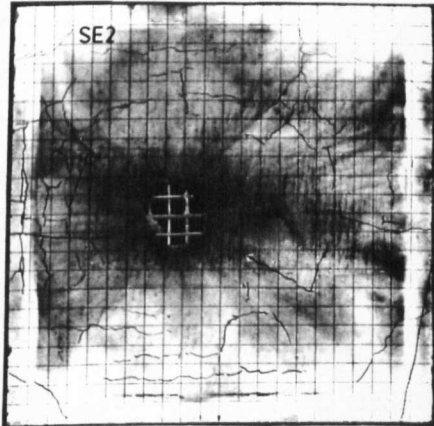


top side

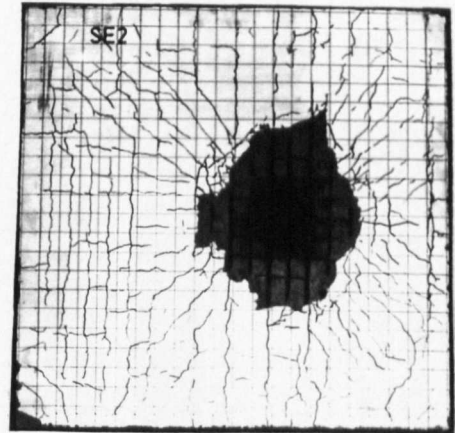


bottom side

SE2

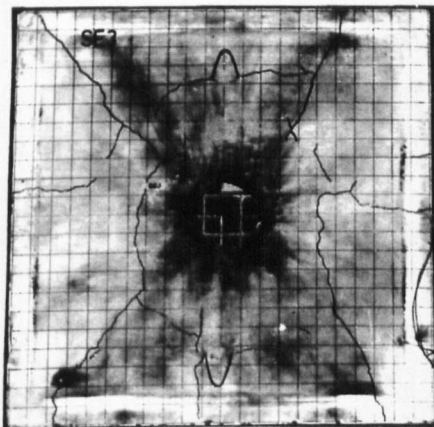


top side

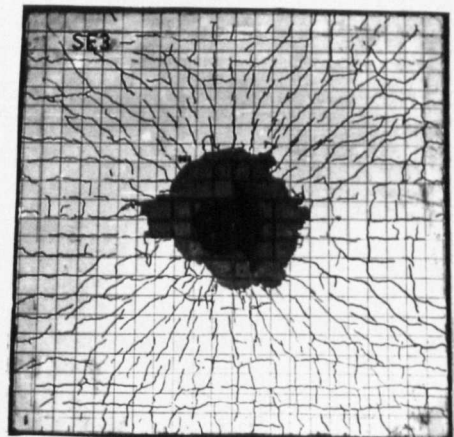


bottom side

SE3



top side



bottom side

IMPULSE TEST

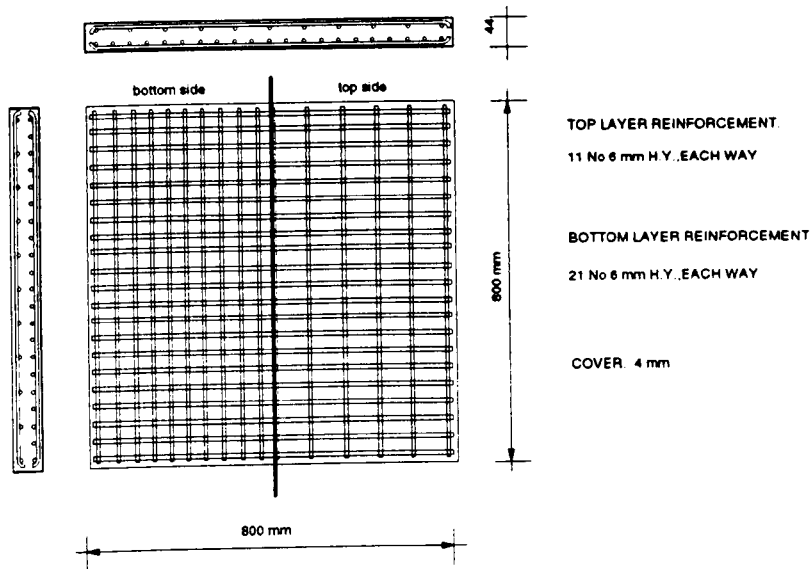
DATE: 14.09.90

SMALL SLAB SE4

AGE OF SPECIMEN: 11 days

Cube compressive strength	N/mm ²	43.3	Cylinder tensile strength	N/mm ²	3.69	Age (days)	11
---------------------------	-------------------	------	---------------------------	-------------------	------	------------	----

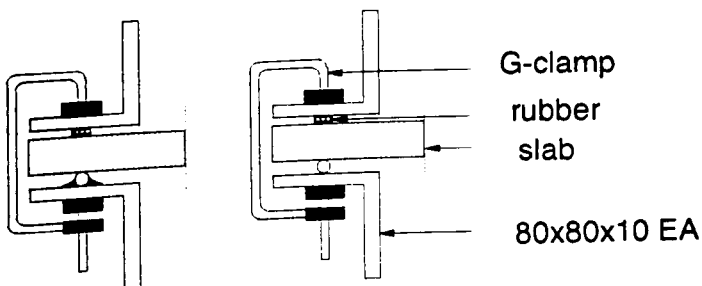
REINFORCEMENT:



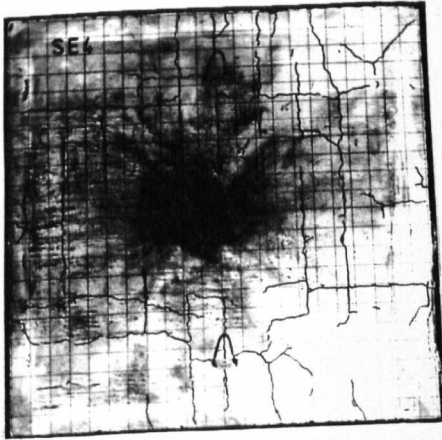
LOADING CONDITIONS:

CHARGE WEIGHT : 78g, PE4
CHARGE SHAPE : Cylindrical
CHARGE DIRECTION..... : Parallel to the specimen
CHARGE POSITION : Central
CLEAR DISTANCE TO THE CHARGE..... : 100mm

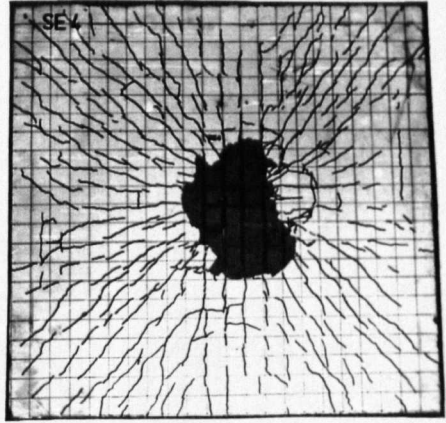
SUPPORTS:



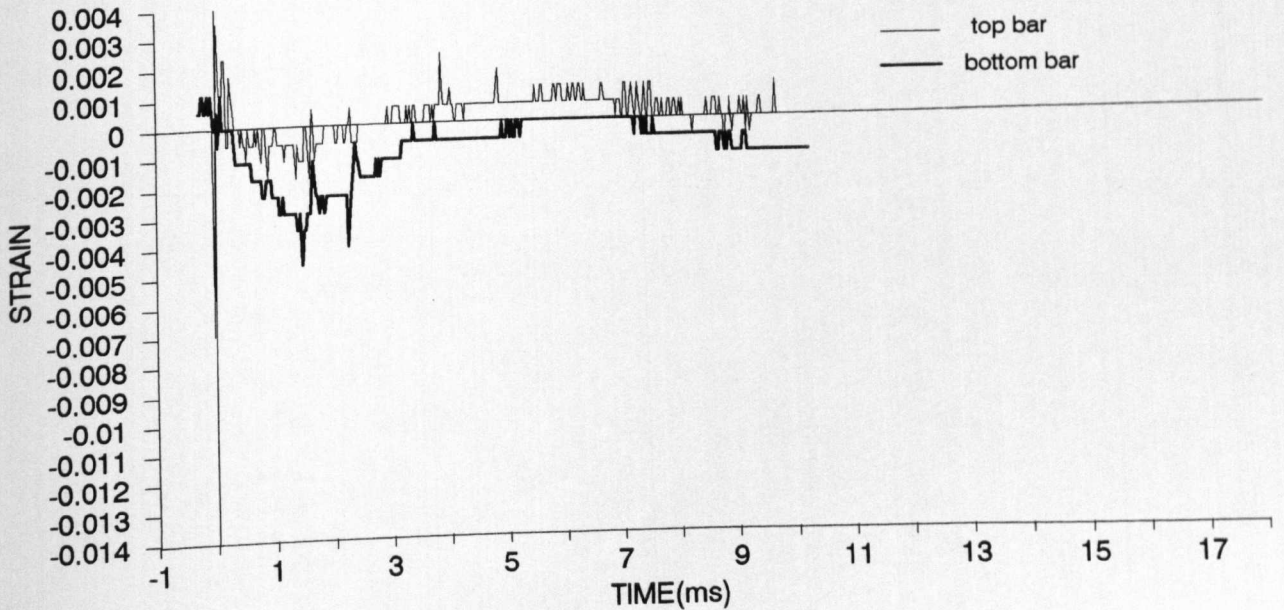
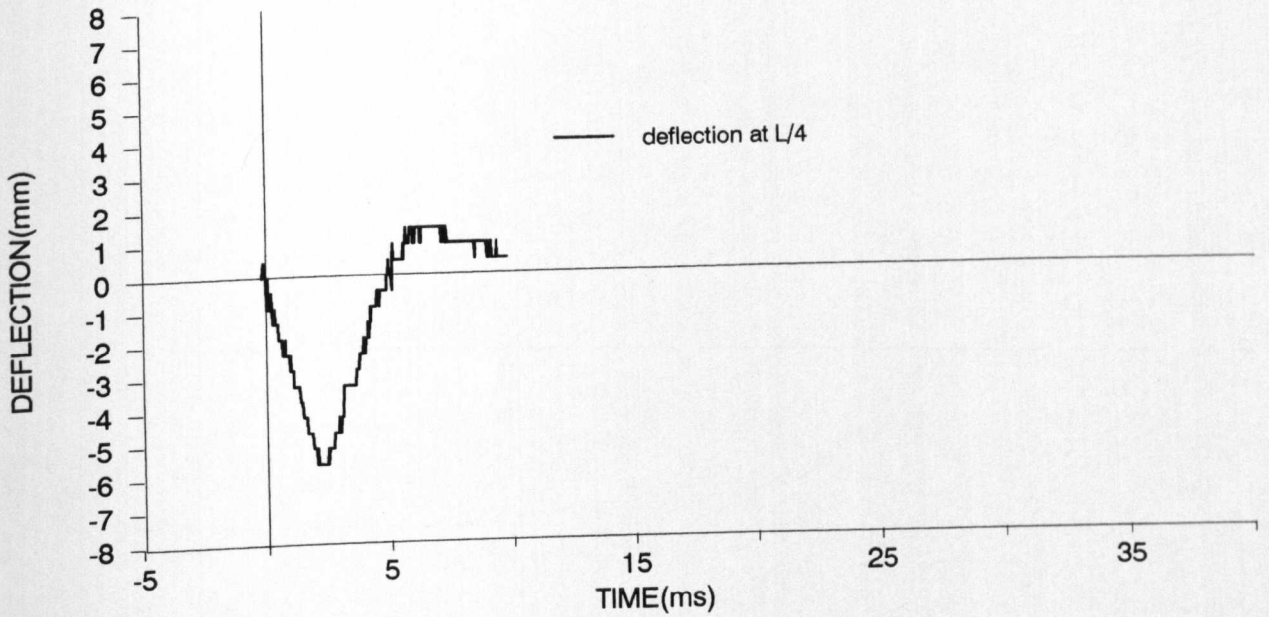
IMPULSE TEST - SMALL SLAB - SE4



top side



bottom side



IMPULSE TEST

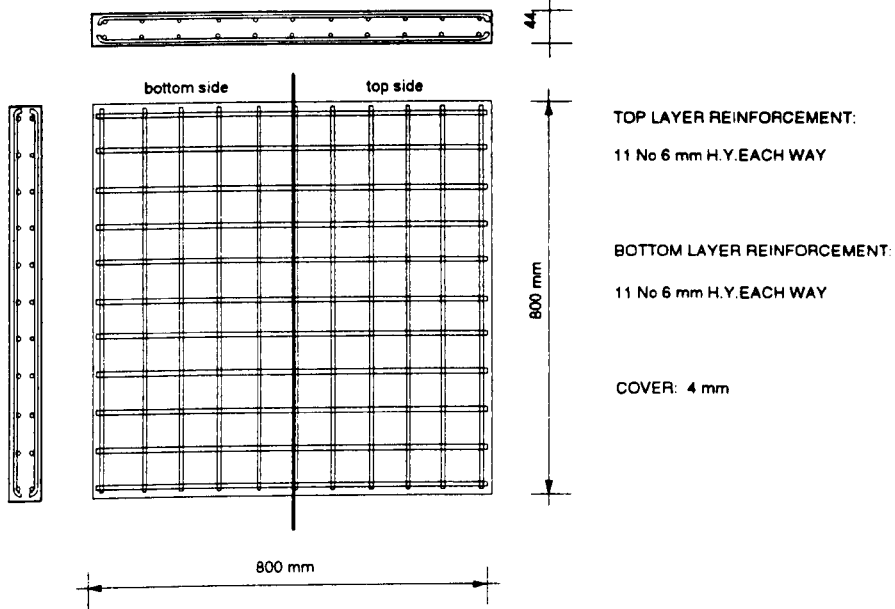
DATE: 18.09.90

SMALL SLAB SE5

AGE OF SPECIMEN: 7 days

Cube compressive strength	N/mm ²	38.4	Cylinder tensile strength	N/mm ²	4.12	Age (days)	8
---------------------------	-------------------	------	---------------------------	-------------------	------	------------	---

REINFORCEMENT:



LOADING CONDITIONS:

CHARGE WEIGHT : 78g, PE4

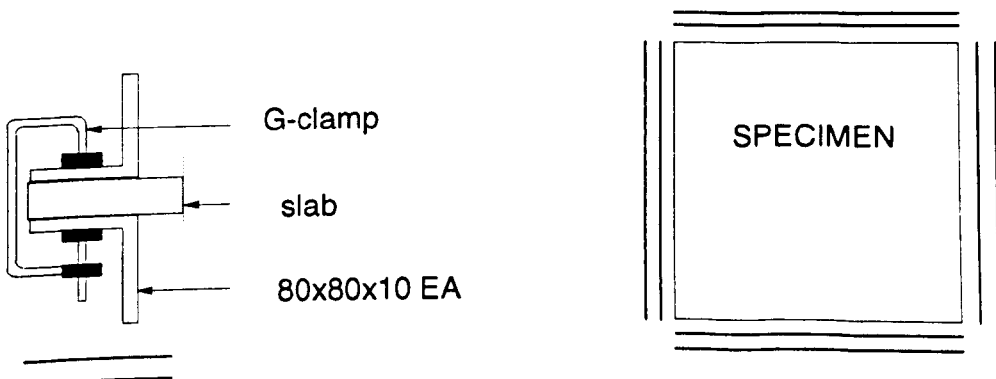
CHARGE SHAPE : Hemispherical

CHARGE DIRECTION..... : Spherical side facing the specimen

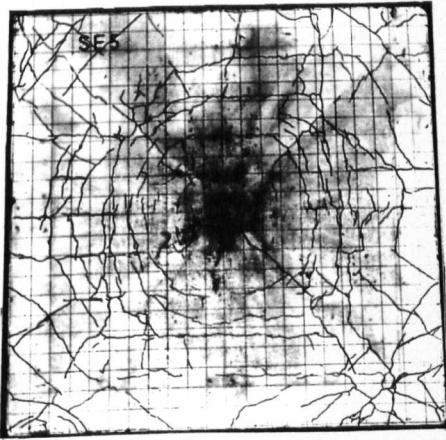
CHARGE POSITION : Central

CLEAR DISTANCE TO THE CHARGE..... : 100mm

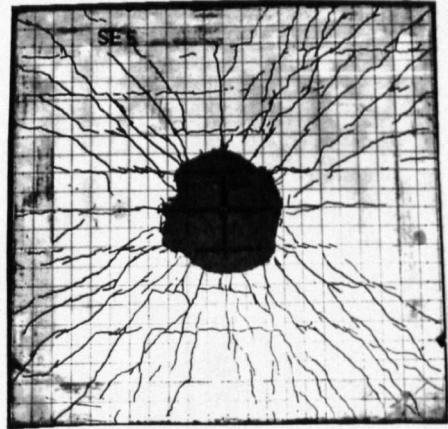
SUPPORTS:



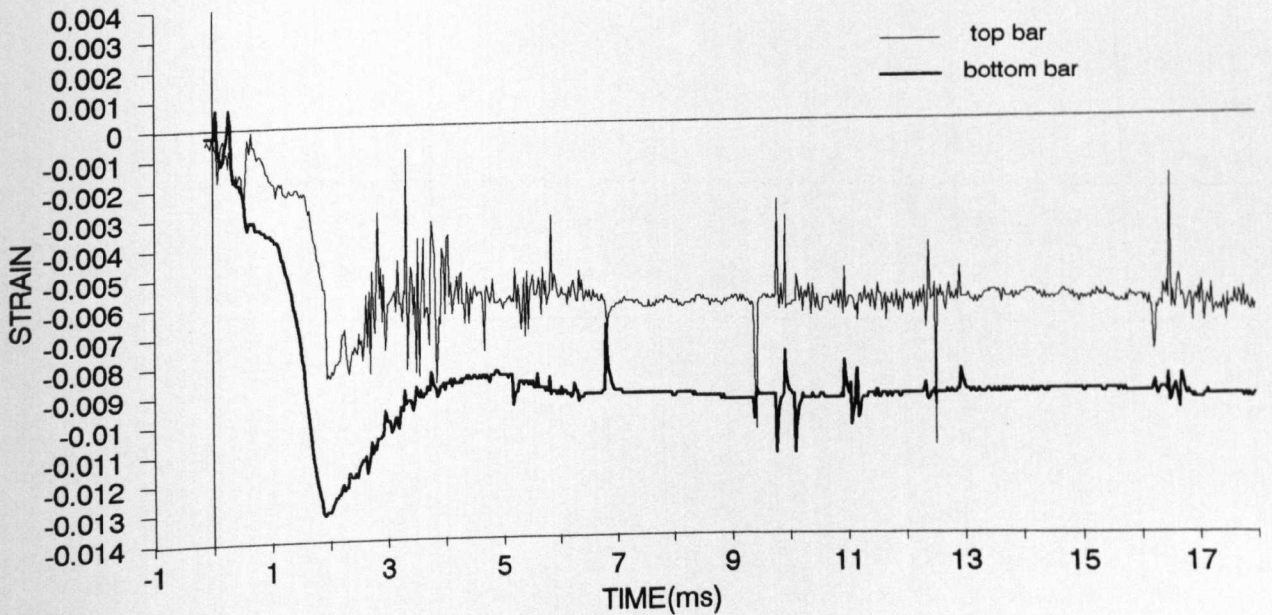
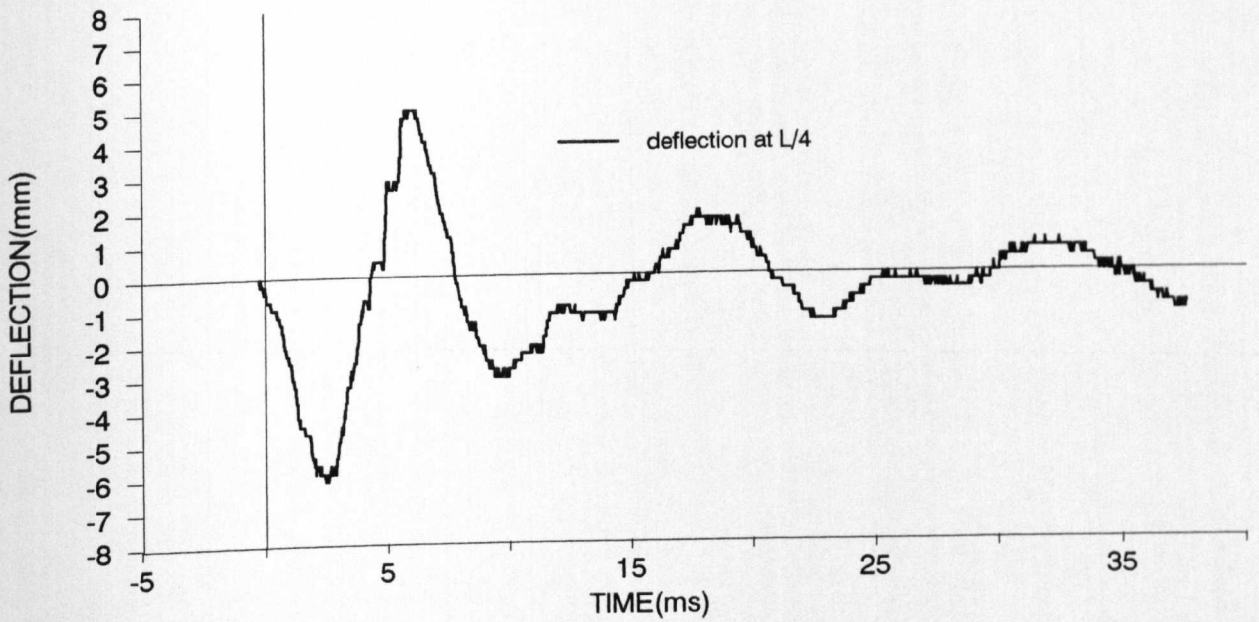
IMPULSE TEST - SMALL SLAB - SE5



top side



bottom side



IMPULSE TEST

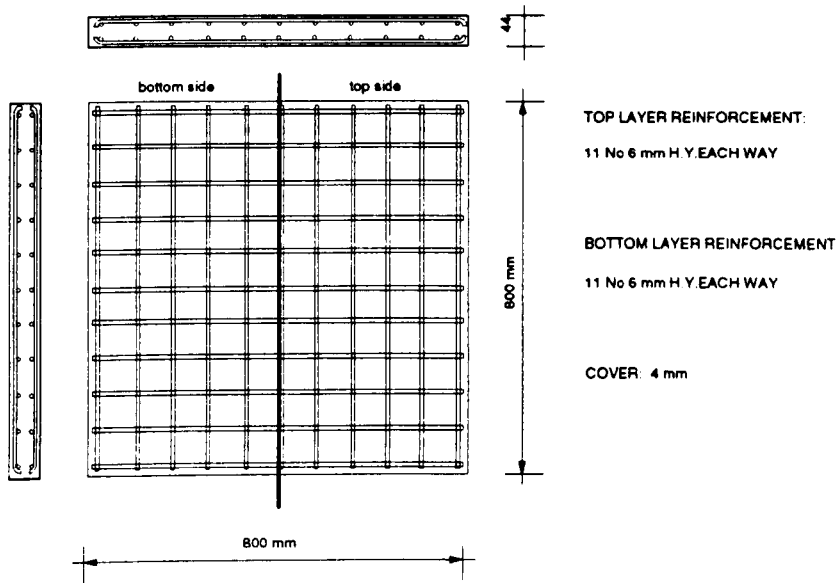
DATE: 18.09.90

SMALL SLAB SE6

AGE OF SPECIMEN: 7 days

Cube compressive strength	N/mm ²	38.4	Cylinder tensile strength	N/mm ²	4.12	Age (days)	8
---------------------------	-------------------	------	---------------------------	-------------------	------	------------	---

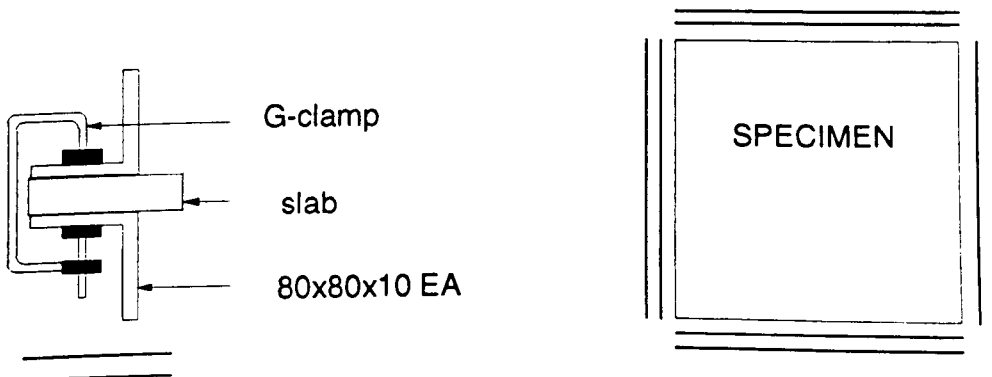
REINFORCEMENT:



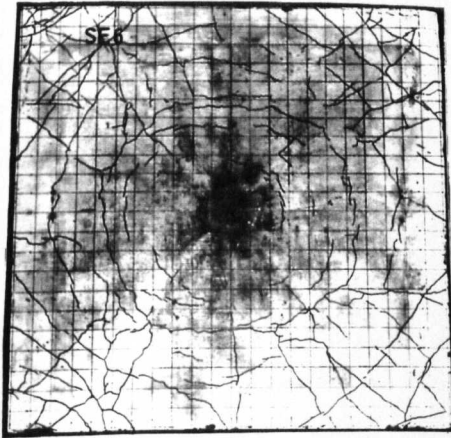
LOADING CONDITIONS:

- CHARGE WEIGHT : 78g, PE4
- CHARGE SHAPE : Hemispherical
- CHARGE DIRECTION..... : Flat side facing the specimen
- CHARGE POSITION : Central
- CLEAR DISTANCE TO THE CHARGE..... : 100mm

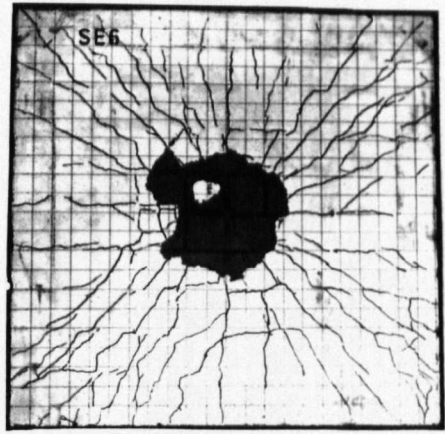
SUPPORTS:



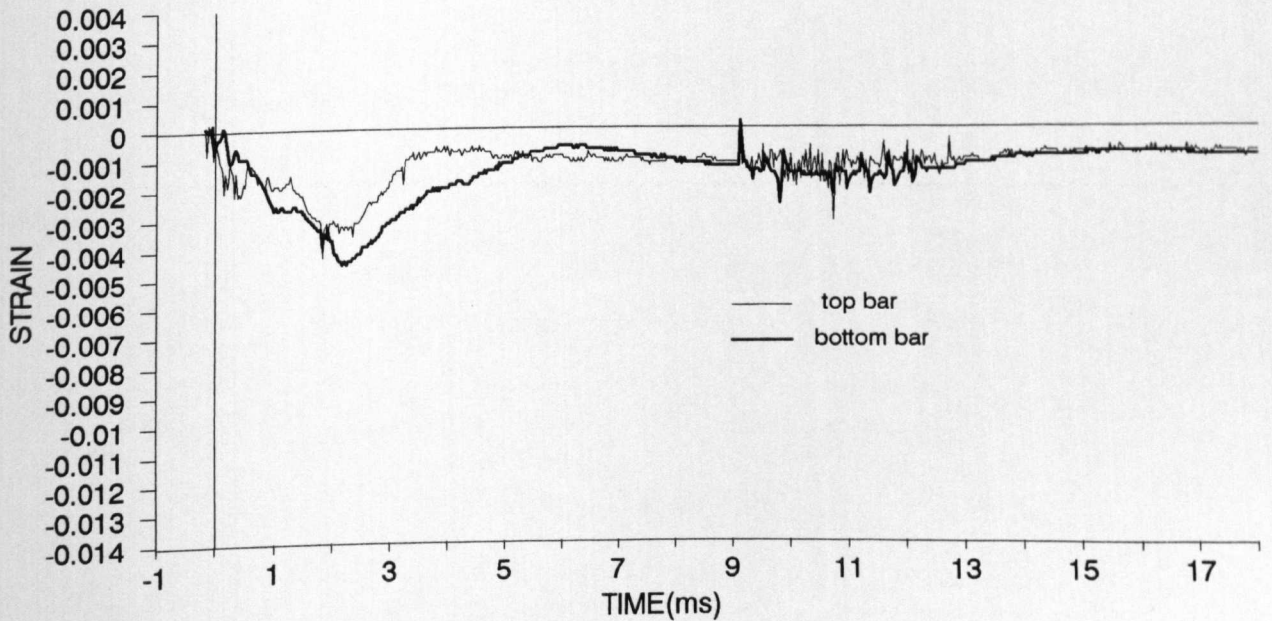
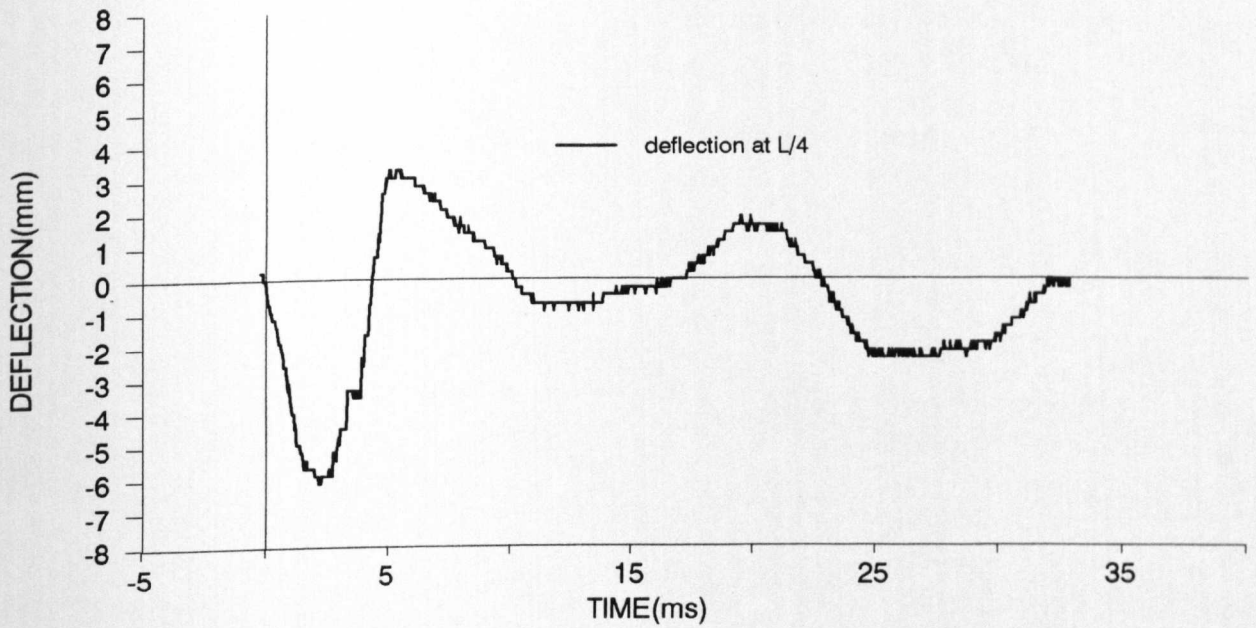
IMPULSE TEST - SMALL SLAB - SE6



top side



bottom side



IMPULSE TEST

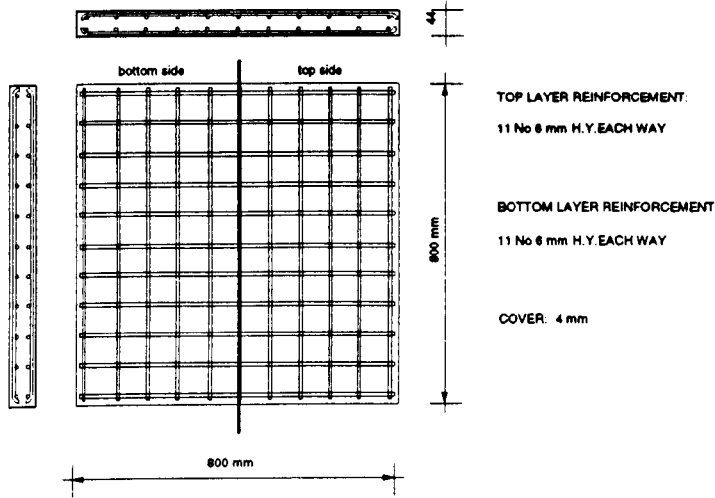
DATE: 27.09.90

SMALL SLAB SE7

AGE OF SPECIMEN: 7 days

Cube compressive strength	N/mm ²	36.8	Cylinder tensile strength	N/mm ²	4.41	Age (days)	7
---------------------------	-------------------	------	---------------------------	-------------------	------	------------	---

REINFORCEMENT:



LOADING CONDITIONS:

CHARGE WEIGHT : 78g, PE4

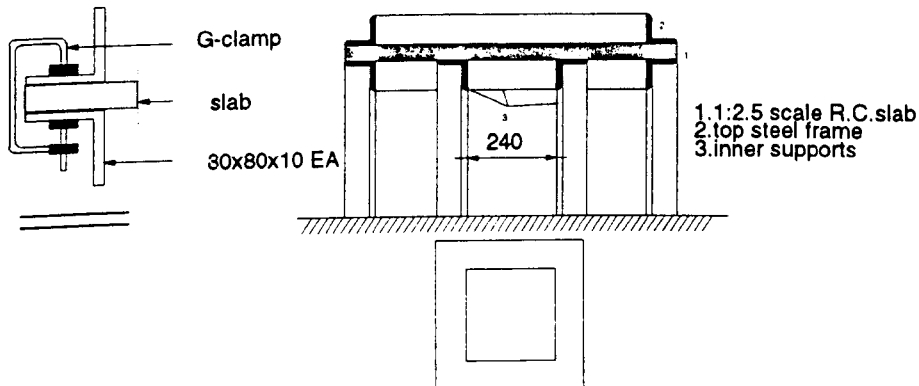
CHARGE SHAPE : Hemispherical

CHARGE DIRECTION..... : Spherical side facing the specimen

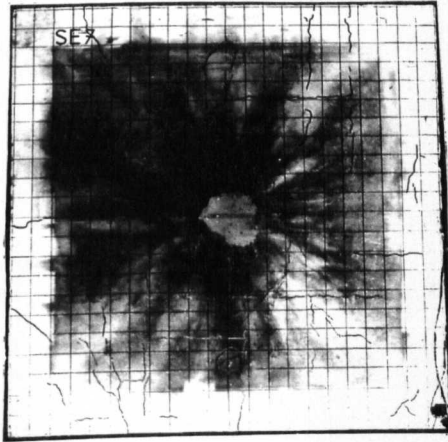
CHARGE POSITION : Central

CLEAR DISTANCE TO THE CHARGE..... : 100mm

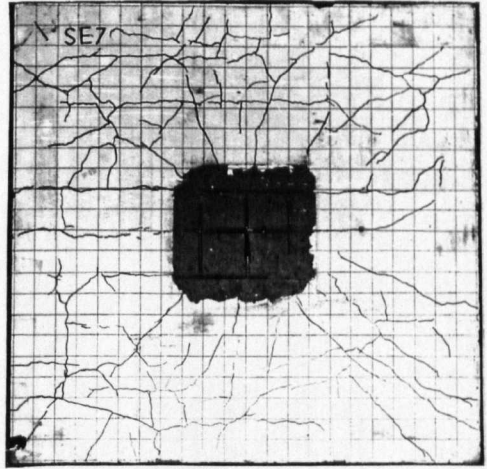
SUPPORTS:



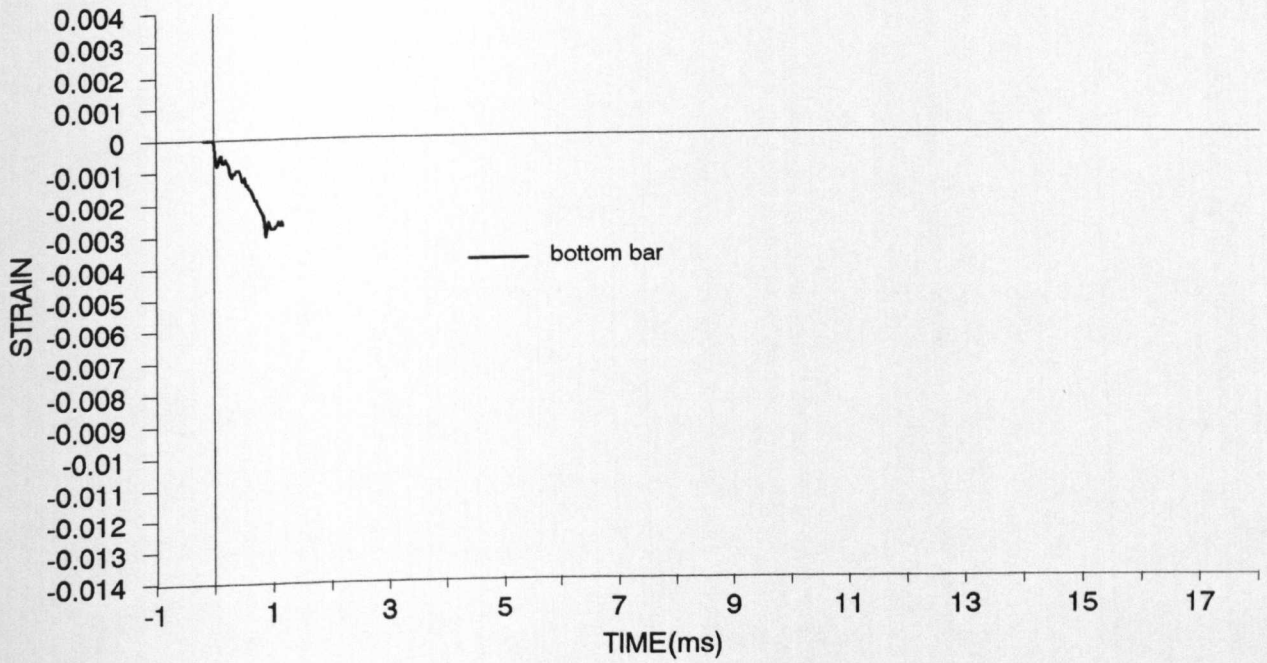
IMPULSE TEST - SMALL SLAB - SE7



top side



bottom side



IMPULSE TEST

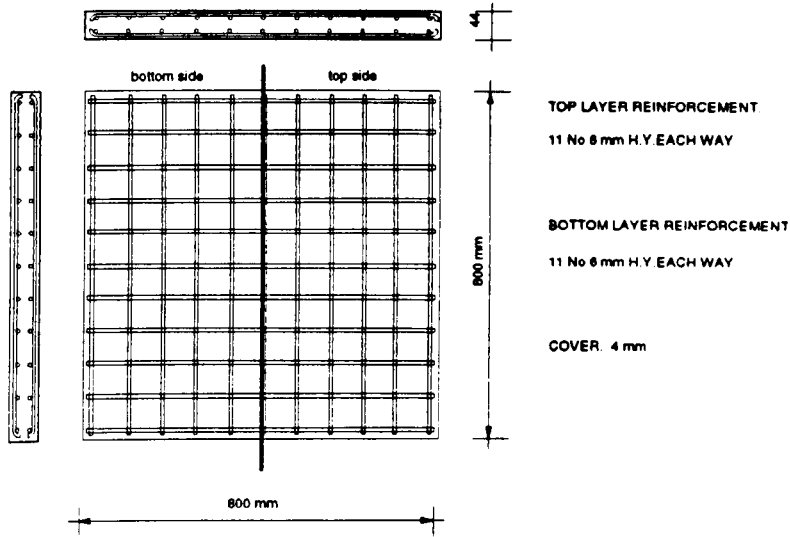
DATE: 27.09.90

SMALL SLAB SE8

AGE OF SPECIMEN: 7 days

Cube compressive strength	N/mm ²	36.8	Cylinder tensile strength	N/mm ²	4.41	Age (days)	7
---------------------------	-------------------	------	---------------------------	-------------------	------	------------	---

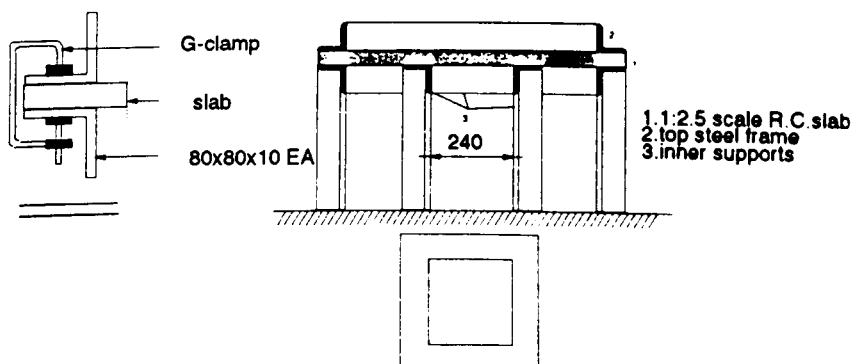
REINFORCEMENT:



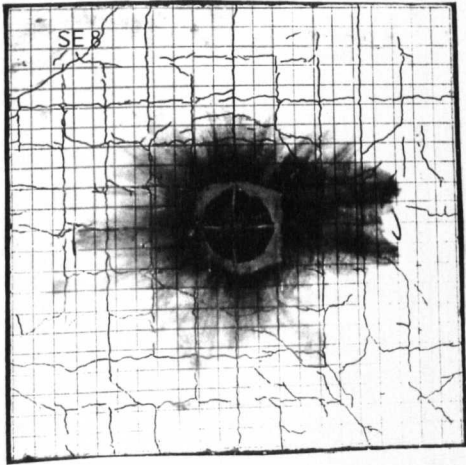
LOADING CONDITIONS:

CHARGE WEIGHT : 78g, PE4
 CHARGE SHAPE : Hemispherical
 CHARGE DIRECTION..... : Flat side facing the specimen
 CHARGE POSITION : Central
 CLEAR DISTANCE TO THE CHARGE..... : 50mm

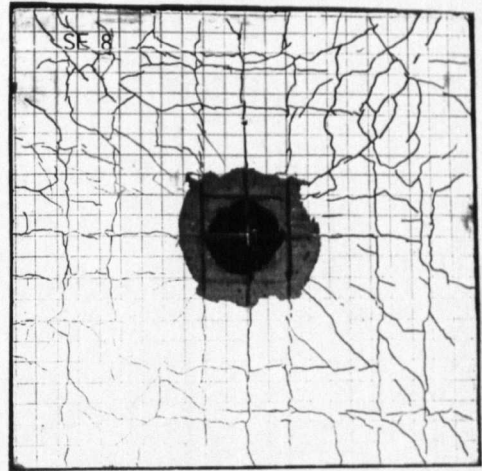
SUPPORTS:



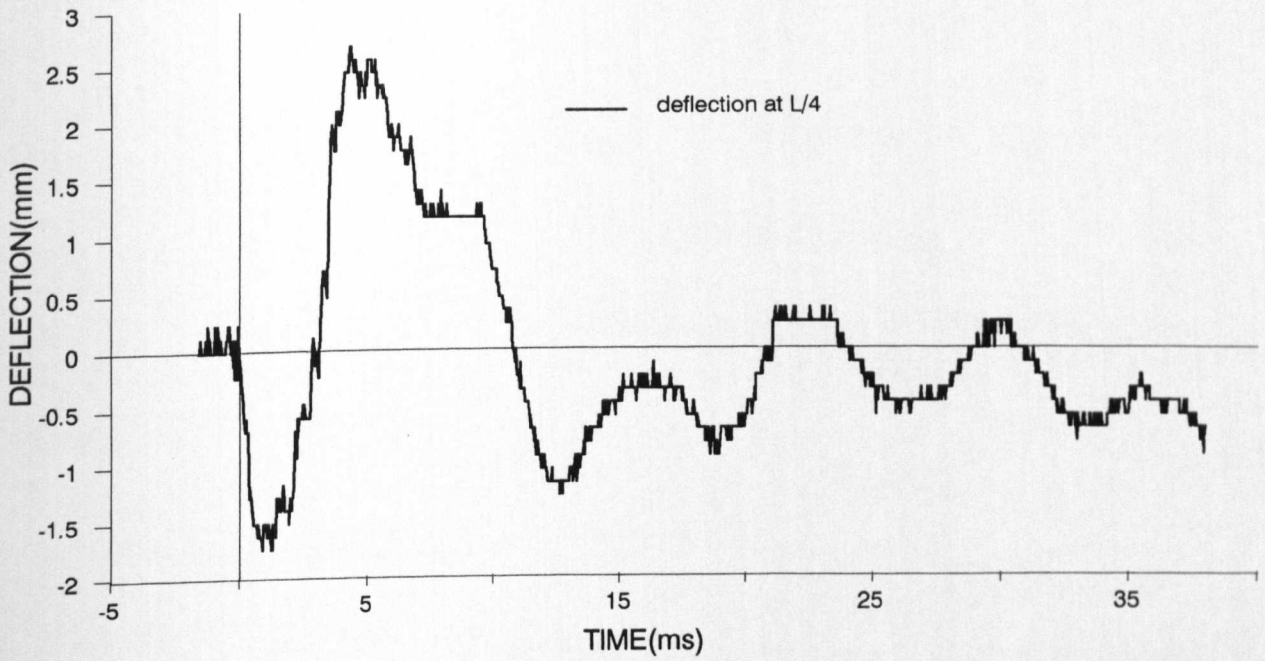
IMPULSE TEST - SMALL SLAB - SE8



top side



bottom side



IMPULSE TEST

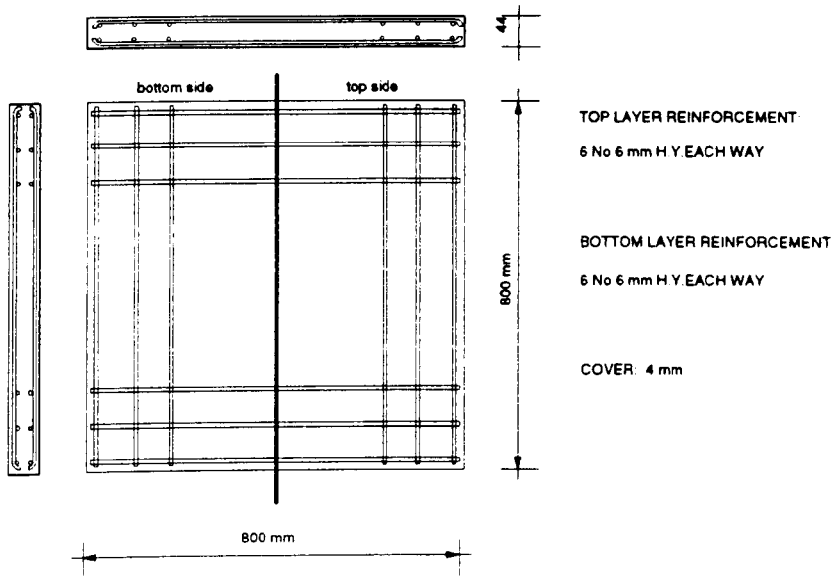
DATE: 27.09.91

SMALL SLAB SE9

AGE OF SPECIMEN: 7 days

Cube compressive strength	N/mm ²	30.4	Cylinder tensile strength	N/mm ²	2.99	Age (days)	7
---------------------------	-------------------	------	---------------------------	-------------------	------	------------	---

REINFORCEMENT:



LOADING CONDITIONS:

CHARGE WEIGHT : 78g, PE4

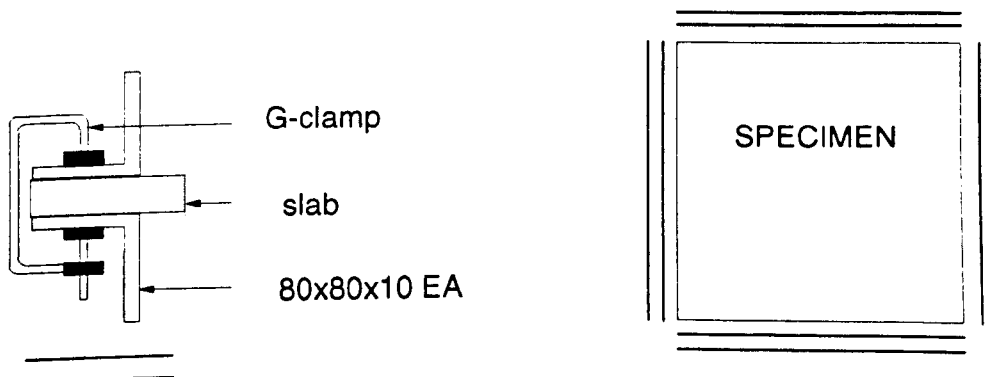
CHARGE SHAPE : Hemispherical

CHARGE DIRECTION..... : Spherical side facing the specimen

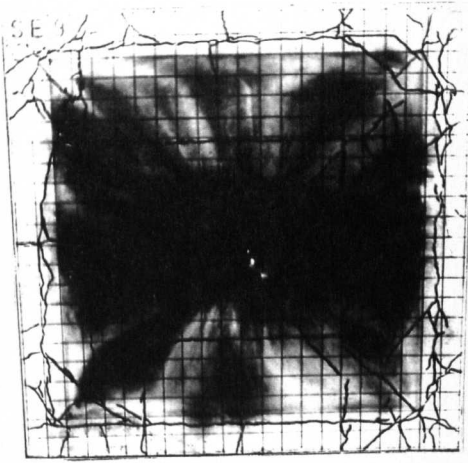
CHARGE POSITION : Central

CLEAR DISTANCE TO THE CHARGE..... : 100mm

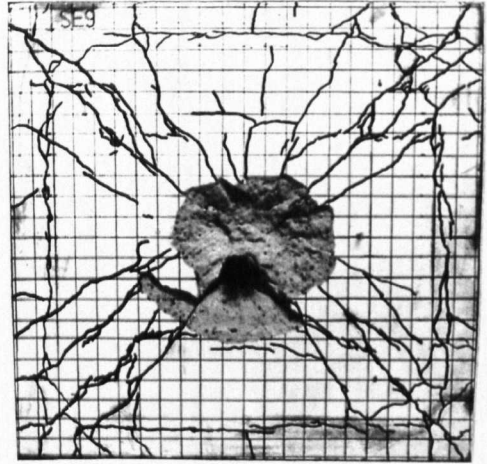
SUPPORTS:



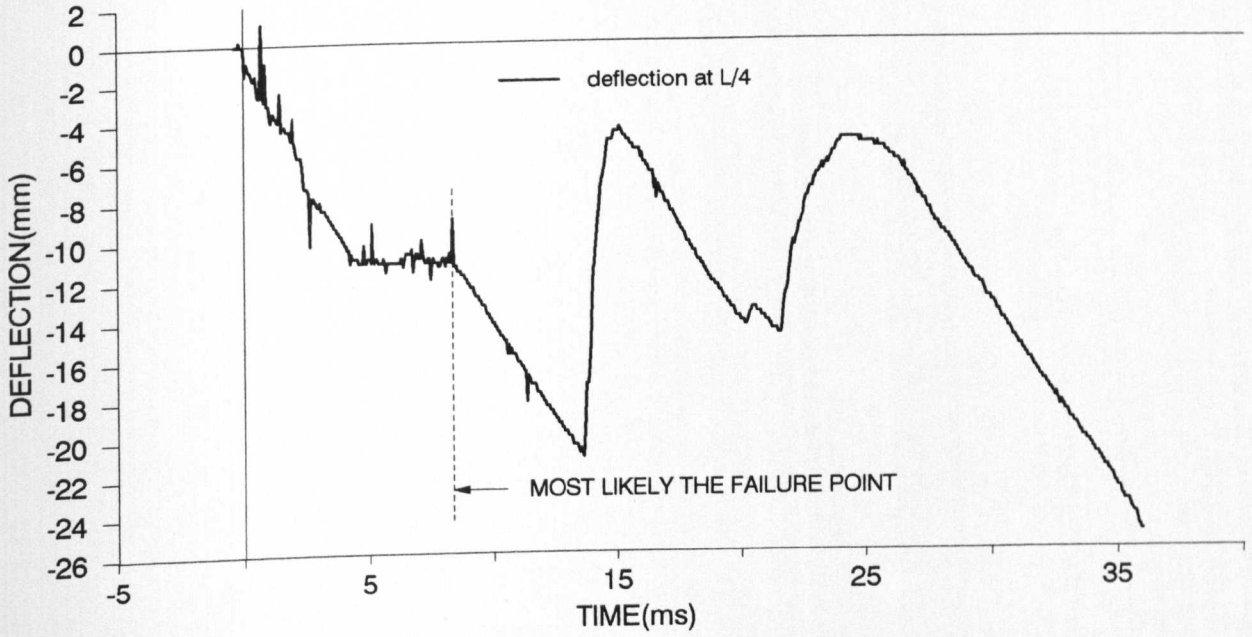
IMPULSE TEST - SMALL SLAB - SE9



top side



bottom side



**DISRUPTION OF THE SIGNAL FOR THE DEFLECTION - TIME TRACES ON
SLABS SE10 TO SE19**

Deflection - time records on slabs SE10 to SE19 have shown unexpected shock peaks in the first couple of milliseconds of the record. A typical example is given in Fig A1. It seems unlikely that these shock peaks represent real slab movement and were probably caused by electrical noise or disruption. When the polarity of the electrical supply to the R.P.D.T. circuitry was changed, Fig A2, the shock peaks were reversed in direction. The results presented in this appendix, for slabs SE10 to SE19, have the traces actually recorded, but the shock peacks are shown with the dotted line, as in Fig A3.

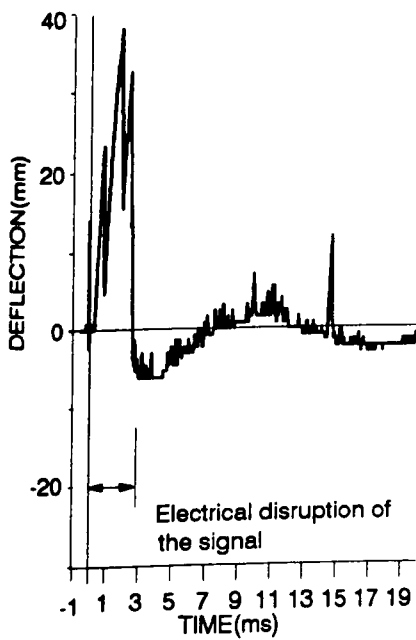


Fig.A1. Positive polarisation of the instrumentation circuitry

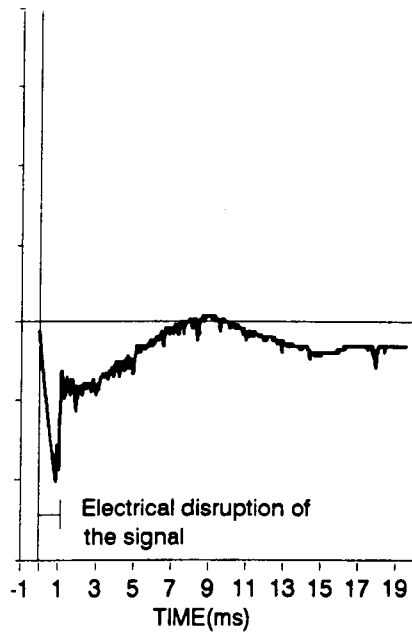


Fig.A2. Negative polarisation of the instrumentation circuitry

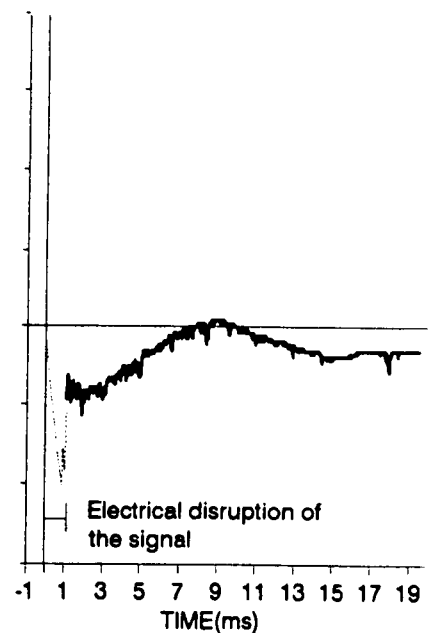


Fig A3. Format of presentation for the slabs SE10 to SE19

IMPULSE TEST

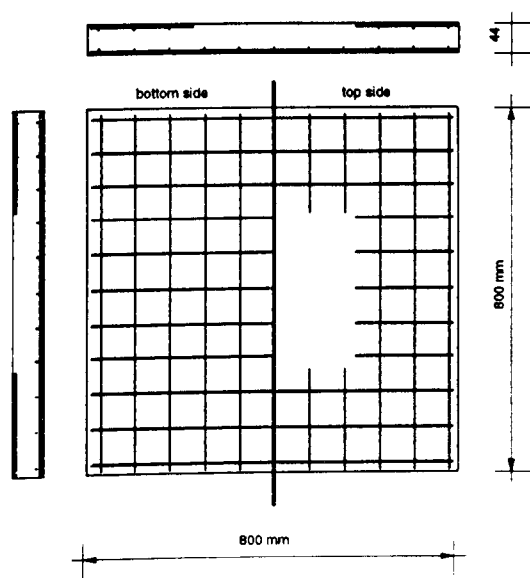
DATE: 27.11.92

SMALL SLAB SE10

AGE OF SPECIMEN: 17 days

Cube compressive strength	N/mm ²	37.33	Cylinder tensile strength	N/mm ²	3.52	Age (days)	17
---------------------------	-------------------	-------	---------------------------	-------------------	------	------------	----

REINFORCEMENT:



TOP LAYER REINFORCEMENT:

R.MESH : 3.15 mm DIAM. / 76.2 mm CENTRES
(WITHOUT CENTRAL REGION 400 X 400 mm)

BOTTOM LAYER REINFORCEMENT:

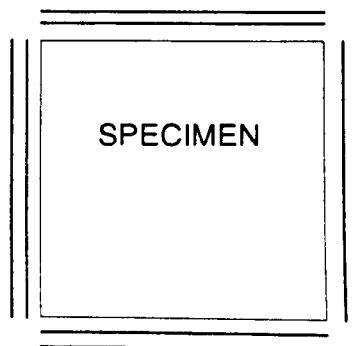
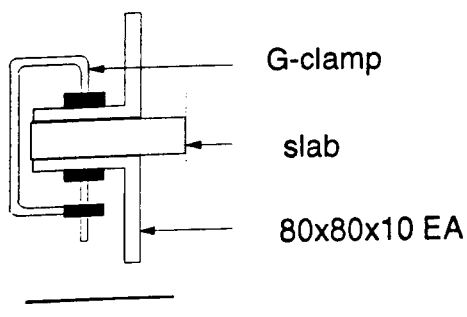
R.MESH : 3.15 mm DIAM. / 76.2 mm CENTRES

COVER: 4 mm

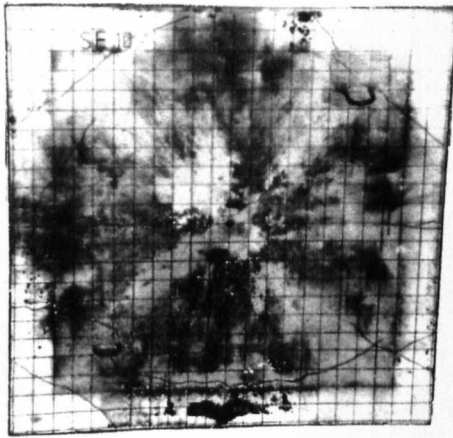
LOADING CONDITIONS:

CHARGE WEIGHT : 78g, PE4
CHARGE SHAPE : Hemispherical
CHARGE DIRECTION..... : Spherical side facing the specimen
CHARGE POSITION : Central
CLEAR DISTANCE TO THE CHARGE..... : 250mm

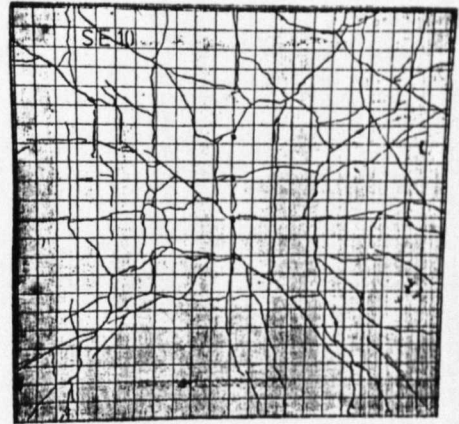
SUPPORTS:



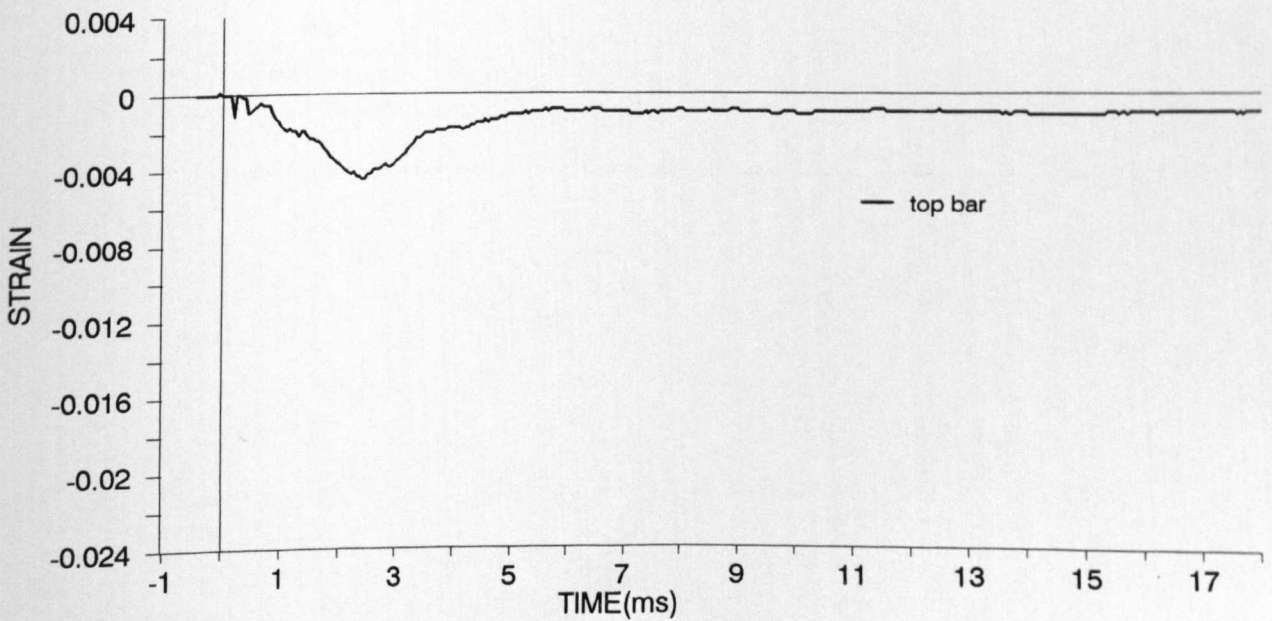
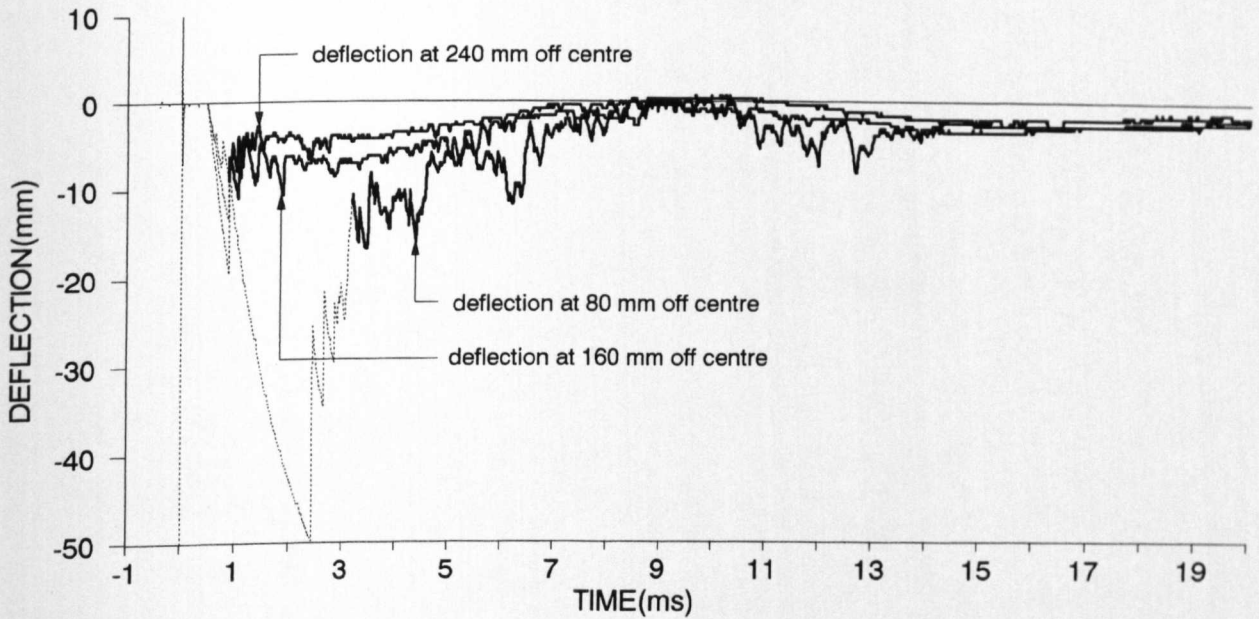
IMPULSE TEST - SMALL SLAB - SE10



top side



bottom side



IMPULSE TEST

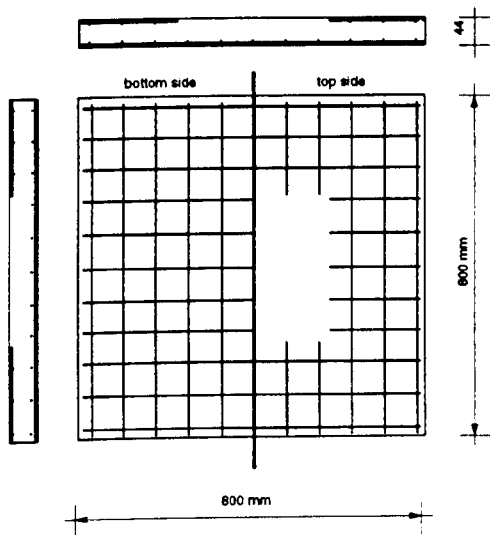
DATE: 1.12.92

SMALL SLAB SE11

AGE OF SPECIMEN: 21 days

Cube compressive strength	N/mm ²	37.33	Cylinder tensile strength	N/mm ²	3.52	Age (days)	17
---------------------------	-------------------	-------	---------------------------	-------------------	------	------------	----

REINFORCEMENT:



TOP LAYER REINFORCEMENT:

R MESH : 3.15 mm DIAM / 76.2 mm CENTRES
(WITHOUT CENTRAL REGION 400 X 400 mm)

BOTTOM LAYER REINFORCEMENT:

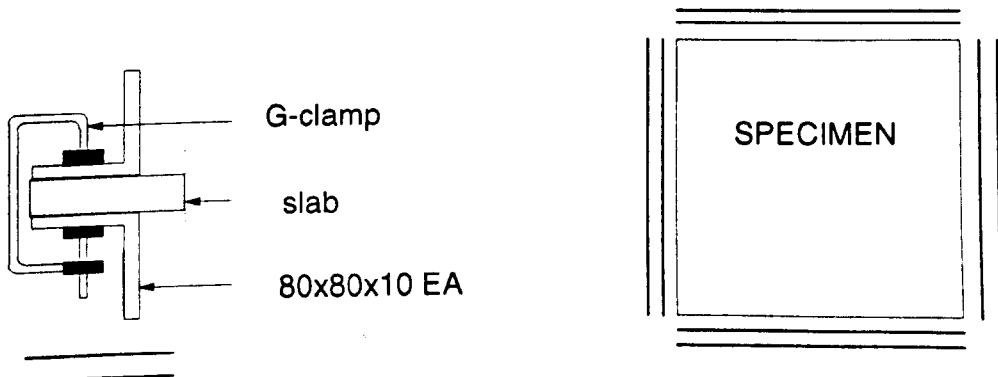
R MESH : 3.15 mm DIAM / 76.2 mm CENTRES

COVER: 4 mm

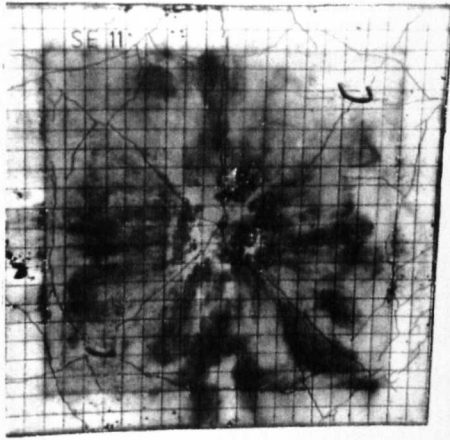
LOADING CONDITIONS:

- CHARGE WEIGHT : 78g, PE4
- CHARGE SHAPE : Hemispherical
- CHARGE DIRECTION..... : Spherical side facing the specimen
- CHARGE POSITION : Central
- CLEAR DISTANCE TO THE CHARGE..... : 200mm

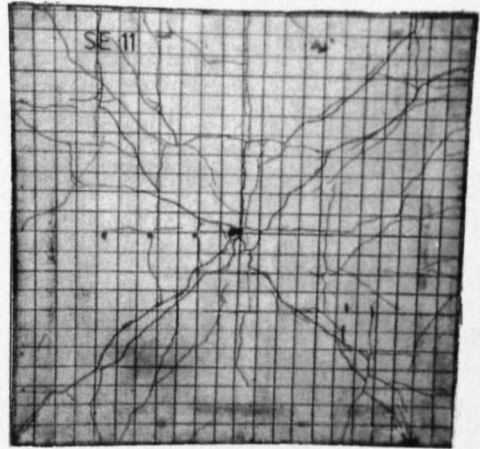
SUPPORTS:



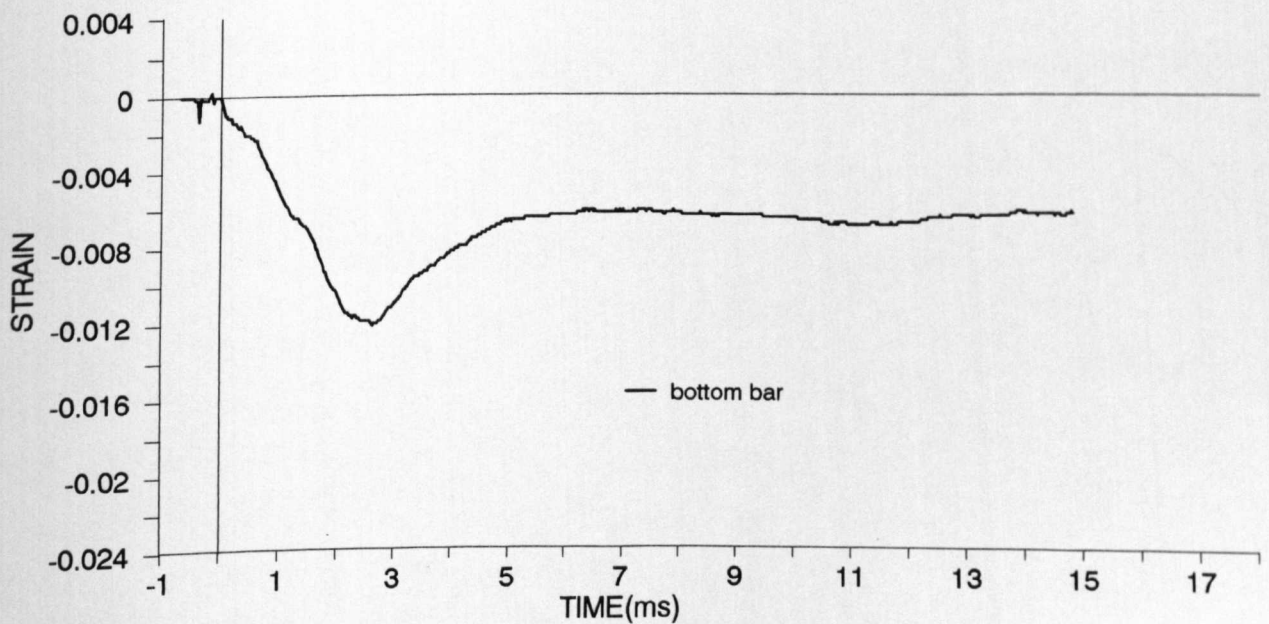
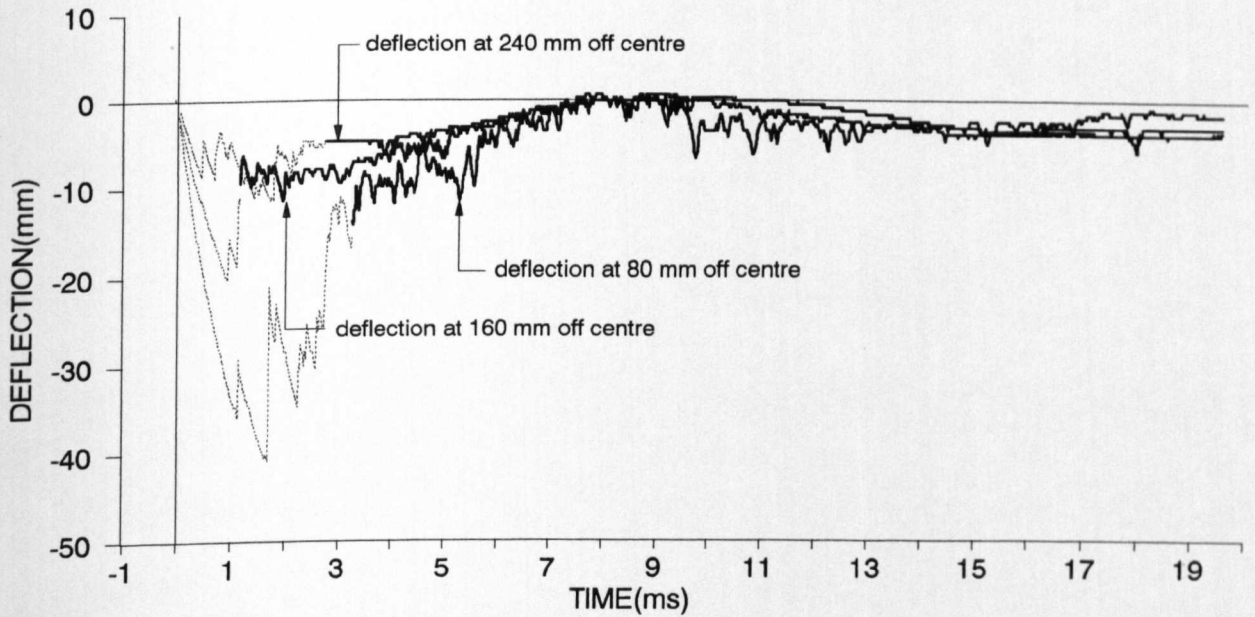
IMPULSE TEST - SMALL SLAB - SE11



top side



bottom side



IMPULSE TEST

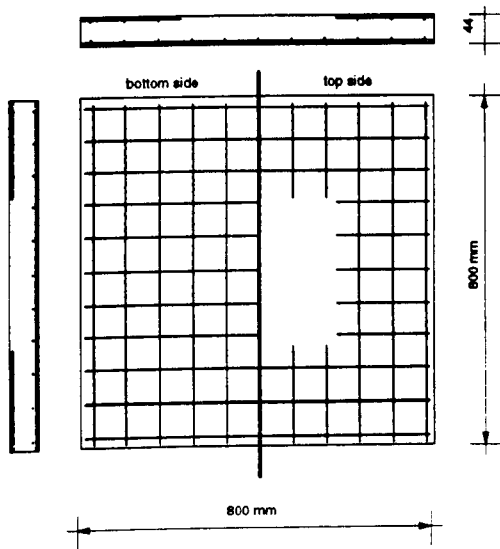
DATE: 2.12.92

SMALL SLAB SE12

AGE OF SPECIMEN: 22 days

Cube compressive strength	N/mm ²	37.33	Cylinder tensile strength	N/mm ²	3.52	Age (days)	17
---------------------------	-------------------	-------	---------------------------	-------------------	------	------------	----

REINFORCEMENT:



TOP LAYER REINFORCEMENT:

R.MESH : 3.15 mm DIAM. / 76.2 mm CENTRES
(WITHOUT CENTRAL REGION 400 X 400 mm)

BOTTOM LAYER REINFORCEMENT:

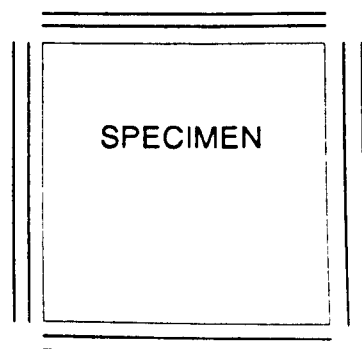
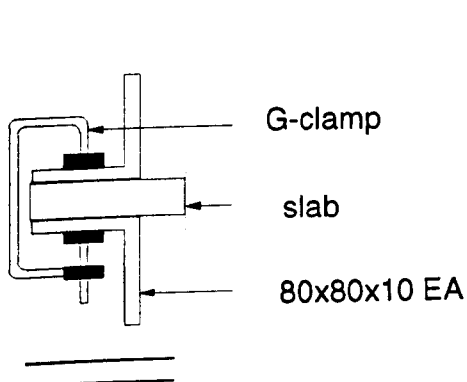
R.MESH : 3.15 mm DIAM. / 76.2 mm CENTRES

COVER: 4 mm

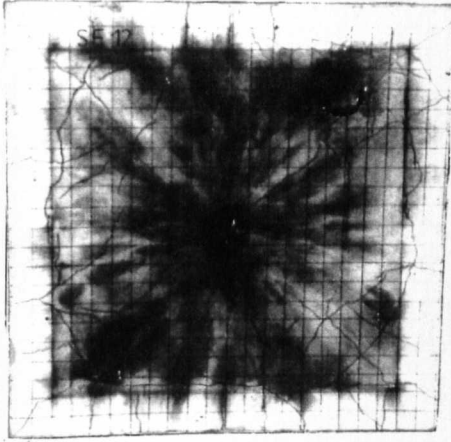
LOADING CONDITIONS:

CHARGE WEIGHT : 78g, PE4
CHARGE SHAPE : Hemispherical
CHARGE DIRECTION..... : Spherical side facing the specimen
CHARGE POSITION : Central
CLEAR DISTANCE TO THE CHARGE..... : 150mm

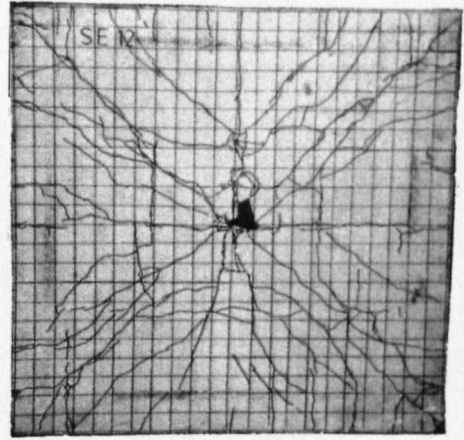
SUPPORTS:



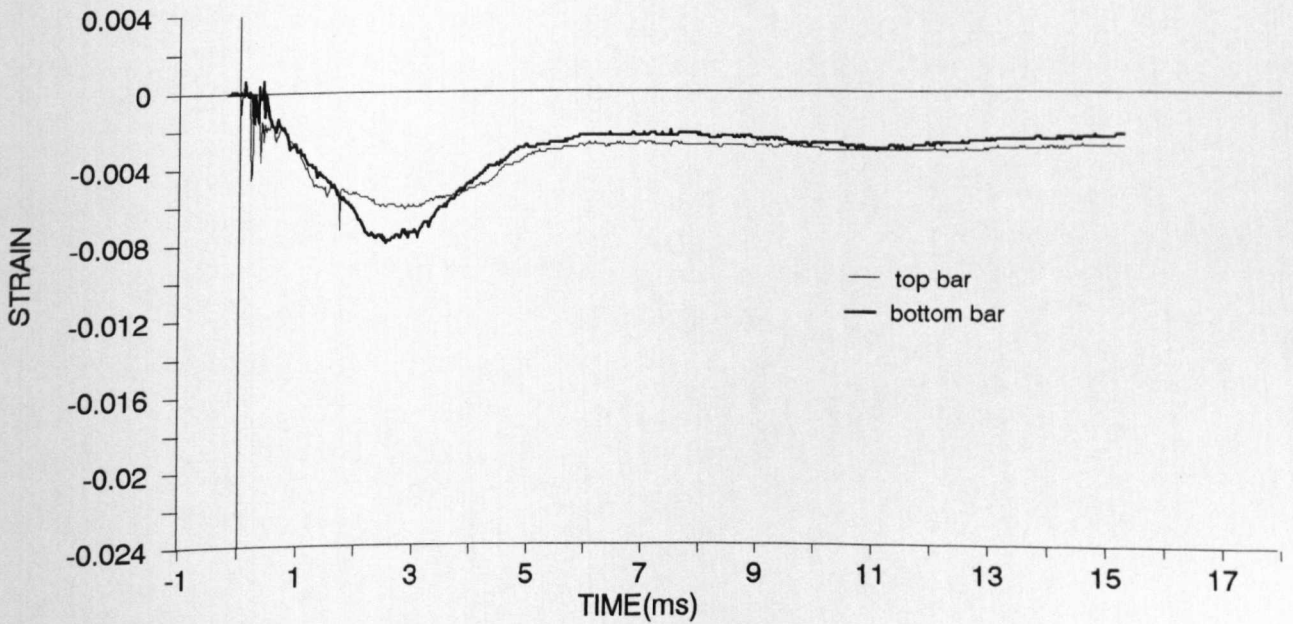
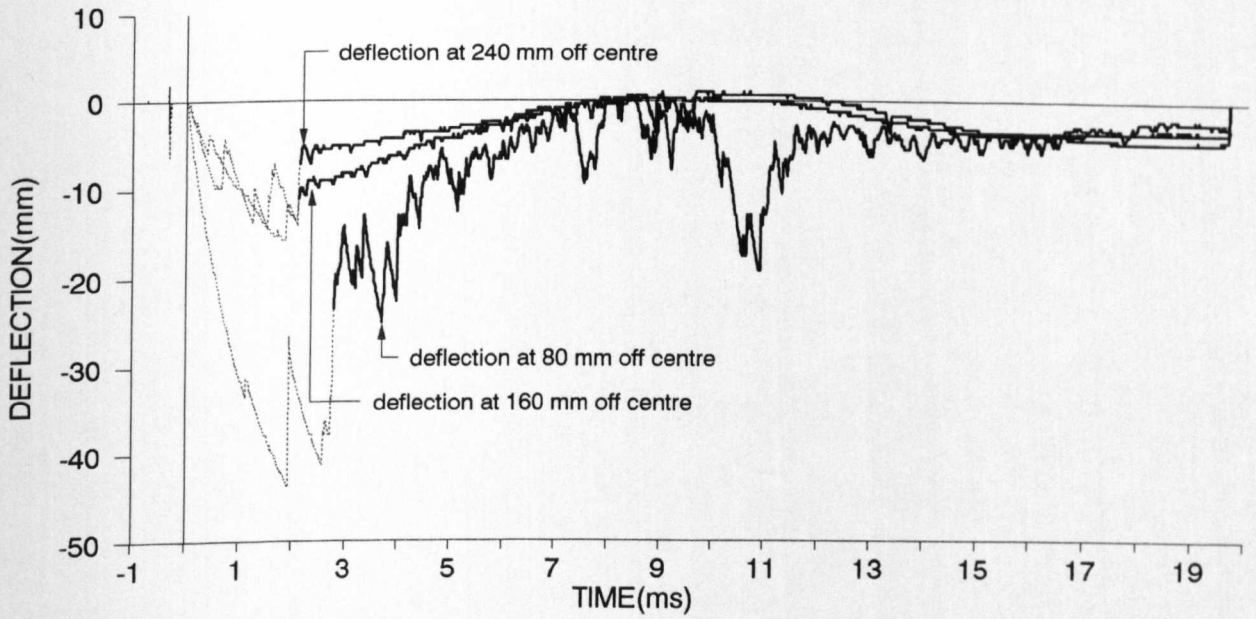
IMPULSE TEST - SMALL SLAB - SE12



top side



bottom side



IMPULSE TEST

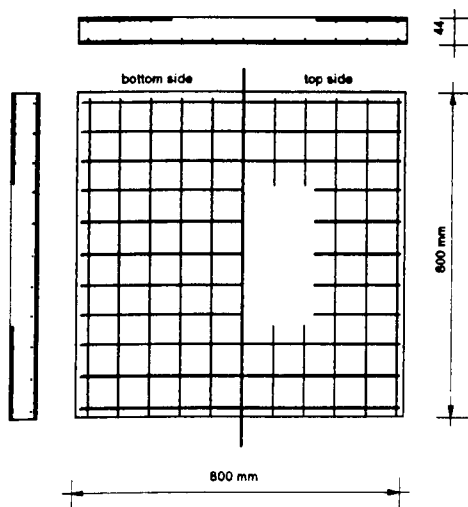
DATE: 18.12.92

SMALL SLAB SE13

AGE OF SPECIMEN: 7 days

Cube compressive strength	N/mm ²	40.7	Cylinder tensile strength	N/mm ²	4.65	Age (days)	10
---------------------------	-------------------	------	---------------------------	-------------------	------	------------	----

REINFORCEMENT:

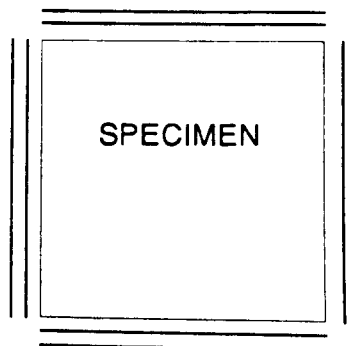
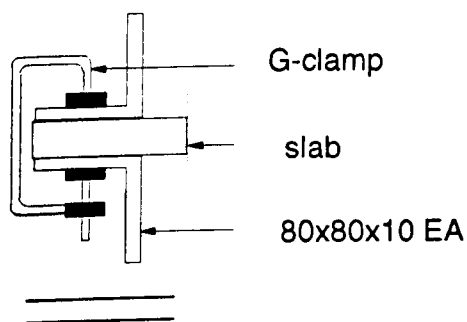


TOP LAYER REINFORCEMENT:
 R.MESH : 3.15 mm DIAM. / 76.2 mm CENTRES
 (WITHOUT CENTRAL REGION 400 X 400 mm)
 BOTTOM LAYER REINFORCEMENT:
 R.MESH : 3.15 mm DIAM. / 76.2 mm CENTRES
 COVER: 4 mm

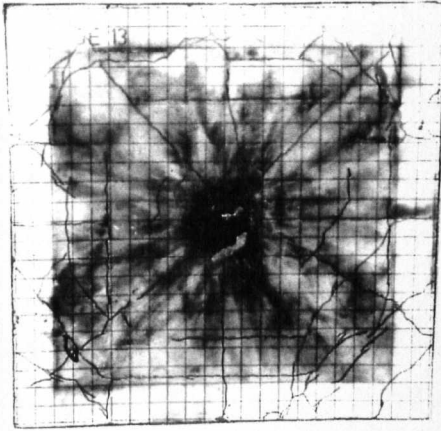
LOADING CONDITIONS:

CHARGE WEIGHT : 78g, PE4
 CHARGE SHAPE : Hemispherical
 CHARGE DIRECTION..... : Spherical side facing the specimen
 CHARGE POSITION : Central
 CLEAR DISTANCE TO THE CHARGE..... : 125mm

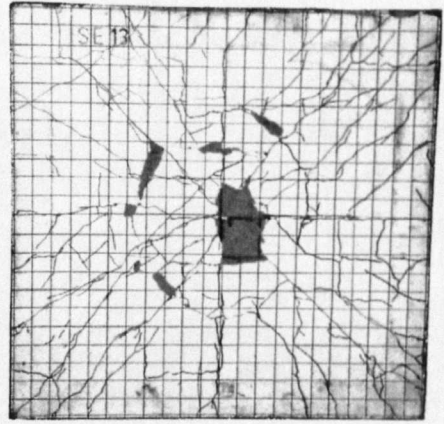
SUPPORTS:



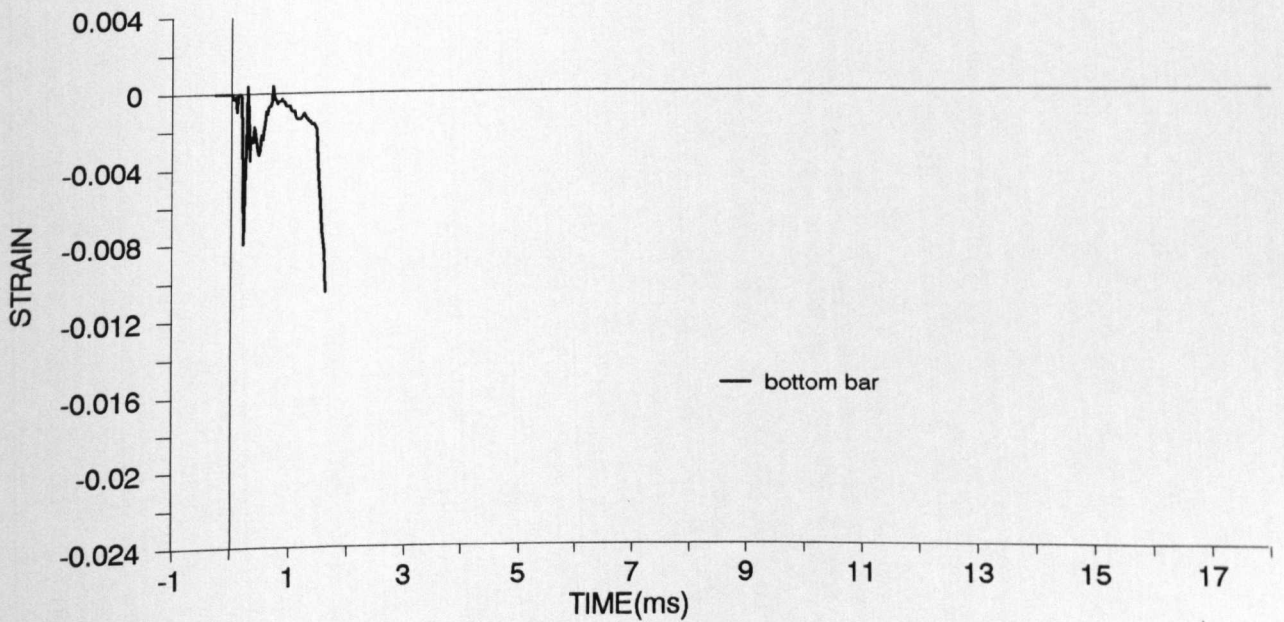
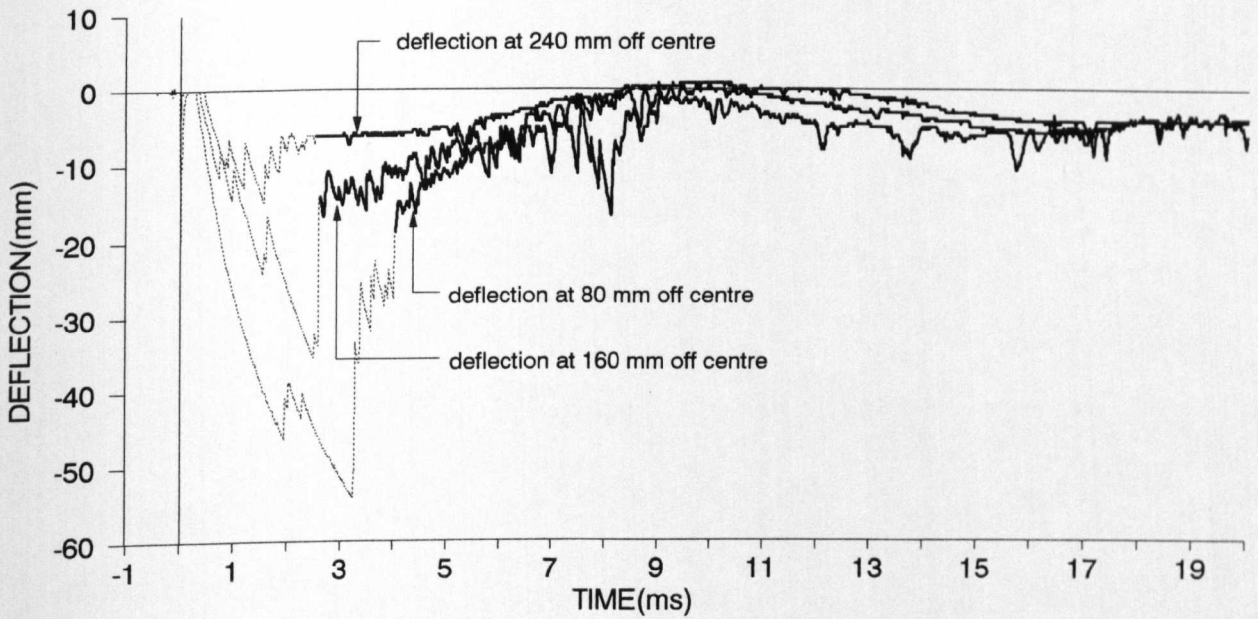
IMPULSE TEST - SMALL SLAB - SE13



top side



bottom side



IMPULSE TEST

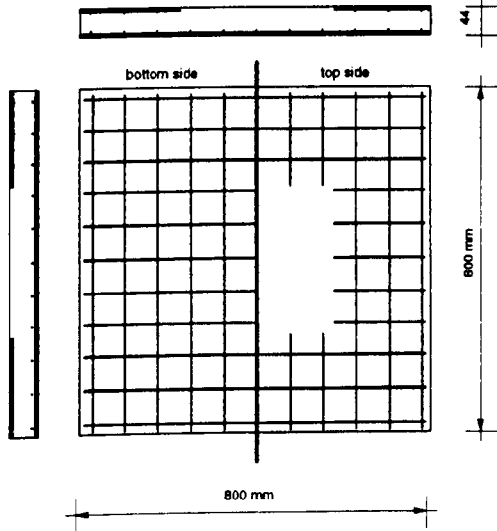
DATE: 21.12.92

SMALL SLAB SE14

AGE OF SPECIMEN: 10 days

Cube compressive strength	N/mm ²	40.7	Cylinder tensile strength	N/mm ²	4.65	Age (days)	10
---------------------------	-------------------	------	---------------------------	-------------------	------	------------	----

REINFORCEMENT:

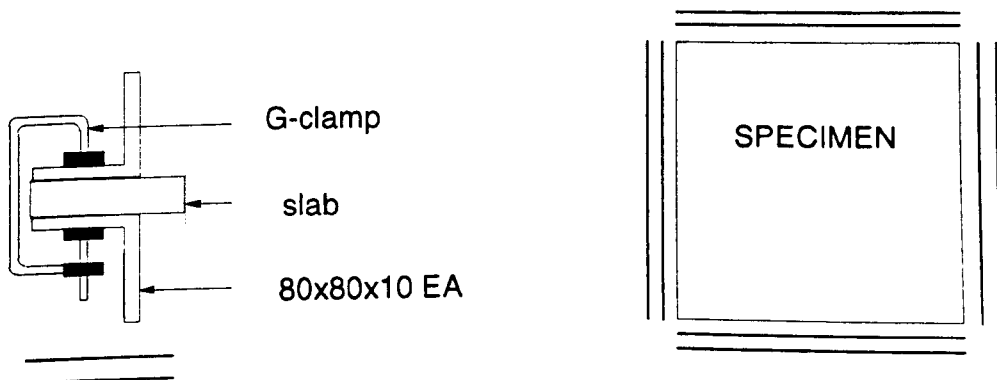


TOP LAYER REINFORCEMENT
 R.MESH : 3.15 mm DIAM. / 76.2 mm CENTRES
 (WITHOUT CENTRAL REGION 400 X 400 mm)
 BOTTOM LAYER REINFORCEMENT
 R.MESH : 3.15 mm DIAM. / 76.2 mm CENTRES
 COVER: 4 mm

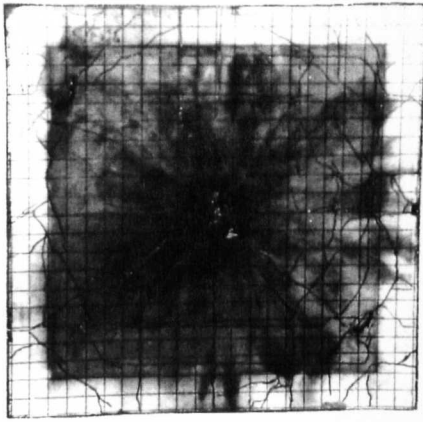
LOADING CONDITIONS:

CHARGE WEIGHT : 78g, PE4
 CHARGE SHAPE : Hemispherical
 CHARGE DIRECTION..... : Spherical side facing the specimen
 CHARGE POSITION : Central
 CLEAR DISTANCE TO THE CHARGE..... : 100mm

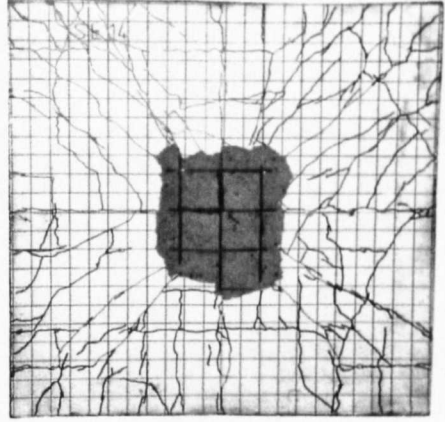
SUPPORTS:



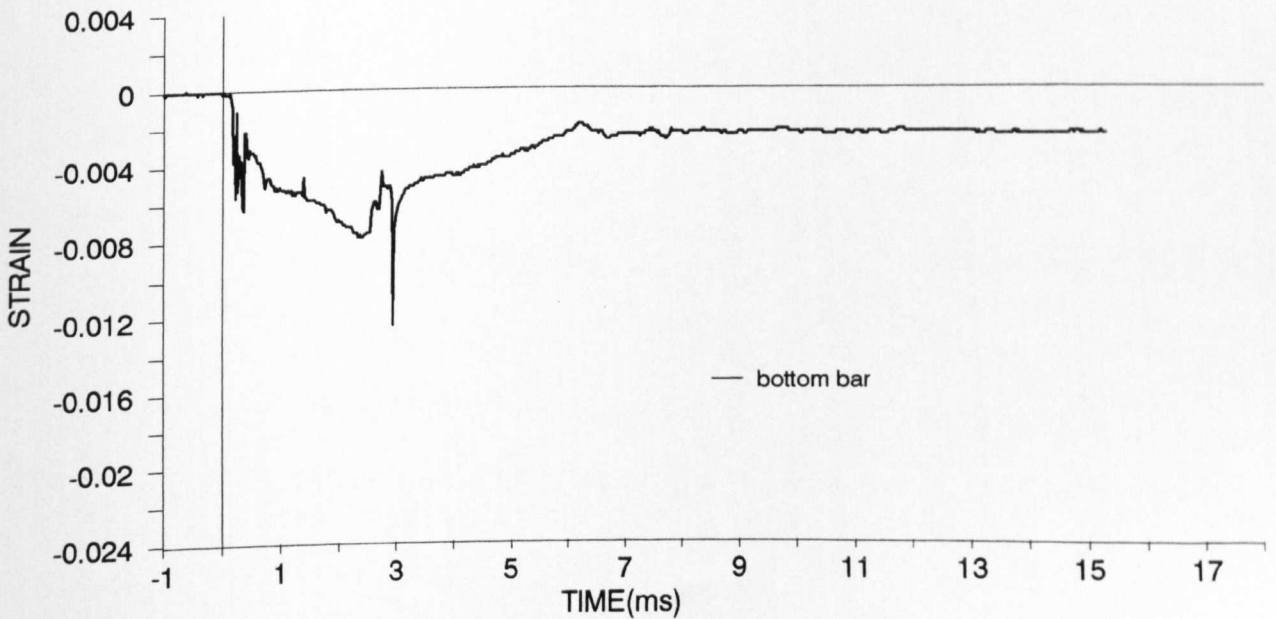
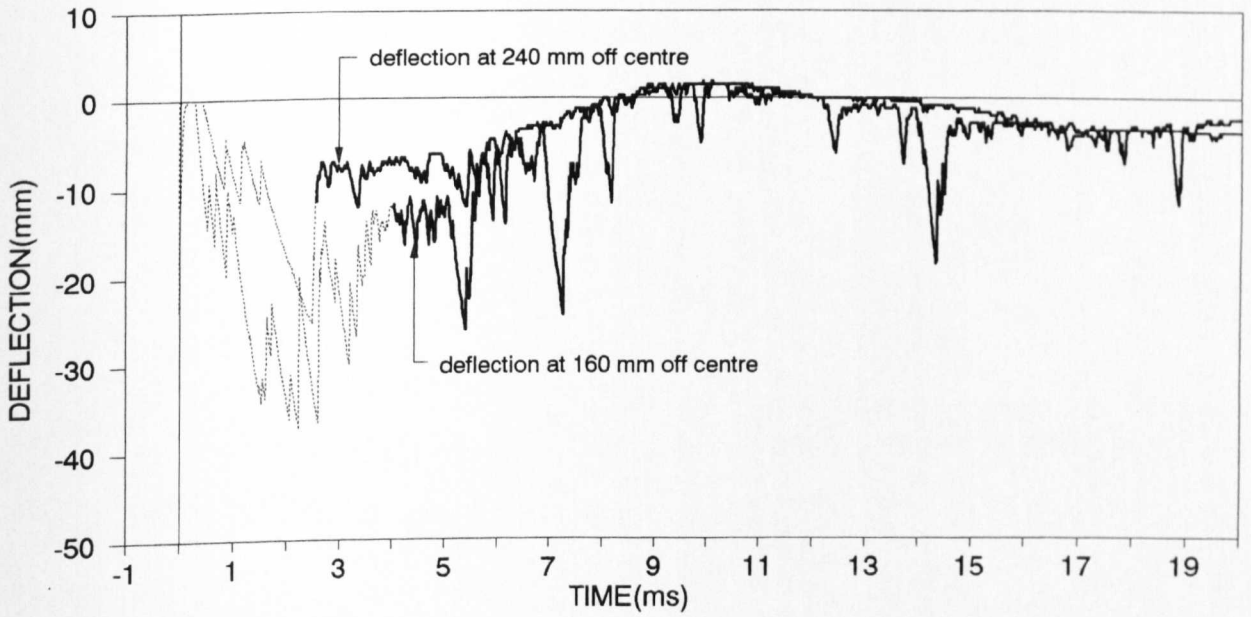
IMPULSE TEST - SMALL SLAB - SE14



top side



bottom side



IMPULSE TEST

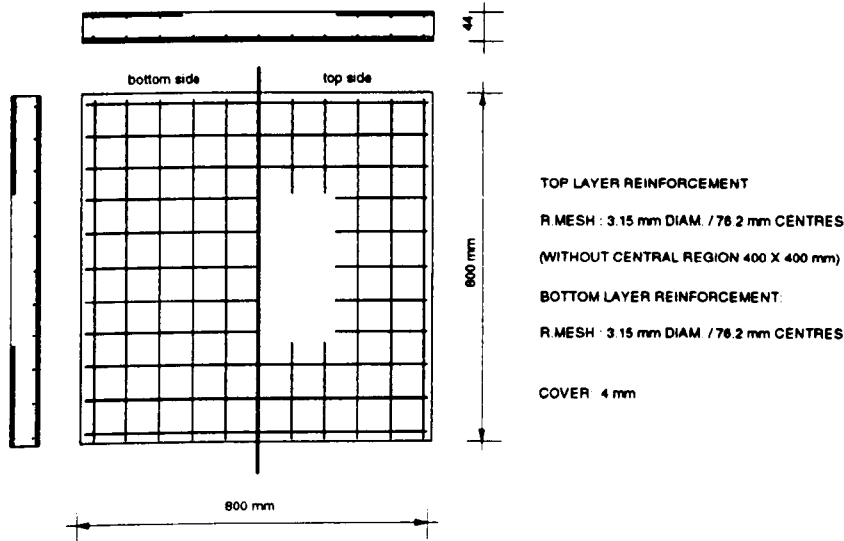
DATE: 21.12.92

SMALL SLAB SE15

AGE OF SPECIMEN: 10 days

Cube compressive strength	N/mm ²	40.7	Cylinder tensile strength	N/mm ²	4.65	Age (days)	10
---------------------------	-------------------	------	---------------------------	-------------------	------	------------	----

REINFORCEMENT:



LOADING CONDITIONS:

CHARGE WEIGHT : 78g, PE4

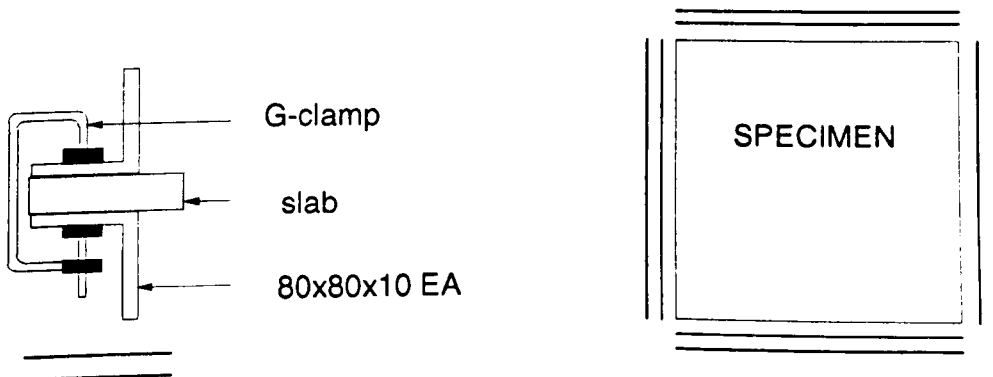
CHARGE SHAPE : Hemispherical

CHARGE DIRECTION..... : Spherical side facing the specimen

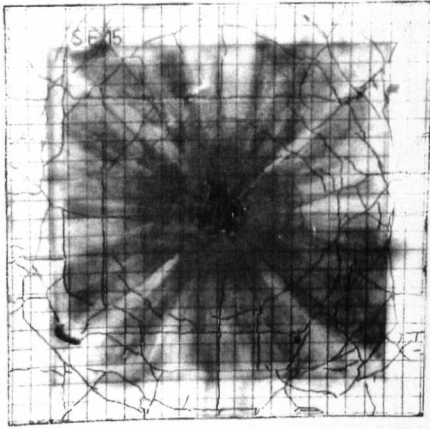
CHARGE POSITION : Central

CLEAR DISTANCE TO THE CHARGE..... : 75mm

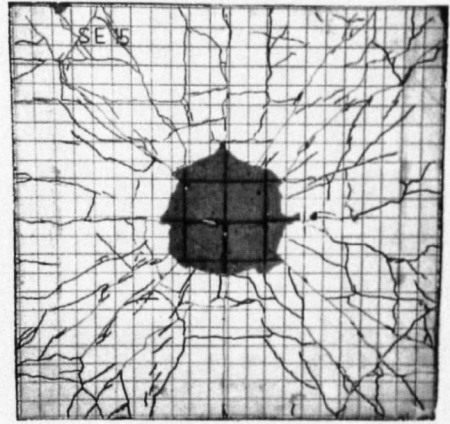
SUPPORTS:



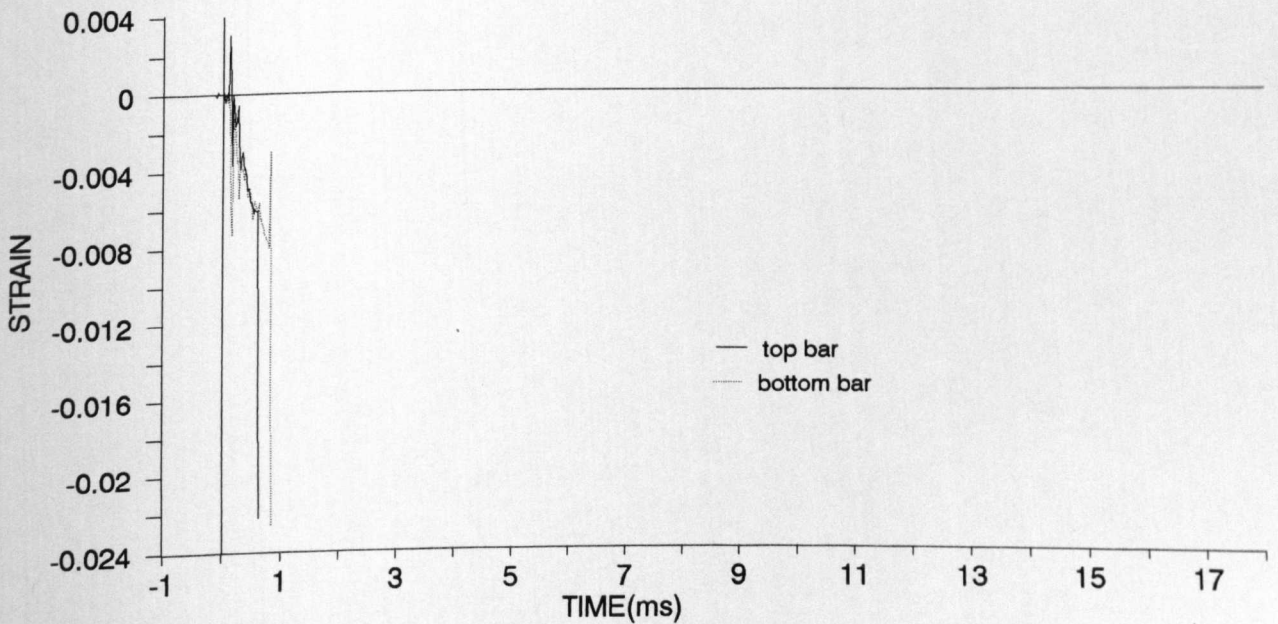
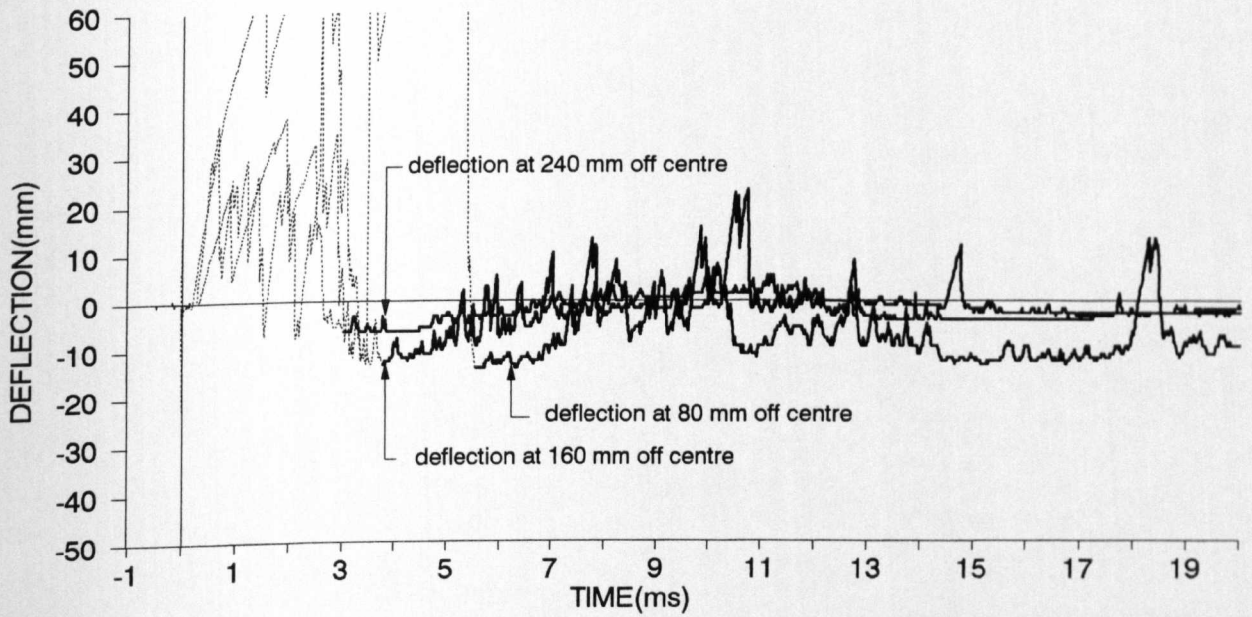
IMPULSE TEST - SMALL SLAB - SE15



top side



bottom side



IMPULSE TEST

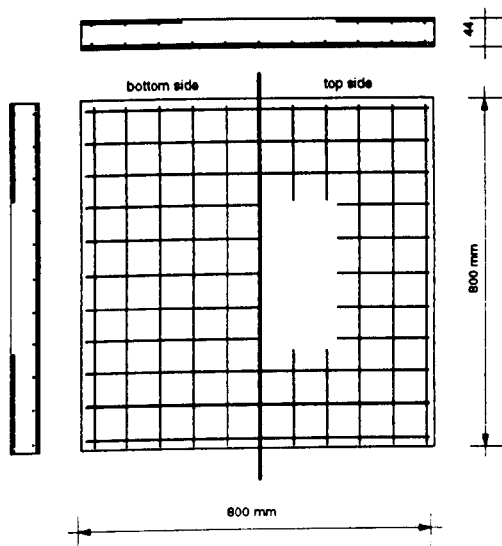
DATE: 15.01.93

SMALL SLAB SE16

AGE OF SPECIMEN: 8 days

Cube compressive strength	N/mm ²	39.33	Cylinder tensile strength	N/mm ²	5.05	Age (days)	8
---------------------------	-------------------	-------	---------------------------	-------------------	------	------------	---

REINFORCEMENT:



TOP LAYER REINFORCEMENT:

R.MESH : 3.15 mm DIAM. / 76.2 mm CENTRES
(WITHOUT CENTRAL REGION 400 X 400 mm)

BOTTOM LAYER REINFORCEMENT:

R.MESH : 3.15 mm DIAM. / 76.2 mm CENTRES

COVER: 4 mm

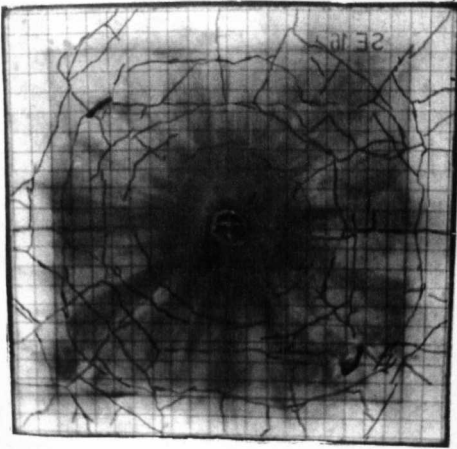
LOADING CONDITIONS:

- CHARGE WEIGHT : 78g, PE4
- CHARGE SHAPE : Hemispherical
- CHARGE DIRECTION..... : Spherical side facing the specimen
- CHARGE POSITION : Central
- CLEAR DISTANCE TO THE CHARGE..... : 60mm

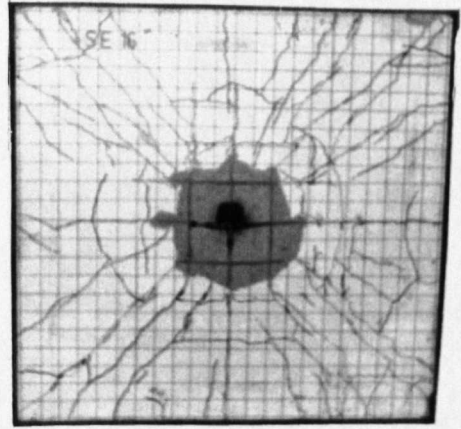
SUPPORTS:



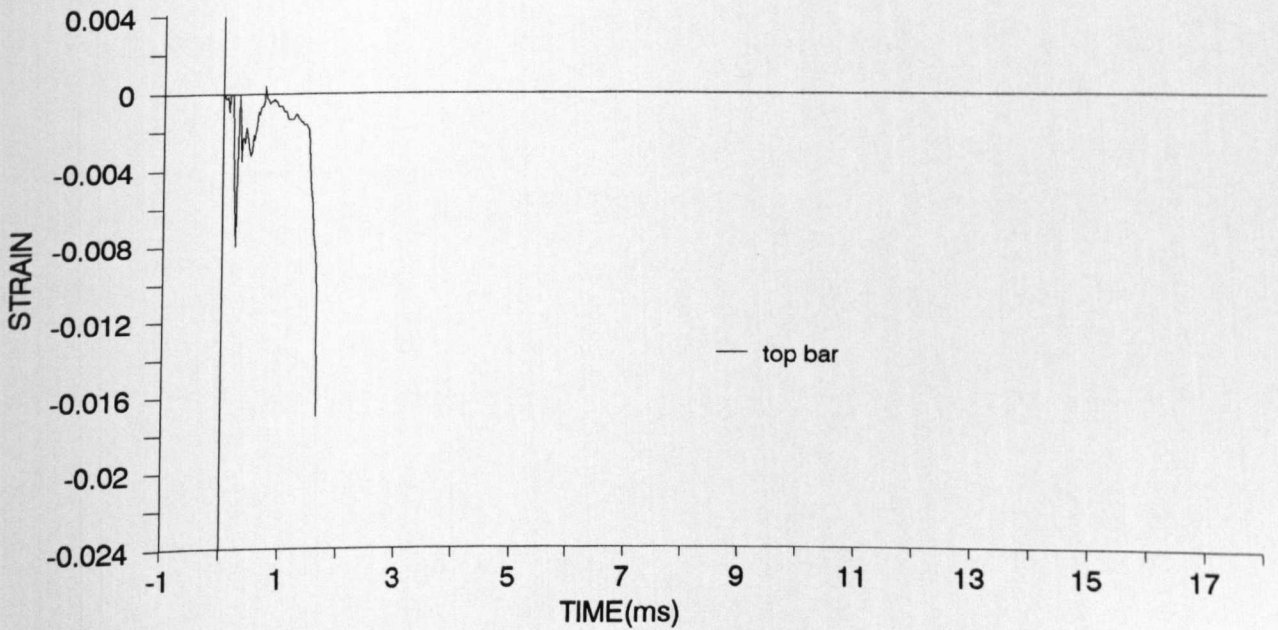
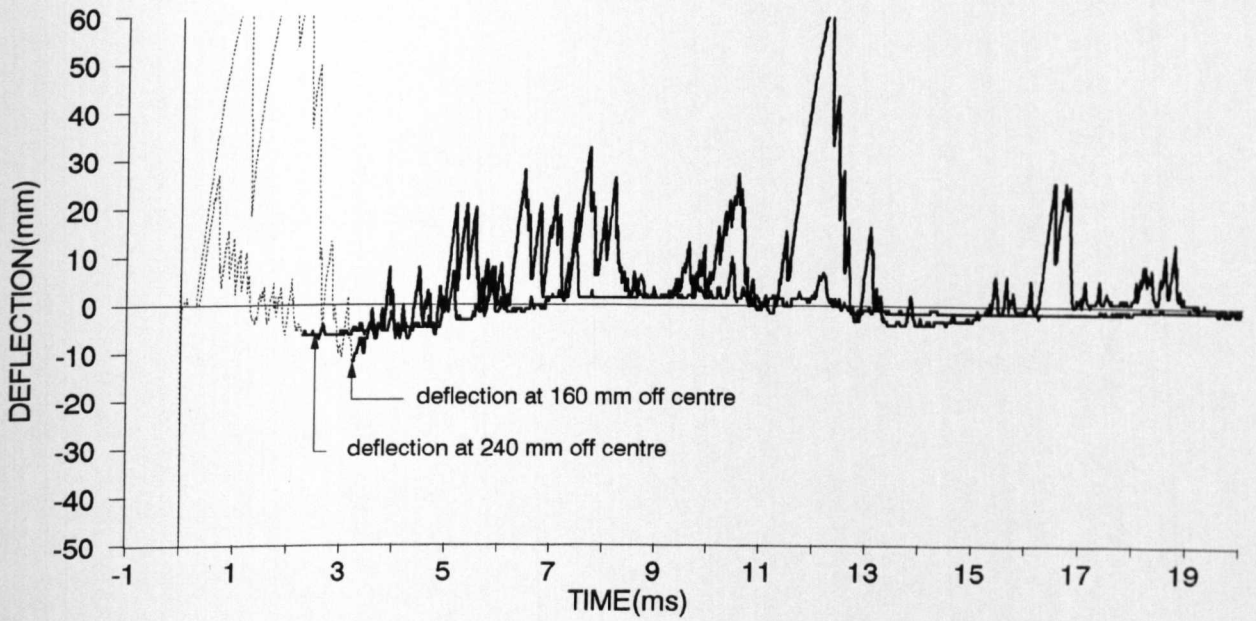
IMPULSE TEST - SMALL SLAB - SE16



top side



bottom side



IMPULSE TEST

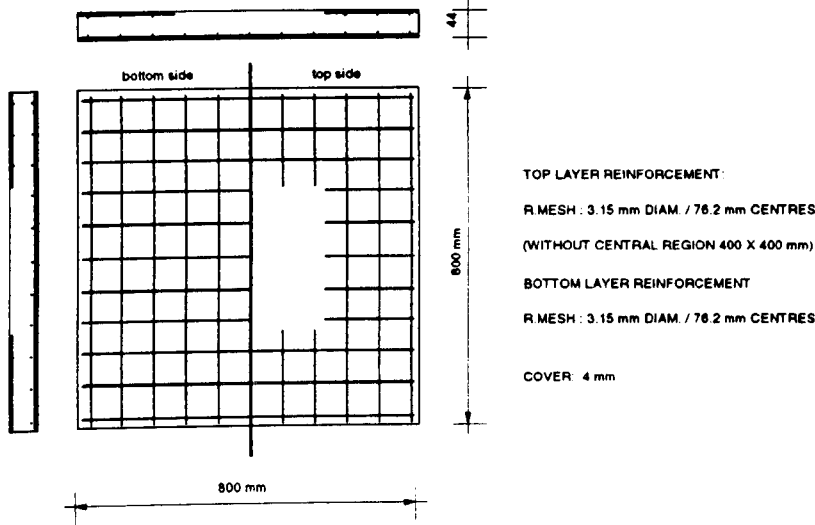
DATE: 18.01.93

SMALL SLAB SE17

AGE OF SPECIMEN: 11 days

Cube compressive strength	N/mm ²	39.33	Cylinder tensile strength	N/mm ²	5.05	Age (days)	8
---------------------------	-------------------	-------	---------------------------	-------------------	------	------------	---

REINFORCEMENT:



LOADING CONDITIONS:

CHARGE WEIGHT : 78g, PE4

CHARGE SHAPE : Hemispherical

CHARGE DIRECTION..... : Spherical side facing the specimen

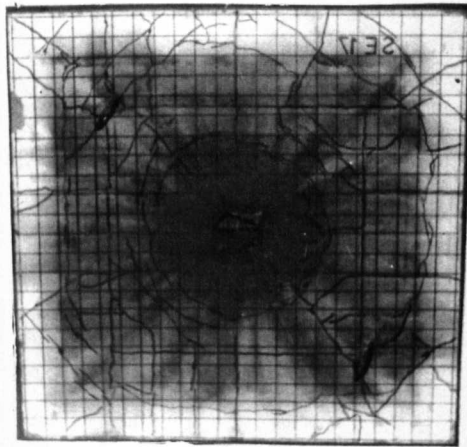
CHARGE POSITION : Central

CLEAR DISTANCE TO THE CHARGE..... : 50mm

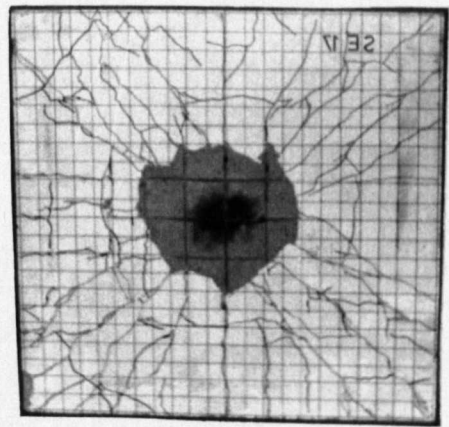
SUPPORTS:



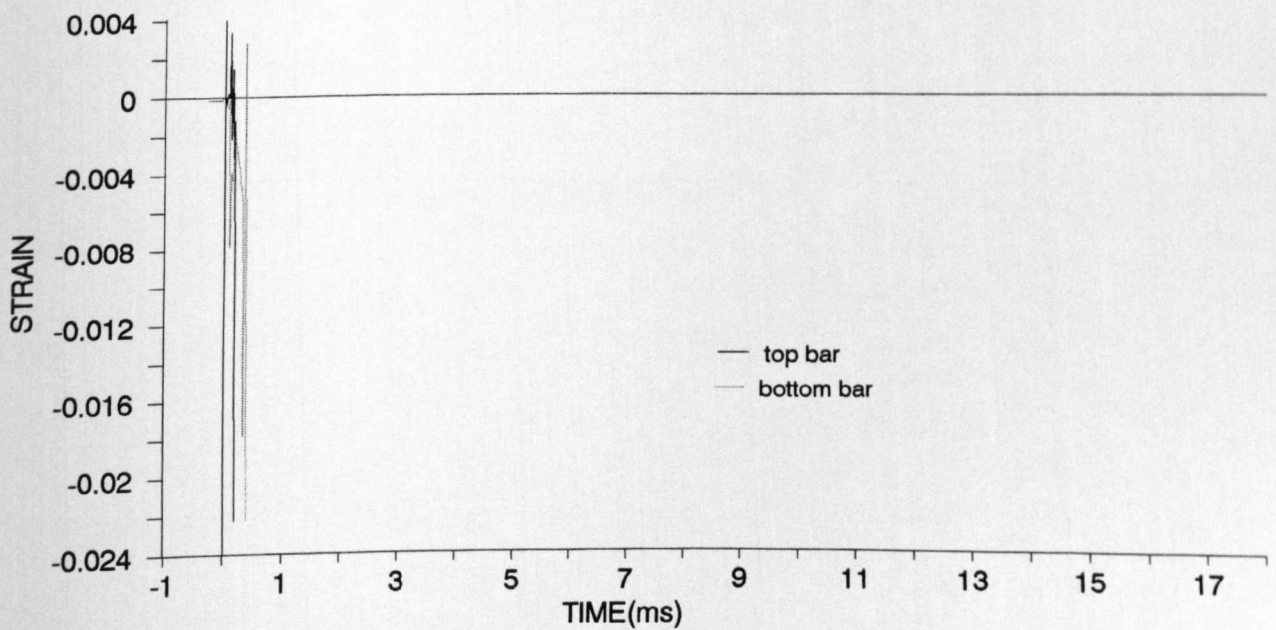
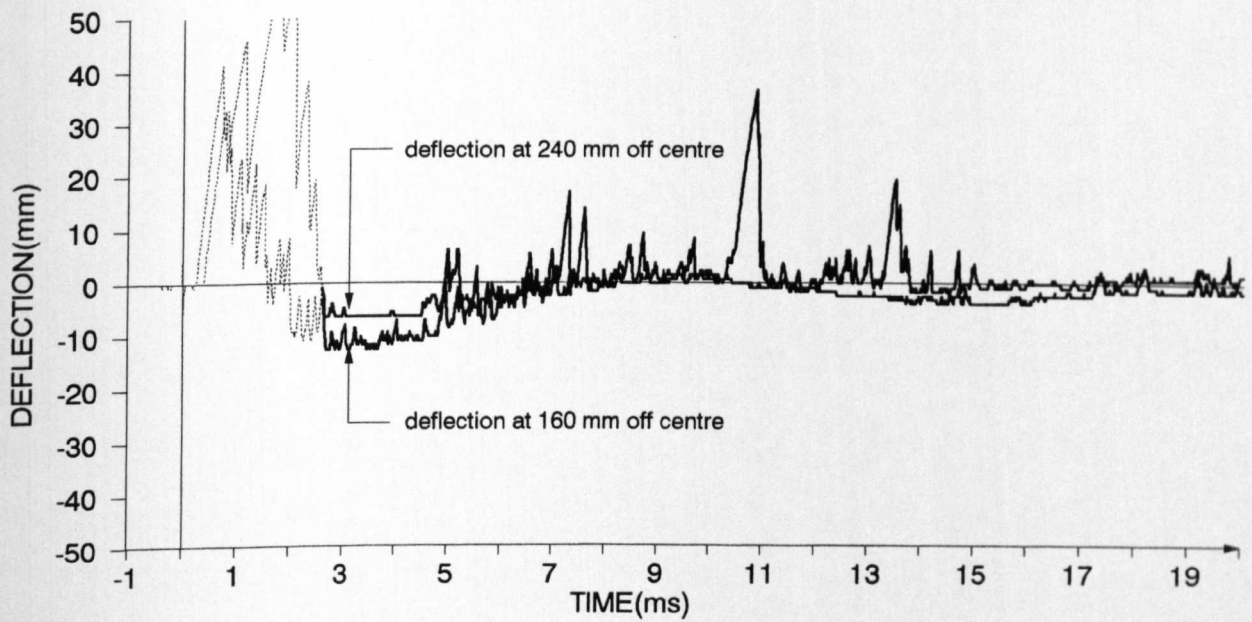
IMPULSE TEST - SMALL SLAB - SE17



top side



bottom side



IMPULSE TEST

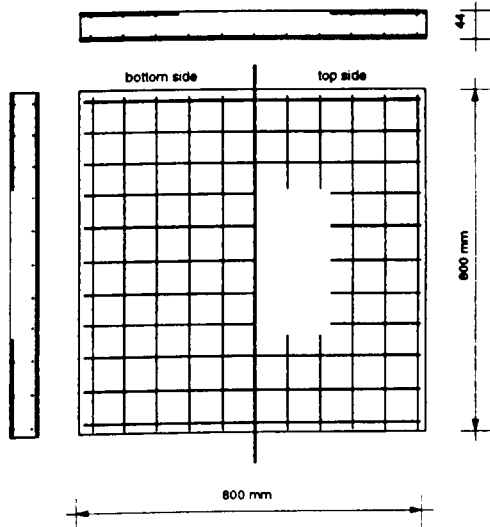
DATE: 18.01.93

SMALL SLAB SE18

AGE OF SPECIMEN: 11 days

Cube compressive strength	N/mm ²	39.33	Cylinder tensile strength	N/mm ²	5.05	Age (days)	8
---------------------------	-------------------	-------	---------------------------	-------------------	------	------------	---

REINFORCEMENT:



TOP LAYER REINFORCEMENT

R MESH : 3.15 mm DIAM / 76.2 mm CENTRES
(WITHOUT CENTRAL REGION 400 X 400 mm)

BOTTOM LAYER REINFORCEMENT

R MESH : 3.15 mm DIAM / 76.2 mm CENTRES

COVER : 4 mm

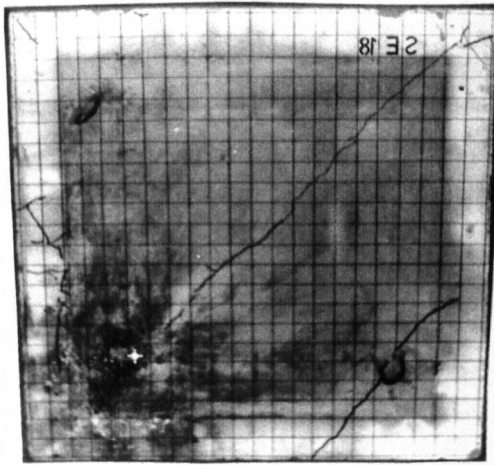
LOADING CONDITIONS:

CHARGE WEIGHT : 78g, PE4
 CHARGE SHAPE : Hemispherical
 CHARGE DIRECTION..... : Spherical side facing the specimen
 CHARGE POSITION : 200mm off centre, each direction
 CLEAR DISTANCE TO THE CHARGE..... : 200mm

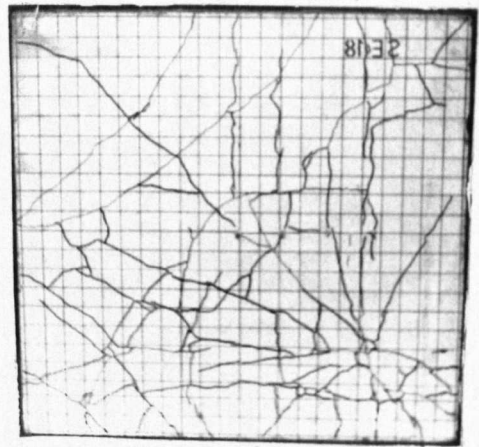
SUPPORTS:



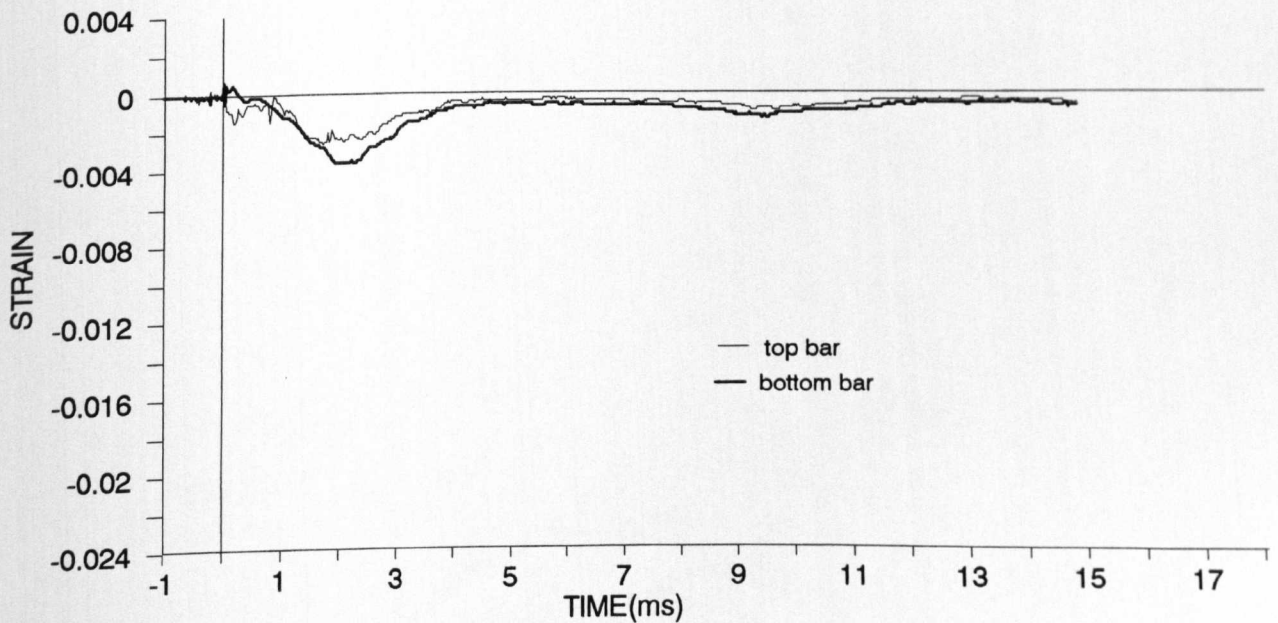
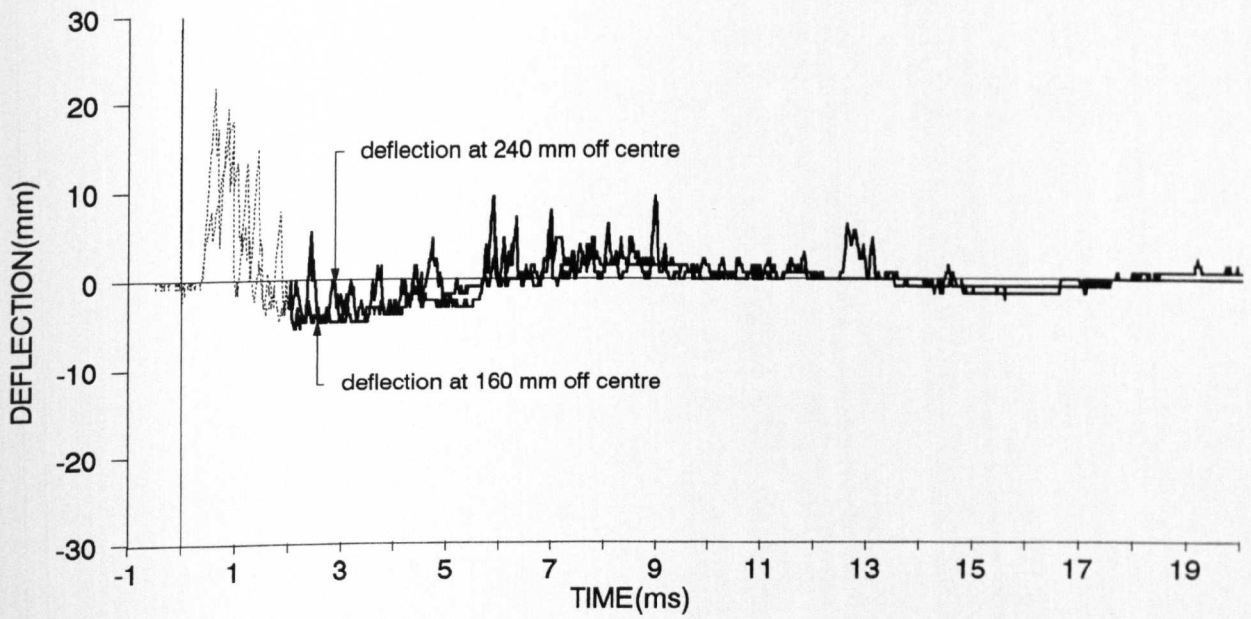
IMPULSE TEST - SMALL SLAB - SE18



top side



bottom side



IMPULSE TEST

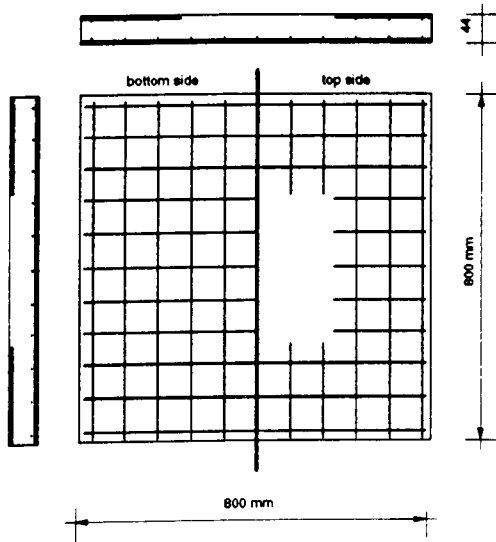
DATE: 1.02.93

SMALL SLAB SE19

AGE OF SPECIMEN: 11 days

Cube compressive strength	N/mm ²	40.0	Cylinder tensile strength	N/mm ²	4.03	Age (days)	11
---------------------------	-------------------	------	---------------------------	-------------------	------	------------	----

REINFORCEMENT:

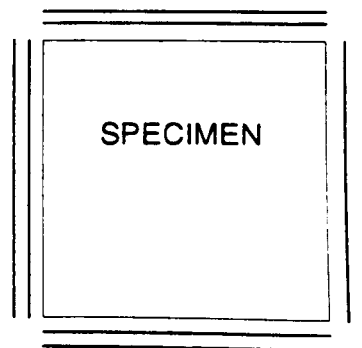
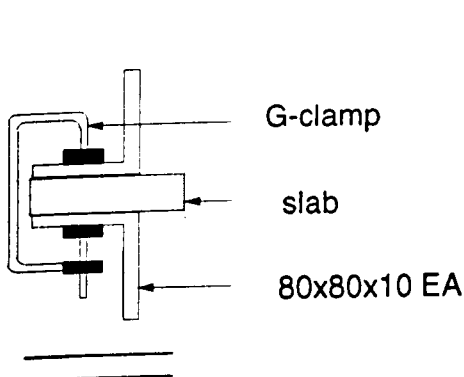


TOP LAYER REINFORCEMENT:
 R.MESH : 3.15 mm DIAM. / 76.2 mm CENTRES
 (WITHOUT CENTRAL REGION 400 X 400 mm)
 BOTTOM LAYER REINFORCEMENT:
 R.MESH : 3.15 mm DIAM. / 76.2 mm CENTRES
 COVER: 4 mm

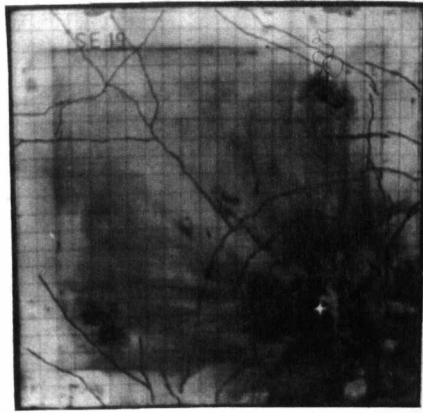
LOADING CONDITIONS:

CHARGE WEIGHT : 78g, PE4
 CHARGE SHAPE : Hemispherical
 CHARGE DIRECTION..... : Spherical side facing the specimen
 CHARGE POSITION : 200mm off centre, each direction
 CLEAR DISTANCE TO THE CHARGE..... : 100mm

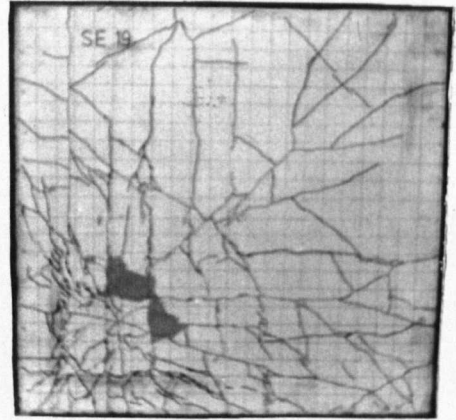
SUPPORTS:



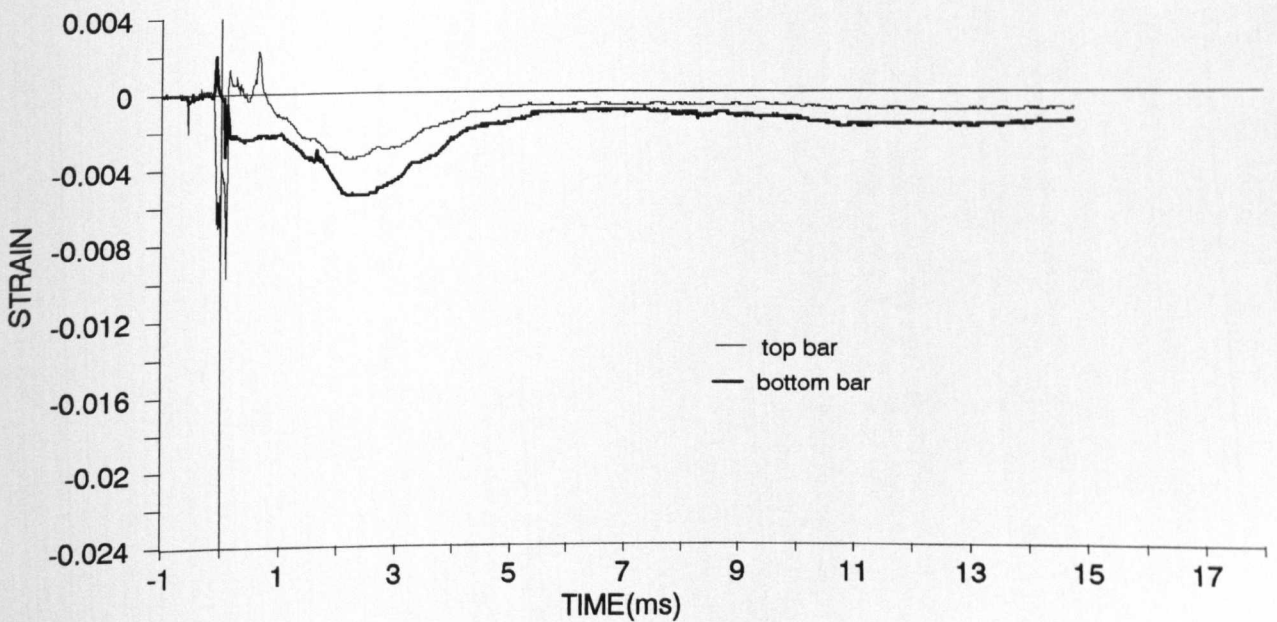
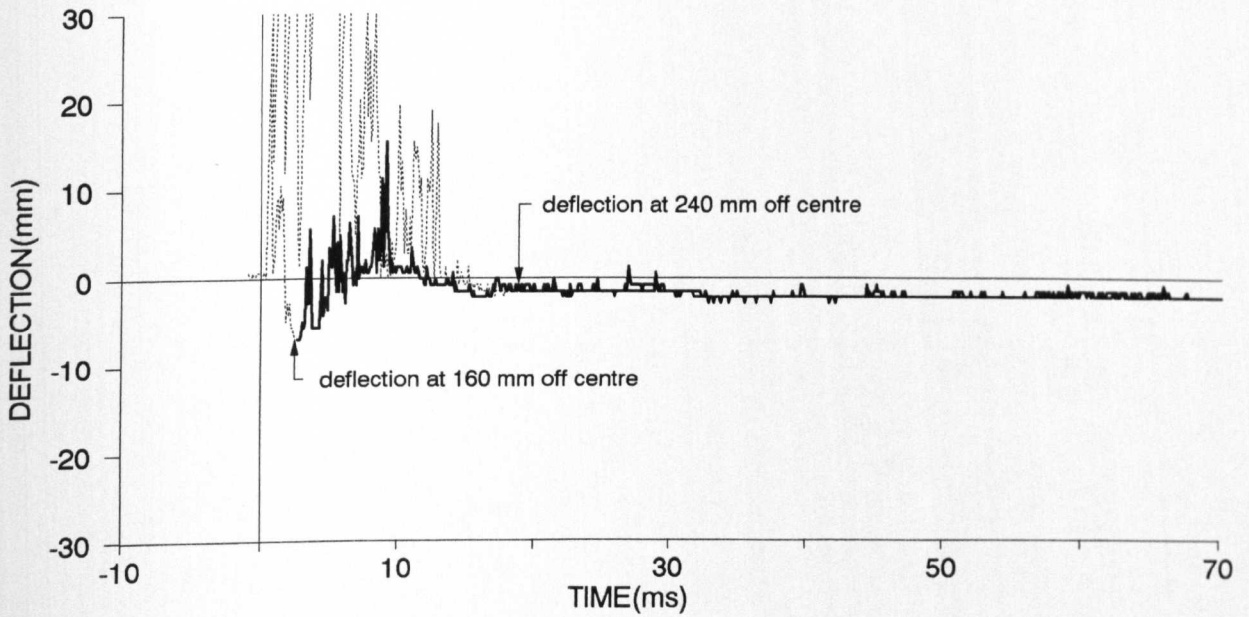
IMPULSE TEST - SMALL SLAB - SE19



top side



bottom side



IMPULSE TESTS

HIGH SPEED FILMS

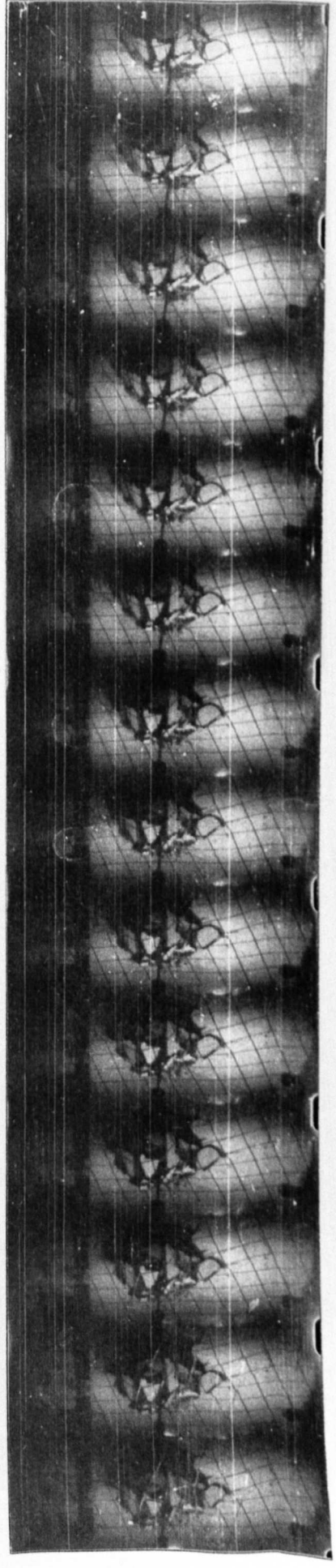
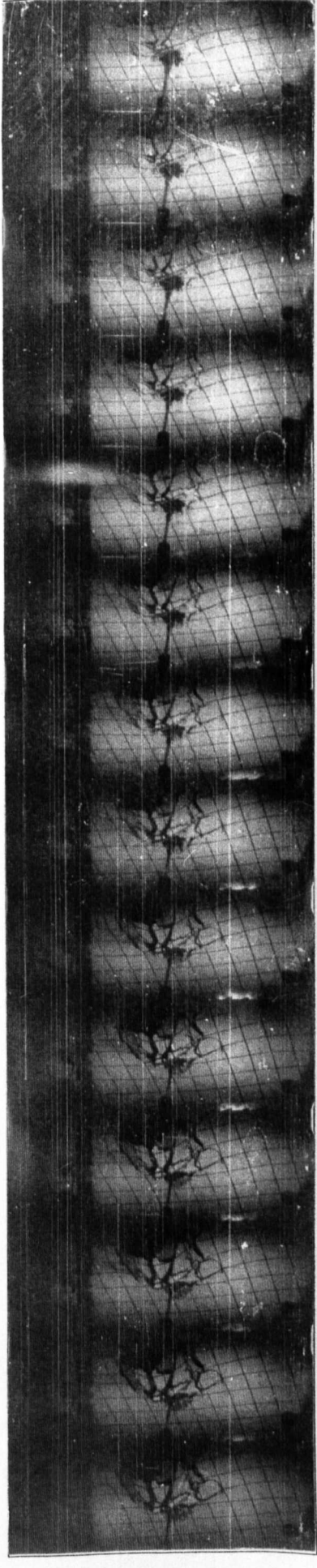
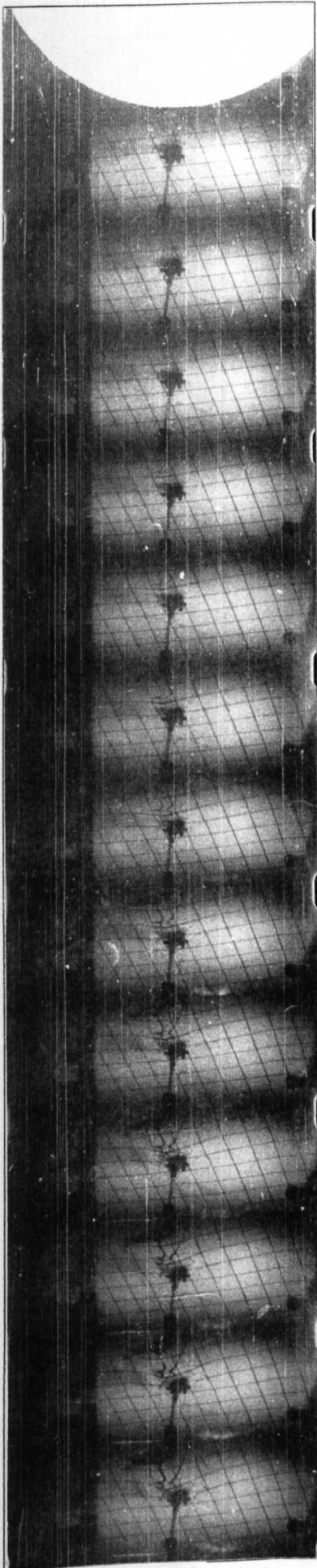
APPENDIX B3

IMPULSE TEST SE4

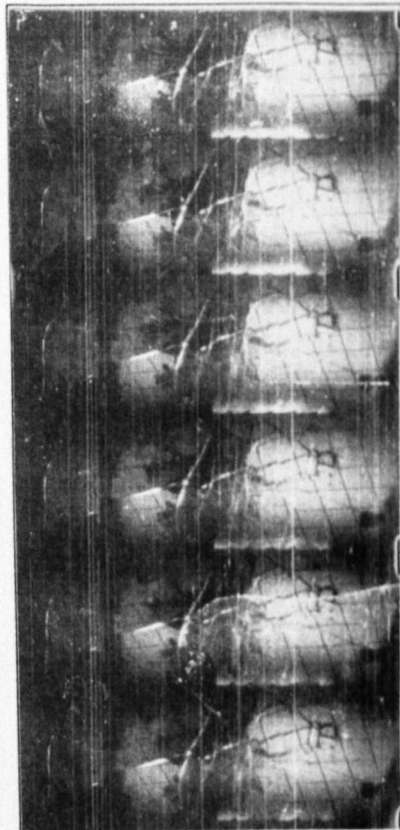
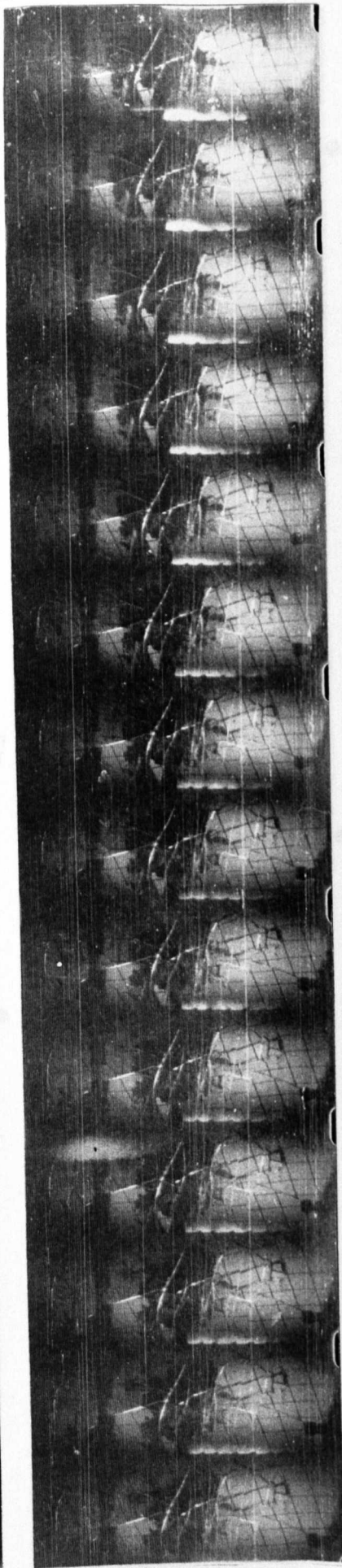
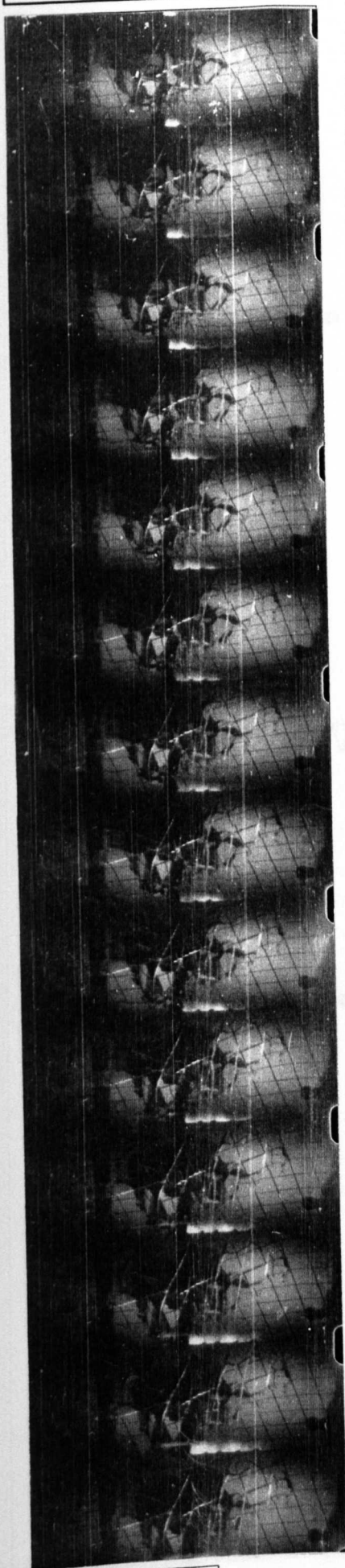
INTERFRAME TIME not available

DETONATION TIME n.a. MSEC. MARKERS-n.a.

1.



GRID SIZE : 36mm X 36mm



GRID SIZE : 36mm X 36mm

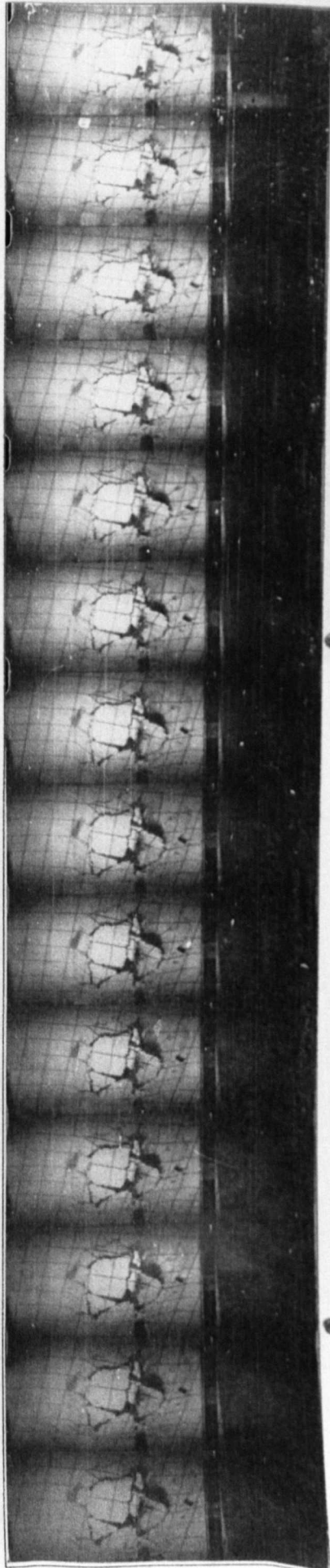
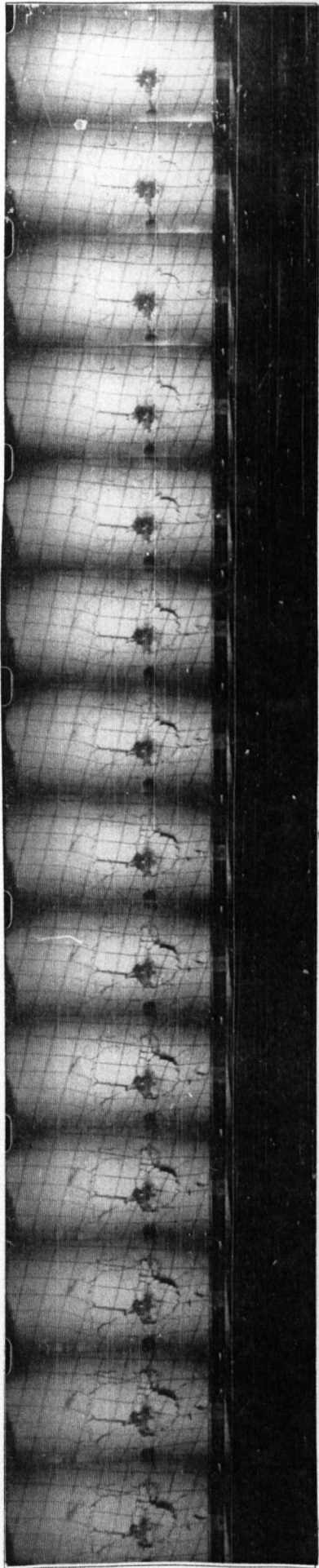
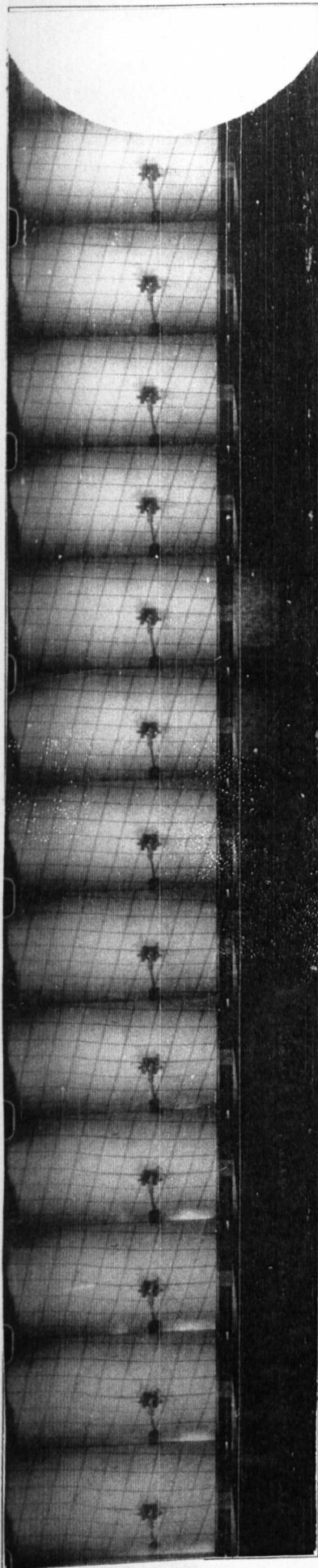
IMPULSE TEST SE5

INTERFRAME TIME 162.38 μ sec

▽ - DETONATION TIME

● - MSEC'S MARKER

1.



GRID SIZE : 36mm X 36mm

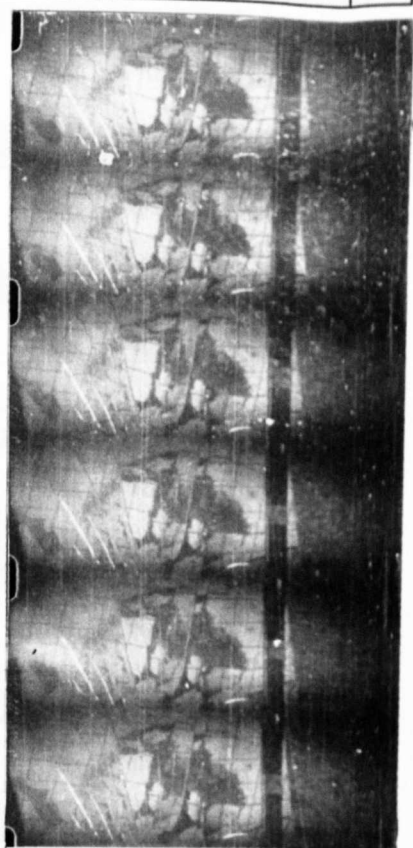
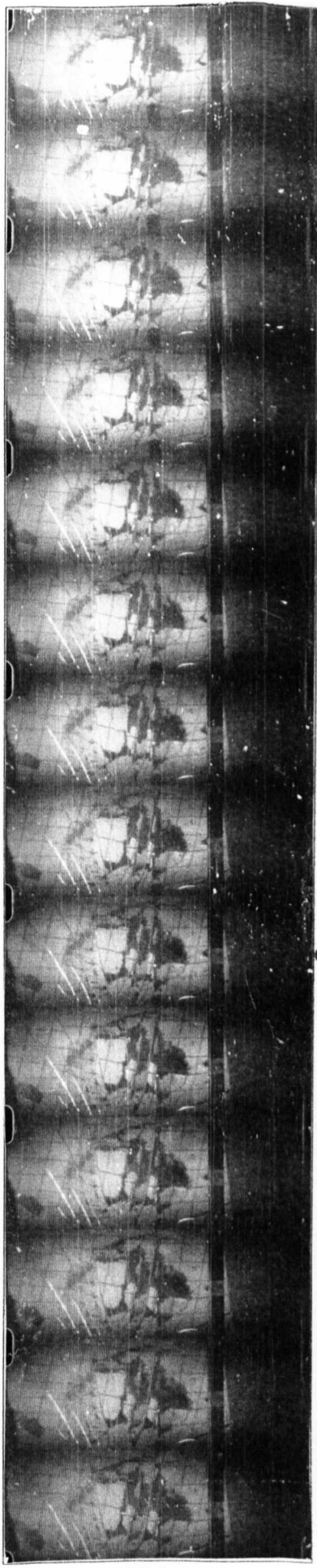
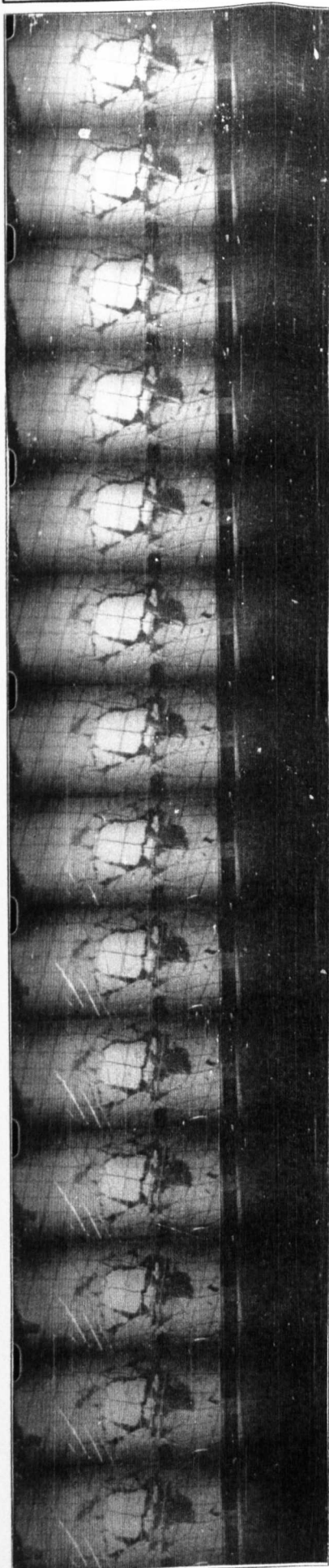
IMPULSE TEST SE5

INTERFRAME TIME 162.38 μ sec

▽ DETONATION TIME

● -MSEC'S MARKER

2.



GRID SIZE : 36mm X 36mm

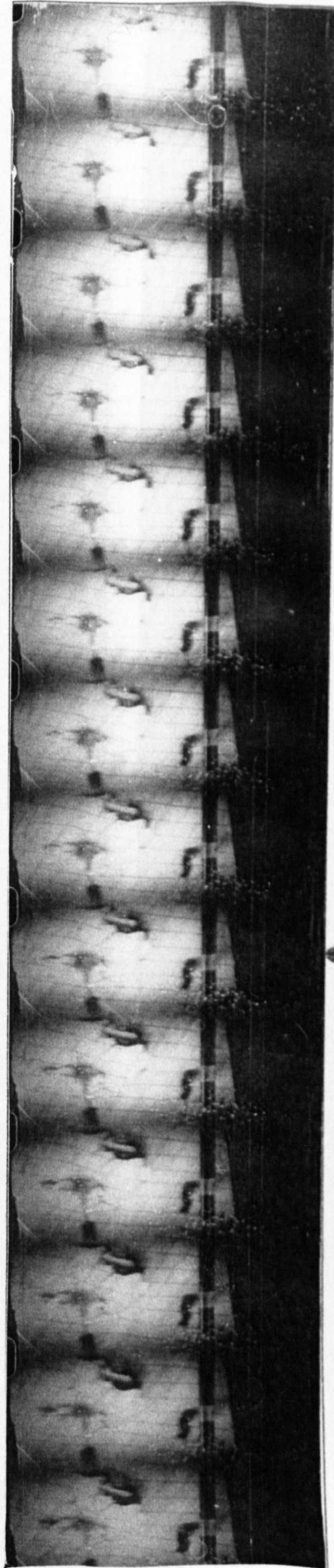
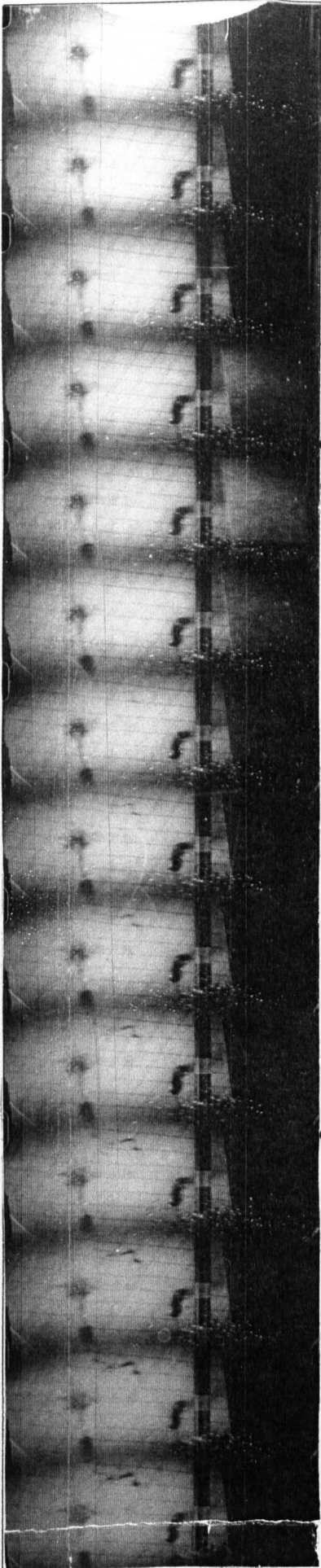
IMPULSE TEST SE6

INTERFRAME TIME 161.29 μ sec

▽ - DETONATION TIME

● - MSEC'S MARKER

1.



GRID SIZE : 36mm X 36mm

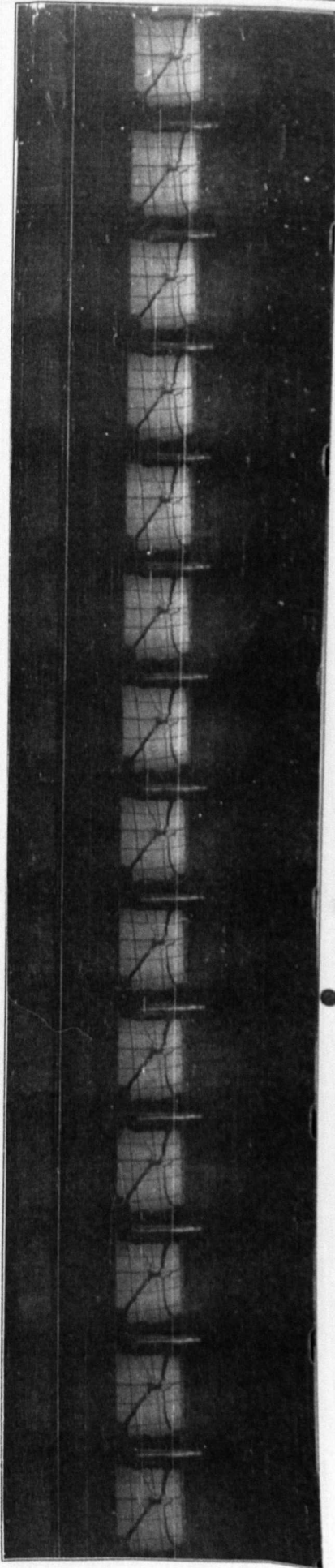
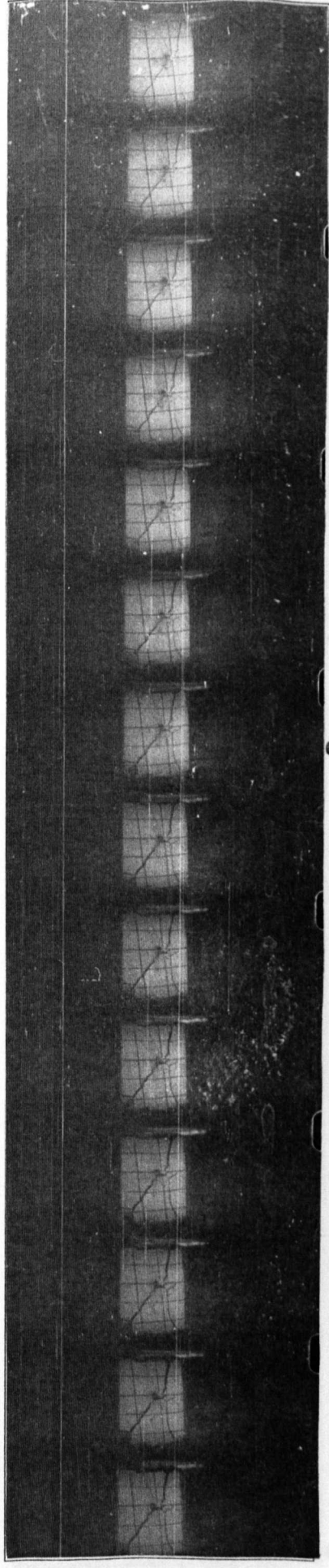
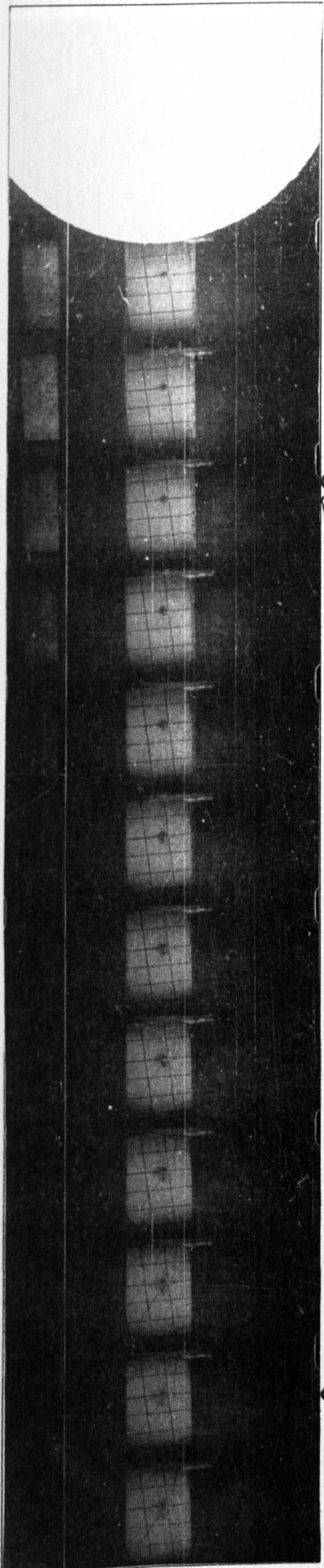
IMPULSE TEST SE7

INTERFRAME TIME 121.76 μ sec

▽ - DETONATION TIME

● - MSEC'S MARKER

1.



GRID SIZE : 36mm X 36mm

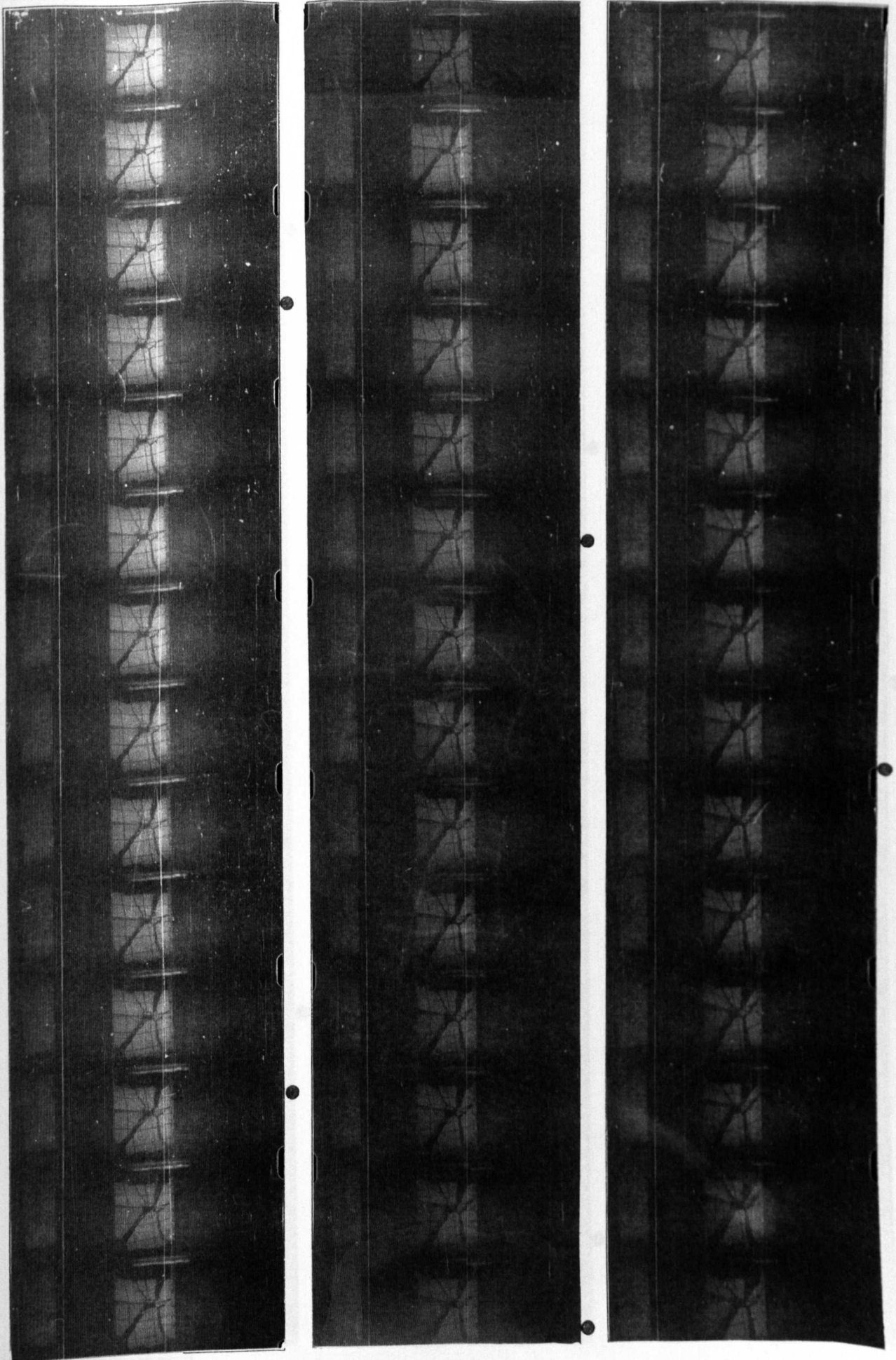
IMPULSE TEST SE7

INTERFRAME TIME 121.76 μ sec

▽ - DETONATION TIME

● - MSEC'S MARKER

2.



GRID SIZE : 36mm X 36mm

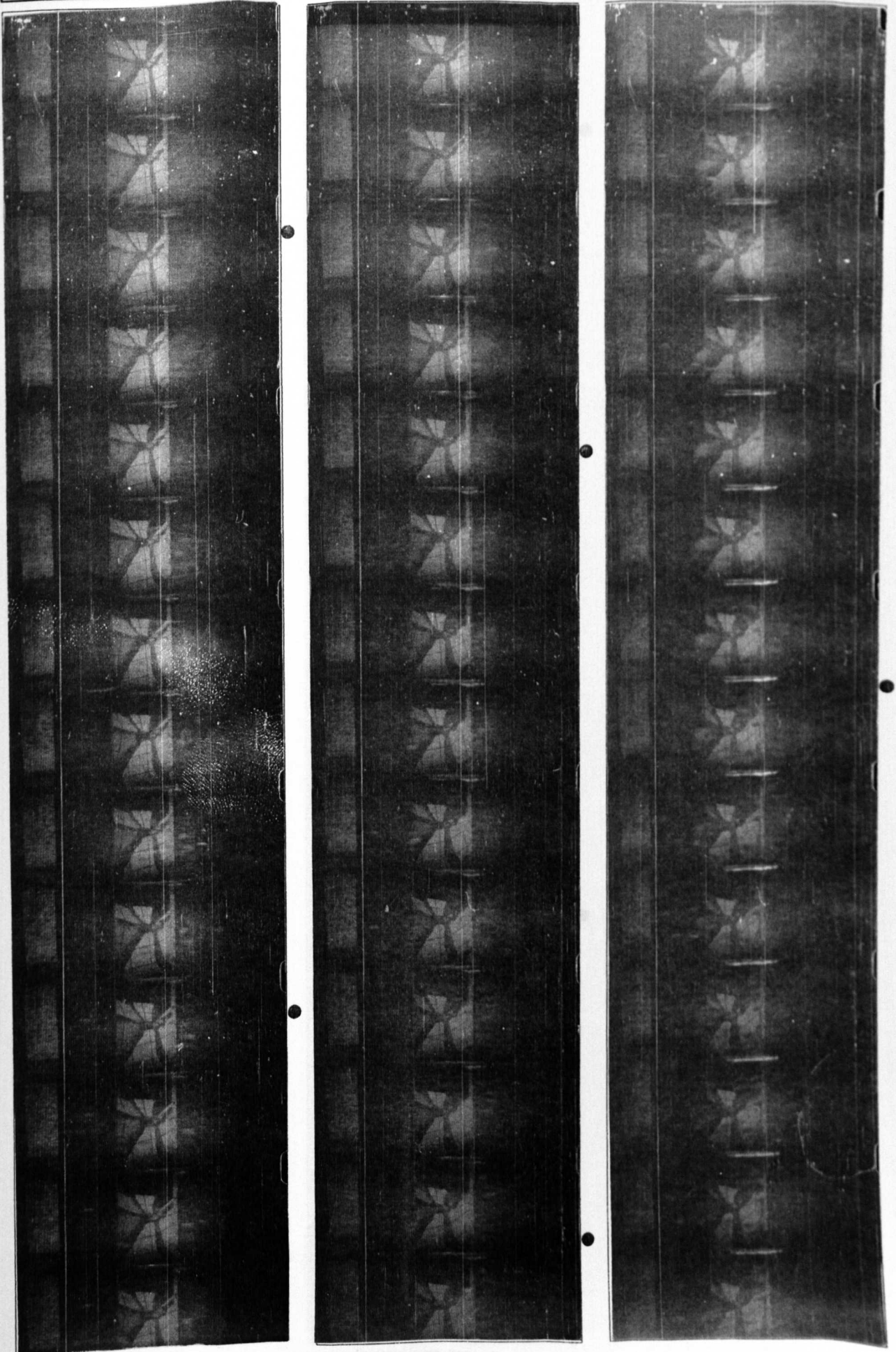
IMPULSE TEST SE7

INTERFRAME TIME 121.76 μ sec

▽ - DETONATION TIME

● - MSEC'S MARKER

3.



GRID SIZE : 36mm X 36mm

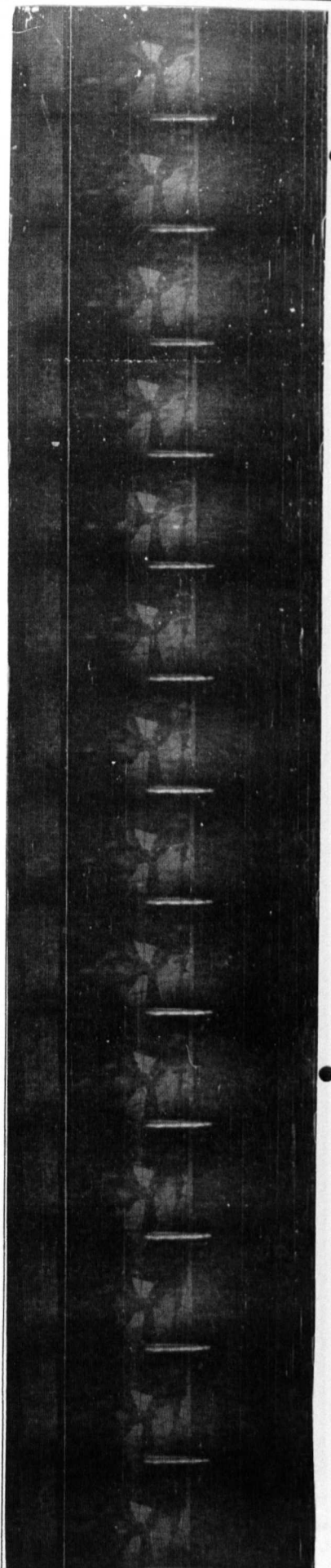
IMPULSE TEST SE7

INTERFRAME TIME 121.76 μ sec

∇ - DETONATION TIME

● - MSEC'S MARKER

4.



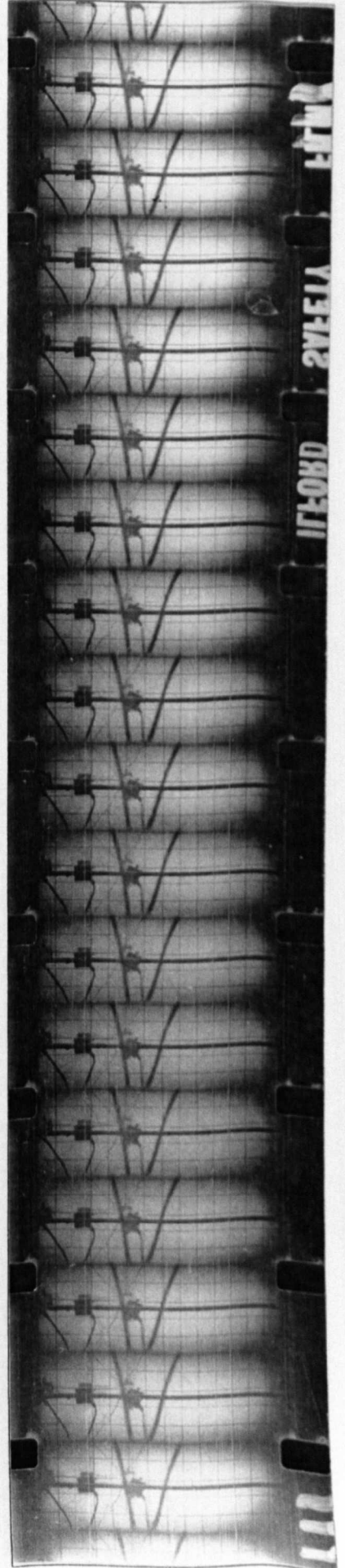
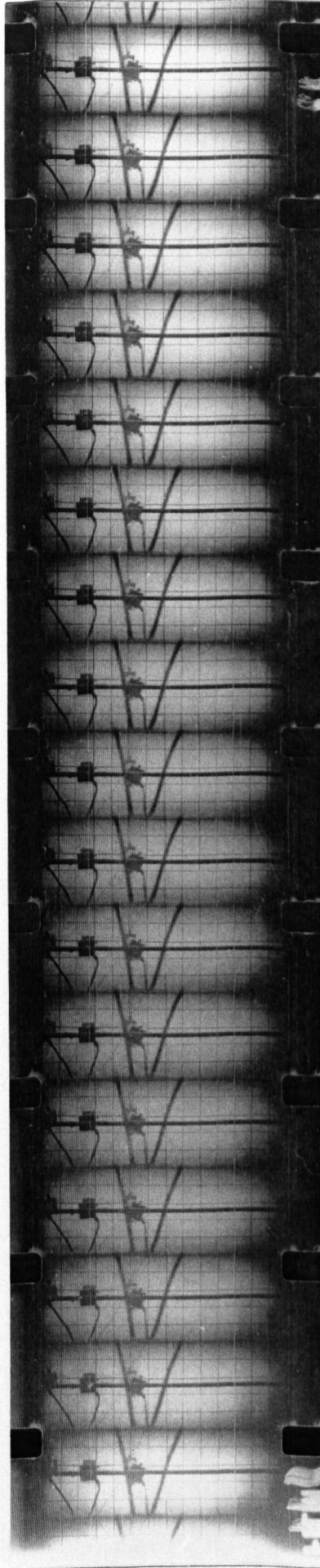
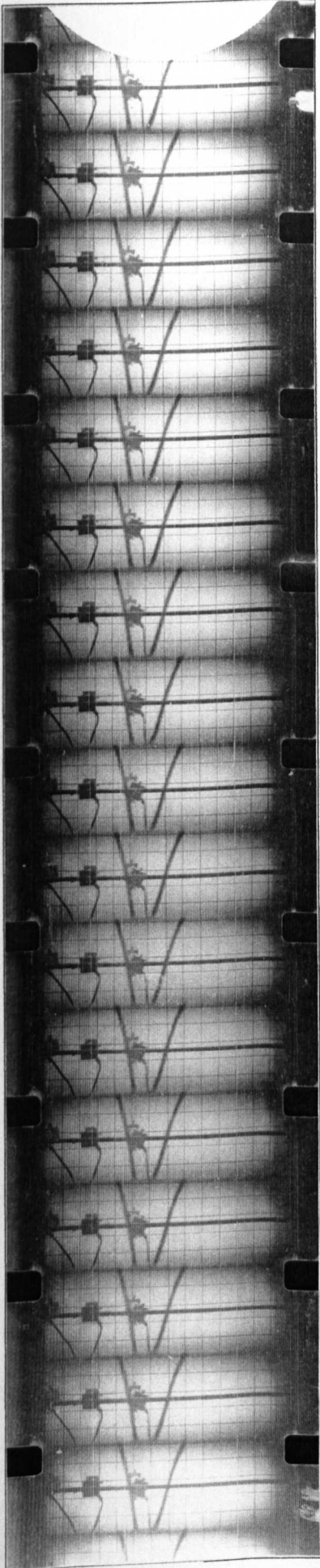
GRID SIZE : 36mm X 36mm

IMPULSE TEST SE13

INTERFRAME TIME not available

DETONATION TIME n.a MSEC. MARKERS-n.a

1.



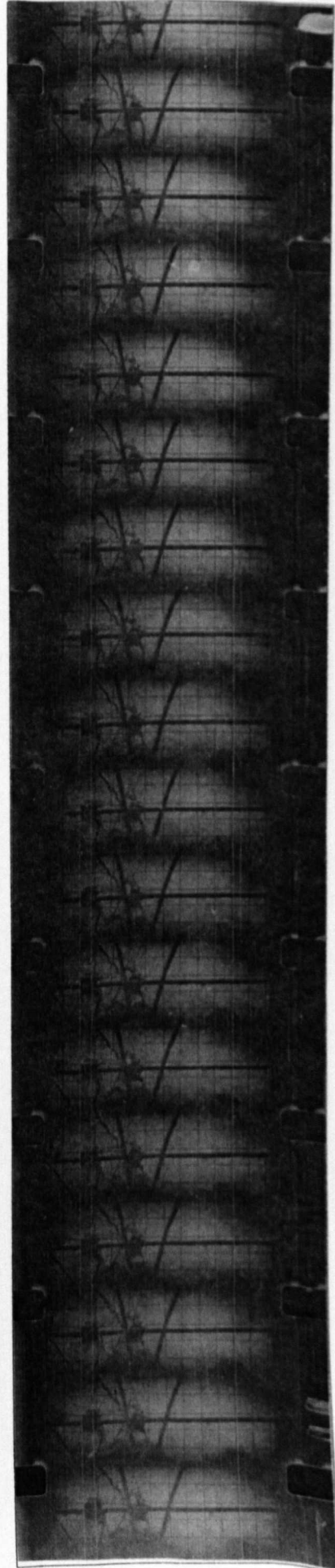
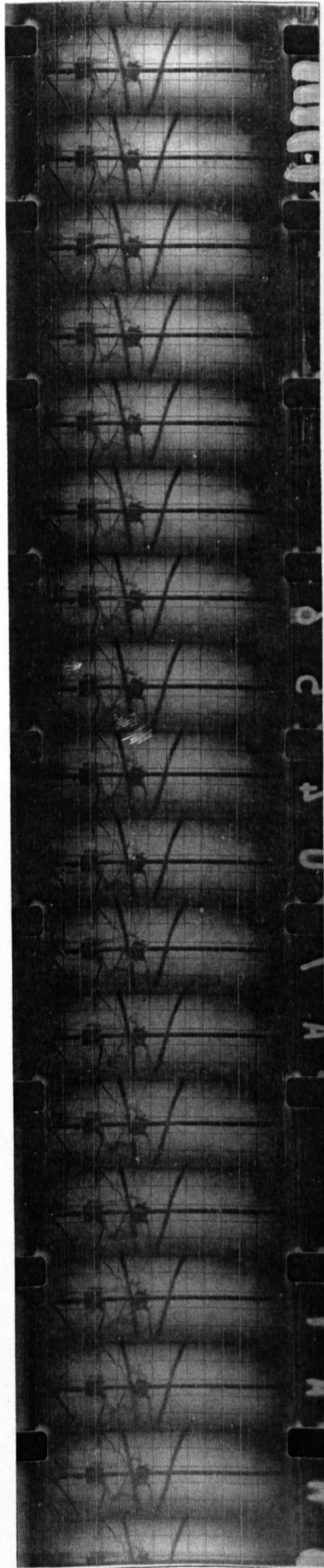
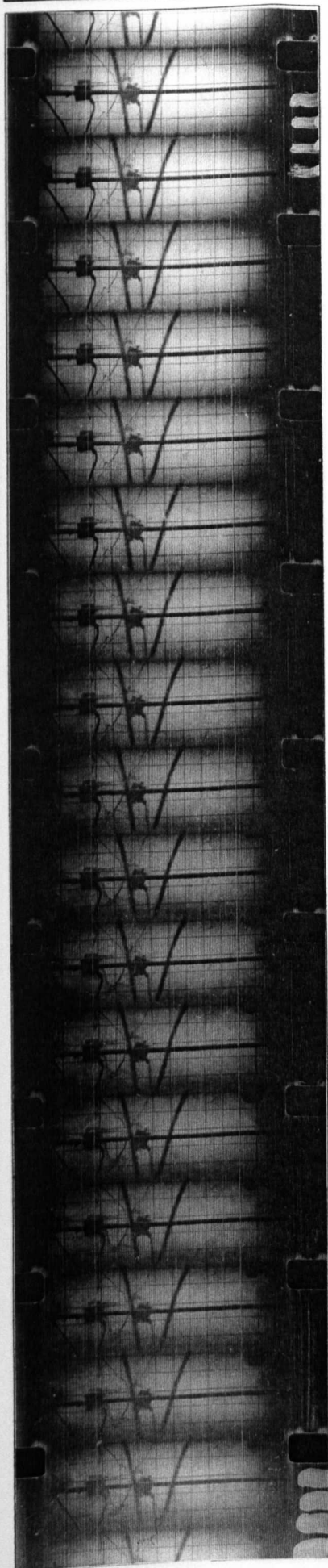
GRID SIZE : 36mm X 36mm

IMPULSE TEST SE13

INTERFRAME TIME not available

DETONATION TIME n.a. MSEC. MARKERS-n.a.

2.



GRID SIZE : 36mm X 36mm

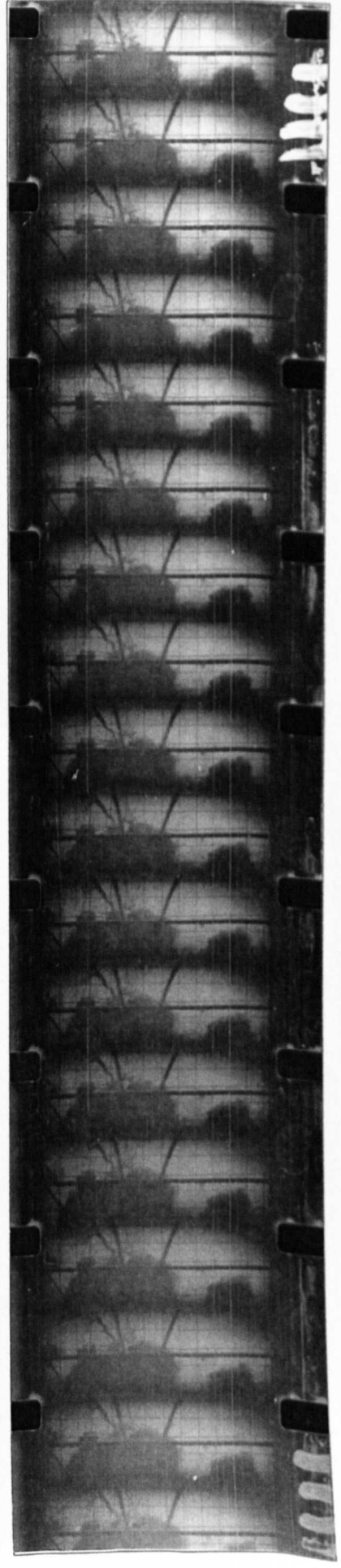
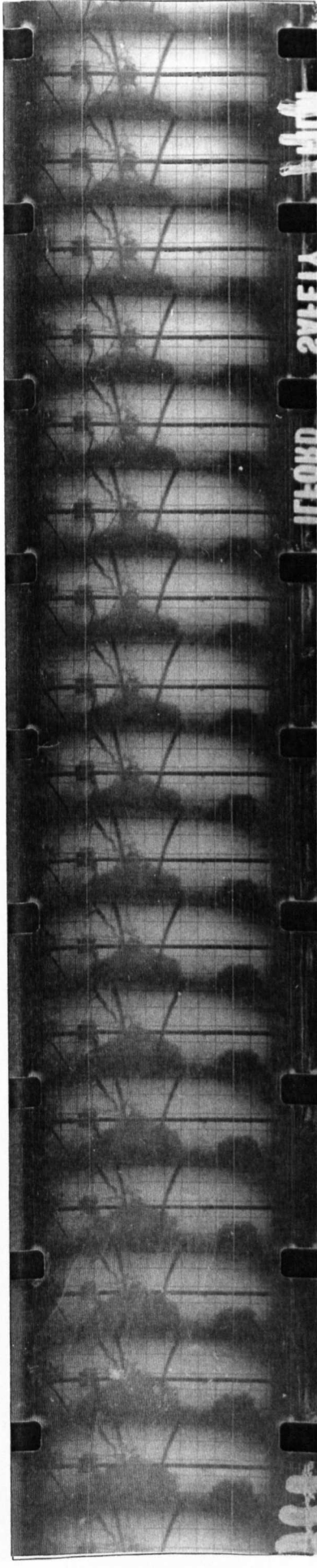
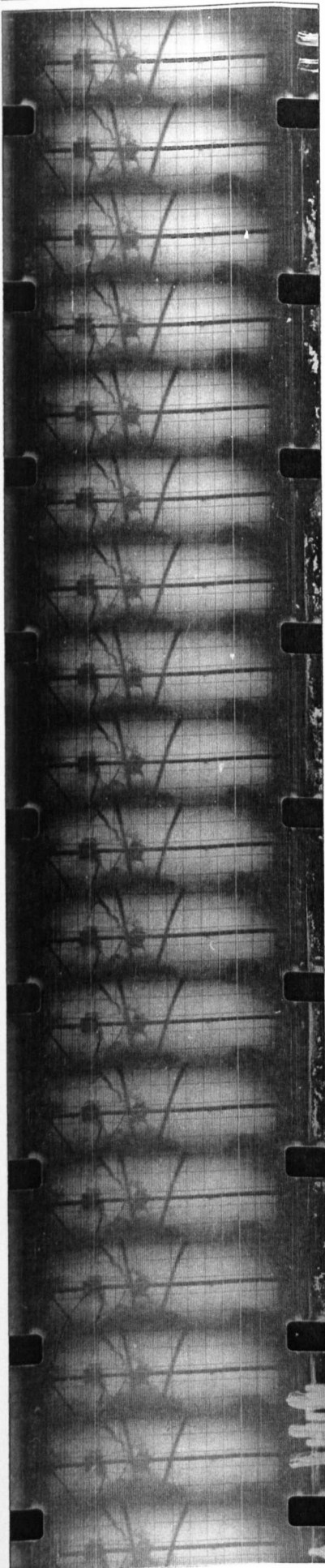
IMPULSE TEST SE13

INTERFRAME TIME not available

DETONATION TIME n.a.

MSEC.MARKERS-n.a.

3.



GRID SIZE : 36mm X 36mm

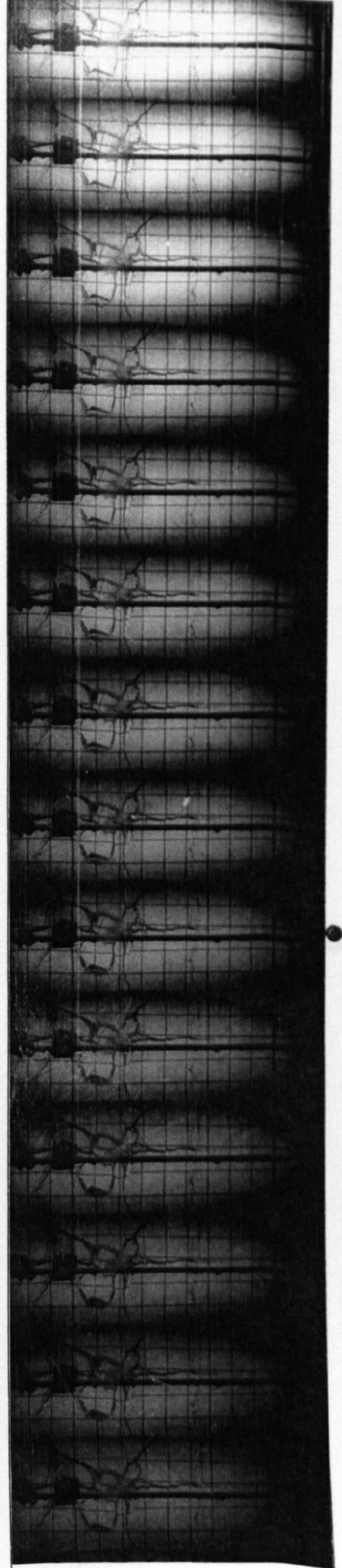
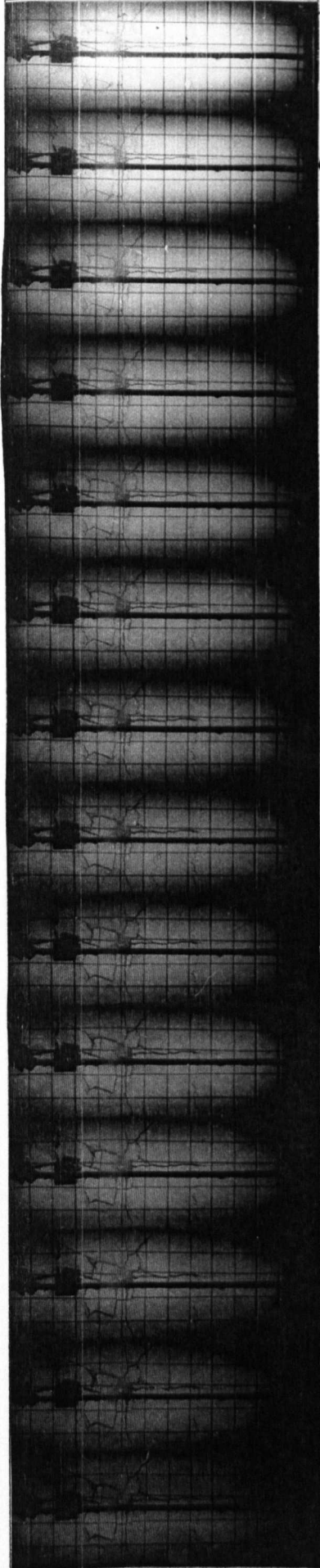
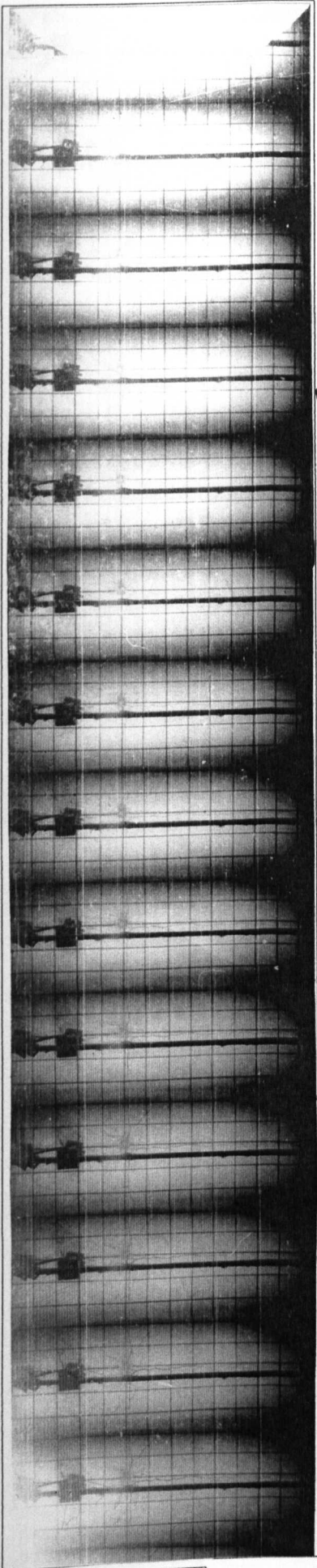
IMPULSE TEST SE14

INTERFRAME TIME 95.81 μ sec

▽ - DETONATION TIME

● - MSEC'S MARKER

1.



GRID SIZE : 36mm X 36mm

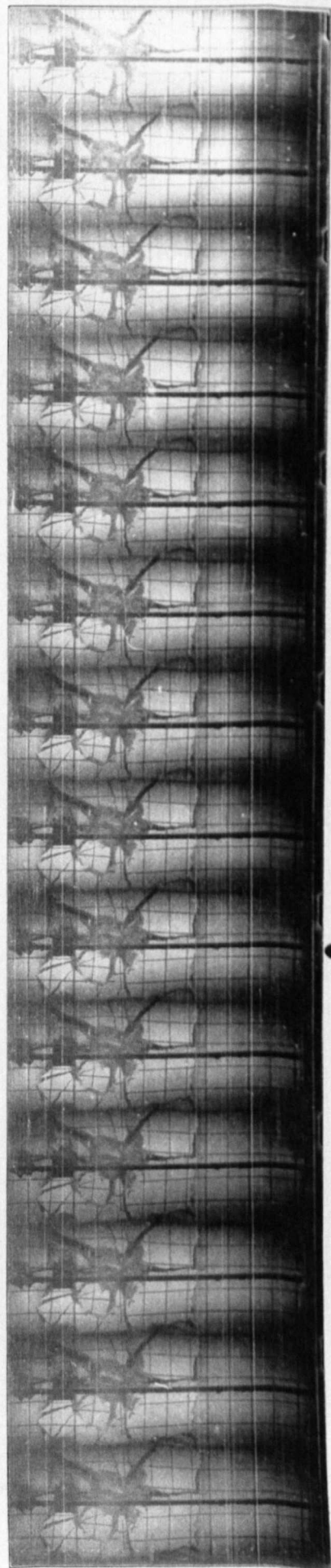
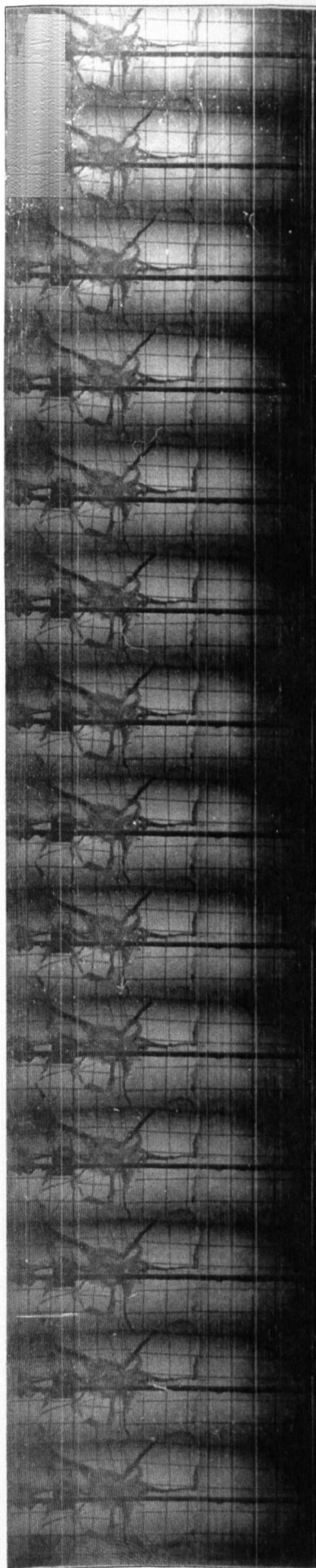
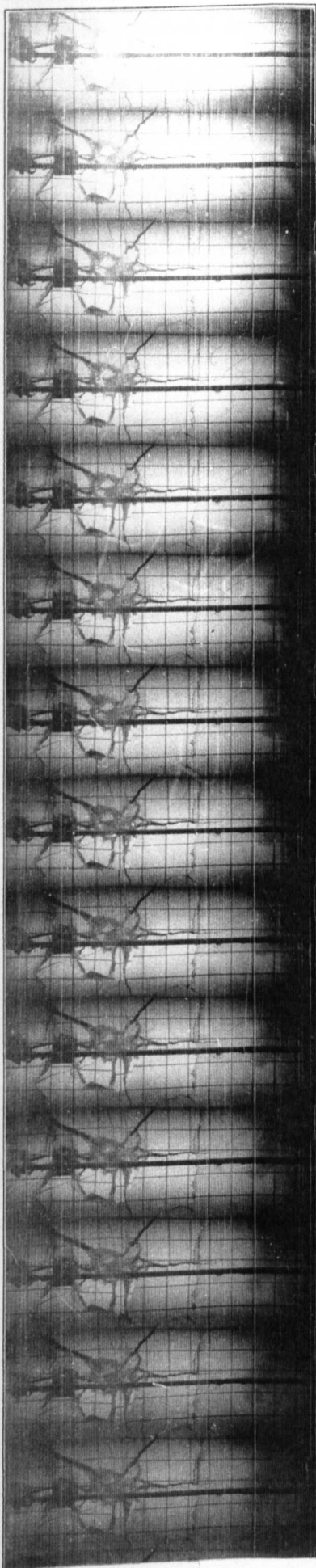
IMPULSE TEST SE14

INTERFRAME TIME 95.81 μ sec

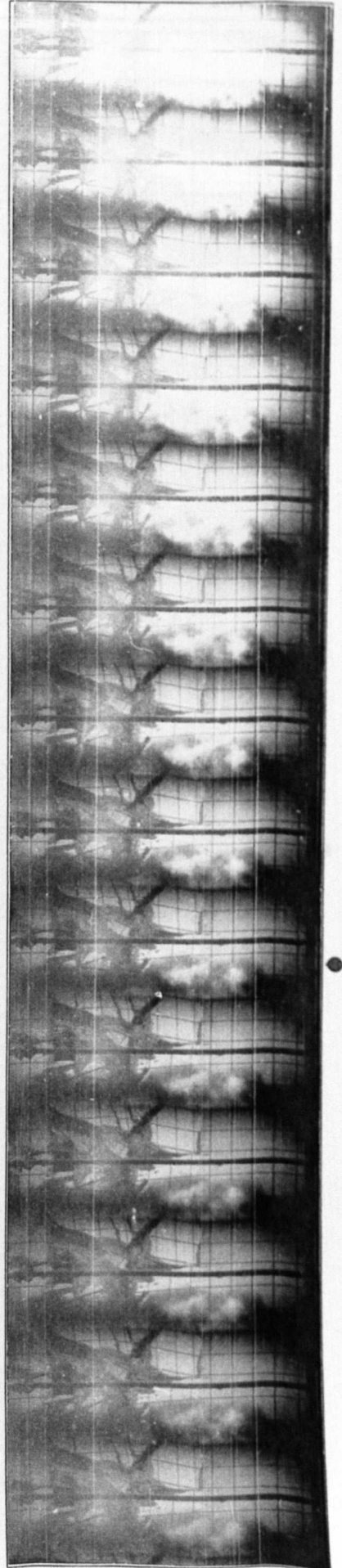
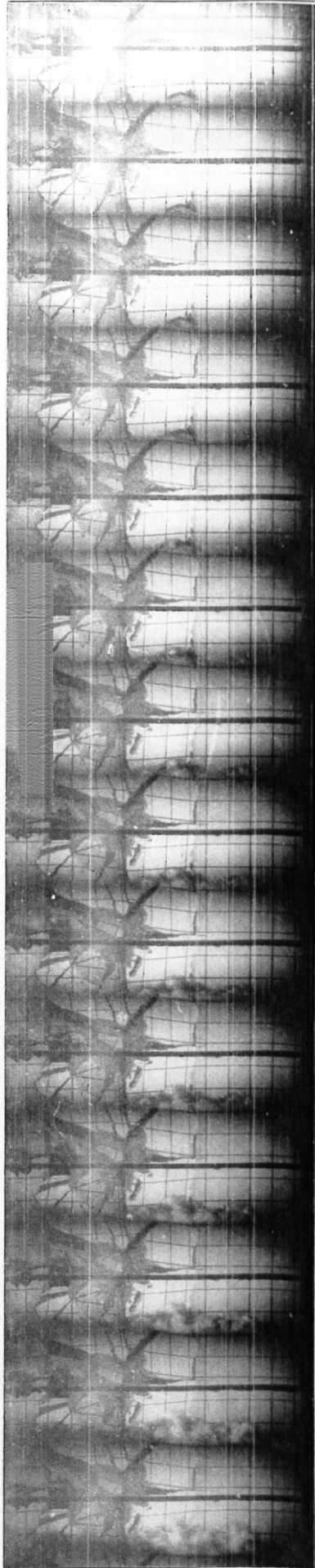
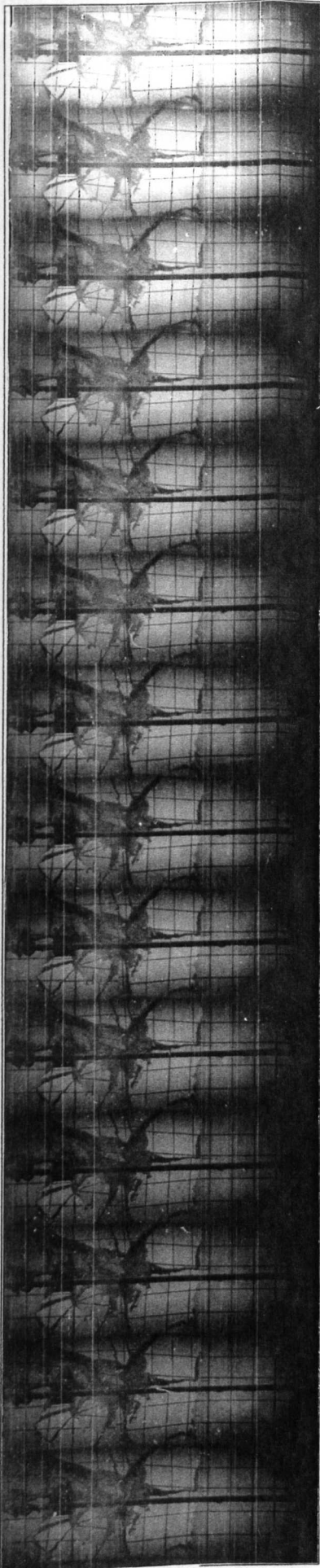
∇ - DETONATION TIME

● - MSEC'S MARKER

2.



GRID SIZE : 36mm X 36mm



GRID SIZE : 36mm X 36mm

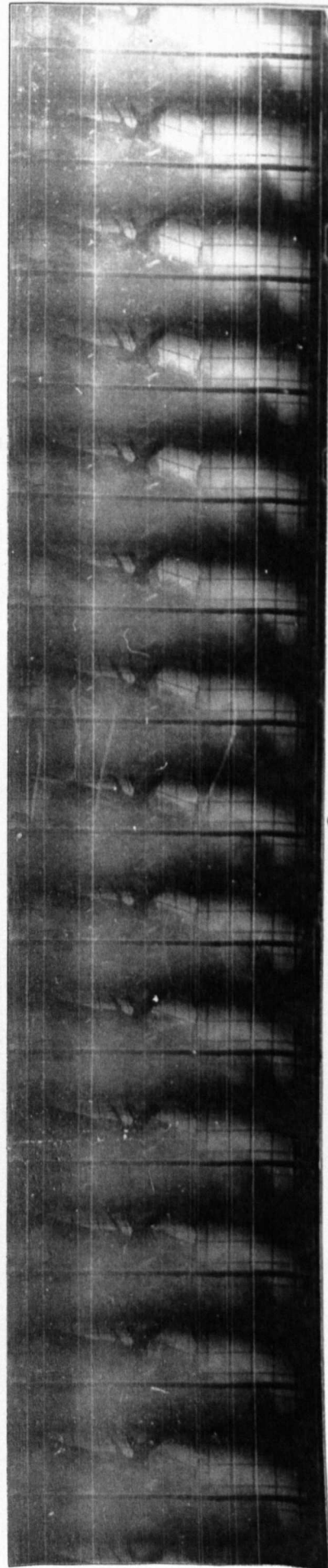
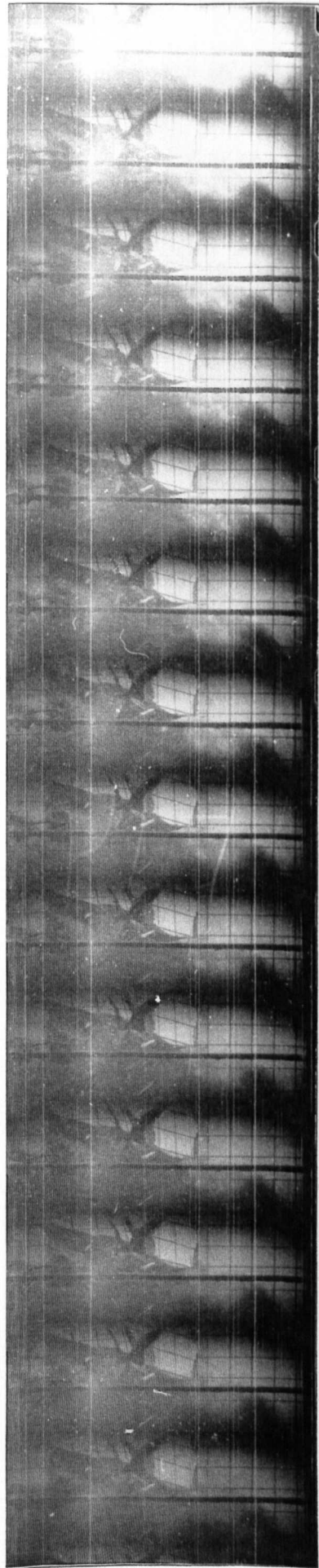
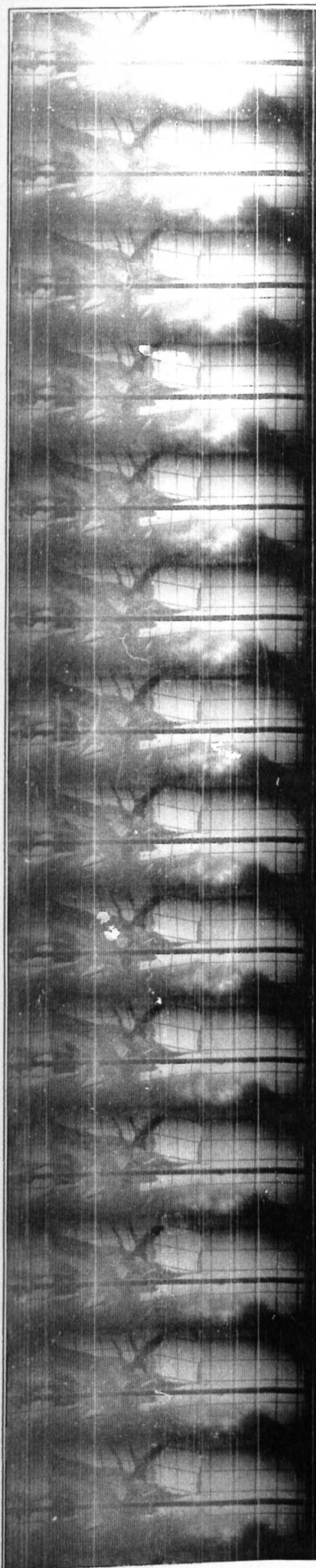
IMPULSE TEST SE14

INTERFRAME TIME 95.81 μ sec

▽ - DETONATION TIME

● - MSEC'S MARKER

4.



GRID SIZE : 36mm X 36mm

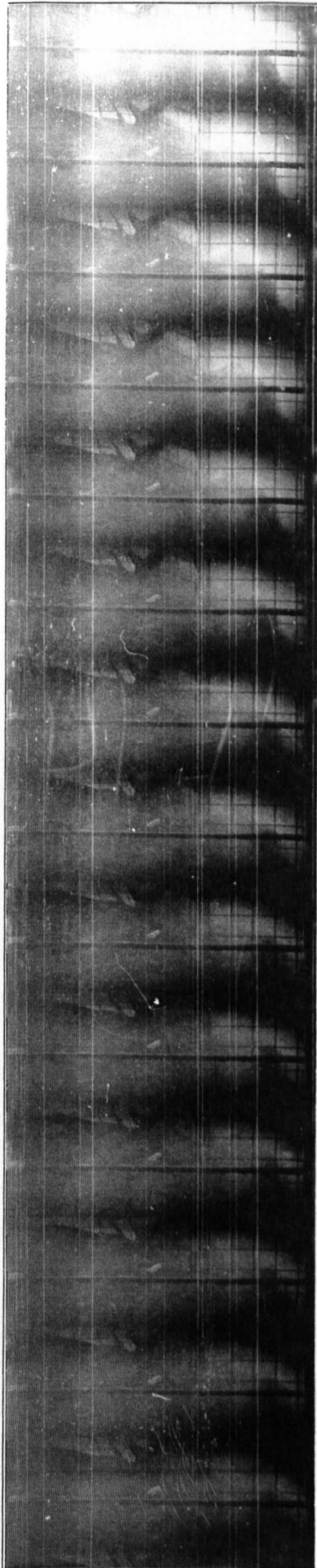
IMPULSE TEST SE14

INTERFRAME TIME 95.81 μ sec

∇ - DETONATION TIME

● - MSEC'S MARKER

5.



GRID SIZE : 36mm X 36mm

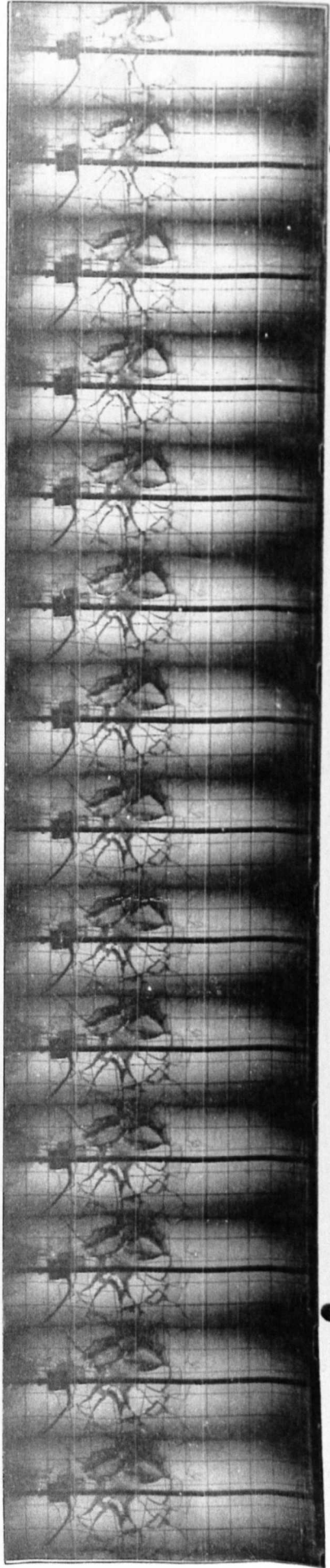
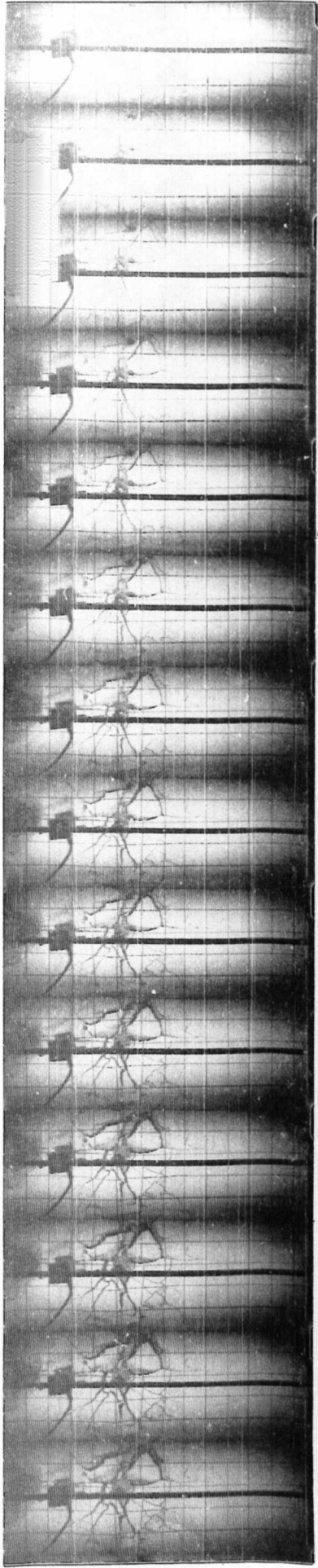
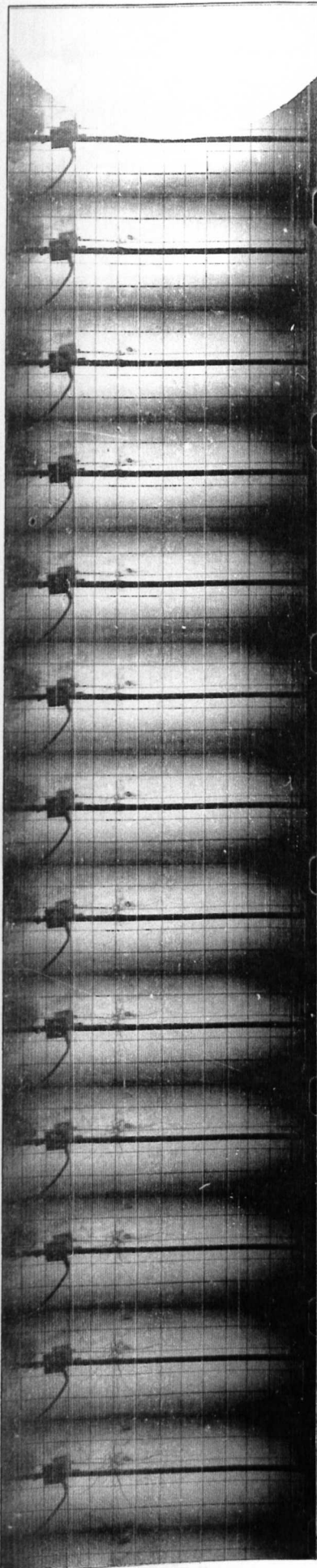
IMPULSE TEST SE15

INTERFRAME TIME 95.01 μ sec

▽ - DETONATION TIME

● - MSEC'S MARKER

1.



GRID SIZE : 36mm X 36mm

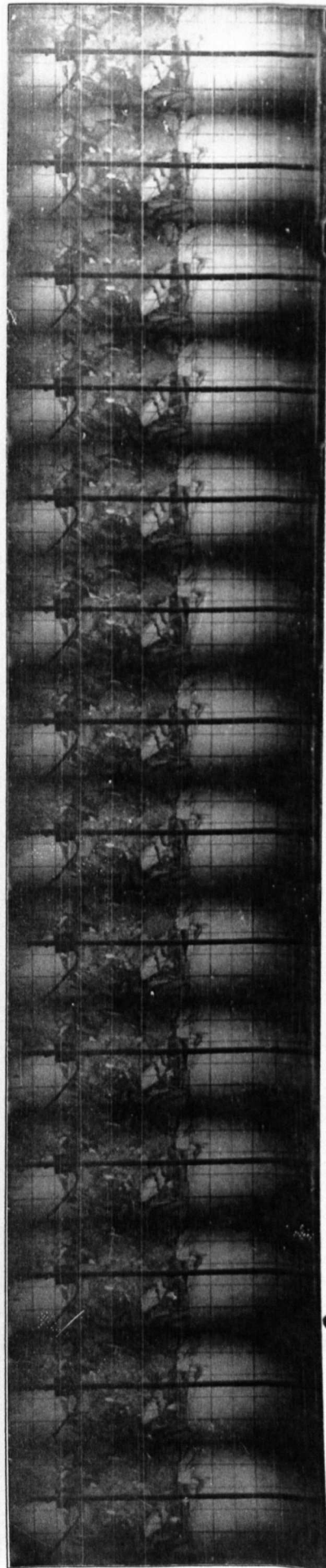
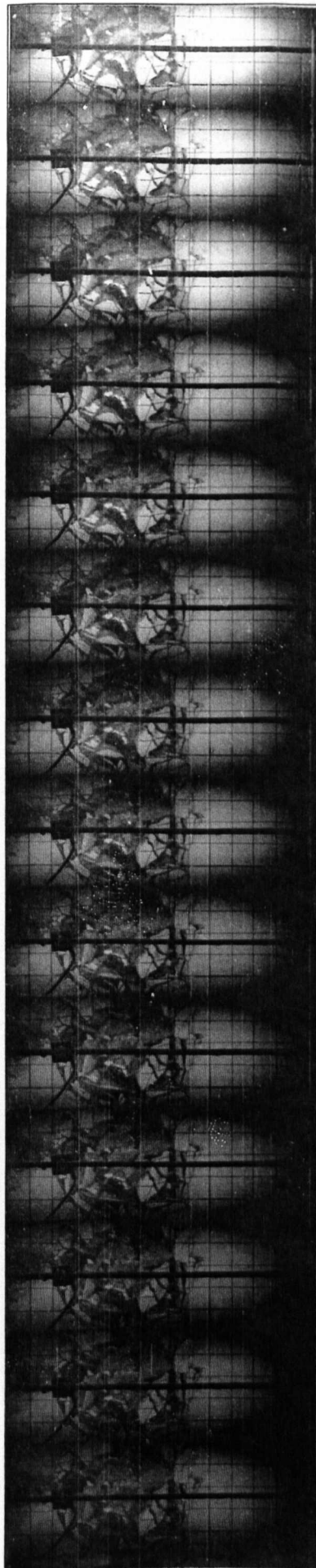
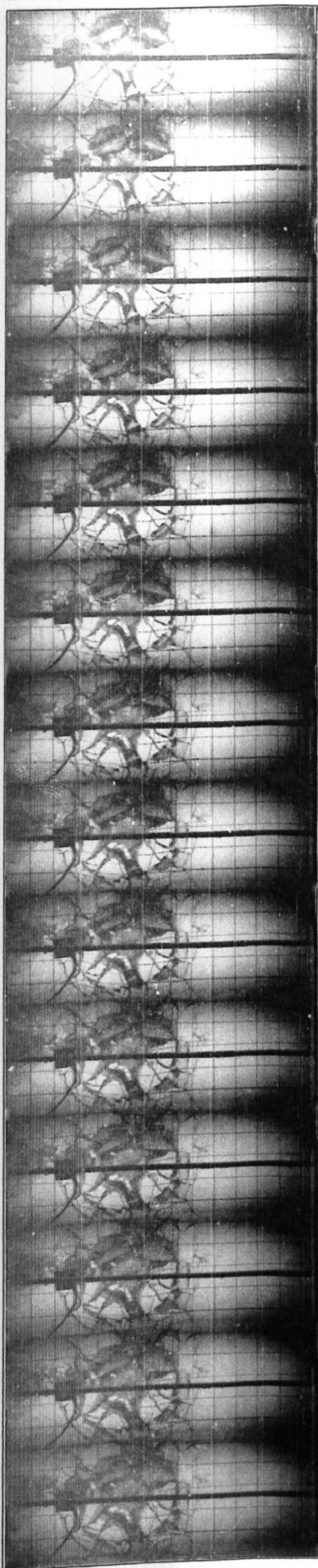
IMPULSE TEST SE15

INTERFRAME TIME 95.01 μ sec

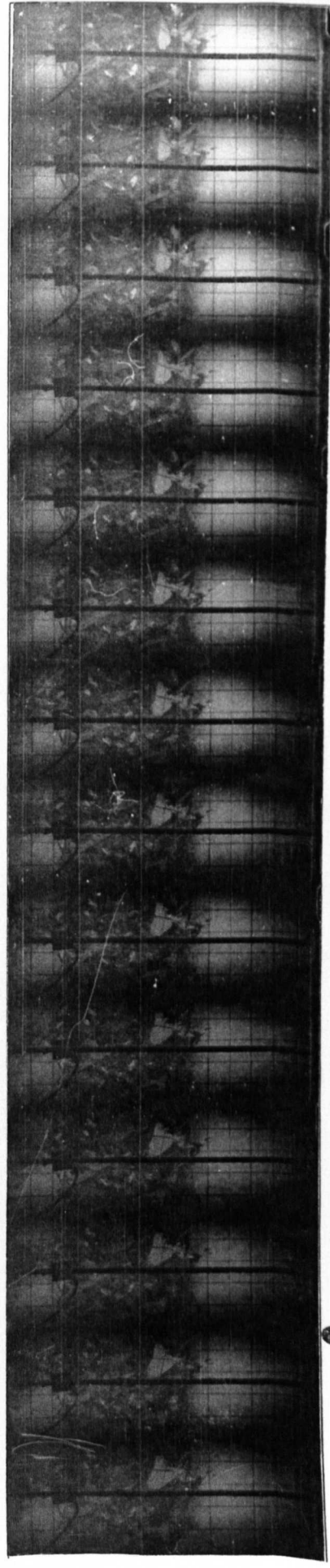
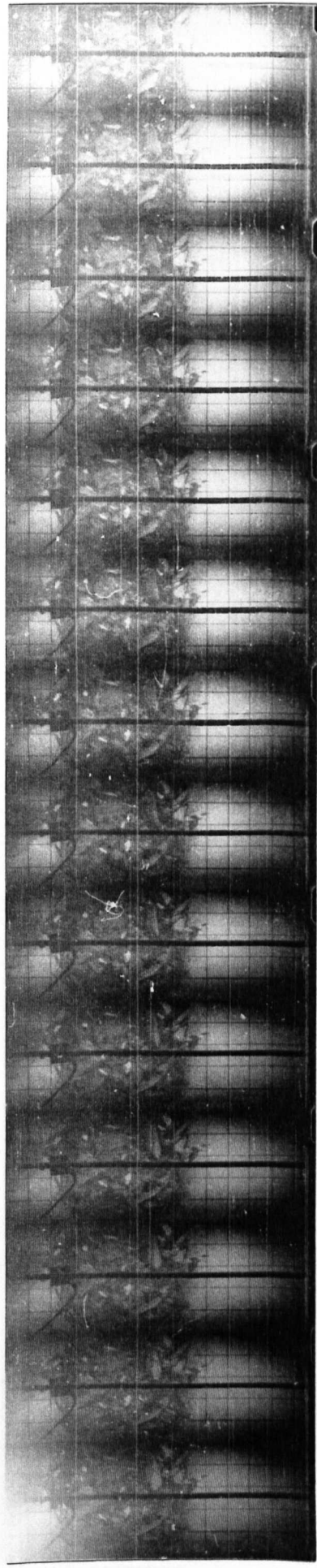
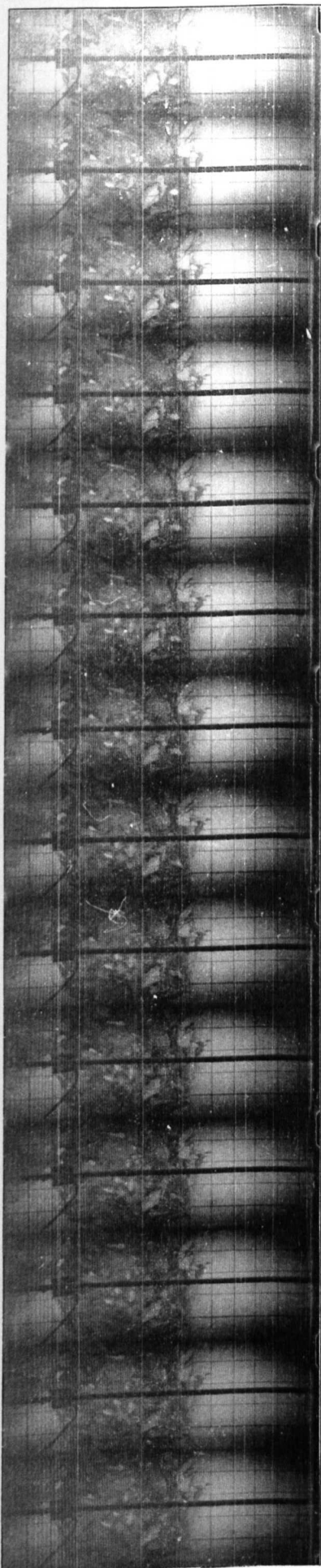
∇ - DETONATION TIME

● - MSEC'S MARKER

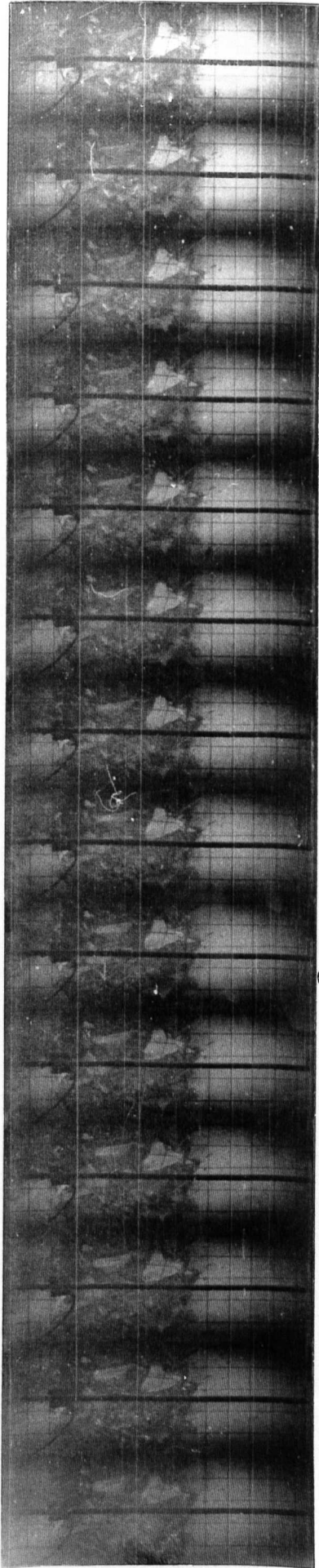
2.



GRID SIZE : 36mm X 36mm



GRID SIZE : 36mm X 36mm



GRID SIZE : 36mm X 36mm

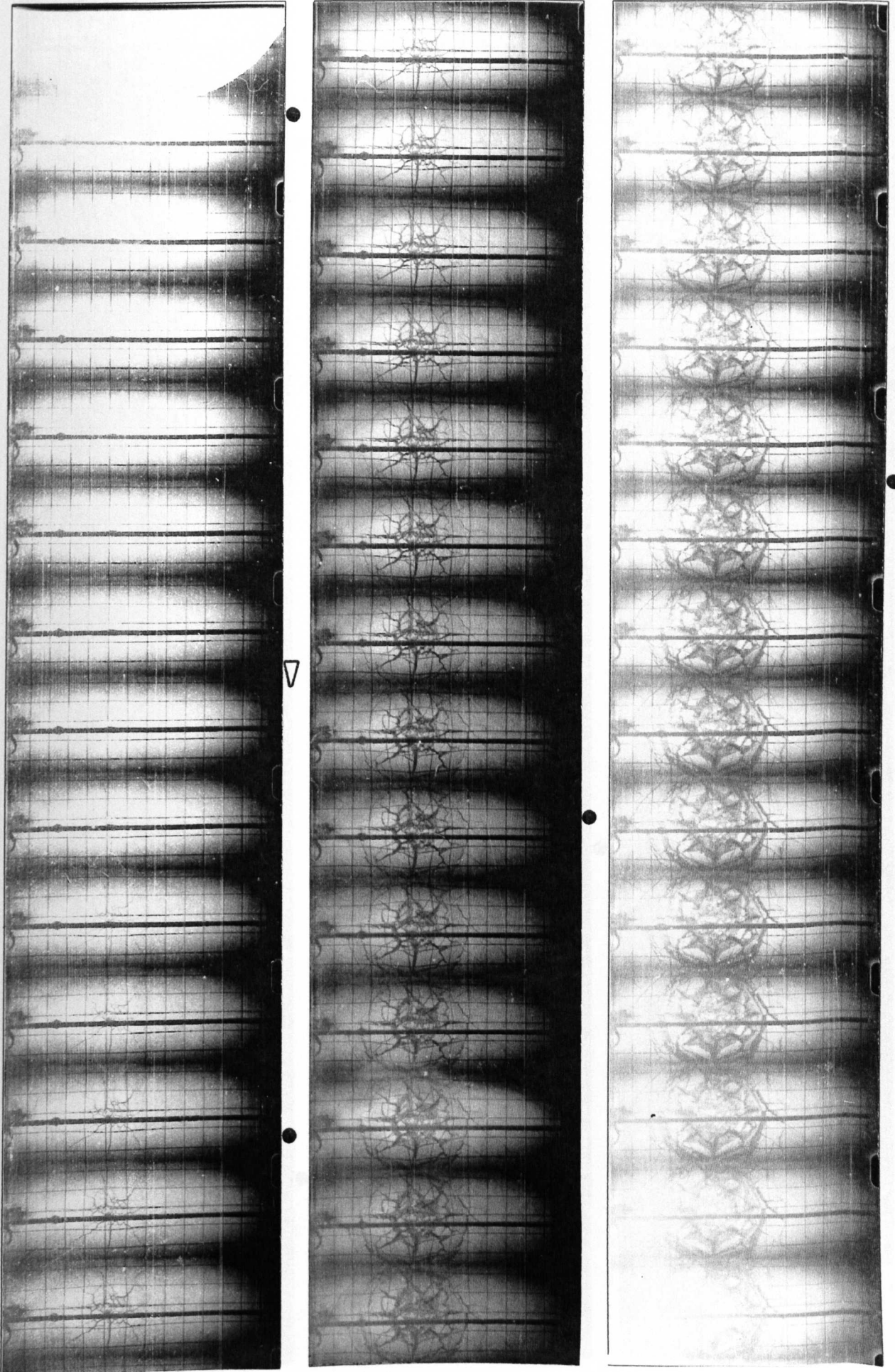
IMPULSE TEST SE17

INTERFRAME TIME 93.70 μ sec

▽ - DETONATION TIME

● - MSEC'S MARKER

1.



GRID SIZE : 36mm X 36mm

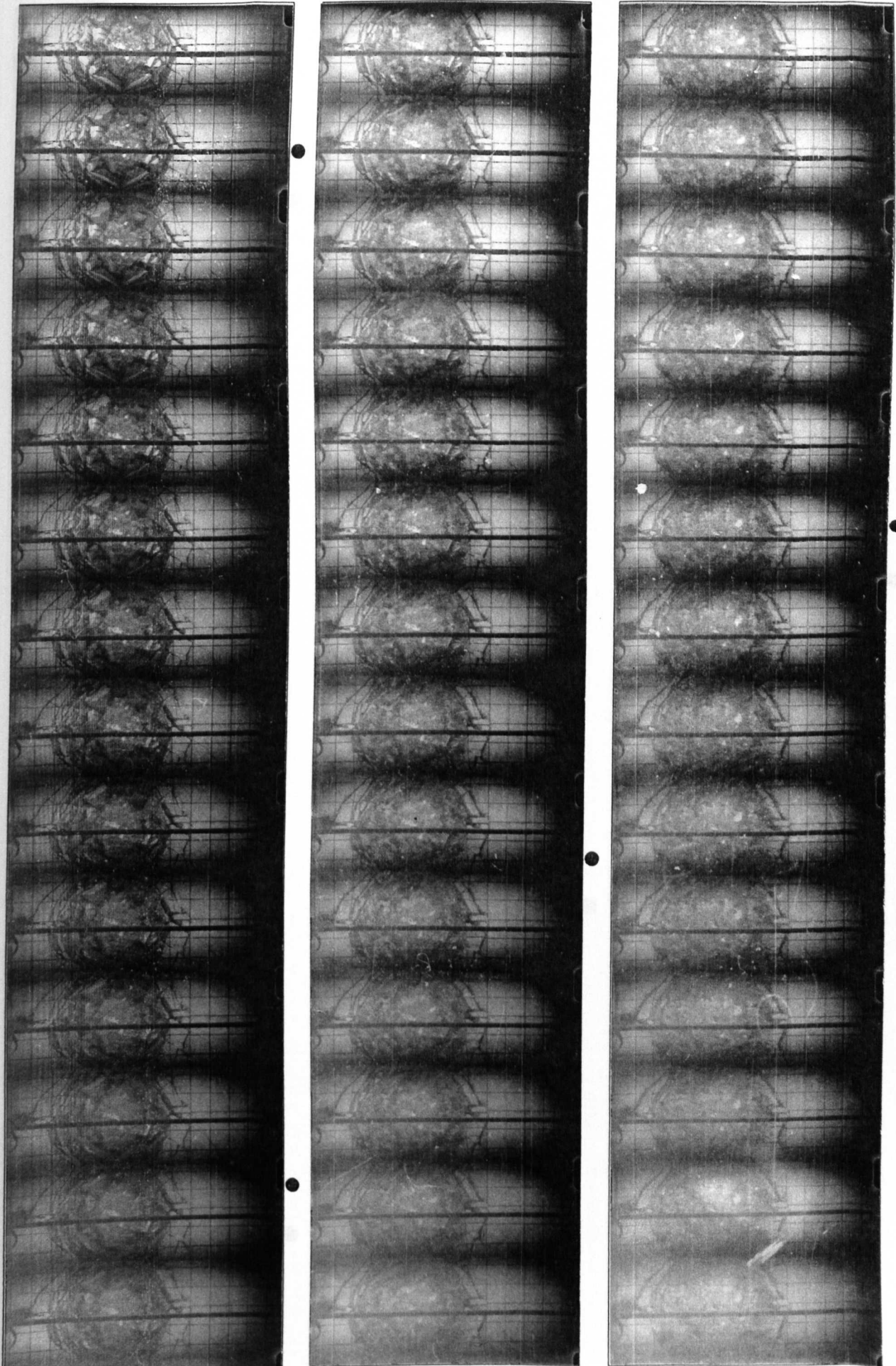
IMPULSE TEST SE17

INTERFRAME TIME 93.70 μ sec

∇ - DETONATION TIME

● - MSEC'S MARKER

2.



GRID SIZE : 36mm X 36mm

IMPULSE TEST SE17

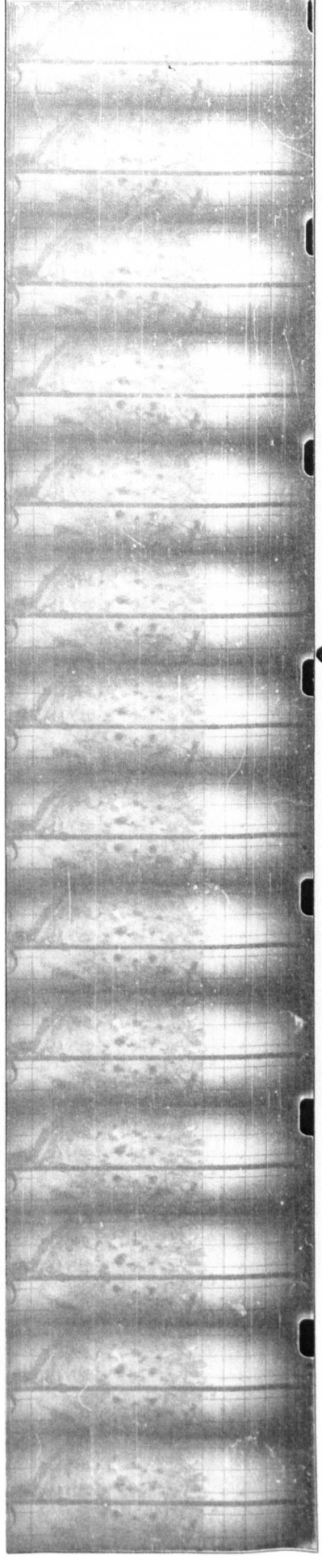
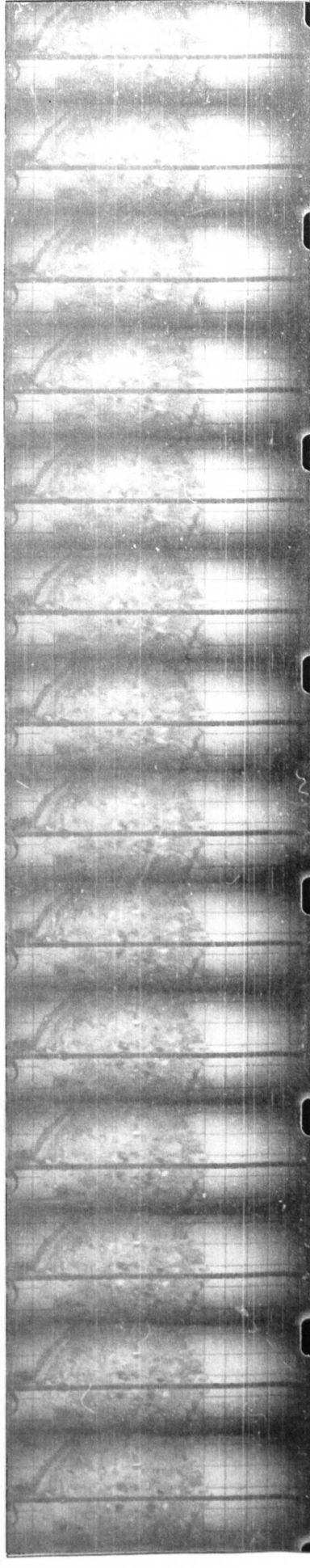
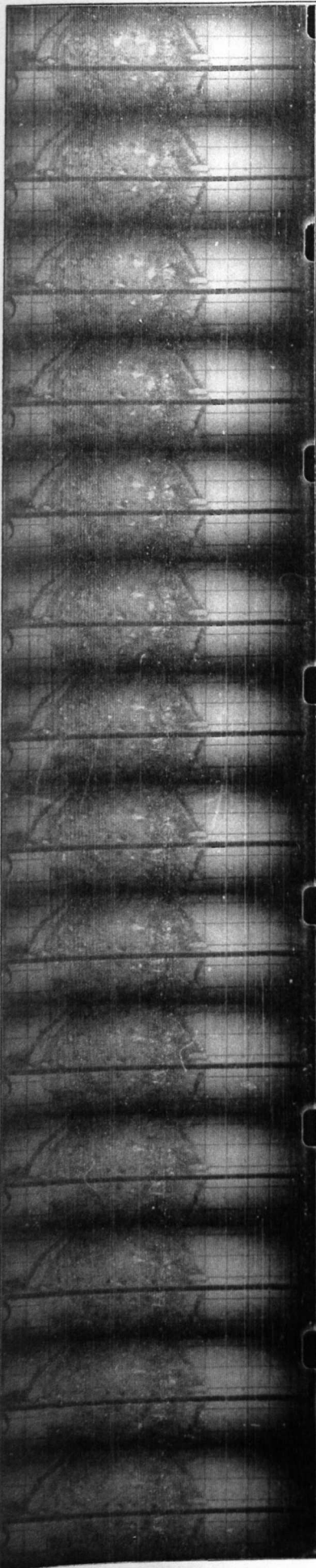
INTERFRAME TIME 93.70 μ sec



DETONATION TIME

●-MSEC'S MARKER

3.



GRID SIZE : 36mm X 36mm

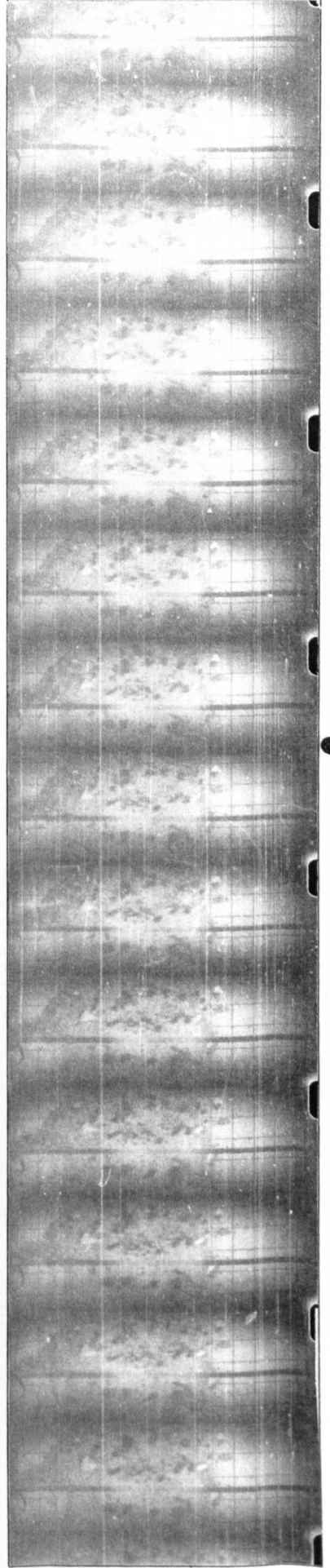
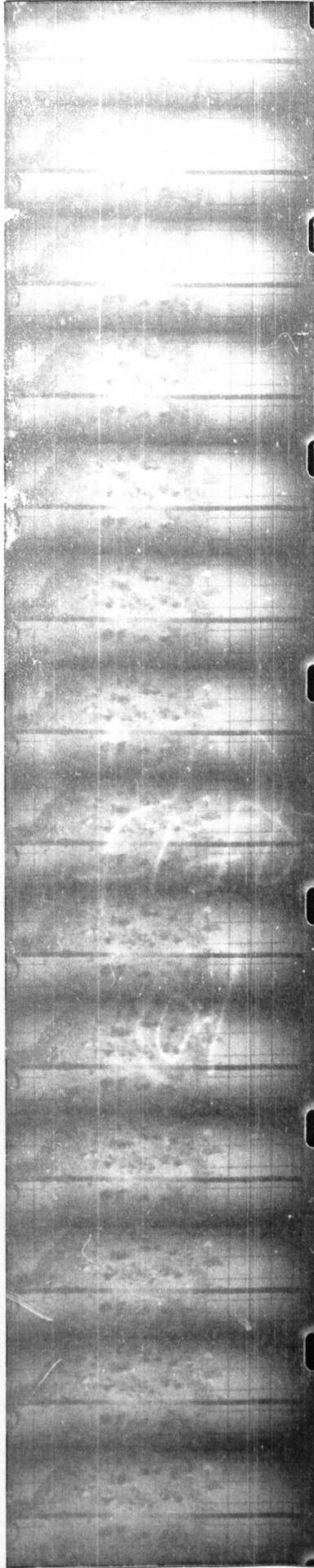
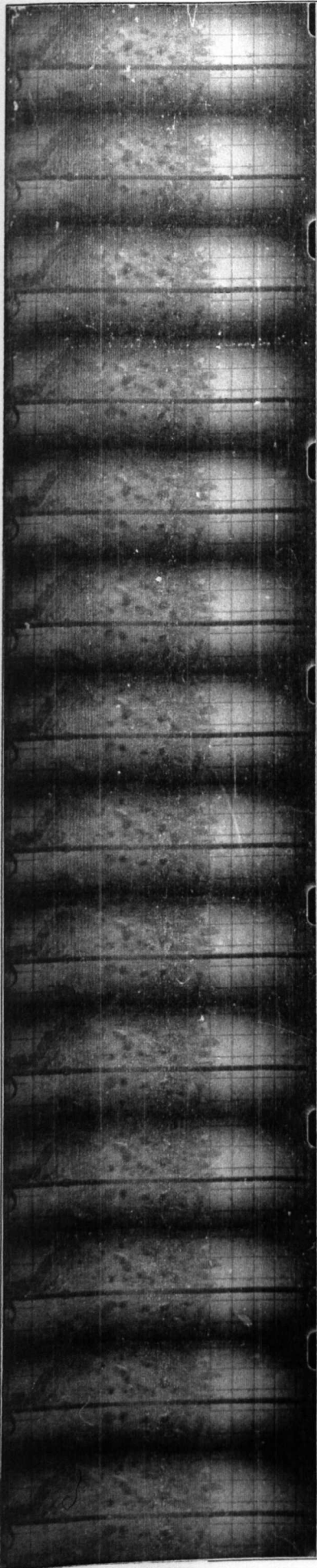
IMPULSE TEST SE17

INTERFRAME TIME 93.70 μ sec

∇-DETONATION TIME

●-MSEC'S MARKER

4.



GRID SIZE : 36mm X 36mm

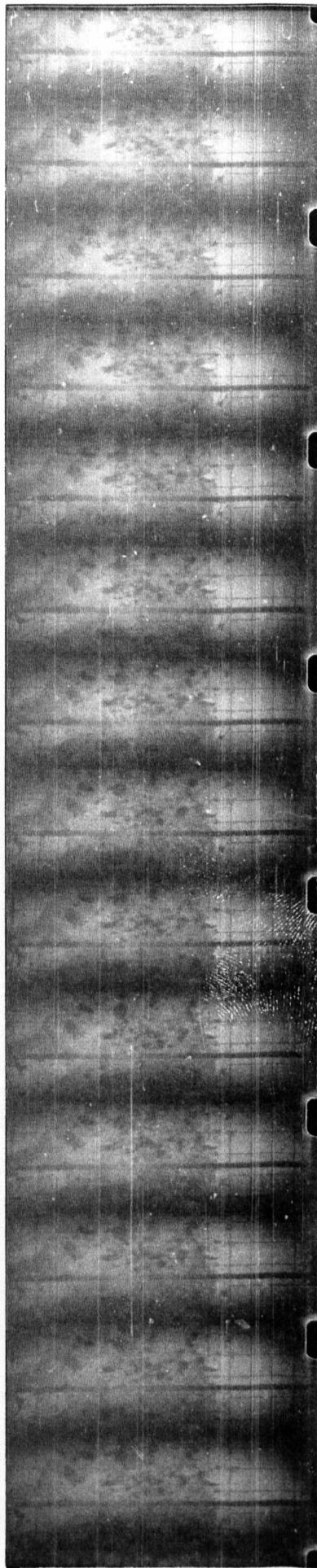
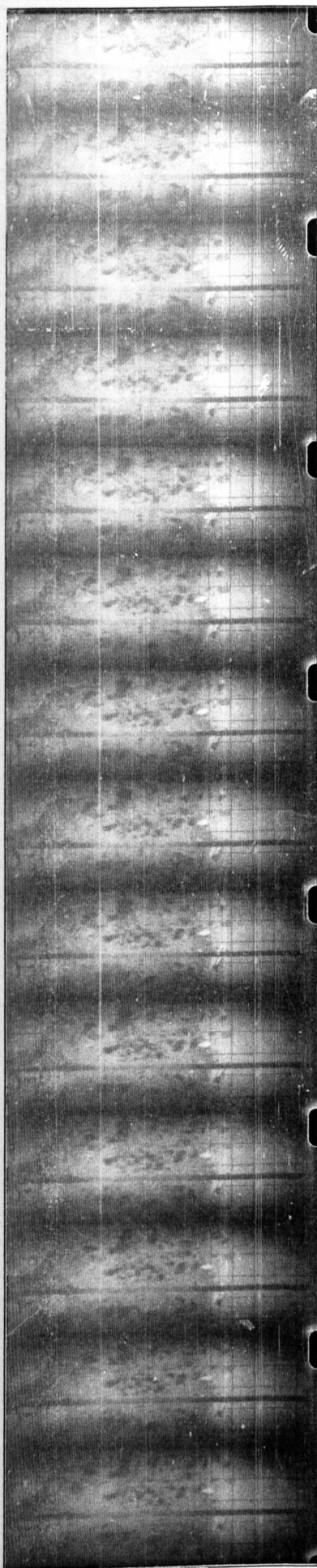
IMPULSE TEST SE17

INTERFRAME TIME 93.70 μ sec

▽-DETONATION TIME

●-MSEC'S MARKER

5.



GRID SIZE : 36mm X 36mm

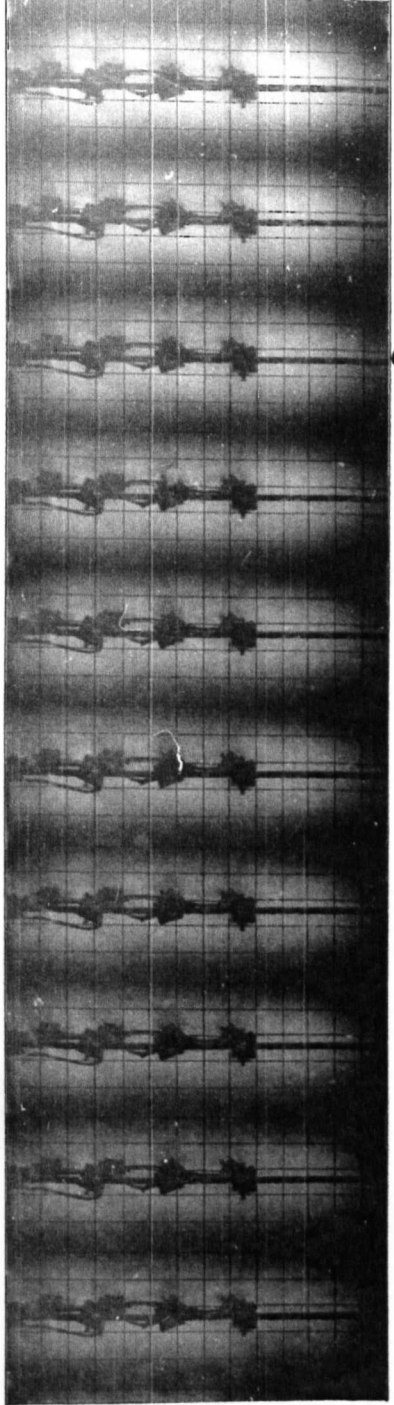
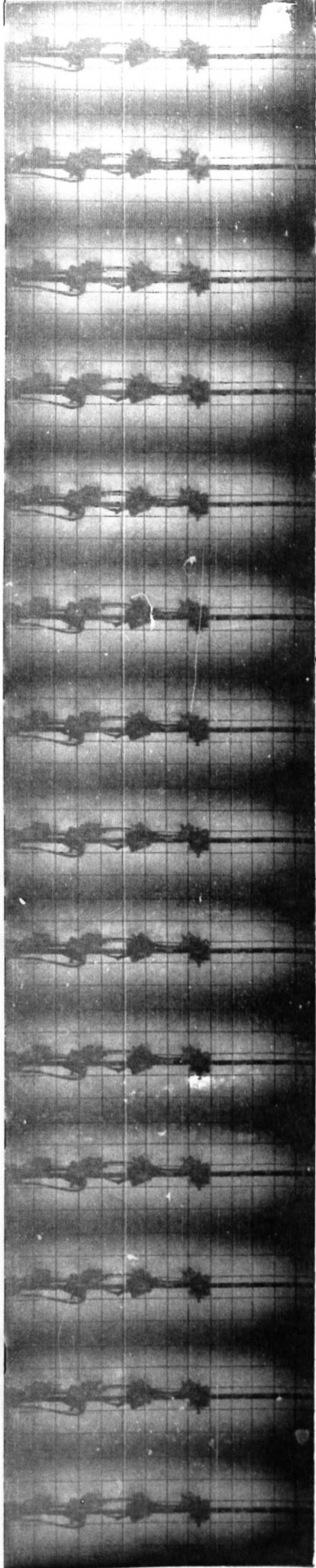
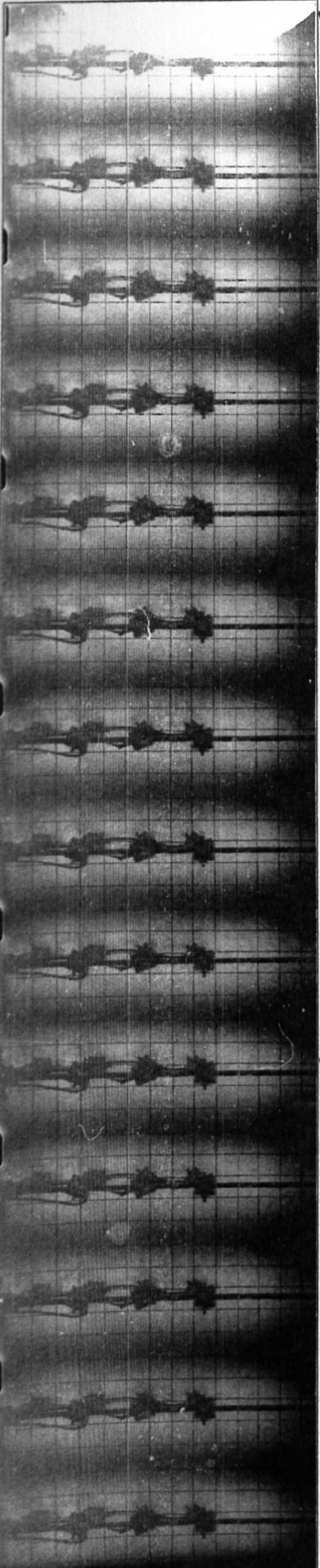
IMPULSE TEST SE18

INTERFRAME TIME 95.24 μ sec

∇ -2.7MSEC AFTER DET

●-MSEC'S MARKER

1.



GRID SIZE : 36mm X 36mm

STATIC TEST RESULTS

1:2.5 SCALE SLABS

APPENDIX C1

STATIC TEST

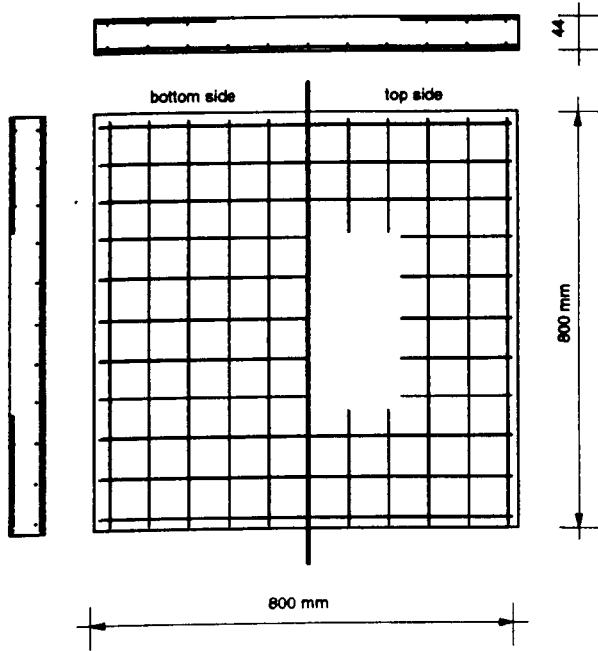
DATE: 24.03.92

SMALL SLAB SS1

AGE OF SPECIMEN: 11 days

Cube compressive strength	N/mm ²	49.5	Cylinder tensile strength	N/mm ²	4.08	Age (days)	12
---------------------------	-------------------	------	---------------------------	-------------------	------	------------	----

REINFORCEMENT:



TOP LAYER REINFORCEMENT:

R.MESH : 3.15 mm DIAM. / 76.2 mm CENTRES

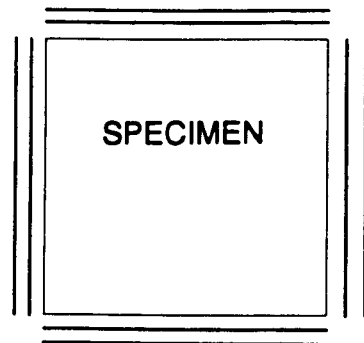
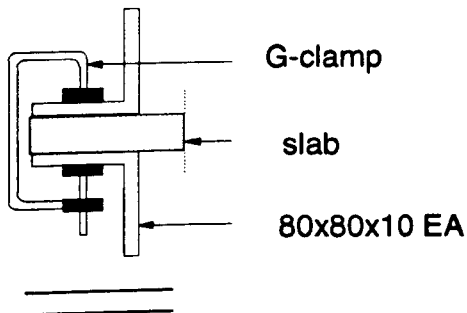
(WITHOUT CENTRAL REGION 400 X 400 mm)

BOTTOM LAYER REINFORCEMENT:

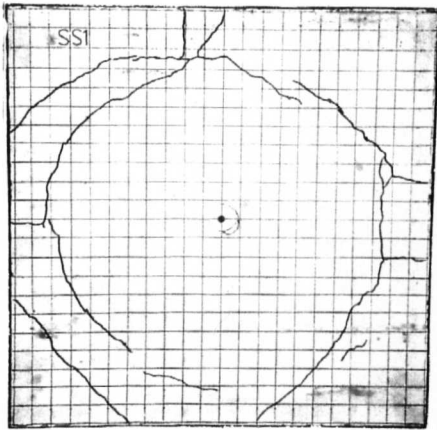
R.MESH : 3.15 mm DIAM. / 76.2 mm CENTRES

COVER: 4 mm

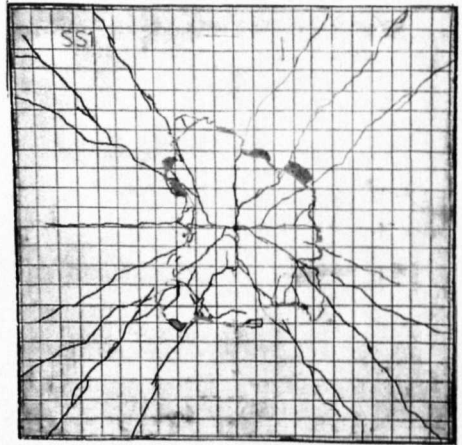
SUPPORTS:



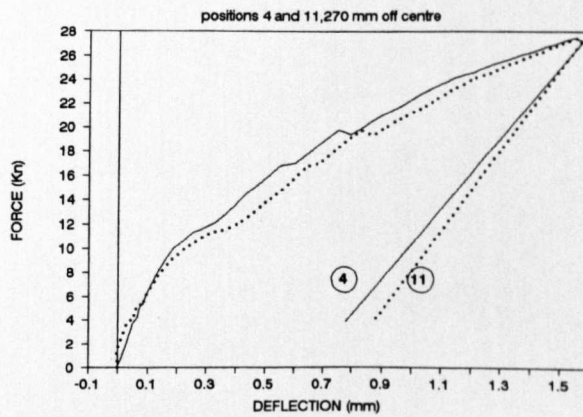
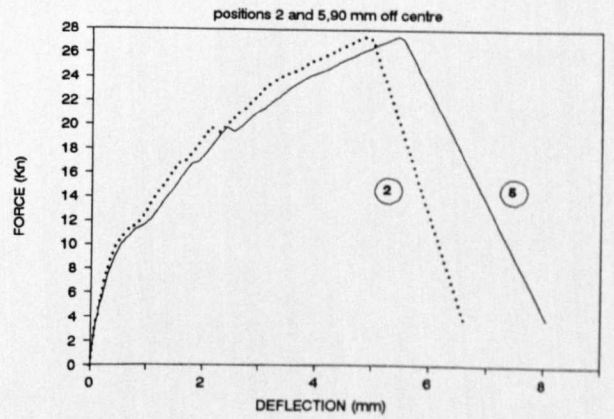
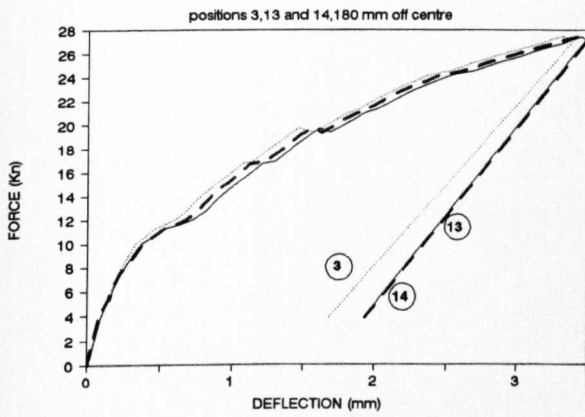
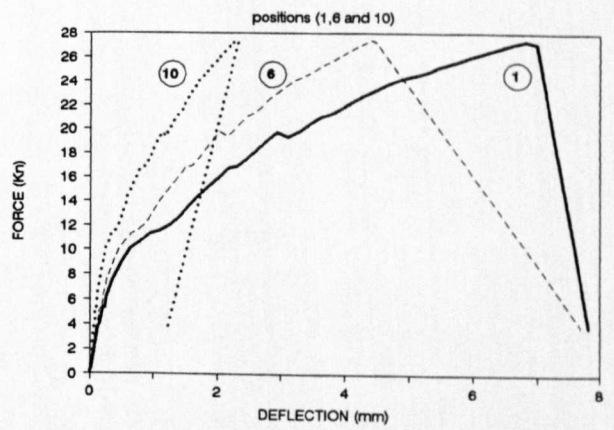
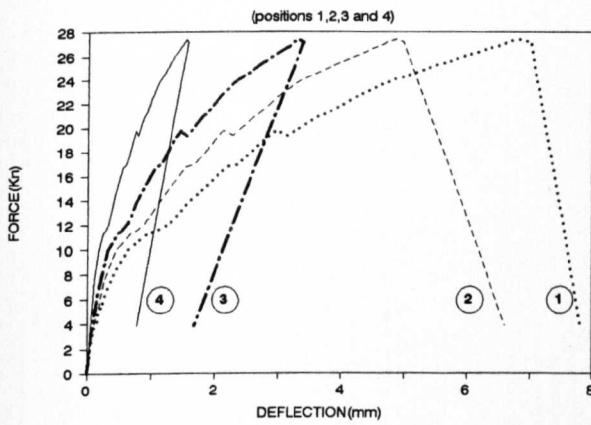
STATIC TEST - SMALL SLAB - SS1



top side



bottom side



STATIC TEST

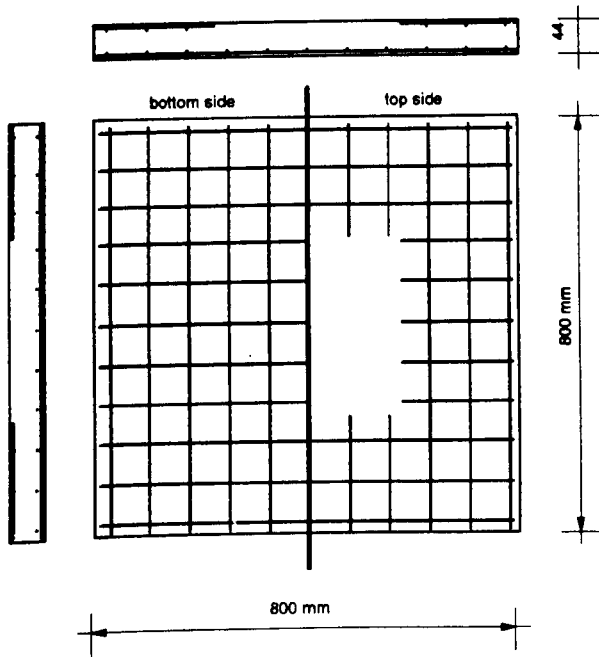
DATE: 25.03.92

SMALL SLAB SS2

AGE OF SPECIMEN: 12 days

Cube compressive strength	N/mm ²	49.5	Cylinder tensile strength	N/mm ²	4.08	Age (days)	12
---------------------------	-------------------	------	---------------------------	-------------------	------	------------	----

REINFORCEMENT:



TOP LAYER REINFORCEMENT:

R.MESH : 3.15 mm DIAM. / 76.2 mm CENTRES

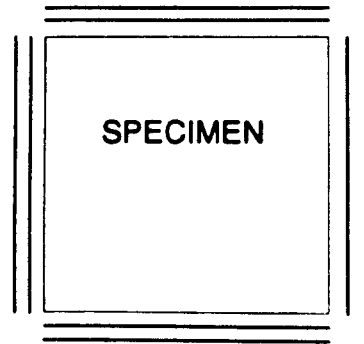
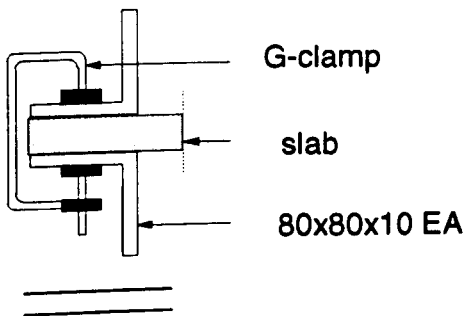
(WITHOUT CENTRAL REGION 400 X 400 mm)

BOTTOM LAYER REINFORCEMENT:

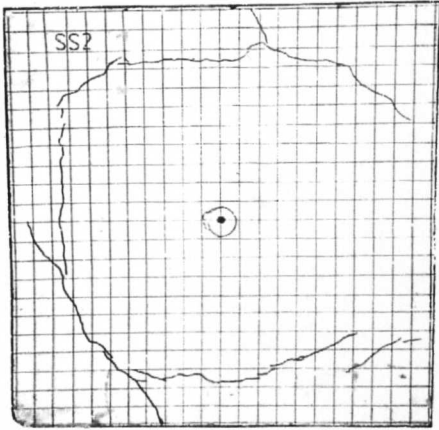
R.MESH : 3.15 mm DIAM. / 76.2 mm CENTRES

COVER: 4 mm

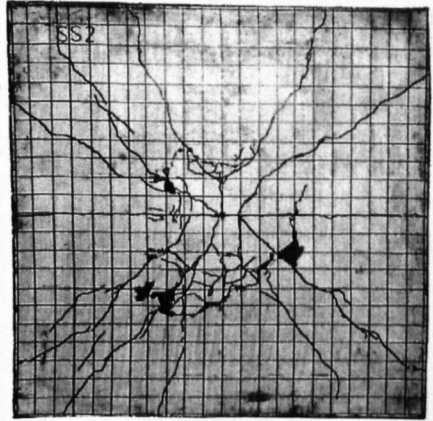
SUPPORTS:



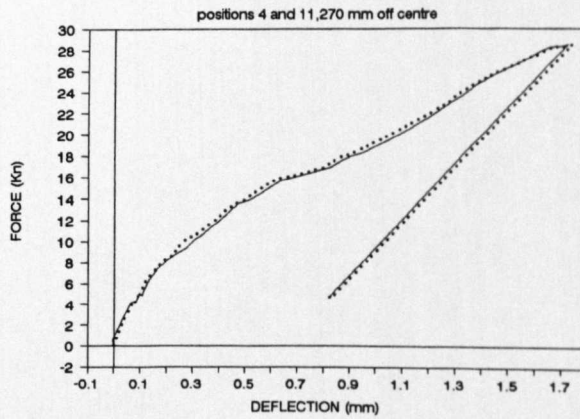
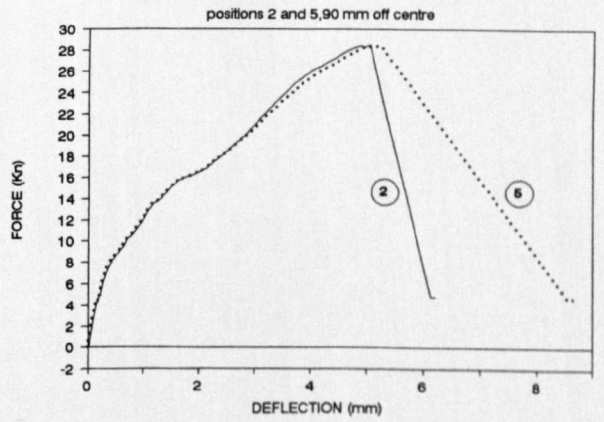
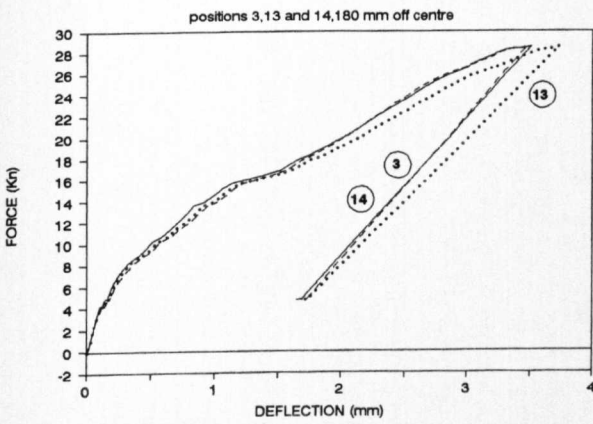
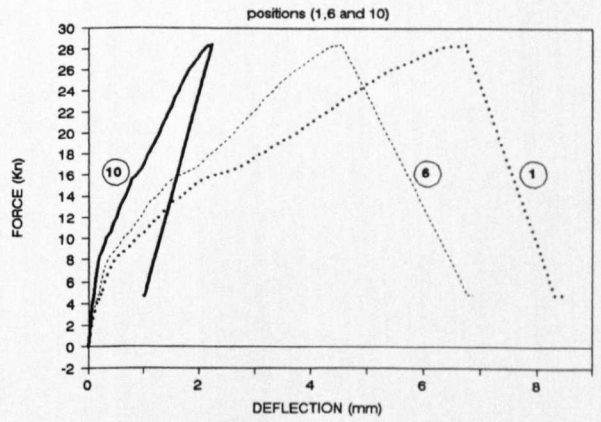
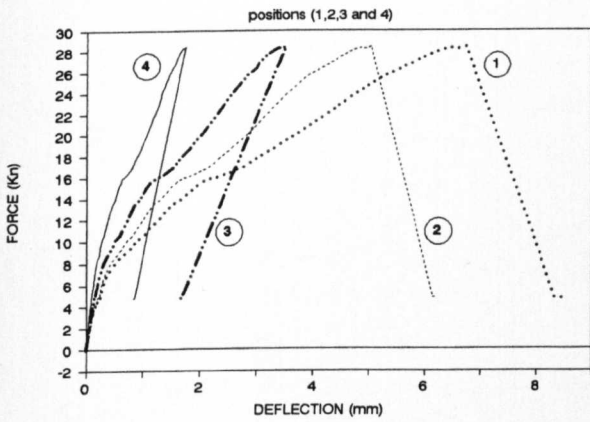
STATIC TEST - SMALL SLAB - SS2



top side



bottom side



STATIC TEST

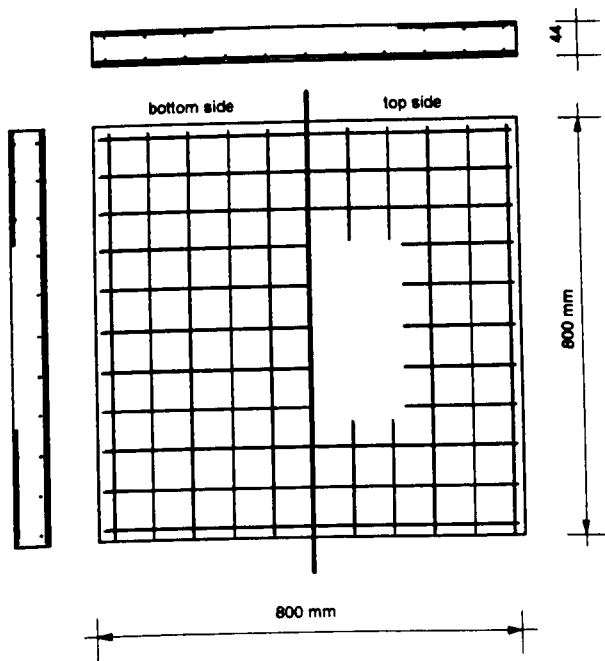
DATE: 15.04.93

SMALL SLAB SS3

AGE OF SPECIMEN: 9 days

Cube compressive strength	N/mm ²	51.6	Cylinder tensile strength	N/mm ²	4.33	Age (days)	10
---------------------------	-------------------	------	---------------------------	-------------------	------	------------	----

REINFORCEMENT:



TOP LAYER REINFORCEMENT:

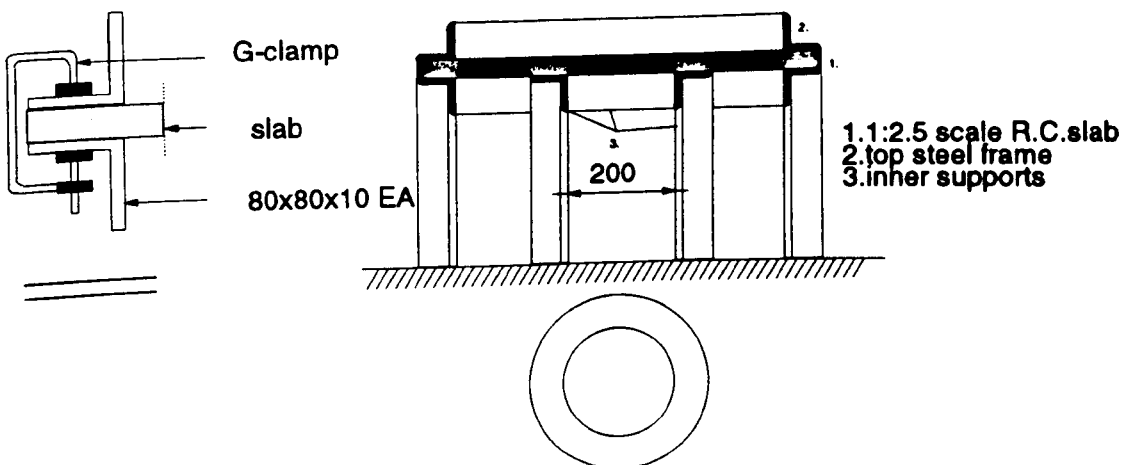
R.MESH : 3.15 mm DIAM. / 76.2 mm CENTRES
(WITHOUT CENTRAL REGION 400 X 400 mm)

BOTTOM LAYER REINFORCEMENT:

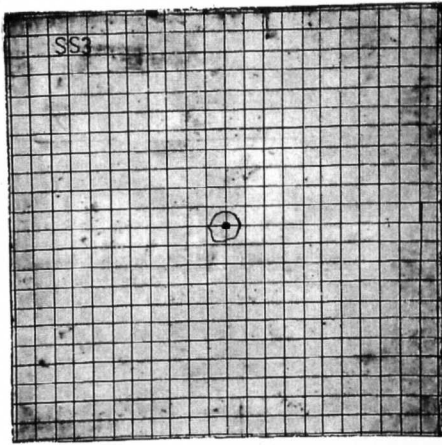
R.MESH : 3.15 mm DIAM. / 76.2 mm CENTRES

COVER: 4 mm

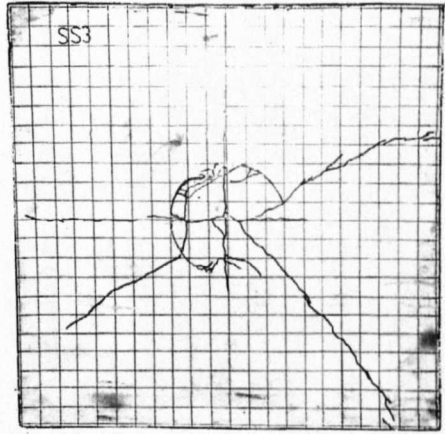
SUPPORTS:



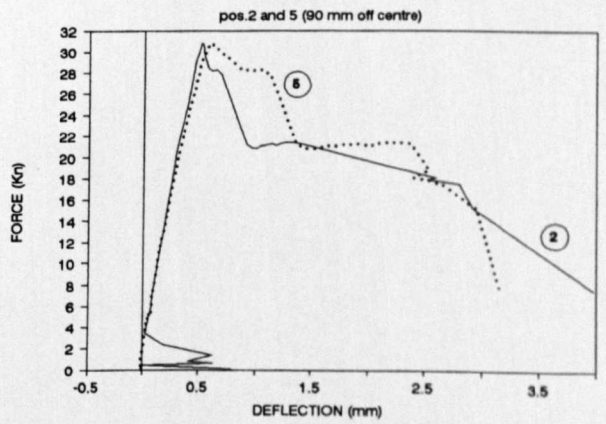
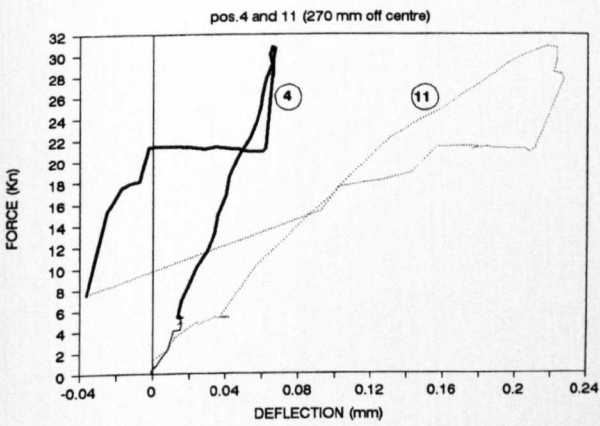
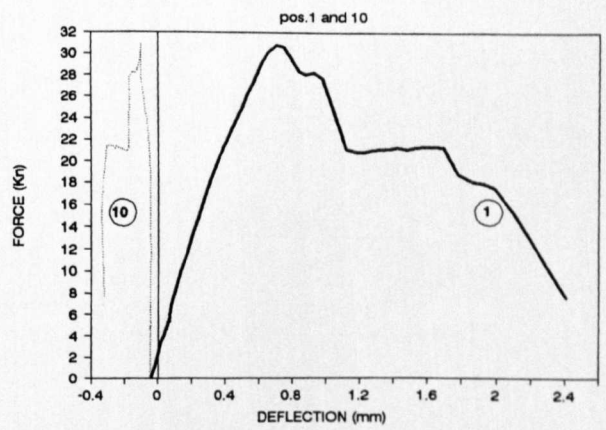
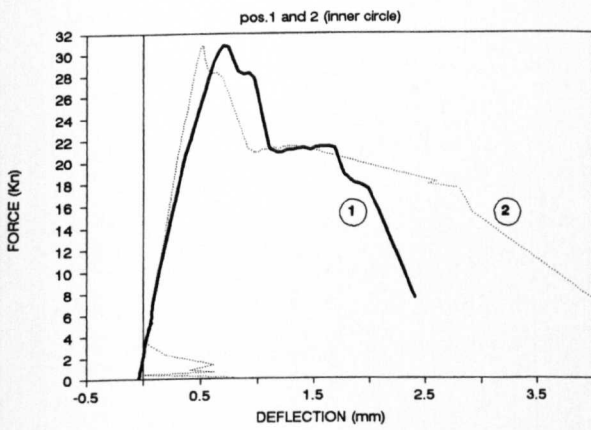
STATIC TEST - SMALL SLAB - SS3



top side



bottom side



STATIC TEST

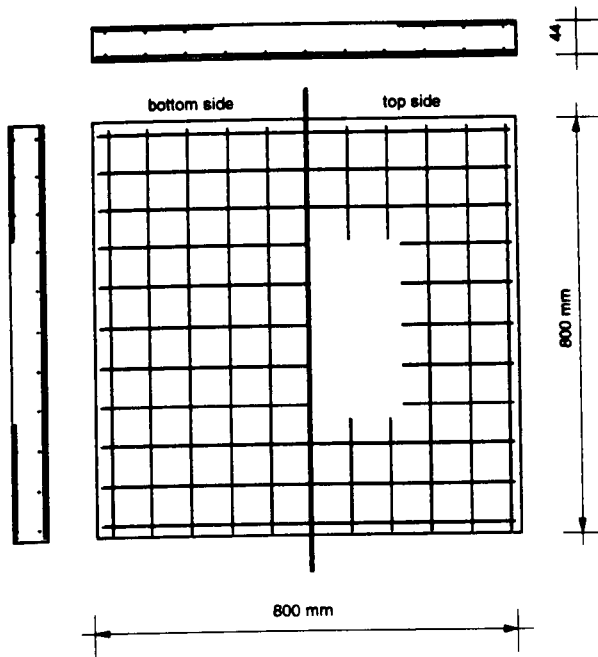
DATE: 16.04.93

SMALL SLAB SS4

AGE OF SPECIMEN: 10 days

Cube compressive strength	N/mm ²	51.6	Cylinder tensile strength	N/mm ²	4.33	Age (days)	10
---------------------------	-------------------	------	---------------------------	-------------------	------	------------	----

REINFORCEMENT:



TOP LAYER REINFORCEMENT:

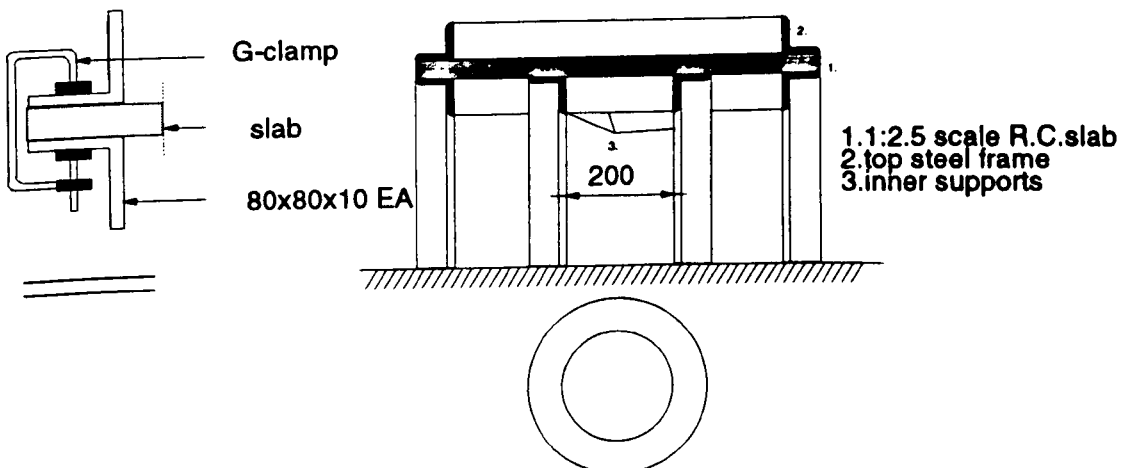
R.MESH : 3.15 mm DIAM. / 76.2 mm CENTRES
(WITHOUT CENTRAL REGION 400 X 400 mm)

BOTTOM LAYER REINFORCEMENT:

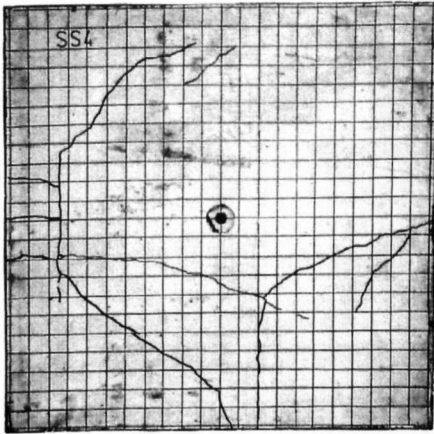
R.MESH : 3.15 mm DIAM. / 76.2 mm CENTRES

COVER: 4 mm

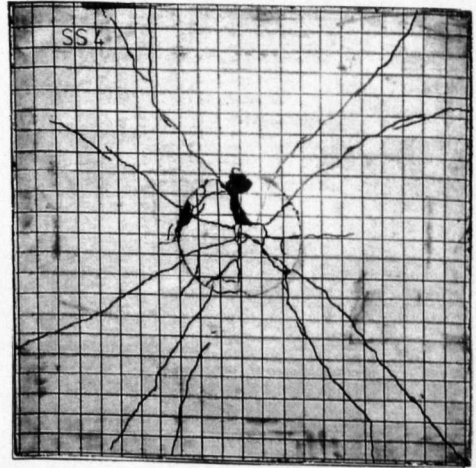
SUPPORTS:



STATIC TEST - SMALL SLAB - SS4

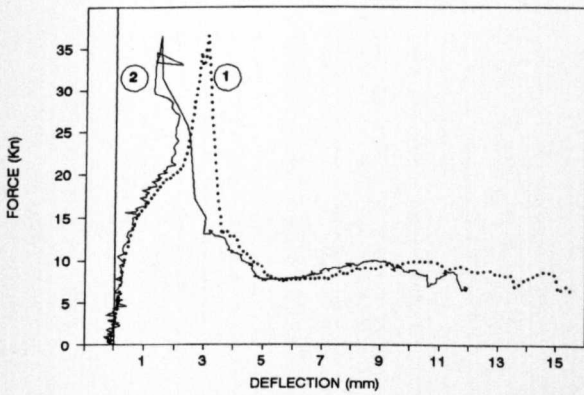


top side

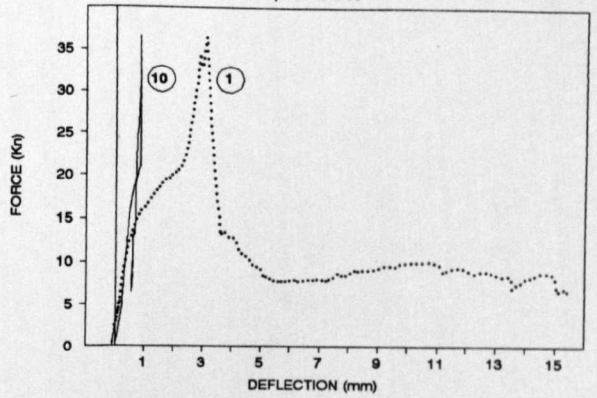


bottom side

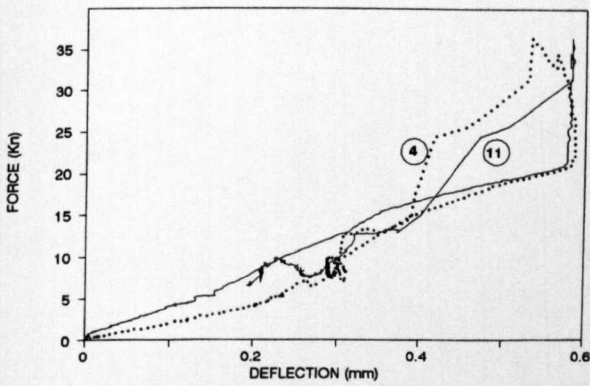
pos.1 and 2 (inner circle)



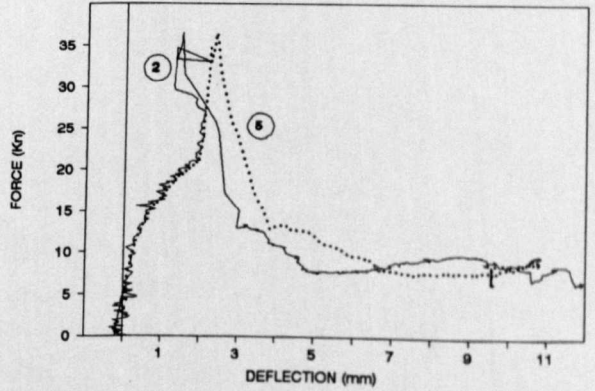
pos.1 and 10



pos.4 and 11 (270 mm off centre)



pos.2 and 5 (90 mm off centre)



STATIC TEST

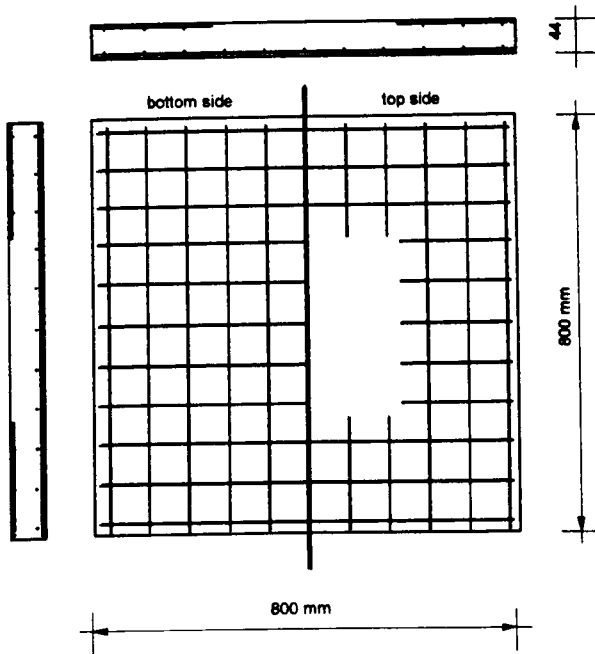
DATE: 16.04.93

SMALL SLAB SS5

AGE OF SPECIMEN: 10 days

Cube compressive strength	N/mm ²	51.6	Cylinder tensile strength	N/mm ²	4.33	Age (days)	10
---------------------------	-------------------	------	---------------------------	-------------------	------	------------	----

REINFORCEMENT:



TOP LAYER REINFORCEMENT:

R.MESH : 3.15 mm DIAM. / 76.2 mm CENTRES

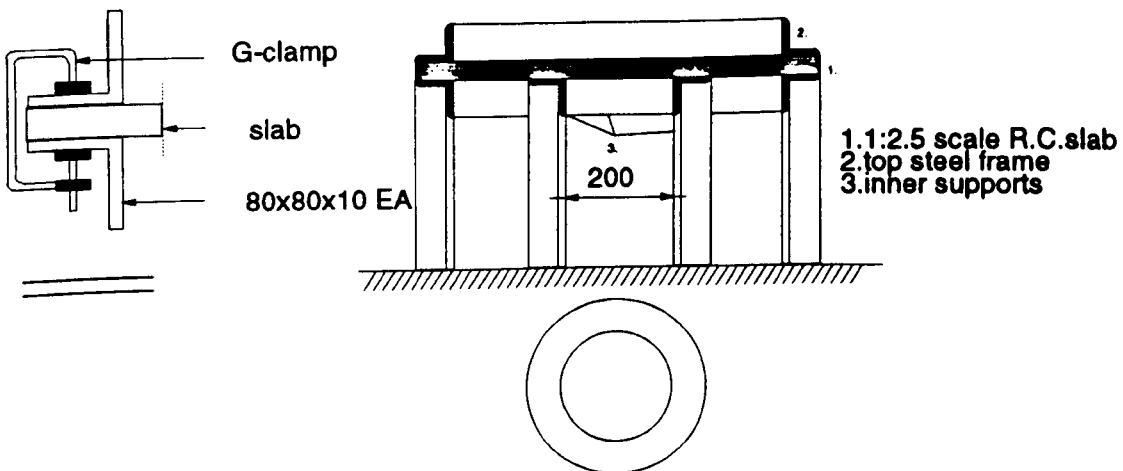
(WITHOUT CENTRAL REGION 400 X 400 mm)

BOTTOM LAYER REINFORCEMENT:

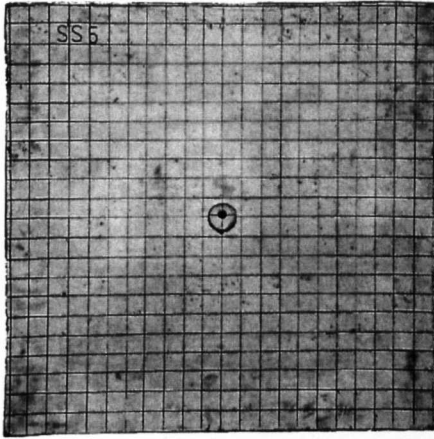
R.MESH : 3.15 mm DIAM. / 76.2 mm CENTRES

COVER: 4 mm

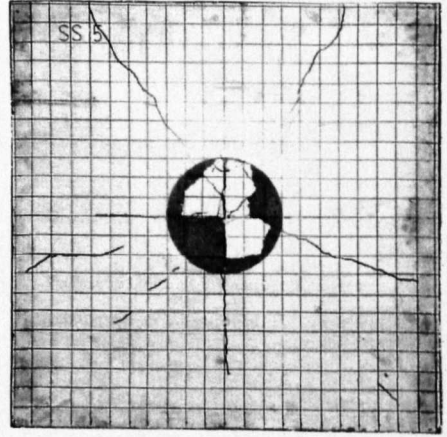
SUPPORTS:



STATIC TEST - SMALL SLAB - SS5



top side



bottom side

